

Sustainable Manufacturing of Next Generation Building Materials Using Microwave Energy

Miguel Angel Calvo-Carrascal, MEng

Thesis submitted to the University of Nottingham for the degree of Doctor of Philosophy

August 2018

ABSTRACT

Global warming and the high energy demands of fossil fuel in industries have led governments to implement legislation aimed towards developing more energy efficient and sustainable processes. In the brickwork industry, the burning of coal and natural gas provides the energy to fire clay bricks in the 900-1200 ^{o}C range into high quality building materials. Microwaves powered by renewable energy sources have been suggested as a sustainable alternative to fossil fuels. Microwave heating has been considered a promising technique for the processing of clays due to the potential energy consumption and carbon footprint reductions, and for its volumetric heating nature, which enables the fast and uniform heating of a load. This could result in improving the mechanical properties of the fired products.

The aims of this project were to develop an understanding of how microwaves interact with clays in order to show whether they could be used to fire clay-based building materials, and to understand how this could be achieved and the parameters that affect it.

The composition of Danish clays was quantified, i.e. quartz, calcite, albite, orthoclase, kaolinite, montmorillonite and muscovite, and their thermal evolution was studied across the firing range. The dielectric properties of clays were measured at 912-2470 MHz and 20-950 ^{o}C in order to investigate the microwave/clay interaction, assess the effects of changing composition, temperature, frequency and material's density on their potential for microwave processing, and provide critical information on the design and scale up of this technology. Relating the mineralogy of a material and its evolution during heating to changes on the dielectric property trends, and thus microwave processability, was examined for the first time in this thesis. Insight into the influence of individual components on the potential for microwave heating was gained from an analogous study on clay constituents.

While the dielectric constants of clays were found to be relatively stable during heating, their loss factors fluctuated with temperature. Free and physically bound water were the dominant dielectric species near room temperature, while their removal halved the loss factors until 350 ^{o}C. Beyond this temperature, a steady increase in the loss factors concurred with the mineral dehydroxylations. The loss factors sharply rose beyond 800 ^{o}C due to sintering effects, while calcite decomposition partially counteracted this growth. Montmorillonite and muscovite were the most microwave absorbing mineral species due to their water affinity and interlayer cation content, enabling the microwave treatment of the whole clay. On the other hand, a frequency shift from 2470 MHz to 912 MHz resulted in a loss factors increase. This is mainly due to the frequency shifting towards the dipolar dispersion area of physically bound water and the zone in which ionic conductivity heating effects dominate.

Mixing rules were used to relate each single mineral to dielectric property variations, and thus rapidly gain knowledge of the microwave processability of any clay across the firing range based on its composition. Böttcher model provided accurate estimations when compared to experimental measurements, and with the same degree of uncertainties at the 912-2470 MHz frequencies and 0.56-0.37 void fraction ranges. The model was expanded for different compositions with clays from Spain, England and Netherlands. This was the first time that mixing rules were successful in estimating mixtures of more than three constituents.

A microwave system was developed with the aim of firing clay products of comparable quality to conventional specimens. The basis of design focused on maximising the thermal uniformity of the clay load. The process design steps involved remodelling the clay load, building heat transfer models of the load, carrying out trials to study whether clays behave as expected from their dielectric properties, i.e. volumetric or selective heating, minimising thermal gradients, and assessing alternative methods for the control of the holding stage. Microwave firing cycles manufactured clays with a thermal uniformity at the height of firing of 1050±55 ^{o}C and reduced processing times to <3 h. This is 92% faster than in brickworks, where conventional samples could not match the heating rates without cracking. High temperature (>800 ^{o}C) mineral reactions went unfinished due to the reduced holding time of the microwave treatment (30 min), which resulted in dimmer surface colorations. Enhanced thermal uniformity and reduced time for densification resulted in specimens with a 12% higher compressive strength, 38% larger water absorption and 7% higher void fraction.

Clay samples three times as big were fired to gain an insight into the scale up of the technique. A tighter process control and higher reproducibility were reported, which is promising for potentially allowing longer holding times in scaled up processes, but the product quality improvement did not change. Looking into an industrial scale up, further work would be required to assess possible design concepts, and an optimal microwave firing process may require complete redesign of the furnace configuration, where several challenges need to be considered, such as brick arrangement, power availability and applicator size and shape. For the purposes of assessing the possible economic and environmental impact of implementing microwave clay firing at industrial scale, one of the most straightforward designs, i.e. retrofitting of an industrial tunnel kiln for microwave processing, was considered. Although energy expenditures would decrease from 11.6 GJ fuel/h to 6.1 GJ electricity/h when using a microwave system for the same throughput, the higher cost of electricity and microwave equipment over conventional burners made the conventional technique more economically feasible. The substitution of natural gas by electricity powered by green energy sources resulted in carbon footprint reductions of >95%, and agreed with the energy policies of numerous countries and supranational organisations worldwide.

ACKNOWLEDGEMENTS

I would like to thank my supervisors Eleanor Binner and Juliano Katrib for their guidance, motivation, and most of all their patience throughout the whole of my PhD.

Special thanks to the researchers, students and technicians from the Faculty of Engineering and particularly from the Microwave Processing Group, whose constructive criticism, feedback and amiable chatter made my time here enjoyable.

I would like to express my deepest gratitude to my parents Angel Luis Calvo and Basilia Carrascal for their continuous encouragement to strive for greatness, to my sister Laura for her constant love and support, to my grandmothers Nieves and Araceli for their unwavering faith in my abilities, and last but not least to my girlfriend Sara Perez for putting up with me all these years.

TABLE OF CONTENTS

ABSTRACT ..... **I**
ACKNOWLEDGEMENTS ..... **III**
TABLE OF CONTENTS ..... **V**
LIST OF TABLES ..... **XIII**
LIST OF FIGURES ..... **XVII**
LIST OF ABBREVIATIONS AND NOMENCLATURE ..... **XXIII**
1 INTRODUCTION **1**
2 AIMS AND OBJECTIVES OF THE RESEARCH **5**
3 CLAY AND ITS PROCESSING **7**
3.1 Introduction 7
3.2 Nature of clays 8
3.2.1 Origins of clays 8
3.2.2 Composition of clays 8
3.2.3 Structure of clays 9
3.2.3.1 Crystalline phase 10
3.2.3.1.1 Clay minerals 10
3.2.3.1.1.1 Kaolinite 11
3.2.3.1.1.2 Muscovite 12
3.2.3.1.1.3 Montmorillonite 12
3.2.3.1.2 Feldspars 12
3.2.3.1.2.1 Orthoclase 12
3.2.3.1.2.2 Albite 13
3.2.3.1.3 Quartz 13
3.2.3.1.4 Calcite 13
3.2.3.2 Non-Crystalline phase 13
3.2.3.3 Mixed-layer minerals 13
3.2.4 Clay characterisation 14
3.2.4.1 X-ray diffraction (XRD) 14
3.2.4.2 X-ray fluorescence (XRF) 15
3.2.4.3 Thermal analyses 15
3.2.4.3.1 Thermogravimetric analysis (TGA) 15
3.2.4.3.2 Differential scanning calorimetry (DSC) 16
3.2.4.4 Scanning electron microscope (SEM) 16

3.2.5 Classification of clays 17
3.3 Conventional processing of clays 18
3.3.1 State of the art processing stages 18
3.3.1.1 Excavation 18
3.3.1.2 Preparation of clay 18
3.3.1.3 Forming of the brick 19
3.3.1.4 Drying 19
3.3.1.5 Firing 19
3.3.1.5.1 Firing zones 20
3.3.1.5.2 State of the art brick firing cycle 21
3.3.2 Physical properties of fired bricks 22
3.3.2.1 Colour and texture 22
3.3.2.2 Compressive strength 23
3.3.2.3 Size variation 23
3.3.2.4 Water absorption 23
3.3.2.5 Durability 23
3.3.3 Thermal transformations of clays 24
3.3.4 Outlook for conventional processing of brick clays 26
3.4 Conclusions 27
4 MICROWAVE PROCESSING THEORY 29
4.1 Introduction 29
4.2 Heating mechanisms in microwave processing 30
4.2.1 Polarisation 31
4.2.1.1 Dipolar polarisation 31
4.2.1.2 Interfacial polarisation 31
4.2.2 Ionic conductivity 32
4.3 Dielectric properties of materials 32
4.3.1 Parameters affecting dielectric properties 33
4.3.1.1 Composition 34
4.3.1.2 Frequency 34
4.3.1.3 Temperature 35
4.3.1.4 Density 36
4.3.2 Dielectric properties of clay materials in the literature 37
4.3.3 Heating equation and penetration depth 41

4.4 Measurement of dielectric properties 42
4.4.1 Open ended coaxial probe 42
4.4.2 Waveguide transmission line 43
4.4.3 Resonant cavity 44
4.5 Estimation of dielectric properties 46
4.5.1 Mixing rules 46
4.5.1.1 Rayleigh 47
4.5.1.2 Böttcher 47
4.5.1.3 Complex Refractive Index (CRI) 48
4.5.1.4 Landau-Lifshitz-Looyenga (LLL) 48
4.5.1.5 Lichtenecker 49
4.5.1.6 Bruggeman-Hanai (BH) 50
4.5.1.7 Sen-Scala-Cohen 50
4.6 Microwave heating equipment 53
4.6.1 Generator 53
4.6.2 Transmission devices 54
4.6.3 Applicators 56
4.6.3.1 Single mode cavities 56
4.6.3.2 Multimode cavities 57
4.6.3.3 Applicator selection criteria 59
4.6.3.3.1 Hot spots and thermal runaway 59
4.6.3.3.2 Arcing 60
4.6.4 Additional waveguide components and systems 60
4.6.4.1 Circulator 61
4.6.4.2 Directional coupler and power meters 61
4.6.4.3 Vector network analyser (VNA) and tuners 61
4.6.4.3.1 Stub tuner 62
4.6.4.3.2 Sliding short 62
4.6.4.4 Microwave leakage seals 62
4.6.4.5 Temperature measurement equipment 63
4.7 Outlook on the microwave heating of clays and clay constituents 63
4.8 Summary of literature review 72
5 MATERIALS AND EXPERIMENTAL TECHNIQUES 75
5.1 Introduction 75

5.2 Materials 75
5.2.1 Materials preparation 76
5.3 Materials characterisation 76
5.3.1 Equilibrium moisture 76
5.3.2 X-ray diffraction 77
5.3.3 Bulk density and void fraction 77
5.3.4 Thermal gravimetric analysis 78
5.3.5 Differential scanning calorimetry 79
5.3.6 Dielectric properties 79
5.3.6.1 Resonant cavity 79
5.3.6.2 Waveguide transmission line 82
5.3.7 Electromagnetic mixing rules 84
5.4 Materials processing 86
5.4.1 System set-up of microwave rig for the firing of clays 86
5.4.2 Microwave heating trials 87
5.5 Quality analysis 90
5.5.1 Conventionally fired clay reference 90
5.5.2 Compressive strength 90
5.5.3 Water absorption and saturation coefficient 91
5.5.4 Shape, size and density variation 91
5.5.5 Colour and texture 92
5.6 Techno-economical assessment of the microwave processing technique 92
5.6.1 Economic assessment 92
5.6.2 Environmental assessment 93
5.7 Conclusions 95
6 CHARACTERISATION OF CLAY MATERIALS 97
6.1 Introduction 97
6.2 Physicochemical characterisation of Danish clays 98
6.2.1 Clay composition 98
6.2.2 Thermal analysis of clays and clay constituents 100
6.2.2.1 Thermogravimetric analysis of Danish clays 100
6.2.2.2 Thermogravimetric analysis of single clay constituents 102
6.2.2.3 Differential scanning calorimetry of Danish clays 103
6.2.3 Conclusions on the physicochemical characterisation of Danish clays 104

6.3 Dielectric property measurements of clays and clay constituents 106
6.3.1 Dielectric properties of red and yellow Danish clays 106
6.3.1.1 Influence of composition on clays dielectric properties 106
6.3.1.2 Influence of void fraction on clay dielectric properties 109
6.3.1.3 Influence of frequency on clay dielectric properties 110
6.3.1.4 Conclusions on the dielectric properties of red and yellow Danish clays .. 112
6.3.2 Dielectric properties of clay constituents 113
6.3.3 Comparative analysis of clay dielectric properties 115
6.3.4 Conclusions on dielectric property measurements of clays and clay constituents 116
6.4 Theoretical estimation of clays dielectric properties 117
6.4.1 Dielectric property estimation of binary clay-air mixtures 118
6.4.2 Dielectric property estimation of multicomponent clay-minerals mixtures . 123
6.4.3 Towards the development of a comprehensive dielectric property predictive tool for clays 128
6.4.4 Conclusions on dielectric property estimations 133
6.5 Conclusions 134
7 MICROWAVE PROCESSING OF CLAYS 137
7.1 Introduction 137
7.2 Design of microwave clay firing system 138
7.2.1 Microwave applicator selection for clay firing 138
7.2.2 Remodelling of raw clay feed for microwave processing 139
7.2.3 Clay temperature monitoring during microwave firing 141
7.2.4 Conclusions on the design of a microwave clay firing system 144
7.3 Commissioning of microwave clay firing system 145
7.3.1 Power distribution in the microwave rig during clay heating 146
7.3.1.1 Power reflections in the microwave system 146
7.3.1.2 Power absorption by the microwave system 148
7.3.1.3 Clay power absorption in the microwave system 149
7.3.2 Validation of heating losses model 152
7.3.3 Thermal uniformity of heated clays 154
7.3.4 Conclusions on commissioning of microwave clay firing system 156
7.4 Development of clay microwave firing cycles 157
7.4.1 Clay firing cycles controlled by sample temperature 158
7.4.2 Clay firing cycles controlled by sample energy needs 160

7.4.3 Thermal uniformity of clays fired using microwave energy 161
7.4.4 Conclusions on the development of clay microwave firing cycles 162
7.5 Quality comparison between microwave and conventional firing 163
7.5.1 Conventionally fired clay reference 164
7.5.2 Compressive strength 165
7.5.3 Water absorption and saturation coefficient 167
7.5.4 Shape, size and density variation 168
7.5.5 Colour and texture 169
7.5.6 Mineralogical evolution 172
7.5.7 Conclusions of microwave-conventional clays quality comparison 173
7.6 Scale up of the clay microwave firing process 174
7.6.1 Understanding the limits of the laboratory scale microwave clay firing system 175
7.6.1.1 Power absorbance and temperature profiles of 25x35 mm clays 175
7.6.1.2 Quality comparison of 25x35 mm fired clays with conventional products 177
7.6.2 Considerations on the scale up of the microwave clay firing system 179
7.6.2.1 Single mode pilot scale processing 180
7.6.2.2 Multimode industrial scale processing 181
7.6.2.2.1 Batch processing 181
7.6.2.2.2 Continuous processing 183
7.6.3 Conclusions on the scale up of the clay microwave firing process 184
7.7 Techno-economical assessment of the processing technique 185
7.7.1 Layout of the conventional and microwave clay firing systems 186
7.7.2 Economic assessment 188
7.7.3 Environmental assessment 191
7.7.4 Legislative assessment 192
7.7.5 Conclusions of the techno-economical assessment 194
7.8 Conclusions 195
8 GENERAL CONCLUSIONS AND FUTURE WORK 199
8.1 Introduction 199
8.2 Clay materials characterisation 199
8.3 Electromagnetic mixing rules estimations of clays dielectric properties 201
8.4 Microwave firing of clays 202
8.5 Techno-economical assessment of the microwave firing technique 203

9 REFERENCES 205

APPENDICES 227

Appendix A: X-ray diffraction spectra of clays 227

Appendix B: Dielectric property measurements 230

Appendix B1: Dielectric properties of clays 230

Appendix B2: Dielectric properties of clay constituents 234

Appendix B3: Dielectric properties of Fibercon wool and Vitcas firebrick 240

Appendix C: Dielectric property estimations 241

Appendix C1: Estimations of binary clay-air mixtures 241

Appendix C1.1: Powder to slab estimations 241

Appendix C1.2: Slab to powder estimations 249

Appendix C2: Estimations of multicomponent clay-minerals mixtures 257

Appendix D: Thermal modelling of microwave trials 271

Appendix D1: Parameters used in the thermal models calculations 271

Appendix D2: Specific heat capacity of Danish clays 271

Appendix D3: Temperature relations and heating losses across clay firing 272

Appendix E: LabVIEW software interface for automatic power input control during microwave heating trials 272

LIST OF TABLES

Table 3.1- Composition ranges of some unfired clay bricks used for building applications in European countries (Jensen, 1978, Jackson, 1973, Oti et al., 2009, González et al., 1998, Bauluz et al., 2003, Vissing, 2004). 9
Table 3.2- Classification of phyllosilicates related to clay minerals. Adapted from (Gillot, 1987) 18
Table 4.1- Published dielectric properties of clays and clay constituents at different conditions of temperature, frequency, moisture and density.*Not Available (NA) is used when temperature is not specified or described as room temperature. 40
Table 4.2- Penetration depths of some common materials at the commonly used processing frequency of 2450 MHz and at room temperature (Püschner, 2015). 42
Table 4.3- Summary table of suitability of various dielectric property measurement techniques for the assessment of clays and clay constituents. 46
Table 4.4- Common mixing rules formulas (Sihvola, 1999, Nelson, 2005). 51
Table 4.5- Summary table of suitability of various electromagnetic mixing rules for the estimation of the dielectric properties of clays and clay constituents. 53
Table 6.1- Quantitative XRD characterisation of the major clay constituents in red and yellow Danish clays, i.e. quartz, calcite, albite, orthoclase and the clay minerals kaolinite, montmorillonite and muscovite. Each sample was measured once, so that deviations for the mineral concentrations range ±2.5% for >60 wt%, ±5% between 60-30 wt%, ±10% between 30-10 wt%, ±20% between 10-3 wt% and ±40% for <3 wt %. 98
Table 6.2- Equilibrium moisture contents of red and yellow Danish clays at different void fractions as solids slabs and powders. For each material, five repeats were made and the standard uncertainty is indicated. 99
Table 6.3- Equilibrium moisture contents of major clay constituents at different void fractions as solids slabs and powders. For each material, five repeats were made and the standard uncertainty is indicated. 100
Table 6.4- T values for the dielectric constants and loss factors between 20-800°C at 2450 MHz of red and yellow Danish clay slabs at void fractions ranging 0.37±0.02 for Vedstaarup yellow, 0.39±0.01 for Hammershoj yellow, 0.40±0.01 for Helligsø red and 0.42±0.03 for Hammershoj red. These results are the average of three repeats. 116
Table 6.5- Comparison between measured dielectric properties of slabs of red and yellow Danish clays at void fractions ranging 0.37±0.02 for Vedstaarup yellow, 0.39±0.01 for Hammershoj yellow, 0.40±0.01 for Helligsø red and 0.42±0.03 for Hammershoj red shown here at certain temperatures across the 20-950 C firing range at 2470 MHz and binary clay-air mixing rules approximations from clay powders at void fractions ranging 0.56±0.03. The standard uncertainties are indicated in the table. 122
Table 6.6- Average estimation errors across the 20-950 °C firing range of the three most suitable mixing rules in the binary clay-air approximations of red and yellow Danish clays at different frequencies and void fractions, i.e. slabs and powders. 123
Table 6.7- Comparison between measured dielectric properties of slabs of red and yellow Danish clays at void fractions ranging 0.37±0.02 for Vedstaarup yellow, 0.39±0.01 for Hammershoj yellow, 0.40±0.01 for Helligsø red and 0.42±0.03 for Hammershoj red shown here at certain temperatures across the 20-950 °C firing range at 2470 MHz and

multicomponent clay-minerals mixing rules approximations from minerals powders at void fractions ranging 0.56±0.04. 127
Table 6.8- Quantitative XRD characterisation of the major clay constituents in red and yellow European clays, i.e. quartz, calcite, albite, orthoclase and the clay minerals kaolinite, montmorillonite and muscovite. Each sample was measured once, so that deviations for the mineral concentrations range ±2.5% for >60 wt%, ±5% between 60-30 wt%, ±10% between 30-10 wt%, ±20% between 10-3 wt% and ±40% for <3 wt %. 128
Table 6.9- Equilibrium moisture contents and void fractions of red and yellow European clays as slabs. For each material, five repeats were made and the standard uncertainty is indicated. 129
Table 6.10- Comparison between measured dielectric properties of slabs of red and yellow European clays at void fractions ranging 0.10±0.01 for Spanish yellow, 0.38±0.01 for Dutch red and 0.30±0.02 for English red shown here at certain temperatures across the 20-950 ºC firing range at 2470 MHz and multicomponent clay/minerals mixing rules approximations from minerals powders at void fractions ranging 0.56±0.04. 132
Table 7.1- Compressive strength of microwaved and conventionally fired 25x20 mm clay specimens in the 20-1050 ºC range with the former processed at different holding times, and standard values from ASTM C62. The microwave data is the average of three repeats, while conventional values are the results of ten repeats. 166
Table 7.2- Cold and boiling water absorption and saturation coefficients of microwaved and conventionally fired 25x20 mm clay specimens with the former processed with a 30 min holding time, and standard values from ASTM C62. These results are the average of three repeats. 168
Table 7.3-Porcentual volume reduction from unfired specimens and bulk densities of microwaved and conventionally fired 25x20 mm clay specimens with the former processed with a 30 min holding time. These results are the average of three repeats. 169
Table 7.4- CIE colour space parameters of unfired, microwaved, conventionally fired, and microwaved + conventionally cooled 25x20 mm red and yellow Danish clays with the former processed with a 30 min holding time. These results are the average of five repeats. 172
Table 7.5- Quantitative XRD characterisation of the major clay constituents in red and yellow Danish clays after microwave firing, conventional firing, and microwave firing + conventional cooling 25x20 mm cylindrical samples in the 20-1050 ºC range. Each sample was measured once, so that deviations for the mineral concentrations range ±2.5% for >60 wt%, ±5% between 60-30 wt%, ±10% between 30-10 wt%, ±20% between 10-3 wt% and ±40% for <3 wt %. 173
Table 7.6- Compressive strength, cold and boiling water absorption, saturation coefficient, volume variation, bulk density and CIE colour space of microwaved and conventionally fired 25x35 mm red and yellow Danish clays, in a 20-1050 ºC range, with the former processed with a 30 min holding time. The conventional and microwave compressive strength data is the result of ten and three repeats. The water absorption, volume and bulk density data is the result of three repeats. The CIE colour parameters data is the result of five repeats. 178
Table 7.7- Quantitative XRD characterisation of the major clay constituents in red and yellow Danish clays after microwave and conventional firing 25x35 mm cylindrical samples in the 20-1050 ºC range. Each sample was measured once, so that deviations for the mineral concentrations range ±2.5% for >60 wt%, ±5% between 60-30 wt%, ±10% between 30-10 wt%, ±20% between 10-3 wt% and ±40% for <3 wt %. 179

Table 7.8- Dimensions, throughput, heating cycle and brick characterisation of a conventional industrial kiln (Køster, 2014, IBSTOCK, 2015, Moesgaard, 2015, Vissing, 2004). 186
Table 7.9- Summary of capital and operational costs of running a conventional and microwave firing of clay bricks at industrial scale based on the assumptions of Table 7.8. . 188
Table 7.10- Summary of capital and operational costs of running a conventional and microwave firing of clay bricks at industrial scale for different countries with contrasting energy supply prices (GOV.UK, 2016a, GOV.UK, 2016b). 190
Table 7.11- Carbon footprint of natural gas and some renewable energy sources from CCalC2 software. 191
Table B.1- Dielectric constants and loss factors between 20-950 ºC at 912 MHz and 2470 MHz for yellow Danish clays slabs measured by the resonant cavity method at void fractions ranging 0.37±0.02 for Vedstaarup yellow and 0.39±0.01 for Hammershoj yellow. These results are the average of three repeats. The standard uncertainties are indicated in the table. 230
Table B.2- Dielectric constants and loss factors between 20-950 ºC at 912 MHz and 2470 MHz for red Danish clays slabs measured by the resonant cavity method at void fractions ranging 0.40±0.01 for Helligsø red and 0.42±0.03 for Hammershoj red . These results are the average of three repeats. The standard uncertainties are indicated in the table. 231
Table B.3- Dielectric constants and loss factors between 20-950 ºC at 912 MHz and 2470 MHz for yellow Danish clays powders with a 0.56±0.03 void fraction measured by the resonant cavity method. These results are the average of three repeats. The standard uncertainties are indicated in the table. 231
Table B.4- Dielectric constants and loss factors between 20-950 ºC at 912 MHz and 2470 MHz for red Danish clays powders with a 0.56±0.03 void fraction measured by the resonant cavity method. These results are the average of three repeats. The standard uncertainties are indicated in the table. 232
Table B.5- Dielectric constants and loss factors between 20-800 ºC at 2470 MHz for red and yellow Danish clays slabs measured by the waveguide technique at void fractions ranging 0.37±0.02 for Vedstaarup yellow, 0.39±0.01 for Hammershoj yellow, 0.40±0.01 for Helligsø red and 0.42±0.03 for Hammershoj red. These results are the average of three repeats. The standard uncertainties are indicated in the table. 232
Table B.6- Dielectric constants and loss factors between 20-950 ºC at 912 MHz and 2470 MHz for Spanish yellow, Dutch red and English red clay slabs measured by the resonant cavity method at void fractions ranging 0.10±0.01 for Spanish yellow, 0.38±0.01 for Dutch red and 0.30±0.02 for English red. These results are the average of three repeats. The standard uncertainties are indicated in the table. 233
Table B.7- Dielectric constants and loss factors between 20-950 ºC at 912 MHz and 2470 MHz for mineral slabs at void fractions ranging 0.32±0.03 for montmorillonite, 0.22±0.07 for muscovite and 0.48±0.02 for kaolinite. These results are the average of three repeats. The standard uncertainties are indicated in the table. 234
Table B.8- Dielectric constants and loss factors between 20-950 ºC at 912 MHz and 2470 MHz for mineral slabs at void fractions ranging 0.09±0.03 for calcite and 0.17±0.01 for quartz. These results are the average of three repeats. The standard uncertainties are indicated in the table. 235
Table B.9- Dielectric constants and loss factors between 20-950 ºC at 912 MHz and 2470 MHz for mineral slabs at void fractions ranging 0.17±0.07 for orthoclase and 0.35±0.06

for albite. These results are the average of three repeats. The standard uncertainties are indicated in the table. 236
Table B.10- Dielectric constants and loss factors between 20-950 °C at 912 MHz and 2470 MHz for mineral powders at void fractions ranging 0.56±0.04 for montmorillonite, muscovite and kaolinite. These results are the average of three repeats. The standard uncertainties are indicated in the table. 237
Table B.11- Dielectric constants and loss factors between 20-950 °C at 912 MHz and 2470 MHz for mineral powders at void fractions ranging 0.56±0.04 for calcite and quartz. These results are the average of three repeats. The standard uncertainties are indicated in the table. 238
Table B.12- Dielectric constants and loss factors between 20-950 °C at 912 MHz and 2470 MHz for mineral powders at void fractions ranging 0.56±0.04 for orthoclase and albite. These results are the average of three repeats. The standard uncertainties are indicated in the table. 239
Table B.13- Average dielectric constants and loss factors of Fibercon 1600 wool and Vitcas grade 30 firebrick at 2470 MHz and across the firing range of 20-950 °C and 20-700 °C, respectively. These results are the average of three repeats using the resonant cavity method. The standard uncertainties are indicated in the table. 240

LIST OF FIGURES

Figure 3.1- Diagram of tetrahedral (A) and octahedral (B) units of a clay mineral lattice (Grim, 1968) and arrangement of two silica layers around an octahedral sheet (C) (Christidis, 2011). 11
Figure 3.2-Sketch of a typical tunnel kiln (Køster, 2014) 21
Figure 3.3-Surface temperature of a clay brick during a typical conventional firing cycle (Køster, 2014). 22
Figure 3.4- Firing diagram of main thermal transformations of major clay constituents (Dunham, 1992, Galan et al., 2013, Heaney, 1994, Chen et al., 2000, McConville and Lee, 2005, Bohor, 1963). 25
Figure 4.1- Propagation of an electromagnetic wave in free space. 30
Figure 4.2- Dielectric properties trends across the frequency range of a typical polar solid with free electrical charges, i.e. concrete. Adapted from Asano et al. (2003). 35
Figure 4.3-Diagram of a coaxial probe measurement process. Adapted from NPL (2003). 43
Figure 4.4-Diagram of a waveguide transmission line connected to a network analyser, with a specimen ready for measurement seen through cut in waveguide. Adapted from ASTM (2014b). 44
Figure 4.5-Diagram of TM_{01} resonant cavity with a dielectric specimen inside a sample holder seen through cut in cavity. Adapted from NPL (2003). 45
Figure 4.6-Comparison of estimated dielectric constants of a binary mixture with a contrast of $\varepsilon_i/\varepsilon_m=100$ at different contents of inclusions with common Power-law models. Adapted from Sihvola (1999). Where εm and εi, are the complex dielectric permittivity of the matrix and the inclusions respectively. 50
Figure 4.7-Comparison of the susceptibility, defined as $(\varepsilon-\varepsilon_m)/(\varepsilon_i-\varepsilon_m)$, of Rayleigh dielectric constants estimations at different contents of inclusions with constituents of different dielectric properties (A), and comparison of estimated dielectric constants with Rayleigh formula of a mixture with a contrast of $\varepsilon_i/\varepsilon_m=50$ at different contents of inclusions and for various particle shapes (B). Adapted from Sihvola (1999). 52
Figure 4.8- Diagramatic aerial (A) and side view (B) of a multi-cavity magnetron microwave generator. Adapted from Thostenson and Chou (1999). 54
Figure 4.9- Distribution of the electric and magnetic fields in a hollow rectangular waveguide with TE_{10} and TM_{11} propagation modes. Adapted from Marcuvitz (1951). 55
Figure 4.10- Diagram of electromagnetic field interaction with a centrally located cylindrical sample and a sliding short seen through cuts in rectangular TE_{10} single mode cavity. Adapted from Mehdizadeh (2015). 57
Figure 4.11- Damping of the mode patters in an empty multimode cavity (f_1,f_2) as a dielectric specimen is loaded in the applicator (f_1',f_2')(A) and three-dimensional distribution pattern of power density in a loaded rectangular cavity (B). Adapted from Metaxas and Meredith (1983) and Mehdizadeh (2015). 59
Figure 4.12- Typical loss factor evolution with temperature of a substance which is susceptible of causing a thermal runaway. 60
Figure 5.1- Aerial (A) and side (B) views of unfired 25x35 mm yellow and 25x20 mm red clay cylinders. 76

Figure 5.2- Experimental set-up of the resonant cavity used for the dielectric property measurement of clays and clay constituents as powders and 19.2±1.0x3.2±0.4 mm cylindrical slabs (A) with added schematics (B).....81
Figure 5.3- Schematics of waveguide transmission line rig used for the dielectric property measurement of 34.3±0.6x90.1±0.7 mm clay bricks. 83
Figure 5.4- Alternatives for the mixing rules predictions of the dielectric properties of clays in mineral-clay mixtures that can be experimentally validated ,i.e. powder minerals to powder clays (A), mineral slabs to powder clays (B), powder minerals to clay slabs (C) and mineral slabs to clay slabs (D). 85
Figure 5.5- Schematic of single mode microwave rig designed for clay heating trials at 2450 MHz. Sample and insulation are seen through cut in waveguide. 86
Figure 5.6- Axonometric view of firebrick crucible plus its cap without wool insulation and loaded with a 25.0±0.5x20.1±0.3 mm red clay sample.....87
Figure 5.7- The reflection scattering parameter S_{11} at different frequencies read by a network analyser for 25.0±0.5x20.1±0.3 mm red clay cylinders showing an optimal cold matching (A) and a broad matching of the microwave field with the load in order to maximise its thermal uniformity (B). 88
Figure 5.8- Display of IR sensor for heating trials where power input is controlled by the clay temperature. 89
Figure 5.9- Schematics of the algorithm of the LabVIEW software interface used to control the power absorbed by the clay samples during microwave heating trials. 90
Figure 5.10- Main interface of CCaLC2 software used for the calculation of the environmental impact of the clays firing process using microwave energy and gas firing. 95
Figure 6.1- Average mass change and derivative mass change versus temperature across the temperature range of 25-1000ºC at 20ºC/min in a N_2 atmosphere for yellow (A) and red (B) Danish clays. These results are the average of three repeats. Standard deviations average for the weight and derivate weight around ±0.29 and ±0.002 for Hammershoj red, ±0.20 and ±0.003 for Helligsø red, ±0.39 and ±0.004 for Vedstaarup yellow, and ±0.47 and ±0.003 for Hammershoj yellow. 101
Figure 6.2- Average mass change and derivative mass change versus temperature across the temperature range of 25-1000 ºC at 20 ºC/min in a N_2 atmosphere of major clay constituents, i.e. montmorillonite, muscovite (A), kaolinite and calcite (B). These results are the average of three repeats. Standard deviations average for the weight and derivate weight around ±0.07 and ±0.001 for kaolinite, ±0.12 and ±0.001 for montmorillonite, ±0.16 and ±0.002 for muscovite, and ±0.64 and ±0.015 for calcite. 103
Figure 6.3- Average heat flow versus temperature across the temperature range of 25-1000 ºC at 20 ºC/min in a N_2 atmosphere for yellow (A) and red (B) Danish clays. These results are the average of three repeats. Standard deviations average around ±0.007 for Vedstaarup yellow, ±0.011 for Hammershoj yellow, ±0.014 for Helligsø red and ±0.010 for Hammershoj red. 104
Figure 6.4- Updated firing diagram of main thermal transformations of major clay constituents taking place in the red and yellow Danish clays studied. Reactions are divided into transformations proven to occur (Green), transformations that cannot be proven to individually take place (Red), and previously undiscovered mineral arrangements (Green with diagonal stripes). 105
Figure 6.5- Average dielectric constants and loss factors across firing between 20-950 ºC at 2470 MHz for yellow (A) and red (B) Danish clays slabs at void fractions ranging 0.37±0.02

for Vedstaarup yellow, 0.39±0.01 for Hammershoj yellow, 0.40±0.01 for Helligsø red and 0.42±0.03 for Hammershoj red. These results are the average of three repeats. 109
Figure 6.6- Average dielectric constants and loss factors across firing between 20-950 ºC at 2470 MHz for yellow (A) and red (B) Danish clays powders with a 0.56±0.03 void fraction. These results are the average of three repeats. 110
Figure 6.7- Average dielectric constants and loss factors across firing between 20-950 ºC at 912 MHz for yellow (A and C) and red (B and D) Danish clay slabs (A-B) at void fractions ranging 0.37±0.02 for Vedstaarup yellow, 0.39±0.01 for Hammershoj yellow, 0.40±0.01 for Helligsø red and 0.42±0.03 for Hammershoj red, and powders (C-D) at void fractions ranging 0.56±0.03. These results are the average of three repeats. 111
Figure 6.8- Average dielectric constants and loss factors across firing between 20-950 ºC at 2470 MHz for mineral slabs at void fractions ranging 0.32±0.03 for montmorillonite, 0.22±0.07 for muscovite (A), 0.48±0.02 for kaolinite, 0.09±0.03 for calcite, 0.17±0.01 for quartz (B), 0.17±0.07 for orthoclase and 0.35±0.06 for albite (C). These results are the average of three repeats 114
Figure 6.9- Continued. 121
Figure 6.10- Alternatives for the mixing rules predictions of the dielectric properties of clays in clay-minerals mixtures that can be experimentally validated, i.e. powder minerals to powder clays (A), mineral slabs to powder clays (B), powder minerals to clay slabs (C) and mineral slabs to clay slabs (D). 124
Figure 6.11- Average dielectric constants (Left) and loss factors (Right) across firing between 20-950 ºC at 2470 MHz for Danish clay slabs at void fractions ranging 0.37±0.02 for Vedstaarup yellow, 0.39±0.01 for Hammershoj yellow, 0.40±0.01 for Helligsø red and 0.42±0.03 for Hammershoj red, and mixing rules approximations from mineral powders at void fractions ranging 0.56±0.03 for yellow (A-D) and red (E-H) clays. These experimental results are the average of three repeats. 125
Figure 6.12- Average dielectric constants (Left) and loss factors (Right) across firing between 20-950 ºC at 2470 MHz for European clay slabs at void fractions ranging 0.10±0.01 for Spanish yellow, 0.38±0.01 for Dutch red and 0.30±0.02 for English red, and mixing rules approximations from mineral powders at void fractions ranging 0.56±0.03 for yellow (A-B) and red (C-F) clays. These experimental results are the average of three repeats. 130
Figure 7.1- Front view of the choked WR-430 brass waveguide used in the 2450 MHz clay microwave heating trials. 139
Figure 7.2- Average penetration depth between 20-950 ºC at 2470 MHz for yellow and red Danish clays slabs at void fractions ranging 0.37±0.02 for Vedstaarup yellow, 0.39±0.01 for Hammershoj yellow, 0.40±0.01 for Helligsø red and 0.42±0.03 for Hammershoj red. These results are the average of three repeats. 141
Figure 7.3- Sketch of the assumed homogeneous distribution of mineral constituents and the focalised heat generation inside a clay cylinder under microwave radiation. 142
Figure 7.4- Generator output frequency spectrum compared to clay load coupling band. Adapted from Gerling (2000). 147
Figure 7.5- Reflected power moving average trends from microwave heating trials at constant incident powers ranging 100-300 W for 80 min on 25x20 mm cylindrical specimens of red (A) and yellow (B) Danish clays at void fractions ranging 0.37±0.02 for the yellow and 0.40±0.01 for the red specimens. These results are the average of three repeats. 148
Figure 7.6- Clay absorbed power+heating losses moving average trends from microwave heating trials at constant incident powers ranging 100-300W for 80 min on 25x20 mm

cylindrical specimens of red (A) and yellow (B) Danish clays at void fractions ranging 0.37±0.02 for the yellow and 0.40±0.01 for the red specimens. These results are the average of three repeats. 149
Figure 7.7- Clay net absorbed power moving average trends from microwave heating trials at constant incident powers ranging 100-300W for 80 min on 25x20 mm cylindrical specimens of red (A) and yellow (B) Danish clays at void fractions ranging 0.37±0.02 for the yellow and 0.40±0.01 for the red specimens. These results are the average of three repeats. 152
Figure 7.8- Measured and estimated temperatures of clay surface (A-B) and insulating wool (C-D) for the validation of the heating losses model used in the microwave heating trials at constant incident powers ranging 100-300W for 80 min on 25x20 mm cylindrical specimens of red (left) and yellow (right) Danish clays at void fractions ranging 0.37±0.02 for the yellow and 0.40±0.01 for the red specimens. These results are the average of three repeats. 154
Figure 7.9- Top view under a thermal camera of 25x20 mm red (A) and yellow (B) clay cylinders after around 65 min of microwave heating at 300 W with added temperature legend, where (a) is the clay, (b) is the firebrick and (c) is the insulating wool. Standard deviations average for the clay surface temperatures for the red and yellow samples around ±83.8 ºC and ±110.8 ºC, respectively. The microwave feed is to the right of the samples. 155
Figure 7.10- Side view of feed facing surfaces of 25x20 mm cylinders of yellow (A) and red (B) Danish clay after around 65 min of microwave heating at 300 W. Partial melting and a thermal gradient pattern are recognised from bloating and colour differences on the clay surface. 156
Figure 7.11- Typical net clay absorbed power moving average trend (A) and clay surface temperature profile (B) from 170 min microwave firing trials at 2450 MHz and at a variable incident power, starting at 200 W, indirectly controlled by the temperature of the clay surface on 25x20 mm cylinders of red Danish clay at a 0.40±0.01 void fraction. 159
Figure 7.12- Typical net clay absorbed power moving average trends (A) and clay surface temperature profiles (B) from 170 min microwave firing trials at 2450 MHz and at a variable incident power, starting at 200 W, directly controlled by the absorbed power of 25x20 mm cylinders of red and yellow Danish clays at void fractions ranging 0.37±0.02 for the yellow and 0.40±0.01 for the red specimens. 161
Figure 7.13- Top view under a thermal camera of 25x20 mm red (A) and yellow (B) clay cylinders at the end of a 30 min holding stage after microwave firing at variable incident powers, starting at 200 W, directly controlled by the clay absorbed power with added temperature legend, where (a) is the clay, (b) is the firebrick and (c) is the insulating wool. Standard deviations average for the clay surface temperatures for the red and yellow samples around ±33.9 ºC and ±61.1 ºC, respectively. 162
Figure 7.14- Compressive strength evolution of conventionally fired 25x20 mm cylinders of red and yellow Danish clays in the 20-1050 ºC range at different heating rates. These results are the average of ten repeats. 165
Figure 7.15- Side view of 25x20 mm red clay cylinder conventionally fired at a heating rate of 7ºC/min in the 20-1050 ºC range. Surface cracks are clearly noticed and denote the presence of intense structural tensions result of large thermal gradients. 165
Figure 7.16- Side view of 25x20 mm cylinders of red Danish clay at different stages of conventional and microwave treatment in the 20-1050 ºC range. Unfired clay (a), microwave heated up to the start of the mineral dehydroxylations at 350-400 ºC (b), microwave heated up to before sintering at 650-700 ºC (c), conventionally fired (d), and microwave fired (e). 170

Figure 7.17- Side view of 25x20 mm cylinders of red (up) and yellow (down) Danish clays treated conventionally (a), with microwaves (b) and with microwaves plus a conventional cooling (c) in the 20-1050 ºC range. 171
Figure 7.18- Typical net clay absorbed power moving average trends (A), and clay surface and insulating wool estimated and measured temperature profiles of red (B) and yellow (C) clays from 170 min microwave firing trials at 2450 MHz and at a variable incident power, starting at 300 W, directly controlled by the absorbed power of 25x35 mm clay cylinders at void fractions ranging 0.37±0.02 for the yellow and 0.40±0.01 for the red specimens. 177
Figure 7.19- Yearly net cash flows across the service life of a common industrial scale tunnel kiln while performing clay firings using conventional gas firing or microwave energy as operational modes. 189
Figure 7.20- Evolution of Net Present Value of a common industrial scale tunnel kiln for the firing of clay bricks using either microwave energy or gas firing for different energy supply prices found in countries worldwide, i.e. Switzerland, Italy, USA, Norway, and the IEA average. 190
Figure 7.21- Carbon footprint generated by the firing of clays in a common industrial scale tunnel kiln where gas firing or electricity powered by different renewable energy sources are used as the energy supply. 192
Figure A.1- Smoothed XRD spectra of untreated Vedstaarup yellow (A), Hammershoj yellow (B), Helligsø red (C) and Hammershoj red (D) clays. Each sample was measured once, so that deviations for the mineral concentrations range ±2.5% for >60 wt%, ±5% between 60-30 wt%, ±10% between 30-10 wt%, ±20% between 10-3 wt% and ±40% for <3 wt %. Differences between these and the following trends come from the above being produced in Aarhus university department of geoscience while the rest have been produced at the British Geological Survey. 227
FigureA.2- Smoothed XRD spectra of untreated English red (A), Dutch red (B) and Spanish yellow (C). Each sample was measured once, so that deviations for the mineral concentrations range ±2.5% for >60 wt%, ±5% between 60-30 wt%, ±10% between 30-10 wt%, ±20% between 10-3 wt% and ±40% for <3 wt %. 228
Figure A.3- Smoothed XRD spectra of Vedstaarup yellow (left) and Helligsø red (right) clays after a firing cycle between 20-950 ºC on 25x20 mm cylindrical specimens using conventional heating (A-B), microwave energy (C-D), and microwave energy followed by a conventionally controlled cooling cycle (E-F). Each sample was measured once, so that deviations for the mineral concentrations range ±2.5% for >60 wt%, ±5% between 60-30 wt%, ±10% between 30-10 wt%, ±20% between 10-3 wt% and ±40% for <3 wt %. 228
Figure A.4- Smoothed XRD spectra of Vedstaarup yellow (left) and Helligsø red (right) clays after a firing cycle between 20-950 ºC on 25x35 mm cylindrical specimens using conventional heating (A-B) and microwave energy (C-D). Each sample was measured once, so that deviations for the mineral concentrations range ±2.5% for >60 wt%, ±5% between 60-30 wt%, ±10% between 30-10 wt%, ±20% between 10-3 wt% and ±40% for <3 wt %. 229

LIST OF ABBREVIATIONS AND NOMENCLATURE

Abbreviations

BH	Bruggeman-Hanai
Conv	Conventional
CIE	International Commission on Illumination
CRI	Complex Refractive Index
DCF	Discounted Cash Flow
DSC	Differential scanning calorimetry
DTI	Danish Technological Institute
EDS	Energy dispersive x-ray spectrometer
EMC	Electromagnetic compatibility
Est	Estimated
EU	European Union
EUDP	Danish Energy Technology Development and Demonstration Program
IEA	International Energy Agency
IR	Infrared radiation
IRR	Internal rate of return
ISM	Industrial, Scientific and Medical radio bands
LLL	Landau-Lifshitz-Looyenga
Meas	Measured
MLA	Mineral liberation analysis
MW	Microwaves
PB	Payback period
PID	Proportional, Integral, Derivative
PTFE	Poly-tetrafluoroethylene
Q factor	Quality factor
SEM	Scanning electron microscope
TE	Transverse electric
TEM	Transverse electromagnetic
TGA	Thermogravimetric analysis
TM	Transverse magnetic
VNA	Vector network analyser
XRD	X-ray diffraction
XRF	X-ray fluorescence

Nomenclature

a		CIELAB green/red parameter
A_C	(m^2)	Heat exchange area of the clay
A_{Ln}	(m^2)	Natural logarithmic heat exchange area
A_W	(m^2)	Heat exchange area of the insulating wool
b		CIELAB blue/yellow parameter
c	(m/s)	Speed of light in vacuum
Ci_z		Cash inflows at a year z
Co_z		Cash outflows at a year z
C_p	(J/kg K)	Specific heat capacity
Cp_{Avg}	(J/kg K)	Average specific heat capacity between the clay, firebrick and wool
Cp_{iAvg}	(J/kg K)	Average specific heat capacity between two temperatures
dH	(J/kg)	Enthalpy differential
D_p	(m)	Penetration depth
$DSC\ signal$	(W/kg)	Heat flow difference between the sample and the reference sample holder
dt	(s)	Time differential
dT	(K)	Temperature differential
e_c	(m)	Thickness of clay
e_F	(m)	Thickness of firebrick
E_i	(V/m)	Electric field strength inside the material
$erfc$		Complementary error function
e_W	(m)	Thickness of insulating wool
f	(Hz)	Frequency
F		Grey vision factor
f_i		Volume fraction of the inclusions/minerals
f_s	(Hz)	Resonance frequency of the loaded resonant cavity
f_0	(Hz)	Resonance frequency of the empty resonant cavity
Fo	(N)	Applied load
f_1,f_2	(Hz)	Central frequency of resonant modes in an empty cavity
f_1',f_2'	(Hz)	Central frequency of resonant modes in a loaded cavity
H_F	(m)	Distance between the heat source and the wool surface
h_N	(W/m^2 K)	Air natural convection heat transfer coefficient
h_R	(W/m^2 K)	Radiation heat transfer coefficient
H_0		Null hypothesis
H_1		Alternative hypothesis
J_1		First order Bessel function
K_{Avg}	(W/m K)	Average thermal conductivity between the clay, firebrick and wool
K_C	(W/m K)	Thermal conductivity of clay
K_F	(W/m K)	Thermal conductivity of firebrick
K_W	(W/m K)	Thermal conductivity insulating wool
L		Luminance
L_F	(m)	Diameter or height of the firebrick crucible
m	(kg)	Mass
m,n		Mode numbers

Nomenclature

M_D	(kg)	Mass of the dry specimen
M_W	(kg)	Mass of the wet specimen
NPV	(£)	Net present value
ñ		Refractive index
P_A	(W)	Total absorbed power
P_{Am}	(psi)	Ambient pressure
P_b	(psi)	Pressure in the combined two chambers after the gas expansion
P_C	(W)	Power absorbed by the whole microwave system except the clay
P_D	(W/m^3)	Power density
P_H	(W)	Absorbed clay power or power used solely to increase the clay temperature
P_I	(W)	Incident power
P_L	(W)	Heating losses
P_R	(W)	Reflected power
P_y	(psi)	Pressure in the sample chamber before the gas expansion
Q_0		Quality factor of the empty resonant cavity
Q_S		Quality factor of the loaded resonant cavity
r		Rate of return
s		Standard deviation of the cavity measurements
S	(mm^2)	Sample's surface that contacts the device's hammer
t	(s)	Time
T_A	(K)	Temperature of the ambient air
T_C		Critical t value for a certain confidence level (Ω) and a determined number of degrees of freedom $(\varrho - 1)$
T_{CC}	(K)	Temperature of the clay core
T_{CS}	(W/m K)	Temperature of the clay surface
T_{FS}	(K)	Temperature of the firebrick surface
t_i, t_{i+1}	(s)	Timestamps across the heating range
T_i, T_{i+1}	(K)	Clay core temperatures at different timestamp
t_p	(years)	Service life of a plant
T_t		t value of a system
T_{WS}	(K)	Temperature of the wool surface
T_{WSt}	(K)	Face wool temperature at a time t
U	(W/m^2 K)	Global heat transfer coefficient
V	(m^3)	Volume
$\bar{V}_0$	(mm^3)	Volume of a resonant cavity
V_p	(m^3)	Volume of a sample without pores
V_S	(m^3)	Volume of the empty sample chamber
$\bar{V}_S$	(mm^3)	Volume of a resonant cavity sample
V_R	(m^3)	Volume of the reference chamber
w	(%)	Moisture content
W_B	(%)	Maximum water absorption of the boiling test
W_C	(%)	Maximum water absorption of the cold test
$X_{l,m}$		mth root of the first order Bessel function $(J_1(x) = 0)$

Nomenclature

$\bar{x}$		Sample mean of complex dielectric permittivity
z	(years)	Year of service of a plant
α		Media topology parameter of power law mixing rules equations
δ		Saturation coefficient
δ_s	(m)	Skin depth
ΔT	(K)	Temperature variation
ε		Complex dielectric permittivity of a mixture
ε_i		Complex dielectric permittivity of inclusions
ε_m		Complex dielectric permittivity of a matrix
ε_0	(F/m)	Permittivity of free space
ε'		Dielectric constant
ε''		Loss factor
ε*		Complex dielectric permittivity
$\varepsilon^*_{StdClay}$		Standard deviation of the complex permittivity of a clay
ε^*_{Stdi}		Standard deviation of the complex permittivity of a mineral
λ	(m)	Wavelength
λ_a	(m)	Wavelength in air
λ_c	(m)	Wavelength inside clay
λ'_0	(m)	Free space wavelength
μ		Population mean of complex dielectric permittivity
μ_0	(V s/A m)	Permeability of free space
μ*		Complex magnetic permeability
ϑ	(N/mm^2)	Compressive strength
ξ	(m/s)	Phase velocity of light in clay
ρ	(kg/m^3)	Density
ρ_{Avg}	(kg/m^3)	Average density between the clay, firebrick and wool
ρ_b	(kg/m^3)	Bulk density
ρ_p	(kg/m^3)	Particle density
σ	(S/m)	Electrical conductivity
σ_i	(J/K)	Boltzmann constant
ϕ		Void fraction
ϙ		Number of measurements
$ϙ - 1$		Degrees of freedom
Ω		Confidence level of t student analysis

1 INTRODUCTION

Global energy and raw material demands are expected to escalate in line with population growth, which is predicted to increase 16% in the next 15 years, reaching 8.5 billion people by 2030 (UN, 2015). These needs are further boosted by the steadily industrialisation of developing and emerging industrial economies, where the added value of their manufactures quadrupled in the 1990-2014 range, reaching 35.9% of the global market with a net worth of £2662 billion (UNIDO, 2015). Most of the increasing energy demands are currently fulfilled by coal, oil and gas. However, the finite nature of these non-renewable energy sources and the progressive awareness of pollution by the population has boosted the pressure on governments and industries to produce more efficient, sustainable and green processes (Howes, 2010). As a result, significant legislation has been produced by international agencies and supranational departments such as the European Commission, aiming towards reducing or eliminating fossil fuel consumption in industry (ENER, 2010). Furthermore, moving towards green energy sources in order to reduce pollution and carbon footprint through sustainable processes was a major topic in the last two G7 summits (METI, 2016, METI, 2017). Finally, there is a significant effort from individual countries such as Denmark (EFKM, 2011), Iceland (INREAP, 2014) and Costa Rica (MINAET, 2011) to develop processes free of fossil fuels.

One of the industries targeted for energy optimisation is brickworking, which accounts for less than 8000 TW, i.e. beneath 5% of the total world energy consumption in 2012 (EIA, 2016). The predominant processing technique to obtain high quality fired bricks for building applications involves slowly heating large loads of raw bricks in kilns by burning natural gas, coal or oil (Manley, 2016). Despite decades of optimisation, the brick firing process can take between 40-60 h and continues to be completely reliant on fossil fuels. Moreover, variable emissions of carbon monoxide, carbon dioxide, nitrogen and sulphur oxides among others are critically dependent on the type of energy supply (Køster, 2014).

A radical shift in energy consumption, carbon footprint and other environmental effects of the brickmaking technique requires a technological step-change of the process, which microwave heating may provide. Microwave processing is a form of heating that occurs as a result of the electromagnetically induced vibration in individual particles of the workload, as opposed to more conventional processes based on the thermal conductivity of the target material and its surroundings (Meredith, 1998). The underlying motivation for its use can be summarised as the possibility of selectively heating a load across its volume without heating its surroundings or being deterred by the material's thermal conductivity. Consequently, faster processes can take place where the final products may display a higher degree of mechanical strength due to

the lack of thermal distortions (Kitchen et al., 2013). In addition, the energy supply is substituted by electricity that can come from renewable energy sources.

Despite these advantages, microwave processing of ceramic materials such as clays has not yet become widespread at industrial scale, with some specialised exceptions (Ceralink, 2013, C-Tech, 2016b). This occurs because it is uncommon to have an insight of the microwave/material interaction prior to process design and the monitoring and control of microwave processes are still challenging (Clark and Sutton, 1996, Waters et al., 2011). On the other hand, microwave heating systems have been extensively used at laboratory scale in the drying, sintering, synthesis and joining of ceramic materials such as alumina and mullite (Sutton, 1992, Liu et al., 2012, Ebadzadeh, 2010), although in many cases microwave applicators are used together with susceptors or additional conventional heating to control the process.

In this thesis, the effects of microwaves on clays are investigated in order to show their potential for use in brickmaking. The PhD was funded by the Danish Energy Technology Development and Demonstration Program (EUDP) with the eventual motivation of reducing the Danish brickworks industry's heavy reliance on fossil fuels by wholly or partly replacing gas firing with microwave heating.

The layout of this thesis is as follows:

The aims and objectives are presented in Chapter 2. Chapter 3 presents a literature review of clay, covering their origin, structure, characterisation and composition, and describing the state of the art in clay processing techniques using conventional heating, including its limitations. The theoretical aspects of microwave heating such as heating mechanisms, penetration depth, dielectric properties and the parameters that affect them are presented in Chapter 4, along with published dielectric property values for several clays and clay constituents. Moreover, common microwave heating equipment and dielectric property measurement techniques are presented, and previous work on the microwave processing of clay-like materials is commented upon, highlighting gaps and opportunities. In Chapter 5, the clay materials used in this project and the experimental procedures and methodologies followed in order to characterise and process the samples are described, e.g. dielectric properties and microwave heating trials respectively. Experimental measurements of the dielectric properties of various Danish red and yellow clays and clay minerals as a function of temperature, void fraction, composition and frequency are presented in Chapter 6, and these results are used to assess the clays' microwave heating potential. A tool for dielectric property predictions based on clay mineralogy is developed and validated with numerous European clays. Chapter 7 reports the development of a small-scale microwave firing apparatus to

investigate the behaviour of clays under an electric field, showing how the microwave/material interaction evolves with temperature. Furthermore, microwave clay firing cycles are developed and the quality of the fired products is compared with conventionally processed clays. Additionally, scale up considerations and a brief techno-economical assessment of the industrial scale microwave technique are provided. Finally, a summary of the findings of the project and a discussion regarding future research for the optimisation of the microwave firing of clays is presented in Chapter 8.

2 AIMS AND OBJECTIVES OF THE RESEARCH

Microwave heating is of interest for its potential to provide a step-change reduction in energy use and carbon dioxide emissions in the brickwork industry. However, ceramic materials (including clays) are known to be poor microwave absorbers, and to date microwave firing/sintering has only been achieved through the addition of microwave absorbing materials or the use of a supplementary conventional heating source, i.e. microwave susceptors and hybrid heating respectively. These measures potentially counteract the advantageous features of microwave heating, e.g. use of a sustainable energy source, selective heating of the load, reduced energy requirements and faster heating, suppressing the potential for it to enable a step-change in the brickwork industry. The aim of this project is to develop an understanding of how microwaves interact with clays in order to show whether they alone can be used to fire clay-based building materials, and if so, to understand how this can be achieved. This understanding will help to determine the potential to use microwave heating in the production of clay building materials.

The specific objectives of this study are:

- Determine whether common European clays can be fired by microwaves, and if this proves possible, how this is affected by other parameters such as temperature, which constituents are responsible for the heating and quantify their effect on clays' potential for microwave heating.
- Determine if building materials of comparable quality to conventionally fired bricks can be produced using microwave heating alone.
- Assuming the technical feasibility of the process is established by the previous objectives, investigate the economic, environmental and legislative assessment of the potential to use electromagnetic heating in the production of building materials.

3 CLAY AND ITS PROCESSING

3.1 Introduction

Clay is a porous, naturally occurring rock generally composed of one or more clay minerals, large quantities of quartz and several other constituents such as feldspars, calcite and iron oxides (Jensen, 1978). This ceramic is one of the oldest building materials on earth together with stone and wood (Grim, 1968). Its suitability for this task derives from its plasticity at the appropriate water content and the fact that it hardens when dried or fired (Guggenheim and Martin, 1995). Conventional industrial manufacturing of clay bricks for building applications involves the gradual heating of the raw materials to around 1000 ºC (Manley, 2016) in order to avoid significant thermal gradients that can result in cracks and fractures (Køster, 2014). The firing process is further lengthened by the characteristically low thermal conductivity of clay (Dondi et al., 2004), resulting in the need for large installations for the continuous production of bricks.

Despite years of improvement and optimisation in the brickwork industry, the process is still largely based on empirical knowledge built up over generations at each brickworks and only for their specific raw material and product profile. The average energy cost of 2.6 MJ/kg of fired material is mainly provided by coal, oil and natural gas (Køster, 2014). This consumption is the result of long processing times and is responsible for greenhouse gas emissions ranging 57-95 kg CO_2/GJ depending on the type of fuel used (Køster, 2014). The current process creates several challenges in a world that is progressively focusing on green energy sources and targeting pollution and carbon footprint as a health hazard of global interest (ENER, 2010).

The aim of this chapter is to present a thorough review of the nature of clays, their characterisation and state of the art in industrial processing techniques. In this chapter, the origin and the mineral composition of natural clays are detailed. Additionally, the structural arrangements and thermal evolution of clay forming minerals and their characterisation methods are outlined. Finally, the conventional clay processing methodology at a brickworks level is comprehensively detailed and its limitations assessed, together with a catalogue of the most relevant physical characteristics of the fired products that define their quality.

3.2 Nature of clays

3.2.1 Origins of clays

Clays can be formed in nature by four major processes: sedimentation, diagenesis/low-grade metamorphism, hydrothermal alteration and weathering, where the last is the primary source of clays (Gillot, 1987, Simonson, 1959). Here, the raw material is generally solid bedrock, which undergoes physical, chemical, and sometimes biological stresses through thousands of years in contact with Earth's atmosphere. This results in its break down and the formation of new constituents, so that at the end of the process the newly formed clay deposit has two differentiated types of constituents (Gillot, 1987, Millot, 1970):

- Primary clay minerals: Remnants of the rock-forming minerals, the most common are feldspars and quartz, which are the most abundant minerals in earth's continental crust.
- Secondary clay minerals: Called simply clay minerals from this point forward, they constitute the solid phase that substitutes the primary rock-forming minerals in the weathering process.

3.2.2 Composition of clays

Clays are heterogeneous multicomponent systems with solid, gaseous and liquid phases. In clay deposits, the last two are usually air and water, respectively. The latter presents itself as H_2O or OH and can be classified based on the energy required to remove it from the clay system (Güven and Pollastro, 1992, Guggenheim and van Groos, 1992):

- Chemically bound water – Strongly bonded water as OH that comprises the structural units of the mineral layer lattice and the junctions between sheets. It is eliminated in dehydroxylation reactions.
- Physically bound water – H_2O that is poorly bonded to the minerals. It is located in the mineral interlayer or on the external surfaces and pores of the materials, where the latter is referred to as free water or moisture. It is removed in dehydration reactions and drying, respectively.

The solid phase can be divided into clay minerals and non-clay minerals owing to the importance of the former on the characteristics of clays (Velde, 2013). Clay minerals are hydrous aluminosilicates of variable chemical formula mainly found in the <2 μm fraction of clays (Gillot, 1987, Guggenheim and Martin, 1995). A wide range of species can be found depending on their origins, but commonly kaolins, smectites and micas constitute the three main mineral families in building bricks (Keeling, 1963, Jensen, 1978). Illite is also

commonly mentioned; this is a vaguely defined term subject to debate due to its structural and chemical similarities with mica (Keeling, 1963, Velde, 1977, Rieder et al., 1998, Gillot, 1987). To avoid misinterpretation, in this work illite will be treated as synonymous with mica. The non-clay minerals consist of feldspars, quartz and carbonates, where the last often appears in the form of calcite and to a lesser extent as dolomite (Reeves et al., 2006). Small quantities of iron oxides can also be found, often in the form of hematite, and a wide range of impurities such as sulphates, phosphates, halides and organic matter may be detected (Reeves et al., 2006, Keeling, 1963).

The compositional ranges of some unfired clay bricks in different European countries are presented in Table 3.1. It is clear that clay composition varies greatly among countries and even within the same state, mainly due to clay genesis and history. Compositional differences are often further aggravated in brickworks, as specific combinations of additives are mixed with the raw materials focusing on improving the technical characteristics of the future fired bricks. As a result, clay compositions gravitate further away from the ideal brick body, i.e. 55% quartz, 25% kaolin and 20% mica (Reeves et al., 2006). Nevertheless, non-clay minerals still make up around half of the clay's composition, with small quantities of feldspars and a highly variable presence of calcite often decreasing the overall quartz contribution, and where the presence of dolomite tends to be residual. In addition, mica and kaolin are usually complemented with smectite which can compose as much as 50% of the clay.

Table 3.1- Composition ranges of some unfired clay bricks used for building applications in European countries (Jensen, 1978, Jackson, 1973, Oti et al., 2009, González et al., 1998, Bauluz et al., 2003, Vissing, 2004).

Country	Spain	Denmark	United Kingdom
Clay Constituent	**Quantity (%w/w)**		
Kaolin	0-17	3-22	9-16
Smectite	0-27	2-51	0
Mica	15-62	2-16	35-53
Feldspars	1-7	8-18	2-6
Quartz	20-40	30-60	18-31
Calcite	0-35	0-23	2-19

3.2.3 Structure of clays

Clay lacks any type of repeatable organizational arrangement due to its heterogeneity. Thus, its structure is a result of its constituents and their combinations. The solid phase of clays is almost always composed of more than two solid constituents, so that the clay mixture can be polycrystalline and polyamorphous, without a sharp dividing line between the two states. The

crystalline components are inorganic minerals and the amorphous may be either organic or inorganic (Grim, 1968).

3.2.3.1 Crystalline phase

3.2.3.1.1 Clay minerals

Clay minerals constitute most of the crystalline state and their structures are normally taken as the representative of this phase (Guggenheim and Martin, 1995, Gillot, 1987). Clay minerals belong to the family of the phyllosilicates, also called sheet silicates, due to their layer structure based on the repetition of two types of structural unit which compose their atomic lattices (Murray, 2006), as shown in Figure 3.1.

- A sheet of closely packed oxygens or hydroxyls in which divalent or trivalent cations such as aluminium, iron or magnesium are embedded in octahedral coordination, in a way that they are equidistant from six oxygens or hydroxyls.
- A hexagonal network of silica tetrahedrons, where the silica atom is equidistant from four oxygens or hydroxyls.

In order to form the layer structure, the silica tetrahedrons form a hexagonal sheet network of platy shape, while the octahedrons coordinate to give another sheet. Then, with replacements of OH and O the layers arrange in a planar single layer. Depending on the cations in the octahedral coordination and the number of silica layers, the arrangements vary. The resultant structures generally have a net negative layer charge that will tend to be offset with cation exchanges and water molecules between the sheets, often causing distortions in the lattices (Grim, 1968, Reeves et al., 2006).

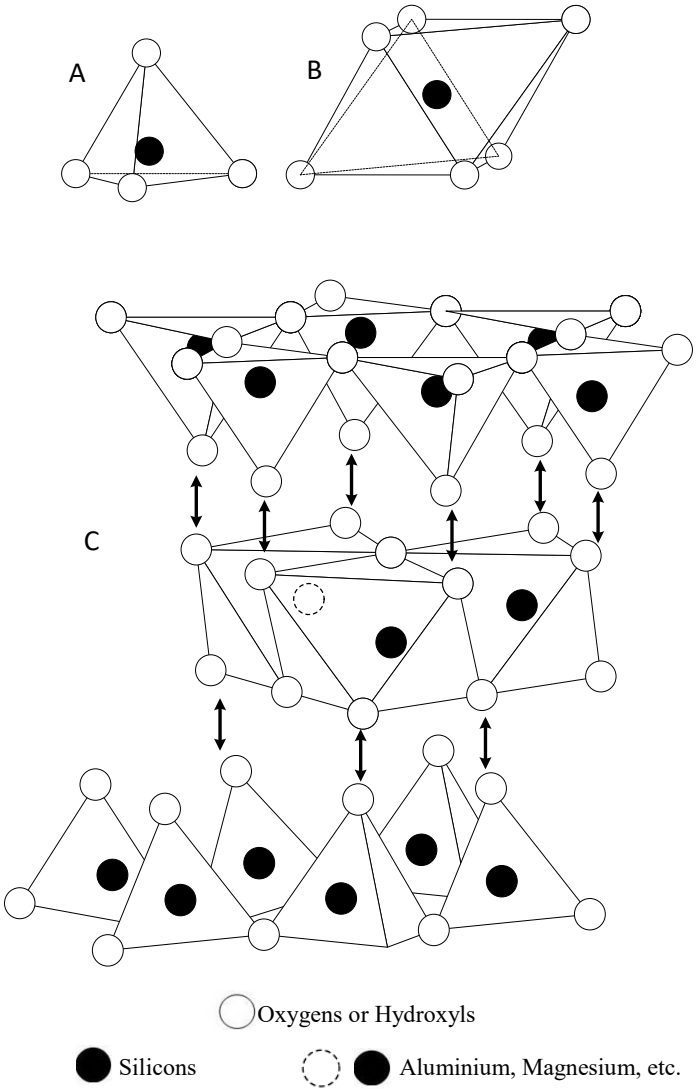


Figure 3.1- Diagram of tetrahedral (A) and octahedral (B) units of a clay mineral lattice (Grim, 1968) and arrangement of two silica layers around an octahedral sheet (C) (Christidis, 2011).

Kaolin, smectite and mica families encompass several mineral species with similar chemical formula but different structures, so that the most abundant and characteristic species of each are chosen to represent them, i.e. kaolin-kaolinite, smectite-montmorillonite and mica-muscovite (Gillot, 1987, Jensen, 1978, Bailey, 1984). The structure of the major clay minerals is the following:

3.2.3.1.1.1 Kaolinite

This abundant kaolin is composed of one octahedral and one tetrahedral sheet in what it is called a 1:1 layer structure. It has the nomenclature $Al_2Si_2O_5(OH)_4$ which is closely resembled in reality since kaolinite shows little chemical variation and very limited water absorption in

its interlayer. This is caused by the strong bonds between kaolinite layers as a result of its neutral layer charge (Murray, 1993).

3.2.3.1.1.2 Muscovite

The structure of this common mica of formula $KAl_2(Si_3Al)O_{10}(OH,F)_2$ consists of two tetrahedral layers on opposite sides of the octahedral sheet, named 2:1. The negatively charged layers motivate the isomorphous substitution of positively charged interlayer cations to neutralise it. It does not swell when absorbing water, limiting the hydration of its interlayer and keeping a low surface area (Osman and Suter, 2000, Gillot, 1987).

3.2.3.1.1.3 Montmorillonite

Like muscovite, this representative smectite has a 2:1 structure with negatively charged sheets. Montmorillonite is highlighted due to its ability to absorb water, resulting in noticeable size variations due to swelling and shrinking effects with temperature and a noticeable cation exchange capacity caused by the hydrated interlayer cations. These substitutions can also be observed in its empirical formula $(Na,Ca)_{0.3}(Al,Mg)_2Si_4O_{10}(OH)_2$ nH_2O. (Weaver and Pollard, 2011, Grim, 1968).

3.2.3.1.2 Feldspars

Similarly to clay minerals, feldspars refer to a broad field of aluminosilicate species, although it is not usual to differentiate among them in brick clays as seen in Table 3.1. They constitute a solid solution series, where the various species can be typically divided into plagioclase (Na,Ca) and alkali (K,Na) groups depending on their relative Na, Ca and K cation content (Smith and Brown, 1988). Among the three series endmembers, i.e. albite, orthoclase and anorthite, the first two are chosen as the representative species of each group respectively, given the rare occurrence of pure anorthite (Anthony et al., 1995).

3.2.3.1.2.1 Orthoclase

Orthoclase's structure consists of a three dimensional tetrahedral framework of Si, Al and O atoms with potassium in the interstices, having the chemical formula $KAlSi_3O_8$. As other K-rich feldspars, it crystallises in the monoclinic system, where the three vectors that define the mineral lattice are of different length with two of them perpendicular to each other, thus forming a rectangular polyhedron (Deer et al., 2001).

3.2.3.1.2.2 Albite

This endmember of both the plagioclase and alkali solid solution series has the stoichiometric formula of $NaAlSi_3O_8$. Crystalline albite differs from orthoclase in that the substitution of potassium by sodium changes the mineral lattice so that it does not have any perpendicular vectors, belonging then to the triclinic system (Deer et al., 2001).

3.2.3.1.3 Quartz

Despite quartz (SiO_2) abundance in clays as seen in Table 3.1, it does often form part of the amorphous phase as silica (Gillot, 1987). When crystalline, it is part of the hexagonal crystal family and specifically the trigonal system, where at room temperature and atmospheric pressure the lattice forms a rhombohedrum and is known as α-quartz (Davila et al., 2008).

3.2.3.1.4 Calcite

Calcite is the most stable polymorph of calcium carbonate with the formula $CaCO_3$ and shares with α-quartz a rhombohedral crystal lattice (Gunasekaran et al., 2006). However, it is rarely found as a natural crystal, often appearing as different types of scalenohedra, bipyramids that contain scalene triangles, and several twinning structures like fibres or lamellas (Klein et al., 1993).

3.2.3.2 Non-Crystalline phase

In spite of the possibility of having the same composition of a neighbouring crystalline unit, amorphous materials do not show any long range order on the atomic scale. Oxides, silicates and phosphates are the major compounds in the non-crystalline phase, being silica glasses one of the most common of this type (Gillot, 1987).

3.2.3.3 Mixed-layer minerals

As a consequence of the multicomponent nature of clays, interactions among the microstructures of the different clay constituents tend to result in hybrid structural arrangements. The study of mineral interstratifications has been focused on clay minerals due to their occurrence. These interstratifications may occur in various ways (Grim, 1968):

- Discrete mineral particles without a preferred geometrical orientation compared to neighbouring particles.
- Partial or total interstratification of layers, where these have one or more aluminosilicate sheets.

Being based in the same structural unit, the interstratification of layers of clay minerals may give structures as stable as the individual minerals. Furthermore, this interstratification can be random or regular. In the case of the latter, the repetitive stacking on layers in a certain direction results in distinctive microstructural characteristics (Grim, 1968). Interstratification of three or even four minerals are possible, nonetheless arrangements of two minerals are the most common (Millot, 1970). Focusing on building clays, the most reported is mica-smectite (Reeves et al., 2006). Nevertheless, kaolin-mica (Grim, 1968) and kaolin-smectite (BIJHMANN and Grubb, 1991) have also been noticed.

3.2.4 Clay characterisation

It is not common practice for brickworks to have a quantitative insight of the composition of the raw materials, since brick firings are experience driven processes (Køster, 2014) with the main aim of reaching determined standards of compressive strength and water absorption (ASTM, 2013a). Several methods have arisen for the quantitative analysis of clay mineralogy. Yet, clay characterisation remains challenging due to the chemical and structural variability of the clay constituents, especially in the case of random interstratifications and impurities (Brown et al., 1980). Generally, better results are reached by combining several of these techniques (Melo et al., 2001, Mohsen and El-maghraby, 2010, Folorunso et al., 2014). The most common characterisation methods are the following.

3.2.4.1 X-ray diffraction (XRD)

In x-ray crystallography studies, a monochromatic x-ray beam collides with a crystalline solid at varying incident angles, so that the diffracted beams' angles and intensities can be related by Bragg's Law to the spacing between the rows of atoms (Moore and Reynolds, 1989). Given that each crystalline substance has its own characteristic regular atomic structure, comparison of the scattered spectrum with a database of reference minerals enables the identification of the sample mineralogy (Reeves et al., 2006).

X-ray diffraction is the most widespread mineralogy identification technique among all the methods employed in the study of clays, with x-ray powder diffraction being the most used method (Melo et al., 2001, Gillot, 1987, Pevear, 1989, Moore and Reynolds Jr, 1997, Teixeira et al., 2001). Its popularity comes from its usefulness in the non-destructive determination of the relative abundance of mineral species (Reeves et al., 2006), while overcoming the issue of acquiring a sufficiently large crystal to perform the traditional single crystal diffraction analysis (Harris and Cheung, 2004). However, a quantitative determination of each clay constituent is troublesome due to their changing structures and structural arrangements

(Pevear, 1989). Moreover, poorly crystalline or amorphous minerals cannot be reliably identified using this method (Reeves et al., 2006).

3.2.4.2 X-ray fluorescence (XRF)

In this technique, the identification of the clay mineralogy comes from the analysis of fluorescent, also called secondary, x-ray radiation that individual atoms emit as a result of being bombarded with x-rays or electrons. The energy of this secondary radiation is characteristic of the atomic number and the abundance of that element, where the quantitative characterisation of the sample is provided by comparing the net intensities with that of reference materials (Brouwer, 2006, Potts, 1987).

XRF is a versatile and rapid technique that has found widespread application in clay science (Hiraoka, 1994, González et al., 1998, Meseguer et al., 2011, El-Mahllawy and Kandeel, 2014). A limitation comes from its difficulty in recognising atomic elements lighter than sodium (Potts, 1987). Another is that given the number of constituents in clay mixtures and their chemical similarity and variability, e.g. montmorillonite and muscovite, building the mineralogy from the atomic chemistry and reference specimens may be troublesome and require empirical corrections (Jenkins, 2000, Wheeler, 1983, Beckhoff et al., 2007).

3.2.4.3 Thermal analyses

Thermal analyses are based on monitoring the changes that occur on materials as they are heated under controlled conditions. These transformations are often characteristic of a substance and their intensities provide the means for quantifying particular compounds (Gillot, 1987). The quantification comes from monitoring parameters subject to change under a temperature increase such as the sample's mass, enthalpy, temperature difference and emitted gases, i.e. thermogravimetric analysis, differential scanning calorimetry, differential thermal analysis and evolved gas analysis respectively (Morgan, 1993), the first two being the most common thermal methods (Reeves et al., 2006). Analyses of this tier are widely used in conjunction with others such as XRD (Mohsen and El-maghraby, 2010, Shimoda and Sudo, 1960).

3.2.4.3.1 Thermogravimetric analysis (TGA)

As a clay is heated, mass losses occur at particular points during the treatment as a result of its constituents undergoing thermal reactions. Using the TGA method, the temperatures at which a weight loss occurs leads to the identification of each clay constituent (Souza et al., 2005), while the magnitude of that loss can serve as a means of quantifying its presence in the clay mixture (ASTM, 2014c).

Among thermal analysis techniques, TGA is very popular because of its simplicity and versatility (Wróblewski and Ceran, 2016), being widely used in clay studies (Xi et al., 2004, Johari et al., 2010, Pérez-Villarejo et al., 2012). However, a quantitative characterisation using only TGA is rare and it is often just qualitative (Johari et al., 2010) or semiquantitative (Vieira et al., 2008). The reason is that TGA curves or their derivative thermogravimetric curves (DTGA) are not characteristic of a single mineral species (Reeves et al., 2006). It is also particularly important in clays to carefully control the heating cycle in order to avoid or minimise overlapping mass loss peaks (Stucki, 1990). In addition, structural transformations without mass changes such as in the case of polymorphs cannot be monitored.

3.2.4.3.2 Differential scanning calorimetry (DSC)

Thermal reactions of clay constituents may or may not result in a mass loss but none of them go by without an energy change in the form of enthalpy, where these physicochemical transformations can be endothermic or exothermic (Shah and Shroff, 2003). When subjecting a sample and a stable reference material to the same heating cycle, the extra energy or lack thereof needed to keep both at the same temperature due to the sample's thermal transformations is the magnitude monitored by the DSC technique (Wilson, 1987).

DSC is commonly used in conjunction with TGA (Post and Henderson, 2012) as this overcomes its inability to monitor thermal transformations without mass loss. Nonetheless, quantitative mineral data provided by this method is affected by the crystallinity of the minerals and the presence of impurities (Bain and Morgan, 1969).

3.2.4.4 Scanning electron microscope (SEM)

In this type of electron microscopy, the sample surface is bombarded with an electron beam producing low energy secondary electrons and high energy backscattered electrons depending on the type of the collision (Giannuzzi, 2006). The analysis of the latter has proved more successful for the characterisation of clay materials, where the intensity and incident angle of the electron beam, and the intensity of the signal to the backscattered electron detector (BSE) allow the atomic compositional mapping of the sample (Reeves et al., 2006).

Although more common in petrofabric analyses (Gillot, 1987, Cultrone et al., 2005), SEM can also be used for the characterisation of the clay mineralogy. Using the x-ray spectrum resulting from the electron bombardment, an energy dispersive x-ray spectrometer (EDS) can provide the elemental chemistry of the sample (Goldstein et al., 2003, Pavía, 2006), whereas the individual constituents can be quantified with the mineral liberation analysis technique (MLA) as explained by Fandrich et al. (2007). SEM/EDS shares the same limitation as XRF,

which is to infer minerals from their elemental composition. On the other hand SEM/MLA has the problem of differentiating among constituents that are chemically similar in close proximity, like clay minerals (Goodall and Scales, 2007).

3.2.5 Classification of clays

Given the importance and widespread utilisation of clay bricks throughout history, classification methods have emerged depending on the scientific discipline considered. Examples are geological, pedological, ceramic and engineering classifications. In these, clays are categorised based on several parameters such as particle size distribution, moisture and temperature, composition joined with utilisation in pottery, and mechanical properties respectively (Gillot, 1987). The engineering classification is the one usually found when dealing with clays used for building applications and several methodologies (GOBRICK, 2006, GOBRICK, 2007, Jackson, 1973) and standards (ASTM, 2015b, ASTM, 2016, Janz, 2013) have arisen in an attempt to organise them.

However, these classifications often do not take into consideration the mineralogy of the raw materials. Owing to the importance of clay minerals on the overall clay final properties (Velde, 2013), a sensible classification method focused in this phase as proposed by Gillot (1987) can be adapted for the clay mineral groups common in building clays and it is shown in Table 3.2. Firstly, clay minerals are separated based on their layer structure, i.e. the number of tetrahedral layers surrounding the octahedral sheet. Then, they are divided into groups by means of their layer charge, and later into subgroups considering the distribution of cations within the octahedral layer, i.e. when trivalent aluminium (dioctahedral) or a divalent ion such as magnesium (trioctahedral) is the dominant cation. Finally, the distinction of mineral species comes from isomorphous substitutions and from differences in the sheets stacking arrangement while remaining identical in two dimensions (polytypism) (Gillot, 1987).

The presence of these polymorphs that randomly change their composition due to interlayer cations makes their differentiation very challenging, as acknowledged by many authors (Saffer et al., 2001, Castelein et al., 2001, Robinson et al., 2008) who instead of describing each of these phases' species often resort only to refer to their groups or their most common species. This trend is followed in this work by exclusively considering the most representative species of each group, as mentioned above.

Table 3.2- Classification of phyllosilicates related to clay minerals. Adapted from (Gillot, 1987)

Layer Type	Group (x=Charge per formula unit)	Subgroup	Species
1:1	Kaolin-Serpentine x≈0	Kaolinite	Kaolinite, Dickite, Halloysite
		Serpentine	Chrysotile, Lizardite, Amesite
2:1	Smectite x≈0.2-0.6	Dioctahedral Smectite	Montmorillonite, Beidellite
		Trioctahedral Smectite	Saponite, Hectorite, Sauconite
	Mica x≈1	Dioctahedral Mica	Muscovite, Paragonite
		Trioctahedral Mica	Phlogopite, Biotite, Lepidolite

3.3 Conventional processing of clays

Making use of the natural ability of clays to harden when heated in order to produce exceedingly durable building materials, such as bricks, is among the earliest technological operations of mankind (Murad and Wagner, 1998). Several techniques and methodologies have been developed across time for small and industrial scale. In the case of the latter, the state of the art processing methods have variations based on the characteristics of the raw materials used and the type of finished product desired. Yet, all have the following stages in common (DECC&BIS, 2015).

3.3.1 State of the art processing stages

3.3.1.1 Excavation

The raw materials are excavated from clay deposits. During this step the first operation aimed at reducing clay heterogeneity takes place, where the raw material is scraped in layers against to those of the natural sediment with the use of dragline and multi bucket excavators. Aside from deposits, another less common source is the clay sediments left by rivers or floods (Køster, 2014).

3.3.1.2 Preparation of clay

The raw materials are sent to a souring plant or sometimes directly delivered for processing. In the souring plant, they are stored up to several weeks to homogenize their moisture. Then, further mixing takes place as the raw materials are extracted in layers from storage. In this stage the feed is also wetted and crushed to increase its workability and sieved. Furthermore, both in the souring plant and prior to shaping, additives such as iron, other clays, sand and water may be added to the mixture (Køster, 2014, ILO, 1984, Junge, 2000). The justification for their addition varies depending on the specific material. Clay minerals significance comes from the plasticity they provide to the raw clay while also acting as a binder when firing, whereas the presence of quartz adds strength and durability to the clay product and feldspars

act as flux material. Other major components such as calcite and iron oxides add aesthetic characteristics to the fired brick, e.g. colour (Junkala et al., 2013, Reeves et al., 2006)

3.3.1.3 Forming of the brick

At industrial scale, extrusion or soft moulding are both widely spread shaping techniques (Calkins, 2008). In both cases the result is a wet unfired brick with an approximate 2:1 length to width relation and variable thickness (ILO, 1984), e.g. 228x108x54 mm in Denmark (Køster, 2014) and 215x102x65 mm in England (EN, 2003) respectively after firing. When extruded, bricks can be solid or have cells, where the main difference is the faster drying and lower material consumption of the latter. Soft mud bricks are stamped out from a "table", giving less uniform products and being more expensive yet preferred for aesthetic reasons (Køster, 2014). Regardless of the shaping method, these raw bricks may reach up to a 50% porosity (Reeves et al., 2006).

3.3.1.4 Drying

Prior to heating the unfired bricks to high temperatures, a step focused on the minimisation of clay moisture is required given the high free water percentage in the raw materials at this point, i.e. between 7-30% (GOBRICK, 2006), where forced drying is preferred to natural convection. Forced drying most generally takes place in individual chambers or tunnel dryers for batch and continuous operation respectively, where the heating is done by gas firing, exhaust gases or air currents from the firing stage in order to reach a moisture level of around 2-3% (Køster, 2014).

The existence of this stage is justified as the faster heating that occurs during the subsequent firing does not let the free water diffuse to the brick surface before evaporating, resulting in steam trapped inside the bricks. This leads to a pressure build up and ultimately fractures (IBSTOCK, 2015). Hence, a slow drying takes place, requiring 18-40 h and reaching temperatures between 80-120 ºC (IBSTOCK, 2015). Given the significant hygroscopic behaviour of some constituents, the brick will also shrink, usually by 10% (ILO, 1984, GOBRICK, 2006).

3.3.1.5 Firing

The firing of the bricks takes place in a thermally insulated chamber called a kiln. During firing, bricks undergo physicochemical changes where clay particles and impurities are fused together to produce a hard, durable and weather-resistant product; this is usually accompanied by further shrinkage in the range of 2.5-4.0% (GOBRICK, 2006) and a colour change (Keeling, 1963).

Several kiln designs can be seen in the industry, where the tunnel and Hoffman/annular kilns are the most commonly found. In the latter, a semi-continuous firing is performed, where stacks of bricks are divided in furnaces that form a circle or an ellipse surrounding a central continuously moving heat source. Each load is heated separately and sequentially, constantly replacing the fired bricks with a new raw batch (ILO, 1984). They are very variable in size depending on the number of chambers, with total lengths between 70-160 m (Gomes and Hossain, 2003, Singer, 1963). On tunnel kilns as displayed in Figure 3.2, a continuous load is moved towards the heat source on a conveyor belt, moving through a single straight chamber of around 70-170 m long (Vissing, 2003). Tunnel kilns are more popular worldwide due to their around 25-30% lower energy requirements (Køster, 2014). Diversification in kilns depends on the characteristics of the feed and the energy optimisation path selected. Three zones can be distinguished in the firing stage regardless of the kiln system.

3.3.1.5.1 Firing zones

- **Pre-heating zone**

Usually, the energy supply comes from exhaust currents for energy optimisation purposes. This ensures that the residual moisture from the drying stage is eliminated without creating tensions in the brick. In Hoffman kilns, bricks are heated with flue gases from the adjacent furnace (ILO, 1984), whereas in tunnel kilns the air current from the cooling zone (Køster, 2014) is used as seen in Figure 3.2 because exhaust gases from the firing zone may cause discolouration of bricks (Kornmann, 2007).

- **Firing zone**

In this stage, the temperature of the load is slowly raised towards a maximum level defined by parameters such as the kiln and clay type (IBSTOCK, 2015, GOBRICK, 2006). The main justification for the slow profiles is the lower mechanical properties of the fired products achieved otherwise (Kadir and Mohajerani, 2015), as thermal non-uniformities enhanced by the aforementioned clay insulating properties may cause asynchronous volume changes that heighten structural tensions. In this zone, the energy required for the bricks to be fired comes mostly from burning natural gas, coal and liquid fuels such as LPG and oil (Vissing, 2003, IBSTOCK, 2015). In Hoffman kilns, firing starts when the heating source aligns with the load, whereas in tunnel kilns it occurs when the load reaches the burners in the middle of the kiln.

The chosen top firing temperature has to be carefully controlled, given its critical effect on the final brick coloration (ILO, 1984) and since a small degree of melting is desirable to improve

the strength of the final product (Dunham, 1992). Additionally, during most of the firing it is necessary to maintain a constant supply of air to guarantee the elimination of organic compounds, which is easily achieved by increasing the air/fuel ratio in the burners or by introducing preheated air (Houseman and Koenig, 1971a, Køster, 2014). However, in some cases, reducing atmospheres may obtain aesthetically appealing surface colours or textures in the final products (Houseman and Koenig, 1971b).

- **Cooling zone**

A controlled slow cooling stage is necessary in order to avoid the tensions or cracks derived from thermal non-uniformities, which were also crucial during firing, and to control the final coloration of the fired product (GOBRICK, 2006). Injecting a stream of fresh air facilitates the temperature decrease (ILO, 1984), which can be later reused in the drying stage. Another option is for this warmed waste air to be directed towards the pre-heating zone of the kiln. This depends on the process design (Køster, 2014, ILO, 1984).

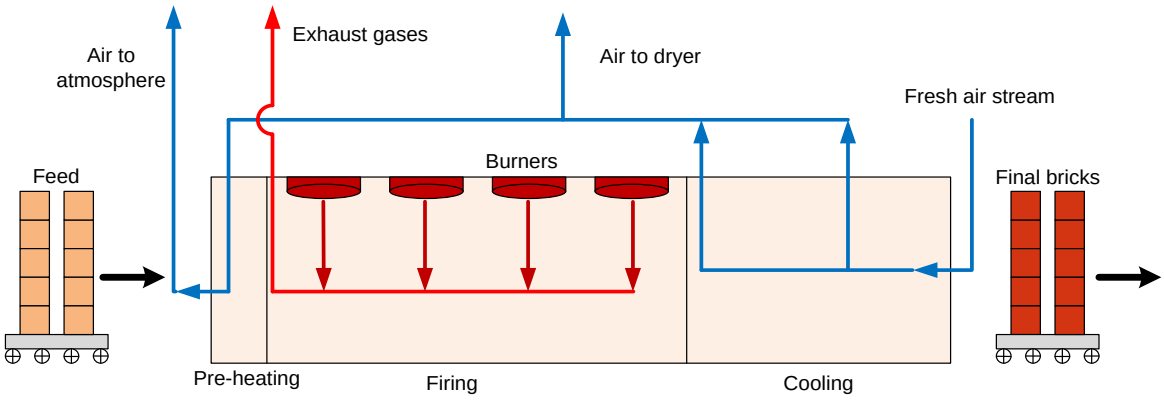


Figure 3.2-Sketch of a typical tunnel kiln (Køster, 2014)

3.3.1.5.2 State of the art brick firing cycle

The optimal processing cycle is that which requires the shortest heating schedule while yielding a product of satisfactory quality. In general, the complete firing of a clay load takes between 10-40 h depending on the process, the kiln and the raw materials (GOBRICK, 2006). A typical firing diagram is shown in Figure 3.3.

Although heating rates can vary greatly to accommodate for the process requirements, longer processing times are more common. Heating rates of around 50-55 ºC/h are ordinary for tunnel kilns to ensure thermal uniformity, with small variations at particular points due to clay exothermic/endothermic reactions (Køster, 2014, Moesgaard, 2015) and swelling/shrinking events (Dunham, 1992). The top temperature for the process varies between 900-1200 ºC (IBSTOCK, 2015). Once this temperature is reached, a 4-6 h soaking period is performed to ensure that the whole feed becomes thermally uniform (Køster, 2014). There are various

options available for the cooling rate depending on the brickworks and the clay type, where in the simplest instance the cooling process is no longer than 10 h of uncontrolled natural air convection (GOBRICK, 2006). In specific cases, some brickworks focus on minimising tensions on cooling by forcing a specific rate such as reported by Moesgaard (2015), i.e. 85 ºC/h until 750 ºC, 20 ºC/h until 500 ºC, 45 ºC/h until 100 ºC and below 100 ºC the bricks are taken out of the kiln and left to be cooled by natural convection.

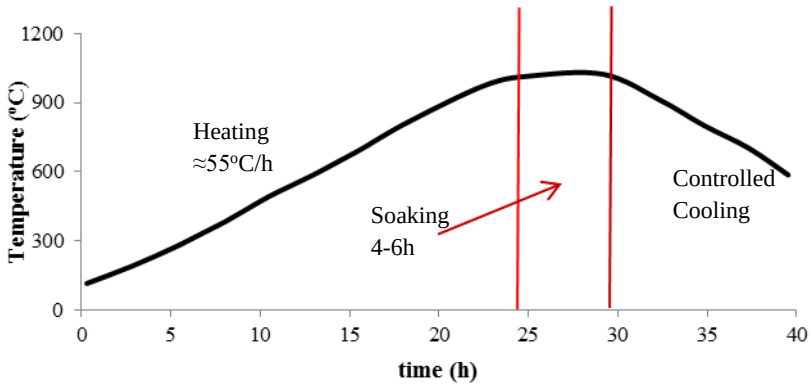


Figure 3.3-Surface temperature of a clay brick during a typical conventional firing cycle (Køster, 2014).

3.3.2 Physical properties of fired bricks

The final characteristics of fired bricks are so critical for the brickworks industry that they are the core of some classifications methods. The most important brick properties can be reduced to colour, texture, size variation, compressive strength, water absorption and durability (GOBRICK, 2006).

3.3.2.1 Colour and texture

These two purely aesthetic characteristics are not determinant in the assessment of the quality of a brick, as they can be repurposed if deemed unsuitable, e.g. from facing to structural bricks. Nevertheless, an appealing colour and texture can be desirable enough to drive forward a specific processing method, such as in the brick shaping stage for soft mud bricks (Køster, 2014). The texture of a brick is assessed qualitatively, normally focusing on the presence of boils, black coring and other imperfections caused by the elimination of gases and volatiles. Generally, darker colours imply larger residence times at higher firing temperatures. However, the surface coloration of a brick can be altered by adding iron oxides or carbonates prior to firing (Junkala et al., 2013, Reeves et al., 2006), giving rise to red and yellow building bricks (Jensen, 1978). In addition, coatings and glazes can achieve distinctive patterns and colorations in the final bricks (GOBRICK, 2006).

3.3.2.2 Compressive strength

The physical strength of a brick is the main parameter adopted to define its suitability to be used in structural applications. The strength of a single brick can range between 8-130 N/mm^2 and it is inversely related to its porosity (Reeves et al., 2006). Thus, strengths can wildly vary depending on the manufacturing method, the heating cycle and the raw materials (GOBRICK, 2006). Standards for building bricks define the minimum compressive strength ranges of single bricks depending on their specific purpose and characteristics, from common buildings to advanced engineering applications, e.g. 8.6-17.2 N/mm^2 (ASTM, 2013a), 15.2-17.2 N/mm^2 (ASTM, 2016) or 75-125 N/mm^2 (EN, 2003).

3.3.2.3 Size variation

Clays tend to shrink during drying and, more importantly, during firing. The initial solid phase expansion is reversed around 600 ^oC (Parsons et al., 1997), where the volume change rates are dependent on the clay composition (Peters and Iberg, 1978). Control of the overall shrinking of the brick comes mainly from the top firing temperature. Excessive shrinkage causes a significant decrease in the mechanical properties of the material, as it is usually the consequence of substantial melting (Karaman et al., 2006). This melting can be inhibited by the addition of silica to the clay before firing (Reeves et al., 2006).

3.3.2.4 Water absorption

Clay bricks can be exposed to water in several ways, such as due to weather conditions or because of direct contact with soil foundations. The absorption of water by the brick is directly affected by its porosity (Khalaf and DeVenny, 2002). Freeze/thawing of pore water can result on the early wear of the brick, which is usually handled by reducing its porosity by means of increased firing temperatures (Johari et al., 2010). The most common absorption tests are based on the quantification of the mass of water absorbed by the brick body in 5 h or 24 h using boiling and cold water, respectively (GOBRICK, 2003). Yet, both large and minimal water absorption can result in a good freeze/thaw resistance, on account of leaving ample space for the water state changes or none at all for water to penetrate into the brick. A better indicator is found in the saturation coefficient, which comes from the 24 h cold and 5 h boiling water absorptions ratio. Low saturation coefficients (<0.78) generally indicate good freeze/thaw resistance (ASTM, 2013a).

3.3.2.5 Durability

The response to environmental and service conditions such as repeated freeze/thawing allows the gradation of building bricks according to their resistance, i.e. severe weathering, moderate

weathering and negligible weathering (ASTM, 2013a). Each grade can be assessed by its own limits of compressive strength, water absorption, and saturation coefficient, or by compressive strength and freeze/thaw cycles (GOBRICK, 2003).

3.3.3 Thermal transformations of clays

Several physicochemical transformations occur to clays when raising their temperature. In general terms, the basics of the reactions are widely known and their temperature ranges are agreed to an extent (GOBRICK, 2006, Reeves et al., 2006). However, the yield and selectivity of the various mineral associations possible are not yet fully understood, where the temperatures reached during firing and the heating rates further affect the final mineral assemblages (Dunham, 1992, Bohor, 1963, Chen et al., 2000).

Despite interest in the subject (Murad and Wagner, 1998, Dunham, 1992) and knowledge of some mineral thermal associations such as kaolinite-muscovite (Zhou et al., 2013, Escalera et al., 2014, Lecomte et al., 2007) and kaolinite-quartz-feldspar (Dana et al., 2004, Iqbal and Lee, 2000), at high temperature the parent materials are not easily identified particularly in the case of the chemically similar clay minerals species. Therefore, this work follows the methodology presented by Dunham (1992), where the reactants have grouped all their possible high temperature products. A graphical representation of the mineral thermal reactions is seen in Figure 3.4, where in the x-axis the major clay constituents are presented and in the y-axis the firing temperatures can be seen.

Regarding the clay minerals phase, their similar structure ensures they undergo the same set of thermal reactions, starting with their loss of free water at 100 ^{o}C and physically bound water between 150-350 ^{o}C (Grim, 1968). Chemically bound water loss starts between 350 ^{o}C and 600 ^{o}C, depending on the strength of microstructural bonds. Here, cations of the interlayers of montmorillonite and muscovite structures are released to the clay matrix due to their crystallinity collapse, with kaolinite retaining its long range order as metakaolinite (McConville and Lee, 2005).

Although most thermal transformations are endothermic, around 800-850 ^{o}C the amorphous dehydroxilated structures start sintering. The associated atom diffusion of this characteristically exothermic process causes porosity reduction and grain growth (Dejonghe and Rahaman, 2003), which together with the high temperatures triggers recrystallisations of compounds like spinels, γ-alumina and small amounts of mullite around 900 ^{o}C, (Dunham, 1992). The final fired brick minerals like mullite, cordierite, corundum, cristobalite, leucite, sanidine and anorthite appear above 1000 ^{o}C (Dunham, 1992, Chen et al., 2000, McConville and Lee, 2005)

Regarding the other clay constituents, any hydrocarbons burn off around 450 ºC (Dunham, 1992). Quartz undergoes a reversible structural inversion to β-quartz at 573 ºC where it expands considerably, later recrystallising into cristobalite (Heaney, 1994, Davila et al., 2008). Calcite thermally decomposes around 750 ºC (Galan et al., 2013) and the resultant quicklime is very reactive, thus contributing to the exothermic formation of several constituents such as pyroxenes, wollastonite, gehlenite and anorthite by cross reaction with kaolinite and other clay constituents (Dunham, 1992, Zhu et al., 1994). Iron oxides appear when temperatures around 800 ºC are reached (Jensen, 1978). This is because they are present in clay minerals structures forming nodules, so that when mineral structures collapse they are released to the clay mixture generally as haematite (Murad and Wagner, 1998, Keeling, 1963). Feldspars show high thermal stability throughout firing. Together with other constituents that tend to melt around 1000-1050 ºC, such as mica, they conform the bulk of a glassy phase sought for its binding properties. Variable quantities of other constituents will also join this melt instead of recrystallising (Dunham, 1992).

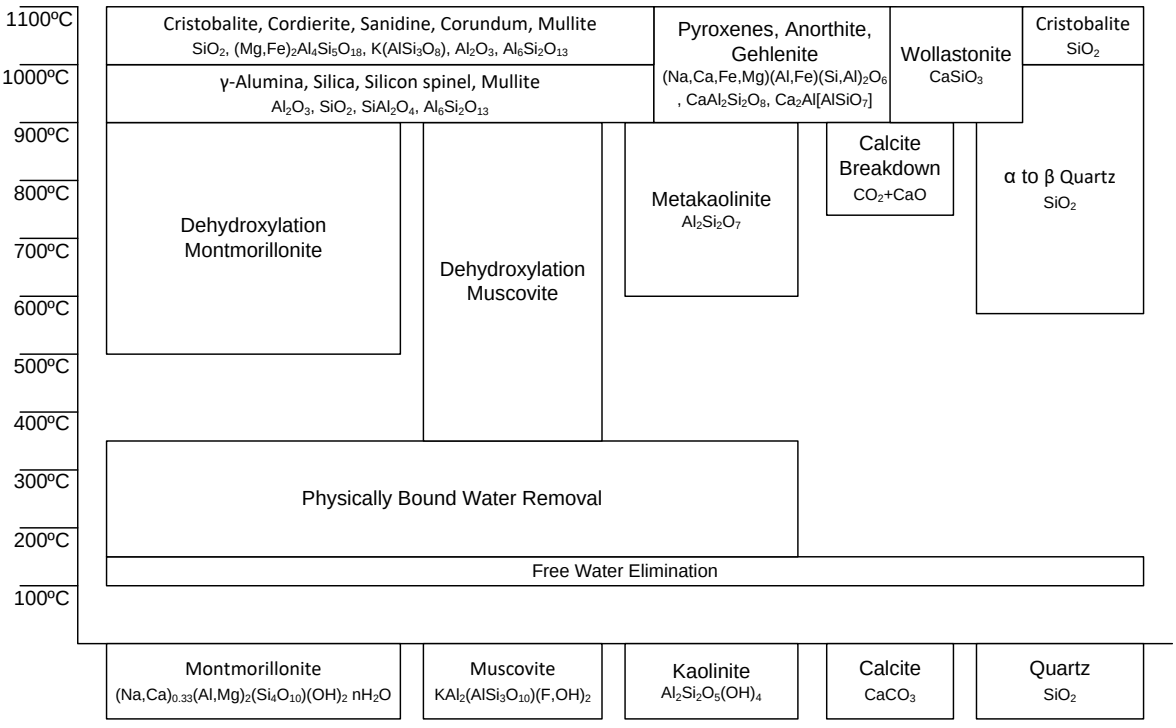


Figure 3.4- Firing diagram of main thermal transformations of major clay constituents (Dunham, 1992, Galan et al., 2013, Heaney, 1994, Chen et al., 2000, McConville and Lee, 2005, Bohor, 1963).

These physicochemical transformations, if not performed with a certain degree of uniformity over the whole clay body, may result in a quality decrease in the final product as a result of fractures and deformations. There are some points across the heating/cooling cycles where minimisation of the thermal gradients becomes critical (CeramicArtDaily, 2005). The first being the free moisture elimination, where the fast heating of bricks in a kiln below free water

evaporation temperatures (100 ^{o}C) can cause water to be trapped as steam inside the brick, causing tensions and fractures. Around 220-270 ^{o}C and particularly during cooling, crystalline cristobalite suddenly shrinks in what is also termed cristobalite inversion. This causes stresses that might result in cracks under a fast cooling rate (Stevens et al., 1997).

Quartz inversion is widely considered to be the most critical point of the process, given the high quantities of quartz in clays. Around 573 ^{o}C, quartz changes from α to β crystal structure, suddenly expanding around 2% volumetrically and causing major stresses. This inversion is reversed on cooling (Dunham, 1992). Across the heating process and up to 800 ^{o}C, carbonaceous materials have been progressively oxidised. If carbonaceous impurities have not been burnt before reaching this temperature, they will be sealed in the brick, causing bloating and black coring. Furthermore, at this temperature the calcite decomposition also takes place, liberating carbon dioxide upon its breakdown. A slow heating is needed for completely removing the organic matter and letting the CO_2 escape respectively, thus avoiding mechanical stresses (CeramicArtDaily, 2005). Finally, the top firing temperature is generally specific for each clay composition so as to reach some degree of melting. However, careful control of the top temperature is needed to avoid substantial melting of constituents like micas and feldspars, which can ruin the quality of the final product (Reeves et al., 2006).

3.3.4 Outlook for conventional processing of brick clays

Brickworks are one of the most basic and yet essential industries for economic development in many countries. In the European Union, around 78% of the construction sector is centred on making buildings. Between the last decade of the 20th century and 2006, there was an increasing construction output; between 2006 and 2013, the economic crisis known as the "Global Financial Crisis" caused a general decrease of manufacturing activities of around 11%. Nonetheless, since 2015 the recovery of economic activity is also causing a recovery of the construction sector (Eurostat, 2017b). In other countries such as the U.S.A., construction domestic value peaked in 2008 with £1 trillion, a figure that is not expected to be reached again until 2018 (FMI, 2015). At the other side of the world, China was not as affected by the crisis and its construction sector doubled its GDP contribution in the 2006-2011 period, reaching £ 5512 billion (EUSME, 2013).

In parallel with the western countries' building recovery and the constant increase of the Asian market, awareness of the population regarding the environmental effects related to industrial activities have resulted in worldwide agreements and legislation towards reducing fossil fuel consumption in industries and its associated environmental effects, such as in the case of the G7 (METI, 2016, METI, 2017), supranational agencies (ENER, 2010, Howes, 2010) or individual countries (MINAET, 2011, EFKM, 2011, INREAP, 2014).

Extensive modifications of the brickmaking process were performed throughout the 20th century to reduce energy consumption (Køster, 2014), such as exhaust currents recirculation, evolution to continuous processing and replacement of coal by natural gas. Despite these advances, clay firings take between 10-40 h, while energy consumption has stabilised around 2.6 MJ/kg of fired material and the process is still reliant on fossil fuels. Greenhouse gas emissions are also significant, ranging from 57-95 kg CO_2/GJ, and are heavily dependent on the type of fuel used (Køster, 2014, Moesgaard, 2015). This means that 675122 tonnes of CO_2 were released to the atmosphere in 2012 due to the UK brickmaking industry alone, with natural gas supplying around 83% of the 3028 GWh required (DECC&BIS, 2015) to produce 1459 millions of bricks (BIS, 2013) out of the nearly 1391 billion worldwide brick production (Zhang, 2013).

Several attempts have been made in recent years to further optimise the brickmaking process in energy costs and carbon emissions. Examples are situating the brickworks adjacent to the clay deposit to minimise pollution due to transport, favouring electricity powered by renewable sources over fossil fuels when possible (Manley, 2016), using alternative feeds such as industrial wastes (Zhang, 2013) and minimising particle emissions through the use of scrubbers, vacuums and filtering systems (GOBRICK, 2006). Yet, the radical reduction in energy use and carbon footprint necessary in order to meet the future legislation requirements is unlikely to be achieved without fundamentally changing the brickmaking process (DECC&BIS, 2015). Here is where microwave energy can be used in order to provide for the needed technological step-up of the brickmaking process.

3.4 Conclusions

Clays are heterogeneous materials in which the presence of major components, i.e. quartz, calcite, kaolinite, montmorillonite, muscovite, plagioclase and alkali feldspars, and impurities is strongly influenced by clay genesis and history. This also affects the possible associations between constituents, which are particularly important among clay minerals due to them sharing the same structural units, and further increases the complexity of the mixture. Thus, despite the numerous characterisation techniques used, e.g. XRD, XRF, SEM, TGA, DSC, the structural and compositional characterisation of clays remains challenging.

Several brickmaking techniques and methodologies have been developed over time, yet the main stages remain common, i.e. excavation, preparation of clay, forming of the brick, drying and firing. Process optimisation focusing on minimising thermal non-uniformities has resulted in the brick firing duration range between 10-40 h with controlled heating rates and soaking times, e.g. 50-55 ºC/h heating rate and 4-6 h soaking time. In the end, the quality of the fired materials is graded based upon characteristics such as colour, texture, size variation,

compressive strength, water absorption and durability, which depends on the raw material composition and the manufacturing method.

The brickworking process is critically reliant on empirical knowledge, and thus during firing the yield and the selectivity of the numerous reaction paths possible are only known in general terms. This is mainly the case for physicochemical transformations taking place after 800 ^{o}C. As a consequence, it is usual to focus on process output, linking reactions to critical temperatures where tight control of the heating rates is necessary to achieve a high quality product, e.g. quartz inversion at 573 ^{o}C.

Brickworking is an essential industry worldwide, and it has undergone a great deal of optimisation in order to minimise energy requirements and costs and address worldwide environmental concerns. However, energy costs are around 2.6 MJ/kg of fired material where fossil fuels are the main energy source, thus contributing to significant greenhouse emissions of around 57-95 kg CO_2/GJ. Although further optimisation attempts such as using waste materials as feeds are underway, microwaves' ability to provide a volumetric heating can bypass clays' limiting thermal conductivity. Consequently, a significant reduction of processing times and energy consumption without causing thermal stresses to clay bricks is attainable. The subsequent drop in emissions can be further minimised by the substitution of fossil fuels by electricity powered by renewable resources. The drastic step change in the brick making techniques caused by the utilisation of microwave energy is the only realistic opportunity to cope with increasingly strict environmental legislations and the dwindling fossil fuels resources (Køster, 2017).

4 MICROWAVE PROCESSING THEORY

4.1 Introduction

In the review of the state of the art of brick firing techniques using a conventional energy supply, the limiting nature of clay thermal conductivity was identified. The demand of thermal uniformity on a substance characterised by its thermal insulating properties (Dondi et al., 2004) results in energy intensive treatments characterised by long processing times, which are required for a successful brick firing. On the other hand, the interaction of a microwave field with a substance allows for a uniform energy delivery across its volume without thermal conductivities or other heat diffusion limitations, due to the direct interaction of its molecules with the electromagnetic field (Meredith, 1998).

Microwaves are a form of electromagnetic energy belonging to the non-ionizing spectrum, which comprises the 300 MHz to 300 GHz frequency band. Microwave energy has traditionally been used in telecommunications applications as well as heating (Meredith, 1998, Metaxas and Meredith, 1983). Interest in microwave heating has flourished since World War II as advantageous benefits were found from the microwave/materials interaction (Osepchuk, 2002), such as in the food, rubber and ceramic industries (Jones et al., 2002). In the case of the last sector, its popularity is mainly justified by quality improvements on the final products, such as higher strength, and lower processing times when compared with established conventional heating methods (Clark et al., 2005, Katz, 1992).

Despite the wide array of ceramics subjected to microwave heating, where notable among them are clay constituents such as kaolinite (Navarro et al., 2014), muscovite (Faeghi-Nia and Ebadzadeh, 2012) and montmorillonite (de Lima Santana et al., 2015), and even entire clay mixtures (Menezes et al., 2007), most of these reports are of small scale laboratory research. Few microwave systems have been developed at an industrial level for the processing of ceramics (Dunn, 2015, Clark et al., 2005, CORDIS, 1999). The prime reasons for this are the reticence of industries to modify well known processes, and the lack of availability and high cost of large scale microwave processing equipment. Moreover, fossil fuel supplies are generally cheaper than electricity. There are also technological barriers to the scale up of these processes, since the often insufficient analysis of the specimens curtail the understanding of their behaviour under the microwave field.

This behavioural knowledge is critical for process design and optimisation, making it critically reliant on experimentation and prone to result in failed attempts otherwise. Consequently, a high level of investment is required to develop a process, as commonly the addition of microwaves requires a complete redesign of the whole process and not just a

retrofit. Particularly in the case of clays, their granular and often heterogeneous nature favours the appearance of hot spots and thermal gradients, which can hinder the quality of the final product (Clark et al., 2005, Clark et al., 2000, Shaheen et al., 2012, Yoshikawa, 2011, Jones et al., 2002, Robinson et al., 2014, Robinson et al., 2012).

The aim of this chapter is to provide a justification of the advantages offered by the application of microwaves for the firing of traditional ceramics such as clays over conventional processing methods. In this chapter, the heating mechanisms that result from microwave/material interaction are detailed. This is followed by the quantification of the material response to the electromagnetic field through the complex dielectric permittivity, where its main parameters are described. Next, an explanation of the most widespread dielectric property measurement techniques and estimation methods, and an inventory of the main types of microwave applicators and other common microwave equipment are provided. Finally, a review of previous studies on the microwave heating of clays and their minerals assesses the gaps and limitations of the state of the art in this area.

4.2 Heating mechanisms in microwave processing

Electromagnetic energy such as microwaves can be divided in two oscillating magnetic and electric field components, which are perpendicular to each other and to the wave's direction of propagation. Assuming a Cartesian coordinate system, the propagation of an electromagnetic wave through free space is clearly represented in Figure 4.1, where its wavelength can be related to its frequency using Eq. 4.1 (Regier et al., 2016),

$$\lambda = \frac{c}{f} \qquad \textbf{4.1}$$

where λ (m) is the wavelength, c (m/s) is the speed of light in vacuum (2.998x10^8 m/s), and f (Hz) is the frequency of the wave. Consequently, the distance for a full wave oscillation in the microwave spectrum ranges between 1 mm-1 m.

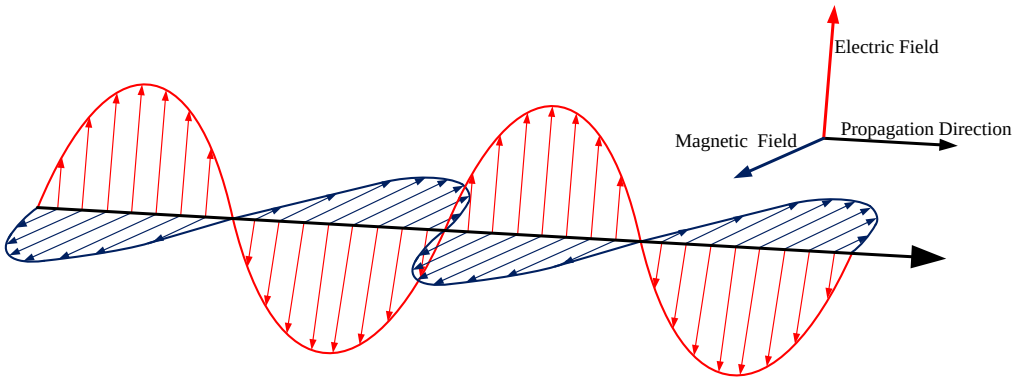


Figure 4.1- Propagation of an electromagnetic wave in free space.

It is worth noting that the wave propagation shown in Figure 4.1 can be described as transverse electromagnetic (TEM), since both the electric and magnetic fields are perpendicular to the field propagation (Meredith, 1998). However, when travelling inside some microwave transmission equipment such as a metallic waveguide, certain boundary conditions apply, e.g. the electric field terminates at the surface of the waveguide. As a result, wave propagation in these situations is either transverse electric (TE) or transverse magnetic (TM). In the case of the former, only the magnetic field propagates along the direction of the wave, while for TM waves it is the electric field (Chan and Reader, 2000, Metaxas and Meredith, 1983).

Regardless of the configuration of the wave propagation, upon it colliding with a certain material the molecular response of that substance to the electromagnetic field determines its ability to convert electromagnetic energy into heat. There are two main ways in which materials can enact this conversion at microwave frequencies, namely through polarisation and ionic conductivity effects (Metaxas and Meredith, 1983).

4.2.1 Polarisation

Under an alternating electric field, the bound charged particles in a material respond by aligning with the field, leaving their equilibrium positions and rotating, forming induced dipoles. Several polarisation mechanism arise depending on the type of bound charges excited, be they electrons, atoms, molecules or interfaces in heterogeneous systems. Thus, these species interact via electronic, atomic, dipolar or interfacial polarisation (Metaxas and Meredith, 1983). In the microwave range only the last two are significant enough for heating purposes (Peng and Hwang, 2015).

4.2.1.1 Dipolar polarisation

Dipolar polarisation is the mechanism that contributes most significantly to the heating in the microwave range, usually dominating above 1 GHz. The degree of heat generated is directly dependant of the ability of the particles to polarise and align with the electric field, where dipoles not efficiently following it and thus lagging behind result in heat generation due to collisions and frictions among them. This is affected both by the material's characteristics and the frequency of the field (Metaxas and Meredith, 1983).

4.2.1.2 Interfacial polarisation

This form of polarisation arises in interfaces, contact areas or grain borders between different components of heterogeneous systems. Space charge can accumulate in these areas, causing field distortions that give way to heating (Peng and Hwang, 2015). Although not as common

as dipolar polarisation, interfacial polarisation normally occurs when a set of conducting particles is embedded in a non-conducting medium (Metaxas and Meredith, 1983). In the context of clays, their granular and multicomponent nature typically present iron impurities which are surrounded by the overall electrically insulating clay matrix (Jensen, 1978). This hints at the presence of this type of polarisation. As a result, it is probable the appearance of strong heating effects at the grain borders and mineral interlayers that may cause thermal gradients in the clay and even degenerate into partial melting.

4.2.2 Ionic conductivity

As opposed to the rotational response of dipoles, free charge carriers such as ions can move accompanying the field oscillations. In their movement, they collide with each other generating heat by ohmic effects (Clark and Sutton, 1996). Ionic conductivity is usually the main heating mechanism for materials with even just small amounts of free charge carriers. However, its effect starts decaying above 100 MHz, in the end falling behind dipolar heating at frequencies depending on the material's characteristics (Meredith, 1998). Despite clays being overall poor electrical conductors, the significant degree of free moving cations present during stages such as sintering, as discussed in the previous chapter, may attain for a noticeable ionic heating effect.

4.3 Dielectric properties of materials

In order for any substance to generate heat through the mechanisms described above, it is a requirement that microwave energy is absorbed by the material to some extent. Materials under the influence of microwave energy display a wide range of responses to the electromagnetic field. These responses can be broadly divided according to textbooks into three groups based on their electrical/magnetic properties (Maizza et al., 2014):

- Opaque: Also called conductors, electromagnetic waves do not penetrate this type of substances and are reflected.
- Absorbing: The energy is absorbed to a certain degree as it goes through the specimen.
- Transparent: Electromagnetic energy passes through the material with little to no attenuation. Those which show this type of response are termed low loss materials.

Quartz and Teflon are notable examples of transparent materials, as they display low proficiency in absorbing microwaves and transforming them into heat. On the opposite corner, the high degree of electrical conductivity displayed by most metals makes them microwave opaque. In between these extremes, water constitutes the most common example

of an absorbing substance, as the polar nature of its molecular bond enables an efficient dipolar polarisation based heating (Tiwari et al., 2016). Ceramics like clay usually belong to the transparent and absorbing groups (Maizza et al., 2014), where these and other substances that can absorb microwave energy are termed dielectric materials (Jones et al., 2002).

In the case of multicomponent heterogeneous systems like clays, a combination of responses may take place. Some clay constituents may display an absorbing nature while others are microwave transparent. This would give rise to a selective heating of the former, which in turn conventionally heat the surrounding transparent minerals. Another option is that the transparent and absorbing minerals are homogeneously distributed in the clay matrix, or that all clay constituents have an identical interaction with the microwave field. This would result in the volumetric heating of the whole clay, since microwave energy completely bypasses heat diffusion limitations like low thermal conductivities. Either a selective or a volumetric heating are the two main options that govern the behaviour of microwave processes. In the case of the microwave firing of clays, their volumetric heating is preferred, as selective heating may result in thermal gradients that can hinder product quality. Understandably, identifying which clay constituents heat and quantifying their microwave heating potential is crucial.

A more quantitative approach to the behaviour of a dielectric material under an electromagnetic field comes from the study of its complex magnetic permeability (μ^*) and complex dielectric permittivity (ε^*) (Metaxas and Meredith, 1983). Only the latter is considered in this work, given the negligible magnetic response expected in clays from their minor iron or other ferromagnetic minerals content (Reeves et al., 2006). The complex dielectric permittivity is composed of a real part called the dielectric constant (ε'), which measures the capability of the material to be polarised. The imaginary part is an effective loss factor (ε'') that describes the ability of the material to transfer the electromagnetic energy into heat. These are commonly collectively termed dielectric properties (Chandrasekaran et al., 2012).

4.3.1 Parameters affecting dielectric properties

The response to an electric field is inherent to a material and so are its dielectric properties. However, it has been previously discussed how frequency changes favour some heating mechanisms over others, which is reflected in the dielectric properties. Analogously in clays, the composition of their solid and liquid phases will also exert a strong influence over the final dielectric response. Furthermore, the macrostructure of major constituents, their bulk density, particle size distribution and grain orientation will also add in for a specific set of dielectric properties for each temperature across the firing range (Metaxas and Meredith,

1983, Ryynänen, 1995). Given the complexity and variability of clays, innumerable structural arrangements are possible. This is also true regarding particle size distributions and grain orientations. However, these are usually not critical for defining a material's dielectric behaviour (Metaxas and Meredith, 1983), so they are not considered here.

4.3.1.1 Composition

As stated in Chapter 3, clays are multicomponent materials with solid and liquid phases that arrange randomly as a result of their genesis and history. Logically, the final dielectric response of a clay is mainly defined by its major constituents, which can show a dissimilar microwave response, such as in the case of the transparent quartz (Church et al., 1988) and the more absorbent kaolinite (Orzechowski et al., 2006). Additionally, the free and physically bound water contents are especially important, as their presence may exert a large influence on the clay dielectric response due to their comparably high dielectric properties (Kaatze and Behrends, 2002), even when present in residual amounts. Hence, the dielectric properties of clays are expected to significantly change across brickworks.

4.3.1.2 Frequency

Except in very low loss materials, dielectric properties are usually dependant on the frequency of the applied electric field (Nelson, 1994). In the case of clays, this translates into an asymmetrical evolution of the dielectric properties of some of their constituents with frequency, e.g. major low loss constituents like quartz are largely unaffected by a frequency change (Church et al., 1988) while for some clay minerals like montmorillonite its complex dielectric permittivity can be more than doubled (Kobusheshe, 2010, Saltas et al., 2008).

Interfacial polarisation effects have not been usually found in clays or their constituents in the microwave range despite the likelihood of their appearance (Sternberg and Levitskaya, 2001, Church et al., 1988). Hence, the dielectric behaviour of clay may result from a conductive response, dipolar response or a mix of both that is characteristic of the material at that frequency. An example of a substance that shows both types of responses is presented in Figure 4.2, where the y-axis displays the dielectric properties trends while the x-axis shows the frequency range. Although in this case conduction and dipolar effects are clearly distinguished, the overlapping of both often occurs as shown in Metaxas and Meredith (1983).

Initially, the lower the frequency, the more dominant the ionic conductivity heating mechanism. Its decay is represented by the progressive decrease of the loss factor with frequency. This occurs because the increasingly faster reversals of the electric field are more arduously followed by the ions, thus generating less effective collisions and consequently less

heat (Meredith, 1998). On the contrary, the bound charges have had ample time to follow the electric field during this range, but at higher frequencies they also start to lag behind it. This time lag is known as relaxation time (Thostenson and Chou, 1999). The lag is marked by the decrease of the dielectric constant and an increase of the loss factor, as the dipoles store less energy and generate more heat. A peak response to the electric field and maximum heat generation is seen as a Gaussian bell in the loss factor, also termed dispersion zone, and it is related to the relaxation time of the material considered. From this point forward, further frequency increments limit the ability of the bound charges to create heat (Metaxas and Meredith, 1983).

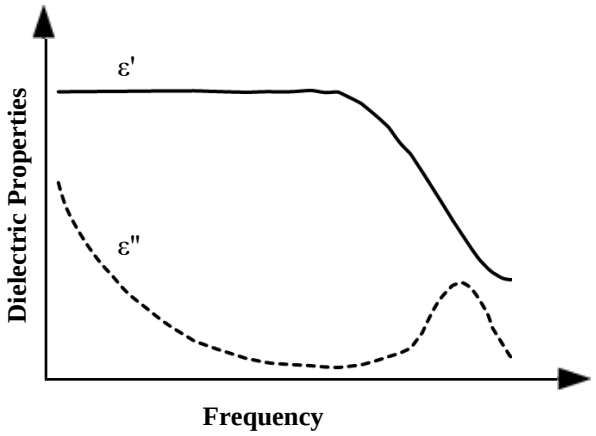


Figure 4.2- Dielectric properties trends across the frequency range of a typical polar solid with free electrical charges, i.e. concrete. Adapted from Asano et al. (2003).

It is worth noting that having found a processing frequency that delivers the optimal dielectric properties for a specific microwave heating, it may very well occur that it is not available for heating purposes. As the microwave technology spread in communications, legislation was brought forward in order to avert interferences. The Industrial, Scientific and Medical radio bands (ISM) define those frequencies at which microwaves can be used for purposes other than telecommunications (Regier et al., 2016). The most widespread frequency is that of 2450 MHz, where others are used to a lesser extent such as 433.92 MHz, 915 MHz and 5800 MHz, (Mingos and Baghurst, 1991, ERC, 2000).

4.3.1.3 Temperature

The temperature increase of a material entails a weakening of its intermolecular forces and an increased thermal agitation (Dinulović and Rašuo, 2011). The lower movement hindrance and higher particle agitation naturally results in the case of free charges in more effective collisions and thus higher loss factors. On the other hand, the behaviour of dipoles with temperature depends on their dispersion zone. If working at a frequency past their dispersion peak, the dipoles impede each other's movements. Therefore, the larger space for the

molecules to rotate means a more effective heat generation and higher loss factors. On the contrary, larger intermolecular spaces before reaching the optimal relaxation time decrease the potential for effective collisions and thus the loss factor. Consequently, the temperature influence can be visually ascertained as a shift of the trends of dielectric properties, like those of Figure 4.2, to higher frequencies (Nelson 1994).

Although the effects of the heating mechanisms on the dielectric properties with increasing temperature are clear, the numerous physicochemical transformations that clay constituents undergo on heating, seen in Figure 3.4, may distort these dielectric trends. For example, in low loss solids with little moisture such as clays at the start of firing, it has been found that the loss factor increases with temperature, completely opposite to what would happen at higher moisture contents (Tinga, 1969).

An explanation is that most of the free water behaves to a lesser extent as physically bound water, which arises typically in granular materials (Trabelsi and Nelson, 2006). Specifically in porous systems like clays, this can be understood as most of the moisture forming a monolayer bound to the materials' structure in their pores (Metaxas and Meredith, 1983). The loss factor increase with temperature is then justified by the dipolar dispersion area for bound water being at a lower frequency than the common 2450 MHz used in processing (Metaxas and Meredith, 1983, Feng et al., 2002), i.e. ≈1000 MHz for clay soils (Hoekstra and Delaney, 1974, Rankin and Singh, 1985). This peaks when the growing thermal agitation of the water particles frees them from the clay, behaving then like free moisture. At that point the loss factor starts decreasing as it happens with free water (Kaatze and Behrends, 2002).

4.3.1.4 Density

Considerations of density, or its analogous terms porosity and void fraction, in a dielectric such as clay can simplify and substitute the more challenging study of the macromolecular structure of each constituent and their possible associations (Nelson, 1994). Higher dielectric properties have been generally found upon bulk density increments in substances such as clay soils (Velazquez-Marti et al., 2005), and for many minerals some of which are present in clays such as muscovite, feldspars and hematite (Nelson et al., 1989). This is explained by the presence in these materials of a gas phase, i.e. air, which also contributes to the final dielectric properties of the mixture. As density increases, crystalline and amorphous entities are packed tighter leaving less space for the admittance of air, e.g. in clay minerals interlayers, where air is conventionally treated as a completely transparent substance (Meredith, 1998). As a sample's density is an easy to control parameter, several studies have arisen looking forward to obtain a quantifiable estimation of the dielectric properties change with density for several materials (Dube and Parshad, 1970, Nelson, 1994, Nelson et al., 1989).

4.3.2 Dielectric properties of clay materials in the literature

In order to successfully understand a material's thermal evolution and thus predict the appearance of unwanted effects such as hot spots, knowledge of its dielectric properties prior to microwave processing is critically important. Moreover, they can serve to design an applicator that guarantees an optimal energy delivery, and in general inform if a material is even a viable candidate for microwave treatment. It is worth noting the generally accepted limits for microwave processing range between $0.01 \leq \varepsilon'' \leq 5$ as defined by Metaxas and Meredith (1983).

In the case of clay mixtures, awareness of the dielectric properties of their major constituents is even more crucial, since the dielectric response of such a naturally multicomponent material is determined by its individual components. In addition, the variable and wide range of species that can be harboured in clays may result in mixtures with remarkably contrasting microwave heating potentials. Hence, a dielectric properties assessment of clay constituents allows the identification of the main species that enable the microwave treatment of clays.

Unfortunately, data of the dielectric properties of clays in the literature is limited, probably due to the experience-based nature of the processes in which it is the main raw material. An exception is made for soils because of their importance in telecommunications applications (Hoekstra and Delaney, 1974) and for their hydrological, agricultural, biological and biogeochemical characteristics (Wang and Qu, 2009, Cihlar and Ulaby, 1974). Studies for some specific minerals have also been produced due to their potential use as insulating coatings, transducers and capacitors or for specialised processes of great added value for the metallurgic industry (Young and Frederikse, 1973). However, this interest is commonly focused in metals and ores (Tikhonov et al., 2010, Arlt et al., 1985, Azad et al., 2006).

Some selected values of dielectric properties of clays and minerals found in the literature are presented in Table 4.1. Among the numerous parameters that affect these properties, frequency is one of the most carefully monitored, as an optimal processing frequency is often sought for sensing, absorption, etc. (Hoekstra and Delaney, 1974). On the other hand, the focus on the preservation of the natural state of these materials explains that except for some specific studies, as mentioned above, and for particular minerals (Nelson et al., 1989), density considerations are generally disregarded. In addition, there is a consistent lack of temperature control, with most studies performed near room temperature (Nelson et al., 1989) and only a handful going above 100 ^{o}C (Orzechowski et al., 2006). This means dealing with moisture contents, which are tightly controlled in soils (Cihlar and Ulaby, 1974) although in minerals the interest does not often go beyond oven drying them. Considerations of particle size

distributions, grain orientations and structural arrangements are almost always disregarded, probably following the same reasoning as in this work.

As a result, large variations in the dielectric properties have been reported for similar materials with some displayed in Table 4.1. Regarding clays, an example of contrasting dielectric properties due to a different mineralogy is evident in the case of Avra and Brookhaven soils, which have an order of magnitude of difference in the losses due to their lossy iron and transparent silica content, respectively (Sternberg and Levitskaya, 2001). Free water is the only major clay constituent purposely studied, where in these generally low loss materials a 20% moisture content can increase the dielectric constant and loss factor by one and two orders of magnitude regardless of frequency. At lower moisture percentages, i.e. 2%, this influence is still significant with around 40% change for the constants and having the losses raised tenfold (von Hippel and Morgan, 1955).

Much less impact comes from a frequency change, being mostly significant for moist soils due to the strong dipolar polarisation of water (von Hippel and Morgan, 1955). Comparing the dielectric properties with temperature is complicated considering the moisture influence. Yet, at 10 ^{o}C the losses can go down one order of magnitude and the dielectric constants decrease 14-50% compared to room temperature values, which is consistent with the moisture-temperature behaviour discussed before. Finally, it is not usual to study density effects although in some cases it is monitored (Gadani, 2012).

Focusing on the clay constituents, it can be seen the significant contrast in the dielectric response of minerals such as quartz and calcite on one side and the clay minerals phase on the other. Moisture effects are still expected to be critical, even in the constituents with higher dielectric properties. Nonetheless, minerals are often studied oven dried and moisture studies are not the norm. The opposite occurs with frequency, remaining as engaging as in bulk clays although its influence is barely noticeable in the dry minerals (Campbell and Ulrichs, 1969).

Temperature changes can cause variations of up to two orders of magnitude in the losses of minerals like kaolinite. However, its influence is hard to be separated from thermal reactions. In the case of density, a constant increase of the dielectric properties occurs with decreasing porosity, e.g. 9% and 40% for the constants and losses in a 22% denser muscovite and 16% for the dielectric constants while doubling the losses for a 16% denser albite. Remarkably, the aforementioned challenging characterisation of mineral species sometimes results in their erroneous labelling, as in the case of the muscovite of Nelson et al. (1989) which is more likely an hydrated phlogopite-mica when compared with Church et al. (1988).

Looking at the microwave heating limits above, it is clear that clays have large amounts of microwave transparent materials regardless of the processing conditions, such as quartz, calcite and some of the feldspars. On the other hand, the clay minerals phase appears to be composed of moderate microwave absorbers, resulting in clays that drift around the processability limit. Therefore, it is the presence of clay minerals, i.e. kaolinite, muscovite and montmorillonite, which enables the microwave processing of clays. This means that during microwave processing, the clay minerals phase may heat faster on account of its better microwave coupling and in doing so; they will then conventionally heat through conduction the comparably transparent minerals in their surroundings. It is worth noting that added to the general lack of dielectric properties data at temperatures beyond room temperature, there is a total absence of any correlation between dielectric properties and the mineral transformations of Figure 3.4. This is particularly important in the case of the clay minerals, as they are thermally unstable beyond 350 ^{o}C and their structure and composition undergo important transformations that may significantly affect their coupling with microwave energy (Grim, 1968).

Table 4.1- Published dielectric properties of clays and clay constituents at different conditions of temperature, frequency, moisture and density.*Not Available (NA) is used when temperature is not specified or described as room temperature.

Clay, clay constituent or soil	ε'	ε''	Frequency (MHz)	Temperature (ºC)*	Bulk density (g/cm^3)	Moisture (%w/w)	Reference
Avra soil	2.95	0.100	900	NA	-	Oven dry	(Sternberg and Levitskaya, 2001)
	2.93	0.120	1000	NA	-	Oven dry	
Brookhaven soil	2.52	0.071	900	NA	-	Oven dry	
	2.51	0.055	1000	NA	-	Oven dry	
Clay soil	2.38	0.047	300	NA	-	Dry	(von Hippel and Morgan, 1955)
	2.27	0.034	3000	NA	-	Dry	
	20.0	1.040	300	NA	-	20.9	
	11.3	2.830	3000	NA	-	20.9	
Loamy soil	2.47	0.016	300	NA	-	Dry	
	2.44	0.003	3000	NA	-	Dry	
	3.52	0.210	300	NA	-	2.2	
	3.53	0.140	3000	NA	-	2.2	
Silty clay	8.30	0.805	500	10	-	10	(Hoekstra and Delaney, 1974)
	12.50	3.052	500	24	-	10	
	5.50	1.250	4000	10	-	10	
	6.30	2.155	4000	24	-	10	
Kaolinite	2.14	0.030	1000	NA	0.832	2.5	(Orzechowski et al., 2006)
	2.11	0.130	4000	NA	0.832	2.5	
	2.01	0.060	1000	400	0.832	2.5	
	1.91	0.120	4000	400	0.832	2.5	
	2.32	0.000	1000	800	0.832	2.5	
	2.19	0.020	4000	800	0.832	2.5	
	2.421	0.111	2450	20	-	-	(Kobusheshe, 2010)
	2.046	0.000	2450	400	-	-	
	1.658	0.000	2450	800	-	-	
Montmorillonite	4.490	1.110	2450	20	-	-	
	1.957	0.015	2450	400	-	-	
	2.80	0.040	1	NA	-	-	(Saltas et al., 2008)
Muscovite	4.23	0.001	900	NA	-	-	(Church et al., 1988)
	4.46	0.003	1000	NA	-	-	
	1.63	0.006	1000	NA	0.45	Oven dry	(Nelson et al., 1989)
	1.62	0.005	2450	NA	0.45	Oven dry	
	1.78	0.008	1000	NA	0.55	Oven dry	
	1.77	0.007	2450	NA	0.55	Oven dry	
Phlogopite	2.1	0.014	1000	NA	0.7	Oven dry	
	2.04	0.011	2450	NA	0.7	Oven dry	
	2.36	0.039	1000	NA	0.86	Oven dry	
	2.31	0.022	2450	NA	0.86	Oven dry	
Albite	2.61	0.024	1000	NA	1.25	Oven dry	
	2.61	0.020	2450	NA	1.25	Oven dry	
	3.03	0.052	1000	NA	1.45	Oven dry	
	3.02	0.048	2450	NA	1.45	Oven dry	
Orthoclase	4.5	0.000	900	NA	-	-	(Church et al., 1988)
	4.4	0.000	1000	NA	-	-	
Calcite	26.0	0.001	900	NA	-	-	
	27.5	0.001	1000	NA	-	-	
Quartz	3.94	0.001	900	NA	-	-	
	3.89	0.001	1000	NA	-	-	
	2.82	0.02	9300	NA	-	-	(Florek and Lovas, 1995)
Hematite	3.61	0.303	1000	NA	1.5	Oven dry	(Nelson et al., 1989)
	3.50	0.237	2450	NA	1.6	Oven dry	
	4.08	0.396	1000	NA	1.8	Oven dry	
	3.98	0.316	2450	NA	1.8	Oven dry	

4.3.3 Heating equation and penetration depth

It has been discussed above that frequency, density, temperature and composition condition the microwave heating potential of a substance through changes on its dielectric properties, where specifically the loss factor indicates the efficiency at heat generation. Understandably, the quantification of the degree of energy capable of being dissipated inside of a target material per time unit will be directly dependent on this parameter among others. In Eq. 4.2 the formulation of this power dissipation, also termed power density, is shown (Metaxas and Meredith, 1983),

$$P_D = {}^{P_A}/_{V} = 2\pi f \varepsilon_0 \varepsilon'' E_i^2 \qquad \textbf{4.2}$$

where P_D (W/m^3) is power density, P_A (W) is the total absorbed power, V (m^3) is the volume of the sample, f (Hz) is the frequency of the electric field, ε_0 (F/m) is the permittivity of free space (8.85x10^{-12} F/m), $\varepsilon''$is the loss factor of the sample and E_i (V/m) is the electric field strength inside the material.

As expected, power dissipation is directly dependant on the loss factor, but also on the processing frequency. Nonetheless, electric field strength has the biggest effect as the power density increases with the electric field squared. The conclusion that can be extracted here and that will be developed later in this chapter is that working at higher frequencies while the losses remain constant would result in a safer heating process, as lower electric field strengths would be necessary to reach the desired power dissipation (Meredith, 1998). As a consequence, the use of microwaves is advised over working at lower frequencies such as those in the radiofrequency range.

With the objective of achieving volumetric heating, the evenly distribution of the electric field across the sample is of vital interest (Metaxas and Meredith, 1983). Electromagnetic waves traversing through a dielectric load undergo a certain degree of attenuation in their amplitude as power is being dissipated in the material. The waning electric field strength will translate looking at Eq. 4.2 in lower power density, where the power attenuation is exponential from the sample's surface. A term called penetration depth, formulated in Eq. 4.3, is put forward to quantify the distance at which the decay of power has reached 36.8% of its value at the surface of the material (Meredith, 1998),

$$D_p = \frac{\lambda_0'}{2\pi(2\varepsilon')^{0.5}}\left[\left(1+\left(\frac{\varepsilon''}{\varepsilon'}\right)^2\right)^{0.5} - 1\right]^{-0.5} \qquad \textbf{4.3}$$

where $\varepsilon'$is the dielectric constant of the sample and λ_0' (m) is the free space wavelength of the microwave energy.

It can be observed in Eq. 4.3 that the power attenuation rate is critically dependant on the dielectric properties. A clearer display of their effect on the penetration depth of some common materials is presented in Table 4.2. Here, it can be seen how low loss materials, such as quartz and Teflon, have high penetration depths as their transparency ensures poor power absorption. On the other hand, there might be penetration depth issues in lossier materials like water and moist organics. Similarly, limited penetration depths are also observable in ceramics with a large content of clay minerals such as porcelains. A small penetration depth may prove to be the most important limiting factor in the processing of clays. From Eq. 4.3, it is clear that the most straightforward solution to processing challenges due to power attenuation is to work at lower frequencies, given their inverse dependence with the penetration depth.

Table 4.2- Penetration depths of some common materials at the commonly used processing frequency of 2450 MHz and at room temperature (Püschner, 2015).

Material	Penetration Depth (cm)
Water	1.4
Bread	2-5
Paper	20-60
Wood	8-350
Quartz	16000
Teflon	9200
Porcelain	56

4.4 Measurement of dielectric properties

The first step in the design of an appropriate microwave heating process for clays is to gain a deep insight into their dielectric properties and those of their major constituents across the firing range, and at the chosen processing frequencies and bulk densities. However, it has been seen in Table 4.1 that dielectric properties data of these materials in the literature is scant and at times it falls in contradictions. The latter point is to some extent understandable, as the expertise of the operator, the employed technique and the measurement conditions, e.g. frequency and sample shape, among others strongly affect the resultant dielectric properties (NPL, 2003). In order to obtain reliable and precise dielectric properties data, several measurement methods have been developed across time, where their suitability is determined by the particular sample characteristics, such as shape and porosity, as well as the target frequency range and temperature (Jha et al., 2011).

4.4.1 Open ended coaxial probe

The coaxial probe consists of a cut off section of a transmission line where its open end is pressed against a dielectric specimen as seen in Figure 4.3. A TEM travelling wave circulates

through the coaxial line and up to the dielectric material, where its reflection by the specimen is critical in the dielectric properties calculation.

The technique is widely used in clay soils mostly due to its simplicity and versatility (Velazquez-Marti et al., 2005), as commercial probes often can work in the 10-10000 MHz range with an uncertainty as low as of 3% (NPL, 2003, NPL, 2017). Moreover, the samples require little to no preparation since the dielectric properties are measured by just contacting one of its surfaces and the method is non-invasive (NPL, 2003, Jha et al., 2011).

In granular samples like clays, air gaps become an important source of measurement errors. Additionally, uncertainties due to sampling may occur with these heterogeneous materials, given the small sample size needed. Furthermore, in low loss dielectrics, errors may come from measuring the sample container (NPL, 2003). Finally, although no temperature limits are considered, measurements at clay firing temperatures cannot be reached, since it is a contact based technique and the probe can be damaged and even melt.

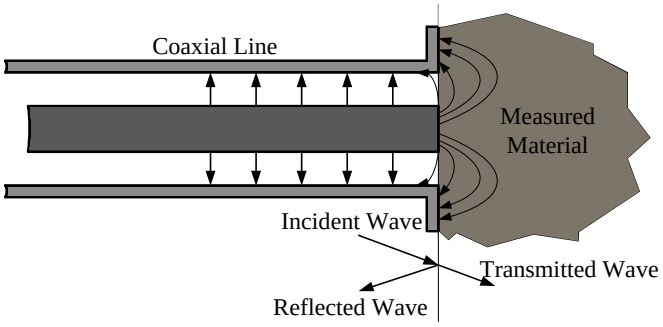


Figure 4.3-Diagram of a coaxial probe measurement process. Adapted from NPL (2003).

4.4.2 Waveguide transmission line

When using this non-destructive method, the sample is enclosed in a vertically or horizontally oriented hollow metallic structure called waveguide, which will be discussed in more detail later in this chapter. Both sides of the waveguide are connected to a network analyser, as seen in Figure 4.4, which measures the degree of reflection and transmission of an electromagnetic signal fired towards the dielectric specimen, thus allowing for the calculation of its dielectric properties (Jha et al., 2011).

The need for larger sample sizes than the coaxial probe generally justifies its higher degree of accuracy, having uncertainties of around 0.5% in optimum circumstances of minimal heterogeneities or air gaps issues. In addition, a broader range of temperatures can be studied as waveguide materials can be heat resistant, e.g. brass (Jha et al., 2011, NPL, 2003). It is documented its use in the study of clay constituents such as silica (Ebara et al., 2006).

This method is not as popular as the coaxial probe. A reason is that it has a more laborious and time consuming sample preparation, since an important source of measurement uncertainties derives from the dielectric not completely filling the cross-section of the waveguide. Additionally, the frequency coverage is restricted depending on the size of the waveguide, and clay firing temperatures, i.e. above 900 ºC, still cannot be reached (Jha et al., 2011, NPL, 2003).

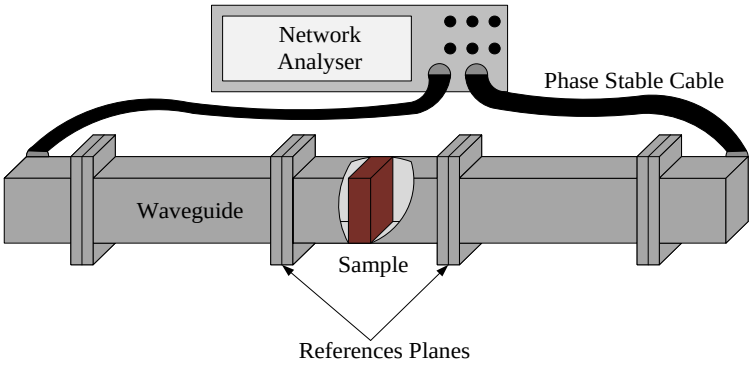


Figure 4.4-Diagram of a waveguide transmission line connected to a network analyser, with a specimen ready for measurement seen through cut in waveguide. Adapted from ASTM (2014b).

4.4.3 Resonant cavity

The measurement cavity is often a hollow TM cylinder as displayed in Figure 4.5, where the travelling wave bounces between its two ends. Based on the resonant cavity perturbation theory, upon the introduction of a load small enough to uphold for the assumption of constant electric field strength across the cavity, there is a change in its resonant frequency and quality factor. The latter parameter relates the stored and dissipated energy per cycle and gives an idea of the excellence of the measurement. Together, their often less than 5% change can be linked to the dielectric constant and the loss factor of the specimen, respectively (NPL, 2003).

This multi-pass technique results in the repeatable and sensitive measurement of liquid or solid low loss materials, as the wave passes several times through the dielectric before being completely absorbed. Being particularly suitable for frequencies generally above 600 MHz (Marland et al., 2001, Sheen, 2005), uncertainties as low as 1-2% for the dielectric constants and around 5% for the loss factor are achievable (ASTM, 2013b, Sheen, 2005, Carter, 2001). As a result, this method has been widely used in measuring low loss dielectrics such as clay shales (Al-Harahsheh et al., 2009), and clay minerals like vermiculite (Katrib et al., 2015). In addition, since the load cannot touch the cavity walls, measurements beyond firing temperatures are possible (ASTM, 2013b, Al-Harahsheh et al., 2009).

Yet, there might be sampling related uncertainties, where sample preparation can be laborious and even challenging depending on the material characteristics (Jha et al., 2011). Moreover, uncertainties higher than 50% in the complex permittivity calculation are found if the frequency and quality factor shift are larger than 10%, due to sample size or the dielectric being too lossy. Something similar occurs if the material is so transparent that $\frac{\varepsilon''}{\varepsilon'} < 10^{-3}$. Additionally, broadband measurements are not possible as the radius of the cavity determine the available resonant frequencies (NPL, 2003, Sheen, 2005).

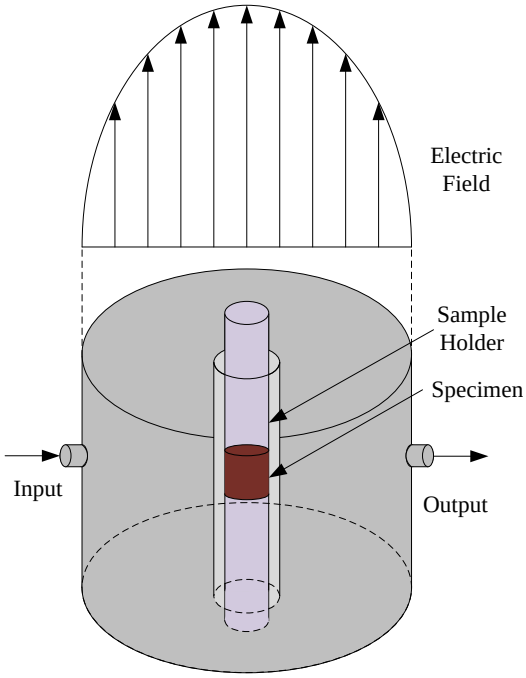


Figure 4.5-Diagram of TM_{01} resonant cavity with a dielectric specimen inside a sample holder seen through cut in cavity. Adapted from NPL (2003).

A summary of the dielectric property measurement techniques with their advantages and disadvantages for the assessment of clays and their constituents is presented in Table 4.3. It is clear that the resonant cavity is the only one that can provide dielectric properties data across the whole clay firing range, while the coaxial probe will most likely struggle with the granular and porous clay structure. However, in both cases the small samples needed for the analysis might require additional validation so as to ensure that the measurements are statistically representative of a whole clay brick, due to clays' typical heterogeneity. The measurement of specimens large enough to embody the whole population can only take place using the waveguide transmission line.

Table 4.3- Summary table of suitability of various dielectric property measurement techniques for the assessment of clays and clay constituents.

Measurement technique	Advantages	Disadvantages
Open ended coaxial probe	Simple, versatile, wide frequency range.	Large errors in granular materials, small samples are unrepresentative of the population, unable to perform measurements in firing range.
Waveguide transmission line	Highly accurate, samples are representative of the population, broad range of temperatures available.	Challenging and critical sample preparation, restricted frequency coverage, cannot reach firing temperatures.
Resonant cavity	Highly accurate for low loss materials, measurements in the firing range are feasible.	Challenging sample preparation, restricted frequency coverage, small samples are unrepresentative of the population.

4.5 Estimation of dielectric properties

In spite of selecting the most accurate and reliable dielectric property measurement techniques for the assessment of clays and their constituents, the high variability of clay composition results in a nearly infinite amount of natural and synthetic clays. This in turn would force a similar number of measurements in order to reach a significant understanding of their potential for microwave heating. On top of that, the accuracy of many of the measuring techniques relies on laborious sample preparations and the training of the operator.

A solution to overcome the challenge of measuring all the possible mineral configurations present in clays is the estimation of their dielectric properties. Extrapolation techniques have been used for reporting the dielectric properties of a material at different densities (Nelson, 2005, Bal and Kothari, 2010) and statistical methods and artificial neural networks have been analogously employed, considering among others moisture contents (Boyacı et al., 2009). Nevertheless, achieving the characterisation of multicomponent heterogeneous mixtures with respect to their individual constituents comes through the utilisation of electromagnetic mixing rules (Sihvola, 1999, Nelson and You, 1990).

4.5.1 Mixing rules

In mixtures, dielectric properties offer an averaged, also termed effective, response of the entire system to microwave energy. Although straightforward in homogeneous media such as water, in the case of heterogeneous systems like clays this entails that their dielectric properties come from a certain assemblage of those of their individual constituents. These species can be understood as discrete homogeneous media within the clay mixture. The interest in electromagnetic mixing rules derives from their ability to predict the dielectric behaviour of a heterogeneous material based on knowledge of its composition and the dielectric properties of its component parts (Sihvola, 2000).

Mixing rules are algebraic formulae that allow for the calculation of the dielectric properties of a mixture as a function of the dielectric properties of its constituents and their volume fractions. This is of great interest regarding brick clays, since it enables the prediction of their dielectric properties across the firing range and at different frequencies or densities. The first case is achievable from knowledge of the clay mineralogy and dielectric properties of its constituents in the same temperature range, whereas similar estimations at different frequencies require the minerals measured at those same frequencies. Estimations at variable densities come from the consideration of material/air mixtures, where the air content represents the material's void fraction.

There are numerous mixing equations available, where each was originally derived by considering some particular and distinctive aspect of the microwaves/material interaction or characteristics of the mixture such as particle shape (Sihvola, 1999). Nonetheless, in some cases different initial considerations lead to the same formula (Mallet et al., 2005, Polder and Van Santen, 1946). A selection of commonly used mixing rules, summarised in Table 4.4, is discussed below. Regardless of the background of their formulation, their importance lies on the fact that all have been successfully used in the estimation of dielectric properties of clays and their constituents, or similar materials such as soils or rocks.

4.5.1.1 Rayleigh

Also called Maxwell Garnett, this equation takes the approach of dividing a mixture in a series of inclusions embedded in a matrix. Its formulation is based on the comparatively higher electric field inside an inclusion with respect to the external one due to the particle's polarisation. Although specific for spherical particles, it can be modified to account for different shapes. Yet, the original formula is often used unless dealing with some very specific geometries like discs and needles (Sihvola, 2000).

The popularity of this commonly used mixing rule comes from its broad applicability, even being suited for calculations in multicomponent mixtures (Sihvola, 1999). It has been successfully applied to powders and rocks (Campbell and Ulrichs, 1969). However, limitations arise as increasing amounts of inclusions deteriorate its performance (Mallet et al., 2005).

4.5.1.2 Böttcher

This formula can also be found in the literature as Polder–van Santen or Bruggeman (Sihvola, 2000). Its original derivation was based in the consideration of the electric field inside a spherical particle in a homogenised medium, where the field and its associated polarisation

are compared with respect to the environment and the individual constituents of the mixture (Böttcher, 1945, Sihvola, 1999, Looyenga, 1965). Later, its applicability has been extended for any shape as long as the material is low loss (Polder and Van Santen, 1946).

Each component is treated symmetrically by not considering a matrix-inclusions system, thus this formula can be used in multicomponent mixtures without increased uncertainties at higher concentrations of inclusions like with Rayleigh (Sihvola, 2000). On the contrary, it is especially suitable for highly concentrated mixtures as a result of its derivation. Additionally, better predictions are obtained as the packing density of the medium is increased (Polder and Van Santen, 1946). This formula has shown a good performance approximating the dielectric properties of low loss crystalline materials and powders (Dube and Parshad, 1970, Tuhkala et al., 2013), where the main source of uncertainties is the presence in the mixture of lossy constituents like water (Polder and Van Santen, 1946, Sihvola, 1999).

4.5.1.3 Complex Refractive Index (CRI)

This mixing rule was originally derived by considering how an electromagnetic wave is attenuated as it propagates through an inhomogeneous medium composed of a matrix and small particle inclusions (Birchak et al., 1974). The simplicity of its formulation and the lack of any considerations regarding the inclusion's shape have resulted in CRI being extended for calculations of the dielectric properties of mixtures of any particle shape, and without the need of differentiating between a matrix and inclusions. Similarly to Rayleigh and Böttcher, it can easily be extended for multicomponent mixtures.

Originally formulated for soil sensing purposes (Birchak et al., 1974), it has been widely used in granular and porous materials (Ajo-Franklin et al., 2004) such as limestone (Nelson, 2005) and soils (Brovelli and Cassiani, 2008, Singh and Rankin, 1986). Due to its versatility, the precision of CRI approximations can be surpassed by mixing rules specifically derived for certain conditions (Nelson, 2005, Nelson and You, 1990). This is countered by empirically modifying the α exponential away from 0.5 since it is understood as the media topology with respect to the applied field (Regalado, 2004), where 0.65 is considered the best match for clay soils (Brovelli and Cassiani, 2008).

4.5.1.4 Landau-Lifshitz-Looyenga (LLL)

Having a very similar formulation to CRI, it allows for the consideration of a family of mixing rules termed Power-law models (Sihvola, 1999). As in Böttcher, its physical background comes from studying the electric field inside a spherical particle in a homogeneous medium. However, in this case the particles are not pure but a mixture

(Looyenga, 1965). Like CRI, it can be used for multicomponent mixtures (Sihvola, 1999) and for substances of different shapes (Landau et al., 1961). Thus, it has been used in estimations of the dielectric properties of dispersive systems composed of powders and porous structures (Tuncer, 2005), like mica, feldspar (Nelson et al., 1989) and rocky ores (Robinson and Friedman, 2003).

On the other hand, increasing uncertainties are reached in mixtures with high dielectric properties contrast (Scheller et al., 2009). Furthermore, lower estimation values are obtained compared with CRI as a result of its formulation, as exemplified in Figure 4.6. Here, it is presented in the y-axis the dielectric constants estimation using common Power-law equations for different volume fractions of a constituent in a binary mixture displayed in the x-axis. Although inclusions are not considered in these formulas, the term is often used when referring to a minor component (Sihvola, 1999).

4.5.1.5 Lichtenecker

Originally developed by Lichtenecker and Rother (1931), this special case of the Power-law family is obtained when taking the product instead of the sum of the complex permittivities, while the α exponential is null and is substituted by the volume fraction of each constituent (Sihvola, 1999). Starting from assessing a range for the dielectric property estimation as defined by the Power-law equation with $\alpha = -1$ and $\alpha = 1$, i.e. Wiener bounds (Sihvola, 1999), and considering two finely dispersed and well-mixed phases where their topology is neither parallel nor in series, the final Lichtenecker formula is reached (Goncharenko et al., 2000).

Low α values are related with a higher porosity in a material, which explains Lichtenecker's widespread use in soils for moisture sensing applications (Regalado, 2004, Leao et al., 2015). This equation gives the lowest estimations of the Power-law formulas considered as observed in Figure 4.6. However, although having all the advantages of being a Power-law equation, it does not cope well with dry solids (Regalado, 2004) or heterogeneous mixtures (Simpkin, 2010, Goncharenko et al., 2000).

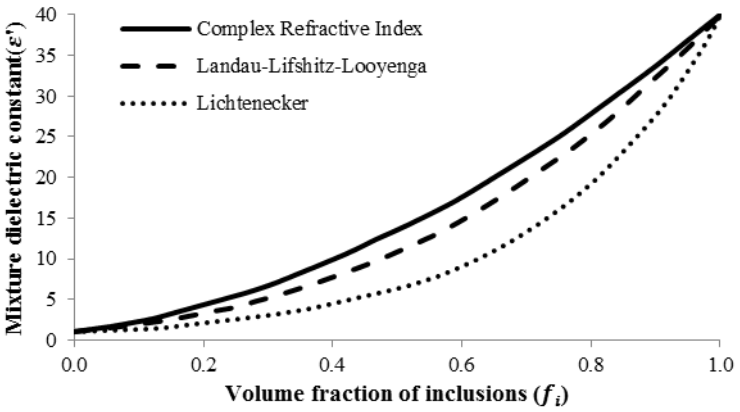


Figure 4.6-Comparison of estimated dielectric constants of a binary mixture with a contrast of $\varepsilon_i/\varepsilon_m$=100 at different contents of inclusions with common Power-law models. Adapted from Sihvola (1999). Where εm and εi, are the complex dielectric permittivity of the matrix and the inclusions respectively.

4.5.1.6 Bruggeman-Hanai (BH)

Also called Bruggeman non-symmetric (Sihvola, 1999). This rule comes from considering the dielectric dispersion caused by particle interactions in a heterogeneous medium consisting on a mixture of substances of different dielectric properties, e.g. an emulsion of concentrated particles. As opposed to the previous formulas, the interactions between particles that cause effects such as interfacial polarisation are the main focus of the derivation (Hanai, 1960). This can be especially useful in materials prone to this effect such as granular or porous dielectrics. (Metaxas and Meredith, 1983).

As Rayleigh equation, it has been successfully applied to powders (Nelson, 2005) and rocks (Campbell and Ulrichs, 1969, Bussian, 1983). Moreover, it is valid for any particle shape and is inherently non-symmetrical. However, it is only applied to binary mixtures (Sihvola, 1999) and its performance decreases for lower amounts of inclusions (Sen et al., 1981).

4.5.1.7 Sen-Scala-Cohen

This complementary formula to Bruggeman-Hanai is reached by interchanging the phases and the volume fractions of the matrix and the inclusions (Sihvola, 1999). However, while Bruggeman-Hanai focuses on higher concentrations of inclusions, Sen-Scala-Cohen does the opposite by being better at estimating diluted mixtures. The approach is to divide the mixture in cells with homogeneous dielectric properties and a homogeneous local field, thus forming a homogeneous medium. Then, interactions between cells progressively build up the mixture.

As Bruggeman-Hanai, it has been applied to some rock types, and similarly it is only applicable to binary mixtures. It is noteworthy to mention that in solids, pore geometry aspects have been averaged when dividing the mixture in cells, resulting in increased estimation uncertainties depending on the mixture characteristics (Sen et al., 1981).

Table 4.4- Common mixing rules formulas (Sihvola, 1999, Nelson, 2005).

Mixing Model	Equation	
Rayleigh	$\frac{\varepsilon-\varepsilon_m}{\varepsilon+2\varepsilon_m}=\sum_{i=1}^{n} f_i\frac{\varepsilon_i-\varepsilon_m}{\varepsilon_i+2\varepsilon_m}$	**4.4**
Böttcher	$\sum_{i=1}^{n} f_i\frac{\varepsilon_i-\varepsilon}{\varepsilon_i+2\varepsilon}=0$	**4.5**
Complex Refractive Index	$\varepsilon^{0.5}=\sum_{i=1}^{n} f_i\varepsilon_i^{0.5}$	**4.6**
Landau-Lifshitz-Looyenga	$\varepsilon^{1/3}=\sum_{i=1}^{n} f_i\varepsilon_i^{1/3}$	**4.7**
Lichtenecker	$\varepsilon=\prod_{i=1}^{n}\varepsilon_i^{f_i}$	**4.8**
Bruggeman-Hanai	$\frac{\varepsilon_i-\varepsilon}{\varepsilon_i-\varepsilon_m}=(1-f_i)\left(\frac{\varepsilon}{\varepsilon_m}\right)^{1/3}$	**4.9**
Sen-Scala-Cohen	$\frac{\varepsilon-\varepsilon_m}{\varepsilon_i-\varepsilon_m}=f\left(\frac{\varepsilon}{\varepsilon_i}\right)^{1/3}$	**4.10**

Where ε_m, ε_i, and ε are the complex dielectric permittivity of the matrix, the inclusions and the mixture, and f_i is the volume fraction of the inclusions.

In some cases, the exact estimation of the dielectric properties is laborious or challenging. Thus, ranges for the estimated dielectric properties can be defined, where Wiener bounds were mentioned above. Tighter limits are possible, such as those of Hashin-Shtrikman. However, these are not often needed unless the suitable mixing rules are very complex or for statistical studies (Sihvola, 1999, Bal and Kothari, 2010).

An aspect often disregarded when considering the selection of the most adequate mixing rule is the dielectric properties contrast between the different constituents, which can constitute an important source of uncertainties for some, e.g. Landau-Lifshitz-Looyenga. Commonly, when mixtures have constituents of high dielectric strength, the matrix/inclusions or inclusions/inclusions contribution to the overall complex permittivity is not done in an equal basis. The influence of increasing quantities of these stronger dielectrics on the overall complex permittivity will be lower than weaker dielectrics as seen for Rayleigh in Figure 4.7A. Here, the y-axis shows the susceptibility of an estimated dielectric constant of a mixture to variable amounts of inclusions with different dielectric strengths displayed on the x-axis.

Something similar can be extracted when taking into consideration the geometry of the particles. In Figure 4.7B, the estimated dielectric constants of some specific shapes, i.e. discs, needles and spheres, are presented against different inclusions contents. It can be seen that the shape of the particles influences their contribution towards the dielectric constant of the mixture on account of the different polarisabilities of each shape. The trends of Figure 4.6 and

Figure 4.7B can be further influenced by the microwave processability of the target mixture, where for example the presence of very lossy inclusions can result in predicted dielectric constants higher than those of the matrix or the constituents alone. This source of errors is generally minimal for low loss substances, so that when considering clay materials as presented in Table 4.1 this effect can most likely be discarded (Sihvola, 1999).

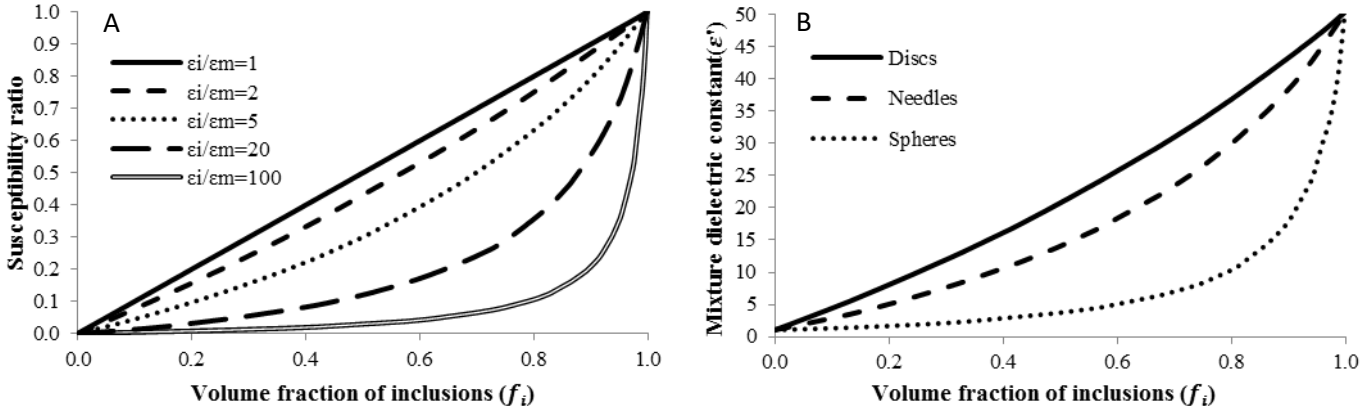


Figure 4.7-Comparison of the susceptibility, defined as (ε-εm)/(εi-εm), of Rayleigh dielectric constants estimations at different contents of inclusions with constituents of different dielectric properties (A), and comparison of estimated dielectric constants with Rayleigh formula of a mixture with a contrast of εi/εm=50 at different contents of inclusions and for various particle shapes (B). Adapted from Sihvola (1999).

Ultimately, despite knowledge of the composition of the clay mixture, considerations of the dielectric contrast of their constituents as per Table 4.1 and Figure 4.7, and the assessment of the particular advantages/disadvantages of each mixing rule in clay-like materials summarised on Table 4.5, the complex nature of clays offers no assurance that some or any of these mixing rules will offer precise dielectric estimations. Hence, an a priori assumption or justification of the formulas most likely to succeed is unfeasible.

Table 4.5- Summary table of suitability of various electromagnetic mixing rules for the estimation of the dielectric properties of clays and clay constituents.

Mixing formula	Advantages	Disadvantages
Rayleigh	Broad applicability Applied to powders and rocks	Considers the mixture as a matrix with inclusions Increasing amounts of inclusions deteriorate its performance
Böttcher	Considers each component symmetrically Suitable for highly concentrated mixtures Better predictions at higher packing densities Applied to low loss crystalline materials and powders	Performance decrease due to the presence of lossy constituents
Complex Refractive Index	Broad applicability Easy empirical modification to match the material's topology Considers each component symmetrically Applied to soils, granular and porous materials	Less accurate than more specific mixing rules
Landau-Lifshitz-Looyenga	Considers each component symmetrically Easy empirical modification to match the material's topology Applied on powders, porous systems and clay constituents	Increased uncertainties when constituents have high dielectric contrast Concentrated systems deteriorate its performance
Lichtenecker	Considers each component symmetrically Easy empirical modification to match the material's topology Applied to soils and porous systems	Does not cope well with dry solids
Bruggeman-Hanai	Considers interactions between constituents Acknowledges interfacial polarisation Applied to granular and porous dielectrics Increasing amounts of inclusions improve its performance	Considers the mixture as a matrix with inclusions Not inherently a multicomponent equation
Sen-Scala-Cohen	Considers interactions between constituents Acknowledges interfacial polarisation Applied to various rock types	Considers the mixture as a matrix with inclusions Not inherently a multicomponent equation Increasing amounts of inclusions deteriorate its performance

4.6 Microwave heating equipment

Once the dielectric properties of clays and their constituents are obtained through measurements or estimations and a detailed understanding of their implications for the processing is reached, the next step is the microwave processing of the clays. In order to do so, there are a variety of system configurations, where the characteristics of the treatment and the load are critical in the process design (Clark and Sutton, 1996). Nevertheless, all possible arrangements have in common a source of microwaves that produces the electromagnetic energy, transmission lines to guide it and an applicator where the microwave energy is applied to a load (Thostenson and Chou, 1999).

4.6.1 Generator

The conversion of electricity to microwave energy at the desired power and frequency is achieved by several devices such as klystrons, travelling wave tubes and magnetrons (Saltiel

and Datta, 1999), where the last one is currently the most widely used given its superiority in efficiency, versatility and lower costs (Meredith, 1998). Various designs are available, with the most common being the multi-cavity magnetron seen in Figure 4.8 (Saltiel and Datta, 1999).

A magnetron is a diode-type electronic vacuum tube consisting of a cathode and an anode, where the latter is at a comparatively high potential creating a strong electric field. Upon heating the cathode with a DC current, loosely bound electrons are released and then accelerated towards the anode. However, the presence of an external magnet causes a magnetic field orthogonal to the electric field, which forces the electrons to travel in a spiral. As the resultant electron cloud passes through the resonant cavities that form the anode, these oscillate at frequencies determined by their size. At this point, critical cooling features are needed for the anode to maintain its integrity. Finally, a coupling probe forms an electromagnetic wave at a fixed frequency from combining all the oscillations and transfers them to a transmission line (Thostenson and Chou, 1999, Saltiel and Datta, 1999, Meredith, 1998)

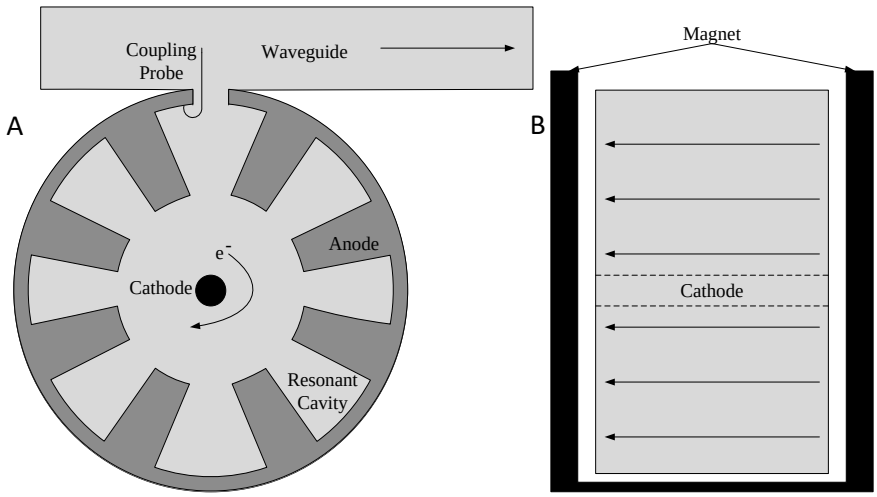


Figure 4.8- Diagramatic aerial (A) and side view (B) of a multi-cavity magnetron microwave generator. Adapted from Thostenson and Chou (1999).

4.6.2 Transmission devices

Guiding the electromagnetic waves from their source towards the load is usually carried out by coaxial lines or waveguides. Nevertheless, although the former is widely used near the radio frequency range, it incurs in large conduction losses when approaching 2450 MHz. Thus, waveguides are the main transmission line in the microwave range (Thostenson and Chou, 1999). These hollow tubes, commonly rectangular in shape, have metallic walls and

low loss air within them that ensure little transmission losses (Saltiel and Datta, 1999). Inside them, waves can propagate in the TE or TM modes (Chan and Reader, 2000).

Regarding the field configuration in the waveguide, each of these modes have specific orders of propagation depending on their mode numbers (m,n), which indicate the number of half cycles of sinusoidal variation of intensity of the field within the waveguide in the transversal axes to the wave propagation (Metaxas and Meredith, 1983, Chandrasekaran et al., 2012). Several $TE_{m,n}$ or $TM_{m,n}$ modes can form in a waveguide, with the lowest frequency mode being called the dominant mode. Waveguide dimensions are precise and standardised so that only the dominant mode can propagate, having as a result different field patterns depending on the dominant mode numbers (Chan and Reader, 2000, Metaxas and Meredith, 1983) as seen in Figure 4.9. Here, the magnetic and electric field configurations of common propagation modes in a rectangular waveguide are displayed, i.e. TE_{10} and TM_{11}, where the former is most widespread (Meredith, 1998, Thostenson and Chou, 1999).

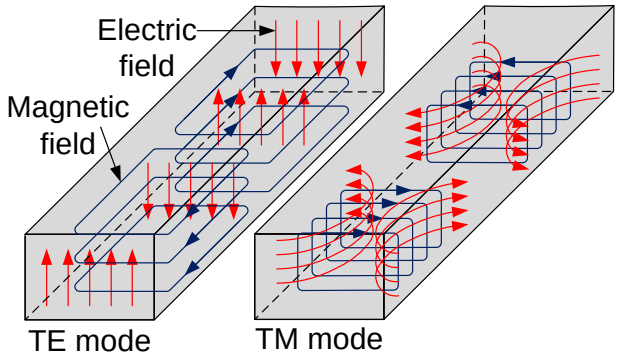


Figure 4.9- Distribution of the electric and magnetic fields in a hollow rectangular waveguide with TE_{10} and TM_{11} propagation modes. Adapted from Marcuvitz (1951).

As well as maximising the electromagnetic wave propagation, waveguide design is also focused towards minimising ohmic losses (Chan and Reader, 2000). In conductors with a high-frequency current flowing through them, there is a deterrent to its flow that increases as it goes deeper into the material. A term called skin depth, seen formulated in Eq. 4.11, is used to quantify the distance at which the current density decay has reached 36.8% of its value at the surface of the material (Metaxas and Meredith, 1983),

$$\delta_s = \sqrt{\frac{1}{\sigma \pi f \mu_0}} \qquad \textbf{4.11}$$

where δ_s (m) is the skin depth, σ (S/m) is the material's electrical conductivity, f (Hz) is the frequency of the field and μ_0 (V s/A m) is the permeability of free space (1.26 10^{-6} V s/A m).

4.6.3 Applicators

The interaction between the guided electromagnetic wave and the load occurs in the applicator. Several types are available depending on the materials to be processed, such as travelling wave, near-field and resonant (Chan and Reader, 2000). Resonant applicators, also termed cavities, have characteristically high field strengths which as per Eq. 4.2 means that they are distinctly suited for processing low loss materials like clays (Thostenson and Chou, 1999, Bykov et al., 2001). They consist of a closed chamber with metallic walls that often has thermal insulation (Bykov et al., 2001).

As in the resonant cavity measurement technique explained above, a standing wave pattern is formed inside the applicator, where the TE or TM wave passes several times through the dielectric before being completely absorbed (Saltiel and Datta, 1999). The resultant electric field distribution determines the temperature gradients within the dielectric (Thostenson and Chou, 1999), and is affected by parameters such as the operating frequency, specimen size and shape, dielectric properties, physicochemical changes undergone during processing, and crucially by the applicator design (Chan and Reader, 2000).

4.6.3.1 Single mode cavities

This type of applicator characteristically supports only one resonant mode at the source's frequency. Consequently, the size of the cavity is of the order of one wavelength, where the mode coupling efficiency is critically dependent on the maintenance of the wave's required frequency band range as determined by the microwave generator (Thostenson and Chou, 1999). Here, the electric field distribution can be calculated analytically, thus allowing for the precise characterisation of the non-uniform electric field distribution.

Single mode cavities present only one electric field strength maximum in the TE_{10} case, also called hot spot. By knowing the location of that hot spot and placing the dielectric in that area, optimum heating is possible (Metaxas and Meredith, 1983). Cavities can be of various shapes, those with a rectangular or circular cross-section being the most common (Chandrasekaran et al., 2012). An example is displayed in Figure 4.10, where a TE_{10} rectangular waveguide has been transformed into a single mode cavity by shorting the microwave propagation with a sliding short. The hot spot of the resultant wave pattern is centred on the sample holder containing the load, thus achieving optimal heating.

In general, single mode cavities establish higher electric fields than other applicators for the same amount of power applied, which is particularly efficiently when carrying out processes with low loss materials (Metaxas and Meredith, 1983). However, the maximum treatable

volume is limited to the cavity size, which is narrowed by the processing frequency, and then often further restricted around the field maximum in order to ensure uniform and optimal processing (Chan and Reader, 2000). Size restrictions and field non-uniformity pose challenges in the scale up of single mode processes, being then mainly employed in ceramic joining or similar specific applications (Thostenson and Chou, 1999, Chandrasekaran et al., 2012). On the other hand, the characteristics of single mode applicators are widely appreciated in the laboratory scale for microwave/material studies (Saltiel and Datta, 1999) and ceramic sintering (Lee and Case, 1999, Zhao et al., 2000) among others.

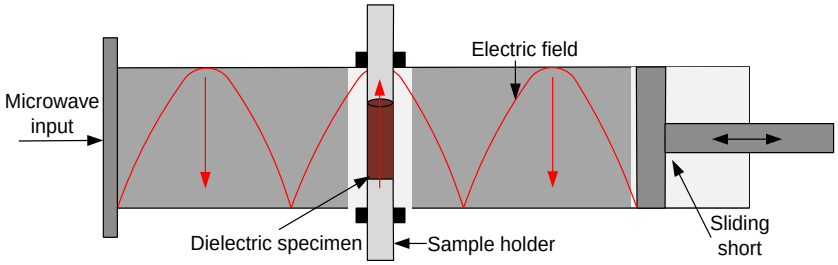


Figure 4.10- Diagram of electromagnetic field interaction with a centrally located cylindrical sample and a sliding short seen through cuts in rectangular TE_{10} single mode cavity. Adapted from Mehdizadeh (2015).

4.6.3.2 Multimode cavities

The size of a multimode cavity is large compared with the wavelength of the microwaves in at least two dimensions. As a result, various standing waves originate, forming a pattern where several resonant modes are sustained at the same time (Katz, 1992, Metaxas and Meredith, 1983). The number of possible resonant modes is directly dependant on the size of the cavity, where its design is often critically reliant on empirical knowledge and trial and error. This is justified by the complexity of accurately deducing the resultant field distribution of a number of modes, given the importance of affecting parameters such as the nature of the dielectric, feeds position and source's frequency (Thostenson and Chou, 1999, Chan and Reader, 2000).

A major feature of multimode applicators is the possibility of achieving a uniformly distributed electric field across the cavity due to the overlapping of the resonant modes, allowing for the homogeneous heating of the load (Metaxas and Meredith, 1983). Figure 4.11A presents a qualitative representation of the mode patterns within the cavity. Each resonant mode has a certain Q factor and resonant frequency in the empty cavity, which are changed when a load is introduced. Hereby, the electric field strength is dampened causing some degree of overlap across the modes (Metaxas and Meredith, 1983). Consequently, the highest possible number of modes is desired to reach uniform heating, which is achieved by increasing the size of the cavity or the operating frequency (Chandrasekaran et al., 2012).

The result of the modes overlapping is more easily seen in the three-dimensional power distribution pattern of Figure 4.11B. As a consequence of the specific nature of each microwave process, e.g. penetration depth issues and capital costs, the complete overlapping of the modes usually does not occur. Consequently, the presence of regions of low and high electric field intensity in the cavity, termed hot and cold spots respectively, is easily recognisable. This can result in the uneven heating of the dielectric (Chan and Reader, 2000, Metaxas and Meredith, 1983).

Instead of further increasing the number of modes to ensure the thermal uniformity of the load on heating, some accessories such as turntables and mode stirrers are frequently added to multimode applicators (Chan and Reader, 2000). The latter is generally a metal fan, that when introduced in the applicator creates a secondary field pattern, which couples with the primary electric field providing a more uniform heating. Their design and application are based on empirical knowledge (Metaxas and Meredith, 1983). On the other hand, a turntable is based on the movement of the workload around the applicator. A reduction of hot spots and increased heating uniformity is reached as the material is moved around the standing waves, since it is subjected to different field intensities cyclically. As for the mode stirrers, there is no analytical procedure to calculate its impact on the heating efficiency (Meredith, 1998).

Multimode ovens are the most commonly used type of microwave applicators, as they are suited for processing large or complex shaped samples where a high degree of uniform heating is desirable (Saltiel and Datta, 1999, Thostenson and Chou, 1999). As such, they have been widely used in the heating of ceramics (Xie et al., 1995, Menezes and Kiminami, 2008, Pendola and Saha, 2014, Pereira et al., 2016) and ores (Mishra et al., 2006, Agrawal, 2006). Moreover, their versatility derived from their low cost, ease of construction and low sensitivity to product position or geometry translates in an easier scale up to the industrial stage, having the domestic kitchen microwave as the most widespread example (Metaxas and Meredith, 1983, Chan and Reader, 2000, Chandrasekaran et al., 2012).

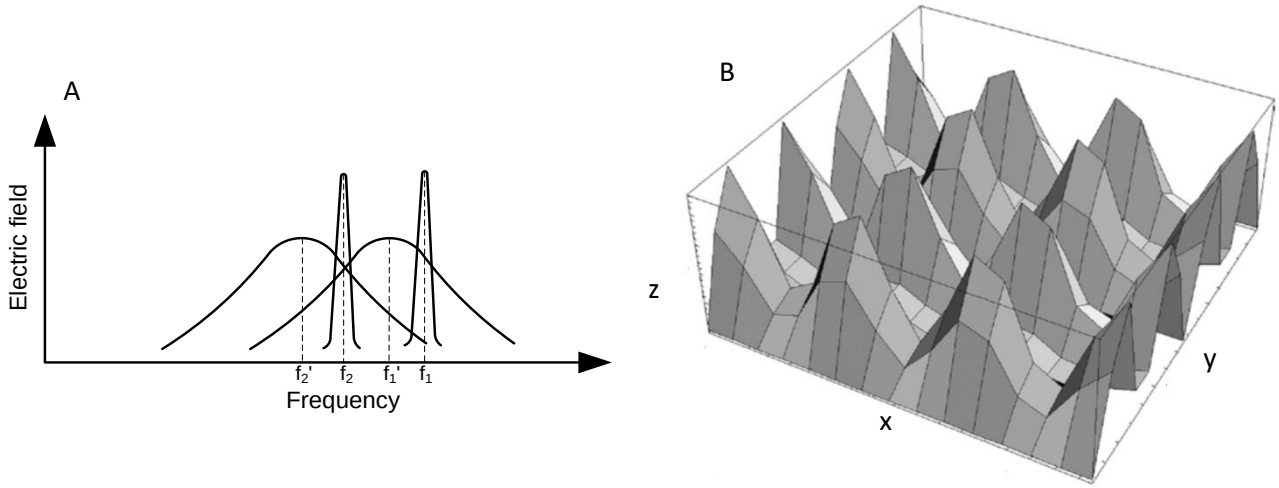


Figure 4.11- Damping of the mode patters in an empty multimode cavity (f_1,f_2) as a dielectric specimen is loaded in the applicator (f_1',f_2')(A) and three-dimensional distribution pattern of power density in a loaded rectangular cavity (B). Adapted from Metaxas and Meredith (1983) and Mehdizadeh (2015).

4.6.3.3 Applicator selection criteria

Although resonant applicators have been found the most suitable for the heating of specimens with low dielectric properties, each cavity has its advantages and disadvantages depending on the specific characteristics of the process and the load. As mentioned before, single mode produces high electric field strengths that result in fast heating rates of small loads while multimode are more versatile and can treat larger specimens. Nevertheless, when exposing any material to microwaves, some important quality and safety considerations may skew the focus of the applicator selection and design.

4.6.3.3.1 Hot spots and thermal runaway

It can be safely assumed that when a heterogeneous material such as clay, whose forming constituents have contrasting dielectric properties, is exposed to microwave energy, several thermal gradients will take place across its volume. Hence, different areas will heat at different rates as defined by Eq. 4.12, which results of the combination of the common sensible heating equation (Coulson et al., 1996) and the power density equation,

$$\frac{\Delta T}{t} = \frac{2\pi f V \varepsilon_0 \varepsilon'' E_i^2}{m C_p} \qquad \textbf{4.12}$$

where m (kg) is the mass of the load and C_p (J/kg K) is its specific heat capacity.

These hotter areas correspond with zones of high electric field strength and are denominated hot spots, as seen previously. It is critical that these can conventionally heat their surroundings in order to achieve the volumetric heating of the load. Yet, it can happen that the heat diffusion is impeded because the material is a thermal insulator or it becomes one due to

thermal transformations during processing. Another situation is that power dissipation in the hot spot exceeds the heat transmission to its surroundings because its loss factor increases with temperature, similarly to how it is shown in Figure 4.12. It is noteworthy to mention that clays comply with both cases. At this point, an uncontrollable increase in the heating rate and temperature of that particular part of the material occurs, i.e. thermal runaway, which leads to a decrease in the product quality or even damage to the microwave equipment (Das et al., 2009, Meredith, 1998).

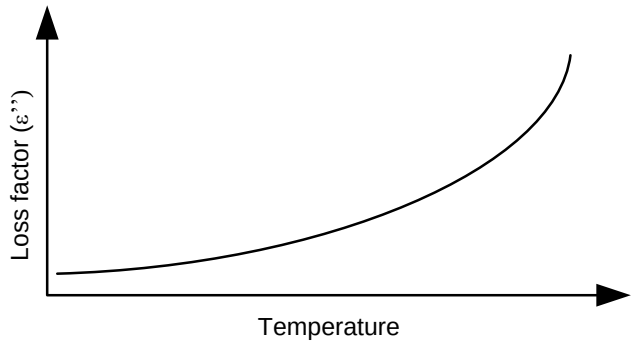


Figure 4.12- Typical loss factor evolution with temperature of a substance which is susceptible of causing a thermal runaway.

4.6.3.3.2 Arcing

Looking at Eq. 4.2, it is clear that in order to achieve a high degree of heating in a low loss solid at a fixed frequency the most straightforward solution is to increase the electric field strength within the material. This field however is always lower or equal to the one outside the load, where several factors can increase this difference, e.g. dielectric with sharp edges can concentrate the field locally. Given a field strong enough, air in the vicinity can be broken down into ionized particles (Meredith, 1998). The specific value depends upon many parameters such as atmosphere, temperature and pressure, being around 2.9 MV/m for dry air at 2450 MHz (Gandhi, 1981). This ionization is problematic because it turns the gas into an electrically conductive medium, becoming a low resistance electrical path and substantially increasing the local power dissipation. The arc produced by microwave energy causes a subsequent violent temperature rise that can damage the load and the applicator if the microwave feed is not stopped. Logically as per Eq. 4.2, arcing is more common at lower microwave frequencies and in the radiofrequency range given the higher fields necessary to achieve the same power density (Metaxas and Meredith, 1983).

4.6.4 Additional waveguide components and systems

Other additional components can be added to the basic generator-waveguide-applicator configuration. Their presence is often justified to achieve an optimal delivery of energy to the

load or for safety reasons, whereas in other cases process control is the main driving factor for their addition.

4.6.4.1 Circulator

Usually when processing low loss materials or when the applicator is empty, reflected energy can return to the magnetron causing damage. A solution is the installation of a circulator, which is commonly a three port transmission line where one is connected to the applicator and another to the microwave source. The waves reflected from the applicator are deviated towards the third port that is connected to a dummy load, e.g. water, which absorbs the excess energy. Although found as a separate piece of equipment, they are almost always included in the microwave generator appliance (Thostenson and Chou, 1999, Metaxas and Meredith, 1983).

4.6.4.2 Directional coupler and power meters

For the purposes of process optimisation and control, it is important to reliably quantify the power absorbed by the load. Power meters are instruments capable of measuring electrical power at microwave and radio frequencies. Although several models exist, they all have in common a power sensor connected to the microwave transmission line and a transducer that delivers power readings to a dedicated software (Boonton, 2015).

Along the microwave transmission line, a directional coupler is recognised as a four port circuit. Two ports are connected to the magnetron-applicator line, while a small proportional amount of forward and reflected waves are separated towards the remaining ports and measured by the power meters located there, giving an idea of the power absorption in the system (Meredith, 1998, Thostenson and Chou, 1999).

4.6.4.3 Vector network analyser (VNA) and tuners

Once the microwave applicator has been selected and the load has been placed within it, it is of interest to investigate whether the specimen is located in the area of maximum electric field for accomplishing both an efficient and uniform microwave heating. A vector network analyser is an instrument that combines the attributes of a microwave source and a spectrum analyser. When connected to the rig substituting the magnetron, it is capable of measuring the network parameters of the system in a determined frequency range, e.g. reflected power, giving information of the matching between the microwave source and the load (Dunsmore, 2012, Metaxas and Meredith, 1983).

In order to locate the specimen in the area of maximum electric field, the alternative to physically moving the load is the utilisation of components called tuners. These are used to match the load with the microwave energy, minimising the amount of reflected power through the adjustment of the electric field distribution (Thostenson and Chou, 1999, Regier et al., 2016). There are two types of widespread use.

4.6.4.3.1 Stub tuner

Forming part of the transmission line, its main difference with a regular waveguide is the variable number of adjustable screws inserted on top of it. Each is connected to a stub that can vertically move inside the waveguide, thus modifying the field distribution. This device is used for fine tuning and it is especially effective when automated, allowing for the dynamic modification of the field to account for the changing dielectric properties of the load during processing (Golio, 2000, Srivastava and Gupta, 2006).

4.6.4.3.2 Sliding short

This manually or automatically controlled line termination typical of single mode applicators is commonly used in rectangular waveguides like that in Figure 4.10. Essentially, it consists of a conductive wall or piston that electrically contacts the applicator walls perfectly, effectively becoming a short circuit. Combined with a plunger or screws, the short can move along the cavity broadly modifying the electric field distribution inside it in order to optimise energy delivery to the load (Golio, 2000, Meredith, 1998).

4.6.4.4 Microwave leakage seals

Especially in high power open ended microwave systems, leakage of microwaves can pose a serious safety problem, where the maximum permitted emissions range 1-5 mW/cm^2 when measured at a distance of 5 cm from the applicator wall (ICNIRP, 2009, Meredith, 1998). Microwave leakage is often found in doors, inlet/outlet ports and other openings of an applicator (Metaxas and Meredith, 1983).

In laboratory scale systems, leakage minimisation is usually achieved by adding to the openings below cutoff attenuation ducts, commonly termed chokes. These are essentially either a cylindrical or rectangular duct whose geometry quickly diminishes the wave amplitude, ensuring the attenuation of the microwave signal prior to leaving the system (Mehdizadeh, 2015). Relatedly, multimode systems generally use quarter wavelength chokes as a door seal, where through the characteristic properties of a quarter wavelength, discussed elsewhere (Metaxas and Meredith, 1983), there is a virtual short circuit that minimises leakage despite the presence of dirt or small gaps between the door and the cavity wall (Chan

and Reader, 2000). Finally, in the case of industrial scale processes, their openings may be too big to allow for efficient wave attenuation. Hence, it is commonly added to the choke conduction resonant/reflective stubs, or an absorbing material lining, e.g. double corrugated chokes and ferrite materials respectively, or a combination of both. Choke design is tabulated upon working parameters such as the microwave frequency and the size of the hole (Catalá-Civera et al., 2006, Mehdizadeh, 2015).

4.6.4.5 Temperature measurement equipment

The high temperature treatment of inorganic materials has attracted a lot of attention towards the precise monitoring of heat transfer processes during heating (Bykov et al., 2001, Saltiel and Datta, 1999, Chandrasekaran et al., 2012), where often the main drivers are the minimisation of hot spots and thermal runaways (Metaxas and Meredith, 1983, Nüchter et al., 2004). Among the available monitoring methods, shielded thermocouples and fibre optics sensors are widely used due to their cost effectiveness and accuracy respectively. However both constitute contact-based sensors, thus still influencing the electric field distribution to a small degree (Nüchter et al., 2004, Saltiel and Datta, 1999). A contactless solution would be the use of IR sensors.

However, none of the available alternatives manages to solve the fundamental challenge of temperature sensing during microwave processing, namely that the volumetric heating of the load is not ideal and its core tends to be hotter than the monitored surface. The justification for this thermal gradient may be the heating losses from the specimen to a cooler ambient, penetration depth issues or the particular shape of the treated specimen (Vadivambal and Jayas, 2010, Hossan et al., 2010). Consequently, conservative temperature values will be obtained when monitoring a microwave process. Moreover, in the context of multicomponent heterogeneous materials with contrasting coupling with the microwave field like clays, the measured temperatures can only be understood as a biased attempt to the average temperature of the system.

4.7 Outlook on the microwave heating of clays and clay constituents

Despite considering ceramic materials as thermal insulators, microwave heating has attracted lots of attention in this sector. This is underpinned by more than 5500 research papers since 2010. This is explained by microwaves' direct energy delivery at a molecular level without constraints such as thermal conductivity, e.g. ≈ 0.49 W/m K for clay at room temperature (Dondi et al., 2004), which translates into a minimisation of thermal gradients (in a homogeneous material) and a reduction of structural tensions.

The aim of this section is to provide a review of previous work on the microwave processing of clay materials in order to assess what was the underlying motivation for using microwaves, which techniques and system configurations were capable of delivering successfully heated products, what challenges to the microwave processing were identified and how were they overcome. This section starts by addressing investigations where microwaves were used to heat clays at small/laboratory scale. Next, studies on the microwave processing at laboratory scale of each of the major clay constituents as single minerals are presented. Finally, previous work on the microwave firing of clays at industrial scale is detailed.

Many studies have been conducted and there are already several review papers published in the area of microwave processing of ceramics (Benavente et al., 2015, Borrell et al., 2014, Agrawal, 2010, Singh et al., 2016, Kim et al., 2012, Bhattacharya and Basak, 2016, Mandal and Sen, 2017). However, the field of ceramic materials is large and while there is significant ongoing development of new microwave treatments to produce complex ceramic materials with superior properties, e.g. $CaCu_3Ti_4O_{12}$, ZrB_2–B_4C, Si_3N_4–Y_2O_3–Al_2O_3, TiN–AlN and Al-B_4C (Das et al., 2009, Oghbaei and Mirzaee, 2010, Zgalat-Lozinskii, 2015, Ghasali et al., 2016), there is less interest in the microwave processing of traditional ceramics such as clays (Menezes et al., 2007, Binner and Vaidhyanathan, 2009). An explanation might be that most of the microwave processes implemented are driven by economic factors, either to improve process throughput or to make it economically feasible (Rybakov et al., 2013), while the clays sector is a mature market and conservative towards changes (Køster, 2014). Another reason may be the critical importance of the applicator design for achieving an optimal energy delivery and scale up, availability of high power generators, and the homogeneity and variability of the raw materials.

The microwave heating of clays can be divided into “low” and “high” temperature processing. Low temperature processing deals with the drying of clay’s moisture (Hammouda and Mihoubi, 2014, Itaya et al., 2005). However, the heating is driven by the presence of moisture and the clay’s temperature increase is secondary. On the other hand, the high temperature microwave treatment of clays has been extensive in the field of porcelains, where sanitary ware, electrical or dental porcelain are among the most common final products (Pendola and Saha, 2014, Menezes et al., 2007, Medeiros et al., 2015, Satapathy, 2009, Lerdprom et al., 2017, Santos et al., 2013, Monteiro et al., 2011, Pereira et al., 2016, Harabi et al., 2016). For this type of applications, the aim is to achieve the fast sintering of a specimen of complex shape while avoiding thermal stresses. In these studies, the addition of microwaves takes place in order to increase the heating rate, so clays are heated up to around 1200 ^{o}C in less than 120 min as opposed to the more conventional 8-12 h.

Looking at the dielectric properties of major clay constituents of Table 4.1, clays can be regarded as low loss materials. This would explain why most of these studies use susceptors. The most common susceptors used for ceramic processing are carbon based materials and metal oxides, either lining the surface of the load or as the sample's support (Lasri et al., 2000, Bhattacharya and Basak, 2016, Acevedo et al., 2015, Bhattacharya and Basak, 2017, Li et al., 2018, Borrell et al., 2014). Susceptors are high loss materials, and therefore strong microwave absorbers, e.g. SiC $\varepsilon'' \approx 0.4\text{-}1.71$ at 2450 MHz and at room temperature (Zhang et al., 2002, Heuguet et al., 2013). As a result of adding a susceptor to the load, its potential for microwave processing is improved (Bhattacharya and Basak, 2016). In clays processing, SiC is the most frequently employed (Santos et al., 2013, Monteiro et al., 2011, Bhattacharya and Basak, 2017, Thuault et al., 2014, Santana et al., 2017).

The fact that the susceptor is the one actually coupling with the microwave field results in the clay being heated conventionally by the susceptor, normally through conduction. This can cause localised heating in contact surfaces, giving rise to hot spots and thermal gradients. Consequently, the benefits of the volumetric heating of the clay may be reduced. Nevertheless, in general the quality of the treated products has been found to be comparable to conventional porcelains, e.g. porosity, hardness, flexural strength.

The suggestion that clays cannot be successfully heated with the sole use of microwave energy, extracted from these studies, is mainly driven by the constant use of susceptors and should be considered in context with the materials and microwave systems used for the processing. Although ceramics under a microwave field tend to heat progressively better as they get hotter, particularly above 900 ^{o}C, they usually display a low coupling with microwave energy at low temperatures (<300 ^{o}C) (Tiwari et al., 2016, Medeiros et al., 2015). The addition of susceptors helps on improving that coupling at the early stages of the microwave treatment. Added to this, almost all published microwave-clay studies use single or multimode resonant cavities. However, these are generally not specifically designed for the materials to be treated, e.g. single mode rectangular or cylindrical waveguides and modified domestic ovens. As a result, these systems cannot provide the necessary high electric field intensities that would heat the clays without the need for heating aids.

It is also worth noting that although in ceramics processing better microwave/material coupling has been found at higher frequencies, e.g. 7-8 GHz (Jadhav et al., 2015) and 22 GHz (Kishimoto et al., 2015), the overwhelming majority of clays heating experiments take place at 2450 MHz. This may be explained by the desire of the authors of avoiding issues of electromagnetic compatibility, as this ISM frequency is universally valid (ERC, 2000). Another option is that the most readily available commercial microwave equipment works at

this frequency (Metaxas and Meredith, 1983). This approach in the use of susceptors and non-specialised microwave applicators results in a lack of quantitative understanding of the microwave/material interaction and how this influences the electric field distribution and the heating performance of any system.

As a direct consequence of the lack of a specialised microwave design, the major challenge in the manufacturing of clay products using microwave energy is the presence of thermal gradients during processing. The nature of the electromagnetic waves distribution in a microwave applicator leads to the formation of areas of high and low electric field strength (Mehdizadeh, 2015), which are the main cause of the heating non-uniformities. Moreover, the susceptor-clay arrangement may further increase the temperature profiles imbalance. Added to the subsequent hindering of the product mechanical properties due to structural tensions, the clay may start melting given a substantial enough hot spot. This can easily develop into thermal runaway since molten ceramics are essentially molten ionic salts that ought to present an enormous degree of microwave coupling due to their ionic conductivity (Gheribi et al., 2018, Reddy and Adams, 2017).

Some previous works used single mode cavities in an attempt to improve the thermal uniformity of the system (Lerdprom et al., 2017, Harabi et al., 2016). The highest degree of uniformity was reached by aligning the clay specimen with the area of high electric field intensity. However, single mode applicators severely constrain the sample's size depending on the frequency of interest, as seen in Section 4.6.3. Thus, they are not the most suitable choice for scale up. Other authors relayed on the added uniformity obtained by the overlapping modes of a multimode applicator. This also enabled the processing of larger loads (Pendola and Saha, 2014, Satapathy, 2009, Santos et al., 2013, Monteiro et al., 2011, Pereira et al., 2016). However, issues with the thermal uniformity of the system persisted, e.g. surface cracks still appeared on the load. Different research studies proposed additional solutions. In Monteiro et al. (2011), besides using SiC as the base of the load and the lining of the cavity walls, table turners and mode stirrers were added to heat utilitarian porcelain cups over 1200 ^{o}C. The minimisation of the thermal gradients was readily visible in the elimination of structural tensions that caused the breakage of the load. Going beyond the addition of mode stirrers and table turners, Santos et al. (2013) focused on homogenising the electric field distribution in its microwave oven by using a multiple generator configuration. The multimode cavity used for heating porcelain tableware was fed through WR-340 rectangular waveguides by 6 magnetrons working at 1 kW. The microwave sintered porcelains showed similar impact resistance, porosity, water absorption, and phase compositions to conventionally sintered porcelains.

A critical and often overlooked parameter prone to affect the thermal uniformity of the microwave treatments is the clays' composition. Porcelains are generally composed of only three major minerals whose composition can vary greatly. The most common species are kaolin, feldspars and quartz (Boussak et al., 2015, Barrachina et al., 2017, Njindam et al., 2018, Harabi et al., 2016). Given the significant dielectric contrast among clay constituents presented in Table 4.1, the generation of significant thermal gradients within the clay body is to an extent inevitable unless its heterogeneity is minimised. Among the major clay constituents identified in building clays, the clay minerals phase, i.e. kaolinite, montmorillonite and muscovite, appears to display the highest potential for microwave processing, according to Table 4.1. Robinson et al. (2014) reached a similar conclusion when performing the extraction of oil from low and high grade tar sands using microwave energy. Apparently, only the presence of clay minerals enabled the microwave processing of oil sands beyond free and physically bound water removal (>250 ^{o}C), as they were selectively heated by the microwaves and in turn conventionally heated the rest of the sand. This processing approach can easily take place in building clays, as per Table 3.1 they can present large amounts of clay minerals.

Looking into the species that make up building clays, their major constituents have been subject to single-mineral microwave treatments. This is explained by the technological importance of some of their resultant products, as they are used as insulators, catalysts, optical instruments, etc. One of the most prominent species investigated is the clay mineral kaolinite. This mineral is a precursor in the synthesis of zeolites (Abdullahi et al., 2017, Jamil and Youssef, 2016, Fahmy et al., 2016) and cordierite (Akpinar et al., 2015, Song et al., 2016b). Yet, the main reason for the interest in this mineral comes from its use in the synthesis of mullite (Navarro et al., 2014, Zhang et al., 2014, Hammouda and Mihoubi, 2014, Thuault et al., 2014, Taurino et al., 2017, Akpinar et al., 2012, Ebadzadeh, 2010). Mullite is a high temperature constituent of clays, as seen in Figure 3.4, which is commercially sought due to its fracture toughness, low thermal expansion and conductivity, high creep resistance and corrosion stability (Navarro et al., 2014, Cividanes et al., 2010, Sarkar et al., 2012).

Conventionally, mullite is synthesised from aluminosilicate precursors, normally kaolinite pressed powders, by heating them to temperatures ranging 1200 ^{o}C to 1600 ^{o}C in cycles that last between 2-8 hours (Pereira et al., 2014, Sadik et al., 2014, Santana et al., 2014, Sahraoui et al., 2016, Bagchi et al., 2010). The utilisation of microwave energy for the mullite synthesis reduces the length of the treatment to less than 40 min and subsequently the energy consumption. A clear example of the potential of microwaves for the fast processing of clay materials comes from Zhang et al. (2014). This author reports microwave heating cycles on kaolinite where the load reaches 1200 ^{o}C as fast as in 2 min and without the addition of

susceptors. This is achieved in a single mode rectangular TE_{10} waveguide, while working at 550-1000 W and at the frequency of 2450 MHz.

In general, the treatment of kaolinites relates to that of clays in the utilisation of commonplace single mode (Zhang et al., 2014, Akpinar et al., 2012) and multimode (Navarro et al., 2014, Thuault et al., 2014, Taurino et al., 2017) cavities and the utilisation of the 2450 MHz frequency, probably for the same reasons mentioned for clays. Moreover, the kaolinite treatment is sometimes multicomponent, as alumina is often added in a 1:1 to 1:2 ratio to fuel the mullite synthesis, since it forms up to 70% of mullite stoichiometry (Navarro et al., 2014). Nevertheless, a major difference has been pointed out in the work of Zhang et al. (2014). Namely, susceptors are not mandatory for the fast heating of kaolinite over 1000 ºC. For this mineral, the addition of SiC susceptors has been justified for increasing the thermal uniformity of the load. This is explained by the SiC heating from the outside to the inside of the material, while microwaves tend to heat the core of a substance more than its surface due to heating losses of the sample to the ambient. The minimisation of heating non-uniformities provided by microwaves is critical, as it resulted in improvements of the microstructure and mechanical properties of the products through their uniform densification.

In Thuault et al. (2014), the effect of the addition of susceptors on the thermal uniformity of complex 16x11x3.5 cm kaolin pieces was investigated. Direct microwave heating of the load in a multimode cavity at 6 kW beyond 1000 ºC led to its highly non-uniform sintering, with the presence of hot-spots and non-sintered zones. On the other hand, the addition of SiC susceptors managed to reduce the magnitude of the thermal gradients, and the products sintered completely and without shape distortions. In this work, the potential of microwave energy to achieve energy savings was also reported, as the 34 kWh necessary for the conventional sintering were reduced to around 6 kWh. Furthermore, in Thuault et al. (2014) the enhanced densification effects of microwave processing were recognised, as microwaved products presented 96% of the ideal pore-less density while keeping fine sized grains. As a thumb rule, conventional means reach a limit at 95% densification unless significant grain growth is allowed (Anggono, 2005, Sadik et al., 2014, Bodhak et al., 2011).

The effect of the microwave processing can also be seen in Akpinar et al. (2012) in the toughness of the final products. The rapid heating to 1500º C using SiC susceptors managed to avoid triggering a large degree of grain growth that would take place otherwise, and so microwaved samples almost doubled the conventional products toughness.

Other clay minerals present in building clays such as montmorillonite have also been used to synthesise mullite using microwave energy (Santana et al., 2014, Gomes et al., 2010, Santana et al., 2017, de Lima Santana et al., 2015). However, this has been investigated to a lesser

extent. The reason is that most montmorillonite treatments really take place on bentonites, a mineral whose mayor constituent is montmorillonite but that can also present impurities such as kaolinite and iron oxides (Gonçalves et al., 2015). Moreover, montmorillonite stoichiometry is more variable than that of kaolinite (Grim, 1968). As a result, this synthesis path produced mullite not as pure as that achieved when using kaolinite as the raw materials, e.g. up to 98% (Ebadzadeh, 2010).

The change of raw materials does not affect the microwave process, as montmorillonite powders were reported to be heated near 1600 ºC in less than 30 min, commonly using domestic multimode ovens at 2450 MHz. As in the case of kaolinite, SiC susceptors were often added to increase the microwave coupling at low temperatures. However, de Lima Santana et al. (2015) proved that this mineral could be heated to sintering temperatures in under 20 min without the need for heating aids. Santana et al. (2017) reported that microwaved specimens differed from conventionally processed ones in their lower grain growth resultant of the shorter heat treatment, which hints towards the higher mechanical properties of the microwaved mullite.

Montmorillonite is also used in the manufacturing of pillared interlayer clays. These have attracted attention as adsorbents and catalysts. Conventional processing methods consist on the intercalation of inorganic polyhydroxylated species of Al, Zr, Ti, Fe with a montmorillonite matrix through its calcination in the 350-750 ºC range (Sun et al., 2006, Martinez et al., 2017). Utilisation of microwave energy has been found to hasten the pillared composite synthesis down to 15 min (Laysandra et al., 2017, González et al., 2017, Chemat-Djennia et al., 2016). As above, treatments generally took place in domestic multimode ovens at 2450 MHz. It is worth noticing the absence of susceptors in the processing. However, it is possible that the interlayered mineral species acted as such, as they appeared in a 10-30 mmol/g montmorillonite ratio.

The last of the clay minerals found in building clays, i.e. muscovite, has not attracted the same degree of attention for microwave processing as an individual species. Probably due to its comparatively higher thermal stability than the other clay minerals but with more stoichiometry variation than kaolinite (Grim, 1968, Reeves et al., 2006). The microwave treatment of shales and bedrocks composed to a large extent of muscovite for the extraction of vanadium has been reported (Yuan et al., 2017, Wang et al., 2018b, Wang et al., 2018a). Conventionally, direct acid leaching and roasting of the raw materials at around 850 ºC is used for processing times as long as 3 h (He et al., 2007, Liu et al., 2010). The utilisation of microwaves provided higher extraction yields in treatments ranging 30-150 min due to its improved heat diffusion across the load. However, in the heating of the specimens in

commercial multimode ovens at 2450 MHz, the uneven heating of the load was reported. Yuan et al. (2017) noted upon treatments in the 700-950 ºC range that vanadium leaching decreased with the progressive sintering of the muscovite. In conventional trials this took place beyond 950 ºC, but in microwave samples it occurred in the 700-900 ºC range. This is an example of hot spots generation, subsequently causing the localised sintering of the muscovite. These hot spots may have been generated or enhanced by microwave absorbent carbon, which is usually contained within the raw materials and probably acted as a susceptor.

One of the few examples of muscovite heated as a single mineral by microwaves is seen in Faeghi-Nia and Ebadzadeh (2012). This author aimed to compare the proficiency of conventional (electric furnace) and microwave (multimode oven at 900 W and 2450 MHz) processing to produce tough composites of low thermal conductivity by thermal treatments in the 600–1050 ºC range for 10 min. The machinability of microwaved samples was proved to be superior as it displayed grains with an aspect ratio of 10 compared with that of conventional samples, which had a 5 aspect ratio and reported cracks across the load surface. It is noteworthy that the microwave treatment took place in the absence of susceptors.

The study of the other major clay forming minerals, calcite, feldspars and quartz, is scant. Single-mineral microwave treatments of these species are uncommon. This may be explained by their low microwave coupling seen in their dielectric properties of Table 4.1. As such, calcite has been processed with microwave energy accompanied by with other components that focus the microwave coupling, e.g. bacterial cellulose (Stoica-Guzun et al., 2013), pyrite (QIN and DAI, 2015), galena (Like and Jun, 2016), polyol (Yu et al., 2015), hydroxyapatite (Chen and Leng, 2015), and other aluminosilicates (Petri Jr et al., 2017).

An example of microwave energy selectively delivered to only calcite is seen in Hwang et al. (2014). This author used microwaves to calcine calcite at 950 ºC in order to synthesise CaO. The microwave treatment took place in a 3 kW rotary microwave kiln at a 3º angle rotation working at 2450 MHz, and managed to produce high purity CaO (98%) at 1/8 of the time required by the conventional process. However, the low microwave coupling of calcite was noted as SiC susceptors were required to heat the load. This was also confirmed by Lu et al. (2017) when submitting different rock forming minerals to 3 min microwave trials in a 2 kW multimode oven working at 2450 MHz. Here, the lack of susceptors translated in the calcite load not increasing its temperature at all.

The microwave treatment of single quartz loads is also uncommon. This is mainly due to quartz being considered as a microwave transparent material (Metaxas and Meredith, 1983, Meredith, 1998). This was recently confirmed by Shang et al. (2014) when investigating the microwave absorption of silica sands with 1-5% moisture content during drying at 2450 MHz,

as the microwave/sand coupling greatly diminished with decreasing moisture. Furthermore, the extensive work of Lu et al. (2017) mentioned above also proved that quartz has a microwave absorbance comparable to that of calcite without the use of susceptors. Any minimal improvement on its coupling may have been caused by the presence of lossier impurities or moisture within its matrix. Nevertheless, this does not mean that this material is unfit to be heated by microwaves, as Eremeev et al. (2018) managed to heat silica spheres to temperatures of up to 1300 ºC at a 60°C/min rate. This was achieved by the use of a higher processing frequency, i.e. 24 GHz, in a 3.5 kW multimode oven, and using susceptors.

Finally, previous work on the microwave heating of feldspars is the most scant of all the mineral species studied, as it is usually accompanied by quartz and calcite among others (Salakjani et al., 2017, Hartlieb et al., 2018, Akpinar et al., 2017, Snellings et al., 2016). Another reason for the lack of attention to this clay material comes from its formulation, as feldspars form a solid solution series where the distinction among the available species is challenging (Smith and Brown, 1988). This is particularly important regarding the presence of impurities or structural arrangements that may fundamentally modify their behaviour under the microwave field. Regarding the microwave heating of feldspars in the clay firing range, the thermal stability feldspars show between 20-1050 ºC, seen in Section 3.3.3, may also explain why the treatment of this material using only microwaves is of little interest. In the previously mentioned work of Lu et al. (2017), some potassium and alkali feldspars showed a behaviour to microwave radiation akin to that of calcite and quartz. A successful microwave-feldspar treatment is exemplified by the work of Liu et al. (2016). Here, microwaves where used together with conventional heating to manufacture potassium merlinoite from K-feldspar of >90% purity and potassium hydroxide. The microwave treatment lasted for 4 min and heated the load to 140-180 ºC in a multimode oven working at 2450 MHz. The addition of microwaves enhanced reaction kinetics, increasing the reaction rates 3-4 times compared with the conventional hydrothermal synthesis.

All the microwave/clay materials works described above take place at a small/laboratory scale. Despite designs for the scale up of microwave processes being available for clay materials (Dunn, 2015, Clark et al., 2005), few specialised companies such as Ceralink Inc and C-Tech Innovation have consistently delivered industrial scale microwave systems for ceramic materials. At the beginning of this chapter, the main reasons that justify the reticence for scaling up microwave processes were detailed. It is worth noting that in these industrial scale processes, microwaves have been always used in combination with conventional means, i.e. electrical or gas firing. As opposed to laboratory scale studies, industrial scale activities generally try to optimise energy use and reduce environmental footprint (Køster, 2014).

Therefore, adding extra mass in the form of susceptors will increase heat requirements and also add extra process steps/waste streams, which increments processing costs.

Looking at each company's main underlying motivation for using microwaves, the main objective in the case of the CerMAT system of Ceralink is to achieve thermal uniformity while optimising energy efficiency through shorter heating cycles (Ceralink, 2013), whereas C-Tech additionally aims for the reduction of firing temperatures and carbon footprint (C-Tech, 2016b, C-Tech, 2016a). C-tech were involved in the industrial development of a microwave system for the firing of ceramic tiles (CORDIS, 1999). A single layer roller kiln powered by gas firing was retrofitted with the addition of a 40 kW microwave generator at the preheating stage with the aim of reducing 3% the energy needs of the process. Furthermore, the microwave input caused a 32% productivity increase. However, the thermal gradients reported for laboratory scale persisted here, and thus the mechanical properties of the fired products did not surpass that of conventionally processed tiles.

4.8 Summary of literature review

In Chapter 3, the heterogeneous nature of clays and the variability of their constituents among deposits were addressed. In spite of this, industrial brickmaking techniques are similar in many ways although critically reliant on empirical knowledge. As with other ceramics, heat transfer limitations dominate the firing of clays, especially at critical temperatures. So, uniform heating is achieved by tight temperature control, increasing the processing times up to 40 h and establishing slow heating rates of around 55 ^{o}C/h. The quality of the brick is assessed by characteristics such as colour, texture, size variation, compressive strength, water absorption and durability, but it is not based on its mineralogy, as the numerous reaction paths during firing are only known in general terms. Lastly, despite extensive optimisation attempts energy costs average around 2.6 MJ/kg of fired material where fossil fuels are the main energy source, thus additionally contributing to significant greenhouse emissions of around 57-95 kg CO_2/GJ.

In order to overcome thermal limitations and avoid the use of fossil fuels, microwaves can be considered as the energy source for clays. The first step in the microwave system design ought to be the study and quantification of clays dielectric properties. Among available measuring techniques, resonant cavity, waveguide transmission line and coaxial probe appear to be the most suitable for assessing clays, where it is critical to control parameters such as composition, density, temperature and frequency. Previous dielectric property studies on clays and their constituents are incomplete, probably due to the specialised nature of microwave metrology equipment and expertise. An alternative is the estimation of clay dielectric properties from their forming minerals through mixing rules equations, which has been

successfully applied to clay materials in the past (Brovelli and Cassiani, 2008, Nelson et al., 1989). Previous studies demonstrated that clays are composed of microwave transparent materials like quartz, calcite and feldspars, while the clay minerals phase contains moderate microwave absorbers that will probably be selectively heated during processing.

Microwave energy has been widely regarded as an alternative heating method in the ceramics sector. One of the reasons for the utilisation of microwaves is the direct coupling of microwave energy with the material, overcoming heat transfer limitations due to low thermal conductivities and thus allowing the fast heating of large and complex shaped loads with minimal thermal gradients. Another is the generally improved mechanical properties of the material as a consequence of its enhanced densification and homogenous grain distribution, where the reduced processing times also caused lower grain growth. Traditional ceramics such as clays have been generally out of the scope of the microwave treatment, being mostly studied in the porcelains sector. On the contrary, clay minerals like kaolinite, montmorillonite and to a lesser extent muscovite have enjoyed much more attention as their processing often ends with products of technological importance and therefore, higher commercial value. Finally, species like quartz, calcite and feldspars are hardly ever addressed for microwave processing due to their microwave transparency.

Despite the wide utilisation of microwaves on clays and related materials, microwave processing is generally based on empirical knowledge and experience. So, rather than designing an applicator for the optimal heating efficiency and handling of the load, multi-purpose equipment is often used where single mode and particularly multimode resonant cavities are the most employed. Additionally, in most works there is a lack of a dielectric characterisation of the raw materials. As a result, there is limited understanding of the interaction of clay materials with microwaves, which limits the optimum use of microwaves and causes the poor design of microwave reactors. Consequently, uneven heating is one of the main challenges of these processes. Furthermore, although there are reported instances of clays and clay minerals being successfully heated solely with microwave energy, microwave/material coupling issues at low temperatures are commonplace and are dealt by adding susceptors like SiC.

The lack of understanding regarding microwave/clay interactions, together with the contradictions found in previous work regarding the suitability of microwave energy to produce heated clays of quality comparable to that of conventional products, results in very few instances of clay materials being treated with microwaves at industrial scale. Although energy savings are reported in these cases, a step-change on the quality of the fired products from conventional techniques has not been reached.

This thesis addresses the limitations in the current state of the art in microwave-clay processing, with the specific aim of developing an understanding of how microwaves interact with clays in order to show whether they alone can be used to fire clay-based building materials, and to understand how this can be achieved. This understanding will help to determine the potential to use microwave heating in the production of clay building materials.

The specific objectives of this study are:

- Determine whether common European clays can be fired solely by microwaves, investigate how this is affected by other parameters such as temperature, identify the main constituents contributing to this heating and quantify their effect on clays' potential for microwave heating.
- Determine if building materials of comparable quality to conventionally fired bricks can be produced using microwave heating alone.
- Investigate the economic, environmental and legislative assessment of the potential to use electromagnetic heating in the production of building materials.

5 MATERIALS AND EXPERIMENTAL TECHNIQUES

5.1 Introduction

In the previous two chapters, the literature related to the characterisation and conventional processing of clays in brickworks. Moreover, the microwave theory and previous work on the microwave processing of clays and clay constituents have also been reviewed. In order to fulfil the aim and objectives enumerated in Chapter 2, this information has been applied into the design and performance of a number of characterisation and microwave heating experiments regarding clays and their constituents. The aim of this chapter is to enumerate the materials handled in this thesis and describe the methodology of the experiments undertaken.

This chapter starts with a description of the clay materials used in this project, followed by the pre-treatments they underwent to become specimens fit for the ensuing studies. Subsequently, the methodologies of these materials' characterisation are described. First, clays and their constituents' liquid and solid phases were quantified through moisture and X-ray diffraction analyses. An investigation of their porosity was possible from insight into their bulk density and void fraction provided by manual volume measurements and a helium pycnometer. Knowledge of clays evolution with temperature was obtained from thermal gravimetric and differential scanning calorimetry analyses. The microwave/clay interaction was quantified through dielectric property measurements using a resonant cavity, a transmission waveguide and mixing rules predictions. After clay characterisation, the methodology of their microwave heating trials is explained. Then, the different methods used for the quality analysis of the fired products are detailed. Finally, the economic and environmental viability of an industrial scale microwave clay firing system are discussed. Further justification of some of the paths pursued can be found on their respective results sections in Chapter 6 and Chapter 7.

5.2 Materials

The main raw materials investigated in this work were red and yellow Danish clays commonly used in building applications from the Strøjer Tegl, Randers Tegl A/S and Helligsø Teglværk brickworks. Specifically, the varieties of Helligsø red, Hammershoj red, Vedstaarup yellow and Hammershoj yellow, which were provided by the Danish Technological Institute (DTI). Additionally, other European clays from brickworks remaining anonymous for confidentiality reasons were studied, i.e. Spanish yellow, Dutch red and English red. Major clay constituents were also used in the investigation. Sweden's calcite, Norway's albite and Pakistan's orthoclase were provided by Richard Tayler Minerals, while 99.97% pure quartz

was supplied by Multi-Lab. Regarding the clay minerals, Fithian muscovite, Upton montmorillonite and Larmor kaolinite, described in American Petroleum (1951), were dispensed by the department of geoscience of the University of Aarhus. Upon reception, all specimens were subjected to a moisture homogenisation, which consisted in an oven drying at 110±5 ºC for 14±2 h, followed by a 20 min cooling down in a desiccator as per ASTM D2216.

5.2.1 Materials preparation

Solid slabs and powders of clays and single clay constituents were required for the characterisation studies. Powders capable of passing through a <150 μm sieve mesh were obtained through crushing unfired bricks and large mineral chunks using a KHD Humboldt Wedag AG for 60 s. Then, representative powdered samples of 1 g were obtained using a Rotary Micro Riffler following ASTM B215. Manual shaping of clay and mineral chunks through the use of hammer, chisel and metal file provided 19.2±1.0x3.2±0.4 mm cylinders for resonant cavity dielectric property measurements, 20.3±0.6x20.1±0.5x20.4±0.5 mm cubes for moisture and density analyses, and 34.3±0.6x90.1±0.7 mm prisms for waveguide dielectric property measurements.

Regarding the microwave heating trials, cylindrical clay specimens were manually extruded from clay slurry using sharp edged hollow metallic rings. The slurry was delivered at the same moisture conditions as in brickworks (≈20% water content) and was wedged as explained by Clark (1983) to eliminate internal porosity prior to shaping. The resultant clay cylinders of sizes 25.0±0.5x20.1±0.3 mm and 25.2±0.6x35.3±0.4 mm were hardened through an oven drying at 110±5 ºC for 14±2 h. Imperfections were later removed though filing. The final specimens are displayed in Figure 5.1.

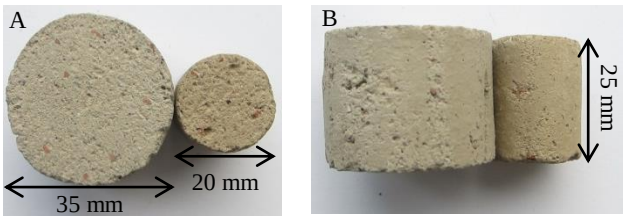


Figure 5.1- Aerial (A) and side (B) views of unfired 25x35 mm yellow and 25x20 mm red clay cylinders.

5.3 Materials characterisation

5.3.1 Equilibrium moisture

Both clay and clay constituents were subjected to a moisture measurement following ASTM D2216. Five samples of every material as cubes and powders were used for the analysis. The powdered samples ranged 20-30 g. Drying took place in a conventional oven set

at 110±5 ºC for 14±2 h. Afterwards, the specimens were cooled down for 20 min in a desiccator. The moisture computation on a dry basis was attained using Eq. 5.1,

$$w = \frac{M_W - M_D}{M_D}\ 100 \qquad \textbf{5.1}$$

where w (%) is moisture content, M_W is the mass of the wet specimen and M_D (kg) is the mass of the dry specimen.

5.3.2 X-ray diffraction

A quantitative assessment of the mineralogical composition of unfired, conventionally and microwave fired clays was carried out using a PANalytical X'Pert Pro series diffractometer. Equipped with a cobalt-target tube and a X'Celerator detector, this device operated at 40 kV and 20 mA. Each powdered sample was scanned within a 2θ (º) range of 4.5º-85º at 2.06°/min. Diffraction data was analysed using a PANalytical X'Pert HighScore Plus version 4.6 software coupled to a PDF-4+ mineral database of the International Centre for Diffraction Data (ICDD). Phase quantification was achieved using the Rietveld refinement technique (Snyder and Bish, 1989). A single measurement was performed for each red and yellow sample. Hence, errors for the mineral concentrations ranged ±2.5% for >60 wt%, ±5% between 60-30 wt%, ±10% between 30-10 wt%, ±20% between 10-3 wt% and ±40% for <3 wt %. Phases with concentrations below 1% were assigned a value of <1%, since the associated error became too large (Hillier et al., 2001).

Prior to the measurements, clay powders were sampled into ≈4.5 g portions. These were then micronised under deionised water with 10% corundum (American Elements-PN:AL-OY-03-P) for 10 min, in order to provide a finer and uniform particle-size for powder XRD analysis. The addition of corundum served both as an internal standard for the quantifications and for the detection of amorphous species. After oven drying at 55±5 ºC for 14 ±2 h, the powders were spray-dried following Hillier (1999) and loaded onto stainless steel sample holders.

The typically overlapping peaks of some clay minerals were taken into account by repeating the experiences on powders that had been additionally glycolated and heated at 400 ºC and 600 ºC, as described by Brindley (1955) and Hathaway (1956). In doing so, the chlorite-kaolinite and montmorillonite-muscovite pairs were respectively separated.

5.3.3 Bulk density and void fraction

The common bulk density determination using water immersion as described by ASTM C128 was not feasible in this case, since clay disaggregates in water. Alternatively, five cubes of clays and clay constituents of known dimensions, thanks to manual calliper measurements,

had their mass weighted in a conventional mass balance. Bulk density could be then calculated from Eq. 5.2. Three repeats were performed per sample,

$$\rho = \frac{M_D}{V} \quad \textbf{5.2}$$

where ρ (kg/m^3) is density, M_D (kg) is dry mass and V (m^3) is volume.

Void fraction was computed following ASTM D5550. Five powdered specimens of each clay and mineral ranging 4-6 g had their particle volume, i.e. bulk volume minus the pores volume, measured ten times by employing the gas displacement method using an Accupyc 1330 Helium pycnometer. Solid slabs were not used in the experiences due to the probable presence of closed pores.

The system consists of a pressure transducer and two chambers, where one contains the sample and the other serves as an internal reference. During processing, the sample chamber is pressurized with the inert gas, where its molecules rapidly fill pores as small as one angstrom in diameter. Once stabilised, the gas is allowed to expand into the reference chamber and the pressure drop is recorded. The pressure drop difference caused by the presence of a sample serves to calculate its volume using Eq. 5.3 (Malczyk, 2007),

$$V_p = V_S + \frac{V_R(P_b - P_{Am})}{P_y - P_b} \quad \textbf{5.3}$$

where V_p (m^3) is the volume of the material without pores, V_S (m^3) is the volume of the empty sample chamber, V_R (m^3) is the volume of the reference chamber, P_{Am}, P_b and P_y (psi) are the ambient pressure, the pressure in the combined two chambers after the gas expansion and the pressure in the sample chamber before the gas expansion, respectively.

Knowledge of V_S and V_R was obtained through empty and reference measurements. The reference used was stainless steel spheres of a combined 6.37102 cm^3. Substitution of the calculated volumes into Eq. 5.2 provided the particle density of the specimens while Eq. 5.4 provided the void fraction,

$$\phi = \frac{\rho_b}{\rho_p} \quad \textbf{5.4}$$

where ϕ is the void fraction and ρ_b and ρ_p (kg/m^3) are the bulk and particle density respectively.

5.3.4 Thermal gravimetric analysis

Mineral transformations on temperature of the clay mixtures and the single clay constituents that incur in mass losses were studied through thermogravimetric analyses, which were

accomplished in a TA Q500 Thermo-gravimetric analyser (TGA). The system is a computer controlled furnace that contains a precision balance and a series of sample holders. Prior to the tests, these platinum holders were cleaned in a methane flame and tared. Dried powders of each sample ranging 20-50 μg were tested three times in the temperature range of 25-1000 ºC, following ASTM E1131. An N_2 atmosphere was selected in order to relate to the low oxygen conditions found at the height of conventional brick firing. A heating rate of 20 ºC/min was chosen, as slower rates could have forced the broadening and agglomeration of different reaction peaks and faster rates might have hindered the completion of the reactions (Stucki, 1990, Sanders and Gallagher, 2002).

5.3.5 Differential scanning calorimetry

A differential scanning calorimetry (DSC) study was used to quantify thermal transformations on clays that occur without an associated mass loss. Analyses on ≈10 mg dry powders were performed three times using a TA Instruments Q600 SDT. The rig consists of a furnace divided in two isolated chambers with a platinum sample holder each, where one has the sample and the other is empty and acts as the reference. In order to be complementary to the TGA trials, experiences took place in the 25-1000 ºC range with a 20 ºC/min rate and in a N_2 atmosphere. Before the start of the trials, the system ran the same cycle without a sample so as to build up the background signal of the sample holders.

The DSC technique was also used to determine clays' specific heat capacity. Due to the absence of a solid standard material in that temperature range (Sabbah et al., 1999), instead of following ASTM E1269 the specific heat capacity was calculated attending to its formulation as described by Stucki (1990) and seen in Eq. 5.5,

$$Cp = \frac{dH}{dT} = \frac{dH/dt}{dT/dt} = \frac{DSC\ signal}{DSC\ heating\ rate} \qquad \textbf{5.5}$$

where Cp (J/kg K) is specific heat capacity, dH (J/kg) is the enthalpy differential for a temperature variation dT (K), dt (s) is a time differential and $DSC\ signal$ (W/kg) is the heat flow difference between the sample and the reference sample holder.

5.3.6 Dielectric properties

5.3.6.1 Resonant cavity

The dielectric properties of powders and cylindrical slabs of clays and clay constituents were measured in triplicate at the close to industrial ISM microwave frequencies of 912 MHz and 2470 MHz by using the cavity perturbation method. Justification for the selection of this technique can be extracted from Chapter 4. The experiment set-up used for the measurements

is shown in Figure 5.2. The system is centred on a water cooled copper resonating cylindrical TM applicator of 58 mm height and 578 mm internal diameter, with an integrated furnace that enables high temperature measurements, an electric motor that moves the sample holder between them and a vector network analyser (VNA) that monitors the frequency and quality factor shift. These two parameters are used in the calculation of the dielectric properties. The VNA obtains their values by sending electromagnetic signals into the cavity and measuring the reflected and transmitted waves.

First, the resonant frequency and quality factor of the undisturbed cavity were determined by room temperature measurements with the empty sample holder inside of the cavity, which was a fussed quartz hollow tube of 4 mm internal diameter with an interior seal. Then, dry cylinders or powders ranging 0.3-0.9 g were loaded to the holder and inserted into the cavity until maximum perturbation was reached, according to the VNA. In the case of powders, all materials were compacted to the same void fraction for later comparison purposes. Due to the interest on processing low porosity clays in brickworks, the minimum void fraction of the least compressible substance was chosen, i.e. ≈56%. Mechanical compression was avoided so as to reduce sample anisotropies; the quartz tube was manually tapped on a fabric surface instead.

Measurements took place at room temperature and from 50 ºC up to 950 ºC with a 50 ºC step change. Soaking times of 10 min and an average 4.59±1.94 ºC/min heating rate were used to ensure thermal uniformity. The top firing temperature (≈1050 ºC) could not be reached on account of the sample holder melting beyond 1000 ºC. Alumina tubes were used in order to solve the issue. However, at high temperatures these reacted with the clay samples and were lossier than them. Also, due to alumina opaqueness, the powders compaction could not be controlled without corrupting the sample. Ultimately, the dielectric properties were calculated using the perturbation equations Eqs. 5.6-5.7 shown below (Al-Harahsheh et al., 2009),

$$\varepsilon' = 1 + 2J_1^2(X_{l,m})\frac{\bar{V}_0}{\bar{V}_S}\frac{f_0 - f_s}{f_0} \quad \textbf{5.6}$$

$$\varepsilon'' = J_1^2(X_{l,m})\left(\frac{1}{Q_S} - \frac{1}{Q_0}\right) \quad \textbf{5.7}$$

where J_1 is the first order Bessel function, $X_{l,m}$ is the mth root of the first order Bessel function ($J_1(x) = 0$), $\bar{V}_0$ and $\bar{V}_S$ (mm^3) are the volumes of the cavity and the sample respectively, f_0 and f_s (Hz) are the resonance frequencies of the empty and loaded cavity, Q_0 and Q_S are the quality factors of the empty and loaded cavity.

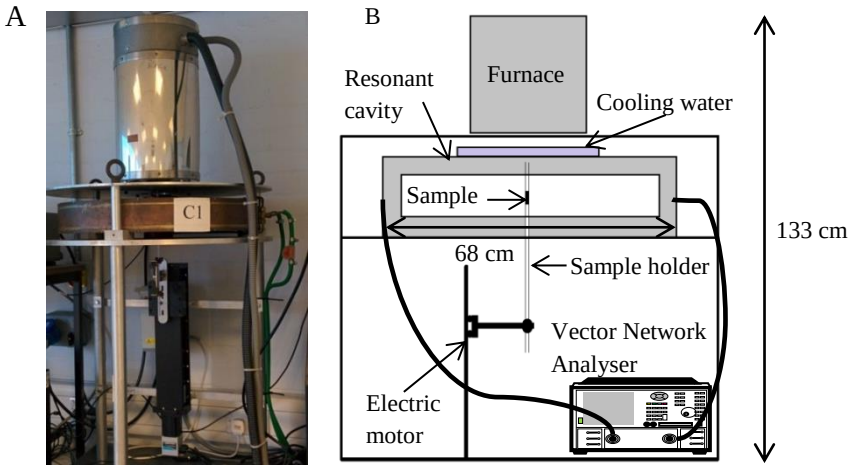


Figure 5.2- Experimental set-up of the resonant cavity used for the dielectric property measurement of clays and clay constituents as powders and 19.2±1.0x3.2±0.4 mm cylindrical slabs (A) with added schematics (B).

The measured data could have been influenced by three types of errors. These were errors caused by inherently unpredictable fluctuations in the readings, errors constant or proportional to the true values due to imperfections of the rig or its devices, and deviations from the true values due to the analysed samples not being statistically representative of the whole population of specimens, i.e. random, systematic and misrepresentation errors (Taylor, 1997). The first was accounted by the standard deviation of the measurements, where both carved and powdered specimens surpassed the limits of 1% for the dielectric constant and 5% for the losses proposed by NPL (2003). This was justifiable given their granular and heterogeneous nature.

The possibility of systematic errors on the rig was investigated through the study of a calibration material. Poly-tetrafluoroethylene (PTFE) rods of 3.5±0.1x17±0.4 mm supplied by Sigma-Aldrich were measured at room temperature using the above methodology. This thermoplastic polymer was chosen due to its low loss behaviour, availability and workability. Higher temperatures were not be investigated on account of PTFE low melting temperature (Price and Jarratt, 2002) and the thermal stability of the clay dielectric properties. In the literature, PTFE dielectric properties at 2450 MHz average around ε'=2.05±0.04 and ε''=0.002±0.001 (Ma et al., 1997, Andrade et al., 1992, Metaxas and Meredith, 1983).The cavity PTFE dielectric properties circled around ε'=2.10±0.03 and ε''=0.001±0.001. Since the uncertainty range of measured and literature values overlapped each other, no error offset could be attributed to a systematic error.

Given the heterogeneous nature of clays and the small size of the analysed samples, it was possible that the dielectric properties of the measured specimens did not align with those of the entire clay population. This was tested by investigating the statistical significance of the cavity results. Following from the symmetrical configuration of the standard deviation of the dielectric measurements, it could be safely assumed that the dielectric properties follow a

normal probability distribution. However, the utilisation of this distribution was impractical since this method requires of a large pool of sample measurements, e.g. >100, to safely compute the standard deviation of the entire population. Instead, a Student's T probability distribution was sought, as it is specifically formulated for estimating population parameters from small sample sizes (Peck et al., 2015). Specifically, a two-tailed t-test was used trying to refute that the cavity measurements aligned with the average of the entire population. This can be mathematically expressed as,

$$H_0: \mu = \bar{x} \quad vs. \quad H_1: \mu \neq \bar{x} \tag{5.8}$$

where H_0 is the null hypothesis and H_1 is the alternative hypothesis, $\bar{x}$ is the sample mean and μ is the population mean, which corresponds to a full brick.

The lack of statistical evidence to reject the validity of the null hypothesis occurs when,

$$-T_C \leq T_t \leq T_C \tag{5.9}$$

where T_t is the t value of the system, and T_C is the critical t value for a certain confidence level (Ω) and a determined number of degrees of freedom ($\varrho - 1$).

T_t was calculated following Eq. 5.10, while T_C was extracted from conversion tables (Peck et al., 2015). In this case, Ω =0.05 was stablished for a 95% confidence range due to its standard use,

$$T_t = \frac{\bar{x} - \mu}{s/\sqrt{\varrho}} \tag{5.10}$$

where s is standard deviation of the cavity measurements and ϱ is the number of measurements.

5.3.6.2 Waveguide transmission line

The dielectric properties of clay half bricks were measured in triplicate at the ISM microwave frequency of 2450 MHz using the waveguide transmission technique. Its utilisation was legitimised by the need of obtaining data from the clay population (μ) in order to validate the cavity results above. In this case, large brick shaped clay specimens were assumed to be valid representatives of the whole clay population. The waveguide rig set up is displayed in Figure 5.3. The rig revolves around two WR-284 brass waveguides, which are located inside a conventional furnace and whose ends are connected to a VNA. In order to protect the inner workings of the latter from the high temperatures reached in the TE_{10} cell, water cooling flanges and aluminium waveguides that separate the VNA connectors from the heat source were added.

Upon fully 2-port calibrating the VNA using the SOL algorithm, i.e. short, open and load calibration, the sample was placed in the middle of the brass waveguides. Measurement of the transmitted and reflected signals, namely their scattering parameters, took place at room temperature and from 200 ºC up to 800 ºC with a 200 ºC step change and 30 min of soaking times. Temperatures as high as in the resonant cavity could not be reached, as the brass waveguides would start melting around 900 ºC (Davis, 2001). Finally, the clay dielectric properties were calculated from measured data using the Newton–Raphson method (NPL, 2003).

While systematic and random errors were also present using this methodology, the increment of the sample size ensured that the specimens were representative of the whole clay population. The existence of a systematic error within the rig was tested by room temperature measurements of Foamglas T4 provided by Foamglas.uk. Using the resonant cavity at 2470 MHz, the standard values obtained averaged around ε'=1.31±0.03 and ε''=0.723±0.079 (Rodriguez Oyarzun, 2017), while the waveguide data was ε'=1.18±0.14 and ε''=0.560±0.089. As before, the uncertainty ranges of standard and waveguide measurements overlapped. The order of magnitude increase of the uncertainty range for the waveguide measurements was justified by the added error of measuring a porous granular material using this technique and the comparably higher accuracy of the resonant cavity method, as explained in Chapter 4.

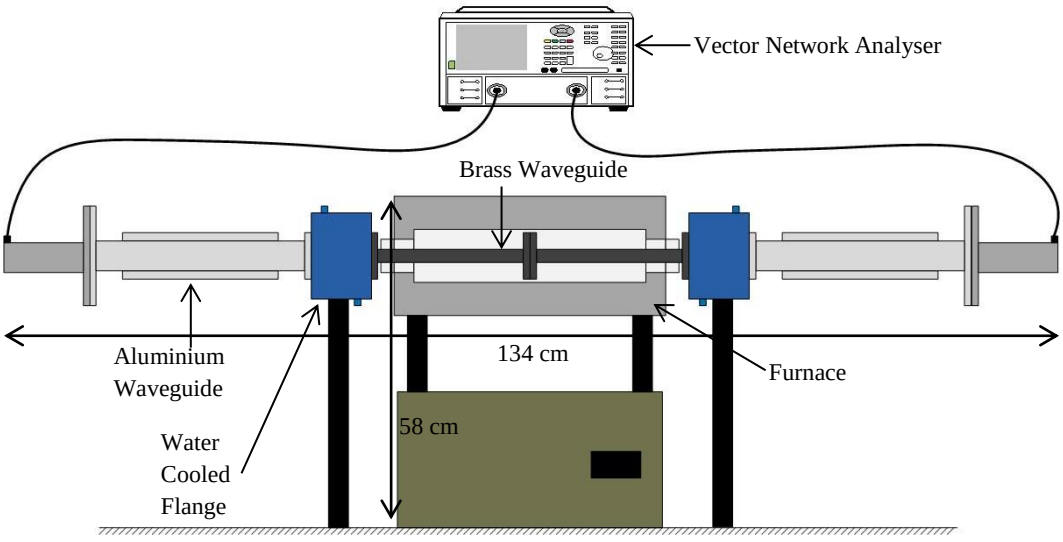


Figure 5.3- Schematics of waveguide transmission line rig used for the dielectric property measurement of 34.3±0.6x90.1±0.7 mm clay bricks.

5.3.7 Electromagnetic mixing rules

A predictive model for the estimation of the dielectric properties of clays from the dielectric properties of their constituents and their volume fractions was built using a mixing rules theoretical model. There are a wide range of mixing formulas in the literature and more details can be found in Sihvola (1999). In this work, Bruggeman-Hanai, Sen-Scala-Cohen, Lichtenecker, Landau-Lifshitz-Looyenga, Complex Refractive Index, Böttcher and Rayleigh were tested. The basis for their selection can be found in Chapter 4. An indication of an error threshold for the estimations could not be found in the literature. Instead, a conservative approach was followed as the error limit was set as the average measurement deviations of powders and clay slabs at 2470 MHz.

At first, binary clay-air mixtures were considered in an attempt to simplify the clays by not taking into consideration their mineralogy. As a result, the analysis was focused on predictions at different densities and frequencies across firing. Structurally, the system was understood as a clay matrix with air inclusions, where the latter's complex permittivity is by convention $\varepsilon'=1$, $\varepsilon''=0$ (Meredith, 1998), and its volume fraction was the porosity/void fraction of the clay. Therefore, through the modification of the air content, predictions at any density were enabled using the mixing rules of Table 4.4. Experimentally, clay powders data was used to estimate clay slabs and vice versa at both 912 MHz and 2470 MHz. The accuracy of the method was tested against measured values. The uncertainty range of the estimations could be assumed to be the same as that of the measured dielectric properties at the target void fraction. Otherwise, unreasonable errors for the estimations were obtained.

The assumption of the meaninglessness of the clay composition on the dielectric property predictions was proven by comparing the simplified model against building up the clay mixtures from their major mineral constituents. Among the available paths shown in Figure 5.4, only path C was interesting beyond the validation of the method. This was justified from the estimation of clays at their most desired state of a slab (brick) using easy to handle free flowing mineral powders. Further justification of the paths selection can be seen in Chapter 7.

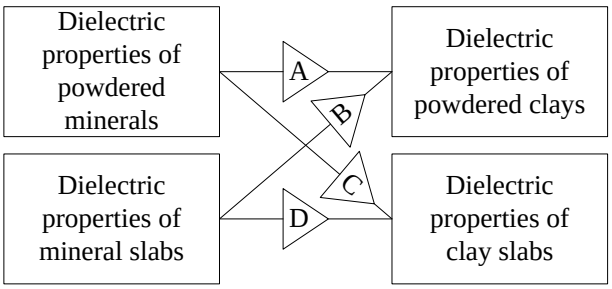


Figure 5.4- Alternatives for the mixing rules predictions of the dielectric properties of clays in mineral-clay mixtures that can be experimentally validated ,i.e. powder minerals to powder clays (A), mineral slabs to powder clays (B), powder minerals to clay slabs (C) and mineral slabs to clay slabs (D).

Initially, the procedure mimicked that of the clay-air mixtures, i.e. minerals as a mineral-air blend, so the dielectric properties of the single minerals at the void fraction of the target clay were computed in the same fashion. Combination of all the minerals using again Table 4.4 equations rendered the clay dielectric properties, where the volume fractions of each mineral were taken from the clays' XRD data at room temperature. No high temperature XRD spectra were used for high temperature estimations due to the inability of separately monitoring each mineral species during heating, particularly during the crossed reactions at the end of firing. The same reason justified the utilisation of only room temperature porosity values.

Despite its high loss factor, free water was not considered in the clay composition due to its early disappearance and the overall dryness of the samples. Yet, significant loss deviations at room temperature caused by moisture differences between powders and slabs were likely to occur, due to the linear relation between loss factor and free water content in low loss materials (Metaxas and Meredith, 1983). Hence, at the material-air calculation step, the predicted loss factors of powders or slabs below 150 ºC were cross multiplied by the moisture of the target powders or slabs in what can be called a moisture fix for the estimated loss factors.

The uncertainty of the mineral to clay estimations was related to a combination of all powdered clay constituents deviations. Given the linear combination of their dielectric properties to build up the clay, the general equation of error propagation for additions displayed in Eq. 5.11 was applied,

$$\varepsilon^*_{StdClay} = \sqrt{\sum_i f_i {\varepsilon^*_{Stdi}}^2} \qquad \textbf{5.11}$$

where $\varepsilon^*_{StdClay}$ is the standard deviation of the complex permittivity of the clay, f_i and $\varepsilon^*_{Stdi}$are the volume fraction and standard deviation of the complex permittivity of each mineral.

5.4 Materials processing

5.4.1 System set-up of microwave rig for the firing of clays

A microwave rig has been designed for the firing of clays. A detailed description of the design process can be encountered at the beginning of Chapter 7. The schematic of the system used for performing microwave heating trials on red and yellow Danish clays at 2450 MHz is presented in Figure 5.5.

First, a 2 kW Sairem microwave generator functioned as the energy source. A circulator with a water load was located next to protect the generator from the foreseeable large degree of reflections the low loss materials incurred into. Precise forward and reflected power readings were obtained from the use of two Agilent U2004A 9 kHz-6 GHz USB Power meters attached to a directional coupler. Power data was continuously monitored in a computer with the help of a N1918A Power Analysis Manager. An automatic 3-stub tuner and a sliding short encircled the applicator in order to control and optimise the microwave/material matching. In order to protect all devices and their inner workings from the strong heat flows generated during firing, water cooled flanges were positioned at both sides of the cavity. A choked WR-430 brass waveguide working at the TE_{10} mode was employed as the applicator. Finally, a NEC thermal camera with a 20-2000 ºC range oversaw the temperature of the specimen across firing through the cavity choke.

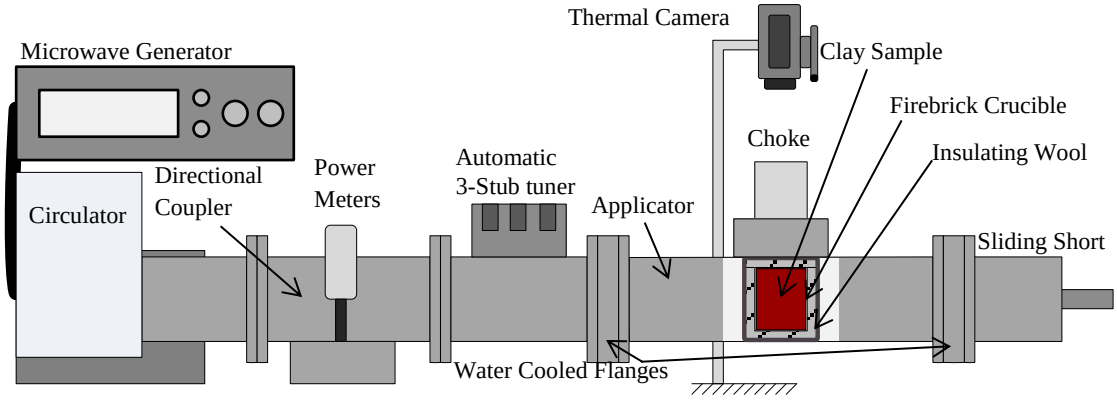


Figure 5.5- Schematic of single mode microwave rig designed for clay heating trials at 2450 MHz. Sample and insulation are seen through cut in waveguide.

The brass applicator would melt at the height of firing, i.e. ≈1050 ºC, so the sample was insulated with Fibercon 1600 wool blanket. However, direct contact with the clay could set it on fire on the event of the specimen melting. Hence, a Vitcas grade 30 insulating firebrick crucible, which is thermally stable up to 1600 ºC, was machined to be the structural support of the sample and separate it from the wool. Besides their thermal stability, both materials are

less microwave absorbent than the clay samples. Their dielectric data tables are displayed in Appendix B3. The firebrick with a loaded sample can be seen in Figure 5.6. Its dimensions were constrained by the inner diameter of the choke.

Having the smallest possible air gap between the firebrick and the clay was crucial in order to increase the thermal conduction exchange area and homogenise the temperature of the clay surface. Added to that, both the firebrick and particularly the wool insulation shifted the thermal shock with the ambient air away from the sample, reducing the magnitude of its thermal gradients. Finally, volatiles and other gases result of the clay thermal evolution were safely eliminated without a pressure build up in the crucible, due to its natural porosity and a minor slack between the cap and the collar.

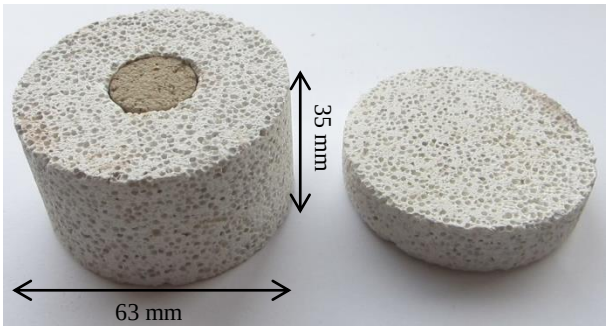


Figure 5.6- Axonometric view of firebrick crucible plus its cap without wool insulation and loaded with a 25.0±0.5x20.1±0.3 mm red clay sample.

5.4.2 Microwave heating trials

The microwave treatment of clay cylinders was divided into commissioning trials and the development of microwave firing cycles. Prior to any of the trials, the rig was cold matched in order to optimise the energy delivery to the clay specimen. A VNA calibrated with an Agilent 85031 B 7 mm calibration kit was connected to the loaded rig before the directional coupler. The S11 scattering parameter was monitored while the microwave/material matching was modified through the use of the stub tuner and the sliding short. Following from the basis of design of the system, justified in Section 7.2, an optimal energy delivery was not as critical as a more uniform energy distribution that would ensure thermal uniformity of the clay load. Hence, a broad matching approach such as the one shown in Figure 5.7B was selected. This also ensured that no readjustment of the sliding short or the 3-stub tuner was needed mid-heating. Afterwards, the microwave generator was reconnected to the rig so that the heating trials could take place.

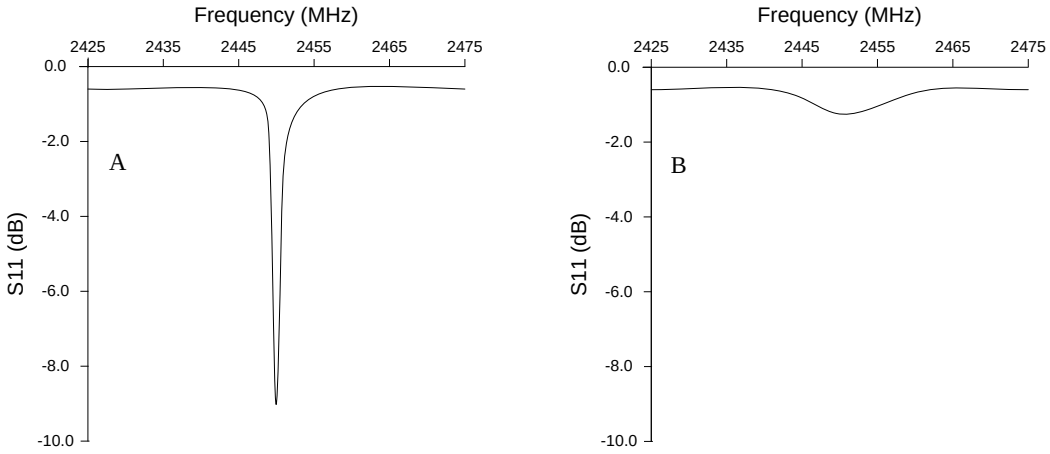


Figure 5.7- The reflection scattering parameter S_{11} at different frequencies read by a network analyser for 25.0±0.5x20.1±0.3 mm red clay cylinders showing an optimal cold matching (A) and a broad matching of the microwave field with the load in order to maximise its thermal uniformity (B).

The response of the clay cylinders to microwave radiation between 20-1050 ^{o}C was tested by performing commissioning heating trials to red and yellow clay cylinders. These took place at constant incident powers ranging 100-500 W for 80 min and at 2450 MHz. The length of the experiences was chosen to allow for a larger number of experiments per working day without unnecessarily hastening the thermal reactions. The heating was halted upon the specimens melting, which was recognisable in the power diagrams as an almost vertically declining reflections trend. Three repeats took place per sample. The power distribution in the system can be understood as presented in Eq. 5.12,

$$P_H = P_I - P_R - P_C - P_L \quad \textbf{5.12}$$

where P_H(W) is the absorbed clay power or power used solely to increase the clay temperature, P_I (W) is the incident power, P_R (W) is the reflected power, P_C (W) is the power absorbed by the whole microwave system except the clay and P_L (W) is the heating losses.

While input and reflected powers were measured and the heating losses were estimated as described in Section 7.2.3, additional experimentation was necessary to quantify the power absorbed by the microwave system. After each of the heating trials at constant power input described above, the sample was removed and the microwave power input proceeded with an empty crucible. From this point forward, power absorption in the rig was due to system absorption from the crucible and the wool. Without the sample, the crucible+wool cooled down, giving information of the system power absorbance across the whole heating range. Due the size contrast between the sample and the crucible+wool, no noticeable change to the broad matching of Figure 5.7B was observed.

Once the performance of the specimens was understood and inconsistencies with the dielectric properties trends were taken into account, heating cycles reminiscent of those found

in brickworks were developed for both clay types in order to carry on complete clay firings at 2450±15 MHz. A different approach was followed for each of the three stages of firing, i.e. heating, holding and cooling, which is further developed in Section 7.4. The lowest power input from the above trials that could put specimens in the firing range was chosen, i.e. 200 W and 300 W for the 25.0±0.5x20.1±0.3 mm and 25.2±0.6x35.3±0.4 mm samples, respectively. Regarding the cooling, an analogous slow rate was desired, which was reached through power input modification. Similarly, power regulation was needed during the holding stage in order to minimise any heating or cooling around the top temperature, i.e. ≈1050ºC. At this stage, samples underwent soaking times of 0 min, 10 min, 20 min, etc. for a later quality analysis.

Power input control could be dependent on the temperature of the material or its energy needs. In the case of the former, the attachment of a Sariem remote GMP 20 generator command unit to the microwave source allowed for an automatic power input control around a set of clay temperatures or heating rates. Temperature measurements came from an IR sensor affixed to the control box, as seen in Figure 5.8, instead of the thermal camera of Figure 5.5. Temperature control around the targets was achieved by a PID controller associated to the control box. The K values were proportional=1.0, integral=3.0 and derivative=0.2. Regarding the soaking, a target of 1050 ºC was set for the clay surface temperature, whereas for the cooling a ≈5 ºC/min rate was established. Given the novelty of microwave cooling, in the event of an ineffectual control of the rates, natural air convection was the only other viable alternative. Each trial was repeated three times for the small red cylinders only, as it is elaborated further in Chapter 7.

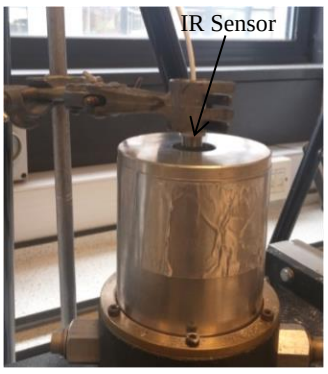


Figure 5.8- Display of IR sensor for heating trials where power input is controlled by the clay temperature.

Alternatively, the soaking stage was also attempted to be controlled by the energy needs of the clay, which summed up to minimising the clay absorbed power defined in Eq. 5.12. Therefore, all of the power delivered to the clay was used on staving off the heating losses and being absorbed by the rest of system. Manual power control at this stage was arduous due to the clay instability at the height of firing and the high probability of melting. Thus, a LabVIEW interface (2016 edition) was developed to act as the PID loop described above.

The designed loop can be seen in Appendix E, while a simplified diagram of the algorithm is shown in Figure 5.9. Power readings were received every second via the power meters from Agilent U 2000 drivers. A power input reduction or increase of 10 W was set in case the absorbed power deviated from the set point more than 5 W, which were the minimum possible power change achievable by the microwave generator and the empirically determined acceptable range of absorbed power deviations respectively. The set point represents the power delivered to the clay ($P_H + P_L$) that fulfils $P_H \approx 0$, which ranged 30-36 W and 43-45 W for 25x20 mm and 25x35 mm cylinders. The resultant new power input was fed to the microwave generator through an Agilent PSG MXG driver. The power control cycle was automatically refreshed at the same rate as the power meters input. A microwave cooling was attempted by stabilising the clay temperature at narrow intervals, i.e. ≈50 ºC until 500 ºC, during the cooling stage in order to ensure thermal uniformity in the clay. As before, natural air convection was to be used if the former proved unfeasible. Three repeats took place for every clay type and size.

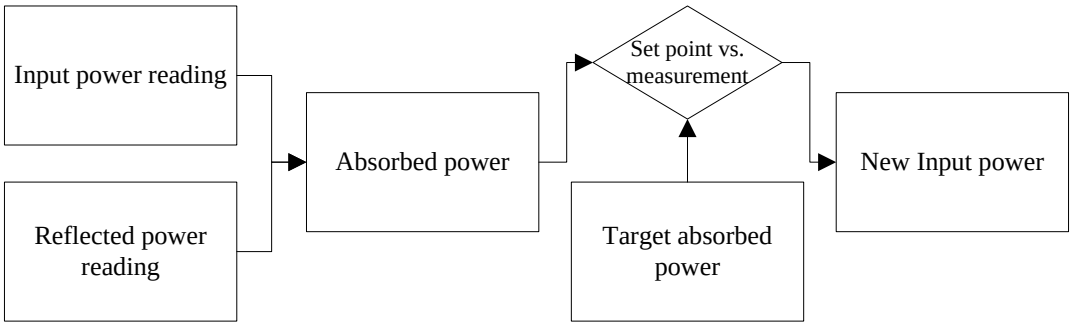


Figure 5.9- Schematics of the algorithm of the LabVIEW software interface used to control the power absorbed by the clay samples during microwave heating trials.

5.5 Quality analysis

5.5.1 Conventionally fired clay reference

Red and yellow 25x20 mm and 25x35 mm clay cylinders were conventionally fired in a Carbolite LMF furnace with a 3216 programmable controller following a common industrial heating cycle as the one presented in Chapter 3, i.e. 0.92 ºC/min up to 1050 ºC, 4 h soaking and then a cooling of 1.42 ºC/min until 750 ºC, 0.33 ºC/min until 500 ºC and 0.75 ºC/min until 100 ºC (Moesgaard, 2015). Similar experiences at increasing heating rates between 1-10 ºC/min were also performed to test the possibility of unlocking faster heating cycles in samples smaller than a brick without causing significant tensions to the specimens.

5.5.2 Compressive strength

The compressive strength of the fired clay cylinders was studied in an INSTRON 5960 Dual Column testing system, which performed uniaxial compressive strength analyses on ten

conventionally and three microwave processed 25x20 mm and 25x35 mm red and yellow Danish clays. The procedure was analogous to the indicated in BS EN 772-1. A metallic hammer with a flat surface descended on the clay specimen with a loading rate of 0.05 N/mm^2/s. This rate was justified by ASTM C62, foreshadowing the brick compressive strength to be lower than 10 N/mm^2. The first load failure was used for the calculation of the compressive strength of the material, as seen in Eq. 5.13, while following failures were considered plastic deformation,

$$\vartheta = \frac{Fo}{S} \quad \textbf{5.13}$$

where, ϑ (N/mm^2) is the compressive strength of a material, Fo (N) is the applied load and S (mm^2) is the sample's surface that contacts the device's hammer.

5.5.3 Water absorption and saturation coefficient

The determination of the maximum water absorption of a substance was performed for both the boiling and cold alternatives. Three samples of conventionally and microwave fired red and yellow Danish clays at 25x20 mm and 25x35 mm sizes were dried for 14±2 h at 110±5 ºC and cooled down for 20 min in a desiccator as described previously. Then, they were submerged in a thermal bath filled with water at room temperature. In the case of the cold test, the sample was removed after 24 h as per ASTM C62. On the other hand, the boiling analysis followed BS 3921. The bath was heated up to 90-95 ºC under an hour and kept at that temperature for 5 h. Then, the water was left to cool and the specimens were subsequently removed. Next, they had their surface water wiped off and their moist mass measured, enabling the calculation of their water content absorption using the same formula applied for the moisture content computation, i.e. Eq. 5.1.

As per ASTM C62 the saturation coefficient is calculated using Eq. 5.14,

$$\delta = \frac{W_C}{W_B} \quad \textbf{5.14}$$

where δ is the saturation coefficient, W_C and W_B (%) are the maximum water absorption of the cold and boiling tests respectively.

5.5.4 Shape, size and density variation

The identification of shape changes between fired and raw samples was focused on the visual identification of bloating and torsions that could have been caused by an exceedingly fast and thermally inhomogeneous firing, respectively. Three red and yellow clay cylinders of both sizes were studied before and after conventional and microwave treatment, where a level was

used on their sides and top-bottom surfaces in order to uncover undesirable faults. On the other hand, volume and bulk density divergences between both processing methods were assessed using the same methodology described in Section 5.3.3.

5.5.5 Colour and texture

Regarding the texture of the fired products, BS 3921 offers no specification for their analysis. Thus, a qualitative assessment of visual defects and differences between three samples of both clay types and sizes fired conventionally and using microwaves was used instead. Similarly, there is no colour standard for clay bricks or similar materials. Alternatively, the general standard of colorimetry CIE 15 was followed. Three samples of unfired, conventionally fired, microwave fired, and microwave fired plus conventionally cooled using a brickworks cycle red and yellow Danish clays at both sizes had their CIELAB colour space parameters studied at five points across their surface using a FRU WR18 portable colorimeter. These are the luminance "L" and the colour opponents "a" and "b", which represent green/red and blue/yellow respectively. The first ranges between 0-100 and describes the darkest black and the brightest white respectively, whereas "a" and "b" run in a ±100 range, where green and blue are the negative values.

5.6 Techno-economical assessment of the microwave processing technique

A theoretical study comparing the microwave and conventional clay firing methodologies at industrial scale was developed, with the aim of uncovering possible advantages of the former processing technique. An economic study focused on the costs of both processing methodologies. An environmental impact study centred on both techniques carbon footprint followed. The comparison between both processing techniques was focused on the firing stage of the kiln/applicator, which is where the substitution of conventional gas firing by microwaves took place. The other stages of the process, such as the drying, pre-heating and cooling, were assumed to remain largely unchanged, both for the sake of simplicity and due to energy optimisation purposes, e.g. exhaust currents recirculation. Further justification of the methodology applied can be seen Section 7.7.

5.6.1 Economic assessment

An estimation of the economic potential of the industrial microwave treatment of clays over conventional methods was addressed through a discounted cash flow (DCF) study of both. This widespread budgeting analysis tool evaluates economic return as a sequence of cash flows over a specified amount of time (Lutz, 2001). There are several DCF variations depending on the particularities of the project, e.g. net present value (NPV), internal rate of

return (IRR) and payback period (PB) (Bierman Jr and Smidt, 2012, Ryan and Ryan, 2002). The first one was selected for this project due to its popularity, widespread utilisation and supply of the most accurate estimations of the potential economic return of a project (Žižlavský, 2014, Bierman Jr and Smidt, 2012, Chiesa and Frattini, 2009).

The NPV approach subtracts outgoing cash flows (costs) from cash inflows (benefits) over a period of time. A null NPV translates in the return of the investment at the end of the project, whereas a positive NPV means profits on top of the investment, and a negative NPV implies losses (Chiesa and Frattini, 2009). Through the principle of the time value of money, future cash flows are discounted by an amount dependent on a rate of return as seen in Eq. 5.15. The rate of return can be understood as the profit from an investment over a period of time and it is a value determined by the investors (Ryan and Ryan, 2002),

$$NPV = \sum_{z=0}^{t_p} \frac{Ci_z - Co_z}{(1+r)^z} \qquad \textbf{5.15}$$

where NPV (£) is the net present value, r is the rate of return, t_p (years) is the service life of the plant and Ci_t and Co_t (£) are the summation of cash inflows and cash outflows at a year z.

Since the present economic analysis was not driven by profit but by the comparison of different processing techniques, the r value was a constant for both defined as the rate of return that caused a NPV=£ 0 for the conventional heating technique. Moreover, an average service life similar to chemical plants, i.e. t_p=40 years (Ludwig, 1997), was selected for the economic study despite brickworks continuously operating beyond even 100 years (Køster, 2014). Finally, costs such as staff wages, taxes, plant start up, interest rates, equipment repair and installation were disregarded for the sake of simplicity, as they could be assumed equal for the conventional and microwave settings. Thus, only the capital costs regarding the price of the main equipment, the operational costs regarding the energy supply and the benefits derived from the brick sales were taken into consideration. Data from experimental results was complemented by input from previous works.

5.6.2 Environmental assessment

The environmental impact of an industrial process can be addressed by a wide number of indicators, such as aquatic eutrophication, human toxicity, resource depletion, particulate matter emission, photochemical ozone formation and carbon footprint (Laurent et al., 2012). Following from the focus on the energy supply of the clay firing process, carbon footprint was chosen as the most suitable indicator for quantifying the environmental impact of the clay firings. Its selection was justified by the direct effect of the fossil fuels burning during firing

on the greenhouse gases. Carbon footprint quantifies as CO_2 equivalents the main six greenhouse gasses included in the Kyoto Protocol, i.e. CO_2, CH_4, N_2O, HFCs, PFCs and SF_6 (UN, 1998), as well as CO, NOx and SOx (Ercin and Hoekstra, 2012). This parameter was also chosen in other works which focused on the conventional firing of clay materials (Kulkarni and Rao, 2016, Quinteiro et al., 2012, Quinteiro et al., 2014).

The carbon footprint of a process is usually covered under a life cycle assessment, whose popularity for the analysis of industrial activities has made it thoroughly standardised (ISO, 2006a, ISO, 2006b, BSI, 2011c). Added to that, numerous software tools have arisen to hasten these assessments, e.g. PEMS (Menke et al., 1996), openLCA (Ciroth, 2007), GaBi (Hendrickson et al., 1997), EIO-LCA (Hendrickson et al., 1998), CCalC (Djekic et al., 2014). In this study, the standalone version of CCalC, also termed CCalC2 and seen in Figure 5.10, was used because of its free availability, versatility and the quality of its two databases (Manchester, 2007). This version follows the standards ISO 14044 and PAS2050 (Manchester, 2016). As such, the standard life cycle analysis methodology was followed, where the main topics were goals and scope definition, functional unit, system boundary, data quality, life cycle inventory analysis, life cycle impact assessment and interpretation of results (ISO, 2006a, ISO, 2006b, BSI, 2011c).

The objective of this study was to determine and compare the environmental impact, through the study of the carbon footprint, of the conventional and microwave firing of clay bricks in order to assess possible advantages of the latter at industry level. The functional unit of the analysis, i.e. the main unit the assessment is built upon, was the hourly brick production. Regarding system boundaries, the whole industrial clay firing process seen in Chapter 3 was narrowed down to the firing stage as mentioned above. Thus, the raw materials, storage and use stages seen in the software's interface in Figure 5.10 were disregarded. Finally, the life cycle inventory, which deals with collecting information of the system energy supply and its data quality were obtained when defining the layout of the system. This is expanded in Chapter 7.

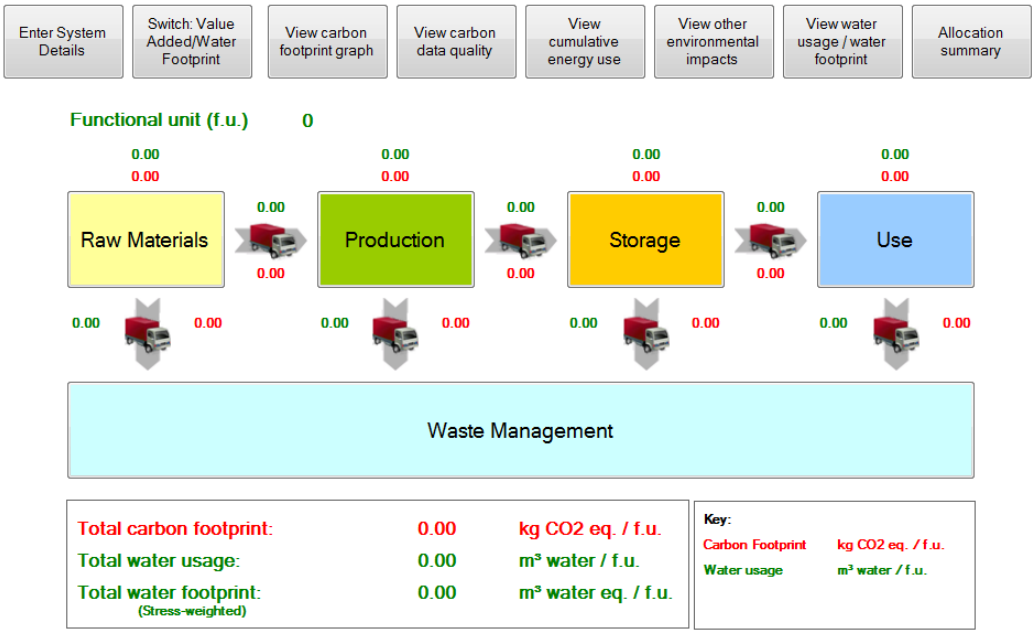


Figure 5.10- Main interface of CCaLC2 software used for the calculation of the environmental impact of the clays firing process using microwave energy and gas firing.

5.7 Conclusions

The materials used and the techniques applied in their analysis and processing in order to fulfil the aims and objectives of this project have been explained in this chapter. Red and yellow clays from Denmark are the focus of the study, together with their major mineral constituents, i.e. montmorillonite, kaolinite, muscovite, quartz, calcite, albite, orthoclase.

These materials underwent a number of characterisation studies, being the first a X-ray diffraction analysis in order to quantify clays mineralogy. Next, both clays and their minerals had their equilibrium moisture, bulk density and void fraction measured as solid slabs and free flowing powders. Additionally, their thermal evolution was investigated through the TGA and DSC techniques in the 25-1000 ^{o}C range in order to assess their physicochemical transformations on heating. Finally, the dielectric properties of clays and clay constituents were measured at the frequencies of 912 MHz and 2470 MHz across 20-950 ^{o}C for both slabs and powdered samples using the cavity perturbation method. This data was later validated through additional dielectric measurements in the 20-800 ^{o}C range of brick sized clay specimens using the waveguide method at 2450 MHz. Furthermore, a tool using mixing rules was developed for the estimation of clay dielectric properties from the dielectric properties and volume fractions of their constituents. The predictive tool was later validated assessing other European clays from Spain, England and Netherlands.

A single mode resonant cavity microwave system for the firing of 25x20 mm and 20x35 mm cylinders of red and yellow clays at 2450 MHz was designed and commissioned. First, the

probable appearance of events unaccounted by the dielectric properties trends was assessed through 80 min exploratory trials at constant incident power ranging 100-500 W. Afterwards, complete firings were carried out in heating cycles reminiscent of those found in brickworks through power input regulation, where power control could be based on the temperature of the specimen or its energy needs. The fired products had their quality parameters, i.e. compressive strength, mineralogy, shape, size, density, water absorption, saturation coefficient, colour and texture, compared with conventionally treated samples. In the end, the specific techniques used on addresing the economic and environmental viability of an industrial scale microwave clay firing system were detailed.

The order of appearance of the methods explained in this chapter is mimicked by the results chapters that follow. The focus of Chapter 6 is the characterisation of the clay materials and the development of the electromagnetic mixing tool. On the other hand, the microwave trials and the assessment of the potential of this processing technique in the industrial scale are discussed in Chapter 7.

6 CHARACTERISATION OF CLAY MATERIALS

6.1 Introduction

It has been seen in Chapter 4 how on many occasions the potential advantages of microwaves over conventional heating methods are counteracted by microwave/material coupling issues, thermal gradients and hot spots, which translates into poorly optimised processes and decreased product quality. The development of industrial scale microwave firing processes has therefore been hindered by the lack of a scale up methodology using comprehensive knowledge of clay material characteristics, such as dielectric properties, as the starting point for the design of microwave cavities and microwave heating cycles. For example, dielectric properties can be used to predict the influence of microwave-absorbing phases on the spatial distribution of the electric field across the load, and the effect of the processing frequency or a materials' density on its microwave heating potential. Furthermore, the common use of susceptors, additional conventional heating, mode stirrers and turntables in order to develop successful processes (Thuault et al., 2014, Menezes et al., 2007, Satapathy, 2009, Mizuno et al., 2004) creates doubts about the potential of microwave energy to fire clays without the help of heating aids and the conditions at which that firing can happen.

The aims of this work in this chapter are to investigate microwave/clay interactions in order to ascertain whether microwave energy alone can fire clays and to determine the effect of parameters that might affect it, such as composition, density, temperature and frequency. In this chapter, the solid and liquid phases of clays used in the brick making industry were quantified and their evolution across 25-1000 ^{o}C was studied. Data from these analyses was used to explain the behaviour of the dielectric properties of clays across firing, which in turn determines their microwave firing potential. An investigation of the dielectric properties of different clay types during heating in the 20-950 ^{o}C range as powders and solid slabs at 912 MHz and 2470 MHz quantified the effect of influencing parameters like composition, frequency and density. Additionally, the dielectric property measurement of clay constituents allowed the recognition of the dominant dielectric phases that may enable successful microwave treatments. Finally, a tool capable of estimating the dielectric properties of clays based on their composition was developed, thus extending the knowledge of microwave/clay interactions to other clay mixtures without the need for further dielectric measurements.

6.2 Physicochemical characterisation of Danish clays

6.2.1 Clay composition

As previously shown in Chapter 3, clays are multiphasic heterogeneous systems that can be composed of a wide array of minerals, which translates into an infinite amount of possible clay mixtures. Together with the contrasting dielectric response of the major clay constituents seen in Table 4.1, it can be deduced that a clay's potential for microwave firing is critically dependent upon the specific composition of its solid and liquid phases. The former consists of the various mineral species present in clays, while free water forms the majority of the liquid phase (Güven and Pollastro, 1992). Therefore, an assessment of the nature of the red and yellow Danish clays used in this project is crucial in order to relate composition to the response of clays to microwave energy.

The mineralogical composition of Danish clays from different geological deposits is presented in Table 6.1. The X-ray diffraction methodology used is explained in Section 5.3.2, while the diffraction patterns can be seen in Appendix A. Chlorite, dolomite and other minor constituents contributing to ≤1% of the clay are not shown. Consistent with previous work (Jensen, 1978, González et al., 1998, Vissing, 2004), the main difference between red and yellow clay types is their calcite content, accounting for more than 20% of yellow clays while often being absent in red specimens. Furthermore, red clays tend to have the largest clay minerals fraction, ranging from 32-38%, compared with the 20-29% of the yellow specimens.

Table 6.1- Quantitative XRD characterisation of the major clay constituents in red and yellow Danish clays, i.e. quartz, calcite, albite, orthoclase and the clay minerals kaolinite, montmorillonite and muscovite. Each sample was measured once, so that deviations for the mineral concentrations range ±2.5% for >60 wt%, ±5% between 60-30 wt%, ±10% between 30-10 wt%, ±20% between 10-3 wt% and ±40% for <3 wt %.

Clay	Quartz (%)	Calcite (%)	Orthoclase (%)	Albite (%)	Kaolinite (%)	Montmorillonite (%)	Muscovite (%)
Hammershoj Yellow	23.9	23.8	7.7	10.4	4.4	19.8	5.5
Vedstaarup Yellow	29.5	21.1	4.5	11.2	2.1	13.2	5.1
Helligsø Red	43.7	0.0	7.1	9.0	3.9	27.1	7.1
Hammershoj Red	31.2	3.6	12.8	17.6	2.6	19.3	10.2

As explained in Chapter 3, the presence of free water in clays is strongly dependent on the availability of pores and contact surfaces. Thus, the equilibrium moisture content in clays is affected by their void fraction, i.e. the degree of empty spaces in the clay matrix that can be filled by substances such as air or water (Grim, 1968). This moisture-void fraction relationship can be easily recognised in Table 6.2 in the powders and solid slabs used in the analyses. Moisture and density measurement methodologies used are described in

Section 5.3.1 and Section 5.3.3, respectively. Regardless of the clay state, the red type presents the highest free water content, being around 28.8% and 78.6% wetter than the yellow specimens as slabs and powders, respectively. This is explained by their larger percentage of clay minerals seen in Table 6.1, as montmorillonite and to a lesser extent muscovite display a notable water affinity (Grim, 1968, Gillot, 1987). This also explains the wetter nature of Hammershoj yellow compared with Vedstaarup yellow and Helligsø red compared with Hammershoj red. The generalised moisture increase noted upon powdering the clays can be related to the 34.6% higher void fractions of the powders, as there is more space for free water.

Table 6.2- Equilibrium moisture contents of red and yellow Danish clays at different void fractions as solids slabs and powders. For each material, five repeats were made and the standard uncertainty is indicated.

Clay	Powder		Slab	
	Moisture (%)	Void fraction (%)	Moisture (%)	Void fraction (%)
Hammershoj Yellow	0.93±0.09	0.56±0.03	0.49±0.02	0.39±0.01
Vedstaarup Yellow	0.62±0.03		0.40±0.02	0.37±0.02
Helligsø Red	1.81±0.39		0.64±0.03	0.40±0.01
Hammershoj Red	1.75±0.25		0.55±0.02	0.42±0.03

As clays are inherently heterogeneous systems, it is misguided to assume that their moisture content is homogeneously distributed across their constituents. The minerals in Table 6.1 may display varying degrees of water affinity. Table 6.3 shows the equilibrium moisture contents of single clay constituents. These can serve to assess the likely moisture distribution within the clays. As expected from previous work, clay minerals have the highest moisture content of all constituents (Gillot, 1987, Murray, 1993, Grim, 1968). Montmorillonite stands out as the wettest species with 1.91% equilibrium moisture as a solid slab and 3.50% as a powder, followed by muscovite with 1.61% and 2.62%, and kaolinite with 0.80% and 1.54% respectively. On the other hand, non-clay minerals are at least four times drier than kaolinite. Consequently, there is a strong moisture imbalance across the clay constituents. This may cause thermal uniformity issues when microwave heating below 100 ^{o}C, given the dielectric contrast between the minerals of Table 4.1 and water (Kraszewski, 1996).

Table 6.3- Equilibrium moisture contents of major clay constituents at different void fractions as solids slabs and powders. For each material, five repeats were made and the standard uncertainty is indicated.

Clay constituent	Powder		Slab	
	Moisture (%)	Void fraction (%)	Moisture (%)	Void fraction (%)
Kaolinite	1.54±0.10	0.56±0.04	0.80±0.02	0.48±0.02
Montmorillonite	3.50±0.24		1.91±0.09	0.32±0.03
Muscovite	2.62±0.22		1.61±0.14	0.22±0.07
Orthoclase	0.14±0.02		0.10±0.01	0.17±0.07
Albite	0.36±0.03		0.21±0.01	0.35±0.06
Calcite	0.23±0.01		0.04±0.01	0.09±0.03
Quartz	0.12±0.01		0.01±0.01	0.17±0.01

6.2.2 Thermal analysis of clays and clay constituents

In the section above, the solid and liquid phases of the studied clay specimens have been quantified at room temperature. However, the configuration of these phases changes across the firing process. The physicochemical transformations of building clays are common knowledge in the brickmaking industry and have been summarised in Figure 3.4. Yet, it is uncertain whether the particular mineralogy of the studied specimens will affect the reaction kinetics, equilibrium conversion in competitive reactions, onset temperature or the yield of these physicochemical transformations. In addition, it is possible that these thermal transformations will affect the dielectric response of clays, and thus their potential for microwave processing. Therefore, it is necessary to extend the investigation on clay composition to the whole firing range.

In this section, a thermogravimetric analysis of red and yellow Danish clays in the 25-1000 ^{o}C range is presented, in order to identify thermal transformations that cause a mass loss. Since several of the expected reactions take place in the same temperature range, an analogous investigation for single clay constituents follows so as to uncover individual reactions that might be difficult to recognise and the effects of mineral associations. Differential scanning calorimetries of clays were used to assess the thermal reactions that do not cause a mass loss.

6.2.2.1 Thermogravimetric analysis of Danish clays

Data from thermogravimetric analyses performed on red and yellow powdered clays between 25 ^{o}C and 1000 ^{o}C at 20 ^{o}C/min in a N_2 atmosphere are presented in Figure 6.1. The methodology of the thermogravimetries is detailed in Section 5.3.4. The x-axis corresponds to the temperatures of the furnace, while the y-axis represents the mass percentage and the mass change percentage with temperature. The mass percentage is used to quantify the mass loss of the clays across firing, whereas the derivative curves are specifically scaled so as to help in the recognition of thermal transformations. Despite mineralogical differences between clays of the same type, their thermal transformations are similar.

The elimination of free water is seen as a peak in both clay types' derivative weight loss curves at 100 ºC, accounting for a 1.5% mass loss in red clays and half as much for yellow specimens. Physically bound water removal takes place between 150-350 ºC. Since the powdering of the specimens loosens the physically bound water to material bond, the physically bound water behaviour approaches that of free water and its signal in the 150-350 ºC range is weakened. This explains why the clays dehydration can only be recognised on the more water absorbent red clays, particularly the Helligsø samples, as a peak around 250 ºC.

In both clay types it is distinguishable a thermal transformation that onsets at 350 ºC and peaks at around 450 ºC. Attending to the clay reactions of Figure 3.4, this corresponds to the combined dehydroxylations of kaolinite, montmorillonite and muscovite. Resolution of their individual peaks is not possible owing to the narrow temperature range. Furthermore, despite muscovite and montmorillonite dehydroxylations often extending until the start of the sintering (McConville and Lee, 2005, Dunham, 1992), it appears that here the dehydroxylations are completed at ≈600 ºC.

Clearly, calcite decomposition is the dominant thermal transformation in yellow clays, judging by their one order of magnitude larger peaks than other transformations at around 700 ºC in Figure 6.1A. The release of CO_2 upon calcite breakdown (Galan et al., 2013) accounts for half of the total mass losses of the yellow specimens across firing, as their 10-12% mass drop contrasts with the up to 6% of the red clays. The absence of identifiable transformations from 800 ºC onwards is explained by the sintering and mineral recrystallisations that take place in this range, typically occurring without mass loss.

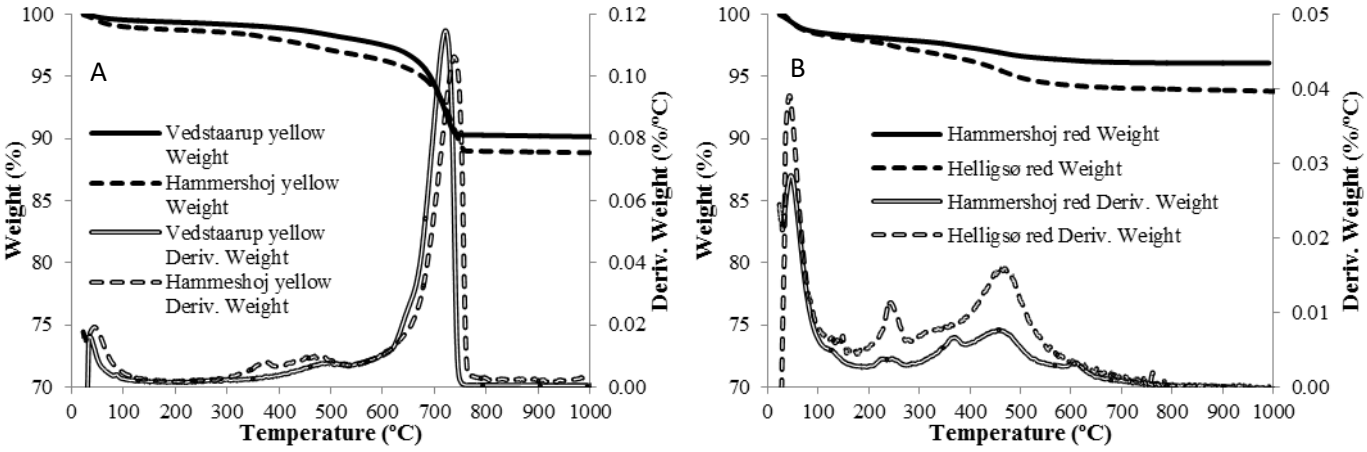


Figure 6.1- Average mass change and derivative mass change versus temperature across the temperature range of 25-1000ºC at 20ºC/min in a N_2 atmosphere for yellow (A) and red (B) Danish clays. These results are the average of three repeats. Standard deviations average for the weight and derivate weight around ±0.29 and ±0.002 for Hammershoj red, ±0.20 and ±0.003 for Helligsø red, ±0.39 and ±0.004 for Vedstaarup yellow, and ±0.47 and ±0.003 for Hammershoj yellow.

6.2.2.2 Thermogravimetric analysis of single clay constituents

A thermogravimetric analysis analogous to that shown in Figure 6.1 is applied to the major clay constituents, i.e. kaolinite, montmorillonite, muscovite, calcite, quartz, orthoclase and albite, in order to identify the single mineral reactions. The results are presented in Figure 6.2. Both feldspars and quartz trends are not displayed due to their thermal stability, as their mass losses average around 0.5% at 1000 ºC.

Consistent with Figure 6.1, free water evaporation is completed at 100 ºC for all species. As shown in Table 6.3, clay minerals have the highest moisture content, where montmorillonite, muscovite and kaolinite lose around 3.4%, 2.2% and 1% of their initial mass after free water removal, respectively. Curiously, none of the studied species show a mass loss at 250 ºC that could correlate to the physically bound water peak recognised in red clays in Figure 6.1B. Given the absence of mineral reactions at this point in the heating, shown by Figure 6.2 and corroborated by Figure 3.4, it is feasible to assume that somehow physically bound water manages to entrench itself in the montmorillonite interlayer. As interstratification is common between clay minerals (Grim, 1968), it is possible that montmorillonite is interstratified with another species when forming the clay, locking the former's structure so as to allow physically bound water inclusion.

Contrary to free and physically bound water elimination, clay minerals dehydroxylations take place at different points during heating since their structural water removal is dependent on the strength of the mineral structures' bonds (Grim, 1968, McConville and Lee, 2005). Kaolinite becomes metakaolinite before 600 ºC, where the summit of the transformation is reached around 500 ºC. Around that temperature, montmorillonite dehydroxylation starts, peaking at 650 ºC. Muscovite shows a two-stage dehydroxylation whose peaks overlap those of the previous minerals, as also demonstrated by American Petroleum (1951). This is possible thanks to the lower reaction rate of micas, as muscovite starts to become amorphous around 350 ºC and finally loses its crystalline structure right before the start of sintering.

Although the clays dehydroxylation peak of Figure 6.1 corresponds to the combination of kaolinite's and the first of muscovite's peaks (Grim, 1968, McConville and Lee, 2005), the second muscovite peak and montmorillonite amorphous transformation around 650 ºC (American Petroleum, 1951) seen in Figure 6.2 are not evident in the clay trends of Figure 6.1. The previous assumption of an interstratified montmorillonite is proved correct here as apparently it interstratifies with muscovite (Reeves et al., 2006). As a result, their reaction parameters are altered, so that either the onset temperature of both dehydroxylations is reduced to that of kaolinite, or the dehydroxylation rate is decreased and takes place over a wider temperature range broadening any possible peak.

It is worth noticing that the single mineral calcite decomposition consistently finishes on average around 40 ºC later than for the yellow clays. Interaction with other constituents may justify the increment of its reaction rate (Galan et al., 2013). The calcite breakdown is clearly the most energetic mineral transformation, as it loses nearly 45% of its initial mass. Moreover, the magnitude of its peak is four times higher that of kaolinite metakaolinization, which in turn more than doubles the other clay minerals dehydroxylations. This is understandable, as muscovite and montmorillonite retain around 91% of their original weight by 1000 ºC despite their array of transformations undertaken, while dehydroxylation effects alone cause kaolinite a nearly 15% mass loss.

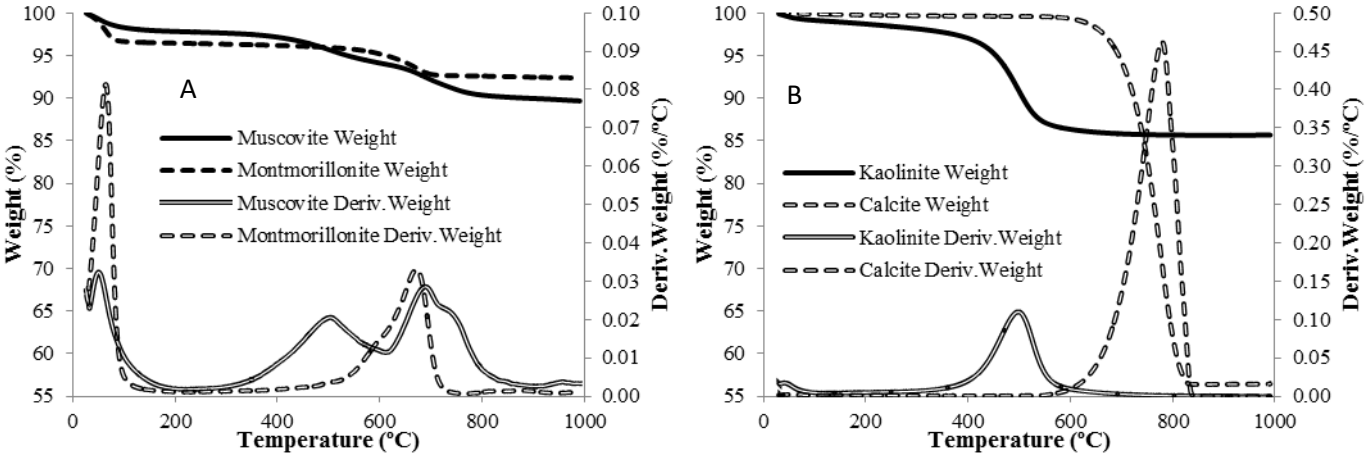


Figure 6.2- Average mass change and derivative mass change versus temperature across the temperature range of 25-1000 ºC at 20 ºC/min in a N_2 atmosphere of major clay constituents, i.e. montmorillonite, muscovite (A), kaolinite and calcite (B). These results are the average of three repeats. Standard deviations average for the weight and derivate weight around ±0.07 and ±0.001 for kaolinite, ±0.12 and ±0.001 for montmorillonite, ±0.16 and ±0.002 for muscovite, and ±0.64 and ±0.015 for calcite.

6.2.2.3 Differential scanning calorimetry of Danish clays

A way to assess the high temperature mineral reactions that occur without mass loss comes from focusing on energy shifts instead on the sample mass, which can be achieved through a Differential Scanning Calorimetry (DSC) study. The DSC curves for red and yellow Danish clays are presented in Figure 6.3, where heat flow is plotted against furnace temperature. The experimental method is detailed in Section 5.3.5. As before, the scales of the heat flows have been modified in order to assist in the recognition of thermal transformations.

As anticipated from the TGA curves above, data for clays of the same type are similar despite mineralogical differences, and previously identified mineral transformations are also recognised here, such as the free water elimination at 100 ºC. The same cannot be said for the physically bound water peak at 250 ºC, probably because the magnitude of the free water elimination peak in red clays masks it. In all clays, quartz inversion (Heaney, 1994, Davila et al., 2008) is noted as a sharp, narrow peak at 570 ºC. Just before that, the first clay minerals

dehydroxylation peak can be seen, corresponding with kaolinite and muscovite (Grim, 1968, McConville and Lee, 2005, American Petroleum, 1951). The combined muscovite and montmorillonite loss of crystallinity (American Petroleum, 1951, Gillot, 1987) is seen as a small peak around 650 ºC for red clays in Figure 6.3B, confirming the assumption that this reaction does take place but it is impeded by mineral interstratifications. This peak appears to be masked by the calcite decomposition peak in the yellow clay trends. With respect to mineral transformations without mass loss beyond sintering, it is seen in both clay types how particularly above 900 ºC a noticeable change of the heat trends matches with the start of the recrystallisations, whose individual identification is still precluded given their number in such a narrow temperature range.

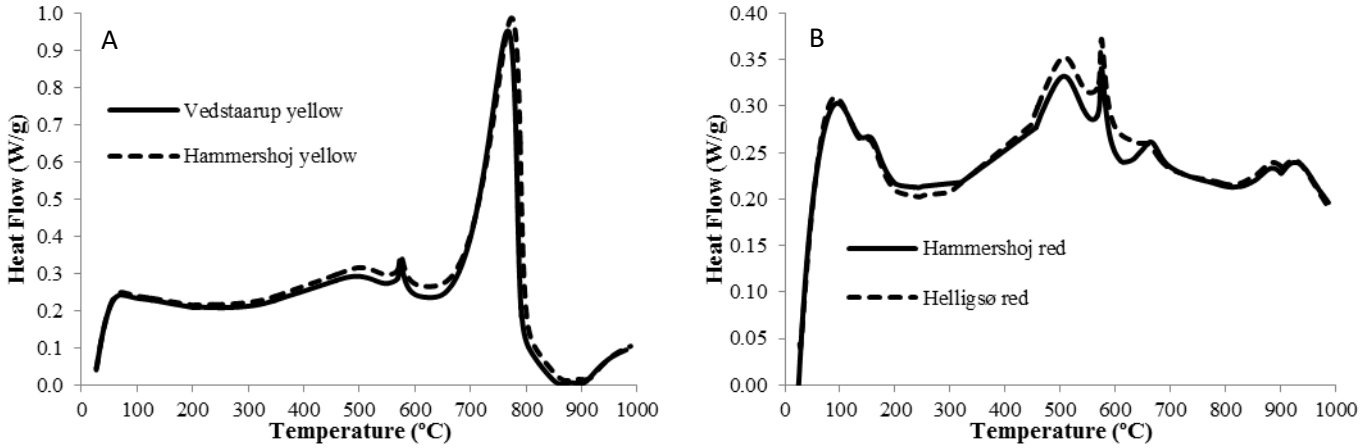


Figure 6.3- Average heat flow versus temperature across the temperature range of 25-1000 ºC at 20 ºC/min in a N_2 atmosphere for yellow (A) and red (B) Danish clays. These results are the average of three repeats. Standard deviations average around ±0.007 for Vedstaarup yellow, ±0.011 for Hammershoj yellow, ±0.014 for Helligsø red and ±0.010 for Hammershoj red.

6.2.3 Conclusions on the physicochemical characterisation of Danish clays

The compositional analyses of the studied Danish clays have served to quantify their specific solid and liquid phases and to gain an insight into their evolution across the firing range. The major clay constituents appear to be kaolinite, montmorillonite, muscovite, calcite, quartz, orthoclase and albite. The rest of the identified species are treated as impurities that form between 2.1-13.3% of the clays. Based on the reported values of the dielectric properties of these clay constituents in Table 4.1, it is reasonable to expect that certain clay components, e.g. clay moisture and clay minerals, may be selectively heated by microwaves, while other phases such as quartz remain relatively microwave transparent, and this could lead to thermal gradients across the clay load during microwave heating. This may be particularly true near room temperature owing to the preferential distribution of water in clay minerals, montmorillonite in particular, which has a moisture content of 1.91% in slab form, compared with the free water content ranging 0.49-0.64% found in the Danish clay slabs tested.

As clays are heated, some of their constituents undergo a series of physicochemical transformations that do not completely match the known clay reactions presented in Figure 3.4. The updated version of the physicochemical transformations of the Danish clays studied is presented in Figure 6.4. Besides the commonly known transformations recognised, such as free and physically bound water elimination at 100 ºC and 250 ºC respectively, clay minerals dehydroxylation between 350-800 ºC, quartz inversion at 570 ºC, calcite decomposition around 750 ºC, sintering at 800 ºC and mineral recrystallisations beyond 900 ºC, There is an identifiable degree of interstratification between montmorillonite and muscovite. Some or all of these thermal reactions may have an effect on the dielectric response of clays, and thus their potential for microwave heating, at different points during firing. Given the similar thermal behaviour between all clays, the performance of red and yellow clays during microwave processing might be similar up to the calcite breakdown, where diverging mass losses resulting from the transformation of calcite to quicklime may occur. Having examined the nature of clays across the firing range and qualitatively assessed their probable responses to microwave energy based on their composition, the next step is to quantify the microwave/material interaction of these clays through dielectric property measurements.

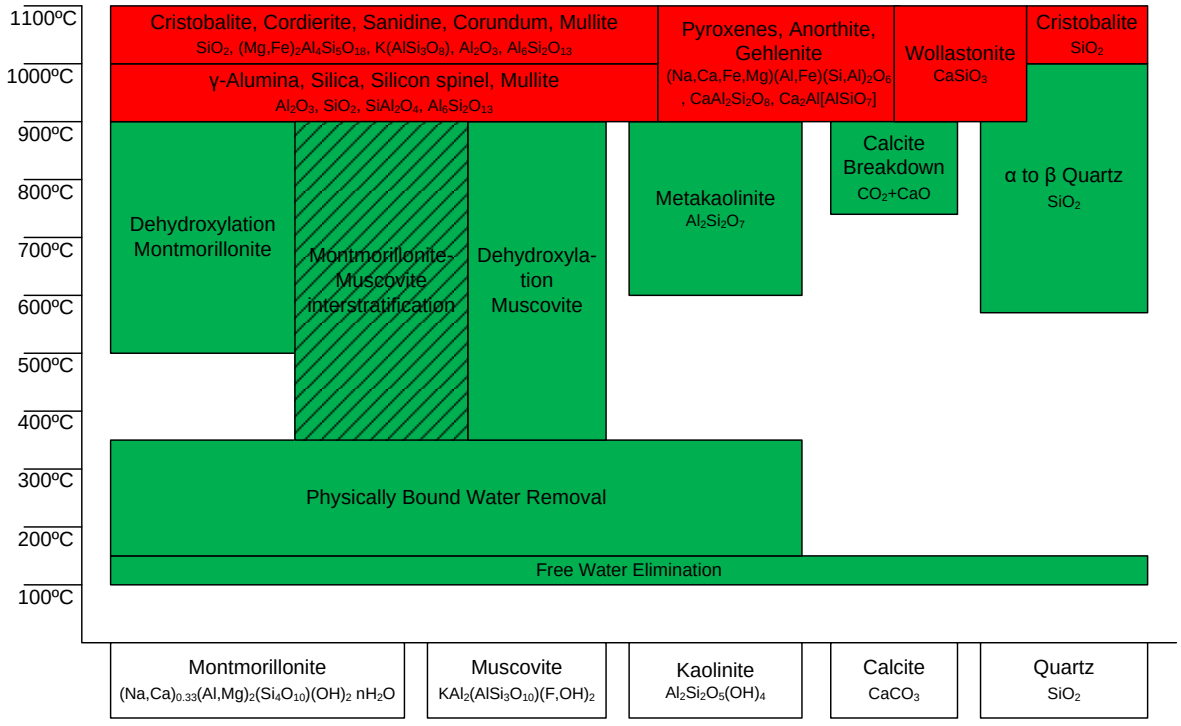


Figure 6.4- Updated firing diagram of main thermal transformations of major clay constituents taking place in the red and yellow Danish clays studied. Reactions are divided into transformations proven to occur (Green), transformations that cannot be proven to individually take place (Red), and previously undiscovered mineral arrangements (Green with diagonal stripes).

6.3 Dielectric property measurements of clays and clay constituents

The investigation into the nature of Danish clays has allowed the formulation of some hypotheses regarding the microwave processing of clays based on their composition. However, these speculations are qualitative. A quantitative insight on the potential for clays to be heated by microwaves requires a comprehensive study of the microwaves/clay interaction. In Chapter 4, it was explained how the dielectric properties of a material describe its response to microwaves and are used to design applicators for an optimal energy delivery (Metaxas and Meredith, 1983). Therefore, the measurement of the dielectric properties of clays can serve to determine the potential for clay firing using microwave energy. Furthermore, modification of the state of these clays or the conditions of the measurements, e.g. red or yellow, slabs or powders and 2470 MHz or 912 MHz, enables the evaluation of the parameters that affect these dielectric properties, such as void fraction, frequency, temperature and composition.

This section starts with the measurement of the dielectric properties of red and yellow clays in the same state as dried unfired bricks, i.e. solid slabs ready for firing, using the cavity perturbation method. Measurements took place between 20-950 ^{o}C at the frequency of 2470 MHz in order to determine the potential for the microwave heating of clays and its variation with temperature. Changes in the dielectric properties with temperature were traced back to the clay mineralogy and their thermal transformations shown in Figure 6.4. Moreover, the influence of changing compositions was addressed by comparing the dielectric properties of red and yellow clays. Next, the same measurements were performed using powdered clay specimens to investigate the influence of void fraction on clay processing, and at 912 MHz to quantify the effect of different processing frequencies. An analogous study focused on the single clay constituents aiming to identify the specific species that may facilitate microwave firing through selective heating. Finally, the statistical significance of the small samples measured by the perturbation method was confirmed by measuring the dielectric properties of half-sized dried unfired bricks at 2450 MHz in the 20-800 ^{o}C range using the waveguide technique.

6.3.1 Dielectric properties of red and yellow Danish clays

6.3.1.1 Influence of composition on clays dielectric properties

Dielectric properties of 19.2±1.0x3.2±0.4 mm cylindrical yellow and red clay slabs measured across the firing temperature range of 20-950 ^{o}C at 2470 MHz and at the void fractions shown in Table 6.2 are presented in Figure 6.5. The y-axis represents the dielectric constant and the loss factor while the x-axis is the temperature of the furnace. The methodologies of the sample preparation and the dielectric property measurements using the resonant cavity

technique are explained in Section 5.2.1 and Section 5.3.6.1, respectively. Tables of the dielectric properties can be found in Appendix B1. The error bars of the measured trends represent a 95% confidence interval.

The dielectric constants and the loss factors display contrasting behaviours upon temperature increase. The former remain stable in the 3.0-4.0 range, while various trend changes are recognisable in the losses that can be related to clays' physicochemical transformations. The stability of the dielectric constants implies a consistent interaction of the electric field with the clay that ought to translate into applicator designs that are non-sensitive to different clay loads (Metaxas and Meredith, 1983, Chan and Reader, 2000, Mehdizadeh, 2015).

As anticipated at the beginning of this chapter, free water moisture is the dominant dielectric phase below 100 ºC due to its comparatively higher loss factor than the mineral species and its superior ability to couple with the microwave field (Kraszewski, 1996). Its effect is seen as a peak around 50 ºC in the losses of both clay types, which is consistent with moisture behaviour in granular materials first as physically bound and later as free water as elaborated in Section 4.3.1.3. In this temperature range, yellow clay from both Vedstaarup and Hammershoj peak at around 0.10, almost doubling Helligsø red while still being surpassed by Hammershoj red with 0.12. This can't be explained by the slab moisture contents in Table 6.2, as the clay with the highest moisture content has the lowest loss. It could be that the marginally lower void fraction of the yellow specimens counteracts their drier nature, but this still doesn't explain why the loss of Helligsø red is lower than Hammershoj red, despite having a higher moisture content and similar void fraction (within error bars). Probably at this point, differences in the spatial arrangements of the minerals in each clay account for the response imbalance.

In the 100-350 ºC range, there is a general decline in the loss factors, reaching 0.026 and 0.040 for the red and yellow types respectively at 300 ºC. This is a result of the absence of mineral transformations and physically bound water removal, which is consistent with the TGA and DSC diagrams of Section 6.2.2. Physically bound water removal is barely recognizable as a peak at 250 ºC.

Above 350 ºC, clay minerals dehydroxylations result in the continuous release of interlayer cations outside the mineral lattices (Grim, 1968). The increase of free charge carriers in the clay matrix and their heightened thermal agitation with temperature explains the observed loss factors escalation, which are similar for all samples regardless of their composition. As expected from its microwave transparency, no noticeable effect of the quartz inversion at 570 ºC is seen in any of the trends.

An inflection point to the loss trends takes place around 800 ºC as sintering begins. This is most evident in red clays, as their slope increases one order of magnitude compared to the previous dehydroxylation stage. The porosity reduction and the enhanced diffusion of charge carriers associated with the sintering process explains the losses increment (Dejonghe and Rahaman, 2003). During this stage, the thermal decomposition of calcite into CO_2 and quicklime takes place, where the subsequent porosity increase competes with the sintering causing a momentary loss stabilisation for yellow clays around 800 ºC and a slower increase with temperature afterwards. On the other hand, the mineral recrystallisations that take place around 900 ºC and the lime reactions do not seem to noticeably affect the trends.

Despite differences in the composition of red and yellow clays, their dielectric properties are similar, where the only clearly recognisably differentiating feature is the calcite decomposition loss stabilisation. In the case of the dielectric constants, it was explained in Chapter 4 that the thermal evolution of a substance's dielectric properties can be understood as their shift to higher frequencies. Hence, their indifference to temperature changes is explained by the stability of the dielectric constants of some of their constituents over a wide frequency range (Nelson et al., 1989, Church et al., 1988). The dielectric constants insensitivity to composition probably comes from the presence of large amounts of low loss materials like quartz and feldspars in all clays, which to a large extent erase trend differences among them. The same reasoning justifies the similarity of the loss factor trends, where only at two points is this likeness disrupted. The first is observed below 100 ºC, which to an extent is caused by differences in free water content, while the second takes place at 800 ºC and is the result of contrasting calcite contents. As a result of the latter, red clays manage to surpass the density imbalance becoming the lossiest clay type until the end of the heating, reaching a maximum difference at 950 ºC as yellow losses as high as 0.145 are at least 40% lower than the red ones.

Looking at the generally accepted limits for the microwave processing of a substance introduced in Chapter 4 , i.e. $0.01 \leq \varepsilon'' \leq 5$ (Metaxas and Meredith, 1983), it can be concluded that all clays are well within the established boundaries and ought to be successfully heated to firing temperatures by microwave energy. However, the loss factor variations with temperature suggest shifts in the potential for microwave heating during processing. Initially, the free water content of clays dominates the microwave heating capacity, while its removal drops the loss factors down to 0.026 in Hammershoj yellow at 350 ºC. Nevertheless, this value still more than doubles the lower threshold for microwave treatment. On the other hand, from this temperature forward, all clays are expected to progressively heat better due to the clay minerals dehydroxylations. Finally, red and to a lesser extent yellow clays ability to heat begins to increase exponentially with temperature beyond 850 ºC, as seen in Figure 4.12,

which is consistent with previous work regarding the microwave heating of ceramics reviewed in Chapter 4.

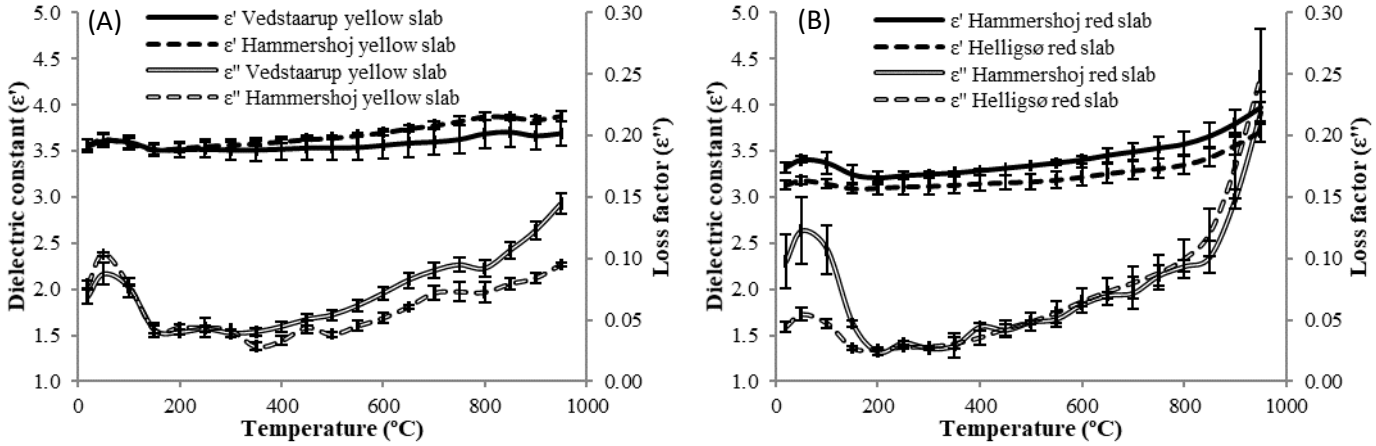


Figure 6.5- Average dielectric constants and loss factors across firing between 20-950 ºC at 2470 MHz for yellow (A) and red (B) Danish clays slabs at void fractions ranging 0.37±0.02 for Vedstaarup yellow, 0.39±0.01 for Hammershoj yellow, 0.40±0.01 for Helligsø red and 0.42±0.03 for Hammershoj red. These results are the average of three repeats.

6.3.1.2 Influence of void fraction on clay dielectric properties

An assessment of the impact of the void fraction/porosity of clays on their dielectric properties across the 20-950 ºC range comes from the comparison of the dielectric trends of the clay slabs of Figure 6.5, at void fractions 0.39-0.42, with those of the same materials at higher void fraction levels, i.e. 0.56. The latter are obtained through the dielectric property measurements of clay powders at 2470 MHz, where the same cavity perturbation methodology applied above and described in Section 5.3.6.1 is used. The resultant dielectric trends are presented in Figure 6.6, while the data tables are located in Appendix B1. The error bars of the measured trends represent a 95% confidence interval.

The results in Figure 6.6 indicate an overall reduction of the dielectric response with the void fraction increase. This is consistent with the larger content of microwave transparent air in the mineral mixtures that form the clays (Meredith, 1998), as it also contributes to the final dielectric properties. The dielectric constants decrease 30% on average. The loss factors drop between 50-70%, where the clays reach values below the processing limit at times with losses as low as 0.007 around 300 ºC. It is to be noted that the moisture increase of all clays upon powdering partially counteracts the loss factor decrease below 150 ºC. The removal of the void fraction differences between clays results in the minimisation of the divergences previously observed in Figure 6.5, which further diminishes the effect of contrasting compositions on the dielectric response.

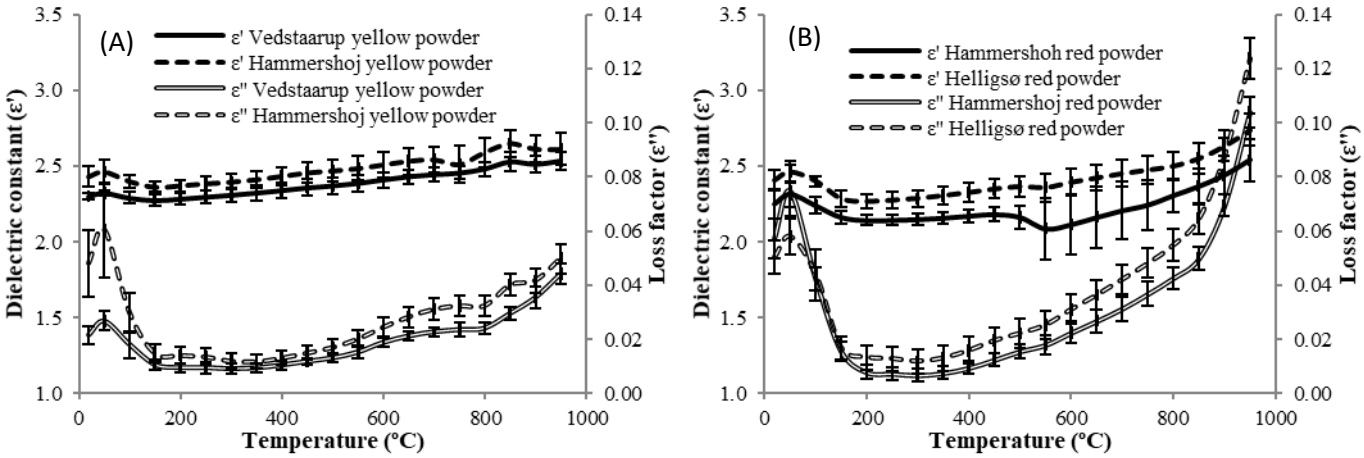


Figure 6.6- Average dielectric constants and loss factors across firing between 20-950 ºC at 2470 MHz for yellow (A) and red (B) Danish clays powders with a 0.56±0.03 void fraction. These results are the average of three repeats.

6.3.1.3 Influence of frequency on clay dielectric properties

Considering the dipolar polarisation and ionic conductivity heating mechanisms, whose typical effects on the dielectric properties across the frequency range are displayed in Figure 4.2, it is clear that clays at 2470 MHz are likely to be heated by both mechanisms. Each heating mechanism is dominant in a certain temperature range. Up to 350 ºC, dipolar polarisation prevails owing to the presence of water, which is a strongly dipolar fluid (Kraszewski, 1996). From this temperature onwards, the losses' steady rise due to the increasing presence and thermal agitation of free charge carriers resembles a conductive response (Metaxas and Meredith, 1983). As a result, a frequency shift may affect differently each area of dominance or modify their ranges of influence, as explained in Chapter 4.

Similarly to data presented for void fraction, the effect of the processing frequency on the dielectric properties of red and yellow Danish clays is investigated by comparing the 2470 MHz dielectric properties of Figure 6.5 and Figure 6.6 with dielectric property measurements of clay powders and slabs at 912 MHz. These trends are shown in Figure 6.7. The methodologies presented in Section 5.2.1 and Section 5.3.6.1 are applied. The error bars of the measured trends represent a 95% confidence interval and the dielectric properties data tables are located in Appendix B1.

Upon the frequency shift to 912 MHz, it is first noted that trend differences between clays remain almost identical, either as powders or solid slabs. This means that the thermal reactions effect on the trends is not magnified nor obscured by the processing frequency. Dielectric constants data for both clay types are particularly indifferent to frequency changes, as only a small increase is distinguished for the red clays around 950 ºC, going as high as 4.5 and 3.1 for slabs and powders, respectively. On the contrary, there appears to be a noticeable increase in the loss factors of all clays across firing regardless of their state.

Peak dielectric losses within the 20-350ºC range are increased from around 0.05-0.10 at 2470 MHz to 0.06-0.14 at 912 MHz for slabs and 0.03-0.07 to 0.05-0.08 for powders. In this range, microwave interactions are still dominated by dipolar polarisation. Previous work in clays and soils (Hoekstra and Delaney, 1974, Rankin and Singh, 1985) has reported relaxation frequencies at around 1000 MHz for physically bound water and tightly held free water. Therefore, the frequency reduction to 912 MHz comes closer to the peak in their dispersion zone, resulting in a loss increase. Understandably, the low equilibrium moisture of clays seen in Table 6.2, i.e. <2%, translates in a moderate loss increment, averaging around 13.7% and 16.3% for red and yellow clays. Conductive effects become more prominent as frequency decreases (Metaxas and Meredith, 1983). Hence, the consequences of the frequency swift are more readily visible in the conductive area of influence. This results in around 30% higher losses at the lower frequency at 300 ºC for both clays, reaching a maximum at 950 ºC more than doubling 2470 MHz values for yellow clays and increasing 91.5% for the red type. An exception is found on powdered Vedstaarup yellow, which presents a more than two-fold loss increment across the whole firing range. This could be caused by its relatively higher proportion of clay minerals than the other yellow specimen and a smaller quartz presence than in the red type, which represent the lossiest and most transparent phases of clays according to Table 4.1.

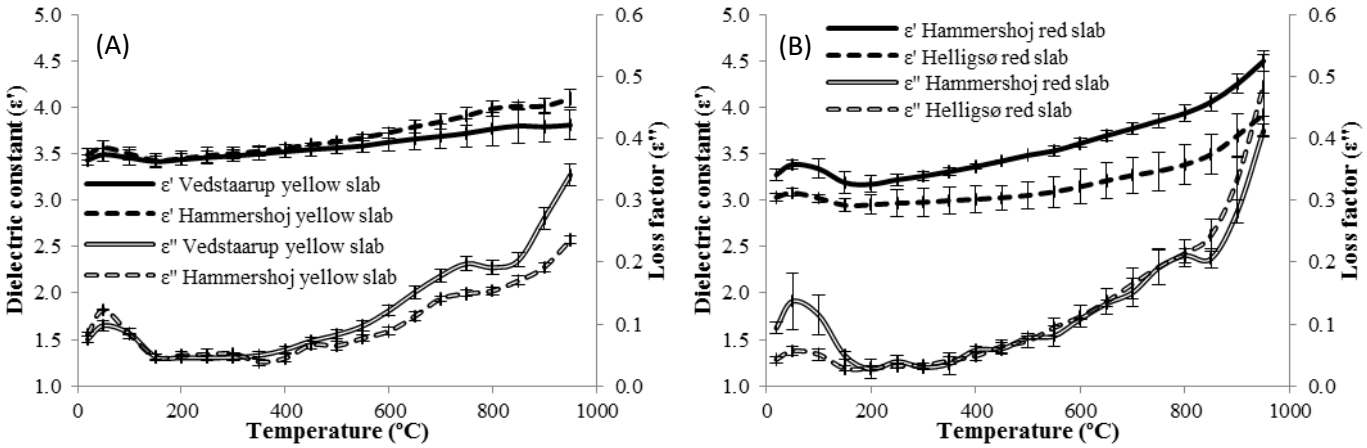


Figure 6.7- Average dielectric constants and loss factors across firing between 20-950 ºC at 912 MHz for yellow (A and C) and red (B and D) Danish clay slabs (A-B) at void fractions ranging 0.37±0.02 for Vedstaarup yellow, 0.39±0.01 for Hammershoj yellow, 0.40±0.01 for Helligsø red and 0.42±0.03 for Hammershoj red, and powders (C-D) at void fractions ranging 0.56±0.03. These results are the average of three repeats.

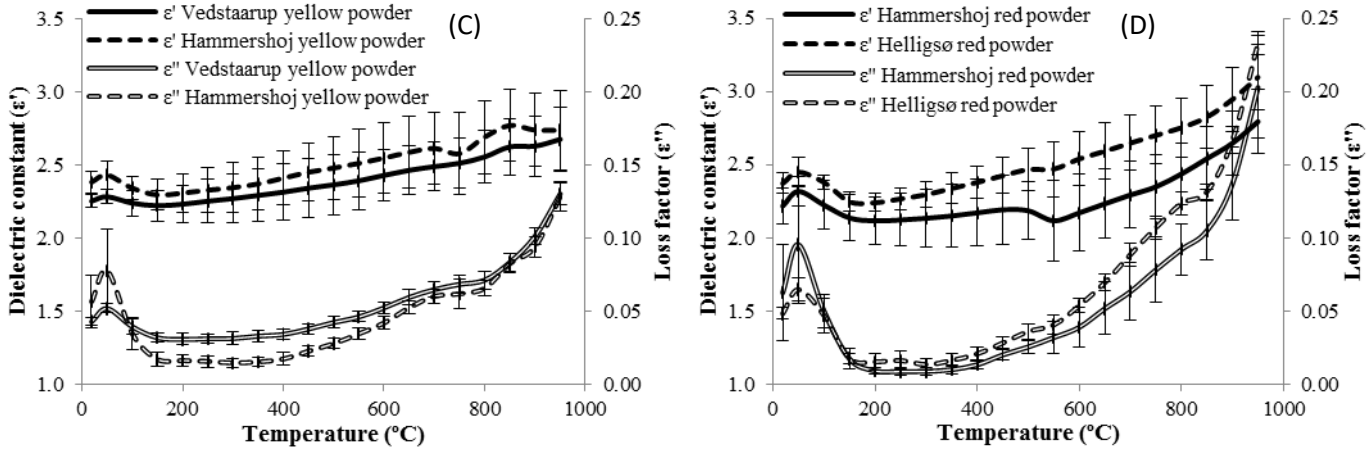


Figure 6.7- Continued.

6.3.1.4 Conclusions on the dielectric properties of red and yellow Danish clays

The study of the dielectric properties of Danish clays provides a comprehensive understanding of the potential for microwave energy to perform clay firings. Red and yellow clays at the same void fractions as unfired bricks and studied at the near to ISM frequency of 2470 MHz display a dynamic response to the microwave field as heating progresses, as seen in the evolution of their loss factor trends. The presence of free and to a lesser extent physically bound water dominate clays' dielectric response at the beginning of the process, while their disappearance reduces the losses down to 0.026-0.040 at 300 °C. From 350 °C, the loss factors increase with temperature. Hence, a more efficient heat generation is expected as clays become hotter. After 800 °C, the escalation of dielectric loss with temperature is hastened by one order of magnitude. During heating, the loss factors of all clays fluctuate in the ranges proposed by Metaxas and Meredith (1983). Thus, it is expected that red and yellow Danish clays can be fired exclusively using microwave energy.

The study of the major parameters that are likely to affect the dielectric properties of clays, namely composition, temperature, void fraction and frequency, has shown that all exert a noticeable influence on the final dielectric response, albeit to various degrees. Among them, the highest influence comes from the constituents' physicochemical transformations with temperature, i.e. water removal, clay minerals dehydroxylations, calcite decomposition and sintering. On the other hand, both clay types display similar loss trends despite mineralogical differences, with only calcite causing a significant difference between them around 800 °C. The inclusion of air in clay's macrostructural spaces, e.g. pores, resulting from a void fraction increase to 0.56 from 0.37-0.42 upon powdering the clay slabs, causes an understandable decline of the dielectric properties. The loss factors decrease on average 60%, while the dielectric constants drop by 30%. Coincidentally, void fraction is the only parameter that noticeable affects the dielectric constants. The frequency shift from 2470 MHz to 912 MHz

boosts the losses of all clays due to approaching the physically bound water relaxation peak below 350 ºC, and increasing the influence of the ionic conductivity effects as the material heats after water removal.

It is worth noting that the dielectric properties shown above are the global response of the system to the microwave field, as clays are understood as homogeneous entities in the context of the measurements. However, the heterogeneity of the clays seen in Table 6.1, their constituents' contrasting dielectric properties in Table 4.1, and the preferential distribution of moisture in the clay minerals as described in Table 6.3 suggests the selective heating of the most microwave absorbing species, rather than the uniform dielectric response according to the clay dielectric properties presented in Figure 6.5-6.7. A study of the dielectric properties of the major clay constituents is therefore necessary to clarify the likelihood of the two possible heating paths.

6.3.2 Dielectric properties of clay constituents

Insight into the effect of composition on the microwave/clay interaction obtained above has not individually addressed the influence of each major clay constituent, so it is unknown which mineral species control the microwave processing. A study of the dielectric properties of the major clay constituents across firing can help uncover the dominant dielectric species. Furthermore, the minerals' assessment also serves to investigate the previously mentioned possibility of an uneven heating profile across the clay volume under microwave firing.

The dielectric properties of slabs of kaolinite, montmorillonite, muscovite, orthoclase, albite, calcite and quartz at different void fractions seen in Table 6.3, and measured in the 20-950 ºC range at 2470 MHz are displayed in Figure 6.8. The axis scales have been modified to enable the recognition of thermal changes. Data tables of their complex dielectric permittivity are present in Appendix B2. As before, the error bars represent a 95% confidence interval. The measurement methodology can be seen in Section 5.3.6.1. Slabs are selected for the analysis since the dielectric properties increment with density, seen for the clays above, provides for a more straightforward recognition of thermal transformations. However, their diverging void fractions hamper a completely quantitative assessment. The dielectric trends of powders and the 912 MHz analyses are presented in Appendix B2, but are not discussed here as the constituents' behaviour with frequency and void fraction is analogous to that of clays.

Figure 6.8 shows that, similarly to clays, most dielectric constants are relatively stable with temperature in a 3.0-5.6 range. However, minor changes found in the trends of some species, i.e. clay minerals and calcite, can be related to thermal reactions. For example, in Figure 6.8B kaolinite metakaolinization (McConville and Lee, 2005) causes a sudden 7% dielectric

constant decrease around 550 ºC, while in Figure 6.8A montmorillonite and muscovite sintering (Dejonghe and Rahaman, 2003, Dunham, 1992) boosts their dielectric constants 19% and 37% respectively in the 800-950 ºC range. Moreover, in Figure 6.8B the dielectric constant of calcite drops from 8.33 at 800 ºC to 6.19 at 950 ºC following its decomposition (Galan et al., 2013). It can be argued that the absence of evidence of this transformation in the clay dielectric properties is because they are masked by the other forming minerals due to their thermal stability (Dunham, 1992, Galan et al., 2013, Heaney, 1994, Chen et al., 2000, McConville and Lee, 2005, Bohor, 1963).

In the case of the losses, the non-clay minerals quartz and calcite can be considered microwave transparent, only becoming moderate microwave absorbers, i.e. ε''>0.01 (Metaxas and Meredith, 1983), at 950 ºC and after 600 ºC, respectively. The feldspars albite and orthoclase leave the transparency range after 100 ºC, with a maximum loss of around 0.052 at 950 ºC. Clay minerals have the highest loss factors. Montmorillonite is the most absorbing species and is expected to become the dominant microwave phase after free water removal, with losses between 0.214 at room temperature and 1.487 at 950 ºC. As explained in Chapter 3, this is due to its interlayer cation content and exceptional water affinity, as its 50 ºC free water loss peak is shifted to 100 ºC and it joins with another that reaches a maximum around 300 ºC, marking its dehydration. The comparatively drier muscovite is the second most absorbing mineral due to its moderate interlayer cations content, with losses averaging around 0.147 until sintering raises them four-fold at top temperature. Finally, kaolinite's lack of water and free charges explains why its losses are one order of magnitude lower than muscovite's and approach those of the non-clay minerals.

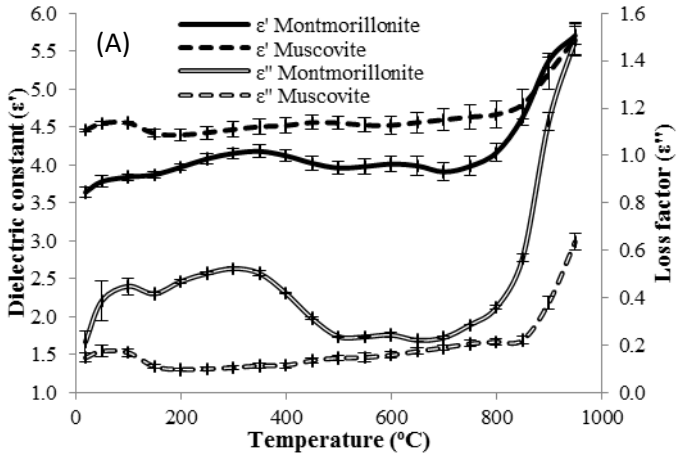


Figure 6.8- Average dielectric constants and loss factors across firing between 20-950 ºC at 2470 MHz for mineral slabs at void fractions ranging 0.32±0.03 for montmorillonite, 0.22±0.07 for muscovite (A), 0.48±0.02 for kaolinite, 0.09±0.03 for calcite, 0.17±0.01 for quartz (B), 0.17±0.07 for orthoclase and 0.35±0.06 for albite (C). These results are the average of three repeats.

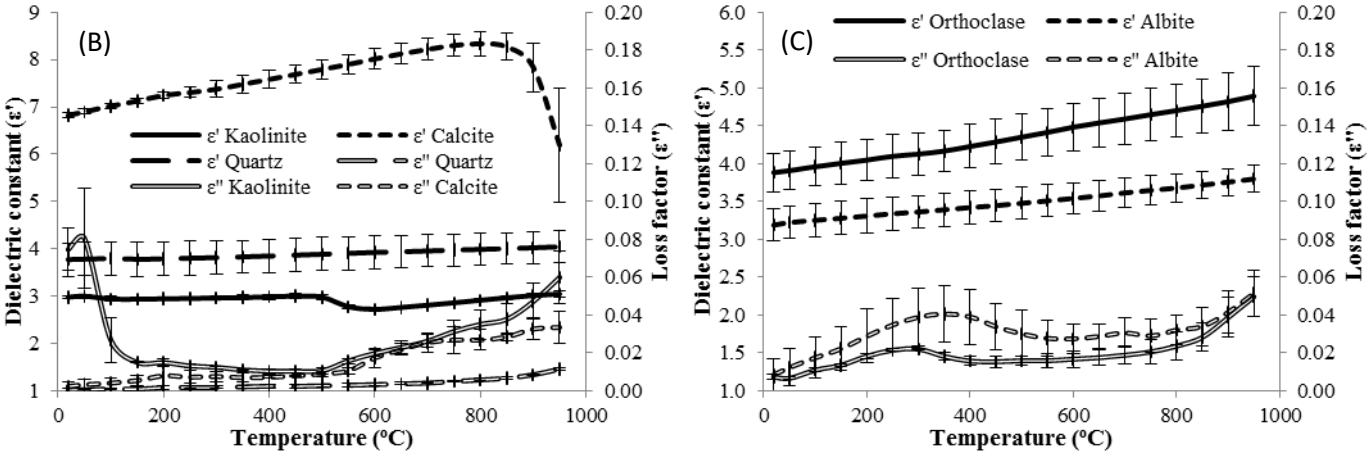


Figure 6.8- Continued.

From the results of Figure 6.8, it is reasonable to expect that some phases within clays may heat selectively and therefore that the clay dielectric properties reported in Section 6.3.1 may not represent the real behaviour of clays under microwave heating. Instead, it is possible that the comparatively better microwave coupling of montmorillonite and muscovite will result in their selective heating. This is also evidenced by the similarities in the trends of the loss factors of these clay minerals and the clays. Based on the dielectric property measurements reported here, clay mineral lumps could heat faster than the surrounding components, subsequently conventionally heating the more transparent species that surround them, creating hot spots and thermal gradients. Nevertheless, it is also possible that the clay constituents are to an extent homogeneously distributed in the clays matrix. Consequently, the clay dielectric property diagrams above would be closer to the real microwave/material behaviour. A final confirmation of the validity of either of these hypotheses comes from the microwave heating trials on clays covered in the next chapter.

6.3.3 Comparative analysis of clay dielectric properties

The heterogeneous and multicomponent nature of clays means that the dielectric properties of the small samples measured using the cavity perturbation method may not be representative of a whole brick, regardless of the efficiency of the sampling. A Student's T two tailed statistical analysis is developed in Section 5.3.6.1 in order to prove that the previous measurements of small clay samples align with the mean of the population. In this case, the average dielectric properties of the population are extracted from measuring half bricks in the 20-800 ºC range at 2450 MHz using the waveguide technique, whose values can be seen in Appendix B1.

Table 6.4 presents the T values of Eq. 5.10 for the dielectric properties of Danish clays at different temperatures during firing. Considering the number of measurements and the desired

degree of confidence, i.e. 3 and 95%, the boundary T_C can be extracted from a conversion table (Peck et al., 2015), having a value of ±4.303. It is straightforward that at all temperatures the calculated T values fall within the range designated by T_C. Hence, there is not enough statistical evidence to accept the hypothesis that the average dielectric properties of the samples investigated (cavity results) are different from the average of the population (waveguide results). Consequently, the dielectric property measurements of clays obtained from the resonant cavity are statistically representative of the whole population of Danish clays.

Table 6.4- T values for the dielectric constants and loss factors between 20-800ºC at 2450 MHz of red and yellow Danish clay slabs at void fractions ranging 0.37±0.02 for Vedstaarup yellow, 0.39±0.01 for Hammershoj yellow, 0.40±0.01 for Helligsø red and 0.42±0.03 for Hammershoj red. These results are the average of three repeats.

T (ºC)	Vedstaarup Yellow		Hammershoj Yellow		Hammershoj Red		Helligsø Red	
	ε'	ε''	ε'	ε''	ε'	ε''	ε'	ε''
20	4.298	4.037	0.550	-3.337	-1.788	-0.536	4.298	4.038
200	2.250	-2.394	0.717	3.191	-0.642	2.382	2.250	-2.395
400	-3.347	-3.435	2.848	-3.455	-1.927	-3.336	-3.347	-3.435
600	-3.589	3.849	2.141	-3.647	-3.668	-1.694	-3.589	3.850
800	-4.107	-3.445	4.199	-3.906	-2.215	-2.353	-4.107	-3.445

6.3.4 Conclusions on dielectric property measurements of clays and clay constituents

The dielectric properties of red and yellow Danish clays and their major clay constituents have been investigated across the firing range of 20-950 ºC and at the frequencies of 912 MHz and 2470 MHz. The clay and mineral specimens have been studied at different void fractions as solid slabs and powders. Data obtained from these resonant cavity measurements has been proved statistically representative of the whole population of Danish clays. The dielectric properties of clays at the same void fraction as unfired bricks convey that these materials can be successfully fired using microwave energy, as they are at all times over the minimum processing threshold stablished by Metaxas and Meredith (1983).

The potential for microwave firing fluctuates across firing, which is caused by clays' composition and their evolution with temperature. Free and physically bound water ensure the microwave heating near room temperature, while their removal drops the microwave heating potential until the start of the clay minerals dehydroxylations at 350 ºC. Beyond this temperature, there is a continuous improvement of the heat generation as clays get hotter, which is further enhanced after sintering at 800 ºC. Among clay constituents, montmorillonite and muscovite are the dominant dielectric species after free water removal due to their water affinity and interlayer cations content, displaying losses between one and two orders of magnitude higher than the non-clay minerals. As a consequence, there is uncertainty about

whether microwaves may selectively heat these constituents which in turn heat the rest of the clay, or the whole system is heated volumetrically as indicated by the clay dielectric properties. Both clay types share similar dielectric trends up to calcite decomposition at 800 ^{o}C regardless of their mineral differences. This may be the result of the homogenising effect of the low loss phases, which form around 64.3% of the clays.

Besides composition and temperature, void fraction and frequency also affect the final dielectric response. A void fraction increase of 34% can be understood as the addition of transparent air inclusions to the clay matrix, justifying why the dielectric constants and loss factors drop by 30% and 60%, respectively. On the other hand, a frequency shift to 912 MHz causes a general loss factors increase, as the system approaches the dipolar dispersion area of physically bound water and the zone of ionic conductivity heating effects dominance.

A quantitative insight into the potential for microwaves to successfully fire Danish clays has been presented. Moreover, the influence of parameters like temperature and composition has been determined. The next step is to apply the knowledge gained from these measurements to develop a tool to predict the dielectric response of other clays. This would enable the prediction of dielectric properties based on knowledge of the physical and chemical characteristics of the clay (moisture content, mineral composition and void fraction). The value of such a tool would be that brickworks would be able to assess if clay from a new source or a recently developed synthetic clay would be suitable for heating, and whether and how the furnace operating parameters should be changed to achieve the desired heating profile. In addition, knowledge of the likely variation in dielectric constant of clay loads would inform furnace design. This approach would avoid the necessity to carry out high temperature dielectric property measurements for every possible clay material, which requires specialised equipment and expertise, along with significant time investment.

6.4 Theoretical estimation of clays dielectric properties

In the pursuit of assessing the potential for microwave processing of clays, it is worth noting that industries like brickworks and non-technical specialists won't generally undertake the measurement of the dielectric properties of their chosen clays. The justification is that the available measuring methodologies presented in Chapter 4 are time-consuming and require a high level of technical expertise and specialised equipment. A fast and simple alternative to the dielectric property measurements of clays consists of their estimation through the use of electromagnetic mixing rules. The development of a mixing rules predictive tool unlocks the possibility of evaluating the microwave heating potential of any natural or synthetic clay. Although this cannot be directly used on controlling the firing process, it enables the quantification of the individual effect of a mineral on the clay dielectric response, which aids

in the formulation of new brick mixtures for microwave processing. This is particularly interesting in the context of developing new clays for product quality or energy optimisation purposes.

A number of mixing rules, shown in Table 4.4, have been chosen based on their previous success when applied to clays, clay constituents or similar materials. There are two available alternatives for the clay dielectric trends estimation, namely a binary or multicomponent approach. The similarity of red and yellow clay dielectric properties despite mineralogical differences opens the possibility of disregarding any mineralogy, treating these materials as binary clay-air mixtures. This streamlines the mixing model as now any clay can be estimated from its void fraction and the dielectric properties of Figure 6.5-6.7. The multicomponent alternative consists of using the mineralogy and void fraction of the target clay instead, so the dielectric properties of clay constituents can be combined to form the desired clay.

Despite previous work on clay materials, no error threshold that certifies the success of the predictions has yet been established. In this study, a conservative approach is taken so that the error limit is set as the standard deviation of the measurements for clay powders and slabs at 2470 MHz, i.e. 5.1% deviation for the dielectric constants and 18.8% for the loss factors. This means that in order for the estimations to be considered adequate, they must fall under the uncertainty ranges of the cavity measurements.

This section starts with the dielectric property estimations of red and yellow Danish clay slabs and powders across 20-950 ^{o}C at 912 MHz and 2470 MHz using the binary clay-air approach, i.e. estimations come from the dielectric properties of clay powders and slabs, respectively. Disregarding the clays' mineralogy focuses the estimations on predictions of clay dielectric properties at different void fractions. The suitability of this model is validated by comparing the accuracy of its predictions with the estimations resultant of estimating clay powders and slabs from the combination of the dielectric properties of mineral powders and slabs, respectively. Next, the validity of the successful model is expanded to cover clays of the whole of Europe, where the boundaries for achieving accurate predictions are addressed.

6.4.1 Dielectric property estimation of binary clay-air mixtures

The most common approach when applying mixing rules to any material consists of using its dielectric properties as a powder to perform estimations of lower void fraction mixtures, e.g. solid slabs (Nelson, 2005, Nelson et al., 1989, Boyacı et al., 2009). This is the most logical approach, as obtaining specimens of some natural materials at specific densities can be challenging while powders are fairly easy to manipulate. Consequently, the mixing rules study is focused on estimating clay slabs from powders, while the results of the reversed

procedure are presented in Appendix C1, and the same for 912 MHz predictions. This is justified by the mixing rules generally not taking into consideration frequency (Sihvola, 1999) and clay dielectric properties not being significantly affected by a frequency shift. The fact that minerals are not considered in the binary approach means that the estimations are focused on dielectric property predictions at different densities.

The results of estimating the dielectric properties of the clay slabs from Figure 6.5 using the clay powders of Figure 6.6 are displayed in Figure 6.9. Only the most accurate mixing rules are displayed here for clarity purposes, i.e. Lichtenecker, Böttcher and Sen-Scala-Cohen, while the full tables of the estimations can be seen in Appendix C1. An explanation of these rules comparatively better accuracy than the rest is provided below. The y-axis represents the measured and estimated dielectric constants and loss factors, while the x-axis is the temperature of the material. The binary clay-air predictions methodology described in Section 5.3.7 has been followed. The error bars of the estimations have not been added for clarity and are assumed to have the same error as the experimental powder measurements, as extrapolation of powders' deviations to lower volume fractions render unreasonable errors.

In the first place, it is observed that measured and estimated dielectric constants of red and yellow clays do not share the same trends. This is expected from the different slopes observed between powders and slabs. Nevertheless, the values of measurements and estimations are similar for both clay types due to the dielectric constants' thermal stability. An exception is the case of Hammershoj red in Figure 6.9E, where a sudden trend shift in all the estimations around 550 ^{o}C which resembles the metakaolinization effect causes deviations of up to 15%. Its appearance is explained by the magnification of minor trend variations from the powder measurements upon a void fraction reduction, although this clay does not have a larger concentration of kaolinite than the other specimens attending to Table 6.1.

Estimated and measured loss factor trends look almost identical after free water removal. However, the accuracy of the mixing rule predictions differs across the clays considered. In yellow clays, all predictions in Figure 6.9B clearly underestimate Vedstaarup losses across the whole temperature range, peaking at 50 ^{o}C with the real values doubling the estimations. In Hammershoj in Figure 6.9D, approximation errors are comparatively minimal beyond 300 ^{o}C, while averaging around 36% below this temperature. This is explained by the larger physically bound water presence on the solid slab compared with the powders, and indicates that the moisture fix described in Section 5.3.7 is inadequate to completely compensate the moisture imbalance between powders and slabs. This limitation in the binary estimations is common to all clays, as red specimens display their estimated and measured values within error bars for most of the firing excepting around 50 ^{o}C. Their larger moisture content results

in a predictably larger uncertainty at this point, with Helligsø and Hammershoj presenting deviations close to 58% and 66%, respectively.

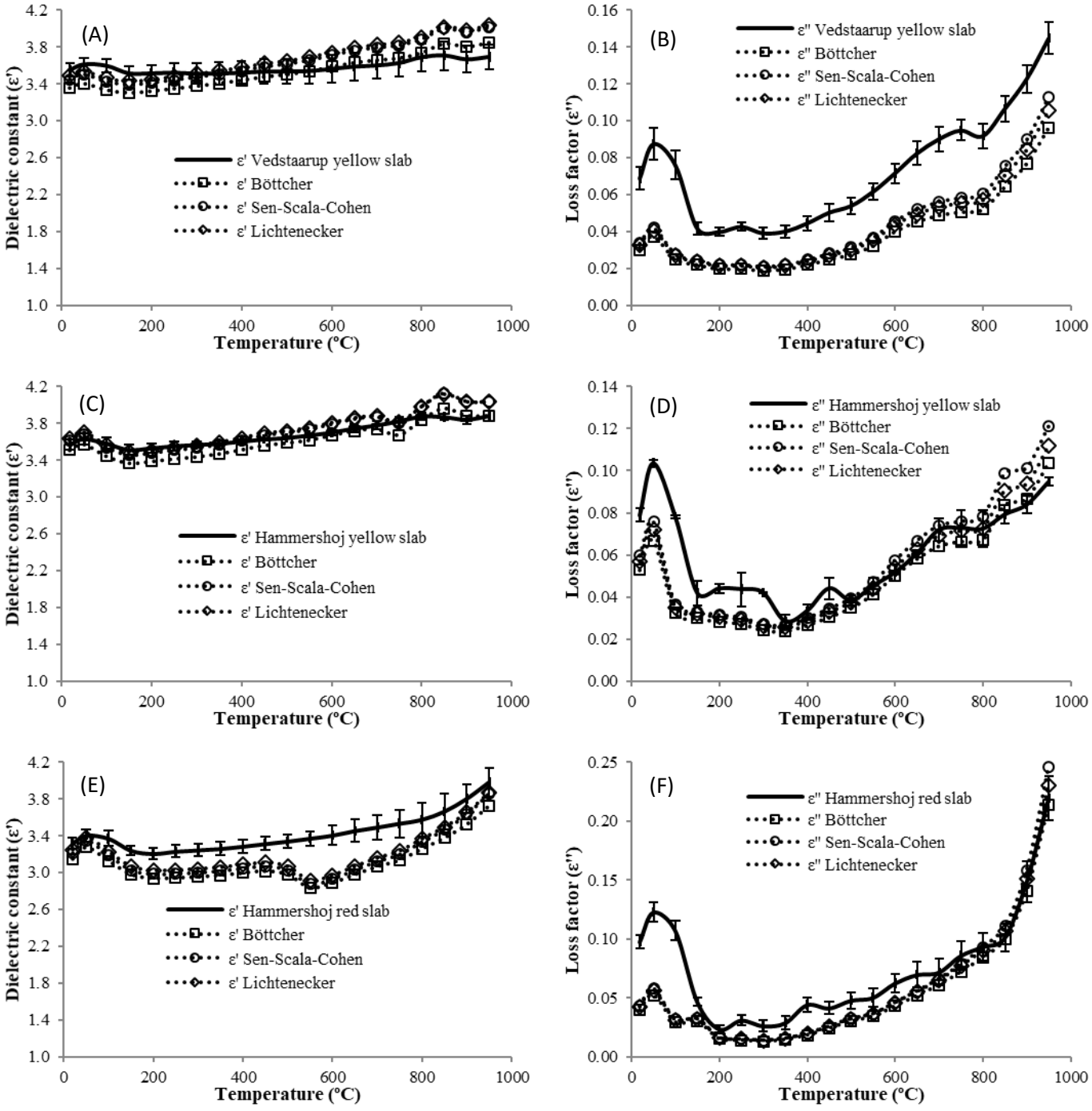


Figure 6.9- Average dielectric constants (Left) and loss factors (Right) across firing between 20-950 ºC at 2470 MHz for Danish clay slabs at void fractions ranging 0.37±0.02 for Vedstaarup yellow, 0.39±0.01 for Hammershoj yellow, 0.40±0.01 for Helligsø red and 0.42±0.03 for Hammershoj red, and mixing rules approximations from clay powders at void fractions ranging 0.56±0.03 for yellow (A-D) and red (E-H) clays. These experimental results are the average of three repeats.

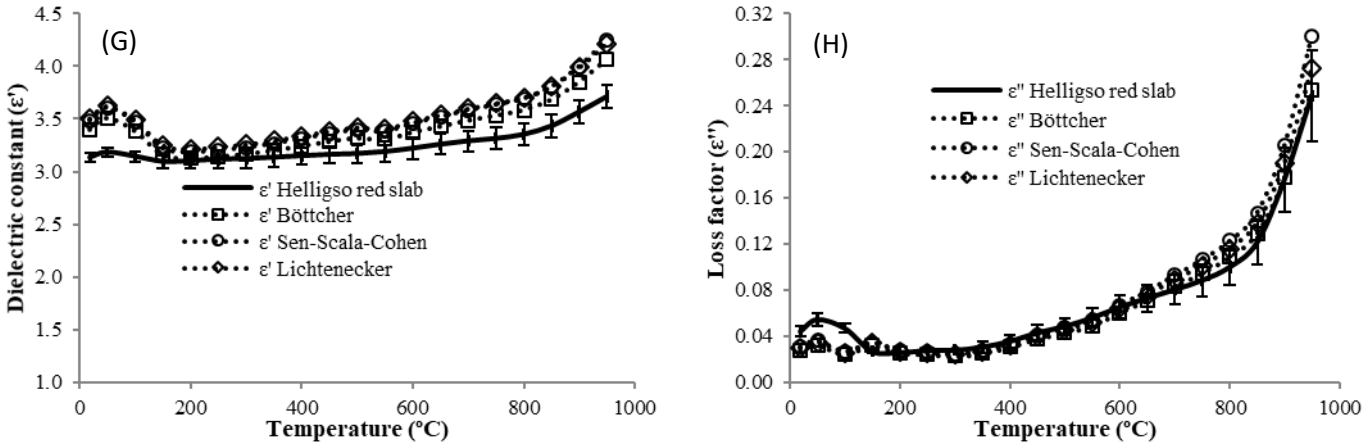


Figure 6.9- Continued.

The performance of each individual mixing rule is better understood by looking at Table 6.5. Here, the measured dielectric properties are compared with the mixing rule approximations at selected temperatures, while the full firing range is displayed in Appendix C1. Lichtenecker appears to give on average the best fit to the complex dielectric permittivity, closely followed by Böttcher and Sen-Scala-Cohen. The suitability of the first is consistent with its widely spread use on moist and porous soils (Regalado, 2004, Leao et al., 2015), while Böttcher accuracy is explained by its focus on low loss and crystalline specimens (Dube and Parshad, 1970). Despite the numerous interactions among clay constituents (Grim, 1968), usage of Sen-Scala-Cohen does not provide a significant improvement over the other rules, probably because here clays are considered in bulk as an aluminosilicate compound.

Regarding the other mixing equations, the large dielectric contrast between the voidless clay and air that form the mixture would explain the comparatively poorer performance of Landau-Lifshitz-Looyenga, while Bruggeman-Hanai has the same problem as Sen-Scala-Cohen but with the added challenge of lacking interfacial polarisation effects that drive its derivation (Hanai, 1960). Finally, more versatile formulas like the two versions of the Complex Refractive Index and Rayleigh proved to give the worst results, especially in the case of the latter, probably because it fares better in dilute media. Considering the CRI equations, the semi-empirical α=0.65 version turns out to be the worst despite its reported better match for clay soils (Brovelli and Cassiani, 2008).

Table 6.5- Comparison between measured dielectric properties of slabs of red and yellow Danish clays at void fractions ranging 0.37±0.02 for Vedstaarup yellow, 0.39±0.01 for Hammershoj yellow, 0.40±0.01 for Helligsø red and 0.42±0.03 for Hammershoj red shown here at certain temperatures across the 20-950 C firing range at 2470 MHz and binary clay-air mixing rules approximations from clay powders at void fractions ranging 0.56±0.03. The standard uncertainties are indicated in the table.

Clay	T (ºC)		Measured Values	Complex Refractive Index	Landau-Lifshitz-Looyenga	Bruggeman-Hanai	Böttcher	Lichtenecker	Rayleigh	Sen-Scala-Cohen	Complex Refractive Index α=0.65
Vedstaarup Yellow	20	ε'	3.55	3.15	3.24	3.17	3.36	3.49	3.08	3.45	3.08
		ε"	0.069	0.025	0.027	0.025	0.030	0.033	0.023	0.034	0.024
Hammershoj Yellow		ε'	3.57	3.28	3.38	3.30	3.51	3.63	3.21	3.61	3.21
		ε"	0.079	0.044	0.047	0.044	0.053	0.057	0.041	0.060	0.042
Helligsø Red		ε'	3.13	3.20	3.28	3.21	3.40	3.51	3.13	3.48	3.13
		ε"	0.044	0.024	0.025	0.024	0.028	0.030	0.022	0.031	0.023
Hammershoj Red		ε'	3.32	2.98	3.06	3.00	3.15	3.25	2.93	3.21	2.93
		ε"	0.098	0.034	0.036	0.034	0.040	0.042	0.032	0.043	0.032
Vedstaarup Yellow	350	ε'	3.51	3.19	3.29	3.21	3.41	3.54	3.12	3.50	3.12
		ε"	0.040	0.017	0.018	0.016	0.019	0.021	0.015	0.022	0.016
Hammershoj Yellow		ε'	3.58	3.25	3.34	3.27	3.47	3.59	3.18	3.57	3.18
		ε"	0.028	0.020	0.021	0.020	0.024	0.026	0.019	0.027	0.019
Helligsø Red		ε'	3.13	3.03	3.10	3.05	3.20	3.30	2.97	3.27	2.97
		ε"	0.031	0.021	0.023	0.021	0.025	0.027	0.020	0.028	0.020
Hammershoj Red		ε'	3.26	2.83	2.89	2.85	2.97	3.06	2.78	3.02	2.78
		ε"	0.029	0.013	0.014	0.013	0.015	0.016	0.012	0.016	0.012
Vedstaarup Yellow	950	ε'	3.69	3.56	3.69	3.58	3.85	4.03	3.46	4.01	3.47
		ε"	0.145	0.079	0.085	0.078	0.095	0.106	0.072	0.113	0.074
Hammershoj Yellow		ε'	3.88	3.59	3.71	3.61	3.88	4.03	3.49	4.03	3.50
		ε"	0.095	0.085	0.091	0.084	0.104	0.112	0.078	0.121	0.080
Helligsø Red		ε'	3.71	3.75	3.87	3.76	4.06	4.22	3.63	4.24	3.65
		ε"	0.249	0.207	0.223	0.205	0.254	0.272	0.190	0.301	0.196
Hammershoj Red		ε'	3.98	3.47	3.58	3.49	3.73	3.87	3.38	3.86	3.39
		ε"	0.219	0.176	0.190	0.176	0.214	0.230	0.162	0.246	0.167

A summary of the average deviations of the estimations for every route and frequency for the three best mixing rules is presented in Table 6.6. Comparing Lichtenecker, Böttcher and Sen-Scala-Cohen average errors on Figure 6.9 estimations, i.e. powder to slab at 2470 MHz, with the established accuracy thresholds above; only Böttcher shows an acceptable dielectric constant prediction while the rest surpass the error limits. Considering each clay type, yellow clays dielectric constants deviations averaging around 2.9% are twice as accurate as their red counterparts, no doubt due to Hammershoj red trend differences. On the contrary, yellow clays loss estimations are 29.7% less accurate, coming from the underestimation of Vedstaarup values.

The independence of the mixing rules from frequency explains the similarity of 912 MHz results, where the main difference is the almost two fold increment of the dielectric constants estimation errors. No better predictions were obtained using the reversed route at either 912 MHz or 2470 MHz, as the nature of the free water fix developed in Chapter 5 now boosts

the estimation errors below 350 ºC. Consequently, deviations average at 5.7% and 50.2% at 2470 MHz and 6.6% and 47.0% at 912 MHz for the dielectric constant and the loss factor, which are far from the required accuracy.

Table 6.6- Average estimation errors across the 20-950 ºC firing range of the three most suitable mixing rules in the binary clay-air approximations of red and yellow Danish clays at different frequencies and void fractions, i.e. slabs and powders.

	Frequency (MHz)	912			2470		
Route	**Mixing Rule**	**Böttcher**	**Lichtenecker**	**Sen-Scala-Cohen**	**Böttcher**	**Lichtenecker**	**Sen-Scala-Cohen**
Powder to slab	**ε'(%)**	7.9	8.3	8.6	5.0	5.3	5.4
	ε''(%)	29.0	26.7	27.5	29.6	26.6	26.6
Slab to powder	**ε'(%)**	6.7	6.6	6.5	4.8	6.5	4.7
	ε''(%)	52.6	46.0	42.5	56.4	49.1	45.2

The generally inadequate accuracy of the estimations could be interpreted as a poor choice of the mixing rules if it was not for the similarity between all the estimated values. An explanation might be the microstructural differences between the powder and slabs, which cannot be overcome by the mixing equations. However, that justification falls short given the at times successful estimations of the dielectric constants across most of the firing. Another possibility is that the previous assumption of the irrelevance of clay mineralogy on the accuracy of the dielectric estimations is incorrect, given the large degree of deviations caused by the moisture content and certain mineral reactions. Consequently, the accuracy of Figure 6.9 estimations needs to be contrasted with those obtained by building the clays from their individual minerals.

6.4.2 Dielectric property estimation of multicomponent clay-minerals mixtures

The procedure used to build the clays from their constituents, described in Section 5.3.7, can be summarised as predicting the dielectric properties of the individual clay constituents at the void fraction of the target clay, and then combining all of them to form the final mixture. In the case of the first step, the same methodology used for the clay-air estimations above is applied. There are several estimation routes available to build the clay. These were summarised in Figure 5.4, which has been replicated here again in Figure 6.10 for clarity purposes. The alternatives shown are powder minerals to clay slabs (C), mineral slabs to powder clays (B), mineral slabs to clay slabs (D) and powder minerals to powder clays (A). The last two will most likely provide the highest degree of accuracy, as the added uncertainty in the estimations caused by the void fraction differences is minimised. Yet, their usefulness is limited. In the first case, finding all the major minerals at void fractions similar to that of

the targeted clays is challenging, while for the latter there is little interest in predictions regarding free flowing clay powders. This last point can be also argued when addressing the mineral slabs to powder clays route, with the added inconvenience of void fraction disparities, thus leaving only the powder minerals to clay slabs course (C). This is justifiably the best option, as clays are estimated at their desired state, while working with mineral powders minimises the appearance of uncertainties due to structural particularities, e.g. montmorillonite-muscovite interstratification.

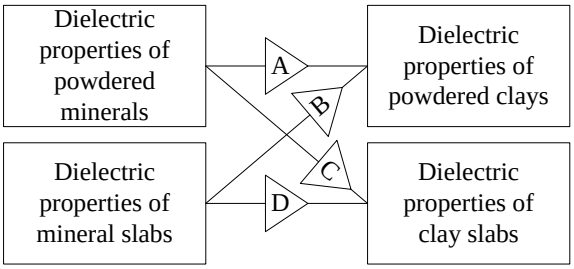


Figure 6.10- Alternatives for the mixing rules predictions of the dielectric properties of clays in clay-minerals mixtures that can be experimentally validated, i.e. powder minerals to powder clays (A), mineral slabs to powder clays (B), powder minerals to clay slabs (C) and mineral slabs to clay slabs (D).

The results of estimating the dielectric properties of clay slabs of Figure 6.5 from measured mineral powders presented in Appendix C2 at 2470 MHz are displayed in Figure 6.11. Estimations at 912 MHz are presented in Appendix C2 following the reasoning used for the binary predictions above. Analogously to Figure 6.9, only Sen-Scala-Cohen, Lichtenecker and Böttcher estimations are shown for clarity purposes, while the others can be seen in Appendix C2. The error bars of the estimations represent a 95% confidence interval. These are calculated following Eq 5.11 and are not present for clarity.

At a first glance, it is obvious that building the clays from their individual constituents provides estimations significantly closer to the real values than when using the binary approach of Figure 6.9. In the dielectric constants, the enhancement of the estimations is predominantly seen in Hammershoj red. For this clay, the previously observed deviations past 550 ^{o}C due to kaolinite metakaolinization are removed, while the constant underestimation of the measured trend is constrained in the 150-550 ^{o}C range, with a ±0.25 deviation. The reason for this improvement is mainly due to evading the direct build-up of the clay structures from their powders, as minor trend differences found in powders are magnified and become an important source of uncertainties, e.g. the metakaolinization mentioned above.

There is a clear improvement in the accuracy of the loss factors estimations. The consistent underestimation of the Vedstaarup yellow and Hammershoj yellow free and physically bound water fuelled deviations are eliminated. Now most of the estimations are within error bars of the measured losses for the majority of the firing. This can be attributed to both eliminating

the boost to trend deviations, and the improvement of the water fix. This is caused by the low moisture content of clays compared to the clay minerals, and the increased importance of the dry non-clay minerals. Curiously, despite the lack of physically bound water on the powdered minerals, its small peak around 250 ºC found on Hammershoj yellow is almost perfectly recreated by Böttcher. On the other hand, the influence of the clay minerals phase would explain how the estimated loss trends overcome the calcite decomposition stabilisation in yellow clays, behaving closer to red clays beyond 900 ºC and thus engaging in deviations of at least 38% in this range. Red clays approximations are particularly improved for the free water approximations similarly to the yellow type, being within error bars except in the case of Hammershoj red, whose originally huge free water deviation is not completely eliminated, doubling its estimated values below 150 ºC.

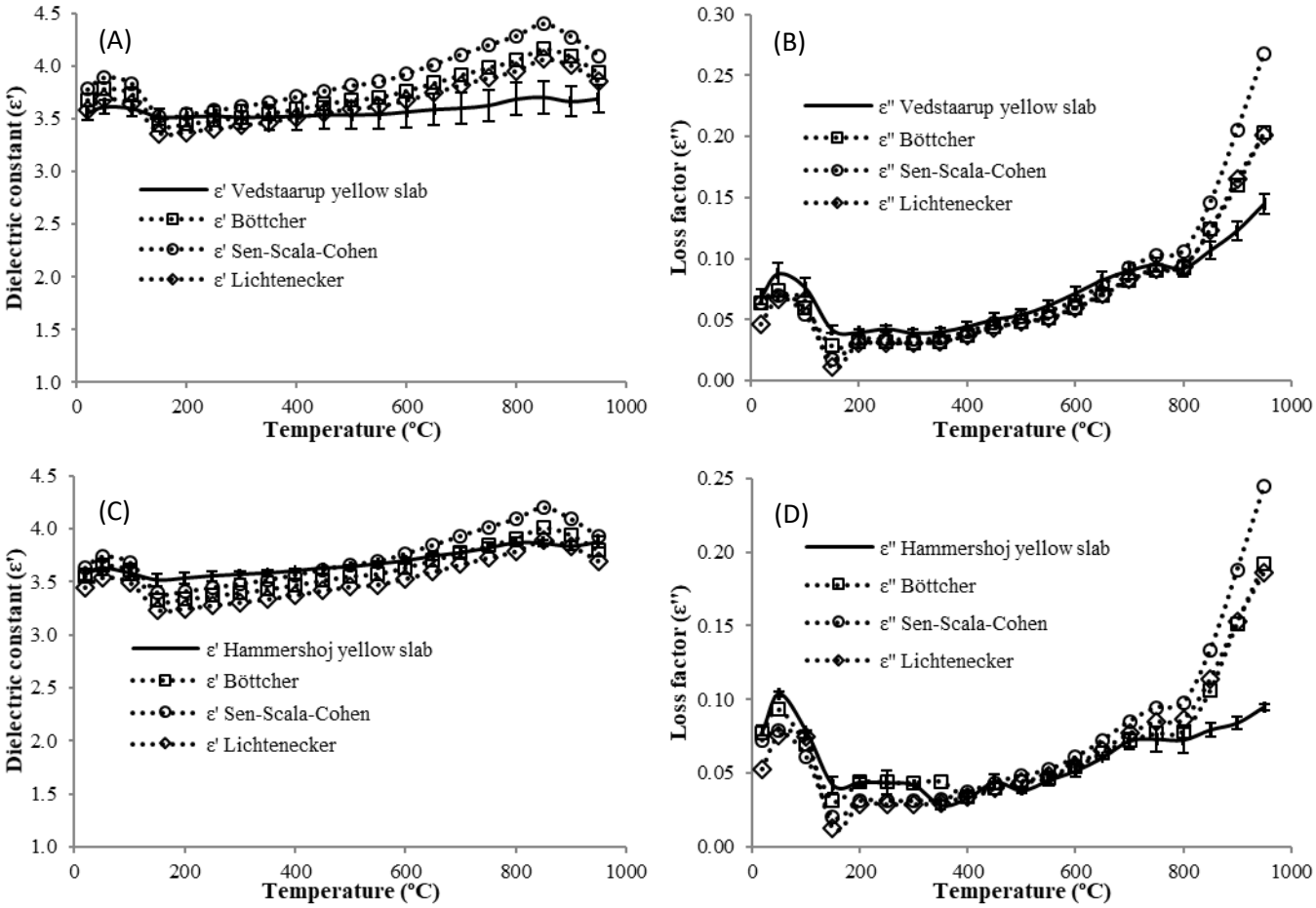


Figure 6.11- Average dielectric constants (Left) and loss factors (Right) across firing between 20-950 ºC at 2470 MHz for Danish clay slabs at void fractions ranging 0.37±0.02 for Vedstaarup yellow, 0.39±0.01 for Hammershoj yellow, 0.40±0.01 for Helligsø red and 0.42±0.03 for Hammershoj red, and mixing rules approximations from mineral powders at void fractions ranging 0.56±0.03 for yellow (A-D) and red (E-H) clays. These experimental results are the average of three repeats.

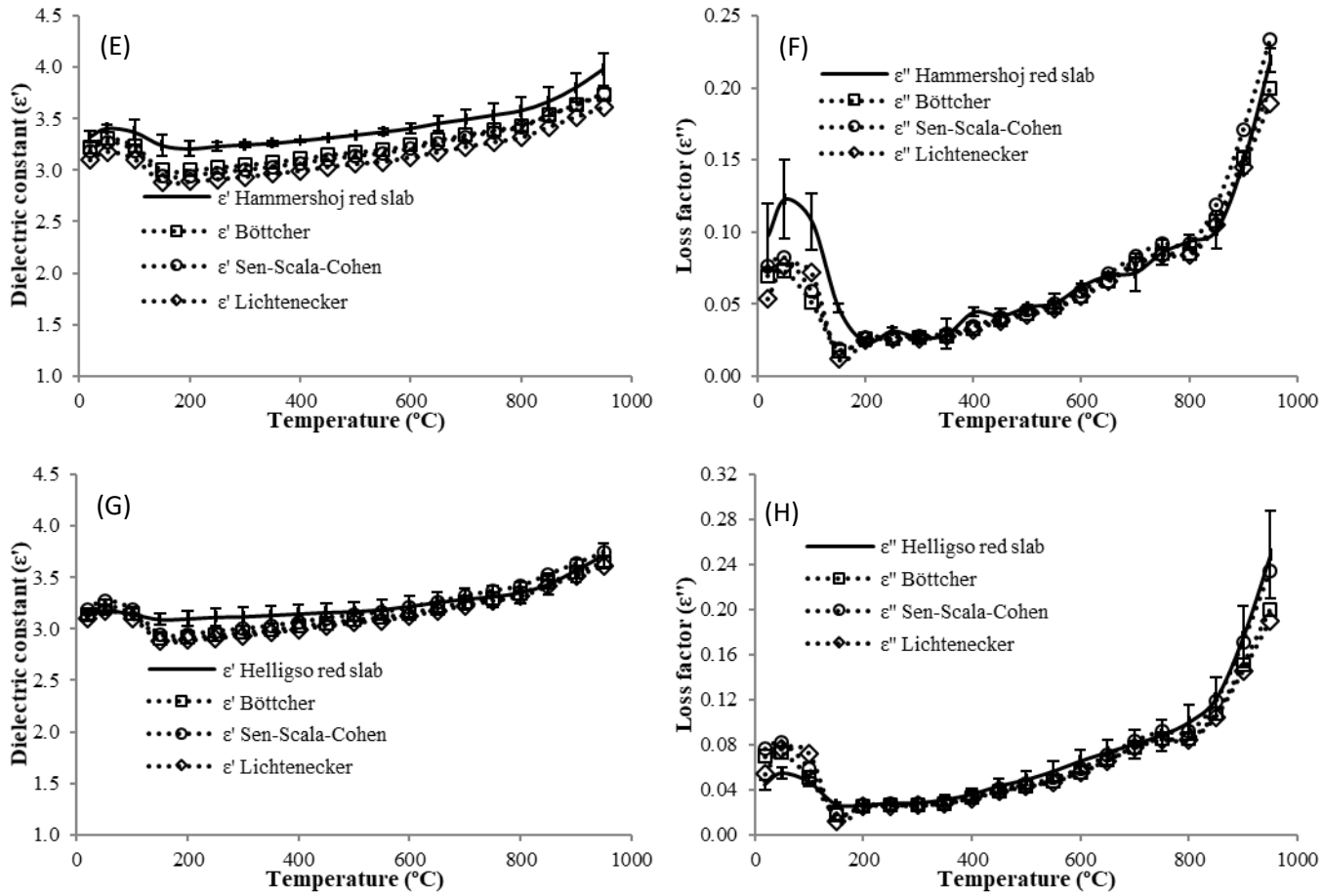


Figure 6.11– Continued.

A study of the precision of each mixing rule is displayed in Table 6.7. Consistently with the binary clay-air estimations, Böttcher, Lichtenecker and Sen-Scala-Cohen provide the most accurate approximations. This is unexpected in the case of the last two since Lichtenecker does not typically fare well with heterogeneous dry mixtures and Sen-Scala-Cohen is not strictly derived for multicomponent mixtures. In any case, Böttcher displays the highest level of accuracy in average for the dielectric constants and loss factors estimations. The assessment of each individual major constituent has surprisingly posed no advantage for the other Power-law equations and Rayleigh, to a point where even Bruggeman-Hanai surpasses them, when like Sen it is not suitable for multicomponent mixtures. Several parameters may account for their disappointing performance, such as the large dielectric contrast between the constituents or the lack of a primary mineral species that could act as a matrix.

Comparing Böttcher results with those of Table 6.5, prediction errors in the dielectric constants decrease on average 24% while almost halving for the loss factors. As a result now both the dielectric constants and the losses are within the established error thresholds. Coincidentally, this is the only mixing rule that manages to fulfil those requirements, as although Lichtenecker and Sen-Scala-Cohen come close by giving on average acceptable

dielectric constant estimations, their loss errors fluctuate around 21.1%. Examining results for the different clay types, yellow clays are closer to the acceptability limits with an average deviation of 3.9% for the dielectric constants and 18.3% for the losses. On the other hand, red clays have 3.7% and 15.2%, respectively. The similarity on the dielectric constants errors stems from their general unresponsiveness to affecting parameters, while the worse loss predictions accuracy in yellow clays is probably caused by Hammershoj yellow deviations above 900 ºC.

Table 6.7- Comparison between measured dielectric properties of slabs of red and yellow Danish clays at void fractions ranging 0.37±0.02 for Vedstaarup yellow, 0.39±0.01 for Hammershoj yellow, 0.40±0.01 for Helligsø red and 0.42±0.03 for Hammershoj red shown here at certain temperatures across the 20-950 ºC firing range at 2470 MHz and multicomponent clay-minerals mixing rules approximations from minerals powders at void fractions ranging 0.56±0.04.

Clay	T (ºC)		Measured Values	Complex Refractive Index	Landau-Lifshitz-Looyenga	Bruggeman-Hanai	Böttcher	Lichtenecker	Rayleigh	Sen-Scala-Cohen	Complex Refractive Index α=0.65
Vedstaarup Yellow	**20**	ε'	3.55	3.12	3.07	3.40	3.68	3.59	3.28	3.78	3.11
		ε''	0.069	0.041	0.038	0.039	0.064	0.046	0.042	0.064	0.038
Hammershoj Yellow		ε'	3.57	3.037	2.97	3.30	3.55	3.45	3.19	3.63	3.03
		ε''	0.079	0.048	0.045	0.046	0.078	0.053	0.050	0.072	0.044
Helligsø Red		ε'	3.13	2.82	2.80	2.98	3.14	3.10	2.90	3.18	2.82
		ε''	0.044	0.057	0.048	0.049	0.069	0.054	0.056	0.077	0.048
Hammershoj Red		ε'	3.32	2.82	2.80	2.98	3.23	3.10	2.90	3.18	2.82
		ε''	0.098	0.057	0.048	0.049	0.069	0.054	0.056	0.077	0.048
Vedstaarup Yellow	**350**	ε'	3.51	3.01	2.96	3.30	3.55	3.47	3.19	3.66	3.01
		ε''	0.040	0.024	0.025	0.026	0.032	0.032	0.024	0.035	0.023
Hammershoj Yellow		ε'	3.58	2.93	2.87	3.20	3.43	3.33	3.11	3.52	2.93
		ε''	0.028	0.023	0.024	0.025	0.045	0.030	0.023	0.032	0.023
Helligsø Red		ε'	3.13	2.70	2.68	2.86	2.99	2.96	2.79	3.03	2.69
		ε''	0.031	0.023	0.024	0.024	0.028	0.028	0.022	0.029	0.023
Hammershoj Red		ε'	3.26	2.70	2.68	2.86	3.08	2.96	2.79	3.03	2.69
		ε''	0.029	0.023	0.024	0.024	0.028	0.028	0.022	0.029	0.023
Vedstaarup Yellow	**950**	ε'	3.69	3.31	3.27	3.63	3.94	3.86	3.49	4.10	3.29
		ε''	0.145	0.164	0.165	0.167	0.203	0.201	0.150	0.267	0.161
Hammershoj Yellow		ε'	3.88	3.21	3.16	3.52	3.80	3.70	3.40	3.93	3.20
		ε''	0.095	0.156	0.156	0.160	0.192	0.186	0.144	0.245	0.155
Helligsø Red		ε'	3.71	3.23	3.22	3.41	3.65	3.61	3.31	3.74	3.20
		ε''	0.249	0.163	0.165	0.163	0.199	0.190	0.150	0.234	0.160
Hammershoj Red		ε'	3.98	3.23	3.22	3.41	3.74	3.61	3.31	3.74	3.20
		ε''	0.219	0.163	0.165	0.163	0.199	0.190	0.150	0.234	0.160

Following the tendency observed on the binary mixtures, the modification of the processing frequency does not noticeably modify the accuracy of the estimations. In this case, yellow clays deviations for the dielectric constants and loss factors average around 4.8% and 17.4%, respectively. Red clays on the other hand have 6.4% lower dielectric constants errors and half the deviation in loss predictions when compared with 2470 MHz values. This means that a dielectric properties predictive tool has been successfully developed based on Böttcher

mixing rule, which can provide estimations of red and yellow clay slabs from their mineral species composition and their dielectric properties as powders regardless of the processing frequency and with the same degree of accuracy as cavity perturbation measurements. However, due to the similar mineral composition of the Danish clays, their similar dielectric property trends and the wide variation of clay mineralogy across countries, further analyses are needed to completely validate the predicting tool.

6.4.3 Towards the development of a comprehensive dielectric property predictive tool for clays

Confirmation of the validity of the Böttcher predictive model comes from testing the accuracy of the estimations with clays from other European countries, namely two red specimens from the Netherlands and England, and one yellow clay from Spain. Naturally, prior to performing dielectric property estimations, it is necessary to determine the mineralogy of these clays plus their void fraction and moisture content, as was done at the beginning of this chapter. The mineralogy results are presented in Table 6.8, where the same XRD methodology presented in Section 5.3.2 is applied. The results demonstrate the compositional variability found in clays from different sources. The most outstanding observation is that as opposed to Danish clays, the Spanish, Dutch and English specimens show an almost total lack of montmorillonite and feldspars. This may significantly affect their ability to be microwave heated, given that montmorillonite is the dominant dielectric mineral species.

Table 6.8- Quantitative XRD characterisation of the major clay constituents in red and yellow European clays, i.e. quartz, calcite, albite, orthoclase and the clay minerals kaolinite, montmorillonite and muscovite. Each sample was measured once, so that deviations for the mineral concentrations range ±2.5% for >60 wt%, ±5% between 60-30 wt%, ±10% between 30-10 wt%, ±20% between 10-3 wt% and ±40% for <3 wt %.

Clay	Quartz (%)	Calcite (%)	Orthoclase (%)	Albite (%)	Kaolinite (%)	Montmorillonite (%)	Muscovite (%)
Spanish Yellow	41.3	36.2	<1.0	2.4	2.4	<1.0	14.0
Dutch Red	84.7	<1.0	<1.0	<0.1	3.2	<1.0	10.5
English Red	53.4	<1.0	<1.0	<1.0	25.8	<1.0	15.4

Considerations of the moisture and general porosity of these specimens are presented in Table 6.9 following the procedures detailed in Section 5.3.1 and Section 5.3.3. The disappearance of montmorillonite accounts for a reduction of around 0.1% of the total moisture mass found in the Dutch and English red clays, while the Spanish yellow moisture is nearly half of that of its analogous Danish.

Table 6.9- Equilibrium moisture contents and void fractions of red and yellow European clays as slabs. For each material, five repeats were made and the standard uncertainty is indicated.

Clay	Slab	
	Moisture (%)	Void fraction (%)
Spanish Yellow	0.25±0.01	0.10±0.01
Dutch Red	0.30±0.04	0.38±0.01
English Red	0.32±0.02	0.30±0.02

The same method applied for the dielectric property measurements of Danish clays was used when measuring European clay slabs in the 20-950 ºC range at 2470 MHz and 912 MHz. Estimations of the dielectric properties of slabs of European clays at 2470 MHz following the multicomponent clay-minerals methodology and using the dielectric properties of mineral powders applied above are presented in Figure 6.12. As before, only Sen-Scala-Cohen, Lichtenecker and Böttcher estimations are displayed here, while the full data tables can be seen in Appendix C2 with the 912 MHz results.

ore focusing on the accuracy of the estimations, it is worth addressing the differences in dielectric properties between the Spanish, Dutch and English clays and the Danish samples, which result from their contrasting mineralogy. On the Spanish yellow specimen, its 41% larger calcite content than the other yellow clays explains why its dielectric constant resembles that of pure calcite. Moreover, its three-fold lower void fraction than the English and Dutch specimens justifies the Spanish sample between 1.5-2 times higher losses at all times. On the other hand, the elimination of montmorillonite causes the English and Dutch red clays to have up to one order of magnitude lower losses at top temperature when compared with their Danish counterparts. Despite the 44.8% larger amount of quartz in the Dutch clay, both English and Dutch red specimens share almost identical dielectric property trends. The lowered loss response in the British sample might be caused by the interstratification of its abundant kaolinite content in muscovite, impeding the dielectric response of the dominant dielectric, i.e. muscovite in the absence of montmorillonite.

Assessing the mixing rule estimations, it appears that building the clays from their individual minerals gives results analogous to those of the Danish clays of Figure 6.11. For the dielectric constants, the kaolinite-muscovite interstratification might explain the slight underestimation of the measured values beyond 850 ºC in the English red, peaking at 950 ºC with a minimum 7.9% deviation. Logically, this discrepancy cannot be adequately reproduced by the combination of powdered single minerals. In addition, the calcite content in the Spanish clay exerts a major influence on the estimated trends in a similar way to the pure calcite mineral estimations, so errors of up to 26.4% are found around 800 ºC.

In the losses, most of the estimations are within error bars for the red clays, while for the yellow sample there is some dispersion of the estimated values. The estimated trends of both red clays behave markedly different from each other near room temperature. It appears that some equations such as Sen-Scala-Cohen, and to a lesser degree in the English clay Böttcher, do not assess the water peak at 50 ºC, having instead steadily decreasing loss trends. This unexpected behaviour could be caused by the larger quartz content in theses clays. Its dry structure will tend to produce no peaks due to free water, while the absence of montmorillonite negates any counterbalance. The same effect is observed for the Spanish clay. In addition, its sharp loss stabilisation around 800 ºC is not accurately mimicked by any rule, probably because of the influence of its large quartz and muscovite content adding in to mask it in the estimations.

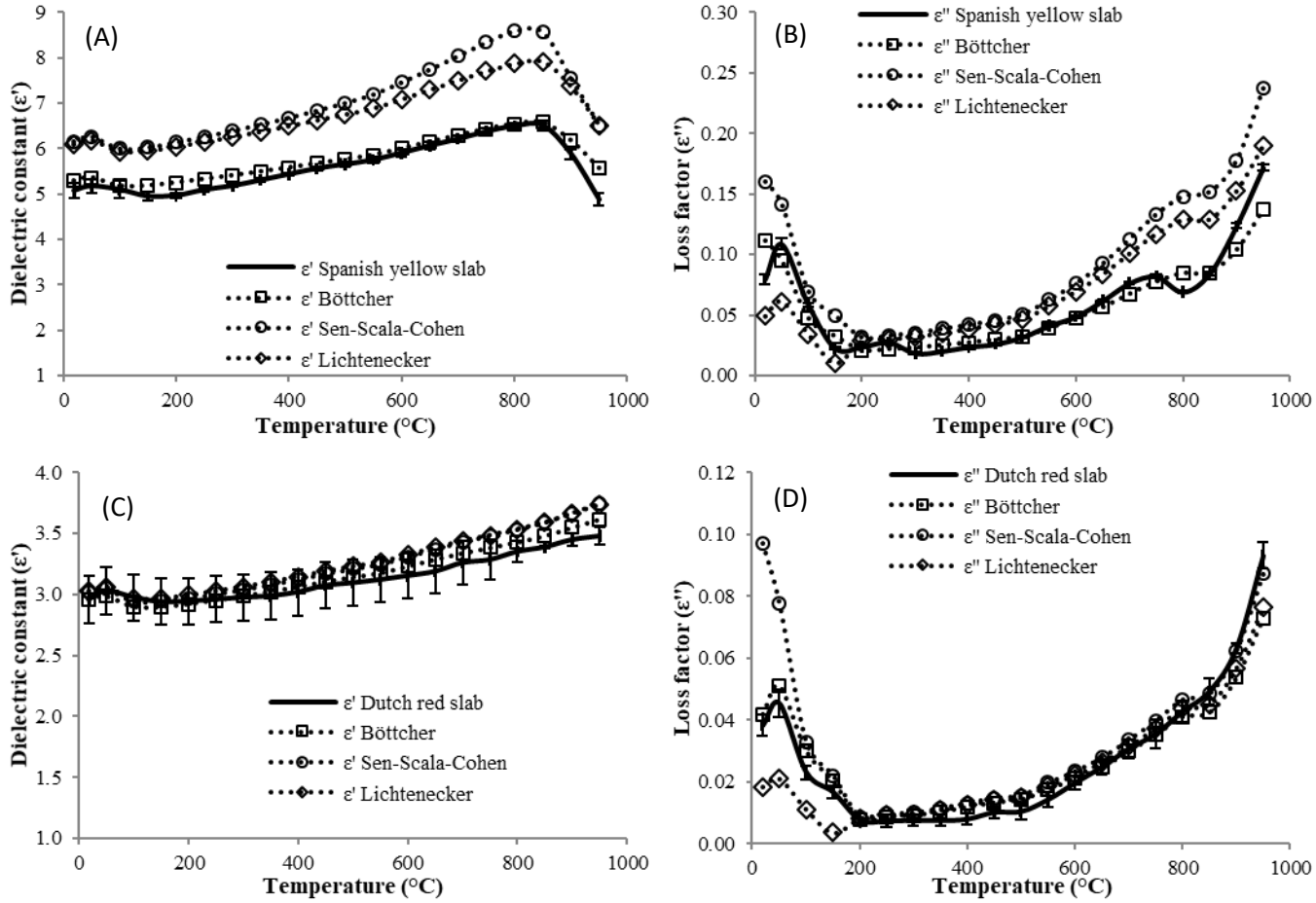


Figure 6.12- Average dielectric constants (Left) and loss factors (Right) across firing between 20-950 ºC at 2470 MHz for European clay slabs at void fractions ranging 0.10±0.01 for Spanish yellow, 0.38±0.01 for Dutch red and 0.30±0.02 for English red, and mixing rules approximations from mineral powders at void fractions ranging 0.56±0.03 for yellow (A-B) and red (C-F) clays. These experimental results are the average of three repeats.

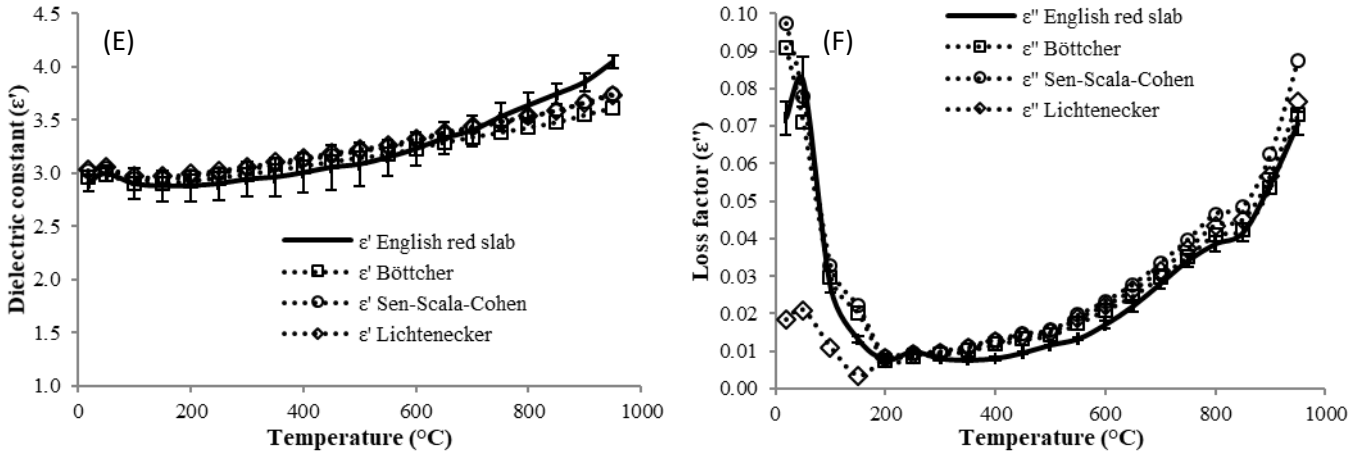


Figure 6.12- Continued

The performance of each mixing rule is better seen in Table 6.10. Böttcher continues being on average the most accurate mixing rule, while among the others only Lichtenecker's red clays dielectric constants approximations fulfils the accuracy requirements with an average 3.8% deviation. Assessing Böttcher accuracy in each clay type separately, both red clays have very similar deviations for the dielectric constants and the loss factors, being these 2.3% and 18.1%, respectively. Curiously, these values correlate better to the yellow Danish clays than to their red counterparts, and the reason probably stems from the more low loss behaviour of these clays due to their lack of montmorillonite. On the contrary, the Spanish yellow one resembles the Danish red clays with dielectric constants and loss deviations of 3.4% and 15.9%, as its muscovite at low porosity most likely mimics the montmorillonite of the Danish specimens.

Table 6.10- Comparison between measured dielectric properties of slabs of red and yellow European clays at void fractions ranging 0.10±0.01 for Spanish yellow, 0.38±0.01 for Dutch red and 0.30±0.02 for English red shown here at certain temperatures across the 20-950 ºC firing range at 2470 MHz and multicomponent clay/minerals mixing rules approximations from minerals powders at void fractions ranging 0.56±0.04.

Clay	T (ºC)		Measured Values	Complex Refractive Index	Landau-Lifshitz-Looyenga	Bruggeman-Hanai	Böttcher	Lichtenecker	Rayleigh	Sen-Scala-Cohen	Complex Refractive Index α=0.65
Spanish Yellow	**20**	ε'	5.07	4.42	4.65	4.68	5.29	6.09	4.39	6.16	4.23
		ε''	0.080	0.079	0.030	0.027	0.111	0.049	0.077	0.160	0.024
Dutch Red		ε'	2.96	2.76	2.81	2.81	2.96	3.03	2.73	3.02	2.71
		ε''	0.038	0.074	0.016	0.015	0.091	0.018	0.070	0.097	0.015
English Red		ε'	2.91	2.76	2.81	2.81	2.96	3.03	2.73	3.02	2.71
		ε''	0.072	0.074	0.016	0.015	0.042	0.018	0.070	0.097	0.015
Spanish Yellow	**350**	ε'	5.30	4.57	4.82	4.83	5.49	6.37	4.52	6.53	4.36
		ε''	0.020	0.018	0.021	0.019	0.025	0.035	0.016	0.039	0.016
Dutch Red		ε'	2.99	2.80	2.86	2.86	3.02	3.10	2.78	3.08	2.75
		ε''	0.007	0.009	0.009	0.009	0.010	0.011	0.008	0.011	0.008
English Red		ε'	2.96	2.80	2.86	2.86	3.02	3.10	2.78	3.08	2.75
		ε''	0.008	0.009	0.009	0.009	0.010	0.011	0.008	0.011	0.008
Spanish Yellow	**950**	ε'	4.87	4.60	4.88	4.90	5.56	6.51	4.60	6.52	4.38
		ε''	0.172	0.101	0.115	0.101	0.137	0.190	0.087	0.237	0.091
Dutch Red		ε'	3.48	3.28	3.37	3.34	3.62	3.73	3.22	3.75	3.20
		ε''	0.093	0.058	0.062	0.058	0.073	0.076	0.053	0.087	0.055
English Red		ε'	4.04	3.28	3.37	3.34	3.62	3.73	3.22	3.75	3.20
		ε''	0.071	0.058	0.062	0.058	0.073	0.076	0.053	0.087	0.055

As in the case of the Danish clays, the accuracy of the estimations at 912 MHz does not significantly differ from the 2470 MHz results. Böttcher deviations on the dielectric constants average around 5.0% and 3.4% for the red and yellow clays, respectively. Finally, their losses estimation errors show a reduction of 1.3% for the English clay, while in the Dutch the improvement is of 10.7%. On the contrary, deviations approaching the error threshold are found for the Spanish yellow clay. Ultimately, the accuracy of the predictive model based on the Böttcher equation for the estimation of the dielectric properties of red and yellow clays of European origin is validated.

The applicability of this formula has in theory no void fraction or frequency boundaries. Regarding the former, dielectric properties for clays at void fractions between 0.10-0.42 have been accurately estimated, which covers most of the range of porosities found in bricks varying between 0.01-0.50 (Reeves et al., 2006). Böttcher has also proven accurate when estimating the dielectric properties of the two major building clay types at various mineralogical configurations, and it is expected to remain so while within the general composition limits given to building clays, i.e. 55% quartz, 25% kaolin and 20% mica (Reeves et al., 2006). Yet, the predicting tool has also been validated for the significant appearance of montmorillonite, feldspars and calcite. However, the presence of constituents with intense thermal reactions, e.g. calcite, especially if they are lossy, might not be

accurately mimicked. Finally, moisture levels equal or lower than those of the clay constituents studied should reduce the appearance of estimation errors near room temperature.

An improvement in the performance of the predictive tool could be achieved by monitoring the clay composition across firing. However, quenching a thermal insulator for compositional analyses without transformations taking place during cooling is challenging. Moreover, the similarity of the different aluminosilicate structures composing clays further complicates their separate identification using techniques such as X-ray diffraction, as mentioned in Chapter 3. Introducing water as a compositional parameter that disappears with temperature may greatly improve the estimations at lower temperatures. However, it will clash with Böttcher's formulation, while deciding at which temperature water effects are effectively eliminated is challenging. This is so far only possible for free water as, physically bound water is not easily trackable in thermal studies done on powders such as TGA or DSC.

6.4.4 Conclusions on dielectric property estimations

In order to avoid performing an infinite number of dielectric property measurements for each possible clay to assess its potential for microwave heating, a tool capable of estimating clay dielectric properties has been developed using electromagnetic mixing rules. Due to the lack of previous studies on multicomponent clay systems, the error thresholds have been set at 5.1% deviation for the dielectric constants and 18.8% for the loss factors, which correspond to the uncertainty range of measured values.

Initially, the similar values of the measured dielectric properties of red and yellow samples hints at the possibility of simplifying the predictive model by disregarding clay composition, thus binary clay-air mixtures are built focusing on estimations at different void fractions and frequencies. Among the mixing rules considered, Böttcher, Lichtenecker and Sen-Scala-Cohen give the most accurate estimations. Their performance is explained by their focus on low loss crystalline specimens, porous and moist materials, and diluted media where inclusions interact with each other, respectively. However, none manage to fulfil the established error thresholds, mainly due to not taking into consideration the clay mineralogy. On the contrary, the combination of the powdered minerals to produce clay slabs at 2470 MHz results in acceptable estimations, with deviations averaging around 3.8% for the dielectric constant and 16.8% for the loss factors when using Böttcher.

The Böttcher predictive tool is still valid at 912 MHz and when tested with other European clays, enabling an analysis of the boundaries for its application. The estimations' accuracy appears minimally affected by the processing frequency. Similarly, the degree of uncertainties is not affected when moving within the void fraction area of 0.10-0.42, which incidentally

covers most of the porosity range of brick clays (Reeves et al., 2006). The tool can adapt to sharp mineralogical variations, e.g. major appearance of montmorillonite or calcite. However, the presence of large quantities of free water (>2%) or intense thermal reactions can negatively influence the effectiveness of the predictions. A solution for the former is the consideration of water as a constituent, while the latter can only be counteracted by limiting the presence of these components. In the case that lossy specimens with a very intense set of thermal reactions are added to the clay mixture, the estimations' uncertainty may go beyond the error thresholds.

6.5 Conclusions

The dielectric properties of red and yellow Danish clays used for building applications and their major constituents have been measured between 20-950 ºC using the cavity perturbation method at different void fractions and at the frequencies of 2470 MHz and 912 MHz. Additional measurements to prove the statistical significance of the cavity method have been performed using the waveguide technique. A study of clay mineralogy has been carried out using XRD, while an analysis of the thermal transformations throughout firing has been implemented for clays and clay constituents using TGA and DSC techniques. A tool for the estimation of the dielectric properties of Danish clays from their mineral composition has been developed via mixing rules and later validated for a wider clay spectrum with other European clays.

The main difference between the two Danish clay types analysed is the significant calcite content (>20%) in yellow clays, whereas red clays appear to have a larger clay minerals fraction and free water content. Among their constituents, clay minerals and calcite stand out for their thermal instability, where their reactions are easily identifiable in the TGA and DSC data between 350-800 ºC and around 800 ºC, respectively. These physicochemical transformations, together with free water removal, are also recognisable in the clays and individual minerals loss factor trends as they strongly influence the potential for microwave processing of clays. On the contrary, dielectric constants are largely stable.

Clay slabs at the same void fraction as unfired bricks are within limits of reasonable microwave firing in the 20-950 ºC range at both 2470 MHz and 912 MHz, despite the abundance of transparent constituents like quartz. This is attributed initially to free and to a lesser extent physically bound water, which are the dominant dielectric phases. After their disappearance, montmorillonite and muscovite are the most absorbing species. This is mainly caused by their water content and interlayer cations. Modification of the void fraction/air inclusions of the specimens caused them to cross the transparency boundary after a 34.6% porosity increase, while moving from 2470 MHz to 912 MHz results in a general loss factors

increase that matches with the system's nearing physically bound water dipolar dispersion zone and the ionic conductivity area of dominance.

Attempting the estimation of the dielectric properties of clays without consideration of their composition results in estimation errors more than two fold higher than the established error limits when considering Böttcher predictions, where this formula one of the most accurate mixing rules. However, when taking into consideration clay mineralogy, estimation errors as low as 3.8% for the dielectric constant and 16.8% for the loss factors when using this formula at 2470 MHz are obtained. The validity of the estimations has been tested by studying other European clays whose predictions also fall within the error thresholds. The effectiveness of this formula for estimating clays is extended to both 2470 MHz and 912 MHz, while also being applicable for most of the porosity range of brick clays, i.e. 0.10-0.42 void fractions. Lastly, mineralogical variations do not appear to damage the accuracy of the model as long as the constituents are drier than montmorillonite and their thermal reactions are less intense than calcite's.

A detailed understanding of the behaviour of clays under an electromagnetic field has been achieved, through deriving the relationship between the dielectric properties of their constituent minerals across the firing range at different void fractions and frequencies. Furthermore, this knowledge has translated into the quantitative estimation of the effects of each mineral constituent upon the dielectric response of a clay mixture by means of a validated tool able to predict the dielectric properties of any natural or synthetic clay based on its composition. This knowledge can now be used to design a microwave system capable of developing clay firing cycles, so as to test the possibility of manufacturing products of similar quality to conventionally produced bricks using microwave heating.

7 MICROWAVE PROCESSING OF CLAYS

7.1 Introduction

In the last two decades, microwave heating of ceramics has been the subject of increasing research efforts (Singh et al., 2016, Borrell et al., 2014, Agrawal, 1998, Das et al., 2009, Bykov et al., 2001). The reason for this is the ability of microwaves to overcome the most crucial limiting factor in their thermal treatment, i.e. a modest thermal conductivity. It has been seen in Chapter 4 that a fast empirical approach often drives these mostly laboratory scale investigations, in order to optimise processing times or product quality. The lack of a comprehensive study of the microwave/material interaction can lead to the unexpected appearance of events such as hot spots and thermal gradients, which reduce the quality of the final products and curtail the possibility of scaling up the microwave processes to industrial scale. In the case of the clays investigated in this project, their physicochemical and dielectric characterisation in Chapter 6 has produced a robust understanding of these materials' response to microwave energy. Consequently, feeding the characterisation data into the development of microwave clay firing experiments can serve to minimise the appearance of these unwanted material effects, leading to microwave fired clays of high quality and paving the road towards a successful scale up of the technique.

The aims of this chapter are to confirm the insight gained in Chapter 6 regarding the potential of microwave energy to heat clays up to firing temperatures (>900 ^{o}C), to assess the quality of fired products manufactured via microwaves and compare them to conventionally fired specimens, and finally to assess the economic, environmental and legislative feasibility of microwaves at industrial scale. In this chapter, the design, commissioning and performance evaluation of a microwave system that manufactures fired products from common red and yellow Danish clays used in building applications is presented. A series of experiments at constant power inputs ranging 100-300 W and at 2450±15 MHz were carried out investigating the either volumetric or selective heating behaviour of the heterogeneous mineral mixtures under microwave energy, while continuously monitoring their temperature and thermal uniformity. Microwave clay firing cycles running for <2.5 h were designed. The resultant fired products were compared with samples fired conventionally using a brickworks cycle through a number of quality parameters, i.e. compressive strength, water absorption, saturation coefficient, shape, size, density, colour, texture and mineralogy. Next, the feasibility of scaling up the technology was discussed. This was underpinned by a techno-economical assessment, which investigated the economic, environmental or legislative advantages of the developed microwave firing technique over the conventional state of the art clay firing methods.

7.2 Design of microwave clay firing system

A drastic modification of the heating methodology from industrial scale brick kilns, discussed in Chapter 3, is required for laboratory scale trials. The main advantage of microwaves over conventional heating is the potential to overcome the thermally insulating nature of clays (Metaxas and Meredith, 1983), which enables a fast and uniform thermal treatment to the load. The latter is the most crucial parameter, as the presence of significant thermal stresses may compromise the quality of the fired products (ILO, 1984, Kadir and Mohajerani, 2015). Consequently, the basis of design of the microwave system is focused towards minimising thermal gradients within the specimens' volume. In brickworks, thermal gradients across the brick stack surface generally range between 80-200 ^{o}C (Nicolau and Dadam, 2009, Køster, 2014, Moesgaard, 2015). In these laboratory scale trials, it is feasible to aim towards temperature differences across the load lower than the industrial kilns range, i.e. <80 ^{o}C. This in turn requires some sort of thermal monitoring of the clay specimens during heating.

In this section, the methodology followed for the selection of the applicator used for volumetric heating and ultimately firing clays using microwave energy is explained. Furthermore, the modifications of the clay feed, necessary in order to gain a fundamental understanding of how clays are heated by microwaves and minimise the presence of thermal gradients, are detailed. Finally, the formulation of the mathematical model used to enable the thermal monitoring of the clays during processing is described.

7.2.1 Microwave applicator selection for clay firing

Given the preliminary nature of the laboratory scale clay heating trials, a batch production system is preferred over the continuous processing found in brickworks. This is because batch production has lower layout requirements and higher degree of flexibility and control of the processing conditions than continuous operation (Robinson et al., 2012, Niu et al., 2015, Green, 2007). Among possible applicator alternatives, the successful processing of clay materials in previous work was achieved through the use of resonant cavities, as discussed in Section 4.7. This is explained by the characteristically high electric field intensities they provide, which according to the power density equation (Eq. 4.2) makes them particularly efficiently in heating low loss materials such as clays (Metaxas and Meredith, 1983, Chan and Reader, 2000).

In Chapter 4, the strengths and weaknesses of single mode and multimode resonant cavities have been thoroughly discussed. Based on the review of the literature on microwave processes on clay materials reported in Section 4.7, it is concluded that although multimode applicators are more widely used, as they can treat large loads with a high degree of thermal

uniformity (Oghbaei and Mirzaee, 2010), their empirical design, coupled with their difficult to characterise and uneven electric field distributions may result in the appearance of large thermal gradients across the samples (Metaxas and Meredith, 1983, Chan and Reader, 2000, Mehdizadeh, 2015). Furthermore, the preliminary and analytical nature of this study justifies a bottom-up approach, which translates in initially assessing samples that might be too small to benefit from the multimode system advantages.

The tight control and characterisation of the distribution of the electric field strength maximum during high temperature ceramic processing, as found by Cheng et al. (2002) and Panneerselvam and Rao (2003), makes single mode operation the best choice in this case. Its main constraint is its uneven electric field distribution, which is counteracted by reducing the sample size to less than half a wavelength of the standing waves of the electromagnetic radiation (Chan and Reader, 2000). In this project, a WR-430 brass waveguide working at the TE_{10} mode, as seen in Figure 7.1, is the selected single mode applicator. The selection of brass instead of the more common aluminium is due to the latter low melting temperature (Davis, 2001) when compared with the high temperatures reached during processing, i.e. ≈1050 ºC. The cavity is choked below the waveguide's cutoff frequency, so as to comply with the health and safety regulations regarding microwave leakage mentioned in Chapter 4. This choke enables the continuous monitoring of the clay thermal evolution.

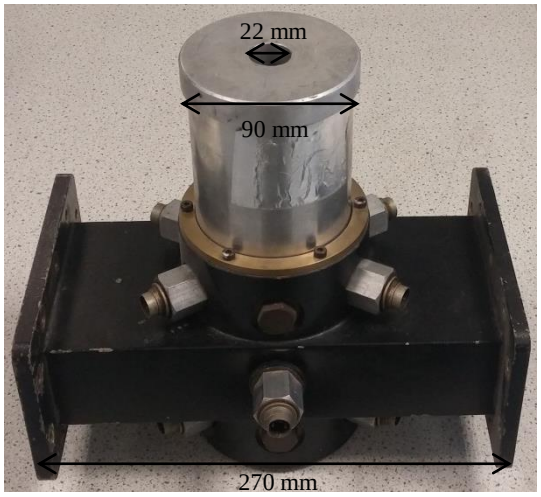


Figure 7.1- Front view of the choked WR-430 brass waveguide used in the 2450 MHz clay microwave heating trials.

7.2.2 Remodelling of raw clay feed for microwave processing

The geometry of the red and yellow clay specimens requires adjustments from a common brick. The main justification for modifying the rectangular prism shape of bricks comes from the necessity of minimising thermal gradients. Material's edges tend to display varying degrees of electric field concentration during microwave processing when compared with the rest of its surfaces (Meredith, 1998). Looking at the power density equation formulated in

Eq. 4.2, this can lead to the uneven heating of the samples and even to thermal runaways and arcing. A straightforward solution would be to shape the specimens as spheres, either by moulding or powder compression. However, this would modify clays internal porosity, macrostructure and surface properties, e.g. shearing, when compared with brickworks bricks. Alternatively, a compromise is reached in building cylindrical samples. Their extrusion from clay slurry detailed in Section 5.2.1, the same as in brickworks, allows clay bricks and cylinders to display the same properties, while still reducing the number of edges.

The dimensions of these cylinders are initially constrained by the single mode applicator, narrowing their size down to less than 122 mm when working at 2450 MHz. Moreover, considerations of power decay across the sample may require to further restrict its volume.

A penetration depth study of red and yellow Danish clays can help in selecting the cylinder's size, where their respective trends are presented in Figure 7.2. The x-axis displays the temperature of the material and the y-axis is the penetration depth. The error bars show a 95% confidence range. The values shown are calculated from applying the penetration depth formula of Eq. 4.3 to the clay dielectric properties of Figure 6.5. Just like clays' dielectric properties, their penetration depth fluctuates with temperature. As expected from their dielectric properties, both clay types have similar penetration depths, maxing at around 1.5 m at 200 ^{o}C and reaching a minimum ranging 0.15-0.40 m at 950 ^{o}C. These values hold important connotations for the process scale up, which will be discussed later. Although at first it appears that there is no danger of thermal non-uniformities due to power attenuation for this single mode system, linear extrapolation of the penetration depths to the top firing temperature (≈1050 ^{o}C) uncovers values as low as 20 mm. Hence, in order to minimise the presence of thermal non-uniformities on account of an uneven electric distribution across the load, its volume is reduced to 25x20 mm. The methodology for the choice of the clay cylinder's height comes from size constraints of the waveguide and the firebrick crucible, and the load's insulation needs

Despite the small size of the clay specimens and the penetration depth study, thermal gradients might still appear due to clay's heterogeneity leading to the spatial variation of the dielectric properties within the sample. In Chapter 6, this has been described as the potential for selective versus volumetric heating as the dominant heating mechanism, which is to be tested in the commissioning stage of the microwave system.

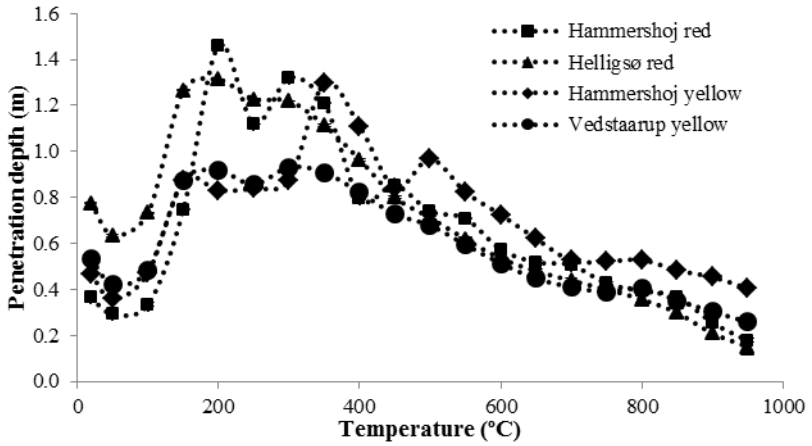


Figure 7.2- Average penetration depth between 20-950 ºC at 2470 MHz for yellow and red Danish clays slabs at void fractions ranging 0.37±0.02 for Vedstaarup yellow, 0.39±0.01 for Hammershoj yellow, 0.40±0.01 for Helligsø red and 0.42±0.03 for Hammershoj red. These results are the average of three repeats.

7.2.3 Clay temperature monitoring during microwave firing

In the processing of clays, their continuous temperature monitoring is crucial for a successful firing. This is explained by the numerous critical temperatures across clay's thermal evolution seen in Chapter 3, and how close the top firing temperature and the start of melting are for these clays, i.e. 1050 ºC and ≈1070 ºC (Mortensen, 2014). Inside the applicator, the clay specimen is placed inside a firebrick crucible and surrounded by wool insulation as described in Section 5.4.1, which act as the structural support of the sample and minimise the presence of thermal gradients between the clay surface and its core, respectively. Hence, direct contact between the thermal camera and the clay is prevented and only the wool can be monitored. To overcome this challenge, an analytical heat loss model that relates the clay and wool temperatures was developed and validated as part of the experimental commissioning process. The model also helped in the calculation of the optimal wool insulation thickness, in order to ensure the maximum thermal uniformity attainable across the clay volume. A simple yet robust analytical model was developed taking into consideration the following assumptions (Coulson et al., 1996).

- Stationary state. System reaches instantaneous thermal equilibrium without tangential heat flows, allows the development of an analytical model.
- Heat losses are independently considered for each axis of a cylindrical coordinates system, enabling the differentiation between sideways and top-bottom heat flows.
- The only heat source is located in the core of a perfectly homogeneous cylinder as seen in Figure 7.3, which accounts for its colder surface and removes the need to model the infinite combinations of mineral distributions in a heterogeneous clay mixture.

These assumptions enable the development of a simplified and analytical temperature model that can adapt to changes in the size and temperature of the load or the microwave rig set up. However, the accuracy of these temperature estimations is low when compared with more specialised numerical modelling methods such as finite differences (Shen et al., 2011).

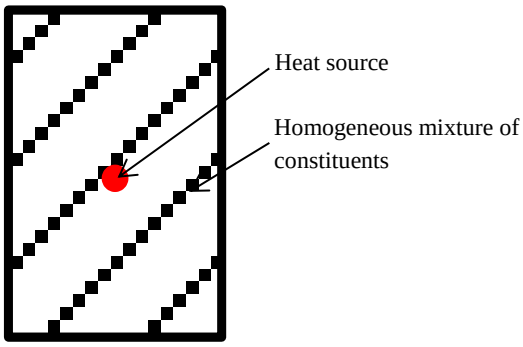


Figure 7.3- Sketch of the assumed homogeneous distribution of mineral constituents and the focalised heat generation inside a clay cylinder under microwave radiation.

Using this method, the relationship between the temperatures of every system component and the insulation thickness can be established by combining the general heat loss (Eq. 7.1), unidirectional conduction (Eqs. 7.2-7.4), and natural convection plus radiation (Eq. 7.5) formulas for stationary state (Coulson et al., 1996),

$$\frac{P_L}{A_{Ln}} = U(T_{CC} - T_A) \quad \textbf{7.1}$$

$$\frac{P_L}{A_{Ln}} = \frac{K_C}{e_c}(T_{CC} - T_{CS}) \quad \textbf{7.2}$$

$$\frac{P_L}{A_{Ln}} = \frac{K_F}{e_F}(T_{CS} - T_{FS}) \quad \textbf{7.3}$$

$$\frac{P_L}{A_{Ln}} = \frac{K_W}{e_W}(T_{FS} - T_{WS}) \quad \textbf{7.4}$$

$$\frac{P_L}{A_{Ln}} = (h_N + h_R)(T_{WS} - T_A) \quad \textbf{7.5}$$

where P_L (W) is the heating losses, U (W/m^2 K) is the global heat transfer coefficient, h_N and h_R (W/m^2 K) are the air natural convection and radiation heat transfer coefficients, K_C, K_F and K_W (W/m K) are the thermal conductivities of clay, firebrick and insulating wool, e_c, e_F and e_W (m) are the thicknesses of the clay, firebrick and insulating wool, A_{Ln} (m^2) is the natural logarithmic heat exchange area of the system, T_{CC}, T_{CS}, T_{FS}, T_{WS} and T_A (K) are the temperatures of the clay core, clay surface, firebrick surface, wool surface and ambient air. The system of equations is internally validated as there are 4 unknown parameters for 5 equations. The value of the thermal conductivities, thicknesses, etc. used in equations in this chapter can be found in Appendix D1 and Appendix D2.

The calculation of the coefficients above comes from Eqs. 7.6-7.9 (Coulson et al., 1996),

$$\frac{1}{U} = \frac{e_c}{K_C} + \frac{e_F}{K_F} + \frac{e_w}{K_w} + \frac{1}{h_N + h_R} \quad \textbf{7.6}$$

$$h_N = 1.35 \left(\frac{T_{WS} - T_A}{L_F/2}\right)^{0.25} \quad \textbf{7.7}$$

$$h_R = \sigma_i F \frac{{T_{WS}}^4 - {T_A}^4}{T_{WS} - T_A} \quad \textbf{7.8}$$

$$A_{Ln} = \frac{A_W - A_C}{\mathrm{Ln}\, {A_W}/{A_C}} \quad \textbf{7.9}$$

where A_C and A_W (m^2) are the heat exchange areas of the clay and wool, L_F (m) is the diameter or the height of the firebrick crucible depending on the plane considered, σ_i (J/K) is the Boltzmann constant and F is the grey vision factor with a conservative value of 0.95.

Given that the thermal camera used for temperature monitoring can only perform discrete recordings at 1 frame/s, an estimation of the full temperature spectrum across firing based on the power readings has been developed in order to allow for heat loss calculations at different points during firing. This allows the estimation of the temperature of the clay load across firing from the system's power readings. This heating profile model uses the aforementioned stationary state assumption and the equation of rate of rise of temperature developed by Metaxas and Meredith (1983). This formula is computed from joining the power density equation (Eq. 4.2), where the experimental power readings are used instead, and the general sensible heating equation (Coulson et al., 1996) in Eq. 7.10,

$$P_H = P_I - P_R - P_C - P_L = m\, Cp_{iAvg} \frac{T_{i+1} - T_i}{t_{i+1} - t_i} \quad \textbf{7.10}$$

where P_H(W) is the absorbed clay power or power used solely to increase the clay temperature, P_I (W) is the incident power, P_R (W) is the reflected power, P_C (W) is the power absorbed by the whole microwave system excepting the clay, m (kg) is the mass of the sample, t_{i+1} and t_i (s) are two timestamps across the heating range, T_{i+1} and T_i (K) are the clay core temperatures at each timestamp and Cp_{iAvg} (J/kg K) is the average specific heat capacity between those two temperatures.

As a result of considering stationary state on a clearly transient system, a correction term in the form of a time lag has to be added. Thermodynamically, it corresponds to the inertia between the temperature increase in the clay core and the wool being affected by the subsequent heat flow. Given that the focalised heat source is several times smaller than that of the sample plus crucible, the analytical solution for a transient heat flow across a semi-infinite sheet can be applied (Coulson et al., 1996), its formulation is presented in Eq. 7.11,

$$\frac{T_{WSt} - T_A}{T_{CS} - T_A} = erfc\left(\frac{H_F}{\sqrt{4\,t\,{K_{Avg}}/{\rho_{Avg}Cp_{Avg}}}}\right) \quad \textbf{7.11}$$

where H_F (m) is the distance between the heat source and the wool surface i.e. the clay+firebrick+wool thickness, $erfc$ is the complementary error function, K_{Avg} (W/m K), Cp_{Avg} (J/kg K) and ρ_{Abv} (kg/m^3) are the average thermal conductivity, specific heat capacity and density between the clay, firebrick and wool, and T_{WSt} (K) is surface wool temperature at a time t (s) since the start of the experiment.

Based on Eq. 7.11, it can be seen that the necessary time lag can be exponentially increased near the temperature equilibrium due to T_{WSt} asymptotic approach towards it. A first order approximation to the steady state would have resulted in different time constants as firing progresses to reach 95% of the equilibrium temperatures, due to their increasing contrast with room temperature. Thus, it has been aimed for constant temperatures 5 ^{o}C lower than those of the equilibrium values, which is where the time lag starts to exponentially increase. As a result, the time lag between the clay core and the wool surface ranges 5-9 mins. Trends of the estimated temperature relations and the heating losses evolution are displayed in Appendix D3.

7.2.4 Conclusions on the design of a microwave clay firing system

A microwave heating system has been designed specifically for the manufacturing of fired clay products with minimal thermal gradients across the load (<80 ^{o}C). The system design can be divided into three main areas, i.e. applicator selection, feed characteristics and thermal monitoring. To our knowledge, this is the first time a microwave clay firing system has been designed using this methodology, and therefore the resulting system is unique in its ability to control the power delivery and temperature of the clay samples. In the first case, the laboratory scale of the heating trials justifies the use of batch operation, among which the utilisation of a single mode resonant system provides high electric field strengths that can aid in the successful firing of the low loss clays and a tight control of the electric field distribution. Specifically, a choked WR-430 brass waveguide working at the TE_{10} mode is chosen.

Clay bricks are subjected to a significant size and shape modification in order to fit in the single mode cavity. First, their shape is changed into a cylinder in order to both preserve the characteristics of a brickworks brick, e.g. porosity, and to reduce the amount of edges that often display electric field concentration and thus cause thermal non-uniformities. Second, the

specimens' size is reduced to 25x20 mm. This is justified by the uneven field distribution of a single mode cavity and by the penetration depth of red and yellow Danish clays, which reach a minimum for red and yellow samples of 0.15 m and 0.40 m respectively at 950 ^{o}C, and a minimum of 20 mm when extrapolated to the top firing temperature.

Thermal monitoring is critical in clay firing given the presence of numerous critical temperatures and the closeness between the top firing temperature and melting, i.e. 1050 ^{o}C and ≈1070 ^{o}C. The insulation of the clay specimens by a firebrick crucible and insulating wool forbids the direct access of the thermal camera to the clay. Instead, its temperatures are estimated by an analytical heat loss model, which relates wool-clay temperatures. Moreover, continuous thermal data logging during the whole length of firing is infeasible, so a heating profile model is built to calculate the temperature profiles across clay firing from power readings. The analytical and stationary state assumptions made when developing both models makes them robust and versatile. However, More accurate temperature estimations may be provided by more specialised numerical models, as the ones used here require correction terms such as a time lag to cope with the transient nature of the firings.

Upon having designed the microwave system for the firing of clays, the next step is the commissioning of the rig in order to investigate if clays can be truly put to firing temperatures with microwave energy and whether the resultant heating is volumetric across the load or selective on the clay minerals.

7.3 Commissioning of microwave clay firing system

The next step in the development of a laboratory scale rig for the manufacturing of fired clay products using microwave energy is evaluating the performance of the designed system. Events such as discrepancies between the dielectric properties of the clay specimens and their behaviour under microwave treatment might appear, and need to be evaluated prior to developing the microwave firing cycles. This particular possibility has also been addressed when investigating the dielectric properties of clays and clay constituents in Chapter 6, where two hypotheses for the heating of clays have been put forward. One option is that the clay minerals' better coupling with microwaves makes them heat selectively and in turn conventionally heat the rest of the clay, probably giving rise to thermal gradients, hot spots and even thermal runaways. The other is that the clay specimen is thoroughly mixed and the heating can be assumed to be uniform across its volume. Experimental validation of the thermal models is also necessary in order to achieve a satisfactory level of temperature monitoring that can help in the production of fired clays. Finally, following from the basis of design of the system, the degree of thermal uniformity in the clay surface needs to be quantified.

This section starts with a study of the power distribution in the clay system during 80 min microwave heating trials on 25x20 mm clay cylinders at a constant power supply ranging 100-300 W and at 2450 MHz. The degree of power reflections and power absorbed by the system are quantified. Furthermore, the power absorbance of the clay specimen across firing is analysed and related to its dielectric properties and thermal transformations. Next, the estimated heating losses and temperature profiles of the microwave system are experimentally validated with periodic temperature recordings of the wool and clay surface. In the end, an investigation of the thermograms of clays at the end of the heating trials serves to determine the level of thermal uniformity achieved by the microwave treatment.

7.3.1 Power distribution in the microwave rig during clay heating

Compared with the vast amounts of energy used in brickworks to fire clays, e.g. 2.6 MJ/kg of fired material (Køster, 2014), the energy requirements to heat the clay samples are very low. A common published value for clay specific heat capacity is 0.96 J/g K (Metaxas and Meredith, 1983), compared with 4.18 J/g K for water. This value contrasts with the average specific heat capacity of 0.20 J/g K measured for the Danish clays at room temperature, which has been calculated using the DSC trends of Chapter 6 as described by Section 5.3.5. This difference is most likely caused by the presence of free water, as adding a 19.1% moisture, i.e. soil's available water capacity (Kutílek and Nielsen, 1994), to the calculated DSC specific heat capacity gives the value in the literature. Either way, this means that the theoretical energy inputs required to heat clays up to 1000 ºC, specifically around 708±11 J/g for red and 740±23 J/g for yellow clays, are nearly four times lower than the actual energy requirements of brickworks; this strengthens the hypothesis that a step change reduction in energy requirements could be achieved if the poor heat transfer properties of clay are overcome through a volumetric heating technology such as microwaves.

However, energy delivery from the microwave generator to the specimen is not necessarily optimal. On top of the heating losses of the clay cylinder, a significant degree of power reflections and power absorption by the system may take place. These energy losses need to be quantified in order to determine the precise amount of microwave energy delivered to the target clay.

7.3.1.1 Power reflections in the microwave system

The measured reflected powers for 25x20 mm cylinders of red and yellow Danish clay heated at 2450 MHz for 80 min at 100-300 W constant incident powers are presented in Figure 7.5. The x-axis represents the processing time while in the y-axis the moving averages within a 120 s range of the power reflections are displayed. The latter is intentionally done for clarity

purposes. For the same reason, no error bars are shown. The methodology of the heating trials is explained in Section 5.4.2. Across all trials from this point forward, only Vedstaarup yellow and Helligsø red have been processed due to the similar dielectric properties and mineralogy within each clay class.

It is clear that at all times there is a high degree of reflections, starting at 80% and going as low as 65% at 80 min when heating at 300 W. An explanation for these reflections behaviour is provided by Gerling (2000). Some characteristics of the microwave generator and the load can significantly affect the overall system performance, i.e. frequency sensitivity of the load, and output frequency stability and spectrum of the generator. Given that the load is a small low loss clay cylinder, the change of power absorption in the system upon loading will be small (high Q factor). Since the single mode pattern of the microwave system is marginally affected by the load, effective heating of the clay cylinder can only be carried out in a narrow band of frequencies. The microwave generator used can be considered as low ripple, which means that it produces a narrow output frequency spectrum. Yet, it cannot match the spectrum of the clay load. This is graphically represented in Figure 7.4. As a result, there are large amounts of power being reflected instead of absorbed.

It is worth noting that this challenge to processing comes mainly from the small spatial size allowed for clay specimens in single mode applicators. This will be probably solved at higher scales primarily by processing larger loads, which will decrease the Q factor of the system and enable a more optimal power delivery. This will be possible thanks to the larger spatial size provided by multimode applicators, as the energy delivery inefficiency of the single mode system is clearly unsuitable for industrial scale processing. This has been already predicted in Chapter 4. However, the justification for using single mode was based on its ability of heating laboratory scale low loss samples, not on the economics of the process (Binner and Vaidhyanathan, 2009).

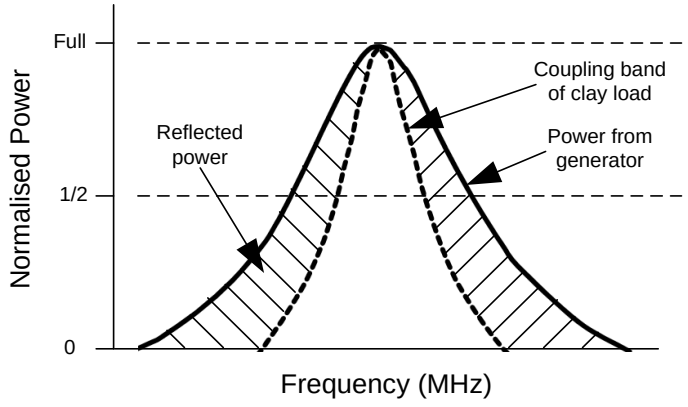


Figure 7.4- Generator output frequency spectrum compared to clay load coupling band. Adapted from Gerling (2000).

The generator and material relation presented in Figure 7.4 is not necessarily stable across the heating treatment. Variations may occur due to a variety of factors in the case of the generator, such as the magnetron operating frequency, while clay dielectric properties have been reported in Chapter 6 to fluctuate during firing. Therefore, the broad matching approach followed, as explained in Section 5.4.2, appears to be a reasonable response to counteract these variations. However, it does not noticeably counteract the high degree of reflections observed. This has been tested by matching the system for an optimal power delivery, where the same degree of reflections is reported. Furthermore, this optimal matching causes larger thermal gradients in the clay, to a point where they can be visually acknowledged. This is seen in the fact that for a power input of 100 W, a hot spot at ≈400 ºC is formed in less than 20 s in the cylinder's centre top while its sides are still unfired.

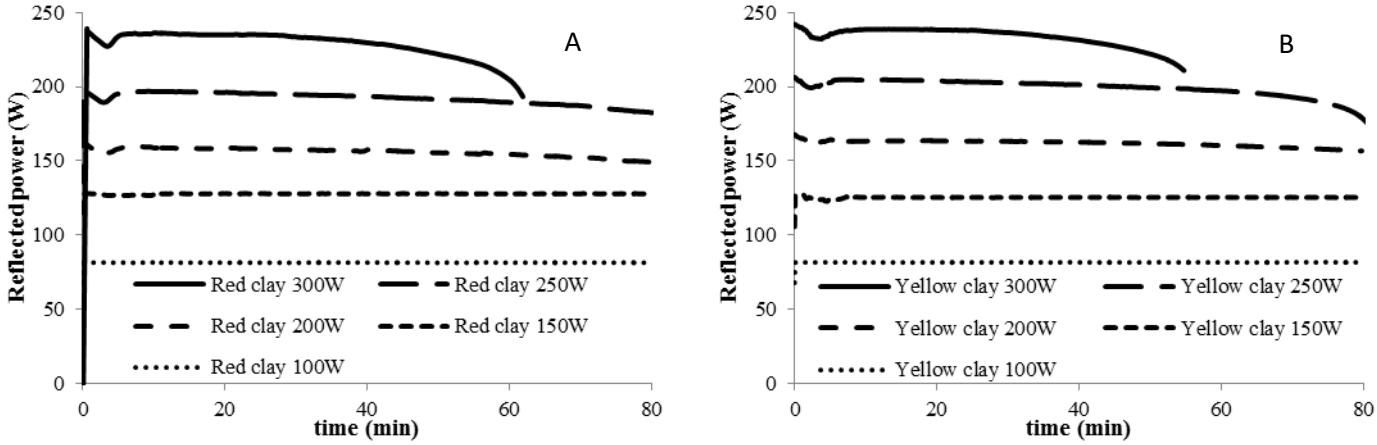


Figure 7.5- Reflected power moving average trends from microwave heating trials at constant incident powers ranging 100-300 W for 80 min on 25x20 mm cylindrical specimens of red (A) and yellow (B) Danish clays at void fractions ranging 0.37±0.02 for the yellow and 0.40±0.01 for the red specimens. These results are the average of three repeats.

7.3.1.2 Power absorption by the microwave system

The power absorbed by the system during heating can be extracted by performing the same trials mentioned above but without loading a sample in the applicator, as described in Section 5.4.2. Subtracting from the power inputs the reflections of Figure 7.5 and the measured system powder absorbance provides the power delivered to clays during the heating trials, i.e. clay absorbed power+heating losses. Trends of the clay absorbed power combined with the heating losses are presented in Figure 7.6. The x-axis is the processing time while the y-axis presents the moving average within a 120 s range of the power trends. As for the power reflections above, no error bars are shown.

Addressing the system power absorption by comparing Figure 7.5 and Figure 7.6 trends, it is certain that the previous assumption of Eq. 5.12 has proven insightful, namely regarding the firebrick crucible and the insulating wool as significant microwave absorbing entities. These

two materials tend to absorb around 93% of the non-reflected power for the 100 W and 150 W trials in both clays. This figure decreases for higher powers at the end of the heating; it goes down to 80% at 200 W, 71% and 64% for red and yellow at 250 W and 68% and 51% for each at 300 W. This reduction is mainly caused by the increasing clay power absorption as the load gets hotter, which in turn is justified by the dielectric properties of Chapter 6. These state that clay coupling with the microwave field progressively improves when getting hotter. Only the crucible+wool/clay volume contrast can explain the noticeable absorbance the system displays, which takes place despite their lower loss factors than the clay load as seen in Appendix B3.

The minimal energy absorption of the clay specimens with respect to the input power, together with their almost trivial energy requirements, result in a heightened sensitivity of the heating rates towards small changes in the system, such as input power or frequency. This negatively affects the reproducibility of the laboratory scale trials.

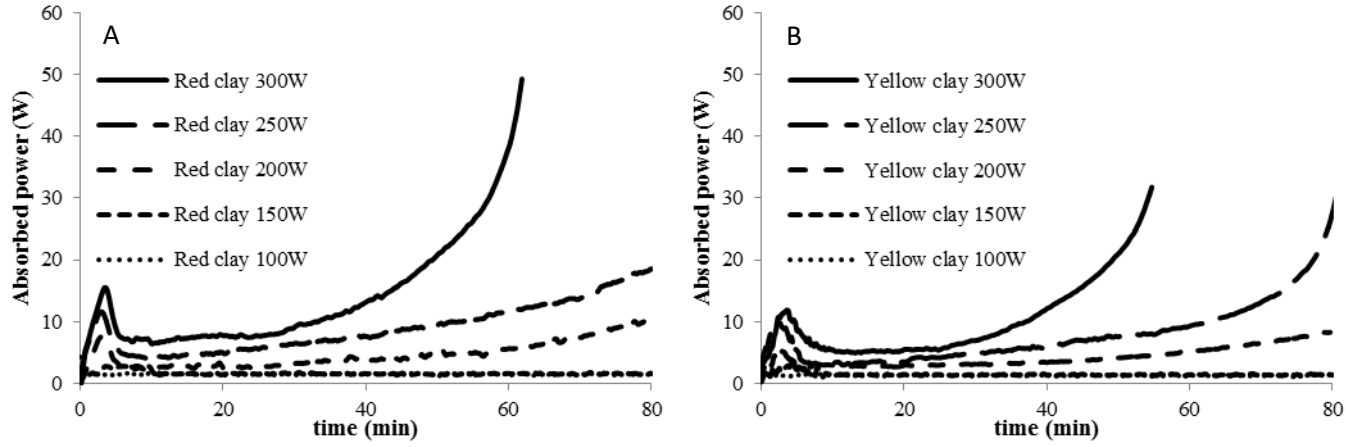


Figure 7.6- Clay absorbed power+heating losses moving average trends from microwave heating trials at constant incident powers ranging 100-300W for 80 min on 25x20 mm cylindrical specimens of red (A) and yellow (B) Danish clays at void fractions ranging 0.37±0.02 for the yellow and 0.40±0.01 for the red specimens. These results are the average of three repeats.

7.3.1.3 Clay power absorption in the microwave system

In order to identify the either volumetric or selective heating of a substance using microwave energy, the quantification of thermal gradients at different sections of the material is often applied, as seen in John et al. (2015), Song et al. (2016a) and Zhang et al. (2017). However, this methodology is not completely suitable for clays since their thermal insulator nature may mask the recognition of the type of heating. Therefore, the volumetric or selective characteristics of the microwave heating of clays are also assessed by contrasting the clays and minerals dielectric properties trends of Chapter 6 with the clay power spectra.

In Figure 7.6, it is seen that the power absorbed by the specimens only roughly resemble the dielectric properties of the red and yellow clays of Chapter 6, mostly due to the effect of the

heating losses graphed in Appendix D3. A more straightforward recognition of the volumetric/selective heating dichotomy comes from removing the power used to overcome the heating losses, leaving only the power absorbed by the clay used to increase its temperature, i.e. net power. The clay net absorbed power trends for the heating trials of Figure 7.5 and Figure 7.6 are seen in Figure 7.7. The x-axis shows the processing time and the y-axis presents the moving average within a 120 s range of the clay absorbed powers. The heating losses of the system are computed from using Eqs. 7.1-7.9, while the temperature profiles are provided by Eqs. 7.10-7.11. Although the thermal models have not been validated yet, at this point it is assumed their suitability for the purposes of recognising clay physicochemical transformations.

Very different power absorption performances are seen in both clays depending on the input power. The flat and nearly null lines found for 100 W and 150 W trials can be assumed to be caused by temperature stagnation beyond water evaporation, as all the absorbed power is used to counter the heating losses when entering the area of worst microwave/material coupling between 150-350 ^{o}C. Using higher power inputs noticeably modifies the power trends. In both clays now appears a clearly defined peak a few minutes into heating, which obviously relates to free water elimination. Logically, its intensity increases as water is eliminated faster with higher applied powers, from the broad and shallow curve below 8 min at 150 W to the peak with almost vertical walls at 300 W. Moreover, the low loss area ranging 150-350 ^{o}C is overcome. This is proven by the steady power absorption increment that at 200 W starts after 30 min for both red and yellow, while understandably commencing earlier at higher power inputs. This concurs with the constant loss factors increase caused by mineral dehydroxylations in clays.

At 300 W for both clays and also at 250 W in the yellow one, a swift transition from the mineral dehydroxylations into sintering, recrystallisations and melting is easily recognisable near the end of the trials in the exponential increase of the absorbed power. The resultant molten ionic salt logically couples so effectively with microwaves that power reflections would be eliminated had the heating not been stopped. Although a small degree of melting is beneficial for obtaining a glassy phase that bounds the mineral structures, the hasty transition to substantial melting compromises the specimen's structural strength (Dunham, 1992, Karaman et al., 2006).

Besides the power absorption differences at the beginning of the heating, both clay types tend to behave similarly and are consistent with the clay dielectric properties of Chapter 6 up to sintering. The fact that the dielectric properties of clay slabs almost perfectly match the clay power absorption trends hints at the volumetric heating (as opposed to selective heating) of

the clay cylinders up to this point. Nevertheless, given the similarities between clay dielectric properties and montmorillonite's and muscovite's, it is feasible that these species have been heated selectively and in turn conventionally raised the temperature of the rest of clay constituents uniformly through conduction effects, resulting in the volumetric heating of the sample regardless. However, these clay minerals have to be homogeneously distributed across the clay volume for the latter to be true. Otherwise, in the analysis of the thermal uniformity of the samples, numerous and significant thermal gradients in all directions will be observed on the clay surface at the end of the heating.

From the start of sintering and until the end of the heating, the resemblance of the power trends to clay dielectric properties and the similarity of both clays power trends decline. Despite yellow clays' lower loss factors beyond sintering, melting is reached around 5-7 min earlier than for its red counterpart. This time difference can be traced back in the latter to a stabilisation of the power absorption easily seen at 300 W between 50-55 min. The only explanation is that there exists a previously undiscovered temperature region where loss factors for red clay, and thus clay power absorption, are moderately stable. This can be understood as interlayer cations having being released from the phyllosilicate structures while sintering has not started yet. The concealment of a high temperature loss factor stable area in red clay dielectric trends might have been caused by the 10 min holding times in the resonant cavity measurements, where possibly sintering has been triggered before taking the measurement.

The lack of a steady clay power absorption stage around 800 ºC in yellow clays may be justified by the effect of the strongly exothermic reactions resultant of the calcite decomposition at 750 ºC, previously seen in the DSC trends of Figure 6.3A. The heat generation provided by these reactions conventionally increases the temperature of nearby minerals. These species are selectively heated by microwaves since their microwave coupling increases with temperature, and subsequently heat through conduction nearby colder minerals creating a thermal gradient. Finally, as a result of the selective heating provided by the calcite decomposition, the sintering stage is promptly triggered. Hence the lack of a flat power trend in yellow clays.

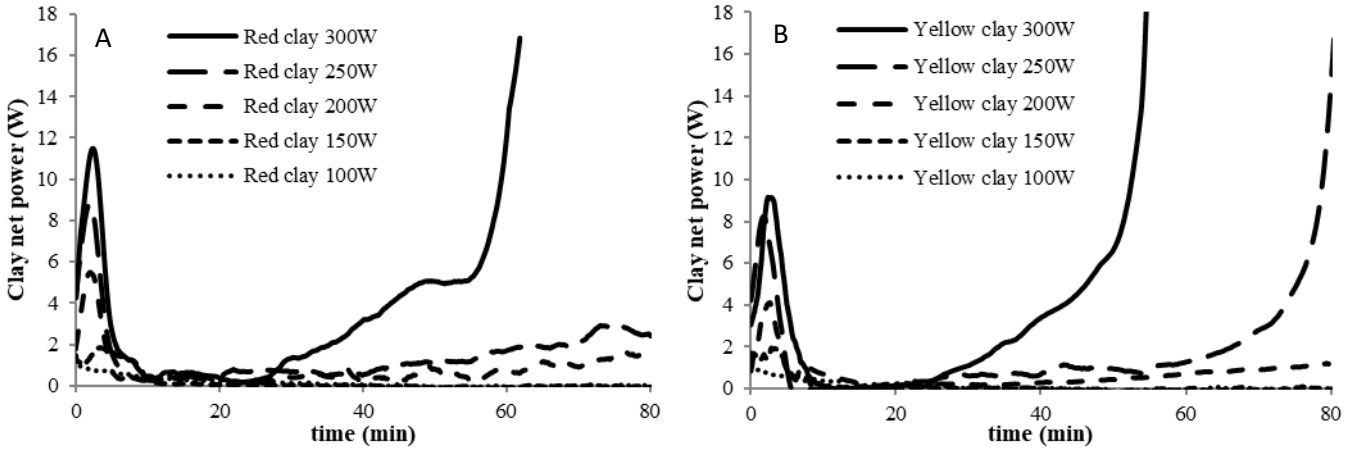


Figure 7.7- Clay net absorbed power moving average trends from microwave heating trials at constant incident powers ranging 100-300W for 80 min on 25x20 mm cylindrical specimens of red (A) and yellow (B) Danish clays at void fractions ranging 0.37±0.02 for the yellow and 0.40±0.01 for the red specimens. These results are the average of three repeats.

7.3.2 Validation of heating losses model

Proof of the validity of the developed thermal models comes from the comparison of the temperature estimations made for the heating trials described above with wool measurements at 10 min intervals and a temperature reading of the clay surface at the end of the trial. The estimated temperature trends and the periodic experimental measurements are presented in Figure 7.8. The x-axis represents the processing time while the y-axis shows the estimated and measured temperatures. The former are displayed as continuous trends while the latter are discrete points. The methodology of the experimental measurements is explained in Section 5.4.2. The error bars of the measurements represent a 95% confidence range. No error bars are shown for the estimations for clarity.

In spite of the simplicity of the thermal models formulations, it is noted that almost all the estimations fall under the error bars of the measured values, which validates the clay thermal reactions discussion above. In the case of the clays surface in Figure 7.8A&B, the consistent overestimation of the measured temperatures is most likely caused by the sharp cooling the specimens undergo in the 1-2 seconds between when the firebrick cap is lifted and the picture is taken. Nevertheless, this difference is beneath the measurements' uncertainties. These uncertainties steadily increase with the clay temperature, maxing for the yellow clay at 300 W with more than 100 ^{o}C due to its fast and uncontrollable development towards melting. Understandably, the degree of these thermal gradients contrasts with the uniformity of the colder 100-150 W results.

Regarding the wool, the flat trends at the beginning of the heating correspond with the time lag from Eq. 7.11. Although agreeing with the measured values, in reality there is most likely a smooth temperature increase in this stage until reaching the end of the time lag. Smaller

temperature deviations than in the clay surface are found on account of the wool's lower temperatures. These deviations range between 1.7-7.5ºC and are mainly caused by the wool's direct contact with air and its relative distance from the heat source, which causes uneven temperature distributions across its surface.

Additional validation of the temperature models can be extracted from the DSC energy requirements to reach 1000 ºC. The energy absorbed by both clays at 100 W and 150 W solely for temperature increase averages around 45.8 J/g and 57.5 J/g for yellow and red, which evidently resembles the 47.3 J/g and 53.6 J/g necessary to reach 100 ºC according to their respective DSC trends. The resemblance tends to break at higher powers. At 200 W it takes 274.1 J/g and 237.2 J/g for red and yellow vs. the 261.9 J/g and 233.1 J/g of the DSC values to reach 428 ºC and 382 ºC, respectively. This is worsened by the exponential advance towards melting seen at 250 W and 300 W. For the former, 514.2 J/g and 528.1 J/g are farther away from the DSC results of 531.5 J/g and 541.1 J/g for red and yellow to nearly reach 730 ºC. Nevertheless, so far all the energy values have fallen under the error bars of the DSC measurements. However, on the 300 W trials the clays start melting, thus going beyond the 1000 ºC DSC values by 20.5% for red clay and by 30.0% for the yellow type.

Finally, it is worth noting the thermal model's only aim is to provide a reasonable average of the temperatures of clays across firing, since information of the thermal uniformity of the specimens is to be obtained from experimental temperature measurements. Hence the uncertainty of measured and estimated values does not need to be comparable.

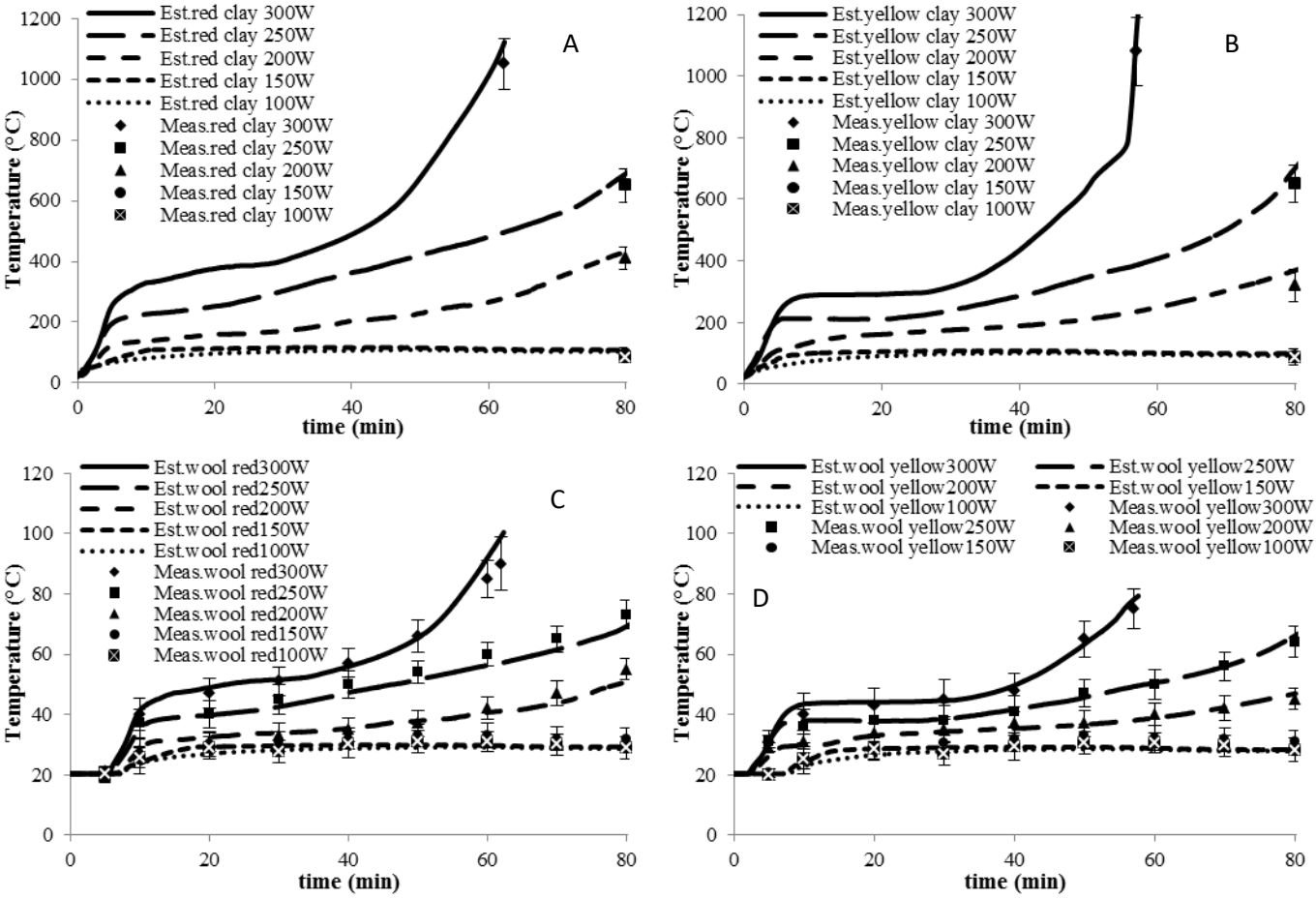


Figure 7.8- Measured and estimated temperatures of clay surface (A-B) and insulating wool (C-D) for the validation of the heating losses model used in the microwave heating trials at constant incident powers ranging 100-300W for 80 min on 25x20 mm cylindrical specimens of red (left) and yellow (right) Danish clays at void fractions ranging 0.37±0.02 for the yellow and 0.40±0.01 for the red specimens. These results are the average of three repeats.

7.3.3 Thermal uniformity of heated clays

In Figure 7.8A&B it has been proven that clays can be heated up to firing temperatures. However, the measured clay surface temperatures portray varying degrees of uniformity depending on the power input. In general, two major and distinct behaviours in the thermal distribution can be distinguished; one where the clays do not surpass 100 ^{o}C and other where they continuously increase their temperature. In the case of the former, the large degree of thermal uniformity present across the clay surface is unequivocal. This is expected considering the more than 60 min of soaking around 100 ^{o}C the samples undergo.

The opposite occurs for higher power inputs, being most marked at 300 W. The presence of an exponential temperature increase renders temperature imbalances in the clay surface larger than 150 ^{o}C. This is better seen in the thermal images of red and yellow specimens at the end of firing at 300 W displayed in Figure 7.9. In both cases, the temperature spectra are not symmetrically distributed from the clay cylinder normal axis, but displaced towards the microwave feed on its right. Thus, the main observable thermal gradient is that formed

between the clay surface facing the microwave feed and its opposing side. The exponential temperature increment both clays undergo at the end of the heating further imbalances the temperature distribution. This maxes out in the yellow clay, probably due to its post-calcite reactions. As a result, part of it has barely reached the firing range whereas its surface facing the microwave feed is about to melt.

On the other hand, red clay displays temperature deviations of around 10% at the height of the heating. The slower approach to melting this clay type presents may justify the higher degree of thermal uniformity observed. The main thermal gradient reported is clearly caused by the effect of the microwave feed on the clay surface facing it and the impossibility of the clay to dissipate the heat to the rest of its volume appropriately due to its insulator nature. Moreover, this thermal gradient is not dependent on its mineralogy or the homogeneity/heterogeneity of its distribution. Therefore, it can be concluded that both clays heat volumetrically when using microwave energy, where only yellow clay displays selective heating at ≈800 ºC due to its calcite content.

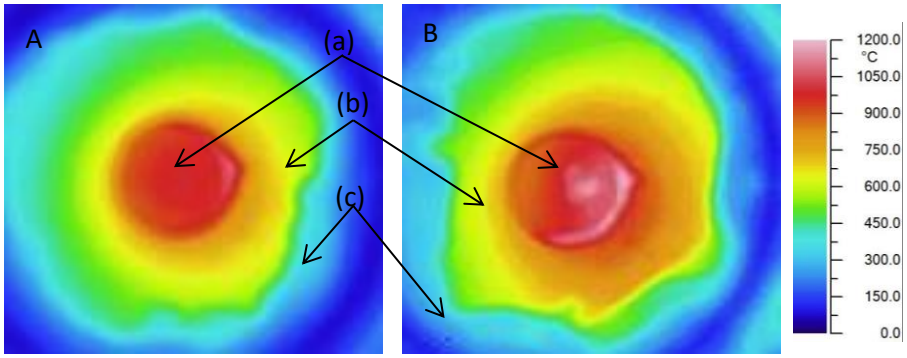


Figure 7.9- Top view under a thermal camera of 25x20 mm red (A) and yellow (B) clay cylinders after around 65 min of microwave heating at 300 W with added temperature legend, where (a) is the clay, (b) is the firebrick and (c) is the insulating wool. Standard deviations average for the clay surface temperatures for the red and yellow samples around ±83.8 ºC and ±110.8 ºC, respectively. The microwave feed is to the right of the samples.

The results of the uneven heating are more clearly seen in Figure 7.10. Here, the localised melting of the clay surface facing the feed and the subsequent thermal gradient surrounding it can be distinguished by colour changes. The effect of the temperature and thermal reactions of the clays' coloration will be discussed later in the chapter. On a positive note, Figure 7.10 further verifies that it is possible to heat clays up to firing temperatures using only microwave energy. The large degree of the thermal gradients witnessed here explain why in previous work in ceramics commented in Chapter 4, hybrid systems, mode stirrers and turntables were used to enhance thermal uniformity and control the process. In the brickworks industry, it has been seen that minimisation of unwanted events, e.g. melting and thermal gradients, which hamper the completion of the firings can be accomplished by the addition of a holding stage.



Figure 7.10- Side view of feed facing surfaces of 25x20 mm cylinders of yellow (A) and red (B) Danish clay after around 65 min of microwave heating at 300 W. Partial melting and a thermal gradient pattern are recognised from bloating and colour differences on the clay surface.

7.3.4 Conclusions on commissioning of microwave clay firing system

A rig designed for the microwave firing of red and yellow clays has been commissioned through the performance of several heating trials at constant power inputs ranging 100-300 W for 80 min at 2450±15 MHz. The suitability of the system to manufacture fired clay products has been proven by investigating the power distribution in the rig, the validation of the thermal models that allow the monitoring of clay temperature during heating, and the thermal uniformity of the processed clay specimens.

These experiments demonstrate, for the first time, that clays can be heated up to firing temperatures and even melting with the sole use of microwave energy. However, not all power inputs manage to heat the specimens beyond 900 ºC. The reason is the far from optimal energy delivery to the sample, causing up to 80% power reflections and between 51-93% of the remaining power is absorbed by the system. The former is the result of heating a small low loss material, while the higher absorbance of the rig comes from the volume contrast between the firebrick and wool insulation when compared with the clay sample. Moreover, a heating choke between 150-350 ºC has been recognised, given the drop of the clays loss factors in this temperature range. Nevertheless, power inputs beyond 200 W are enough for both clay types to overcome it and reach firing temperatures. Regardless of the power input and clays behaviour, the heat loss and heat profiles analytical models provide adequate estimations of the temperatures of the different components of the microwave system, despite the assumptions of stationary state and focal heat generation made among others.

Power absorption behaviour for both clay types agrees with a volumetric heating of the samples, where their power trends are alike until calcite decomposition at 800 ºC. At this point, exothermic reactions from calcite reaction products cause the selective heating of the clay minerals fraction in yellow clays, bypassing an otherwise brief stage of constant power absorption and triggering the clay's sintering. In spite of differences between clays' high temperature behaviour, both swiftly go into melting beyond sintering which causes thermal gradients that can surpass 150 ºC. The main challenge for thermal uniformity comes from the

hot spots that degenerate into melting, which to an extent are caused by clays' characteristic heterogeneity and the dielectric contrast among their constituents. In order to produce fired clays of acceptable quality to be used as building materials, minimisation of these unwanted events is critical. This may be achieved by the addition of a holding stage at the top temperature. As a result, the configuration of what it may be successful a microwave clay firing cycle starts to take shape.

7.4 Development of clay microwave firing cycles

In order to deliver microwaved products of similar quality to conventionally manufactured clays using the designed and commissioned microwave system, heating cycles similar to those found in the industry (Moesgaard, 2015) need to be developed. The justification comes from the importance of controlled heating and cooling rates to minimise thermal gradients in the treated specimens. Moreover, adding a holding stage at the top temperature is crucial in order to minimise thermal gradients and melting. Some alterations from conventional heating cycles have to be made to each of the three stages of firing, i.e. heating, holding, and cooling, when using microwaves as the energy source.

In the first stage, the preliminary nature of the trials favours a simple approach, such as a steady heating rate over a varying one tailored for each critical temperature in clays. Hence, the lowest power input from the above heating experiences that can put the specimens in the firing range has been chosen, i.e. 200 W. Regarding the cooling, an analogous slow rate seems logical in order to minimise structural tensions across clay critical temperatures described in Section 3.3.3. This can be achieved either by natural air convection or power input regulation, as thoroughly discussed in Chapter 5. However, only the former was possible as it will be elaborated later. Finally, the establishment of a holding stage at top temperature is only possible through power regulation.

Power input can be regulated either by the material's surface temperature or by its energy needs. The former appears as the most sensible choice considering how it addresses the crucial importance of the critical temperatures of clays on heating and the top firing temperature on the quality of the final product, while the latter relies on the direct relation between the input and absorbed powers and relates to the energy required to reach the top firing temperature (≈1050 ºC) and complete the mineral transformations. However, the exact energy needs of a specimen over time are determined by parameters that are difficult to accurately measure or tightly control, such as heating losses or clay absorbed power. Thus, it is logical in a first attempt to perform a soaking stage by controlling the temperature of the samples.

In this section, the development of microwave heating cycles for the manufacturing of 25x20 mm fired clays at 2450 MHz is presented. In these cycles, specimens are initially heated with a constant power input of 200 W. Holding stages of 0-30 min are applied to optimise clay thermal uniformity. Control of this stage is first attempted through a PID controller loop, i.e. proportional–integral–derivative, where the determinant parameter is the top temperature of the clay as described in Section 5.4.2. Next, control of the soaking stage through the energy needs of the clay is tested. On the other hand, the cooling has been left to natural air convection. The suitability of the developed firing cycles is assessed based on the degree of thermal uniformity of the fired products.

7.4.1 Clay firing cycles controlled by sample temperature

The moving average of the clay net absorbed power and the clay surface temperature trends of microwaved red specimens for 170 min at 2450±15 MHz are presented in Figure 7.11. The x-axis is the processing time while the y-axis is the estimated clay temperatures and the moving average of the clay absorbed power. An initial power input of 200 W is applied. Power input regulation through a PID loop controlled by the clay temperature provides holding stages up to 30 min long, while the cooling stage is dominated by natural air convection. No error bars have been added for clarity. The methodology of the trials is explained in Section 5.4.2, while the estimated clay temperature profiles are extracted from the measured power spectra and Eqs. 7.1-7.11. Given that the clay temperature cannot be directly monitored, a steady wool temperature of 118 ^{o}C needs to be reached during the holding stage to ensure a clay surface temperature of 1050 ^{o}C.

The clay net power absorption trend during the first 80 min of processing is similar to the 200 W heating trials at constant incident power of Figure 7.7A. A qualitative resemblance to the higher powers of 250 W and 300 W can be established for the following 40 min as the firing progresses, whereas the sample appears to build up to the exponential temperature increase in the 120-140 min range like at the end of the 300 W trend. Although here melting is averted through power modification, instead of a stable soaking stage there can be observed marked temperature oscillations of more than 250 ^{o}C.

It appears that the PID controller struggles to maintain the temperature set point. This is abundantly clear from looking at Figure 7.11A, where the power values sharply alternate between cooling and heating instead of tending to zero. The justification for this undesirable behaviour comes from the indirect control of the clay surface temperature. Given the difference in the magnitude of the temperatures found in the clay and wool, i.e. around 1000 ^{o}C and 100 ^{o}C respectively, the monitoring of the wool's temperature is not sensitive enough to provide a stable holding stage. As a result, the specimens are effectively out of the

firing range at times, meaning a true soaking stage is not reached. Consequently, there is really no point discussing the thermal uniformity of the process. Finally, even though holding times as long as 30 min have been achieved, shortly after that the samples invariably start to melt. This is most likely caused by the overheating caused by the oscillations, triggering the melting of fluxes like feldspars that subsequently melt the entire clay.

The justification for a natural air convection cooling of the samples in the cavity, instead of the power input regulation alternative, comes from the unsuccessful control of the holding stage by the PID and the sensitivity of the clay specimens to minimal power variations. Any attempt of a controlled microwave cooling invariably causes the clays to hastily depart from the firing range straight below sintering (≈600-700 ºC). Moreover, the resultant trends are seldom reproducible. Given the behaviour of yellow clay post-sintering, there is no point for its treatment using this methodology, as power control during the holding and cooling stages would almost certainly be more challenging.

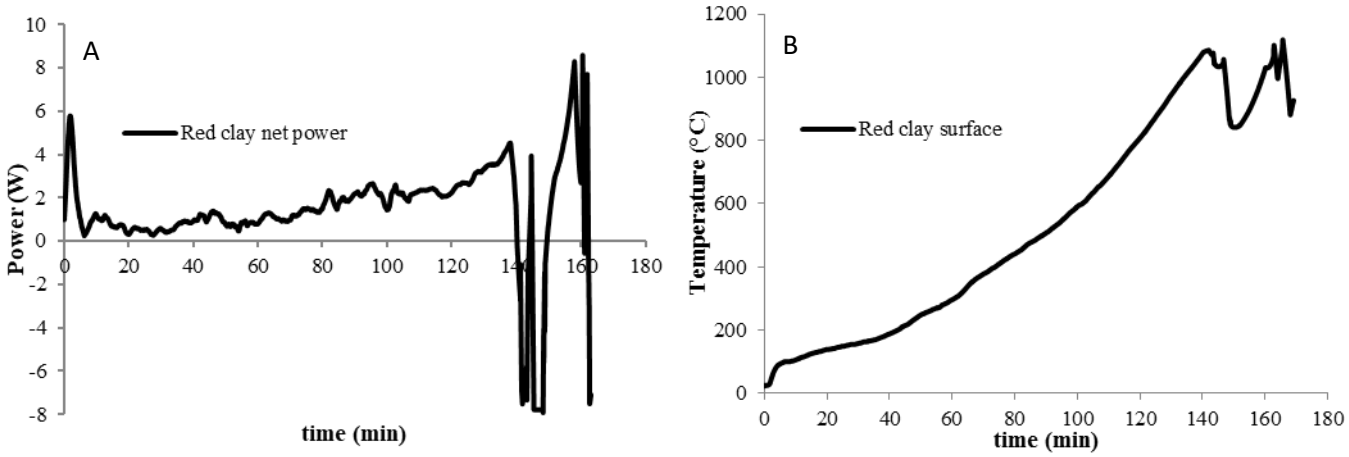


Figure 7.11- Typical net clay absorbed power moving average trend (A) and clay surface temperature profile (B) from 170 min microwave firing trials at 2450 MHz and at a variable incident power, starting at 200 W, indirectly controlled by the temperature of the clay surface on 25x20 mm cylinders of red Danish clay at a 0.40±0.01 void fraction.

A straightforward solution for eliminating the wool-clay temperature dependence that causes the oscillations would be to bring forward a direct temperature measurement of the clay. This can be achieved by substituting the IR sensor by a thermocouple in contact with the clay. However, the thermocouple would interact with the microwave field. Another option is to manufacture a hole in the firebrick so the camera can directly see the clay. Although both cases are feasible in the industrial level, in these laboratory trials there will be an associated heating loss increase and larger thermal gradients. Therefore, to achieve a satisfactory control of the holding stage at this scale, the path of energy needs control appears to be the only viable alternative.

7.4.2 Clay firing cycles controlled by sample energy needs

The moving average of the net clay absorbed power and the clay surface temperature trends of red and yellow Danish clays during microwave firing trials equivalent to the ones above are presented in Figure 7.12. However, in this case instead of a holding stage governed by clay temperatures, an energy needs based control through the development of a LabVIEW loop, explained in Section 5.4.2, is applied. In contrast with the heating trials above, the set point of power delivery to the clay across the holding stage, i.e. absorbed power plus heating losses, is defined by the characteristics of the process and the system. As a result, there is no discrete target of power that stabilises the sample surface temperature around 1050 ºC, but a range instead. Through trial and error experiments, requirements of 30-32 W for red and 34-36 W for yellow clay have been established.

The advantage of this methodology is evident. A tighter restraint on the exponential power increase tendency at sintering is observed in Figure 7.12A for red clay, where power input modification starts around 5 min earlier than in Figure 7.11. This is explained by the straightforward control of the absorbed power, as there is no inertia with respect to the input power. Consequently, the power reversals found in Figure 7.11A strongly contrast with Figure 7.12A small but periodic power rearrangements that gradually minimise the clay absorbed power, signalling the clay temperature stabilisation. Minor power fluctuations can be seen at this point for correction purposes, given that the top temperature is not a stable point. As a result, the previously observed overheating peak at the start of the soaking in Figure 7.11B is here eliminated. The subsequent oscillations that take the clay in and out of the firing stage are also absent.

A similar behaviour is found for the yellow clay. Although these specimens tend faster to melting than the red samples, the LabVIEW control loop is still able to regulate the set absorbed power. However, in doing so the heating does not proceed beyond 850 ºC. It is possible that by decreasing the power input, the selective heating of clay minerals observed at this point is overcome by the heating losses. Given the samples' sensitivity to power changes, no middle point of moderate heating between temperature's stabilisation and melting can be reached. Thus, in order to continue the firing, the system is briefly allowed to manually surpass the absorbed power threshold. The result can be easily distinguished as a peak around 117 min in Figure 7.12B, where the specimens surpass 1100 ºC. Nevertheless, the temperature is promptly stabilised around 1050 ºC after that. It is worth noting for both clays that because of the smoothing of the graphs with the moving average, some power fluctuations are averaged out of the display.

The optimisation of the soaking stage does not translate into the possibility of noticeably longer holding times. The samples still melt randomly before reaching 40 mins of soaking. This means that the temperature oscillations of Figure 7.11B do not hinder the clay melting resistance as much as the top temperature of the firing being close to the clay melting point.

Similar to the previous trials, attempts to control the cooling rate are also unsuccessful. The justification here is that the temperature decline would have to be stabilised at narrow intervals to avoid the generation of thermal gradients, where the associated absorbed powers would be calculated as in the holding stage. The resulting challenge of adequately determining all the power ranges for a material so sensitive to power changes is not justified, considering the relatively small magnitude of thermal gradients expected in such small cylinders when using natural air convection for the cooling.

Regarding energy consumption, both clays' requirements to reach 1050 ºC tend to agree with the DSC results, taking into account that the DSC results cover the 20-1000 ºC range. Comparing both clay types, yellow clay with 804±21 J/g needs around 70 J/g less than the red counterpart.

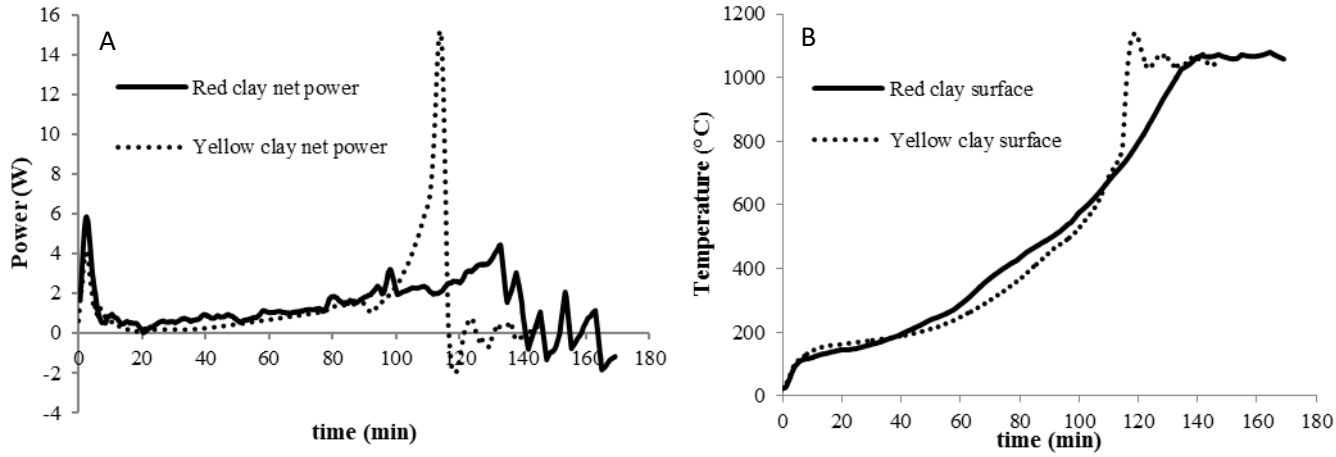


Figure 7.12- Typical net clay absorbed power moving average trends (A) and clay surface temperature profiles (B) from 170 min microwave firing trials at 2450 MHz and at a variable incident power, starting at 200 W, directly controlled by the absorbed power of 25x20 mm cylinders of red and yellow Danish clays at void fractions ranging 0.37±0.02 for the yellow and 0.40±0.01 for the red specimens.

7.4.3 Thermal uniformity of clays fired using microwave energy

Only the thermal uniformity of clays subjected to microwave firing cycles where the power input is controlled by the energy needs is worth being studied. The reason is this system configuration alone manages to provide thermally stable clays at the end of the holding stage. As seen before, the existence of thermal gradients can be more effectively assessed by looking at the thermal images of the surface of red and yellow specimens at the end of the firing cycles. The thermograms of the clays of Figure 7.12 after a 30 min holding stage are

displayed in Figure 7.13. The effect of the holding stage is abundantly clear upon comparison with Figure 7.9, as there is a significant reduction of thermal gradients. The samples are stable around 1050 ºC and the maximum temperature difference in the red and yellow clays is reduced to 40 ºC and 70 ºC respectively. It appears that keeping the samples soaking even for only 30 min allows for the redistribution of the heat and results in the thorough thermal homogenisation of the clays' surface. Additionally, the previously found overheating on the side facing the microwave feed is minimised. However, it is still somewhat recognizable on the yellow clay, as expected from its more vigorous exothermic behaviour post-sintering.

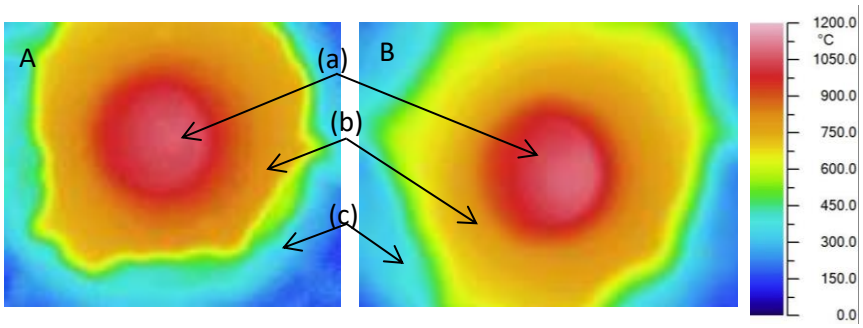


Figure 7.13- Top view under a thermal camera of 25x20 mm red (A) and yellow (B) clay cylinders at the end of a 30 min holding stage after microwave firing at variable incident powers, starting at 200 W, directly controlled by the clay absorbed power with added temperature legend, where (a) is the clay, (b) is the firebrick and (c) is the insulating wool. Standard deviations average for the clay surface temperatures for the red and yellow samples around ±33.9 ºC and ±61.1 ºC, respectively.

7.4.4 Conclusions on the development of clay microwave firing cycles

In the manufacturing of fired clays comparable to brickworks clays while using microwave energy, the development of the microwave firing cycles can be divided in three sections, i.e. heating, holding and cooling. Similarly to what occurs in brickworks (Moesgaard, 2015), a steady heating rate is preferred over a more variable one tailored to the critical temperatures of clays on heating. Power regulation is necessary to establish a holding stage, which has been shown to be critical to achieve thermal uniformity in clays during the microwave system commissioning. Finally, power regulation or natural air convection can be used to cool down the fired products. Microwave controlled cooling has been found infeasible at this laboratory scale, where natural air cooling is used instead.

Two options of power regulation have been found proficient in counteracting clays melting, which invariably occurs after sintering. Both also establish, with various degrees of success, a holding stage that minimises clay thermal gradients, which easily surpass 150 ºC otherwise. One option is where the power input is controlled by the temperature of the clay/wool surface, while the other links power input with the energy needs of the clay via its absorbed power. Both alternatives manage to provide holding stages of up to 30 min until the specimens start to melt, probably due to the closeness of the top firing temperature and the clay melting point. However, the indirect control of the clay temperature through the insulating wool surface

temperature causes temperature oscillations in clays during the holding stage of up to 250 ºC. On the contrary, tight control of the system and a stable holding stage are provided by the energy needs control alternative. Consequently, this methodology provides minimisation of the thermal gradients after soaking for 30 min, with maximum temperature imbalances of 40 ºC and 70 ºC for the red and yellow samples.

The success of the firing cycles has proven that microwave energy alone can heat these multicomponent heterogeneous materials, while also ensuring a tight level of control during the process. Furthermore, the use of microwaves reduces processing times more than 90% when compared with conventional brickworks cycles seen in Chapter 3, although it is unknown what would be the appropriate firing time for a full size brick. The reproducibility of the trials remains challenging due to the power sensitivity of the clay samples, which comes from the high degree of power reflections and power absorbance by the system found in the commissioning stage. Added to this, holding stages as long as in conventional firing cycles are unfeasible as the samples invariably melted after 30 min. Despite these advantages and caveats, it is unknown if the quality of the fired products has been affected positively, negatively or not at all by the use of microwaves. Moreover, the necessary brevity of the holding stage in order to avoid melting may have negative repercussions when attempting the firing of a full brick using only microwaves. Hence, the next step is to compare their properties with those of clays treated under conventional means to assess possible technical advantages of the microwave technique.

7.5 Quality comparison between microwave and conventional firing

In Chapter 3, the quality parameters of fired clays commonly quantified in brickworks have been addressed, i.e. compressive strength, water absorption and saturation coefficient, size variation, durability, colour and texture. In order to contrast the microwave and conventional processing techniques, it is worth also assessing shape, density and mineralogical differences between both methodologies, so as to gain a deeper knowledge of the impact of microwaves on product quality.

A direct comparison between the quality of fired bricks using brickworks heating cycles, and the laboratory scale microwaved clay cylinders investigated above is not possible. This is mainly due to their different geometries, as some crucial quality indicators such as compressive strength are extensive properties, i.e. depend on the volume of the specimen. Moreover, the smaller size of the studied cylinders ought to enable faster heating cycles using conventional methods, without the significant decline in mechanical properties that would occur for full bricks. Therefore, in order to enable a quantitative and sensible quality

comparison, a conventional firing reference using the same clay cylinders employed in the microwave trials has been developed.

This section starts with the manufacturing of a conventionally fired reference using 25x20 mm clay cylinders of the same size as those used in the microwave trials in order to allow for a direct comparison between microwave and conventional firing. The specimens are fired using different cycles, ranging from brickworks to the microwave trials heating rates. Next, both conventionally and microwave fired specimens quality is investigated through several parameters, i.e. compressive strength, water absorption and saturation coefficient, size variation, durability, colour and texture, shape, density and mineralogy, which will indicate any possible advantages or disadvantages of microwave processing over conventional heating methods in terms of product quality.

7.5.1 Conventionally fired clay reference

Although there can be recognised various heating rates during the microwave trials, the average values of 7.8 ^{o}C/min and 9.5 ^{o}C/min found for the red and yellow clays are targeted for the conventional cycles in order to enable a fair comparison. Figure 7.14 presents the evolution of the quality of the conventionally processed clays for increasing heating rates, starting from industrial values, i.e. 0.92 ^{o}C/min. The compressive strength is used as the key quality indicator here. The methodology followed is detailed in Section 5.5.1 and Section 5.5.2. Clays' compressive strength is displayed in the y-axis for different heating rates shown in the x-axis. The error bars show a 95% confidence range. The soaking and the cooling times have not been changed from brickworks' heating cycles since the heating rate is the focus of the investigation, i.e. 4 h soaking and cooling at 85 ^{o}C/h until 750 ^{o}C, 20 ^{o}C/h until 500 ^{o}C, 45 ^{o}C/h until 100 ^{o}C.

A significant compressive strength decrease is observed upon small increases of the heating rate. This sensitivity to heating rate increments has been previously noted in the literature (Mohajerani, 2013) and it most likely lies in the development of structural tensions as clay firing progresses through abundant critical points without ensuring thermal uniformity. The most prominent example is the more than 50% reduction in strength of both clays when increasing the heating rate five-fold from brickworks values. Addressing each clay type, red clay displays at all times a larger degree of compressive strength on average, although the uncertainty of the measurements cancels that divergence except for the fastest heating rate. Here, red clay with 2.86 N/mm^2 has a 32% higher strength than the yellow type. This can be attributed to the difference in calcite content, i.e. 20% in yellow clay vs marginal in red clay, where its decomposition is a major cause of structural tensions (Beruto et al., 2003, Rodriguez-Navarro et al., 2009).

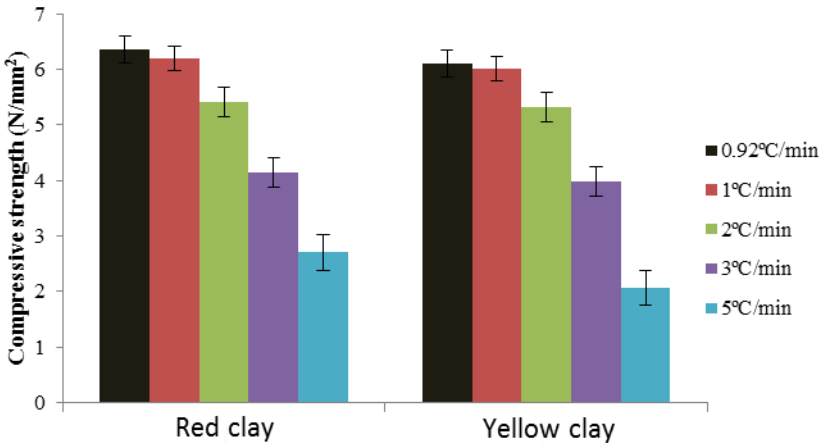


Figure 7.14- Compressive strength evolution of conventionally fired 25x20 mm cylinders of red and yellow Danish clays in the 20-1050 ºC range at different heating rates. These results are the average of ten repeats.

Heating rates above 5 ºC/min are not presented in Figure 7.14. This is mainly due to the appearance of visible fractures across the specimen's surface as seen in Figure 7.15, which indicate a sharp decrease of its mechanical strength. This comes to a point where clay cylinders conventionally processed at 9.5 ºC/min crumble before the application of any compressive load. It appears that the sample size reduction does not aid in unlocking faster conventional processes. Thus, a clear advantage of microwave processing has been discovered, as clays cannot be conventionally fired nearly half as fast as when using microwaves. It is worth noting that this is the case for the laboratory scale samples studied, as for industrial stacks of bricks the allowed heating rates for microwave processing may vary. Understandably in the case of a quality comparison, the compressive strength is more meaningful than the speed of the firing. Thus, clay cylinders conventionally fired at 0.92 ºC/min, i.e. same as in brickworks, are used as the reference for the following quality comparisons in spite of their longer processing time.



Figure 7.15- Side view of 25x20 mm red clay cylinder conventionally fired at a heating rate of 7ºC/min in the 20-1050 ºC range. Surface cracks are clearly noticed and denote the presence of intense structural tensions result of large thermal gradients.

7.5.2 Compressive strength

The compressive strengths of conventionally fired red and yellow Danish clays using a brickworks cycle with a 0.92 ºC/min heating rate, and microwave fired specimens using a heating cycle like that of Figure 7.12 while applying different holding stages ranging 0-

30 min are seen in Table 7.1. The methodology followed is detailed in Section 5.5.2. The need for an in-built standard as argued above is demonstrated by the obvious difference between ASTM C62 standard values and the experimental data.

As expected, the worst strength values are obtained for specimens that do not undergo a holding stage. This comes from the large thermal gradients seen in Figure 7.9 as opposed to the thermal uniformity seen in Figure 7.13, which hint at significant structural tensions in the former. As a result, the non-soaked microwaved samples are found to be 22.3% in the case of the red and 33.7% for the yellow weaker than conventional products.

Higher levels of compressive strength are achieved when having a holding stage that curtails thermal gradients from ±83-110 ºC down to ±34-61 ºC. Even a brief 10 min of stabilisation dwarfs the influence of clay's heterogeneity and allows for a more even densification of the specimens, causing a strength increase of 17.7% and 32.6% for red and yellow respectively over non-soaked specimens. Further soaking improves product quality with decreasing efficiency, as between 20-30 min the strength growth is narrowed down to 5.8%. Similarly, the system stabilisation brought by larger holding times tends to reduce deviations in the results, reaching a one order of magnitude improvement for the yellow clay with a 30 min holding time.

It is worth noting that with the longest soaking time, the microwaved specimens have on average 11.5% for the red and 13.4% for the yellow higher strength than their conventional counterparts. At the same time, yellow clay appears to have 15.7% lower compressive strengths than red clay, which can be explained by its calcite decomposition fuelled thermal gradient near the start of the holding stage. Nevertheless, the uncertainty of the measured values, justified by the challenging reproducibility of the heating experiences, largely negates this difference.

Table 7.1- Compressive strength of microwaved and conventionally fired 25x20 mm clay specimens in the 20-1050 ºC range with the former processed at different holding times, and standard values from ASTM C62. The microwave data is the average of three repeats, while conventional values are the results of ten repeats.

	Building bricks standard (ASTM C62		Experimental									
			Red clay					Yellow clay				
			Conventional	Microwave				Conventional	Microwave			
Holding time (min)	**N/A**		**240**	**0**	**10**	**20**	**30**	**2400**	**0**	**10**	**20**	**30**
Compressive strength (N/mm^2)	**Weathering**		6.37 ±0.29	5.09 ±0.76	5.99 ±0.26	6.78 ±0.31	7.15 ±0.18	6.11 ±0.21	4.35 ±1.23	5.77 ±0.55	6.58 ±0.20	6.99 ±0.11
	Severe	**≥17.2**										
	Moderate	**≥15.2**										
	None	**≥8.6**										

7.5.3 Water absorption and saturation coefficient

The comparison between microwaved and conventionally processed clays with regards to their water absorption, both boiling and cold, and their resultant saturation coefficients are displayed in Table 7.2. The methodology applied can be seen in Section 5.5.3. From the results of Table 7.1, the quality analyses from this point forward are focused on clays subjected to holding times of 30 min. As in the case of compressive strength, the size disparity between conventional bricks and clay cylinders justifies the need for a customised standard.

Microwaved clays have a higher degree of water absorption than their conventional counterparts regardless of the water temperature, i.e. boiling or cold, averaging around 31.6% for the red and 45.3% for the yellow clays. Given the direct relationship of water absorption with porosity (Zhang, 2011), this means that microwaved samples must have larger void fractions. This aligns with heating cycle differences between the conventional and microwave treatments, where the comparable brevity of the latter's holding stage hampers the enhanced densification resultant of volumetric heating. Among clay types, yellow clay consistently absorbs more water than the red counterpart, admitting around 19.2% and 33.4% more water for conventional and microwaved samples respectively. This occurs because of the porosity creation caused by calcite during its decomposition, which makes the fired yellow clay prone to show a larger degree of water absorbance (Galan et al., 2013, Zhang, 2011).

As opposed to the material characteristics reported so far, experimental saturation coefficients (also shown in Table 7.2) have values comparable to industrial bricks standards and enable the assessment of the fired clays durability. This occurs thanks to the intensive nature of this variable, which means that it does not depend on the amount of the material that forms the system. It appears that under ASTM C62, the conventionally manufactured bricks are acceptable for moderate weathering conditions. Microwaved samples have on average a slightly larger saturation coefficient (3.4%), but their error bars overlap with conventional values. This means that structurally, both processing methods present a similar degree of resistance to freezing/thawing mechanisms (ASTM, 2013a).

Table 7.2- Cold and boiling water absorption and saturation coefficients of microwaved and conventionally fired 25x20 mm clay specimens with the former processed with a 30 min holding time, and standard values from ASTM C62. These results are the average of three repeats.

	Building bricks standard (ASTM C62		Experimental			
			Red clay		Yellow clay	
			Conventional	Microwave	Conventional	Microwave
Absorption boiling water 5 h (%)	Weathering		8.9±0.1	12.1±0.2	10.5±0.2	16.5±0.3
	Severe	≤20.0				
	Moderate	≤25.0				
	None	N/A				
Absorption cold water 24 h (%)	Weathering		7.6±0.2	10.7±0.3	9.5±0.3	15.4±0.3
	Severe	≤16.0				
	Moderate	≤22.5				
	None	N/A				
Saturation coefficient	Weathering		0.85±0.01	0.88±0.02	0.90±0.02	0.93±0.02
	Severe	≤0.80				
	Moderate	≤0.90				
	None	N/A				

7.5.4 Shape, size and density variation

As detailed in Section 5.5.4, the recognition of shape distortions in the clay cylinders caused by the processing method is based on a qualitative visual assessment of the fired products. Identification of any torsion, camber or bloating on the small 25x20 mm samples is challenging. Furthermore, these faults are usually generated by uneven thermal distributions within the brick, which in the microwave case have been reduced according to Figure 7.13. The side view of red clays unfired, conventionally fired and at different stages of the microwave treatment presented in Figure 7.16 demonstrate that microwave and conventional firing cause no shape deviations for the sizes studied here. Obtaining the same results at industrial scale will critically depend on the uniformity of the heating procured by microwaves, where a fast and non-uniform heating may cause asymmetrical volume expansions across the clay load. Moreover, the critical elimination of carbonaceous material before 800 ^{o}C, as mentioned in Section 3.3.3, may not be completed and result in the bloating and black coring of the clay load.

A similar problem is found for the quantification of the size variation, given the considerable degree of uncertainty in monitoring the shrinking of small clay cylinders. In Table 7.3, the volume changes on firing using conventional heating and microwave energy have been quantified, where the methodology is explained in Section 5.5.4. Conventionally treated clays shrink around 3.8%, while firing using microwave energy reduces the shrinkage rate and presents divergent volume changes for each clay type. This agrees with the higher water absorption, and therefore porosity, of microwaved clays seen in Table 7.2. On microwaved red specimens, the volume loss has diminished on average by 45.9% while in yellow samples it is reduced only by 15.4%. The lower densification in the latter can be attributed to the pore

creation caused by calcite decomposition. The decline of the samples' shrinkage comes from the shorter holding times, as the briefer the soaking of the samples at top temperature, the lower their volume loss and densification.

Finally, density differences between the conventional and microwaved samples give an insight into their degree of densification. Using the methodology of Section 5.5.4, the bulk density values are presented in Table 7.3. The density of conventionally treated samples is close to 2.3 g/cm^3, i.e. typical industrial bricks' density (Karaman et al., 2006, Faria et al., 2012). However, the same values are not reached by the microwaved samples, as they are on average 6.9% more porous. This lower densification and consequently higher porosity agrees with the higher water absorption and lower volume change caused by the shorter holding times, as discussed above. As expected, the yellow clay displays a 5.8% lower density than its counterpart, which is caused by the void generation resultant of the calcite decomposition.

The fact that microwaved samples display a lower degree of densification due to their shorter processing times would generally be a sign of poor compressive strength in the final product (Ovri and Ndukwe, 2014). However, this method manufactures fired clays of increased mechanical strength instead. The explanation comes from the reduction of thermal gradients that microwaves provide. The strength improvement resultant from the higher degree of thermal uniformity of microwaved clays counteracts and overcomes the compressive strength reduction caused by their lower densification.

Table 7.3-Porcentual volume reduction from unfired specimens and bulk densities of microwaved and conventionally fired 25x20 mm clay specimens with the former processed with a 30 min holding time. These results are the average of three repeats.

	Red clay		Yellow clay	
	Conventional	**Microwave**	**Conventional**	**Microwave**
Volume change (%)	3.7±0.1	2.0±0.2	3.9±0.1	3.3±0.3
Dry bulk density (g/cm^3)	2.06±0.03	1.95±0.03	2.00±0.03	1.84±0.04

7.5.5 Colour and texture

Similar to the analysis of shape changes, texture differences between conventional and microwaved clays can be visually inferred from Figure 7.16. Clearly, the small size of the samples hampers the recognition of any flaws resulting from the treatment. Close examination between both processing techniques shows no significant cracks or flakes for any of the samples, where the only aesthetic defects clearly recognisable are those developed during shaping. It appears that surface characteristics are indifferent to the processing technique.

Focusing on the surface coloration of the samples, in Figure 7.16 the side view of red clays unfired, conventionally fired and at different stages during microwave heating is shown.

Colour changes across firing allow the identification of some physicochemical transformations in the clays. Starting from the leftmost grey unfired cylinder (a), heating it up to the start of clay minerals dehydroxylations causes a sharp darkening of the whole load (b). This change is explained as a direct result of the elimination of organic volatiles, which peaks around 400 ºC (Dunham, 1992). As the dehydroxylations progress, the specimen acquires a reddish coloration, which becomes easily distinguishable at 600 ºC (c). Finally, reaching firing temperatures either conventionally (d) or through microwaves (e) further enhances the intensity of the red colouring.

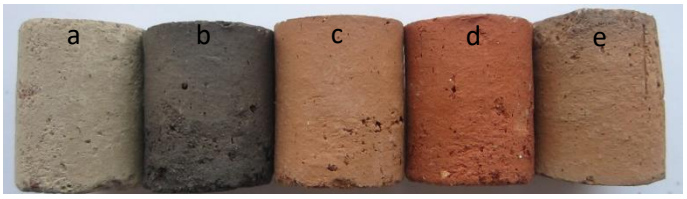


Figure 7.16- Side view of 25x20 mm cylinders of red Danish clay at different stages of conventional and microwave treatment in the 20-1050 ºC range. Unfired clay (a), microwave heated up to the start of the mineral dehydroxylations at 350-400 ºC (b), microwave heated up to before sintering at 650-700 ºC (c), conventionally fired (d), and microwave fired (e).

Given the close relationship between the top firing temperature and clay's coloration (Kreimeyer, 1987), it is interesting to note that conventional treatments consistently provide more intense colours. Since the thermograms of Figure 7.13 prove that 1050 ºC has been reached during microwave firing, the colour disparities might be caused by the significantly shorter holding times and uncontrolled cooling of the microwave heating cycle below firing temperatures. The link between colour intensity and the completion of certain mineral reactions, e.g. hematite formation, discussed in Chapter 3 suggests that some mineral transformations are left incomplete when undergoing a microwave firing cycle.

An assessment of the influence of the processing times on the coloration of clays fired with microwave energy has been detailed in Section 5.5.5. It consists on adding a controlled conventional cooling using the same rates as in brickworks to microwaved clays at the end of their holding stage. The resultant fired products are displayed together with microwaved and conventionally treated specimens on Figure 7.17. The effect of larger holding times has not been investigated due to the aforementioned tendency of both clay types to melt. Clearly, extending the duration of the cooling stage increases the intensity of the red and yellow coloration of both clay types. Although not matching the conventionally treated cylinders, the microwave heated and conventionally cooled specimens establish a middle point between the pure microwaves and pure conventional samples. The fact that the latter's coloration is not reached is probably caused by the different length of the holding stages.

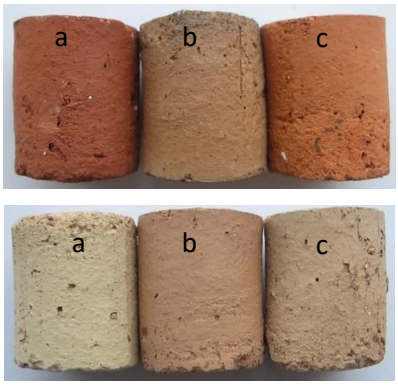


Figure 7.17- Side view of 25x20 mm cylinders of red (up) and yellow (down) Danish clays treated conventionally (a), with microwaves (b) and with microwaves plus a conventional cooling (c) in the 20-1050 ºC range.

A quantitative analysis of the colour disparities of red and yellow fired clays is provided by their CIE colour parameters shown in Table 7.4. As explained in the methodology presented in Section 5.5.5, "L" stands for luminance while "a" and "b" describe the colour opponents green–red and blue–yellow. It can be seen that unfired and processed clays have similar levels of luminance regardless of their type, all clays being fairly light specimens with an average 61% for both clay types. Regarding their colour, unfired specimens stand close to the ideal grey configuration, i.e. a=0, b=0, as expected from being dry untreated clays. Due to its mineralogy, yellow clay "b" value almost doubles that of its red counterpart. Upon conventional firing, the latter unmistakably tends towards a strong red coloration with an "a" factor averaging around 30. The same occurs for the yellow tone of the yellow sample.

Microwaved red samples are redder and yellower than the unfired cylinders but 38.2% and 27.5% less so respectively than conventional specimens on average. Yellow samples appear redder than both conventional and unfired specimens. The best possible explanation is that their black coloration from the organics elimination has not been completely removed, giving that darker appearance to the samples. The addition of conventional cooling to the microwaved samples makes them closer in colour to the conventionally fired clays. The change is less marked in yellow clays, as they are only 10.3% more yellow and a third less red, while red clays are 32% redder and 14% yellower. Surprisingly, the latter's "b" value surpasses that of the conventional specimens. It is hypothesised that this is caused by the luminance contrast between the processing methods used for each sample.

Table 7.4- CIE colour space parameters of unfired, microwaved, conventionally fired, and microwaved + conventionally cooled 25x20 mm red and yellow Danish clays with the former processed with a 30 min holding time. These results are the average of five repeats.

	Red clay				Yellow clay			
CIE parameters	**Raw**	**Conventional**	**Microwave**	**Microwave + Conventional cooling**	**Raw**	**Conventional**	**Microwave**	**Microwave + Conventional cooling**
a	3.7±0.6	29.3±0.7	19.9±0.4	26.4±0.2	-0.4±0.2	-3.6±0.7	9.5±0.7	6.1±0.3
b	5.9±0.9	18.5±0.4	16.2±0.6	21.2±0.3	10.2±0.7	30.6±0.5	23.2±0.2	25.6±0.3
L (%)	67.9±4.1	58±5.7	61±3.2	68±4.2	55±3.3	62±5.0	60±4.7	56±4.5

7.5.6 Mineralogical evolution

An analysis of the mineralogical differences between clays that have been microwaved, conventionally treated, and microwaved and then cooled conventionally is displayed in Table 7.5. The experimental procedure is detailed in Section 5.3.2. In general, the clay minerals phase and calcite completely disappear from the conventionally treated specimens, being replaced by hematite, pyroxenes, sanidine and wollastonite, as expected from Figure 3.4. The last three are only observable for the yellow clay, while hematite forms up to 4.4% of the yellow clay and twice as much of the red one. Hematite appearance in clays has been also reported by Jensen (1978). The presence of other common recrystallised minerals such as mullite, anorthite and corundum is negligible in both clay types. Finally, feldspars stay largely unchanged by the thermal treatment, while there is an up to two-fold increase in quartz compared with unfired clay values reported in Table 6.1. The justification lies on the formation of quartz from unbounded silicates, e.g. aluminosilicates result of the clay minerals decomposition (Dunham, 1992).

Some differences are observed in the microwave fired specimens. First, muscovite is not completely dehydroxilated, forming 4.9% of the yellow clay and nearly twice as much of the red sample. The shorter duration of the microwave firings prevents the most thermally stable clay mineral from completely disappearing (American Petroleum, 1951). This is also observed for calcite in the yellow clay, where its original content has been more than halved. Consequently, no recrystallised minerals are observed in the yellow samples, while the hematite content in red clays is almost five times lower than in the conventionally fired specimens. The failure to complete the thermal reactions of the conventional treatment when using microwave energy aligns with the dimmer coloration of the latter's samples and the brevity of the microwave firings. Nevertheless, their influence on the final compressive strength is minimal because it is counteracted by the larger degree of thermal uniformity microwaves provide. Adding a conventional cooling to the microwave firing creates a middle point between both methodologies, which partially counteracts the shorter processing cycle of

the microwave treatment. The presence of recrystallised minerals is reduced by 1.1% from conventional values for the yellow and curiously increased 17.0% for the red type.

Table 7.5- Quantitative XRD characterisation of the major clay constituents in red and yellow Danish clays after microwave firing, conventional firing, and microwave firing + conventional cooling 25x20 mm cylindrical samples in the 20-1050 ºC range. Each sample was measured once, so that deviations for the mineral concentrations range ±2.5% for >60 wt%, ±5% between 60-30 wt%, ±10% between 30-10 wt%, ±20% between 10-3 wt% and ±40% for <3 wt %.

Clay	Treatment	Quartz (%)	Calcite (%)	Orthoclase (%)	Albite (%)	Muscovite (%)	Hematite (%)	Pyroxenes (%)	Sanidine (%)	Wollastonite (%)
Yellow	Conv	51.9	<1	8.8	11.3	<1	4.4	14.4	3.8	5.4
	MW	65.8	7.1	8.4	10.7	4.9	<1	<1	<1	<1
	MW+ Conv	50.4	<1	9.1	11.9	<1	3.6	15.6	3.1	5.4
Red	Conv	67.4	<1	10.4	12.9	<1	8.6	<1	<1	<1
	MW	69.2	<1	9.8	10.2	9.2	1.5	<1	<1	<1
	MW+ Conv	67.0	<1	8.7	13.7	<1	10.2	<1	<1	<1

7.5.7 Conclusions of microwave-conventional clays quality comparison

Important advantages have been found to the substitution of conventional heating methods by microwave energy in the processing of clays used in common building applications. First, the firing cycle length has been reduced by 92%, where attempts to speed up the conventional treatment result in clay's substantial cracking. Microwaved clays show on average a compressive strength increase of 12.45% after a 30 min holding stage, reaching 7.15 N/mm^2 and 6.99 N/mm^2 for red and yellow respectively. The main factor affecting this improvement is the thermal uniformity brought by the soaking stage. Absence of a holding stage causes a 40.11% compressive strength reduction, becoming worse than conventional samples. The enhanced densification often reported when using microwaves, which improves sample's compressive strength, appears counteracted by the brevity of the holding and cooling stages. This is confirmed by the 16.6-59.6% lower volume shrinkage of microwaved specimens and their average 6.9% lower bulk density. As a direct consequence, microwaved clays display 40% higher levels of boiling and cold water absorption. Nevertheless, microwaved and conventional samples display a similar freeze/thaw resistance on account of their almost identical saturation coefficients, which average around 0.90.

The coloration on the clays' surface allows for the visual recognition of the thermal reactions that are underway during heating until reaching the firing zone. At this point, microwaved clays present dimmer colours than conventional samples. On average on the CIE colour space, the microwaved red and yellow clays are nearly 10 points lower on their red and yellow intensity scales than conventional specimens. This is caused mainly by not having the specimens in the firing range the same amount of time as during conventional processing. Proof comes from subjecting clays to conventionally controlled cooling cycles after

microwave firing, where colour differences with conventional red and yellow samples are halved for their respective eponyms.

By itself, dimmer coloration is not a compelling reason to discard the fired products, as they can be used for other purposes than facing bricks. However, they hint at the possibility of unfinished mineral reactions. This is proved by the presence of 9.2-12.0% of unreacted muscovite and calcite in the microwaved samples, resulting in the near total absence of recrystallised minerals. This contrasts with the total elimination of unfired minerals when firing conventionally. Moreover, up to 28% of the conventional product is made of recrystallised species in the yellow sample and half of that for the red ones. Adding conventional cooling to the microwaved samples mostly solves the issue: the original species are completely eliminated, but the same degree of recrystallised minerals is not reached.

The quality analysis on microwave and conventionally fired clays proves they can be fired faster and have better mechanical properties than conventionally processed samples. However, these benefits have been obtained in the laboratory scale. Furthermore, it is unknown whether longer holding times are achievable without the substantial melting of the samples. A solution would be to optimise the heating cycle. Another would be to add conventional heating sources at the holding stage. A next step in the research would be to scale up the processing technique to fire clay specimens closer to brickworks' loads and assess possible changes to the quality of the fired products.

7.6 Scale up of the clay microwave firing process

The technical advantages found for the application of microwave energy on the firing of clays have been discovered in the laboratory scale, working with specimens more than a hundred times smaller than a common industrial brick. Understandably, it is desirable to extend these results to industrial loads. However, the same degree of quality cannot be expected to be maintained, where changing the process conditions if only to accommodate for brick sized samples will bring new processing challenges. The next step of experimental processing would be to fire bigger clay loads in the developed single mode system in order to quantify quality changes and processing challenges result of the sample volume increase. Furthermore, from the heating trials it is possible to give an insight on the necessary characteristics of an industrial microwave clay firing setting.

In this section, the single mode system developed at the beginning of the chapter is used to process 25x35 mm clays, in order to provide an insight on the material's properties upon a scale up from the 25x20 mm samples fired previously. Next, information on the process conditions obtained for the 25x20 mm and the 25x35 mm specimens is fed into a theoretical

discussion of probable layout alternatives for the microwave firing of single bricks and industrial stacks.

7.6.1 Understanding the limits of the laboratory scale microwave clay firing system

The main target in the design of the heating trials has been to minimise the extent of thermal gradients in the clay samples below <80 ^{o}C, After demonstrating the success of using a 30 min long holding stage in optimising thermal uniformity at the height of firing, it seems feasible that increasing the sample size will not incur into the appearance of significant thermal gradients that will decrease product quality. Thus, the volume of the previously treated clay specimens is increased three-fold, so that clay cylinders of 25x35 mm are used for a new set of microwave heating trials. Heating cycles analogous to those of Figure 7.12 are sought in order to allow for a fair comparison with the 25x20 mm samples.

7.6.1.1 Power absorbance and temperature profiles of 25x35 mm clays

After preliminary heating experiences similar to those of Figure 7.7, the required starting power input is confirmed to be around 300 W. The 50% power increment contrasts with the nearly three-fold mass increase, which can be explained by the modifications imposed on the firebrick crucible. Its thickness reduction in order to allow the fitting of larger samples shifts the behaviour of the system power absorption, where the system holds now 89-47% of the total absorbed power at the beginning and end of the firing. This further modifies the target of absorbed power by the clay to stabilise its surface temperature around 1050 ^{o}C, where now it averages around 43 W and 45 W for red and yellow specimens. On the other hand, increasing the sample size has not reduced power reflections, as they are still high with only between 10% and up to 50% of the input power being absorbed.

The moving average of the clay net absorbed power trends for the firing of red and yellow Danish clay cylinders of 25x35 mm, and their respective surface temperature profiles for firing cycles nearly 170 min long at 2450 MHz and using an initial power input of 300 W are presented in Figure 7.18. The x-axis is the processing time while the y-axis presents the measured and estimated clay surface and wool temperatures, and the moving average of the clay absorbed power. The holding stage is 30 min long and controlled by the material's energy needs, while the cooling is left to natural air convection. The methodology of the experiments is detailed in Section 5.4.2, whereas the estimated temperature profiles come from the application of Eqs. 7.1-7.11.

The mass increase does result to a certain extent in a linear increment of the power needs of the clay, hinting at the absence of any material transformations or other events that may alter

the energy needs of the system at larger scales. This explains the resemblance of the obtained power trends to those of Figure 7.12, albeit to varying degrees. Red clay trends are the most alike, while in yellow specimens this affinity ends around the calcite decomposition. At this point, the sample size increase brings forth lower power sensitivity and thus the possibility of a greater control of the heating process. Hence, progress through this stage gets further away from the exponential absorbed power increase that swiftly derives into melting. This is exemplified by the intensity of its heating power peak, where its 22 W is only 37.8% higher than the 15 W of the 25x20 mm specimens. It is justifiable to hypothesise that further load increases will steadily ease process control, even rendering the calcite decomposition processing issue innocuous when considering an industrial load.

Improvement of power control also enables a smoother transition into the holding stage, which replaces the previous power cut-off especially recognisable on the yellow sample. Both clays show now less frequent power regulation and at longer intervals. Importantly, the holding stage can be safely maintained around 5 more minutes than with the smaller samples without melting issues. This increase of the soaking time could be caused by the enhanced power control or by the increased mass load. In any case, this means that for larger sample sizes, longer holding times are possible.

Regarding the temperature profiles, first of all it is important to note that the developed thermal models are also suitable for the 25x35 mm specimens. Secondly, the consequences of the smoother power control are most evident on the yellow clay. The temperature surge due to the calcite decomposition is eliminated at the pinnacle of the reaction around 750 ^{o}C, which explains the shoulder at that point in the profile of Figure 7.18C. As a result of curbing the reaction before sintering, there is no overheating far beyond 1100 ^{o}C as previously. Finally, the reproducibility of these trials has markedly improved, most likely due to the load size increase. This adds into the consideration that scaling up the process will result in more reproducible and controllable heating cycles.

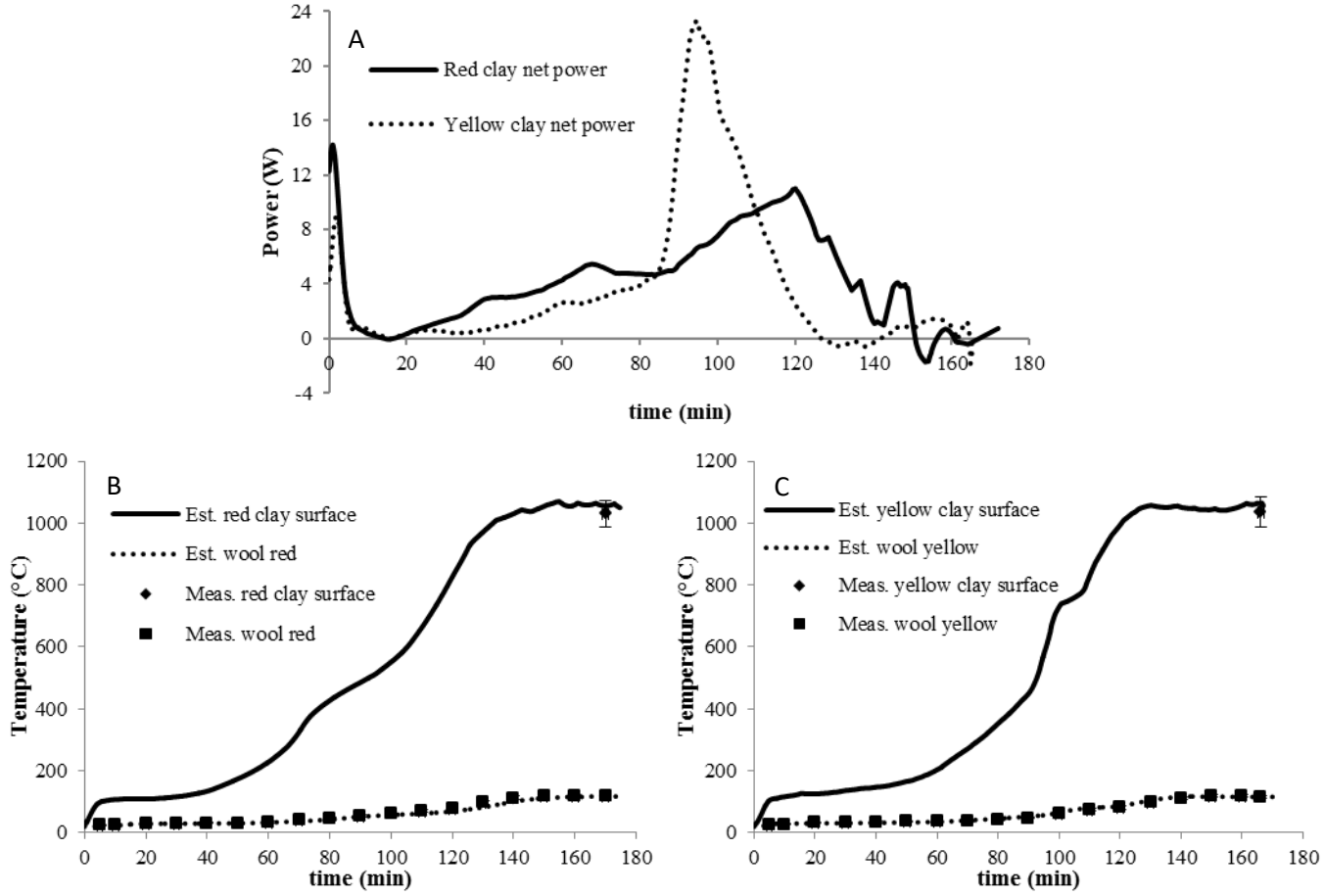


Figure 7.18- Typical net clay absorbed power moving average trends (A), and clay surface and insulating wool estimated and measured temperature profiles of red (B) and yellow (C) clays from 170 min microwave firing trials at 2450 MHz and at a variable incident power, starting at 300 W, directly controlled by the absorbed power of 25x35 mm clay cylinders at void fractions ranging 0.37±0.02 for the yellow and 0.40±0.01 for the red specimens.

7.6.1.2 Quality comparison of 25x35 mm fired clays with conventional products

Despite the size increase, the fired products are still far smaller than industrial bricks. Thus, 25x35 mm reference cylinders are conventionally treated using a brickworks heating cycle as explained in Section 5.4.2. The results of the quality analyses described in Section 5.5 are presented in Table 7.6. Probably the most remarkable result is the average 26.9% increase of the microwaved clays compressive strength from Table 7.1 values. This is mostly due to the sample size increase, since wider specimens result in a broader distribution of the load. In addition, a larger volume translates in a reduced effect of the materials heterogeneity, e.g. quartz clumps, on the overall clay toughness. The fact that both circumstances are unaltered by the processing technique explains why these effects are also visible on the conventional samples, as their toughness improves 23.6% from the smaller cylinders. Ultimately, clay's compressive strength enhancement for microwaved samples of this size averages around 15.8%, which represents a similar improvement to Table 7.1 results. The linear progression of

strength with sample's mass indicates the absence of significant thermal gradients across the clay's volume.

There is a growing divergence between red and yellow compressive strengths as the sample volume increases. Its justification lies on the brevity of the holding stage. The larger yellow samples need longer holding times to overcome pore creation and thermal gradients, which are the result of the selective heating caused by the calcite decomposition, and reach thermal uniformity. The same reasoning also explains their enhanced water absorption, particularly when considering the pore creation aspect. For both cold and boiling water, the increment averages around 52%, while the red clay presents similar absorbance values as the 25x20 mm cylinders.

Curiously, the existence of a noticeably heightened pore fraction in any of the clays is not readily visible when looking at their bulk densities. Both conventional and microwave samples have values akin to those found on the 25x20 mm clays. The surface coloration of the specimens also follows the same trend. It appears that the holding stage is sufficient to ensure thermal uniformity on the clay surface but not enough to reach the same level of densification as in Table 7.1.

Table 7.6- Compressive strength, cold and boiling water absorption, saturation coefficient, volume variation, bulk density and CIE colour space of microwaved and conventionally fired 25x35 mm red and yellow Danish clays, in a 20-1050 ºC range, with the former processed with a 30 min holding time. The conventional and microwave compressive strength data is the result of ten and three repeats. The water absorption, volume and bulk density data is the result of three repeats. The CIE colour parameters data is the result of five repeats.

		Experimental					
		Red clay			Yellow clay		
		Conventional	Microwave		Conventional	Microwave	
Compressive strength (N/mm^2)		8.01 ±0.19	9.50 ±0.23		7.81 ±0.24	9.04 ±0.22	
Absorption boiling water 5h (%)		15.0±0.2	20.8±0.1		16.7±0.3	28.2±0.2	
Absorption cold water 24h (%)		13.3±0.1	19.1±0.3		15.6±0.1	26.9±0.2	
Saturation coefficient		0.89±0.01	0.91±0.01		0.93±0.01	0.95±0.02	
Volume change (%)		2.2±0.2	1.8±0.3		2.6±0.1	2.2±0.2	
Dry density (g/cm^3)		2.10±0.02	1.93±0.04		2.05±0.03	1.89±0.06	
CIE parameters	a	33.6±0.3	21.2±0.8	29.0±0.6	0.3±0.5	7.2±0.9	4.9±0.5
	b	19.0±0.9	15.0±0.2	20.1±0.5	28.1±0.6	24.0±0.3	26.8±0.1
	L (%)	65±4.1	64±4.4	69±2.7	66±2.5	65±3.9	71±6.4

With regards to the evolution of clay mineralogy, in Table 7.7 it is displayed the composition of 25x35 mm clays at the end of a conventional and a microwave firing, measured following Section 5.3.2. Although results of the conventional processing are almost identical to those of Table 7.5, there are some minor differences in the microwave data. Namely, recrystallised minerals now appear on microwaved samples forming up to 6% of yellow clays and in these same specimens the presence of unreacted calcite has increased seven-fold. Explanation for

the latter comes from the lower yield of the thermal reactions suggested by the samples higher volume and same processing time.

Table 7.7- Quantitative XRD characterisation of the major clay constituents in red and yellow Danish clays after microwave and conventional firing 25x35 mm cylindrical samples in the 20-1050 ºC range. Each sample was measured once, so that deviations for the mineral concentrations range ±2.5% for >60 wt%, ±5% between 60-30 wt%, ±10% between 30-10 wt%, ±20% between 10-3 wt% and ±40% for <3 wt %.

Clay	Treatment	Quartz (%)	Calcite (%)	Orthoclase (%)	Albite (%)	Muscovite (%)	Hematite (%)	Pyroxenes (%)	Sanidine (%)	Wollastonite (%)
Yellow	Conv	51.3	<1	9.2	11.9	<1	4.1	15.2	3.1	5.0
	MW	65.5	1.5	8.3	9.6	5.4	2.4	2.2	<1	1.4
Red	Conv	67.0	<1	9.3	13.4	0.6	9.8	<1	<1	<1
	MW	71.8	<1	9.8	10.1	7.0	1.3	<1	<1	<1

7.6.2 Considerations on the scale up of the microwave clay firing system

The basis of the scale up of the clay microwave system is to increase the throughput of fired bricks to a level comparable with commercial conventional systems. For example, in 2009 Demark produced 222 millions of bricks by conventional means, which correspond to around 12.8 millions of bricks/brickworks (Køster, 2014). This entails a significant modification from the microwave applicator used in the heating trials. Additionally, the geometrical requirements of the industrial products, which generally are rectangular prisms with standardised dimensions, e.g. 215x102.5x65 mm, as seen in Chapter 3, must be noted. Investigations on the scale up of microwave heating processes for ceramics are not unusual (Clark et al., 2005, Dunn, 2015). However, they generally entail the consideration of hybrid systems. Due to the great deal of experience necessary for system optimisation, e.g. gas/MW ratio, final designs end up resembling a conventional system with a minor addition of microwave energy that it is not an integral part of the process but just an addition to speed it up (Clark et al., 2005).

The key parameters used in the applicator design of scaled up processes are frequency, the dielectric properties of the specimens, their nature and their handling (Bowman et al., 2007, Mehdizadeh, 2015). Nevertheless, the design focus is often found to be shifted towards the modelling of the electric field distribution and power density from the electromagnetic characterisation, which is enabled by the existence of software computer aids such as COMSOL. In order for microwaves to be truly viable as a process technology, extensive consideration of the material's nature and the processing boundaries that result is critical (Dunn, 2015). In this case where the raw feed is a fundamentally multicomponent, heterogeneous and thermally unstable minerals mixture heated through a wide temperature range, the practical considerations of the clay microwave processing are essentially the limiting factor in the scale up process design. Several alternatives are available for the scale

up process. Here, basic options of single mode and multimode applicators working at either batch or continuous operation are succinctly discussed.

7.6.2.1 Single mode pilot scale processing

Having used a single mode cavity for the clay heating trials above, it is reasonable to further push the boundaries of this system' capabilities. Given the cavity size-frequency dependence mentioned in Chapter 4, moving from 2450 MHz to the industrial frequency of 915 MHz translates in an increase of the cavity size to 0.33 m. Regarding the wavelength inside the material, the clay refractive index can be used for its calculation attending to its general formulation seen in Eq. 7.12 (Adams, 1981). The combination of Eq. 7.12 with Eq. 4.1 provides the relation between the wavelengths inside and outside the material, as displayed in Eq. 7.13. Given that the refractive index of the major clay constituents averages around 1.5 (Weidler and Friedrich, 2007), the wavelength inside the material circles around 0.22 m. This length is clearly enough to fit one full brick,

$$\tilde{n} = \frac{c}{\xi} \qquad \textbf{7.12}$$

$$\tilde{n} = \frac{\lambda_a}{\lambda_c} \qquad \textbf{7.13}$$

where $\tilde{n}$ is the refractive index between air and clay, c (m/s) is the speed of light in vacuum (2.998×10^8 m/s), ξ (m/s) is the phase velocity of light in clay, λ_a (m) is the wavelength of the microwaves in air and λ_c (m) is the wavelength of the microwaves inside the clay.

Given the similarities of clay dielectric properties at both frequencies, as studied in Chapter 6, it is plausible that the processing of full bricks analogous to the heating trials described will be possible if the selected applicator is still a rectangular TE_{10} waveguide. The main challenge during heating is the thermal uniformity of the sample, where some advantages are found to a frequency reduction. The penetration depth is greater at 915 MHz, reaching minimums around 0.24 m and 0.48 m at 950 ^{o}C for red and yellow Danish clays, respectively. The increased heating at the brick edges caused by the electric field concentration can be neutralised to a certain extent with a broad system matching, abundant insulation that prioritises conduction across the brick instead of normal towards the surroundings, and a slow heating rate. Particularly, a tighter control of the last ought to be possible due to the load increase. Nevertheless, these edges will still be more prone to melting than the rest of the brick.

On the other hand, serious disadvantages are found to the industrial application of this particular technique, the first being its small throughput, namely 1 brick/170 min if the processing conditions of Figure 7.18 are maintained. The use of applicators in parallel to reach semi-continuous production would approach the throughput mentioned at the beginning

of this section without a massive plant layout. Its alternative use as a portable brick manufacturer for areas with no gas supply is also impractical given that progressing from the trials above, a 3 kg brick needs an energy supply topping at 30 kW for its full firing. Of course, this is caused due to power reflections and the broad matching. A redesign of the applicator ought to be able to reduce them without endangering the thermal uniformity of the sample during heating. However, the yield of the processing method is still leagues below industrial requirements.

In order to compensate for the lower frequency and reach the same power density, a higher electric field intensity will be required as per Eq. 4.2. This in turn increases the possibility of arcing, especially when considering powder to powder particulate contact and brick edges (Meredith, 1998, Clark et al., 2005). Finally, although processing at 2450 MHz is universally allowed, there may be an issue of electromagnetic compatibility (EMC) working at 915 MHz (Catalá-Civera et al., 2006), as due to its closeness to frequencies used for communications systems it is usually subject to special legislation in the UK and elsewhere. Thus, attention to microwave leakage is critical (OFCOM, 2017).

7.6.2.2 Multimode industrial scale processing

In modifying the manufacturing process to fulfil industrial yields, inspiration from the state of the art conventional methodology can serve as a base onto which add microwave energy. Tunnel and Hoffman kilns, accounting for the conventional batch and continuous production seen in Chapter 3, have been subject to retrofitting studies in order to add microwaves to the gas firing process (Clark et al., 2005, Dunn, 2015, Køster, 2017). In both cases, a straightforward advantage over single mode operation is displayed in the detachment of the processing frequency from the cavity size, allowing for the firing of larger clay loads per cycle. Moreover, temperature sensing is more accessible than in laboratory scale, as procedures used in brickworks can be replicated, e.g. thermocouples at different points in the load (Moesgaard, 2015), while taking into account the possibility of microwave interferences. However, no working pure microwave clay firing design has been yet published, probably due to the microwave/material processing challenges encountered during the trials above.

7.6.2.2.1 Batch processing

The advantages of designing an applicator for batch processing have been detailed in Chapter 4 and in this case are focused around its flexibility. The potential of a batch system has been recognised by others such as the Danish Technological Institute (DTI), who has recently designed a working pilot multimode batch applicator specifically for clay firing using both microwaves and conventional gas firing (Køster, 2017). The arrangement of several of

these applicators in an annular configuration similarly to Hoffman kilns leads to semi-continuous processing that can reach industrial throughputs. In this case, it is straightforward that the conventional heating source at the centre is substituted by at least one microwave generator, whose feed rotates along various loaded multimode cavities. At the same time, the hot exhaust gases can be also transferred to the following applicator to help in conventionally preheating the load. Thus, free water elimination progresses more uniformly. Moreover, it may help to bypass the area of low microwave/material coupling ranging 150-350 ^{o}C. Nevertheless, this may lead to the accumulation of CO_2 and form a reductive atmosphere.

As with the single mode considerations, the main issue is the heating uniformity of the load, which in this case is comprised of hundreds of bricks. Added to the field concentration in bricks' edges, intense local heating may take place between bricks in near contact in a manner reminiscent of interfacial polarisation (Metaxas and Meredith, 1983, Clark et al., 2005), which could easily degenerate into melting or an arc. Moreover, considering a workload of tons of bricks, their thickness is larger than that of the microwave penetration depths. The subsequent inherent exponential heating non-uniformity of the system can be minimised by adding multiple feed points to the cavity, a sensible matching and purposely arranging the bricks in different fashions that homogenise the electric field across the load. Yet, this might not solve the problem completely. It is worth mentioning that thanks to the (to an extent) stability of the clay dielectric properties with temperature and the length of the firing, the continuous tuning of the system for an optimal energy delivery is attainable.

Following from a working design of a single batch applicator for the high temperature heating of ceramics using microwaves (Kimrey Jr, 1990), a solution to avoid non-uniform heating is to drastically increase the cavity size with respect to the feed's wavelength and to add mode stirrers. Additionally, a turntable can be used to further homogenise the field. The other critical parameter to consider is the microwave absorbance of this support. If pure microwave heating is desired, it needs to be transparent. An example material could be cordierite, which is also used in brickworks (Køster, 2017). On the other hand, if the heating deceleration around 150-350 ^{o}C is deemed unacceptable the base can be a susceptor such as the commonly used SiC, although that will only heat the bottom bricks.

Finally, the applicator layout not only affects the capital costs and the thermal uniformity of the load, but the heating losses and the amount of insulation needed. Interior insulation is not advisable, due to its likelihood of catching fire if touching the bricks. Insulation surrounding the outside of the cavity can be used instead, where the exact quantities to be used depend on economic considerations, e.g. importance of decreasing energy expenditure as heating losses

and helping in the elimination of thermal gradients in the load versus the cost of the insulation.

7.6.2.2.2 Continuous processing

Continuous conventional brick manufacturing methods bring additional advantages of higher yields and decreased energy and equipment costs over batch processing (Køster, 2014). The idea of using tunnel kilns described in Chapter 3 to perform microwave firings is not new as they are regarded as the most feasible model to be retrofitted (Dunn, 2015, Clark et al., 2005). Nevertheless, microwaves are generally considered as a side addition to the gas firing as seen in Clark et al. (2005), where in a conventional tunnel microwave feeds are added in the firing area. Conceptually, the system can be easily brought up to be purely microwave powered by eliminating the gas burners, although it may be prove more effective to completely redesign the system. Furthermore, it is not impossible to fathom the microwave cooling of the brick stacks after firing, controlling the power input through the temperature of the load. Yet, conventional cooling through air currents is probably more appealing due to energy optimisation considerations. The same may occur to the pre-heating stage, where if this area is prolonged until the loads are beyond 350 ^{o}C the clay low loss range will have been bypassed altogether.

Compared to batch operation, temperature control is simplified as each subdivision of the firing area has a steady target temperature. These can be maintained by IR or shielded thermocouple sensor loops to the microwave sources, which can be even pulsed power driven for a tight soaking control (Korovin et al., 2004, Clark et al., 2005). The same power matching and insulation considerations as with batch systems remain, with the addition of two major non-isolated openings for the materials loading and unloading.

Although electric field non-uniformities and the need for a specific brick arrangement persist, issues about the thermal imbalance across the load are diminished as workloads on a travelling conveyor inherently eliminate the effect of longitudinal non-uniform heating. However, this entails two additional issues, which are the microwave leakage from both ends of the tunnel and the movement of the load. In the case of the former, despite the reduced possibility of interference with communication devices by working at 2450 MHz, a maximum leakage of 5 mW/cm^2 over an exposure time of 30 s measured at a distance of 5 cm from the equipment must be ensured (BSI, 2011b). This is achieved through the thorough design of chokes at both ends of the tunnel and at any of the openings for temperature sensors.

Regarding the load transportation, rollers or a continuous polymeric conveyor won’t do because they will heat and even melt during processing. A solution would be to use a thick

conductive conveyor such as in Shute et al. (1995). An absorbing or transparent support is needed as in the case for the batch system. Its justification here is for the handling of the brick stack. However, the combined weight of the brick stack and its support denies the utilisation of commonly used rolling or vibrating conveyors. A fix might be to have the brick load on a support that moves on rails etched on the metallic bottom, where the load is pushed through the tunnel by another load behind and so forth. Another solution would be a layout middle point between the Hoffman and tunnel kiln, which is that of a rotating ceramic-based disc applicator as seen in Beneroso et al. (2017). The load is moved on an infinite circular ring while the microwave energy is focused on a narrow section, allowing the existence of preheating and cooling stages.

7.6.3 Conclusions on the scale up of the clay microwave firing process

Significant modifications from the laboratory scale microwave rig designed for clay firing are required to develop a system that can work with industrial throughputs while addressing the particular nature of clays. Challenges such as penetration depth issues and uneven heating due to the brick shaped load may counteract the technical advantages found for microwave processing if unaddressed. Prior to reaching industrial scale, the single mode system can provide results for larger loads than the 20x25 mm cylinders studied here, namely experimentally firing 20x35 mm clays using the same heating cycles.

The use of the same single mode rig is justified by the large degree of thermal uniformity observed in the previous clay microwave firing trials. The increment of the load size results to a certain extent in a linear increase of the power needs, where the power trends remain almost unchanged from 20x25 mm data. Furthermore, a tighter power control is enabled, as the power absorption peak for the calcite decomposition has increased only 37.8%. Moreover, soaking stages longer than 30 min have been unlocked and the reproducibility of the trials has improved upon the sample increase. Minor alterations are reported to the quality of the fired products. The compressive strength enhancement from using microwave energy now averages around 15.8%, while the bigger samples need a longer holding stage to reach thermal equilibrium. This is observed in the enhanced water absorption of microwaved yellow samples, averaging around 52%, and their seven-fold increment of unreacted calcite.

Pushing the limits of the single mode system makes possible the firing a full brick. This requires going down to 915 MHz, where the associated penetration depth increase prevents power attenuation issues across the brick, i.e. minimum 0.24 m and 0.48 m at 950 ^{o}C for red and yellow vs a common brick thickness of 0.07 m. Elimination of thermal gradients comes from balancing electric field concentration in field edges with the use of abundant insulation,

slow heating rate and a broad system matching. However, working at 915 MHz there is a higher possibility of arcing and electromagnetic compatibility issues.

Multimode batch and continuous systems are the only viable option for reaching industrial throughputs. In the first case, several cavities can be arranged to form an annular kiln, where the microwave feed moves across the applicators sequentially firing each batch. The presence of hot gases can be advantageous to pre-heat the clays over their low loss area, i.e. 150-350 MHz. Besides penetration depth issues and electric field concentration in edges, intense heating may occur between bricks in near contact. The resultant thermal gradients are minimised by adding mode stirrers, turntables, microwave feeds and arranging the bricks so as to eliminate penetration depth issues.

The retrofitting of a continuous tunnel kiln is the most feasible option for an industrial microwave clay firing system, as temperature and power control are simplified. Moreover, longitudinal non-uniform heating effects are eliminated for workloads on a travelling conveyor. In addition to microwave leakage at the tunnel extremes and the need for the arrangement of the brick load, an important challenge of the process is the load handling. The two easiest solutions are to move the load on a transparent support sliding over the metallic wall of the applicator, or use a metallic or ceramic disc that turns the applicator in a mixture between tunnel and Hoffman kilns, while still allowing for preheating and cooling stages.

In spite of the numerous paths that can be followed for the scale up of the microwave clay firing process and the discovered technical advantages of microwave processing, it is unknown whether conventional heating is still superior to microwaves in the industrial scale for other reasons, e.g. more cost effective. Thus, a quantitative comparison of the two processing techniques at industrial scale is imperative at this point.

7.7 Techno-economical assessment of the processing technique

Previously in this chapter, the technical advantages of microwaves in the manufacturing of fired clay products have been established and alternatives for the process scale up have been proposed. However, it is unknown if the holding times can successfully be extended to fire whole bricks and if it can be scaled up. Moreover, it is necessary to address whether the microwave process will result in a justifiable advancement over conventional methods at industry level regarding aspects other than the quality of the fired products, i.e. economic, environmental and legislative. Obviously, there are massive limitations to an assessment of an industrial scale microwave clay firing kiln when starting from the laboratory results presented above. Therefore, there is a large degree of uncertainty for the considerations and choices made in this section. Nevertheless, a preliminary investigation of the potential of microwaves

to substitute conventional clay firing methods in brickworks provides a valuable insight of any possible appeal it may possess, besides higher quality products, to drive the scale up of the technique.

In this section, a brief assessment of the potential economic, environmental and legislative advantages provided by the microwave firing of clays over conventional systems is presented.

7.7.1 Layout of the conventional and microwave clay firing systems

In order to ensure a feasible comparison with the conventional processing technique, the simplest hypothetical layout approach akin to those of Dunn (2015) and Clark et al. (2005) is proposed. Namely, a common tunnel kiln is retrofitted by replacing its natural gas burners in the firing zone (Vissing, 2004) with microwave feeds. It is necessary to highlight again that the consideration of a hypothetical kiln will result in a large degree of uncertainties for the results of the following analyses. Considerations on a hybrid configuration have not been assessed given that although it will provide a middle point between the conventional and microwave results, a great deal of experience is necessary to establish the optimal conventional to microwave energy supply ratio in the system. Throughput and dimensions of this kiln and its products under conventional processing can follow that of typical Danish brickworks, as shown in Table 7.8. Using the parameters found in this table and the typical bulk density of bricks mentioned before, i.e. 2.3 g/cm^3 (Karaman et al., 2006), it is trivial to calculate that a production of 1461 bricks/h requires around 11.6 GJ fuel/h.

Table 7.8- Dimensions, throughput, heating cycle and brick characterisation of a conventional industrial kiln (Køster, 2014, IBSTOCK, 2015, Moesgaard, 2015, Vissing, 2004).

Conventional kiln system parameters					
Length kiln (m)	**Nº burners**	**Throughput (bricks/year)**	**Fired brick dimensions (mm)**	**Energy supply (MJ natural gas/kg of fired brick)**	**Heating cycle length (h)**
100	70	12.8 x 10^6	228x108x54	2.6	47.6

Regarding the possible microwave system, further changes to the tunnel kiln are needed beyond the addition of microwave feeds, e.g. choking and extra insulation. Conversely, microwave applicators often require less than one-quarter of the volume of a conventional system when performing the same heat treatment (Dunn, 2015). However, this level of optimisation is best to be covered in detail through an electromagnetic design. For the sake of simplicity, the burners/microwave feeds replacement is the only significant alteration to the kiln considered here.

A crucial modification to the microwave firing rig comes from penetration depth issues, which have been discussed in the previous section. As a result, spacing between bricks is

needed to ensure electric field uniformity across the load. Without further assurances from electromagnetic design, which would be crucial in any real scale up attempt, it can be initially established a brick distribution so that a stack contains ≈60% of the bricks of a conventional one. This specific percentage has been chosen so that the brick throughput of both methodologies is later revealed to be the same, so as to aid in the comparative analysis. The size of a brick stack in a kiln cart varies depending on the kiln size and the desired number of bricks per load (GOBRICK, 2006). Knowledge of the geometry of the kiln allows for the calculation of the brick stack in the conventional system through the intuitive development of Eq. 7.14. The kiln cart data has been extracted by linearly increasing the dimensions of those found in Nicolau and Dadam (2009) in order to fit the conventional brick output. Thus, a stack contains 1398 bricks during conventional processing against 829 bricks in the microwave system.

$$Nº\ Bricks/_{Stack} = \frac{\frac{Bricks}{hour}\ Heating\ cylce\ length}{\frac{Length\ kiln}{Length\ kiln\ cart}} \quad \textbf{7.14}$$

Despite the lower feed of the microwave rig, the heating trials above foreshadow significantly faster firings. First, the heating rate is assumed to follow that of the 25x35 mm samples, i.e. ≈441 ºC/h. Second, the holding time is narrowed down to 1 h while still ensuring thermal uniformity. This comes from doubling the soaking times from the laboratory scale trials, as the 25x20 mm cylinder's thickness is nearly half of that of a standard brick. On the other hand the cooling is unchanged, as it has been previously justified. This translates in microwave firings 28.3 h long. Consequently, the microwave system throughput calculated using Eq. 7.14 is the same as that of the conventional kiln.

With respect to the energy needs of the microwave firing, it appears misguided to extrapolate the consumption from the single mode trials to a multimode tunnel kiln, whose energy demands are supposedly thoroughly optimised. This is justified in the preliminary nature of the laboratory trials, as they show a large degree of reflections peaking at 90% of the input power at times. Alternatively, an estimation of the energy costs is brought forward from the DSC results of Chapter 6. Since microwave power is only applied in the firing zone to preheated bricks at around 100 ºC, subtracting the nearly 48 J/g needed to reach this temperature leaves a cost of around 3.3 GJ/h to heat the clays to ≈1050 ºC.

A similar problematic is found for the extrapolation of the heating losses from the clay cylinders runs; instead data from conventional kilns is used. Heating losses in these kilns range 36.5-46.9% of the total energy consumption due to conduction and exhaust gases convection (Maithel, 2003). The higher value is chosen for the microwave system so as to also cover for any inefficiency in the microwave energy delivery due to power reflections and

system absorbance, which here can assumed to be minimal given the size contrast of the continuous load with the tunnel kiln and the optimal microwave/material matching. The combination of firing the bricks while staving off heating losses averages around 6.1 GJ electricity/h of.

7.7.2 Economic assessment

A summary of the operational and capital costs of the conventional and microwave systems is shown in Table 7.9. The latter costs are related to buying the required equipment, i.e. number of gas burners and microwave generators, while operational costs refer to the energy supply. Regarding the microwave system, its energy needs can be satisfied with different combinations of high powered generators, where more than one optimal arrangement may exist. In this study, a combination of 314 common commercial 6 kW magnetron microwave generators working at 2450 MHz is used, assuming the magnetrons work at a 90% energy conversion efficiency (Council, 1994). These systems can have an individual cost of £ 14,983 (Sairem, 2018b). T300 High-velocity premix gas burners are employed in the conventional kiln, where a single burner may cost £ 2,950 (Duomo, 2018). These are five times cheaper than the microwave generators. This is understandable, as the price of microwave equipment tends to be larger than that of conventional heating systems (Clark and Sutton, 1996, Metaxas and Meredith, 1983).

Among the operational costs, the almost two-fold energy supply reduction from conventional processing is counteracted with the higher tariffs of electricity over natural gas. This is clear when comparing the average £ 20.22 /GJ for electricity in IEA countries in 2016 (GOV.UK, 2016a) with the nearly four times lower natural gas costs circling around £ 6.25 /GJ in the European Union in that same year (Eurostat, 2017a). Regarding benefits, fired bricks can be sold at around £ 0.02 /kg (DHRI, 2018).

Table 7.9- Summary of capital and operational costs of running a conventional and microwave firing of clay bricks at industrial scale based on the assumptions of Table 7.8.

	Conventional processing	**Microwave processing**
Capital cost (£)	70 Gas burners £ 2950 /burner £ $2.1\ 10^5$	314 Microwave generators £ 14983 /generator £ $4.7\ 10^6$
Operational costs(£)	Natural gas fuel £ 6.25 /GJ £ 72.62 /h	Electricity £ 20.22 /GJ £ 123.20 /h
Benefits (£)	Fired bricks sales £ 0.02 /kg £ 94.74 /h	

The assessment of the economic potential of microwave firing comes from a discounted cash flow analysis using the net present value approach (NPV) as explained in Section 5.6.1. An

internal rate of return of 15.2% has been chosen so as to ensure that NPV=£ 0 for the conventional kiln when using Eq. 5.15. This means that the investment has been fully returned upon the end of the project without further benefits. On contrast, the microwave process displays a NPV= £ -3.1 10^5. The economic losses derived from using this technique are easily explained from the contrast between the capital and operational costs of both kiln types in Table 7.9.

A clearer insight into these divergent NPVs is obtained from Figure 7.19, which presents the evolution of the net cash flows for both the microwave and conventional systems across the plant's service life. The x-axis is the years of operation since the plant start up and the y-axis is the net cash flow. It is straightforward that the conventional system pays out the capital costs in year two and starts profiting around £ 1.9 10^5 yearly. On the other hand, mainly due to the fact that electricity costs overcome the benefits of the brick sales, the microwave arrangement continuously loses £ 2.5 10^5 /year. Consequently, at an industrial scale the microwave processing of clays is not as appealing as the conventional methods from an economic point of view.

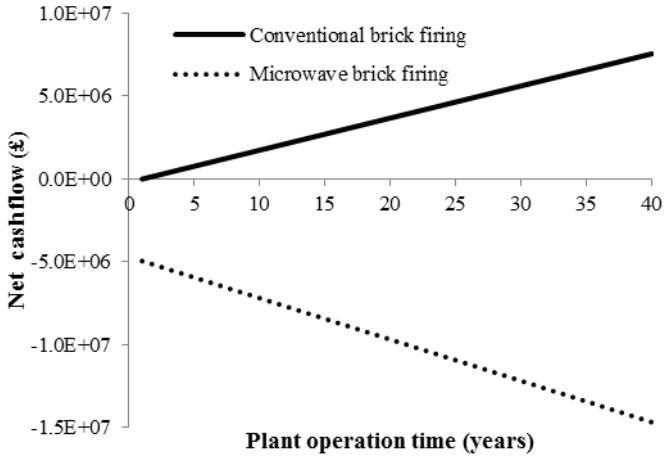


Figure 7.19- Yearly net cash flows across the service life of a common industrial scale tunnel kiln while performing clay firings using conventional gas firing or microwave energy as operational modes.

Obviously, the NPV results and the values from Figure 7.19 will undergo drastic modifications when considering a more in depth economic analysis, where more diverse operational costs, e.g. staff wages, cost optimisation alternatives and the price for the energy supply in specific countries are taken into account.

Natural gas and electricity costs may vary greatly across countries, which may have a determinant influence in the microwave/conventional firing selection. The minimum and maximum energy supply cost across IEA countries is presented in Table 7.10. The order of magnitude of difference between the min/max costs of electricity and natural gas allows the recognition of potential for microwave firing from countries like Norway, whose £ 42.60 /h

electricity cost is nearly three times lower than the IEA average seen above and also 3.5 and 1.7 times cheaper than Switzerland's and the average EU natural gas prices.

Table 7.10- Summary of capital and operational costs of running a conventional and microwave firing of clay bricks at industrial scale for different countries with contrasting energy supply prices (GOV.UK, 2016a, GOV.UK, 2016b).

Energy costs	Conventional processing	Microwave processing
Maximum	Switzerland £ 147.7 /h	Italy £ 183.56 /h
Minimum	USA £ 27.71 /h	Norway £ 42.60 /h

Applying the cash flow analysis seen above to the brick firing process in these countries provides a series of NPV trends in Figure 7.20, which informs of the sensitivity of the process to resources costs. The x-axis is the cost of the energy supply, either gas or electricity, and the y-axis is the net present value. Not even when comparing Norway's and Switzerland's energy supply does the microwave process become as valuable as a conventional one. Furthermore, this gap will unlikely be narrowed by a sudden change of the prices of gas and electricity, given that their price has steadily increased around 37.3% and 59.8% respectively in the last 10 years (GOV.UK, 2016a, GOV.UK, 2016b). The contrast between both alternatives is justified by the 183% higher capital costs of the microwave option. As it has been mentioned above, there may be available better arrangements for the microwave source. Particularly in the best microwave case so far, i.e. Norway, a reduction by 74.4% of the microwave capital costs of Table 7.9 is necessary to match the NPV of Switzerland's conventional kiln. The other possibility of increasing the gas burners cost is unlikely given their use is standardised and has been optimised for tunnel kiln operation since the last quarter of the twentieth century (Køster, 2014).

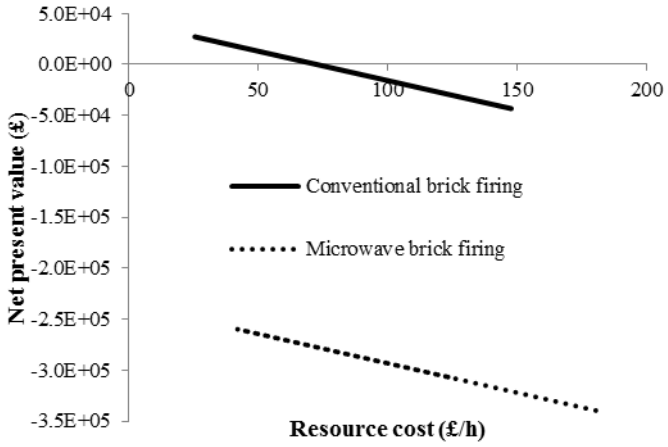


Figure 7.20- Evolution of Net Present Value of a common industrial scale tunnel kiln for the firing of clay bricks using either microwave energy or gas firing for different energy supply prices found in countries worldwide, i.e. Switzerland, Italy, USA, Norway, and the IEA average.

Another alternative is to process the clay bricks at a lower frequency, where higher power generators are more frequent. An example is the possibility of using commercial 100 kW microwave generators while working at 915 MHz (Sairem, 2018a). Following the common assumption of £ 1000/kW at 915 MHz and knowing that 915 MHz magnetrons have efficiencies around 84% (Fermilab, 2018), 21 generators would be able to provide 6.35 GJ/h for a total cost of £ 2.1 10^6. This means that moving to 915 MHz almost halves capital costs compared to the 2450 MHz alternative. Nevertheless, the microwave process is still less economically appealing than the conventional method with NPV= £ -1.5 10^5. Finally, it needs to be mentioned the potential of price premiums for the sustainable production of bricks, which may bridge the gap between the conventional and microwave paths. However, this premium will suffer large variations from country to country.

7.7.3 Environmental assessment

As mentioned in Chapter 3, the energy supply in brickworks is provided by the direct combustion of fossil fuels. The chosen fuel may vary depending on the energy mix of a particular country, e.g. a 32.2%-37.8%-24.2% coal-oil-gas utilisation in Australia (GOV.AU, 2016) versus the 13.5%-4.4%-41.4% of UK (GOV.UK, 2017). Although some brickworks still employ coal or fuel oil as the conventional energy supply, generally natural gas is the most employed (ILO, 1984, Køster, 2014, Martínez-González and Jiménez-Islas, 2014). On the other hand, electricity is required for the microwave process. This electricity can be generated by solar, wind and hydropower energy among others (Bridgwater, 2003, Sengupta et al., 2007, Johansson and Burnham, 1993, Markham, 2015), where their associated carbon footprints from the CCalC2 software are displayed in Table 7.11. The CCalC2 methodology is explained in Section 5.6.2. The natural gas's carbon footprint is one order of magnitude higher than any of the electricity alternatives addressed here. This portrays a significant potential advantage of microwave processing in countries where the energy mix is dominated by renewable energy sources. Other alternatives such as biofuels and coal are also used to produce electricity in thermal power plants. Nevertheless, it is worth noting that the efficiency of their energy supply would be higher if they are directly burned onto the bricks in the kiln.

Table 7.11- Carbon footprint of natural gas and some renewable energy sources from CCalC2 software.

Energy source	Carbon footprint (kg CO_2eq/GJ)	CCalC2 database
Natural gas	62	CCalC
Electricity wind	1.83	CCalC
Electricity solar	5.66	Ecoinvent
Electricity hydropower	6.78	CCalC

Feeding the energy requirements of the microwave and conventional processes calculated in the layout section, and the carbon footprints of Table 7.11 to the CCalC2 software as described in Section 5.6.2 enables the comparison of the environmental impact of both clay firing methodologies. The resultant environmental impact bars can be seen in Figure 7.21. The x-axis displays the energy supply alternatives while their carbon footprint on both clay types is seen in the y-axis. The carbon footprint of the conventional system clearly stands out, peaking at 1212 kg CO_2eq/h and 720 kg CO_2eq/h for the yellow and red specimens. On the contrary, the electricity alternatives considered reach a maximum of 533 kg CO_2eq/h for the hydropower on yellow clays while only being 41 kg CO_2eq/h for the red ones.

The observed disparity between clay types can be attributed to their calcite content. It has been seen in Figure 6.1 that calcite decomposition causes an average 11% mass loss on the yellow Danish clays. This mass loss is CO_2 released to the surroundings, i.e. 492 kg CO_2eq/h for the above throughput, and cannot be minimised by changing the kiln configuration. Consequently, red clays carbon footprint generation ranges 1.6-5.7% of that of the conventional kiln. This comes from removing the carbon footprint of natural gas plus a twofold reduction of the energy needs from the conventional kiln. On the other hand, the CO_2 generation of the yellow specimens only reduces the carbon emissions by slightly more than half during firing upon the transition to a microwave kiln. In conclusion, there will be a significant reduction of the carbon footprint during clay firing when using a microwave system instead of a conventional kiln regardless of the raw material.

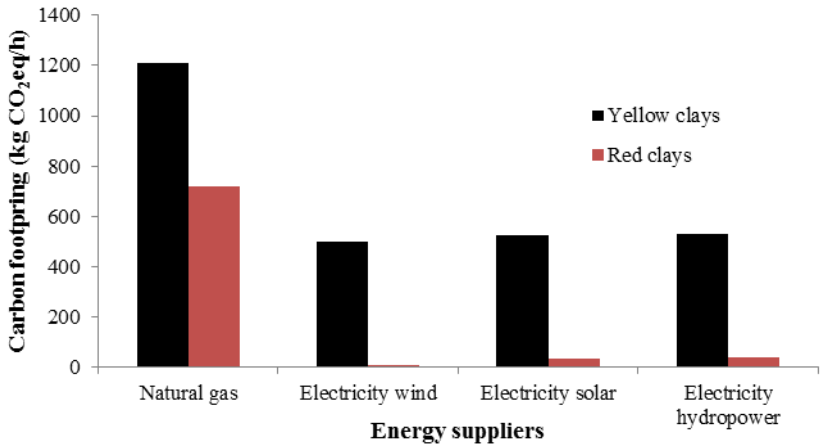


Figure 7.21- Carbon footprint generated by the firing of clays in a common industrial scale tunnel kiln where gas firing or electricity powered by different renewable energy sources are used as the energy supply.

7.7.4 Legislative assessment

On the analyses above, there have been identified two key points that broadly differentiate the firing of clay bricks through conventional gas burning or microwave energy. The first is the substitution of fossil fuels by electricity, where the latter can be powered by sustainable

resources such as wind and solar. The second is the reduction of the carbon footprint of the firing by at least half of that of the conventional kiln when using microwaves. Coincidentally, the sustainability of the energy supply of energy intensive processes in industries and the minimisation of the effects of industrial activity on the environment have been in recent years two major topics of discussion among the population worldwide (Howes, 2010, Noorman and Uiterkamp, 2014, Bilgen and Sarıkaya, 2016). Naturally, governments and supranational agencies have developed a significant amount of statutes and regulations to address these issues.

Regarding the choice of energy supply, natural gas worldwide popularity in brickworks and other industries comes mainly from being cheap, plentiful and versatile when compared with other fossil fuels (Weissman, 2016). However, one of the main drawbacks of natural gas and fossil fuels in general is their finite nature, as they are non-renewable resources (Hartwick, 2013). Together with a consistent rise of natural gas demand of 1.6%/year worldwide from 3.6 10^{12} m^3 in 2016 (IEA, 2017a), natural gas has turned into a resource of crucial geopolitical interest whose price greatly depends on the political stability of the producing countries (Colombo et al., 2016, Bilgin, 2009, Victor et al., 2006).

International agencies and supranational departments, such as the International Energy agency, United Nations, Renewable Energy Policy Network and European Commission, have long been advising towards transitioning into more sustainable energy systems by phasing out fossil fuels through the elimination of their subsidies, investing into sustainable resources such as wind and solar energy and creating task forces for encouraging and promoting renewable energies (Gerasimchuk, 2015, Sawin et al., 2013, Martinot, 2005, Singer et al., 2017, Clini, 2001, Goldemberg, 2006, ENER, 2010, Colombo et al., 2016). As a result, renewable energy sources accounted for almost two-thirds of net new power capacity around the world with almost 165 GW in 2016 (IEA, 2017b), while several countries, such as Brazil, Venezuela, Sudan, Iran, India, Egypt and Saudi Arabia, agreed in 2016 to stop fossil fuels subsidies (Sawin et al., 2013). In the context of this project, it is clear that the substitution of natural gas by electricity in the firing of clays opens new possibilities for the application of sustainable energy sources in the building sector, which follows the worldwide trend of reducing or completely eliminating fossil fuels consumption in industries.

Legislation to address the carbon footprint resulting from industrial activities has been increasingly stringent due to their influence on global warming, also termed climate change (Change, 2015, Seinfeld and Pandis, 2016, Oreskes, 2018). These regulations refer to reducing carbon generation or minimising its release to the ambient, e.g. soil, water, atmosphere. Minimising its release can be understood as part of a system optimisation and is

irrelevant in the context of this comparative assessment. Part of natural gas' popularity over other fossil fuels comes from its around 57 kg CO_2eq/GJ emissions, which nearly halves coal emissions and makes natural gas the cleanest fossil fuel (Køster, 2014). In the clay industry, it has mostly substituted coal as the main energy source since the last half of the 20th century, although the latter continues being used to a minor extent in brickworks (Køster, 2014, Manley, 2016).

Consequently, natural gas has been understood as a "bridge fuel" for achieving a sensible reduction of carbon emissions in between a broader transition between fossil fuels and green energy sources, e.g. solar and wind (Weissman, 2016). A further reduction of industries' carbon footprint, as proposed by international agencies such as the G8/G7, consists on completing the transition towards less carbon-intensive energy sources, i.e. green energies, and stopping the utilisation of fossil fuels (METI, 2016, METI, 2017, Obama, 2017). This solution is the same as the one suggested previously for dealing with the non-renewable nature of fossil fuels, so the organisations named above and their policies and previous works often also discuss carbon footprint and environmental impact alternatives. Added to that, individual countries have taken extra steps to significantly reduce their utilisation of fossil fuels in their industries in order to achieve carbon footprint reductions larger than 50% in a short time frame, such as the United Kingdom (GOV.UK, 2008), Italy (IEA, 2016) and Sweden (Centeno, 2016), or to develop processes completely free of fossil fuels like Denmark (EFKM, 2011), Iceland (INREAP, 2014) and Costa Rica (MINAET, 2011). It is straightforward that the significant reduction of carbon footprint in clay firing upon transitioning to microwave processing, if realised, poses a great advantage towards the development of green processes. Together with the elimination of fossil fuels consumption, the microwave alternative appears to be prepared to meet the demands from both international agencies and national governments in the near future.

7.7.5 Conclusions of the techno-economical assessment

Two methodologies for the firing of clays at an industrial scale have been assessed, i.e. conventional and microwave processing. A common tunnel kiln is the applicator retrofitted to use microwave energy, where the main differences between both methodologies are located in the firing stage. Massive uncertainties have to be taken into account in the model due to the technical uncertainty of how a microwave process would be configured in the industrial scale. In conventional processing, the required 11.6 GJ fuel/h needed for a throughput of 1461 bricks/h is supplied by the direct burning of natural gas in 70 T300 High-velocity premix burners. The same brick production has been achieved by the microwave system upon

substituting the burners with 314 6 kW magnetron microwave generators working at 2450 MHz, where electricity covers an energy demand of 6.1 GJ/h.

Despite the lower energy consumption of the microwave treatment, the price of electricity averaging at £ 20.22 /GJ is more than three times more expensive than natural gas. Moreover, the capital cost of the microwave generators is more than 20 times that of the gas burners. A NPV study on both alternatives reveals that upon repayment of the initial investment for the conventional kiln, through brick sales of £ 94.74 /h, the microwave system has £ $3.1\ 10^5$ of losses. Clearly, conventional clay firing remains the most profitable business model.

The lower energy consumption of the microwave system, plus using electricity as the energy supply instead of natural gas, drops its carbon footprint down to 1.6-5.7% of that of the conventional kiln for red clays, i.e. 720 kg CO_2eq/h. In yellow clays, the calcite decomposition causes an additional 492 kg CO_2eq/h, which increases the microwave carbon footprint to half of the conventional process. Certainly, the microwave system has a lower environmental impact.

The main differences between the microwave and conventional process at an energy policy level are focused on the use of a sustainable form of energy, namely green energies powering electricity, and the drastic reduction of the carbon footprint of the firing. These characteristics strongly align with the worldwide trend across national governments and international agencies of transitioning towards green energy sources that cause a minimal impact to the environment.

Through the previous techno-economic analysis, it can be concluded that the industrial firing of clays using a microwave system is still inferior to conventional kilns in the economic sense. Despite taking into consideration the uncertainty of the model, the results clearly show that no matter how the kiln is configured, capital and operating costs are likely to be significantly higher for the microwave option. However, if microwave technology could be successfully implemented, it poses a great advance over environmental impact concerns and policies pushing for a less polluting industrial activity, due to its drastic reduction of carbon footprint from the elimination of natural gas. Moreover, its substitution with electricity powered by renewable resources falls in line with the enacted energy policies legislated in European countries and generally promoted worldwide.

7.8 Conclusions

The behaviour under microwave radiation of common red and yellow Danish clays used for building applications has been studied in a single mode applicator on 25x20 mm clay

cylinders at constant power inputs in the 100-300 W range. The investigation assessed power evolution, temperature profiles, energy needs and thermal uniformity. Single mode microwave firing trials at variable incident powers starting at 200 W were later performed using cycles reminiscent of those used in brickworks. The quality of the resultant fired products was compared with a conventionally manufactured in built reference due to the size and shape divergence between the 25x20 mm samples and standard bricks, and was based on parameters such as compressive strength, water absorption, saturation coefficient, colour, texture, mineralogical evolution, shape, size and density. An insight on the scale up of the technique was provided experimentally by firing specimens thrice the volume of the original samples and commenting on possible batch and continuous single and multimode systems. Finally, a techno-economic analysis of the microwave and conventional processing technique assessed whether the former provides a justifiable advancement over conventional methods at industry level besides product quality.

The main challenges for the successful microwave heating of 25x20 mm clays are the exponential power absorbance that invariably appears after sintering swiftly leading to melting, and a thermal non-uniformity surpassing 100 ºC at the end of firing. The former is solved by regulating the power input when reaching sintering and the latter is minimised by adding a holding zone similarly to brickworks. A tighter power control is found when adjusting the power input through the clay energy needs as opposed to the clay surface temperature, largely due to the indirect control of the latter. As a result, holding stages of up to 30 min are reached before melting, with an added thermal uniformity improvement (≈55ºC) across the specimens' surface.

Microwaved 25x20 mm clays have 12.45% larger compressive strengths while displaying 6.9% higher porosity. The higher porosity is due to the reduced densification of the microwaved samples caused by the 92% shorter firings, while their enhanced thermal uniformity minimises structural tensions, leading to higher compressive strengths. Larger porosities also concur with the 40% larger water absorption and 16.6-59.6% smaller volume change. In both red and yellow clays, the brevity of the firings results in dimmer products, evidenced visually and by their red and yellow CIE scales being nearly 10 points lower than in conventional specimens. This difference is halved by lengthening the cooling stage conventionally. Similarly, the shorter microwave cycles do not allow for the complete elimination of muscovite and calcite and hinder the appearance of recrystallised minerals. This contrasts with the total elimination of the former and a significant generation of the latter under conventional treatment, where up to 28% of the final product is made of recrystallised species. Using microwaves plus a conventional cooling seems to largely solve the issue as

mineral reactants are eliminated and the recrystallised phase deviates as low as 1.1% from conventional results.

Upon consideration of larger processing scales, the threefold sample volume increase does not significantly alter the quality improvement described above. The only divergences found are caused by the need for longer holding times in order to reach the same level of densification as smaller specimens. Additionally, the massive improvement in process control implies advancement in curbing thermal gradients. Using that same single mode in industrial scale is nevertheless disadvantageous if only due to throughput considerations. Instead, multimode systems appear as the only feasible alternative. A potential configuration is to modify the feeds on Hoffman or tunnel kilns to add microwaves, where multiple feeds, mode stirrers and specific load arrangements counteract the limiting penetration depth that has a minimum of 0.15 m at 950 ^{o}C. Ultimately, the design and operation of pilot or industrial level plant will be the only viable path to prove whether it is technically possible for microwave to fire industrial brick loads given the processing challenges found for small clay cylinders.

A comparison between a theoretical microwave and conventional firing of clays at an industrial level concludes that the former is not economically viable when compared with conventional methods. Nevertheless, the successful substitution of natural gas by electricity powered by renewable energy sources could results in carbon footprint drop of up to 98%. Finally, the use of green energies plus a drastically reduced environmental impact falls in line with the energy policies of numerous institutions worldwide such as the European Commission and the G7/G8. Although the specific results of the analyses may vary given the broad assumptions made, the conclusions are still robust given the large economic and environmental differences between the two processes. Furthermore, hybrid heating may be a suitable processing technique that may attain a middle point between pure conventional or pure microwave firing.

8 GENERAL CONCLUSIONS AND FUTURE WORK

8.1 Introduction

The aim of this research was to gain an understanding of how microwaves interact with clays in order to test whether microwave energy alone could be used to fire clay-based materials. The specific objectives of this study were: to determine whether common Danish building clays could be fired by microwaves, to assess the constituents responsible for the heating and how are they affected by the process parameters; to determine if building materials of comparable quality to conventionally fired bricks could be manufactured using microwave processing alone, and to investigate the economic, environmental and legislative potential of the electromagnetic heating technique in the production of building materials. The general conclusions of the research are summarised below.

8.2 Clay materials characterisation

The microwave/clay interaction was investigated at different conditions of frequency, density, composition and temperature in order to ascertain whether microwave energy could fire clays. For the first time, the mineralogy of a multicomponent heterogeneous material like clay and its evolution during heating has been successfully associated to changes on its dielectric property trends. This is of critical importance as it builds a direct link between the microwave processability of a substance and its constituents, unlocking the possibility of addressing the processing potential of any clay based on its composition.

Clays displayed low free water contents in both their powder and slab states, i.e. 0.6-1.8% and 0.4-0.6%, respectively. Furthermore, this moisture was found to be concentrated in the clay minerals, peaking in montmorillonite at 3.5% and 1.9% as a powder and slab respectively. The uneven free water distribution, together with its comparatively better microwave coupling than clays, hinted towards an uneven microwave heating below 100 ºC. Regarding clay solid phases, the main mineralogical difference between red and yellow types was the significant calcite content (>20%) of yellow specimens. Consequently, all clays exhibited a similar behaviour on heating despite mineralogical differences, i.e. free and physically bound water elimination at 100 ºC and 250 ºC respectively, clay minerals dehydroxylation between 350-800 ºC, quartz inversion at 570 ºC, calcite decomposition around 750 ºC, sintering at 800 ºC and mineral recrystallisations beyond 900 ºC. In addition, there was an identifiable degree of interstratification between montmorillonite and muscovite, which may differentiate powders and slabs heating behaviour.

The dielectric property measurements of clay slabs at 2450 Mhz across the firing range (20-950 ºC) indicated that it should be feasible to fire them using microwave energy. This microwave heating potential fluctuated across the firing range, albeit to varying degrees, depending on the clay's composition, void fraction, temperature, and processing frequency. Although a 34% void fraction increase caused a general 30-60% drop in dielectric properties, and shifting from 2470 MHz to 912 MHz resulted in a general loss factors increase due to the system being brought closer both to a pure conductive response and the physically bound water dispersion zone, the main affecting parameters on clays dielectric properties are their composition and temperature. The physicochemical transformations of clay constituents were recognisable on the clays' loss factor trends whereas dielectric constants remained steady and alike during the thermal treatment, which implies applicator designs non-sensitive to different clay loads. This is of great interest given the variability of clays across deposits.

Free and physically bound water ensured the microwave heating around room temperature, while their removal curtailed the heating potential until the start of the clay minerals dehydroxylations at 350 ºC. Beyond this point, heat generation steadily improved as clays got hotter, which was further enhanced after sintering at 800 ºC. After water elimination, montmorillonite and muscovite became the dominant dielectric species that enabled the heating due to their water affinity and interlayer cations content, showing losses between one and two orders of magnitude higher than the other species. The dielectric contrast between these minerals and the other constituents suggests their selective microwave heating and the subsequent conventional heating through conduction effects of the rest of the clay, which would result in thermal gradients during processing unless the clay constituents are homogeneously distributed.

Future work on clays' characterisation should focus on the high temperature quantification of clay mineralogy, particularly on the recrystallised species beyond 900 ºC. Their identification would provide an understanding of the macrostructural mineral arrangements present around the top firing temperature, which can be later related to the dielectric properties in that range and the clay microwave processing.

Future studies ought to consider monitoring the porosity and the volume change of clay and mineral specimens during heating. This will improve the accuracy of the dielectric properties measurements, providing more precise information regarding the potential for microwave processing of a substance.

Future work should aim towards the characterisation of other clay constituents besides the major ones studied here. Particularly, lossy constituents such as iron oxides should be assessed, given their comparably higher dielectric response with respect to the low loss clays,

and their effect on the generation of hot spots and thermal gradients across the sample should be investigated. This will provide a deeper insight into the nature and possible thermal evolution of the studied clay specimens.

8.3 Electromagnetic mixing rules estimations of clays dielectric properties

A predictive model based on electromagnetic mixing rules was used to estimate the dielectric properties of any clay from their composition. This enabled a quantitative understanding of the effect of single minerals on the microwave processability of a whole clay. In addition to implementing a fast and simple alternative to dielectric property measurements, this tool can be used in the formulation of clay mixtures particularly designed for an optimal microwave processing.

A number of mixing equations were used on the study given their previous success in estimating clay materials, i.e. Complex Refractive Index, Landau-Lifshitz-Looyenga, Bruggeman-Hanai, Böttcher, Lichtenecker, Rayleigh and Sen-Scala-Cohen. The estimations were deemed successful if they were within the error bars of the 2470 MHz clays dielectric property measurements. An initial attempt to simplify clays into binary clay-air mixtures, where the focus was on predicting clays at different void fractions and frequencies, was unsuccessful given that clays cannot be considered homogenous entities. On the other hand, a multicomponent mixture approach where powdered minerals build clays at the same void fraction as unfired bricks resulted in acceptable estimations for Böttcher regardless of frequency. One of the limitations of this model was the absence of free water as a clay constituent. Its effect on the estimations was addressed with a correction term to the losses below 150 ^{o}C. The Böttcher predictive tool was also validated with other clay samples, namely yellow clay from Spain and red clays from England and Netherlands, expanding its applicability to clays of all over Europe.

The estimations' accuracy appeared insignificantly affected by the frequency and void fraction, where the latter covered most of the clay bricks void fraction range, i.e. 0.10-0.42 against 0.01-0.50. The tool could cope with sharp mineralogical variations but the presence of large quantities of free water (>2%) or intense thermal reactions negatively influenced the accuracy of the predictions. This means that a versatile tool as accurate as dielectric properties measurements has been developed for the fast prediction of the dielectric properties of a near infinite amount of clays at a wide void fraction range across firing and at the frequencies of 912-2470 MHz.

Future work on the estimation of clays dielectric properties should investigate the possibility of including free and physically bound water as constituents in the mixing rules to improve

the estimations' accuracy. The main challenges in doing so are the monitoring of free water presence and the quantification and monitoring of physically bound water evolution across firing in the minerals' interlayer.

Future studies should also consider using for the estimations the mineralogy of the clays at each point during firing instead of just the room temperature mineralogy used here. This should boost the estimations accuracy and reliability.

8.4 Microwave firing of clays

A single mode microwave system working at 2450±15 MHz was designed and commissioned for the firing of clay samples. This is the first time that microwave energy alone has been successfully utilised in producing fired ceramic materials (>1000 ^{o}C) whose quality is comparable to that of conventionally treated specimens. The basis of design focused on maximising the thermal uniformity of the clay load (<80 ^{o}C gradients), so as to maximise the quality of the fired products. Hence 25x20 mm clay cylinders were fired in a WR-430 waveguide working at TE_{10}.

Reproducibility of the trials was challenging giving the sensitivity of the load to small power fluctuations. This comes from the up to 80% power reflections when working at 300 W, while the remaining power ranging 51-93% was absorbed by the system instead of the sample. Reflections were caused by the small size of the load and its low loss behaviour, whereas the high system power absorbance came from the volume contrast between the sample and its thermal insulation.

The similarity between the clay power absorption behaviour and the clay dielectric properties indicate the volumetric heating of clays for most of the firing, where selective heating is recognised for the yellow samples beyond calcite decomposition at 800 ^{o}C. This is explained by the exothermic reactions from calcite reaction products, which hastily triggered the clay's sintering. Both clays tended to melting shortly afterwards (<2 min) in the absence of any type of holding stage. While a steady power input of 200 W was used during heating and natural air convection cooled the samples, power control was used to stablish a holding stage that lasted up to 30 min. The power modification was attempted through a control loop monitoring the clay surface's temperature or its energy needs. While the indirect control of clay temperatures through their insulation caused temperature oscillations of up to 250 ^{o}C, the energy needs control alternative provided a stable holding stage and a great minimisation of the thermal gradients after soaking for 30 min, with average temperature imbalances of 33 ^{o}C and 61 ^{o}C for the red and yellow samples around 1050 ^{o}C.

In addition to having firing cycles 90% shorter than in conventional brickworks (<180 min). Microwave fired clays had a 12% increased compressive strength after a 30 min holding stage, reaching 7 MPa. This was mainly achieved by the enhanced thermal uniformity of the microwaved clays brought by the soaking stage. The brevity of this holding stage compared to conventional processing was responsible for a lower volume shrinkage and 7% lower bulk density of microwaved products. Consequently, these displayed 40% higher levels of boiling and cold water absorption, but a similar freeze/thaw resistance with saturation coefficients averaging around 0.90. Additionally, microwaved clays presented dimmer colours than conventional samples. This hinted at unfinished mineral reactions, proven by the presence of 10% of unreacted muscovite and calcite, and the near total absence of recrystallised minerals in the microwaved samples. This opposed the total elimination of the former and the up to 28% recrystallised minerals phase found in conventional samples. A middle point was reached by adding a conventional cooling to the microwaved samples. Finally, a load increase to 25x35 mm presented similar improvements over conventional methods.

Future investigations should aim to optimise energy delivery to the clay sample. Moreover, a modification of the rig and/or sample should take place in order to further optimise energy delivery by reducing power reflections.

Future work on the microwave heating of clays should focus on developing a tailored firing cycle that optimises the length of the firing with the aim of increasing product quality

Future work should investigate the possibility of adding conventional heating at the beginning of the firing (<350 ºC) to aid in the heating at the area of lowest potential for microwave processing and also during the holding stage in order to surpass the 30 min length limit. Alternatively, a reduction of the top firing temperature may aid in surpassing this limit.

8.5 Techno-economical assessment of the microwave firing technique

A techno-economical assessment comparing the conventional and the microwave processing techniques was performed in order to assess any economic, environmental and legislative potential of the latter in the production of building materials at industrial scale. A retrofitted tunnel kiln option was considered for the analyses. The main divergences between both methodologies were located in its firing stage. Massive limitations to an assessment of an industrial scale microwave clay firing kiln when starting from laboratory results were acknowledged. Hence, there is a large degree of uncertainty for the considerations and choices made in this section. This is the first time that the microwave processing of clays at industrial scale has been subjected to a feasibility study.

Despite the lower energy consumption of the microwave rig to produce the same throughput, i.e. 11.6 GJ fuel/h vs. 6.1 GJ electricity/h, electricity costs were three times more expensive than natural gas. Moreover, the microwave generators were more than 20 times more expensive than the gas burners. Upon performing a NPV analysis on both alternatives, the microwave system had £ 3.1 10^5 of losses. A sensitivity analysis revealed that an around 80% decrease of the microwave system capital costs would balance both processing techniques economically. Moreover, switching to cheaper microwave equipment by processing at 915 MHz halved the microwave capital costs. An alternative to make more appealing microwaves would be price premiums for the production of sustainable bricks. Otherwise, conventional clay firing appeared to be the most profitable business model.

The lower energy consumption of the microwave system and its use of electricity as the energy supply instead of natural gas resulted in a lower environmental impact of the microwave technique, where the carbon footprint of the conventional kiln, ranging 720-1212 kg CO_2eq/h, dropped down to 1.6-5.7% of this value for red clays and was halved for yellow clays. At an energy policy level, the use of microwave energy was encouraged in the context of potentially substituting fossil fuels with sustainable green energies (used to produce electricity) while reducing carbon footprint. This aligned with the current policies of national governments and international agencies worldwide. Thus, the microwave clay firing process would be better prepared to cope with future legislation regarding of sustainable energy supplies and reduction of carbon footprint.

Future studies on the scaling up of the processing technique ought to develop an electromagnetic design of an industrial microwave applicator for the optimal clay firing of bricks. Probably, this firing will be a continuous process to increase product reproducibility.

Future work should expand on the life cycle assessment provided here and increase its complexity and sophistication, such as by taking into account for the analyses different possible kiln designs to cope for both processing techniques, prices of microwave equipment specifically designed for being used in clay firing, and address other possible internal rates of return.

9 REFERENCES

ABDULLAHI, T., HARUN, Z. & OTHMAN, M. H. D. 2017. A review on sustainable synthesis of zeolite from kaolinite resources via hydrothermal process. *Advanced Powder Technology,* 28**,** 1827-1840.

ACEVEDO, L., USON, S. & UCHE, J. 2015. Numerical study of cullet glass subjected to microwave heating and SiC susceptor effects. Part I: Combined electric and thermal model. *Energy Conversion and Management,* 97**,** 439-457.

ADAMS, M. J. 1981. *An introduction to optical waveguides*, Wiley New York.

AGRAWAL, D. Microwave sintering, brazing and melting of metallic materials. Sohn International Symposium; Advanced Processing of Metals and Materials Volume 4: New, Improved and Existing Technologies: Non-Ferrous Materials Extraction and Processing, 2006. 183-192.

AGRAWAL, D. 2010. Latest global developments in microwave materials processing. *Materials Research Innovations,* 14**,** 3-8.

AGRAWAL, D. K. 1998. Microwave processing of ceramics. *Current Opinion in Solid State and Materials Science,* 3**,** 480-485.

AJO-FRANKLIN, J., GELLER, J. & HARRIS, J. 2004. The dielectric properties of granular media saturated with DNAPL/water mixtures. *Geophysical Research Letters,* 31.

AKPINAR, S., EVCIN, A. & OZDEMIR, Y. 2017. Effect of calcined colemanite additions on properties of hard porcelain body. *Ceramics International,* 43**,** 8364-8371.

AKPINAR, S., KUSOGLU, I., ERTUGRUL, O. & ONEL, K. 2012. In situ mullite foam fabrication using microwave energy. *Journal of the European Ceramic Society,* 32**,** 843-848.

AKPINAR, S., KUŞOĞLU, I., ERTUGRUL, O. & ONEL, K. 2015. Microwave assisted sintering of in-situ cordierite foam. *Ceramics International,* 41**,** 8605-8613.

AL-HARAHSHEH, M., KINGMAN, S., SAEID, A., ROBINSON, J., DIMITRAKIS, G. & ALNAWAFLEH, H. 2009. Dielectric properties of Jordanian oil shales. *Fuel Processing Technology,* 90**,** 1259-1264.

AMERICAN PETROLEUM, I. 1951. *Reference clay minerals; American Petroleum Institute research project 49. Preliminary reports no. 1-8*, [New York] : [Columbia University], [1951].

ANDRADE, O. M., ISKANDER, M. F. & BRINGHURST, S. 1992. High temperature broadband dielectric properties measurement techniques. *MRS Online Proceedings Library Archive,* 269.

ANGGONO, J. 2005. Mullite ceramics: its properties structure and synthesis. *Jurnal Teknik Mesin,* 7**,** 1-10.

ANTHONY, J. W., BIDEAUX, R. A., BLADH, K. W. & NICHOLS, M. C. 1995. *Handbook of mineralogy, Volume II Silica, Silicates Part 1&2,* Chantilly, Virginia, Mineralogical Society of America.

ARLT, G., HENNINGS, D. & DE WITH, G. 1985. Dielectric properties of fine-grained barium titanate ceramics. *Journal of applied physics,* 58**,** 1619-1625.

ASANO, M., MIURA, N., SUDO, S., HAYASHI, Y., SINYAHIKI, N., YAGIHARA, S., SHIOTSUBO, M., KATO, Y., UOMOTO, T. & ARINO, M. Dielectric relaxation spectroscopy to investigate structured water in mortar. Proceedings of International Symposium of Non-Destructive Testing in Civil Engineering (NDT-CE), 2003.

ASTM 2010. ASTM D2216-Standard Test Methods for Laboratory Determination of Water (Moisture) Content of Soil and Rock by Mass. ASTM International.

ASTM 2011. ASTM E1269-Standard Test Method for Determining Specific Heat Capacity by Differential Scanning Calorimetry. ASTM International.

ASTM 2013a. ASTM C62-Standard Specification for Building Brick (Solid Masonry Units Made From Clay or Shale). ASTM International.

ASTM 2013b. ASTM D2520-13 Standard Test Methods for Complex Permittivity (Dielectric Constant) of Solid Electrical Insulating Materials at Microwave Frequencies and Temperatures to 1650ºC. ASTM International.

ASTM 2014a. ASTM D5550-Standard Test Method for Specific Gravity of Soil Solids by Gas Pycnometer. ASTM International.

ASTM 2014b. ASTM D5568-Standard Test Method for Measuring Relative Complex Permittivity and Relative Magnetic Permeability of Solid Materials at Microwave Frequencies Using Waveguide. ASTM International.

ASTM 2014c. ASTM E1131-Standard Test Method for Compositional Analysis by Thermogravimetry. ASTM International.

ASTM 2015a. ASTM B215-Standard Practices for Sampling Metal Powders. ASTM International.

ASTM 2015b. ASTM C652-Standard Specification for Hollow Brick (Hollow Masonry Units Made From Clay or Shale). ASTM International.

ASTM 2016. ASTM C216-Standard Specification for Facing Brick (Solid Masonry Units Made from Clay or Shale). ASTM International.

AZAD, A. K., ZHAO, Y., ZHANG, W. & HE, M. 2006. Effect of dielectric properties of metals on terahertz transmission in subwavelength hole arrays. *Optics letters,* 31**,** 2637-2639.

BAGCHI, B., DAS, S., BHATTACHARYA, A., BASU, R. & NANDY, P. 2010. Mullite phase enhancement in Indian kaolins by addition of vanadium pentoxide. *Applied clay science,* 47**,** 409-413.

BAILEY, S. W. 1984. *Micas*, Mineralogical Society of America.

BAIN, J. & MORGAN, D. 1969. The role of thermal analysis in the evaluation of impure clay deposits as mineral raw materials. *Clay minerals,* 8**,** 171-192.

BAL, K. & KOTHARI, V. 2010. Permittivity of woven fabrics: A comparison of dielectric formulas for air-fiber mixture. *IEEE Transactions on Dielectrics and Electrical Insulation,* 17.

BARRACHINA, E., CALVET, I., FRAGA, D. & CARDA, J. 2017. Ceramic porcelain stoneware production with Spanish clays purified by means of the removal of iron compounds and organic matter using physical methods. *Applied Clay Science,* 143**,** 258-264.

BAULUZ, B., MAYAYO, M. J., FERNÁNDEZ-NIETO, C., CULTRONE, G. & LÓPEZ, J. M. G. 2003. Assessment of technological properties of calcareous and non-calcareous clays used for the brick-making industry of Zaragoza (Spain). *Applied clay science,* 24**,** 121-126.

BECKHOFF, B., KANNGIEßER, B., LANGHOFF, N., WEDELL, R. & WOLFF, H. 2007. *Handbook of practical X-ray fluorescence analysis*, Springer Science & Business Media.

BENAVENTE, R., PRUNA, A., BORRELL, A., SALVADOR, M., PULLINI, D., PEÑARANDA-FOIX, F. & BUSQUETS, D. 2015. Fast route to obtain Al2O3-based nanocomposites employing graphene oxide: Synthesis and sintering. *Materials Research Bulletin,* 64**,** 245-251.

BENEROSO, D., MONTI, T., KOSTAS, E. & ROBINSON, J. 2017. Microwave pyrolysis of biomass for bio-oil production: Scalable processing concepts. *Chemical Engineering Journal*.

BERUTO, D., VECCHIATTINI, R. & GIORDANI, M. 2003. Solid products and rate-limiting step in the thermal half decomposition of natural dolomite in a CO2 (g) atmosphere. *Thermochimica Acta,* 405**,** 183-194.

BHATTACHARYA, M. & BASAK, T. 2016. A review on the susceptor assisted microwave processing of materials. *Energy,* 97**,** 306-338.

BHATTACHARYA, M. & BASAK, T. 2017. Susceptor-Assisted Enhanced Microwave Processing of Ceramics-A Review. *Critical Reviews in Solid State and Materials Sciences,* 42**,** 433-469.

BIERMAN JR, H. & SMIDT, S. 2012. *The capital budgeting decision: economic analysis of investment projects*, Routledge.

BIJHMANN, C. & GRUBB, P. 1991. A kaolin-smectite interstratification sequence from a red and black complex. *Clay Minerals,* 26**,** 343-358.

BILGEN, S. & SARıKAYA, İ. 2016. Contribution of efficient energy use on economy, environment, and sustainability. *Energy Sources, Part B: Economics, Planning, and Policy,* 11**,** 1166-1172.

BILGIN, M. 2009. Geopolitics of European natural gas demand: Supplies from Russia, Caspian and the Middle East. *Energy Policy,* 37**,** 4482-4492.

BINNER, J. & VAIDHYANATHAN, B. When should microwaves be used to process technical ceramics? Materials Science Forum, 2009. Trans Tech Publ, 51-59.

BIRCHAK, J. R., GARDNER, C. G., HIPP, J. E. & VICTOR, J. M. 1974. High dielectric constant microwave probes for sensing soil moisture. *Proceedings of the IEEE,* 62**,** 93-98.

BIS 2013. Monthly Statistics of Building Materials and Components. Department for Business, Innovation and Skills.

BNZ 2016. Insulating Fire Brick. *In:* BNZ MATERIALS, I. (ed.).

BODHAK, S., BOSE, S. & BANDYOPADHYAY, A. 2011. Densification Study and Mechanical Properties of Microwave-Sintered Mullite and Mullite–Zirconia Composites. *Journal of the American Ceramic Society,* 94**,** 32-41.

BOHOR, B. F. 1963. High-temperature phase development in illitic clays. *Clays and Clay Minerals,* 12**,** 233-246.

BOONTON 2015. PRINCIPLES OF POWER MEASUREMENT A Reference Guide on RF & Microwave Power Measurement. Parsippany, United States: Wireless Telecom Group

BORRELL, A., D SALVADOR, M., MIRANDA, M., L PENARANDA-FOIX, F. & M CATALA-CIVERA, J. 2014. Microwave technique: a powerful tool for sintering ceramic materials. *Current Nanoscience,* 10**,** 32-35.

BÖTTCHER, C. 1945. The dielectric constant of crystalline powders. *Recueil des travaux chimiques des Pays-Bas,* 64**,** 47-51.

BOUSSAK, H., CHEMANI, H. & SERIER, A. 2015. Characterization of porcelain tableware formulation containing bentonite clay. *International Journal of Physical Sciences,* 10**,** 38-45.

BOWMAN, M. D., HOLCOMB, J. L., KORMOS, C. M., LEADBEATER, N. E. & WILLIAMS, V. A. 2007. Approaches for scale-up of microwave-promoted reactions. *Organic Process Research & Development,* 12**,** 41-57.

BOYACı, İ. H., SUMNU, G. & SAKIYAN, O. 2009. Estimation of dielectric properties of cakes based on porosity, moisture content, and formulations using statistical methods and artificial neural networks. *Food and Bioprocess Technology,* 2**,** 353-360.

BRIDGWATER, A. V. 2003. Renewable fuels and chemicals by thermal processing of biomass. *Chemical Engineering Journal,* 91**,** 87-102.

BRINDLEY, G. W. 1955. Identification of clay minerals by X-ray diffraction analysis.

BROUWER, P. 2006. Theory of XRF. *Almelo, Netherlands: PANalytical BV.*

BROVELLI, A. & CASSIANI, G. 2008. Effective permittivity of porous media: A critical analysis of the complex refractive index model. *Geophysical Prospecting,* 56**,** 715-727.

BROWN, G., BRINDLEY, G. W. & BROWN, G. 1980. Crystal structures of clay minerals and their X-ray identification.

BSI 1985. BS 3921-Specification for Clay bricks. British Standards Institution.

BSI 2011a. BS 772-1-Methods of test for masonry units. *Part 1: Determination of compressive strength.* London: British Standards Institution.

BSI 2011b. BS EN 60519-6-Specifications for safety in industrial microwave heating equipment. London: British Standard Institution.

BSI 2011c. PAS 2050 -How to carbon footprint your products, identify hotspots and reduce emissions in your supply chain. London: British Standards Institution.

BUSSIAN, A. 1983. Electrical conductance in a porous medium. *Geophysics,* 48**,** 1258-1268.
BYKOV, Y. V., RYBAKOV, K. & SEMENOV, V. 2001. High-temperature microwave processing of materials. *Journal of Physics D: Applied Physics,* 34**,** R55.
C-TECH. 2016a. *The Cost of Heat in the Ceramic Industry* [Online]. C-Tech Innovation. [Accessed 10 / 11 / 2016].
C-TECH. 2016b. *Microwave-assisted Kilns* [Online]. C-Tech Innovation. Available: http://www.ctechinnovation.com/energy-and-heating/microwave-assisted-kilns/ [Accessed 4 / 11 / 2016].
CALKINS, M. 2008. *Materials for sustainable sites: a complete guide to the evaluation, selection, and use of sustainable construction materials*, John Wiley & Sons.
CAMPBELL, G., JUNGBAUER JR, J., BIDLAKE, W. & HUNGERFORD, R. 1994. Predicting the effect of temperature on soil thermal conductivity. *Soil Science,* 158**,** 307-313.
CAMPBELL, M. J. & ULRICHS, J. 1969. Electrical properties of rocks and their significance for lunar radar observations. *Journal of Geophysical Research,* 74**,** 5867-5881.
CARTER, R. G. 2001. Accuracy of microwave cavity perturbation measurements. *IEEE Transactions on Microwave theory and techniques,* 49**,** 918-923.
CASTELEIN, O., SOULESTIN, B., BONNET, J. & BLANCHART, P. 2001. The influence of heating rate on the thermal behaviour and mullite formation from a kaolin raw material. *Ceramics International,* 27**,** 517-522.
CATALÁ-CIVERA, J., SOTO, P., BORIA, V., BALBASTRE, J. V. & DE LOS REYES, E. 2006. Design parameters of multiple reactive chokes for open ports in microwave heating systems. *Advances in Microwave and Radio Frequency Processing.* Springer.
CENTENO, E. 2016. Sweden´s renewable energy policies towards 2020 and 2030. *In:* ENERGY, S. M. O. E. A. (ed.).
CERALINK. 2013. *MICROWAVE ASSIST TECHNOLOGY (MAT™)* [Online]. CERALINK. Available: http://ceralink.com/MATHome [Accessed 8 / 11 / 2016].
CERAMICARTDAILY. 2005. *Kiln Firing Chart* [Online]. Available: www.ceramicartdaily.net/PMI/KilnFiringChart.pdf [Accessed 3/6/16 2016].
CHAN, T. V. C. T. & READER, H. C. 2000. *Understanding microwave heating cavities*, Artech House Publishers.
CHANDRASEKARAN, S., RAMANATHAN, S. & BASAK, T. 2012. Microwave material processing—a review. *AIChE Journal,* 58**,** 330-363.
CHANGE, I. P. O. C. 2015. *Climate change 2014: mitigation of climate change*, Cambridge University Press.
CHEMAT-DJENNIA, Z., BAKOZ, P. Y. & HAMADA, B. 2016. Catalytic Preparation, Characterization and Performance Isomerization of M-Xylene by Modified Montmorillonite Prepared by Microwave. *Science Journal of University of Zakho,* 1**,** 768-779.
CHEN, C. Y., LAN, G. S. & TUAN, W. H. 2000. Microstructural evolution of mullite during the sintering of kaolin powder compacts. *Ceramics International,* 26**,** 715-720.
CHEN, H. & LENG, S. 2015. Rapid synthesis of hollow nano-structured hydroxyapatite microspheres via microwave transformation method using hollow CaCO3 precursor microspheres. *Ceramics International,* 41**,** 2209-2213.
CHENG, J., AGRAWAL, D., ZHANG, Y. & ROY, R. 2002. Microwave sintering of transparent alumina. *Materials Letters,* 56**,** 587-592.
CHIESA, V. & FRATTINI, F. 2009. *Evaluation and performance measurement of research and development: Techniques and perspectives for multi-level analysis*, Edward Elgar Publishing.
CHRISTIDIS, G. E. 2011. *Advances in the characterization of industrial minerals*, The Mineralogical Society of Great Britain and Ireland.

CHURCH, R. H., WEBB, W. E. & SALSMAN, J. 1988. *Dielectric properties of low-loss minerals*, US Department of the Interior.

CIE 2004. Technical Report Colorimetry. International Commission on Illumination.

CIHLAR, J. & ULABY, F. T. 1974. Dielectric properties of soils as a function of moisture content.

CIROTH, A. 2007. ICT for environment in life cycle applications openLCA—A new open source software for life cycle assessment. *The International Journal of Life Cycle Assessment,* 12**,** 209.

CIVIDANES, L. S., CAMPOS, T. M., RODRIGUES, L. A., BRUNELLI, D. D. & THIM, G. P. 2010. Review of mullite synthesis routes by sol–gel method. *Journal of Sol-Gel Science and Technology,* 55**,** 111-125.

CLARK, D., FOLZ, D., FOLGAR, C. & MAHMOUD, M. 2005. Microwave solutions for ceramic engineers. *The American Ceramic Society*.

CLARK, D. E., FOLZ, D. C. & WEST, J. K. 2000. Processing materials with microwave energy. *Materials Science and Engineering: A,* 287**,** 153-158.

CLARK, D. E. & SUTTON, W. H. 1996. Microwave processing of materials. *Annual Review of Materials Science,* 26**,** 299-331.

CLARK, K. 1983. *The potter's manual*, Book Sales.

CLINI, C. M. S., MARK 2001. G8 Renewable Energy Task Force. G8.

COLOMBO, S., EL HARRAK, M. & SARTORI, N. 2016. The Future of Natural Gas: Markets and Geopolitics. *Books & Reports*.

CORDIS 1999. MICROWAVE ASSISTED GAS FIRING ON A SINGLE LAYER ROLLER KILN FOR MANUFACTURE OF CERAMIC WALL TILES. *In:* SERVICE, C. R. A. D. I. (ed.).

COULSON, J. M., RICHARDSON, J. F., BACKHURST, J. R. & HARKER, J. H. 1996. *Coulson and Richardson's Chemical Engineering Volume 1 - Fluid Flow, Heat Transfer and Mass Transfer* Elsevier.

COUNCIL, N. R. 1994. *Microwave processing of materials*, National Academies Press.

CULTRONE, G., SEBASTIAN, E. & DE LA TORRE, M. 2005. Mineralogical and physical behaviour of solid bricks with additives. *Construction and Building Materials,* 19**,** 39-48.

DANA, K., DAS, S. & DAS, S. K. 2004. Effect of substitution of fly ash for quartz in triaxial kaolin–quartz–feldspar system. *Journal of the European Ceramic Society,* 24**,** 3169-3175.

DAS, S., MUKHOPADHYAY, A., DATTA, S. & BASU, D. 2009. Prospects of microwave processing: an overview. *Bulletin of Materials Science,* 32**,** 1-13.

DAVILA, L. P., RISBUD, S. H. & SHACKELFORD, J. F. 2008. Quartz and Silicas. *Ceramic and Glass Materials.* Springer.

DAVIS, J. R. 2001. *Copper and copper alloys*, ASM international.

DE LIMA SANTANA, L. N., GOMES, J., DA SILVA, V. J., GONÇALVES, W. P., DE LUCENA LIRA, H., DE ARAÚJO NEVES, G. & MENEZES, R. R. Influence of Power and Synthesis Time in the Formation of Mullite Obtained by Microwave Heating. Materials Science Forum, 2015.

DECC&BIS 2015. Industrial Decarbonisation & Energy Efficiency Roadmaps to 2050-Ceramic Sector. Department of Energy and Climate Change and Department for Business, Innovation and Skills.

DEER, W. A., HOWIE, R. A. & ZUSSMAN, J. Rock-forming Minerals: Feldspars, Volume 4A. 2001. Geological Society of London.

DEJONGHE, L. C. & RAHAMAN, M. N. 2003. Sintering of Ceramics. *Handbook of Advanced Ceramics: Materials, Applications, Processing and Properties.*

DHRI. 2018. *Clay brick wholesale* [Online]. Available: https://www.alibaba.com/product-detail/China-factory-of-wholesale-bricks-

clay_60160427382.html?spm=a2700.7724838.2017115.64.7cff65f9xVS1d5 [Accessed 17 / 4 / 2018].

DINULOVIĆ, M. & RAŠUO, B. 2011. Dielectric modeling of multiphase composites. *Composite Structures,* 93**,** 3209-3215.

DJEKIC, I., MIOCINOVIC, J., TOMASEVIC, I., SMIGIC, N. & TOMIC, N. 2014. Environmental life-cycle assessment of various dairy products. *Journal of cleaner production,* 68**,** 64-72.

DONDI, M., MAZZANTI, F., PRINCIPI, P., RAIMONDO, M. & ZANARINI, G. 2004. Thermal conductivity of clay bricks. *Journal of Materials in Civil Engineering,* 16**,** 8-14.

DUBE, D. & PARSHAD, R. 1970. Study of Böttcher's formula for dielectric correlation between powder and bulk. *Journal of Physics D: Applied Physics,* 3**,** 677.

DUNHAM, A. Developments in industrial mineralogy: I. The mineralogy of brick-making. Proceedings of the Yorkshire Geological and Polytechnic Society, 1992. Geological Society of London.

DUNN, M. 2015. Microwave Heating of Ceramics *Ceramic Industry*.

DUNSMORE, J. P. 2012. *Handbook of microwave component measurements: with advanced VNA techniques*, John Wiley & Sons.

DUOMO 2018. T300 Pre-mixed burner *In:* DUOMO (ed.).

EBADZADEH, T. 2010. Effect of mechanical activation and microwave heating on synthesis and sintering of nano-structured mullite. *Journal of Alloys and Compounds,* 489**,** 125-129.

EBARA, H., INOUE, T. & HASHIMOTO, O. 2006. Measurement method of complex permittivity and permeability for a powdered material using a waveguide in microwave band. *Science and Technology of Advanced Materials,* 7**,** 77-83.

EFKM 2011. Energy strategy 2050– from coal, oil and gas to green energy. *In:* ENERGY, D. M. O. C. A. (ed.). København: Danish Government.

EIA 2016. International energy outlook 2016. *In:* ADMINISTRATION, U. E. I. (ed.).

EL-MAHLLAWY, M. S. & KANDEEL, A. M. 2014. Engineering and mineralogical characteristics of stabilized unfired montmorillonitic clay bricks. *HBRC Journal,* 10**,** 82-91.

EN, B. 2003. EN, BS 771-1 Specification for Masonry Units-Part 1: Clay Masonry Units. *British Standards Institute.*

ENER 2010. Energy 2020 A strategy for competitive, sustainable and secure energy. Luxembourg: European Comission.

ERC 2000. Interference from industrial, scientific and medical (ISM) machines. *In:* (CEPT), E. R. C. E. W. T. E. C. O. P. A. T. A. (ed.). Luxembourg.

ERCIN, A. E. & HOEKSTRA, A. Y. 2012. *The United Nations World Water Development Report–N° 4–Carbon and Water Footprints (Concepts, Methodologies and Policy Responses)*, Unesco.

EREMEEV, A., EGOROV, S., SOROKIN, A., BYKOV, Y. V. & RYBAKOV, K. 2018. Apparent viscosity reduction during microwave sintering of amorphous silica. *Ceramics International,* 44**,** 1797-1801.

ESCALERA, E., TEGMAN, R., ANTTI, M.-L. & ODÉN, M. 2014. High temperature phase evolution of Bolivian kaolinitic–illitic clays heated to 1250° C. *Applied Clay Science,* 101**,** 100-105.

EUROSTAT. 2017a. *Natural gas prices for non-household consumers - bi-annual data (from 2007 onwards)* [Online]. Eurostat. [Accessed 17/1/18 2017].

EUROSTAT. 2017b. *Production in construction - monthly data* [Online]. Eurostat. Available: http://appsso.eurostat.ec.europa.eu/nui/show.do?dataset=sts_copr_m&lang=en [Accessed 3/4/17 2017].

EUSME 2013. The construction sector in China. European Union European small and medium-sized enterprises.

FAEGHI-NIA, A. & EBADZADEH, T. 2012. Fabrication of machinable phlogopite–glass composite using microwave processing. *Ceramics International,* 38**,** 2653-2658.

FAHMY, A., YOUSSEF, H. & ELZAREF, A. 2016. Adsorption of Cadmium Ions onto Zeolite-A prepared from Egyptian Kaolin using Microwave. *Int J Sci Res,* 5**,** 1549-1555.

FANDRICH, R., GU, Y., BURROWS, D. & MOELLER, K. 2007. Modern SEM-based mineral liberation analysis. *International Journal of Mineral Processing,* 84**,** 310-320.

FARIA, K. C. P., GURGEL, R. F. & HOLANDA, J. N. F. 2012. Recycling of sugarcane bagasse ash waste in the production of clay bricks. *Journal of Environmental Management,* 101**,** 7-12.

FENG, H., TANG, J. & CAVALIERI, R. 2002. Dielectric properties of dehydrated apples as affected by moisture and temperature. *Transactions-American Society of Agricultural Engineers,* 45**,** 129-136.

FERMILAB 2018. Magnetron Technology Summary. *In:* FERMILAB (ed.).

FLOREK, I. & LOVAS, M. 1995. The influence of the complex electric permittivity and grain size on microwave drying of the grained minerals. *Fizykochemiczne Problemy Mineralurgii***,** 127-134.

FMI 2015. U.S. Markets Construction overview 2016. Raleigh, North Carolina: FMI Corporation.

FOLORUNSO, D., OLUBAMBI, P. & BORODE, J. 2014. Characterization and qualitative analysis of some Nigerian clay deposits for refractory applications. *IOSR Journal of Applied Chemistry,* 7**,** 40-47.

GADANI, D. H. 2012. Dielectric properties of soils in microwave region.

GALAN, I., GLASSER, F. P. & ANDRADE, C. 2013. Calcium carbonate decomposition. *Journal of thermal analysis and calorimetry,* 111**,** 1197-1202.

GANDHI, O. P. 1981. *Microwave engineering and applications*, Pergamon Press.

GERASIMCHUK, I. 2015. Fossil-fuel Subsidy Reform: Critical Mass for Critical Change. Working Paper, May. Austin: University of Texas at Austin.

GERLING, J. F. 2000. Waveguide components and configurations for optimal performance in microwave heating systems. *Gerling Applied Engineering*.

GHASALI, E., ALIZADEH, M. & EBADZADEH, T. 2016. Mechanical and microstructure comparison between microwave and spark plasma sintering of Al–B4C composite. *Journal of Alloys and Compounds,* 655**,** 93-98.

GHERIBI, A. E., MACHADO, K., ZANGHI, D., BESSADA, C., SALANNE, M. & CHARTRAND, P. 2018. On the determination of ion transport numbers in molten salts using molecular dynamics. *Electrochimica Acta,* 274**,** 266-273.

GIANNUZZI, L. A. 2006. *Introduction to focused ion beams: instrumentation, theory, techniques and practice*, Springer Science & Business Media.

GILLOT, J. E. 1987. *Clay in engineering geology*, Elsevier.

GOBRICK 2003. Manufacturing, Classification, and Selection of Brick, Selection, Part 3. *In:* ASSOCIATION, B. I. (ed.) *Technical Notes on Brick Construction 9B.* Reston, Virginia.

GOBRICK 2006. Manufacturing of Brick. *In:* ASSOCIATION, B. I. (ed.) *Technical Notes on Brick Construction 9.* Reston, Virginia.

GOBRICK 2007. Specifications for and Classification of Brick. *In:* ASSOCIATION, B. I. (ed.) *Technical Notes on Brick Construction 9A.* Reston, Virginia.

GOLDEMBERG, J. 2006. The promise of clean energy. *Energy policy,* 34**,** 2185-2190.

GOLDSTEIN, J., NEWBURY, D., ECHLIN, P., JOY, D., FIORI, C. & LIFSHIN, E. 2003. *SCANNING ELECTRON-MICROSCOPY AND X-RAY-MICROANALYSIS*, MINERALS METALS MATERIALS SOC 420 COMMONWEALTH DR, WARRENDALE, PA 15086.

GOLIO, M. 2000. *The RF and microwave handbook*, CRC press.

GOMES, E. & HOSSAIN, I. 2003. Transition from traditional brick manufacturing to more sustainable practices. *Energy for sustainable development,* 7**,** 66-76.

GOMES, J., ROCHA, A., MENEZES, R., NEVES, G., SANTANA, L. & BRASILEIRO, M. Mullite evidence for rapid firing from bentonite clay of Paraíba. Mater. Sci. Forum, 2010. 936-942.

GONÇALVES, W. P., DA SILVA, V. J., GOMES, J., DE ARAÚJO NEVES, G., MENEZES, R. R. & DE LIMA SANTANA, L. N. Influence of the Heating Rate on the Phase and Microstructural Transformations of Smectite Clays. Materials Science Forum, 2015. Trans Tech Publ, 46-50.

GONCHARENKO, A., LOZOVSKI, V. & VENGER, E. 2000. Lichtenecker's equation: applicability and limitations. *Optics Communications,* 174**,** 19-32.

GONZÁLEZ, B., PÉREZ, A. H., TRUJILLANO, R., GIL, A. & VICENTE, M. A. 2017. Microwave-assisted pillaring of a montmorillonite with Al-polycations in concentrated media. *Materials,* 10**,** 886.

GONZÁLEZ, I., GALÁN, E., MIRAS, A. & APARICIO, P. 1998. New uses for brick-making clay materials from the Bailén area (southern Spain). *Clay Minerals,* 33**,** 453-465.

GOODALL, W. R. & SCALES, P. J. 2007. An overview of the advantages and disadvantages of the determination of gold mineralogy by automated mineralogy. *Minerals Engineering,* 20**,** 506-517.

GOV.AU 2016. Australian energy update. *In:* DEPARTMENT OF INDUSTRY, I. A. S. (ed.).

GOV.UK 2008. Climate Change Act 2008 Chapter 27. *In:* KINGDOM, P. O. T. U. (ed.).

GOV.UK 2016a. Industrial electricity prices in the IEA. *In:* DEPARTMENT FOR BUSINESS, E. I. S. (ed.).

GOV.UK 2016b. Industrial gas prices in the IEA. *In:* DEPARTMENT FOR BUSINESS, E. I. S. (ed.).

GOV.UK 2017. Fuel mix disclosure data table. *In:* DEPARTMENT FOR BUSINESS, E. I. S. (ed.).

GREEN, D. W. 2007. Perry's chemical engineering handbook. *McGrawHill Professional Publ*.

GRIM, R. 1968. *Clay Mineralogy,* New York, McGraw-Hill.

GUGGENHEIM, S. & MARTIN, R. 1995. Definition of clay and clay mineral: joint report of the AIPEA nomenclature and CMS nomenclature committees. *Clays and clay minerals,* 43**,** 255-256.

GUGGENHEIM, S. & VAN GROOS, A. 1992. High-Pressure Differential Thermal Analysis (HP-DTA) I. Dehydration reactions at elevated pressures in phyllosilicates. *Journal of Thermal Analysis and Calorimetry,* 38**,** 1701-1728.

GUNASEKARAN, S., ANBALAGAN, G. & PANDI, S. 2006. Raman and infrared spectra of carbonates of calcite structure. *Journal of Raman Spectroscopy,* 37**,** 892-899.

GÜVEN, N. & POLLASTRO, R. M. 1992. *Clay-water interface and its rheological implications*, Clay Minerals Society.

HAMMOUDA, I. & MIHOUBI, D. 2014. Comparative numerical study of kaolin clay with three drying methods: Convective, convective–microwave and convective infrared modes. *Energy Conversion and Management,* 87**,** 832-839.

HANAI, T. 1960. Theory of the dielectric dispersion due to the interfacial polarization and its application to emulsions. *Kolloid-Zeitschrift,* 171**,** 23-31.

HARABI, A., GUERFA, F., HARABI, E., BENHASSINE, M.-T., FOUGHALI, L. & ZAIOU, S. 2016. Preparation and characterization of new dental porcelains, using K-feldspar and quartz raw materials. Effect of B2O3 additions on sintering and mechanical properties. *Materials Science and Engineering: C,* 65**,** 33-42.

HARRIS, K. D. & CHEUNG, E. Y. 2004. How to determine structures when single crystals cannot be grown: opportunities for structure determination of molecular materials using powder diffraction data. *Chemical Society Reviews,* 33**,** 526-538.

HARTLIEB, P., KUCHAR, F., MOSER, P., KARGL, H. & RESTNER, U. 2018. Reaction of different rock types to low-power (3.2 kW) microwave irradiation in a multimode cavity. *Minerals Engineering,* 118**,** 37-51.

HARTWICK, J. 2013. *Non-renewable resources extraction programs and markets*, Routledge.

HATHAWAY, J. C. 1956. Procedure for clay mineral analysis used in the sedimentary petrology laboratory of the US Geological Survey. *Clay minerals bulletin,* 3**,** 8-13.
HE, D., FENG, Q., ZHANG, G., OU, L. & LU, Y. 2007. An environmentally-friendly technology of vanadium extraction from stone coal. *Minerals Engineering,* 20**,** 1184-1186.
HEANEY, P. J. 1994. Structure and chemistry of the low-pressure silica polymorphs. *Reviews in Mineralogy and Geochemistry,* 29**,** 1-40.
HENDRICKSON, C., HORVATH, A., JOSHI, S. & LAVE, L. 1998. Peer reviewed: economic input–output models for environmental life-cycle assessment. *Environmental science & technology,* 32**,** 184A-191A.
HENDRICKSON, C. T., HORVATH, A., JOSHI, S., KLAUSNER, M., LAVE, L. B. & MCMICHAEL, F. C. Comparing two life cycle assessment approaches: a process model vs. economic input-output-based assessment. Electronics and the Environment, 1997. ISEE-1997., Proceedings of the 1997 IEEE International Symposium on, 1997. Ieee, 176-181.
HEUGUET, R., MARINEL, S., THUAULT, A. & BADEV, A. 2013. Effects of the susceptor dielectric properties on the microwave sintering of alumina. *Journal of the American Ceramic Society,* 96**,** 3728-3736.
HILLIER, S. 1999. Use of an air brush to spray dry samples for X-ray powder diffraction. *Clay Minerals,* 34**,** 127-135.
HILLIER, S., SUZUKI, K. & COTTER-HOWELLS, J. 2001. Quantitative determination of cerussite (lead carbonate) by X-ray powder diffraction and inferences for lead speciation and transport in stream sediments from a former lead mining area in Scotland. *Applied Geochemistry,* 16**,** 597-608.
HIRAOKA, Y. 1994. A possible approach to soil discrimination using X-ray fluorescence analysis. *Journal of Forensic Science,* 39**,** 1381-1392.
HOEKSTRA, P. & DELANEY, A. 1974. Dielectric properties of soils at UHF and microwave frequencies. *Journal of geophysical research,* 79**,** 1699-1708.
HOSSAN, M. R., BYUN, D. & DUTTA, P. 2010. Analysis of microwave heating for cylindrical shaped objects. *International Journal of Heat and Mass Transfer,* 53**,** 5129-5138.
HOUSEMAN, J. & KOENIG, C. 1971a. Influence of kiln atmospheres in firing structural clay products: I, maturation and technological properties. *Journal of the American Ceramic Society,* 54**,** 75-82.
HOUSEMAN, J. & KOENIG, C. 1971b. Influence of kiln atmospheres in firing structural clay products: II, color development and burnout. *Journal of the American Ceramic Society,* 54**,** 82-89.
HOWES, T. 2010. The EU's New Renewable Energy Directive (2009/28/EC). *The new climate policies of the European Union: internal legislation and climate diplomacy,* 15**,** 3.
HWANG, D. J., RYU, J. Y., YU, Y. H., CHO, K. H., AHN, J. W., HAN, C. & LEE, J. D. 2014. Characteristics of precipitated calcium carbonate by hydrothermal and carbonation processes with mega-crystalline calcite using rotary microwave kiln. *Journal of Industrial and Engineering Chemistry,* 20**,** 2727-2734.
IBSTOCK 2015. How clay bricks are made *In:* IBSTOCK (ed.) *Technical information sheet a1 design & specification considerations.*
ICNIRP 2009. ICNIRP statement on the "guidelines for limiting exposure to time-varying electric, magnetic, and electromagnetic fields (up to 300 ghz)". *In:* PROTECTION, I. C. O. N.-I. R. (ed.) *Health physics.*
IEA 2016. Energy Policies of IEA Countries Italy 2016 Review

International Energy Agency.
IEA 2017a. GAS 2017 Analysis and Forecasts to 2022. International Energy Agency.
IEA 2017b. Renewables 2017. International Energy Agency.
ILO 1984. *Small-Scale Brickmaking,* Geneva, International labour Office (ILO).

INREAP 2014. The Icelandic National Renewable Energy Action Plan for the promotion of the use of energy from renewable sources. Reykjavik: Ministry of Industries and Innovation.

INSULCON 2014. Technical Datasheet Fibercon 1600 High Alumina Blanket Maximum Performance in Thermal Insulation. *In:* B.V., I. (ed.).

IQBAL, Y. & LEE, W. E. 2000. Microstructural evolution in triaxial porcelain. *Journal of the American Ceramic Society,* 83**,** 3121-3127.

ISO 2006a. ISO 14040 -Environmental management-life cycle assessment-principles and framework. International Organization for Standardization.

ISO 2006b. ISO 14044 -Environmental management -Life cycle assessment -Requirements and guidelines. International Organization for Standardization.

ITAYA, Y., UCHIYAMA, S., HATANO, S. & MORI, S. 2005. Drying enhancement of clay slab by microwave heating. *Drying Technology,* 23**,** 1243-1255.

JACKSON, J. 1973. The alteration characteristics of the Lower Oxford Clay. *Clay Minerals,* 10**,** 113-126.

JADHAV, A. K., NALAWADE, P. R., BUTEE, S. P., BASHAIAH, S. & RAJU, K. J. Hard Materials-Processing 2: Enhancement in Microwave Dielectric Properties of (Zn^ sub 1-x^ Mn^ sub x^)^ sub 2^ TiO%^ sub 4^ Ceramics through Post-Sinter Annealing. European Congress and Exhibition on Powder Metallurgy. European PM Conference Proceedings, 2015. The European Powder Metallurgy Association, 1.

JAMIL, T. S. & YOUSSEF, H. 2016. Microwave synthesis of zeolites from Egyptian kaolin: Evaluation of heavy metals removal. *Separation Science and Technology,* 51**,** 2876-2886.

JANZ, G. J. 2013. *Molten salts handbook*, Elsevier.

JENKINS, R. 2000. X-Ray Techniques: Overview. *Encyclopedia of analytical chemistry*.

JENSEN, E. 1978. The Typical Danish Brick- A Phase Analitycal Study by X-rays. *The Royal Veterinary and Agricultural High School of Denmark***,** 53-63.

JHA, S. N., NARSAIAH, K., BASEDIYA, A., SHARMA, R., JAISWAL, P., KUMAR, R. & BHARDWAJ, R. 2011. Measurement techniques and application of electrical properties for nondestructive quality evaluation of foods—a review. *Journal of food science and technology,* 48**,** 387-411.

JOHANSSON, T. B. & BURNHAM, L. 1993. *Renewable energy: sources for fuels and electricity*, Island press.

JOHARI, I., SAID, S., HISHAM, B., BAKAR, A. & AHMAD, Z. 2010. Effect of the change of firing temperature on microstructure and physical properties of clay bricks from Beruas (Malaysia). *Science of Sintering,* 42**,** 245-254.

JOHN, R. S., BATCHELOR, A. R., IVANOV, D., UDOUDO, O. B., JONES, D. A., DODDS, C. & KINGMAN, S. W. 2015. Understanding microwave induced sorting of porphyry copper ores. *Minerals Engineering,* 84**,** 77-87.

JONES, D., LELYVELD, T., MAVROFIDIS, S., KINGMAN, S. & MILES, N. 2002. Microwave heating applications in environmental engineering—a review. *Resources, conservation and recycling,* 34**,** 75-90.

JUNGE, K. 2000. Additives in the brick and tile industry. *ZI International,* 53**,** 25-26.

JUNKALA, M., SIN, P., TRNÍK, A., BACÍK, P. & STUBNA, I. 2013. Temperature dependence of bricks clay's sound velocity. *Available at:. Downloaded on August,* 23.

KAATZE, U. & BEHRENDS, R. 2002. Dielectric properties of water and aqueous solutions. *Technisches Messen,* 69**,** 5-11.

KADIR, A. A. & MOHAJERANI, A. 2015. Effect of heating rate on gas emissions and properties of fired clay bricks and fired clay bricks incorporated with cigarette butts. *Applied Clay Science,* 104**,** 269-276.

KARAMAN, S., ERSAHIN, S. & GUNAL, H. 2006. Firing temperature and firing time influence on mechanical and physical properties of clay bricks.

KATRIB, J., FOLORUNSO, O., DODDS, C., DIMITRAKIS, G. & KINGMAN, S. W. 2015. Improving the design of industrial microwave processing systems through prediction of the dielectric properties of complex multi-layered materials. *Journal of materials science,* 50**,** 7591-7599.

KATZ, J. D. 1992. Microwave sintering of ceramics. *Annual Review of Materials Science,* 22**,** 153-170.

KEELING, P. S. 1963. *The geology and mineralogy of brick clays*, Brick Development Association.

KHALAF, F. & DEVENNY, A. 2002. New tests for porosity and water absorption of fired clay bricks. *Journal of materials in civil engineering,* 14**,** 334-337.

KIM, J., MUN, S. C., KO, H.-U., KIM, K.-B., KHONDOKER, M. A. H. & ZHAI, L. 2012. Review of microwave assisted manufacturing technologies. *International Journal of Precision Engineering and Manufacturing,* 13**,** 2263-2272.

KIMREY JR, H. D. 1990. Method and device for microwave sintering large ceramic articles. Google Patents.

KISHIMOTO, A., YAMASHITA, K., TERANISHI, T., HAYASHI, H. & SANO, S. 2015. Effect of 24 GHz microwave heating on creep deformation of yttria partially stabilised zirconia ceramics with titania and tin oxide additives. *Ceramics International,* 41**,** 5785-5789.

KLEIN, C., HURLBUT, C. S. & DANA, J. D. 1993. *Manual of mineralogy*, Wiley.

KOBUSHESHE, J. 2010. *Microwave enhanced processing of ores.* University of Nottingham.

KORNMANN, M. 2007. *Clay bricks and rooftiles, manufacturing and properties*, lasim.

KOROVIN, S. D., ROSTOV, V. V., POLEVIN, S. D., PEGEL, I. V., SCHAMILOGLU, E., FUKS, M. I. & BARKER, R. J. 2004. Pulsed power-driven high-power microwave sources. *Proceedings of the IEEE,* 92**,** 1082-1095.

KØSTER, A. 2014. The brick industry in Denmark : An overview of the development of technology and energy consumption. *In:* INSTITUTE, D. T. (ed.). Aarhus: Danish Technological Institute.

KØSTER, A. 2017. Sustainable manufacture of brick and tiles with microwave energy.

KRASZEWSKI, A. 1996. *Microwave aquametry: electromagnetic wave interaction with water-containing materials*, IEEE.

KREIMEYER, R. 1987. Some notes on the firing colour of clay bricks. *Applied clay science,* 2**,** 175-183.

KULKARNI, N. G. & RAO, A. B. 2016. Carbon footprint of solid clay bricks fired in clamps of India. *Journal of Cleaner Production,* 135**,** 1396-1406.

KUTÍLEK, M. & NIELSEN, D. R. 1994. *Soil hydrology: texbook for students of soil science, agriculture, forestry, geoecology, hydrology, geomorphology and other related disciplines*, Catena Verlag.

LANDAU, L. D., LIFSHITZ, E. M., SYKES, J. B., BELL, J. S. & DILL, E. 1961. Electrodynamics of continuous media. AIP.

LASRI, J., RAMESH, P. D. & SCHÄCHTER, L. 2000. Energy conversion during microwave sintering of a multiphase ceramic surrounded by a susceptor. *Journal of the American Ceramic Society,* 83**,** 1465-1468.

LAURENT, A., OLSEN, S. I. & HAUSCHILD, M. Z. 2012. Limitations of carbon footprint as indicator of environmental sustainability. *Environmental science & technology,* 46**,** 4100-4108.

LAYSANDRA, L., SARI, M. W. M. K., SOETAREDJO, F. E., FOE, K., PUTRO, J. N., KURNIAWAN, A., JU, Y.-H. & ISMADJI, S. 2017. Adsorption and photocatalytic performance of bentonite-titanium dioxide composites for methylene blue and rhodamine B decoloration. *Heliyon,* 3**,** e00488.

LEAO, T. P., PERFECT, E. & TYNER, J. S. 2015. Evaluation of Lichtenecker's mixing model for predicting effective permittivity of soils at 50 MHz. *Transactions of the ASABE,* 58**,** 83-91.

LECOMTE, G. L., BONNET, J. P. & BLANCHART, P. 2007. A study of the influence of muscovite on the thermal transformations of kaolinite from room temperature up to 1,100° C. *Journal of Materials Science,* 42**,** 8745-8752.

LEE, K.-Y. & CASE, E. 1999. Microwave sintering of alumina matrix zirconia composites using a single-mode microwave cavity. *Journal of materials science letters,* 18**,** 201-203.

LERDPROM, W., ZAPATA-SOLVAS, E., JAYASEELAN, D. D., BORRELL, A., SALVADOR, M. D. & LEE, W. E. 2017. Impact of microwave processing on porcelain microstructure. *Ceramics International,* 43**,** 13765-13771.

LI, H.-X., LI, B.-W., DENG, L.-B., XU, P.-F., DU, Y.-S. & OUYANG, S.-L. 2018. Microwave-assisted processing of graded structural tailing glass-ceramics. *Journal of the European Ceramic Society,* 38**,** 2632-2638.

LICHTENECKER, K. & ROTHER, K. 1931. Die Herleitung des logarithmischen Mischungsgesetz es aus allgemeinen Prinzipien der stationären Strömung. *Physikalische Zeitschrift,* 32**,** 255-260.

LIKE, Q. & JUN, D. 2016. Analysis on the growth of different shapes of mineral microcracks in microwave field. *Frattura ed Integrità Strutturale,* 10**,** 342-351.

LIU, C., YANG, J., MA, H. & ZHANG, P. 2016. Microwave-assisted and conventional hydrothermal synthesis of potassium merlinoite from K-feldspar. *Advanced Powder Technology,* 27**,** 2121-2127.

LIU, Y.-H., YANG, C., LI, P.-Y. & LI, S.-Q. 2010. A new process of extracting vanadium from stone coal. *International Journal of Minerals, Metallurgy, and Materials,* 17**,** 381-388.

LIU, Y., MIN, F.-F., ZHU, J.-B. & ZHANG, M.-X. 2012. Effect of nanometer Al2O3 powder on microstructure and properties of alumina ceramics by microwave sintering. *Materials Science and Engineering: A,* 546**,** 328-331.

LOOYENGA, H. 1965. Dielectric constants of heterogeneous mixtures. *Physica,* 31**,** 401-406.

LU, G.-M., LI, Y.-H., HASSANI, F. & ZHANG, X. 2017. The influence of microwave irradiation on thermal properties of main rock-forming minerals. *Applied Thermal Engineering,* 112**,** 1523-1532.

LUDWIG, E. E. 1997. *Applied process design for chemical and petrochemical plants*, Gulf Professional Publishing.

LUTZ, R. P. 2001. Discounted cash flow methods. *Handbook of Industrial Engineering: Technology and Operations Management, Third Edition***,** 2331-2359.

MA, J., FANG, M., LI, P., ZHU, B., LU, X. & LAU, N. 1997. Microwave-assisted catalytic combustion of diesel soot. *Applied Catalysis A: General,* 159**,** 211-228.

MAITHEL, S. 2003. Energy utilization in brick kilns. *Indian Institute of Technology, Bombay*.

MAIZZA, G., GRASSO, S. & SAKKA, Y. 2014. Systematic study on densification of alumina fine powder during milliwave sintering at 28GHz. *Journal of Asian Ceramic Societies,* 2**,** 215-222.

MALCZYK, J. 2007. Determination of actual performance of a gas pycnometer versus quoted specifications. *In:* INC., I. (ed.) *Application Note.*

MALLET, P., GUERIN, C.-A. & SENTENAC, A. 2005. Maxwell-Garnett mixing rule in the presence of multiple scattering: Derivation and accuracy. *Physical Review B,* 72**,** 014205.

MANCHESTER, T. U. O. 2007. Carbon calculations over the life cycle of industrial activities. CCaLc 3.1.

MANCHESTER, T. U. O. 2016. CCaLC2 for Windows Manual.

MANDAL, A. K. & SEN, R. 2017. An overview on microwave processing of material: A special emphasis on glass melting. *Materials and Manufacturing Processes,* 32**,** 1-20.

MANLEY, D. 2016. Brick Sustainability Report 2016. London: The Brick Development Association.

MARCUVITZ, N. 1951. *Waveguide handbook*, Iet.

MARKHAM, D. 2015. The Leading Sources of Clean Energy: Wind, Solar, Hydropower & Biomass. *Renewable Energy World*.

MARLAND, S., MERCHANT, A. & ROWSON, N. 2001. Dielectric properties of coal. *Fuel,* 80**,** 1839-1849.

MARTÍNEZ-GONZÁLEZ, G. & JIMÉNEZ-ISLAS, H. 2014. Experimental study of the firing of red clay bricks using liquefied petroleum gas. *Journal of Scientific & Industrial Research,* 73**,** 661-666.

MARTINEZ, J., VOLZONE, C. & GARRIDO, L. 2017. Thermal transformations up to 1200° C of Al-pillared montmorillonite precursors prepared by different OH–Al polymers. *Journal of Thermal Analysis and Calorimetry,* 128**,** 61-69.

MARTINOT, E. 2005. Renewables 2005: Global status report. *Washington, DC: Worldwatch Institute*.

MCCONVILLE, C. J. & LEE, W. E. 2005. Microstructural development on firing illite and smectite clays compared with that in kaolinite. *Journal of the American Ceramic Society,* 88**,** 2267-2276.

MEDEIROS, F. D. S. C., MENEZES, R. R., NEVES, G. A., DE LIMA SANTANA, L. N., FERREIRA, H. S., DE LIMA, D. S. G. & DE LIMA, S. J. G. 2015. Microwave-assisted sintering of dental porcelains. *Ceramics International,* 41**,** 7501-7510.

MEHDIZADEH, M. 2015. *Microwave/RF applicators and probes: for material heating, sensing, and plasma generation*, William Andrew.

MELO, V., SINGH, B., SCHAEFER, C., NOVAIS, R. & FONTES, M. 2001. Chemical and mineralogical properties of kaolinite-rich Brazilian soils. *Soil Science Society of America Journal,* 65**,** 1324-1333.

MENEZES, R. & KIMINAMI, R. 2008. Microwave sintering of alumina–zirconia nanocomposites. *Journal of Materials Processing Technology,* 203**,** 513-517.

MENEZES, R. R., SOUTO, P. M. & KIMINAMI, R. H. G. A. 2007. Microwave hybrid fast sintering of porcelain bodies. *Journal of Materials Processing Technology,* 190**,** 223-229.

MENKE, D. M., DAVIS, G. A. & VIGON, B. W. 1996. *Evaluation of life-cycle assessment tools*, Environment Canada Gatineau, Canada.

MEREDITH, R. J. 1998. *Engineers' handbook of industrial microwave heating*, IET.

MESEGUER, S., JORDÁN, M. M., PARDO, F. & SANFELIU, T. 2011. Geology and application of clays used in Castellon ceramic cluster (NE, Spain). *Journal of Geography and Geology,* 3**,** p132.

METAXAS, A. C. & MEREDITH, R. J. 1983. *Industrial microwave heating,* London, Peter Perigrinus.

METI 2016. G7 Energy Ministerial Meeting. Kitakyushu Initiative on Energy Security for Global Growth: Joint Statement. Kitakyushu.

METI 2017. G7 Energy Ministerial Meeting. Taormina Roadmap for a Gender-Responsive Economic Environment. Taormina.

MILLOT, G. 1970. *Geology of clays : weathering, sedimentology, geochemistry,* New York and berlin, Springer-Verlag

MINAET 2011. VI Plan Nacional de Energia 2012-2030. *In:* MINISTERIO DE AMBIENTE, E. Y. T.-D. S. D. E. (ed.).

MINGOS, D. & BAGHURST, D. 1991. Applications of microwave dielectric heating effects to synthetic problems in chemistry. *Chemical Society reviews,* 20**,** 1-47.

MISHRA, P., UPADHYAYA, A. & SETHI, G. 2006. Modeling of microwave heating of particulate metals. *Metallurgical and Materials Transactions B,* 37**,** 839-845.

MIZUNO, M., OBATA, S., TAKAYAMA, S., ITO, S., KATO, N., HIRAI, T. & SATO, M. 2004. Sintering of alumina by 2.45 GHz microwave heating. *Journal of the European Ceramic Society,* 24**,** 387-391.

MOESGAARD, M. 2015. Sustainable manufacture of brick and tiles with microwave energy: Firing of bricks in tunnel kilns. Danish Technological Institute.

MOHAJERANI, A. Physical and mechanical properties of fired clay bricks incorporated with cigarette butts: Comparison between slow and fast heating rates. Applied Mechanics and Materials, 2013. Trans Tech Publ, 201-204.

MOHSEN, Q. & EL-MAGHRABY, A. 2010. Characterization and assessment of Saudi clays raw material at different area. *Arabian Journal of Chemistry,* 3**,** 271-277.

MONTEIRO, J., VALENTE, M., SANTOS, T., COSTA, L. & SOUSA, J. Microwave radiation: an alternative method to sinter utilitarian porcelain. Microwave & Optoelectronics Conference (IMOC), 2011 SBMO/IEEE MTT-S International, 2011. IEEE, 561-564.

MOORE, D. & REYNOLDS JR, R. 1997. X-ray Diffraction and the Identification and Analysis of Clay Minerals. Oxford University Press, Oxford, England.

MOORE, D. M. & REYNOLDS, R. C. 1989. *X-ray Diffraction and the Identification and Analysis of Clay Minerals*, Oxford university press Oxford.

MORGAN, D. 1993. Thermal analysis—including evolved gas analysis—of clay raw materials. *Applied clay science,* 8**,** 81-89.

MORTENSEN, T. 2014. Firing of clay bricks.

MURAD, E. & WAGNER, U. 1998. Clays and clay minerals: the firing process. *Hyperfine Interactions,* 117**,** 337-356.

MURRAY, H. H. 1993. *Kaolin genesis and utilization: a collection of papers presented at the Keller'90 Kaolin Symposium*, The Clay Minerals Society (CMS).

MURRAY, H. H. 2006. *Applied clay mineralogy: occurrences, processing and applications of kaolins, bentonites, palygorskitesepiolite, and common clays*, Elsevier.

NAVARRO, L. C. R., MENEZES, R. R. & KIMINAMI, R. H. G. A. 2014. Microwave sintering of mullite-Al2O3 from kaolin precursor. *Materials Research,* 17**,** 1575-1580.

NELSON, S., LINDROTH, D. & BLAKE, R. 1989. Dielectric properties of selected and purified minerals at 1 to 22 GHz. *Journal of microwave power and electromagnetic energy,* 24**,** 213-220.

NELSON, S. O. 1994. Measurement of microwave dielectric properties of particulate materials. *Journal of food engineering,* 21**,** 365-384.

NELSON, S. O. 2005. Density-permittivity relationships for powdered and granular materials. *Instrumentation and Measurement, IEEE Transactions on,* 54**,** 2033-2040.

NELSON, S. O. & YOU, T. S. 1990. Relationships between microwave permittivities of solid and pulverised plastics. *Journal of physics D: applied physics,* 23**,** 346.

NICOLAU, V. D. P. & DADAM, A. P. 2009. Numerical and experimental thermal analysis of a tunnel kiln used in ceramic production. *Journal of the Brazilian Society of Mechanical Sciences and Engineering,* 31**,** 297-304.

NIU, G., RUDITSKIY, A., VARA, M. & XIA, Y. 2015. Toward continuous and scalable production of colloidal nanocrystals by switching from batch to droplet reactors. *Chemical Society Reviews,* 44**,** 5806-5820.

NJINDAM, O., NJOYA, D., MACHE, J., MOUAFON, M., MESSAN, A. & NJOPWOUO, D. 2018. Effect of glass powder on the technological properties and microstructure of clay mixture for porcelain stoneware tiles manufacture. *Construction and Building Materials,* 170**,** 512-519.

NOORMAN, K. J. & UITERKAMP, T. S. 2014. *Green households: domestic consumers, the environment and sustainability*, Routledge.

NPL 2003. A Guide to characterisation of dielectric materials at RF and microwave frequencies. London: National Physical Laboratory and the Institute of Measurement & Control.

NPL 2017. Coaxial Sensors for SAR. *In:* CONTROL, N. P. L. A. T. I. O. M. (ed.).

NÜCHTER, M., ONDRUSCHKA, B., BONRATH, W. & GUM, A. 2004. Microwave assisted synthesis–a critical technology overview. *Green chemistry,* 6**,** 128-141.

OBAMA, B. 2017. The irreversible momentum of clean energy. *Science,* 355**,** 126-129.

OFCOM 2017. United Kingdom table of radio frequency allocations 9kHz-105GHz.

OGHBAEI, M. & MIRZAEE, O. 2010. Microwave versus conventional sintering: a review of fundamentals, advantages and applications. *Journal of Alloys and Compounds,* 494**,** 175-189.

ORESKES, N. 2018. The scientific consensus on climate change: How do we know we're not wrong? *Climate Modelling.* Springer.

ORZECHOWSKI, K., SŁONKA, T. & GŁOWINSKI, J. 2006. Dielectric properties of intercalated kaolinite. *Journal of Physics and Chemistry of Solids,* 67**,** 915-919.

OSEPCHUK, J. M. 2002. Microwave power applications. *IEEE Transactions on Microwave Theory and Techniques,* 50**,** 975-985.

OSMAN, M. A. & SUTER, U. W. 2000. Determination of the cation-exchange capacity of muscovite mica. *Journal of colloid and interface science,* 224**,** 112-115.

OTI, J., KINUTHIA, J. & BAI, J. 2009. Engineering properties of unfired clay masonry bricks. *Engineering Geology,* 107**,** 130-139.

OVRI, J. E. O. & NDUKWE, A. I. 2014. The Densification and Diametral Compression Strength of Isi-Ogwuta Clay. *American Journal of Engineering Research,* 3**,** 18-26.

PANNEERSELVAM, M. & RAO, K. 2003. Novel microwave method for the synthesis and sintering of mullite from kaolinite. *Chemistry of materials,* 15**,** 2247-2252.

PARSONS, A., INGLETHORPE, S., MORGAN, D. & DUNHAM, A. 1997. Evolved gas analysis (EGA) of brick clays. *Journal of Thermal Analysis and Calorimetry,* 48**,** 49-62.

PAVÍA, S. 2006. THE DETERMINATION OF BRICK PROVENANCE AND TECHNOLOGY USING ANALYTICAL TECHNIQUES FROM THE PHYSICAL SCIENCES*. *Archaeometry,* 48**,** 201-218.

PECK, R., OLSEN, C. & DEVORE, J. L. 2015. *Introduction to statistics and data analysis*, Cengage Learning.

PENDOLA, M. & SAHA, S. CAD-system dental ceramics sintering using microwaves. Bioengineering Conference (NEBEC), 2014 40th Annual Northeast, 2014. IEEE, 1-2.

PENG, Z. & HWANG, J.-Y. 2015. Microwave-assisted metallurgy. *International Materials Reviews,* 60**,** 30-63.

PEREIRA, D., BIASIBETTI, G., CAMERINI, R. & PEREIRA, A. 2014. Sintering of mullite by different methods. *Materials and Manufacturing Processes,* 29**,** 391-396.

PEREIRA, D., SANTOS, T., NOGUEIRA, R., COSTA, L. C. & ALBERTO, N. 2016. High temperatures (> 1000° C) monitoring during the sintering process in microwave oven using RFBGs. *Optical and Quantum Electronics,* 48**,** 304.

PÉREZ-VILLAREJO, L., ELICHE-QUESADA, D., IGLESIAS-GODINO, F. J., MARTÍNEZ-GARCÍA, C. & CORPAS-IGLESIAS, F. A. 2012. Recycling of ash from biomass incinerator in clay matrix to produce ceramic bricks. *Journal of Environmental Management,* 95**,** S349-S354.

PETERS, T. & IBERG, R. 1978. Mineralogical changes during firing of calcium-rich brick clays. *Ceramic Bulletin,* 57**,** 503-509.

PETRI JR, I., DOS SANTOS, J. M., ROSSI, A. S., PEREIRA, M. S., DUARTE, C. R. & ATAÍDE, C. H. Influence of rock chemical composition in microwave heating and decontamination of drill cuttings. Materials Science Forum, 2017. Trans Tech Publ, 469-473.

PEVEAR, D. R. 1989. *Quantitative mineral analysis of clays*, Clay Minerals Society.

POLDER, D. & VAN SANTEN, J. 1946. The effective permeability of mixtures of solids. *Physica,* 12**,** 257-271.

POST, E. & HENDERSON, J. B. Characterization of Two Different Clay Materials by Thermogravimetry (TG), Differential Scanning Calorimetry (DSC), Dilatometry (DIL) and Mass Spectrometry (MS)-12215. Germany WM Conference, 2012.

POTTS, P. J. 1987. *A handbook of silicate rock analysis*, Springer Science & Business Media.

PRICE, D. M. & JARRATT, M. 2002. Thermal conductivity of PTFE and PTFE composites. *Thermochimica Acta,* 392-393**,** 231-236.

PÜSCHNER. 2015. *Penetration Depths* [Online]. PÜSCHNER MicrowavePowerSystems. Available: http://www.pueschner.com/en/microwave-technology/penetration-depths [Accessed 3 / 6 / 2017].

QIN, L.-K. & DAI, J. 2015. Temperature Distribution and Influential Factors for Ore Particles under Microwave Irradiation. *Mining and Metallurgical Engineering,* 3**,** 032.

QUINTEIRO, P., ALMEIDA, M., DIAS, A. C., ARAÚJO, A. & ARROJA, L. 2014. The carbon footprint of ceramic products. *Assessment of Carbon Footprint in Different Industrial Sectors, Volume 1.* Springer.

QUINTEIRO, P., ARAÚJO, A., OLIVEIRA, B., DIAS, A. C. & ARROJA, L. 2012. The carbon footprint and energy consumption of a commercially produced earthenware ceramic piece. *Journal of the European Ceramic Society,* 32**,** 2087-2094.

RANKIN, D. & SINGH, R. 1985. Effect of clay and salinity on the dielectric properties of rock. *Journal of Geophysical Research: Solid Earth,* 90**,** 8793-8800.

REDDY, M. & ADAMS, S. 2017. Molten salt synthesis and characterization of fast ion conductor Li6. 75La3Zr1. 75Ta0. 25O12. *Journal of Solid State Electrochemistry,* 21**,** 2921-2928.

REEVES, G. M., SIMS, I. & CRIPPS, J. Clay materials used in construction. 2006. Geological Society of London.

REGALADO, C. 2004. A physical interpretation of logarithmic TDR calibration equations of volcanic soils and their solid fraction permittivity based on Lichtenecker's mixing formulae. *Geoderma,* 123**,** 41-50.

REGIER, M., KNOERZER, K. & SCHUBERT, H. 2016. *The microwave processing of foods*, Woodhead publishing.

RIEDER, M., CAVAZZINI, G., D'YAKONOV, Y. S., FRANK-KAMENETSKII, V. A., GOTTARDI, G., GUGGENHEIM, S., KOVAL', P. V., MUELLER, G., NEIVA, A. M. & RADOSLOVICH, E. W. 1998. Nomenclature of the micas. *Clays and clay minerals,* 46**,** 586-595.

ROBINSON, D. & FRIEDMAN, S. 2003. A method for measuring the solid particle permittivity or electrical conductivity of rocks, sediments, and granular materials. *Journal of Geophysical Research: Solid Earth,* 108.

ROBINSON, J., BINNER, E., SAEID, A., AL-HARAHSHEH, M. & KINGMAN, S. 2014. Microwave processing of oil sands and contribution of clay minerals. *Fuel,* 135**,** 153-161.

ROBINSON, J., KINGMAN, S., LESTER, E. & YI, C. 2012. Microwave remediation of hydrocarbon-contaminated soils–Scale-up using batch reactors. *Separation and purification technology,* 96**,** 12-19.

ROBINSON, J., KINGMAN, S. & ONOBRAKPEYA, O. 2008. Microwave-assisted stripping of oil contaminated drill cuttings. *Journal of environmental management,* 88**,** 211-218.

RODRIGUEZ-NAVARRO, C., RUIZ-AGUDO, E., LUQUE, A., RODRIGUEZ-NAVARRO, A. B. & ORTEGA-HUERTAS, M. 2009. Thermal decomposition of calcite: Mechanisms of formation and textural evolution of CaO nanocrystals. *American Mineralogist,* 94**,** 578-593.

RODRIGUEZ OYARZUN, J. 2017. High temperature microwave applicator technologies.

RYAN, P. A. & RYAN, G. P. 2002. Capital budgeting practices of the Fortune 1000: how have things changed? *Journal of business and management,* 8**,** 355.

RYBAKOV, K. I., OLEVSKY, E. A. & KRIKUN, E. V. 2013. Microwave sintering: fundamentals and modeling. *Journal of the American Ceramic Society,* 96**,** 1003-1020.

RYYNÄNEN, S. 1995. The electromagnetic properties of food materials: a review of the basic principles. *Journal of Food Engineering,* 26**,** 409-429.

SABBAH, R., XU-WU, A., CHICKOS, J., LEITÃO, M. P., ROUX, M. & TORRES, L. 1999. Reference materials for calorimetry and differential thermal analysis. *Thermochimica Acta,* 331**,** 93-204.

SADIK, C., EL AMRANI, I.-E. & ALBIZANE, A. 2014. Recent advances in silica-alumina refractory: A review. *Journal of Asian Ceramic Societies,* 2**,** 83-96.

SAFFER, D. M., FRYE, K. M., MARONE, C. & MAIR, K. 2001. Laboratory results indicating complex and potentially unstable frictional behavior of smectite clay. *Geophysical Research Letters,* 28**,** 2297-2300.

SAHRAOUI, T., BELHOUCHET, H., HERAIZ, M., BRIHI, N. & GUERMAT, A. 2016. The effects of mechanical activation on the sintering of mullite produced from kaolin and aluminum powder. *Ceramics International,* 42**,** 12185-12193.

SAIREM 2018a. 100 kW, 915 MHz MICROWAVE GENERATOR Ref: GLP1000KSM56T400ME2IRG3. *In:* SAIREM (ed.).

SAIREM 2018b. Quotation for a 6kW 2.45 GHz microwave generator. *In:* SAIREM (ed.).

SALAKJANI, N. K., NIKOLOSKI, A. N. & SINGH, P. 2017. Mineralogical transformations of spodumene concentrate from Greenbushes, Western Australia. Part 2: Microwave heating. *Minerals Engineering,* 100**,** 191-199.

SALTAS, V., VALLIANATOS, F. & TRIANTIS, D. 2008. Dielectric properties of non-swelling bentonite: the effect of temperature and water saturation. *Journal of Non-Crystalline Solids,* 354**,** 5533-5541.

SALTIEL, C. & DATTA, A. K. 1999. Heat and mass transfer in microwave processing. *Advances in heat transfer,* 33**,** 1-94.

SANDERS, J. P. & GALLAGHER, P. K. 2002. Kinetic analyses using simultaneous TG/DSC measurements: Part I: decomposition of calcium carbonate in argon. *Thermochimica Acta,* 388**,** 115-128.

SANTANA, L., GOMES, J., NEVES, G., LIRA, H., MENEZES, R. & SEGADÃES, A. 2014. Mullite formation from bentonites containing kaolinite: effect of composition and synthesis parameters. *Applied Clay Science,* 87**,** 28-33.

SANTANA, L. N., GOMES, J., MENEZES, R. R., NEVES, G. A., LIRA, H. L. & SEGADÃES, A. M. 2017. Microstructure development in clays upon heat treatment: Kinetics and equilibrium. *Applied Clay Science,* 135**,** 325-332.

SANTOS, T., COSTA, L., HENNETIER, L., VALENTE, M., MONTEIRO, J. & SOUSA, J. 2013. Microwave processing of porcelain tableware using a multiple generator configuration. *Applied Thermal Engineering,* 50**,** 677-682.

SARKAR, S., BANDYOPADHYAY, S., LARBOT, A. & CERNEAUX, S. 2012. New clay–alumina porous capillary supports for filtration application. *Journal of membrane science,* 392**,** 130-136.

SATAPATHY, L. 2009. Microwave assisted sintering of high voltage porcelain materials and its characterization. *J. Ceram. Process. Res,* 10**,** 637-642.

SAWIN, J. L., SVERRISSON, F., SEYBOTH, K., ADIB, R., MURDOCK, H. E., LINS, C., EDWARDS, I., HULLIN, M., NGUYEN, L. H. & PRILLIANTO, S. S. 2013. Renewables 2017 Global Status Report.

SCHELLER, M., WIETZKE, S., JANSEN, C. & KOCH, M. 2009. Modelling heterogeneous dielectric mixtures in the terahertz regime: a quasi-static effective medium theory. *Journal of Physics D: Applied Physics,* 42**,** 065415.

SEINFELD, J. H. & PANDIS, S. N. 2016. *Atmospheric chemistry and physics: from air pollution to climate change*, John Wiley & Sons.

SEN, P., SCALA, C. & COHEN, M. 1981. A self-similar model for sedimentary rocks with application to the dielectric constant of fused glass beads. *Geophysics,* 46**,** 781-795.

SENGUPTA, S., DATTA, A. & DUTTAGUPTA, S. 2007. Exergy analysis of a coal-based 210 MW thermal power plant. *International Journal of Energy Research,* 31**,** 14-28.

SHAH, D. & SHROFF, A. 2003. *Soil mechanics and geotechnical engineering*, CRC Press.

SHAHEEN, M. S., EL-MASSRY, K. F., EL-GHORAB, A. H. & ANJUM, F. M. 2012. Microwave applications in thermal food processing. *The Development and Application of Microwave Heating.* InTech.

SHANG, X., CHEN, J., ZHANG, W., PENG, J., CHEN, H., GUO, S. & CHEN, G. 2014. Dimension optimization for silica sand based on the analysis of dynamic absorption efficiency in microwave drying. *Drying technology,* 32**,** 1608-1613.

SHEEN, J. 2005. Study of microwave dielectric properties measurements by various resonance techniques. *Measurement,* 37**,** 123-130.

SHEN, B., SHIH, A. J. & XIAO, G. 2011. A heat transfer model based on finite difference method for grinding. *Journal of Manufacturing Science and Engineering,* 133**,** 031001.

SHIMODA, S. & SUDO, T. 1960. An interstratified mixture of mica clay minerals. *American Mineralogist,* 45**,** 1069-1077.

SHUTE, M. R., DAINES, P. N. & MEREDITH, R. J. 1995. Microwave ovens having conductive conveyor band and applicator launch section to provide parallel plate electric field. Google Patents.

SIHVOLA, A. 1999. *Electromagnetic mixing formulas and applications*, The Institution of Electrical Engineers, London, UK.

SIHVOLA, A. 2000. Mixing rules with complex dielectric coefficients. *Subsurface Sensing Technologies and Applications,* 1**,** 393-415.

SIMONSON, R. W. 1959. Outline of a generalized theory of soil genesis. *Soil Science Society of America Journal,* 23**,** 152-156.

SIMPKIN, R. 2010. Derivation of Lichtenecker's logarithmic mixture formula from Maxwell's equations. *IEEE Transactions on Microwave Theory and Techniques,* 58**,** 545-550.

SINGER, F. 1963. *Industrial ceramics*, Springer.

SINGER, S., DENRUYTER, J.-P. & YENER, D. 2017. The energy report: 100% renewable energy by 2050. *Towards 100% Renewable Energy.* Springer.

SINGH, R. & RANKIN, D. 1986. Effect of clay on dielectric properties of oil-sand media. *Journal of Geophysical Research: Solid Earth,* 91**,** 3877-3882.

SINGH, S., GUPTA, D. & JAIN, V. 2016. An Energy Efficient Processing Route for Advance Ceramic Composites Using Microwaves. *Advanced Ceramic Materials***,** 97-143.

SMITH, J. & BROWN, W. 1988. *Feldspar Minerals Volume 1 Crystal Structures, Physical, Chemical, and Microtextural properties*, Springer Science & Business Media.

SNELLINGS, R., CIZER, Ö., HORCKMANS, L., DURDZIŃSKI, P. T., DIERCKX, P., NIELSEN, P., VAN BALEN, K. & VANDEWALLE, L. 2016. Properties and pozzolanic reactivity of flash calcined dredging sediments. *Applied Clay Science,* 129**,** 35-39.

SNYDER, R. & BISH, D. L. 1989. Quantitative analysis. *Reviews in Mineralogy and Geochemistry,* 20**,** 101-144.

SONG, C., WANG, Y., WANG, S., CUI, Z., XU, Y. & ZHU, H. 2016a. Non-uniformity investigation in a combined thermal and microwave drying of silica gel. *Applied Thermal Engineering,* 98**,** 872-879.

SONG, L., LI, Z., LI, G., LI, Y., JIANG, S., HUANG, Y. & SHEN, Y. 2016b. Fabrication, sintering and characterization of cordierite glass–ceramics for low temperature co-fired ceramic substrates from kaolin. *Journal of Materials Science: Materials in Electronics,* 27**,** 8504-8511.

SOUZA, G. D., SOUSA, S., TERRONES, L. & HOLANDA, J. D. 2005. Mineralogical analysis of Brazilian ceramic sedimentary clays used in red ceramic. *Cerâmica,* 51**,** 382-387.

SRIVASTAVA, G. P. & GUPTA, V. L. 2006. *Microwave devices and circuit design*, PHI Learning Pvt. Ltd.

STERNBERG, B. K. & LEVITSKAYA, T. M. 2001. Electrical parameters of soils in the frequency range from 1 kHz to 1 GHz, using lumped-circuit methods. *Radio Science,* 36**,** 709-719.

STEVENS, S., HAND, R. & SHARP, J. 1997. Temperature dependence of the cristobalite α-β inversion. *Journal of Thermal Analysis and Calorimetry,* 49**,** 1409-1415.

STOICA-GUZUN, A., STROESCU, M., JINGA, S. I., JIPA, I. M. & DOBRE, T. 2013. Microwave assisted synthesis of bacterial cellulose-calcium carbonate composites. *Industrial crops and products,* 50**,** 414-422.

STUCKI, J. 1990. *Thermal analysis in clay science*, Clay Minerals Society.

SUN, S., JIANG, Y., YU, L., LI, F., YANG, Z., HOU, T., HU, D. & XIA, M. 2006. Enhanced photocatalytic activity of microwave treated TiO2 pillared montmorillonite. *Materials Chemistry and Physics,* 98**,** 377-381.

SUTTON, W. H. Microwave processing of ceramics-an overview. MRS Proceedings, 1992. Cambridge Univ Press, 3.

TAURINO, R., KARAMANOV, A., ROSA, R., KARAMANOVA, E., BARBIERI, L., ATANASOVA-VLADIMIROVA, S., AVDEEV, G. & LEONELLI, C. 2017. New ceramic materials from MSWI bottom ash obtained by an innovative microwave-assisted sintering process. *Journal of the European Ceramic Society,* 37**,** 323-331.

TAYLOR, J. 1997. *Introduction to error analysis, the study of uncertainties in physical measurements*.

TEIXEIRA, S., DE SOUZA, S. & MOURA, C. 2001. Mineralogical characterization of clays used in the structural ceramic industry in west of S. Paulo State, Brazil. *Cerâmica,* 47**,** 204-207.

THOSTENSON, E. & CHOU, T.-W. 1999. Microwave processing: fundamentals and applications. *Composites Part A: Applied Science and Manufacturing,* 30**,** 1055-1071.

THUAULT, A., SAVARY, E., BAZIN, J. & MARINEL, S. 2014. Microwave sintering of large size pieces with complex shape. *Journal of Materials Processing Technology,* 214**,** 470-476.

TIKHONOV, V. V., BOYARSKII, D. A., POLYAKOVA, O. N., DZARDANOV, A. L. & GOLTSMAN, G. N. 2010. Radiophysical and Dielectric Properties of Ore Minerals in 12--145 GHz Frequency Range. *Progress In Electromagnetics Research B,* 25**,** 349-367.

TINGA, W. 1969. Dielectric properties of Douglas fir at 2.45 GHz. *J. Microwave Power,* 4**,** 162-164.

TIWARI, A., GERHARDT, R. A. & SZUTKOWSKA, M. 2016. *Advanced Ceramic Materials*, John Wiley & Sons.

TRABELSI, S. & NELSON, S. O. 2006. Temperature-dependent behaviour of dielectric properties of bound water in grain at microwave frequencies. *Measurement Science and Technology,* 17**,** 2289.

TUHKALA, M., JUUTI, J. & JANTUNEN, H. 2013. Method to characterize dielectric properties of powdery substances. *Journal of Applied Physics,* 114**,** 014108.

TUNCER, E. 2005. The Landau-Lifshitz/Looyenga dielectric mixture expression and its self-similar fractal nature. *arXiv preprint cond-mat/0503750*.

UN 1998. Kyoto protocol to the united nations framework convention on climate change.

UN 2015. World Population Prospects, the 2015 Revision. New York: United Nations Department of Economic and Social Affairs.

UNIDO 2015. Industrial Development Report 2016. The Role of Technology and Innovation in Inclusive and Sustainable Industrial Development. Vienna: United Nations Industrial Development Organization.

VADIVAMBAL, R. & JAYAS, D. 2010. Non-uniform temperature distribution during microwave heating of food materials—A review. *Food and Bioprocess Technology,* 3**,** 161-171.

VELAZQUEZ-MARTI, B., GRACIA-LOPEZ, C. & PLAZA-GONZALEZ, P. 2005. Determination of dielectric properties of agricultural soil. *Biosystems engineering,* 91**,** 119-125.

VELDE, B. 1977. *Clays and clay minerals in natural and synthetic systems*, Elsevier.

VELDE, B. 2013. *Origin and mineralogy of clays: clays and the environment*, Springer Science & Business Media.

VICTOR, D. G., JAFFE, A. M. & HAYES, M. H. 2006. *Natural gas and geopolitics: From 1970 to 2040*, Cambridge University Press.

VIEIRA, C., SANCHEZ, R. & MONTEIRO, S. 2008. Characteristics of clays and properties of building ceramics in the state of Rio de Janeiro, Brazil. *Construction and Building Materials,* 22**,** 781-787.

VISSING, L. 2003. Energy consumption in the Danish brick industry. *ZI International,* 56**,** 21-25.

VISSING, L. 2004. Red firing clays for the danish brick industry. *ZI International,* 57**,** 24-28.

VON HIPPEL, A. R. & MORGAN, S. 1955. Dielectric materials and applications. *Journal of The Electrochemical Society,* 102**,** 68C-68C.

WANG, J.-P., ZHANG, Y.-M., HUANG, J. & LIU, T. 2018a. Kinetic and Mechanism Study of Vanadium Acid Leaching from Black Shale Using Microwave Heating Method. *JOM,* 70**,** 1031-1036.

WANG, J., ZHANG, Y., LIU, T. & HUANG, J. 2018b. Evaluation of Microwave Intensified Vanadium Bearing-High Carbonaceous Shale Acid Extraction Process. *Minerals,* 8**,** 113.

WANG, L. & QU, J. J. 2009. Satellite remote sensing applications for surface soil moisture monitoring: A review. *Frontiers of Earth Science in China,* 3**,** 237-247.

WATERS, L. J., BEDFORD, S. & PARKES, G. M. 2011. Controlled microwave processing applied to the pharmaceutical formulation of ibuprofen. *AAPS PharmSciTech,* 12**,** 1038-1043.

WEAVER, C. E. & POLLARD, L. D. 2011. *The chemistry of clay minerals*, Elsevier.

WEIDLER, P. G. & FRIEDRICH, F. 2007. Determination of the refractive index of particles in the clay and sub-micrometer size range. *American Mineralogist,* 92**,** 1130-1132.

WEISSMAN, S. 2016. Natural Gas as a Bridge Fuel Measuring the Bridge. Center for Sustainable Energy.

WHEELER, B. D. 1983. Chemical analysis of Portland cement by energy dispersive X-ray fluorescence. *Cement, concrete and aggregates,* 5**,** 123-127.

WILSON, M. J. 1987. *A Handbook of determinative methods in clay mineralogy*, Blackie. Chapman and Hall.

WRÓBLEWSKI, R. & CERAN, B. Thermogravimetric analysis in the study of solid fuels. E3S Web of Conferences, 2016. EDP Sciences, 00109.

XI, Y., DING, Z., HE, H. & FROST, R. L. 2004. Structure of organoclays—an X-ray diffraction and thermogravimetric analysis study. *Journal of colloid and interface science,* 277**,** 116-120.

XIE, Z., HUANG, Y., WU, J. & ZHENG, L. 1995. Microwave debinding of a ceramic injection moulded body. *Journal of materials science letters,* 14**,** 794-795.

YOSHIKAWA, N. 2011. *Recent studies on fundamentals and application of microwave processing of materials*, INTECH Open Access Publisher.

YOUNG, K. & FREDERIKSE, H. 1973. Compilation of the static dielectric constant of inorganic solids. *Journal of Physical and Chemical Reference Data,* 2**,** 313-410.

YU, S.-H., LI, H., YAO, Q.-Z., ZHOU, G.-T. & FU, S.-Q. 2015. Preparation of mesoporous calcite with hierarchical architectures. *Materials Letters,* 160**,** 167-170.

YUAN, Y.-Z., ZHANG, Y.-M., LIU, T. & CHEN, T.-J. 2017. Microwave roasting with size grading based on the influence of carbon on vanadium extraction from stone coal via microwave roasting-acid leaching. *RSC Advances,* 7**,** 1387-1395.

ZGALAT-LOZINSKII, O. 2015. Structure of Si3N4–Y2O3–Al2O3 and TiN–AlN composites consolidated in microwaves (2.45 GHz). *Powder Metallurgy and Metal Ceramics,* 54**,** 60-66.

ZHANG, B., LI, J., SUN, J., ZHANG, S., ZHAI, H. & DU, Z. 2002. Nanometer silicon carbide powder synthesis and its dielectric behavior in the GHz range. *Journal of the European Ceramic Society,* 22**,** 93-99.

ZHANG, H. 2011. *Building materials in civil engineering*, Elsevier.

ZHANG, J., LUO, Y., LIAO, C., XIONG, F., LI, X., SUN, L. & LI, X. 2017. Theoretical investigation of temperature distribution uniformity in wood during microwave drying in three-port feeding circular resonant cavity. *Drying technology,* 35**,** 409-416.

ZHANG, L. 2013. Production of bricks from waste materials–A review. *Construction and building materials,* 47**,** 643-655.

ZHANG, Z., QIAO, X. & YU, J. 2014. Microwave selective heating-enhanced reaction rates for mullite preparation from kaolinite. *RSC Advances,* 4**,** 2640-2647.

ZHAO, C., VLEUGELS, J., GROFFILS, C., LUYPAERT, P. & VAN DER BIEST, O. 2000. Hybrid sintering with a tubular susceptor in a cylindrical single-mode microwave furnace. *Acta materialia,* 48**,** 3795-3801.

ZHOU, H., QIAO, X. & YU, J. 2013. Influences of quartz and muscovite on the formation of mullite from kaolinite. *Applied Clay Science,* 80**,** 176-181.

ZHU, H., NEWTON, R. & KLEPPA, O. 1994. Enthalpy of formation of wollastonite (CaSiO 3) and anorthite (CaAl 2 Si 2 O 8) by experimental phase equilibrium measurements and high-temperature solution colorimetry. *American Mineralogist,* 79**,** 134-144.

ŽIŽLAVSKÝ, O. 2014. Net present value approach: method for economic assessment of innovation projects. *Procedia-Social and Behavioral Sciences,* 156**,** 506-512.

APPENDICES

Appendix A: X-ray diffraction spectra of clays

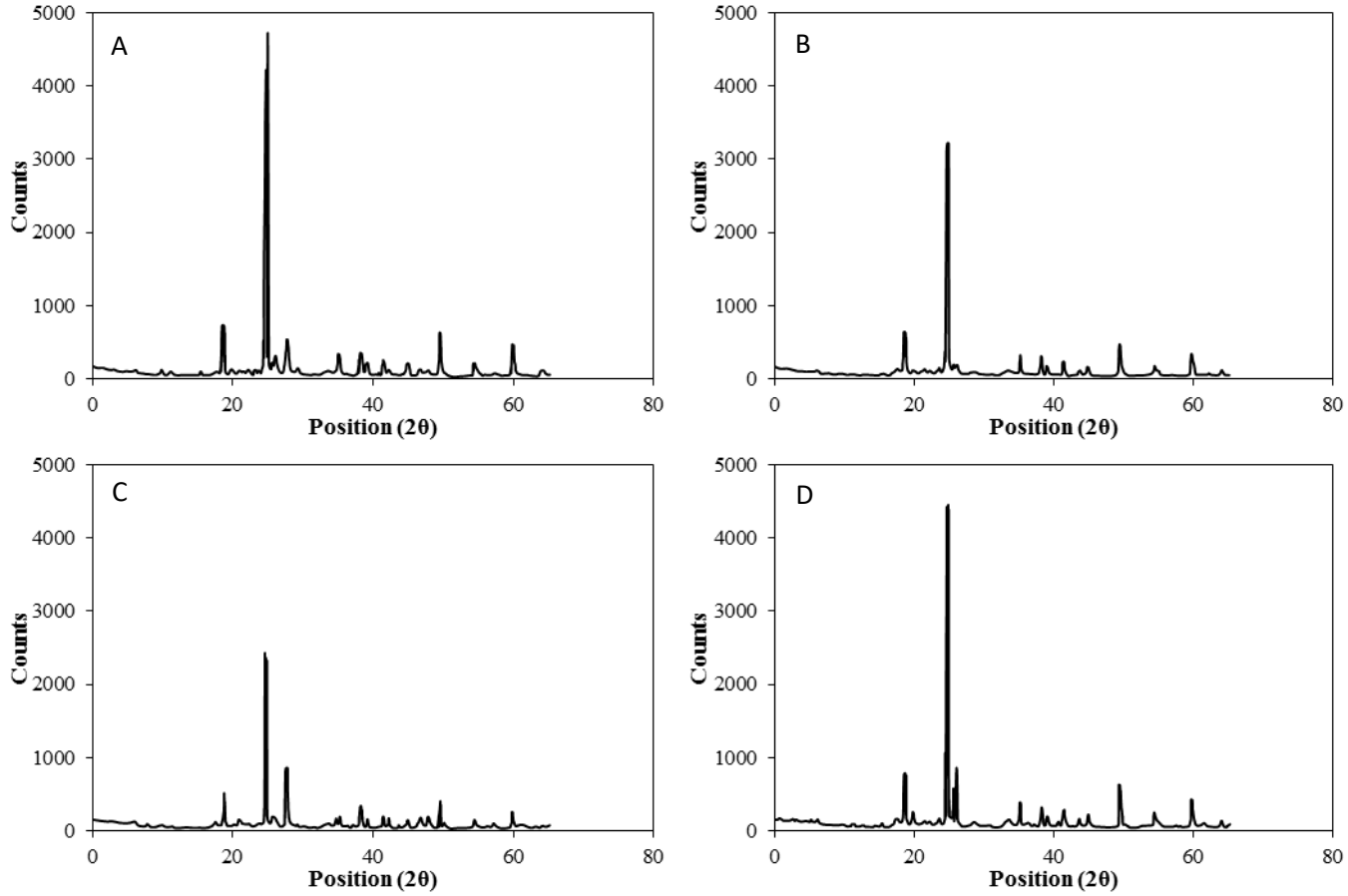
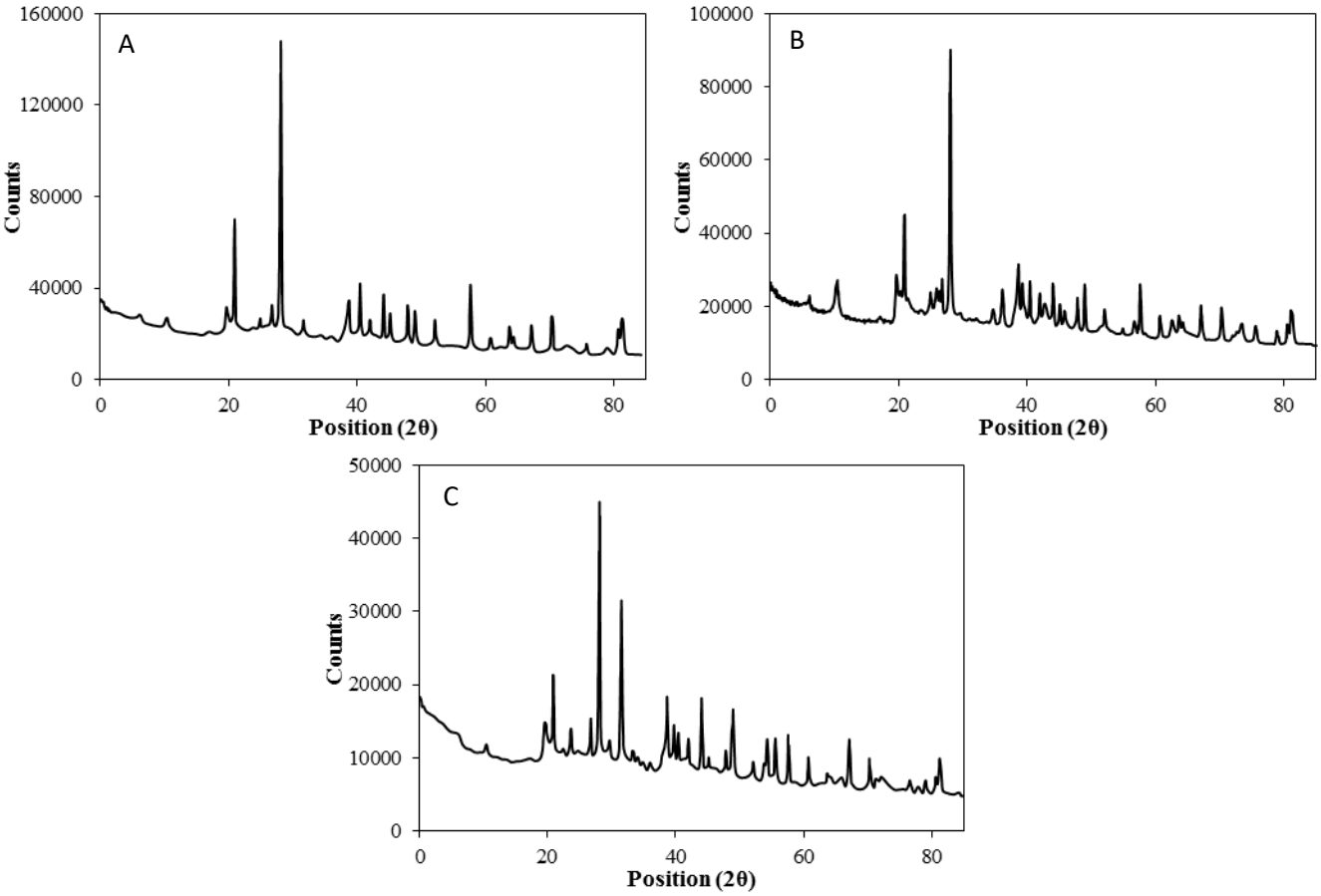


Figure A.1- Smoothed XRD spectra of untreated Vedstaarup yellow (A), Hammershoj yellow (B), Helligsø red (C) and Hammershoj red (D) clays. Each sample was measured once, so that deviations for the mineral concentrations range ±2.5% for >60 wt%, ±5% between 60-30 wt%, ±10% between 30-10 wt%, ±20% between 10-3 wt% and ±40% for <3 wt %. Differences between these and the following trends come from the above being produced in Aarhus university department of geoscience while the rest have been produced at the British Geological Survey.



FigureA.2- Smoothed XRD spectra of untreated English red (A), Dutch red (B) and Spanish yellow (C). Each sample was measured once, so that deviations for the mineral concentrations range ±2.5% for >60 wt%, ±5% between 60-30 wt%, ±10% between 30-10 wt%, ±20% between 10-3 wt% and ±40% for <3 wt %.

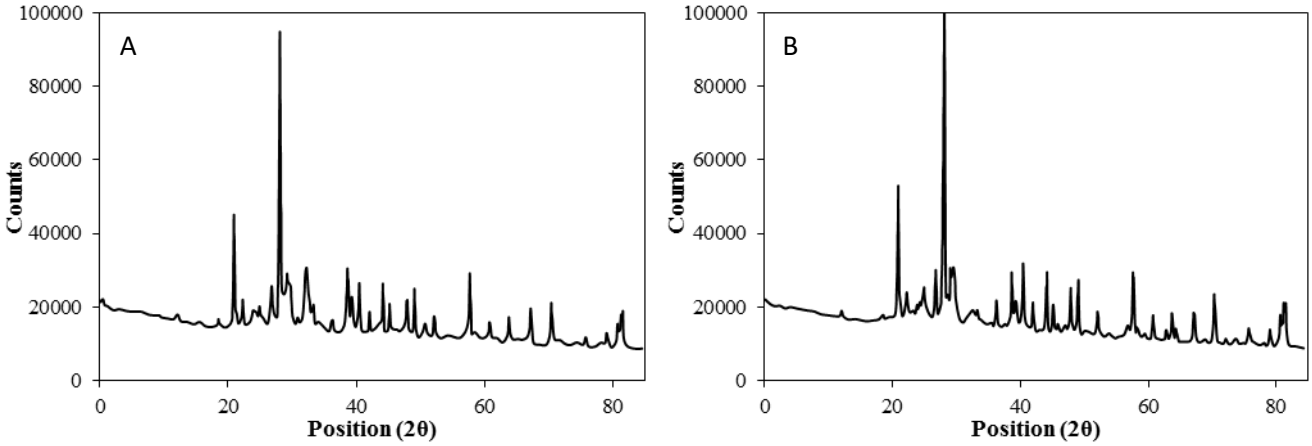


Figure A.3- Smoothed XRD spectra of Vedstaarup yellow (left) and Helligsø red (right) clays after a firing cycle between 20-950 ºC on 25x20 mm cylindrical specimens using conventional heating (A-B), microwave energy (C-D), and microwave energy followed by a conventionally controlled cooling cycle (E-F). Each sample was measured once, so that deviations for the mineral concentrations range ±2.5% for >60 wt%, ±5% between 60-30 wt%, ±10% between 30-10 wt%, ±20% between 10-3 wt% and ±40% for <3 wt %.

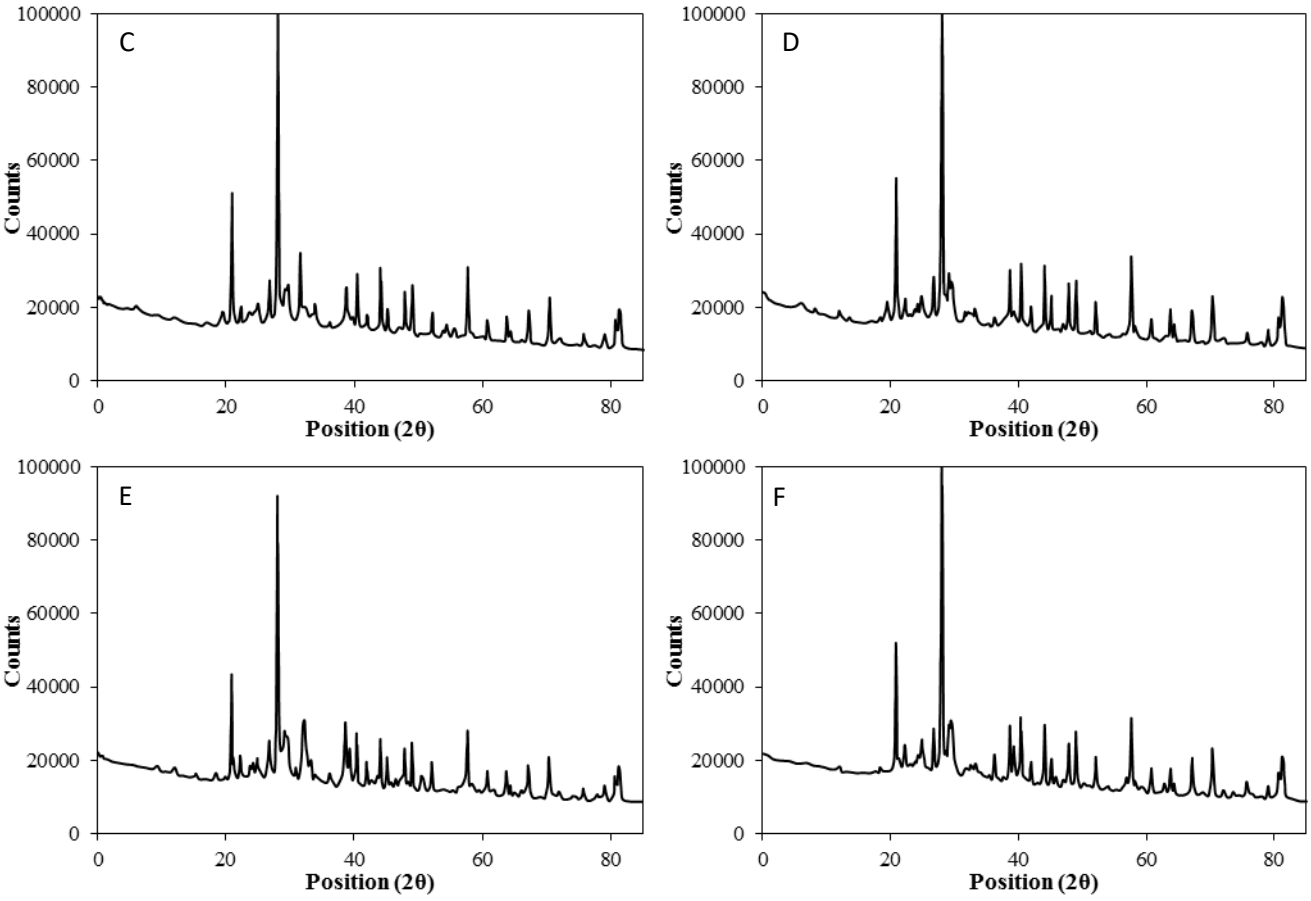


Figure A.3- Continued.

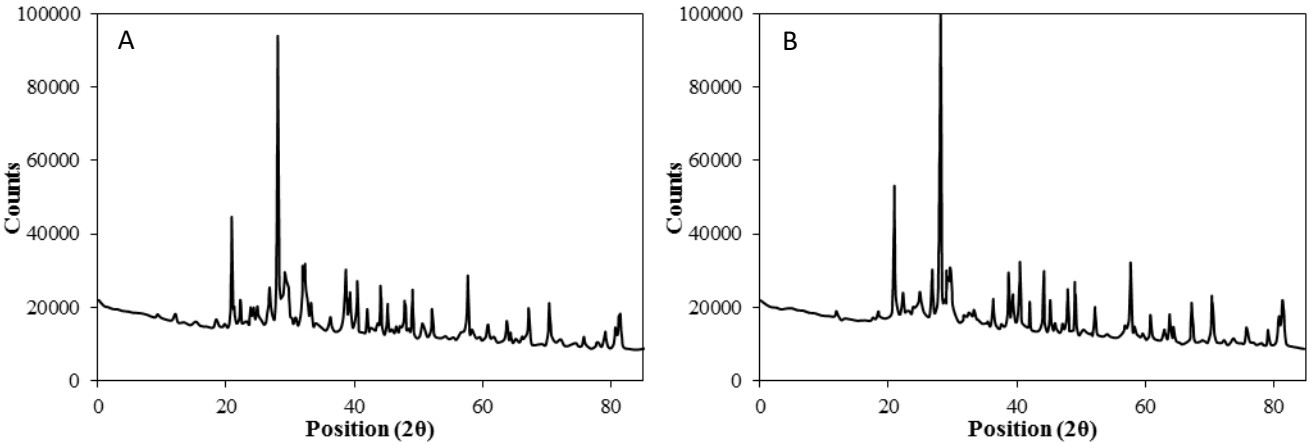


Figure A.4- Smoothed XRD spectra of Vedstaarup yellow (left) and Helligsø red (right) clays after a firing cycle between 20-950 ºC on 25x35 mm cylindrical specimens using conventional heating (A-B) and microwave energy (C-D). Each sample was measured once, so that deviations for the mineral concentrations range ±2.5% for >60 wt%, ±5% between 60-30 wt%, ±10% between 30-10 wt%, ±20% between 10-3 wt% and ±40% for <3 wt %.

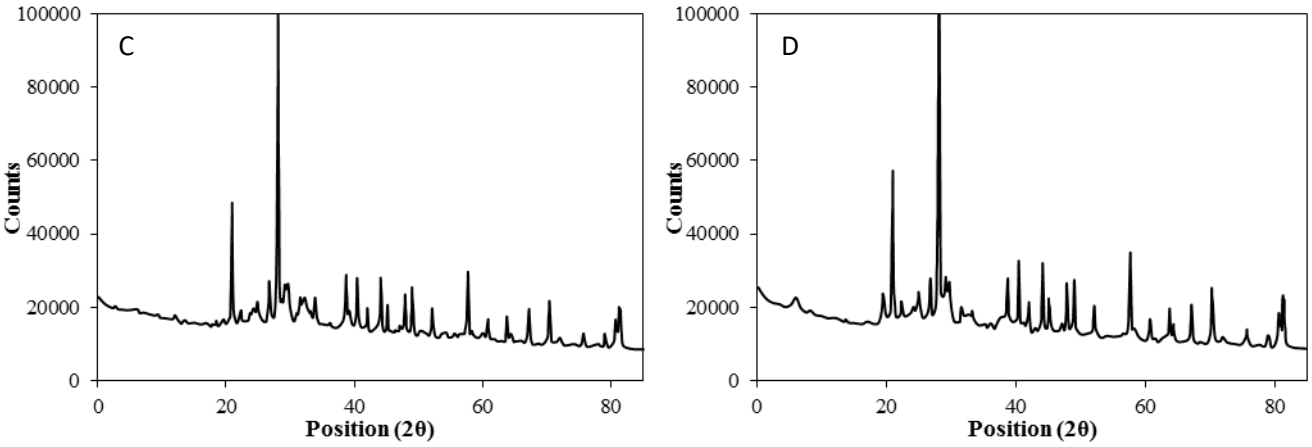


Figure A.4- Continued

Appendix B: Dielectric property measurements

Appendix B1: Dielectric properties of clays

Table B.1- Dielectric constants and loss factors between 20-950 ºC at 912 MHz and 2470 MHz for yellow Danish clays slabs measured by the resonant cavity method at void fractions ranging 0.37±0.02 for Vedstaarup yellow and 0.39±0.01 for Hammershoj yellow. These results are the average of three repeats. The standard uncertainties are indicated in the table.

	Vedstaarup yellow				Hammershoj yellow			
Frequency (MHz)	912		2470		912		2470	
T (°C)	ε'	ε''	ε'	ε''	ε'	ε''	ε'	ε''
20	3.43±0.06	0.075±0.006	3.55±0.07	0.069±0.006	3.49±0.06	0.083±0.003	3.57±0.05	0.079±0.003
50	3.49±0.07	0.098±0.008	3.61±0.07	0.087±0.009	3.57±0.08	0.123±0.002	3.63±0.07	0.104±0.001
100	3.46±0.08	0.085±0.009	3.60±0.07	0.076±0.008	3.50±0.07	0.084±0.001	3.58±0.06	0.078±0.001
150	3.42±0.05	0.048±0.004	3.52±0.07	0.042±0.003	3.43±0.08	0.047±0.005	3.51±0.06	0.042±0.006
200	3.44±0.06	0.046±0.003	3.52±0.08	0.040±0.002	3.45±0.08	0.049±0.006	3.53±0.05	0.044±0.002
250	3.46±0.07	0.046±0.004	3.52±0.10	0.043±0.002	3.48±0.08	0.051±0.008	3.55±0.05	0.044±0.008
300	3.48±0.07	0.046±0.005	3.51±0.11	0.039±0.003	3.50±0.06	0.052±0.001	3.57±0.03	0.042±0.000
350	3.50±0.07	0.049±0.006	3.51±0.12	0.040±0.003	3.53±0.05	0.039±0.007	3.58±0.03	0.028±0.003
400	3.52±0.07	0.059±0.006	3.52±0.13	0.045±0.004	3.56±0.04	0.045±0.006	3.60±0.02	0.033±0.003
450	3.55±0.07	0.073±0.005	3.54±0.13	0.050±0.005	3.60±0.02	0.066±0.006	3.63±0.01	0.044±0.005
500	3.56±0.07	0.083±0.007	3.54±0.13	0.054±0.004	3.63±0.02	0.065±0.008	3.64±0.01	0.038±0.002
550	3.59±0.08	0.097±0.008	3.54±0.14	0.062±0.004	3.68±0.04	0.077±0.006	3.67±0.02	0.045±0.004
600	3.63±0.10	0.122±0.008	3.56±0.15	0.072±0.005	3.73±0.06	0.088±0.006	3.70±0.03	0.052±0.004
650	3.66±0.12	0.151±0.011	3.59±0.15	0.082±0.006	3.79±0.07	0.113±0.007	3.74±0.04	0.061±0.002
700	3.69±0.13	0.178±0.011	3.60±0.15	0.090±0.007	3.84±0.09	0.141±0.005	3.78±0.05	0.072±0.005
750	3.72±0.15	0.198±0.012	3.63±0.15	0.095±0.006	3.91±0.10	0.149±0.005	3.82±0.05	0.073±0.008
800	3.77±0.18	0.191±0.012	3.69±0.15	0.092±0.007	3.99±0.08	0.154±0.006	3.87±0.04	0.073±0.009
850	3.80±0.19	0.203±0.011	3.71±0.16	0.107±0.007	4.01±0.05	0.170±0.007	3.87±0.03	0.079±0.005
900	3.79±0.16	0.271±0.017	3.66±0.15	0.123±0.007	4.01±0.08	0.192±0.008	3.84±0.04	0.084±0.004
950	3.81±0.16	0.341±0.019	3.69±0.13	0.145±0.008	4.10±0.10	0.236±0.006	3.88±0.05	0.095±0.002

Table B.2- Dielectric constants and loss factors between 20-950 ºC at 912 MHz and 2470 MHz for red Danish clays slabs measured by the resonant cavity method at void fractions ranging 0.40±0.01 for Helligsø red and 0.42±0.03 for Hammershoj red . These results are the average of three repeats. The standard uncertainties are indicated in the table.

	Helligsø red				Hammershoj red			
Frequency (MHz)	**912**		**2470**		**912**		**2470**	
T (°C)	**ε'**	**ε''**	**ε'**	**ε''**	**ε'**	**ε''**	**ε'**	**ε''**
20	3.03±0.05	0.043±0.005	3.13±0.05	0.044±0.004	3.27±0.06	0.094±0.009	3.32±0.05	0.098±0.022
50	3.08±0.04	0.057±0.007	3.18±0.05	0.055±0.005	3.39±0.05	0.137±0.046	3.41±0.04	0.123±0.027
100	3.02±0.04	0.051±0.009	3.14±0.05	0.047±0.004	3.34±0.10	0.115±0.033	3.37±0.12	0.107±0.020
150	2.95±0.07	0.028±0.005	3.09±0.06	0.027±0.001	3.19±0.11	0.049±0.007	3.24±0.10	0.047±0.003
200	2.95±0.10	0.029±0.004	3.10±0.07	0.026±0.001	3.17±0.09	0.027±0.015	3.21±0.07	0.024±0.003
250	2.97±0.15	0.032±0.003	3.12±0.08	0.028±0.001	3.22±0.06	0.040±0.010	3.23±0.04	0.031±0.002
300	2.98±0.15	0.033±0.004	3.12±0.09	0.028±0.001	3.26±0.05	0.030±0.003	3.25±0.03	0.027±0.002
350	3.00±0.15	0.041±0.006	3.13±0.09	0.031±0.005	3.31±0.04	0.036±0.018	3.26±0.02	0.029±0.010
400	3.01±0.14	0.049±0.008	3.15±0.08	0.036±0.005	3.36±0.02	0.058±0.005	3.29±0.01	0.044±0.003
450	3.03±0.13	0.064±0.010	3.16±0.08	0.043±0.007	3.42±0.00	0.060±0.009	3.31±0.00	0.042±0.005
500	3.05±0.14	0.073±0.011	3.17±0.09	0.049±0.008	3.49±0.00	0.078±0.002	3.34±0.00	0.048±0.001
550	3.09±0.16	0.094±0.014	3.19±0.09	0.056±0.009	3.53±0.06	0.081±0.016	3.37±0.03	0.051±0.006
600	3.15±0.19	0.112±0.018	3.22±0.10	0.065±0.010	3.61±0.05	0.108±0.002	3.41±0.04	0.063±0.002
650	3.21±0.19	0.136±0.022	3.26±0.10	0.073±0.011	3.70±0.05	0.133±0.005	3.45±0.07	0.070±0.002
700	3.27±0.19	0.165±0.025	3.29±0.10	0.081±0.012	3.77±0.07	0.151±0.023	3.49±0.09	0.072±0.013
750	3.31±0.21	0.192±0.030	3.31±0.10	0.089±0.013	3.86±0.08	0.191±0.028	3.53±0.12	0.086±0.008
800	3.38±0.21	0.214±0.023	3.35±0.11	0.100±0.016	3.94±0.10	0.211±0.012	3.58±0.14	0.094±0.005
850	3.49±0.21	0.244±0.024	3.43±0.10	0.121±0.019	4.06±0.10	0.206±0.016	3.66±0.14	0.101±0.013
900	3.70±0.23	0.334±0.035	3.57±0.11	0.176±0.028	4.25±0.10	0.282±0.018	3.80±0.14	0.149±0.008
950	3.93±0.23	0.485±0.053	3.71±0.11	0.249±0.038	4.50±0.11	0.412±0.011	3.98±0.16	0.219±0.008

Table B.3- Dielectric constants and loss factors between 20-950 ºC at 912 MHz and 2470 MHz for yellow Danish clays powders with a 0.56±0.03 void fraction measured by the resonant cavity method. These results are the average of three repeats. The standard uncertainties are indicated in the table.

	Vedstaarup yellow				Hammershoj yellow			
Frequency (MHz)	**912**		**2470**		**912**		**2470**	
T (°C)	**ε'**	**ε''**	**ε'**	**ε''**	**ε'**	**ε''**	**ε'**	**ε''**
20	2.25±0.04	0.043±0.002	2.30±0.02	0.022±0.003	2.38±0.08	0.056±0.018	2.43±0.07	0.048±0.012
50	2.28±0.05	0.052±0.003	2.32±0.02	0.027±0.004	2.43±0.10	0.078±0.028	2.46±0.08	0.060±0.017
100	2.24±0.09	0.039±0.005	2.29±0.04	0.018±0.005	2.34±0.08	0.035±0.011	2.40±0.04	0.030±0.007
150	2.22±0.10	0.032±0.003	2.28±0.04	0.011±0.002	2.29±0.11	0.017±0.005	2.36±0.03	0.015±0.003
200	2.23±0.13	0.031±0.004	2.28±0.04	0.010±0.002	2.31±0.13	0.016±0.004	2.37±0.04	0.014±0.003
250	2.25±0.15	0.031±0.003	2.30±0.04	0.009±0.002	2.33±0.15	0.016±0.004	2.39±0.05	0.014±0.003
300	2.27±0.17	0.031±0.004	2.31±0.05	0.009±0.002	2.34±0.17	0.015±0.003	2.40±0.05	0.012±0.003
350	2.29±0.18	0.033±0.004	2.32±0.05	0.009±0.002	2.37±0.18	0.015±0.003	2.41±0.05	0.012±0.003
400	2.31±0.19	0.034±0.004	2.34±0.05	0.010±0.002	2.41±0.18	0.017±0.004	2.43±0.06	0.013±0.003
450	2.34±0.20	0.038±0.004	2.36±0.05	0.012±0.001	2.45±0.20	0.023±0.004	2.46±0.07	0.015±0.003
500	2.36±0.20	0.042±0.004	2.37±0.06	0.013±0.002	2.48±0.22	0.028±0.003	2.47±0.07	0.017±0.003
550	2.39±0.20	0.046±0.003	2.39±0.05	0.015±0.002	2.51±0.23	0.034±0.004	2.48±0.08	0.020±0.003
600	2.43±0.18	0.052±0.004	2.41±0.05	0.019±0.002	2.55±0.24	0.042±0.005	2.51±0.09	0.025±0.004
650	2.46±0.16	0.059±0.005	2.43±0.05	0.021±0.002	2.59±0.25	0.052±0.004	2.53±0.09	0.028±0.004
700	2.49±0.16	0.065±0.005	2.44±0.04	0.023±0.002	2.61±0.25	0.060±0.005	2.54±0.09	0.031±0.004
750	2.51±0.17	0.068±0.006	2.45±0.04	0.024±0.003	2.58±0.28	0.062±0.010	2.51±0.13	0.032±0.004
800	2.55±0.18	0.071±0.006	2.48±0.05	0.024±0.002	2.69±0.25	0.066±0.005	2.59±0.09	0.032±0.004
850	2.62±0.19	0.083±0.006	2.53±0.06	0.030±0.002	2.77±0.25	0.082±0.007	2.65±0.09	0.040±0.004
900	2.63±0.21	0.101±0.006	2.51±0.06	0.035±0.004	2.74±0.25	0.094±0.007	2.61±0.09	0.042±0.004
950	2.67±0.22	0.130±0.008	2.53±0.06	0.044±0.004	2.74±0.27	0.128±0.010	2.61±0.10	0.050±0.005

Table B.4- Dielectric constants and loss factors between 20-950 ºC at 912 MHz and 2470 MHz for red Danish clays powders with a 0.56±0.03 void fraction measured by the resonant cavity method. These results are the average of three repeats. The standard uncertainties are indicated in the table.

	Helligsø red				Hammershoj red			
Frequency (MHz)	**912**		**2470**		**912**		**2470**	
T (°C)	**ε'**	**ε''**	**ε'**	**ε''**	**ε'**	**ε''**	**ε'**	**ε''**
20	2.37±0.07	0.048±0.004	2.41±0.06	0.050±0.006	2.22±0.12	0.062±0.033	2.25±0.10	0.057±0.007
50	2.45±0.10	0.065±0.008	2.46±0.07	0.058±0.007	2.32±0.10	0.095±0.040	2.32±0.08	0.075±0.009
100	2.38±0.05	0.047±0.012	2.40±0.03	0.044±0.009	2.22±0.17	0.050±0.012	2.24±0.06	0.042±0.004
150	2.25±0.06	0.018±0.004	2.28±0.05	0.017±0.004	2.14±0.16	0.017±0.007	2.16±0.04	0.016±0.003
200	2.24±0.06	0.015±0.006	2.27±0.05	0.013±0.004	2.12±0.16	0.009±0.002	2.14±0.03	0.008±0.003
250	2.27±0.08	0.016±0.006	2.28±0.05	0.013±0.005	2.12±0.18	0.009±0.002	2.14±0.03	0.007±0.002
300	2.30±0.09	0.013±0.004	2.29±0.06	0.012±0.004	2.13±0.20	0.009±0.003	2.15±0.04	0.007±0.002
350	2.34±0.10	0.016±0.004	2.31±0.06	0.013±0.005	2.15±0.21	0.010±0.003	2.16±0.04	0.008±0.002
400	2.38±0.11	0.021±0.005	2.33±0.06	0.016±0.005	2.17±0.23	0.013±0.003	2.17±0.04	0.010±0.002
450	2.42±0.12	0.028±0.004	2.35±0.06	0.020±0.005	2.19±0.24	0.020±0.003	2.18±0.05	0.013±0.003
500	2.47±0.15	0.036±0.005	2.37±0.07	0.022±0.005	2.19±0.19	0.026±0.004	2.16±0.08	0.016±0.003
550	2.47±0.19	0.041±0.007	2.36±0.09	0.025±0.005	2.12±0.28	0.032±0.011	2.09±0.20	0.018±0.004
600	2.54±0.19	0.054±0.005	2.39±0.09	0.031±0.005	2.17±0.26	0.039±0.014	2.12±0.20	0.023±0.004
650	2.59±0.19	0.069±0.006	2.42±0.09	0.036±0.005	2.23±0.24	0.052±0.018	2.16±0.21	0.027±0.004
700	2.65±0.19	0.089±0.008	2.45±0.09	0.042±0.005	2.29±0.23	0.063±0.020	2.21±0.19	0.031±0.004
750	2.70±0.20	0.107±0.008	2.48±0.09	0.048±0.005	2.35±0.22	0.078±0.023	2.24±0.16	0.037±0.005
800	2.75±0.20	0.124±0.008	2.50±0.10	0.055±0.006	2.44±0.21	0.092±0.018	2.31±0.11	0.043±0.004
850	2.83±0.21	0.132±0.005	2.55±0.10	0.065±0.006	2.54±0.21	0.105±0.020	2.37±0.12	0.050±0.004
900	2.95±0.22	0.167±0.009	2.63±0.10	0.088±0.007	2.65±0.22	0.137±0.025	2.44±0.13	0.069±0.004
950	3.10±0.22	0.233±0.008	2.74±0.10	0.124±0.008	2.80±0.22	0.203±0.035	2.54±0.14	0.104±0.006

Table B.5- Dielectric constants and loss factors between 20-800 ºC at 2470 MHz for red and yellow Danish clays slabs measured by the waveguide technique at void fractions ranging 0.37±0.02 for Vedstaarup yellow, 0.39±0.01 for Hammershoj yellow, 0.40±0.01 for Helligsø red and 0.42±0.03 for Hammershoj red. These results are the average of three repeats. The standard uncertainties are indicated in the table.

	Vedstaarup yellow		Hammershoj yellow		Helligsø red		Hammershoj red	
T (°C)	ε'	ε"	ε'	ε"	ε'	ε"	ε'	ε"
20	3.38± 0.18	0.055± 0.174	3.55± 0.48	0.085± 0.014	3.02± 0.16	0.035± 0.033	3.38± 0.49	0.104± 0.010
200	3.41± 0.42	0.043± 0.157	3.51± 0.41	0.040± 0.014	3.01± 0.24	0.027± 0.012	3.24± 0.60	0.020± 0.023
400	3.77± 0.31	0.052± 0.175	3.57± 0.28	0.040± 0.020	3.31± 0.26	0.047± 0.013	3.30± 0.69	0.050± 0.019
600	3.87± 0.30	0.060± 0.186	3.66± 0.60	0.060± 0.031	3.43± 0.52	0.042± 0.024	3.50± 0.42	0.064± 0.029
800	4.05± 0.31	0.105± 0.287	3.77± 0.39	0.092± 0.043	3.60± 0.47	0.130± 0.032	3.75± 0.20	0.100± 0.034

Table B.6- Dielectric constants and loss factors between 20-950 ºC at 912 MHz and 2470 MHz for Spanish yellow, Dutch red and English red clay slabs measured by the resonant cavity method at void fractions ranging 0.10±0.01 for Spanish yellow, 0.38±0.01 for Dutch red and 0.30±0.02 for English red. These results are the average of three repeats. The standard uncertainties are indicated in the table.

	Spanish yellow				English red				Dutch red			
Frequency (MHz)	**912**		**2470**		**912**		**2470**		**912**		**2470**	
T (°C)	**ε'**	**ε''**	**ε'**	**ε''**	**ε'**	**ε''**	**ε'**	**ε''**	**ε'**	**ε''**	**ε'**	**ε''**
20	5.00± 0.05	0.096± 0.006	5.07± 0.16	0.080± 0.004	3.02± 0.05	0.074± 0.005	2.91± 0.07	0.072± 0.004	2.85± 0.18	0.059± 0.004	2.96± 0.19	0.038± 0.003
50	5.10± 0.07	0.126± 0.007	5.17± 0.16	0.109± 0.005	3.11± 0.03	0.095± 0.011	3.00± 0.07	0.082± 0.007	2.94± 0.18	0.059± 0.005	3.03± 0.19	0.045± 0.004
100	4.98± 0.04	0.065± 0.002	5.09± 0.19	0.058± 0.002	2.95± 0.12	0.049± 0.001	2.90± 0.14	0.027± 0.001	2.87± 0.18	0.039± 0.003	2.98± 0.19	0.023± 0.002
150	4.84± 0.09	0.023± 0.001	4.95± 0.11	0.023± 0.001	2.90± 0.13	0.016± 0.001	2.88± 0.15	0.013± 0.001	2.80± 0.17	0.022± 0.002	2.94± 0.19	0.017± 0.002
200	4.88± 0.12	0.031± 0.001	4.96± 0.06	0.024± 0.001	2.90± 0.13	0.009± 0.001	2.88± 0.14	0.008± 0.000	2.79± 0.17	0.013± 0.002	2.94± 0.19	0.008± 0.002
250	4.86± 0.15	0.040± 0.001	5.09± 0.03	0.028± 0.001	2.98± 0.14	0.007± 0.001	2.90± 0.15	0.010± 0.001	2.79± 0.17	0.008± 0.002	2.96± 0.19	0.007± 0.002
300	4.96± 0.15	0.020± 0.001	5.18± 0.03	0.018± 0.001	3.00± 0.18	0.009± 0.001	2.94± 0.17	0.008± 0.001	2.79± 0.17	0.010± 0.002	2.97± 0.19	0.008± 0.002
350	5.07± 0.15	0.028± 0.002	5.30± 0.04	0.020± 0.001	3.01± 0.21	0.012± 0.000	2.96± 0.18	0.008± 0.001	2.80± 0.17	0.011± 0.001	2.99± 0.19	0.007± 0.002
400	5.20± 0.13	0.038± 0.001	5.43± 0.03	0.024± 0.001	3.10± 0.23	0.018± 0.000	3.00± 0.19	0.008± 0.000	2.86± 0.17	0.017± 0.002	3.02± 0.19	0.008± 0.002
450	5.43± 0.12	0.052± 0.002	5.56± 0.04	0.026± 0.001	3.25± 0.27	0.020± 0.000	3.05± 0.21	0.010± 0.000	2.95± 0.16	0.019± 0.003	3.07± 0.19	0.010± 0.002
500	5.66± 0.08	0.063± 0.002	5.65± 0.05	0.032± 0.001	3.32± 0.28	0.021± 0.001	3.08± 0.21	0.012± 0.000	3.04± 0.15	0.022± 0.003	3.09± 0.19	0.010± 0.003
550	5.78± 0.05	0.083± 0.002	5.75± 0.07	0.041± 0.001	3.47± 0.20	0.025± 0.002	3.15± 0.17	0.013± 0.000	3.13± 0.15	0.027± 0.004	3.12± 0.18	0.014± 0.002
600	5.96± 0.07	0.101± 0.002	5.90± 0.07	0.049± 0.001	3.56± 0.18	0.032± 0.002	3.23± 0.16	0.017± 0.001	3.25± 0.15	0.036± 0.003	3.15± 0.18	0.020± 0.002
650	6.14± 0.08	0.133± 0.003	6.06± 0.07	0.062± 0.001	3.69± 0.15	0.040± 0.002	3.33± 0.15	0.022± 0.001	3.33± 0.15	0.046± 0.003	3.19± 0.18	0.025± 0.002
700	6.32± 0.05	0.160± 0.004	6.21± 0.07	0.076± 0.001	3.84± 0.13	0.049± 0.002	3.40± 0.15	0.028± 0.001	3.43± 0.14	0.051± 0.003	3.26± 0.18	0.031± 0.003
750	6.53± 0.03	0.169± 0.003	6.37± 0.07	0.082± 0.001	4.00± 0.10	0.056± 0.003	3.53± 0.13	0.034± 0.002	3.52± 0.13	0.061± 0.004	3.29± 0.17	0.035± 0.005
800	6.82± 0.06	0.122± 0.003	6.49± 0.05	0.069± 0.001	4.14± 0.06	0.061± 0.002	3.64± 0.12	0.039± 0.002	3.61± 0.06	0.070± 0.005	3.35± 0.09	0.043± 0.004
850	7.12± 0.17	0.177± 0.004	6.50± 0.10	0.084± 0.002	4.24± 0.00	0.076± 0.002	3.74± 0.10	0.042± 0.002	3.66± 0.01	0.079± 0.004	3.39± 0.01	0.049± 0.004
900	6.91± 0.21	0.253± 0.006	5.88± 0.11	0.123± 0.002	4.37± 0.03	0.108± 0.003	3.85± 0.08	0.055± 0.003	3.69± 0.07	0.099± 0.006	3.45± 0.05	0.063± 0.001
950	6.15± 0.25	0.357± 0.006	4.87± 0.14	0.172± 0.002	4.59± 0.06	0.169± 0.004	4.04± 0.06	0.071± 0.003	3.84± 0.10	0.136± 0.008	3.48± 0.07	0.093± 0.004

Appendix B2: Dielectric properties of clay constituents

Table B.7- Dielectric constants and loss factors between 20-950 ºC at 912 MHz and 2470 MHz for mineral slabs at void fractions ranging 0.32±0.03 for montmorillonite, 0.22±0.07 for muscovite and 0.48±0.02 for kaolinite. These results are the average of three repeats. The standard uncertainties are indicated in the table.

	Kaolinite				Montmorillonite				Muscovite			
Frequency (MHz)	**912**		**2470**		**912**		**2470**		**912**		**2470**	
T (°C)	**ε'**	**ε''**	**ε'**	**ε''**	**ε'**	**ε''**	**ε'**	**ε''**	**ε'**	**ε''**	**ε'**	**ε''**
20	2.91± 0.03	0.108± 0.018	2.98± 0.03	0.075± 0.011	3.59± 0.08	0.344± 0.081	3.64± 0.06	0.214± 0.045	4.31± 0.03	0.163± 0.027	4.46± 0.02	0.147± 0.019
50	2.93± 0.05	0.131± 0.045	3.00± 0.04	0.081± 0.026	3.83± 0.11	0.643± 0.134	3.78± 0.07	0.387± 0.083	4.43± 0.05	0.200± 0.029	4.55± 0.03	0.175± 0.023
100	2.84± 0.03	0.039± 0.019	2.94± 0.05	0.027± 0.012	3.97± 0.05	0.696± 0.063	3.84± 0.04	0.449± 0.035	4.46± 0.01	0.188± 0.02	4.56± 0.02	0.169± 0.015
150	2.82± 0.02	0.024± 0.005	2.94± 0.04	0.015± 0.000	4.01± 0.06	0.570± 0.009	3.87± 0.04	0.417± 0.004	4.31± 0.06	0.125± 0.005	4.42± 0.05	0.110± 0.007
200	2.80± 0.07	0.020± 0.001	2.94± 0.03	0.015± 0.002	4.16± 0.08	0.580± 0.015	3.97± 0.04	0.469± 0.008	4.29± 0.09	0.113± 0.006	4.39± 0.07	0.098± 0.007
250	2.79± 0.13	0.013± 0.005	2.95± 0.04	0.013± 0.001	4.29± 0.12	0.610± 0.025	4.08± 0.06	0.503± 0.005	4.34± 0.13	0.112± 0.012	4.43± 0.08	0.100± 0.007
300	2.78± 0.18	0.015± 0.003	2.96± 0.05	0.012± 0.001	4.38± 0.14	0.618± 0.001	4.15± 0.07	0.523± 0.009	4.40± 0.15	0.129± 0.014	4.47± 0.10	0.106± 0.009
350	2.78± 0.21	0.013± 0.004	2.97± 0.06	0.011± 0.000	4.40± 0.16	0.598± 0.013	4.18± 0.08	0.503± 0.01	4.46± 0.16	0.142± 0.013	4.51± 0.11	0.114± 0.010
400	2.80± 0.22	0.012± 0.002	2.99± 0.06	0.010± 0.001	4.31± 0.18	0.526± 0.007	4.12± 0.08	0.420± 0.004	4.50± 0.17	0.159± 0.009	4.52± 0.11	0.115± 0.011
450	2.83± 0.23	0.012± 0.005	3.00± 0.06	0.010± 0.001	4.17± 0.18	0.471± 0.01	4.02± 0.09	0.313± 0.005	4.59± 0.16	0.209± 0.010	4.56± 0.10	0.136± 0.010
500	2.82± 0.23	0.016± 0.002	2.98± 0.05	0.011± 0.002	4.09± 0.19	0.434± 0.007	3.96± 0.09	0.237± 0.004	4.64± 0.16	0.235± 0.011	4.55± 0.09	0.146± 0.012
550	2.66± 0.23	0.024± 0.009	2.78± 0.05	0.016± 0.001	4.14± 0.22	0.494± 0.007	3.98± 0.10	0.236± 0.002	4.65± 0.17	0.259± 0.022	4.53± 0.09	0.148± 0.020
600	2.64± 0.22	0.028± 0.005	2.72± 0.03	0.020± 0.002	4.23± 0.24	0.513± 0.021	4.01± 0.10	0.243± 0.009	4.69± 0.21	0.298± 0.014	4.52± 0.11	0.158± 0.013
650	2.71± 0.21	0.033± 0.006	2.76± 0.03	0.023± 0.003	4.23± 0.26	0.479± 0.014	3.99± 0.12	0.221± 0.004	4.77± 0.24	0.340± 0.026	4.56± 0.13	0.175± 0.012
700	2.80± 0.17	0.043± 0.007	2.81± 0.02	0.026± 0.003	4.20± 0.28	0.506± 0.009	3.91± 0.12	0.232± 0.003	4.85± 0.27	0.391± 0.026	4.60± 0.14	0.190± 0.010
750	2.89± 0.12	0.053± 0.007	2.86± 0.01	0.031± 0.006	4.36± 0.28	0.652± 0.013	3.98± 0.12	0.286± 0.001	4.93± 0.30	0.449± 0.033	4.63± 0.16	0.207± 0.013
800	2.98± 0.09	0.063± 0.013	2.92± 0.03	0.035± 0.008	4.65± 0.29	0.817± 0.022	4.16± 0.12	0.358± 0.009	5.01± 0.32	0.463± 0.036	4.67± 0.17	0.214± 0.014
850	3.07± 0.07	0.069± 0.017	2.97± 0.04	0.038± 0.008	5.37± 0.27	1.216± 0.066	4.63± 0.11	0.567± 0.016	5.18± 0.36	0.449± 0.035	4.80± 0.19	0.222± 0.018
900	3.16± 0.07	0.096± 0.020	3.01± 0.04	0.047± 0.009	6.68± 0.28	2.443± 0.109	5.38± 0.10	1.144± 0.039	5.77± 0.39	0.771± 0.057	5.21± 0.21	0.379± 0.026
950	3.24± 0.08	0.136± 0.029	3.05± 0.06	0.060± 0.014	7.43± 0.34	3.285± 0.184	5.70± 0.12	1.487± 0.067	6.52± 0.40	1.289± 0.058	5.67± 0.21	0.636± 0.036

Table B.8- Dielectric constants and loss factors between 20-950 ºC at 912 MHz and 2470 MHz for mineral slabs at void fractions ranging 0.09±0.03 for calcite and 0.17±0.01 for quartz. These results are the average of three repeats. The standard uncertainties are indicated in the table.

	Calcite				Quartz			
Frequency (MHz)	**912**		**2470**		**912**		**2470**	
T (°C)	**ε'**	**ε''**	**ε'**	**ε''**	**ε'**	**ε''**	**ε'**	**ε''**
20	6.33± 0.05	0.002± 0.004	6.82± 0.06	0.002± 0.002	3.59± 0.33	0.000± 0.002	3.77± 0.35	0.000± 0.001
50	6.39± 0.05	0.002± 0.003	6.90± 0.05	0.003± 0.003	3.60± 0.33	0.000± 0.002	3.78± 0.35	0.001± 0.001
100	6.51± 0.05	0.002± 0.004	7.02± 0.06	0.004± 0.003	3.61± 0.34	0.001± 0.003	3.80± 0.35	0.001± 0.000
150	6.61± 0.04	0.003± 0.002	7.13± 0.06	0.005± 0.003	3.59± 0.34	0.001± 0.001	3.78± 0.36	0.001± 0.001
200	6.72± 0.05	0.008± 0.008	7.24± 0.06	0.008± 0.005	3.58± 0.33	0.000± 0.001	3.79± 0.36	0.002± 0.001
250	6.78± 0.11	0.009± 0.007	7.30± 0.11	0.007± 0.003	3.59± 0.32	0.001± 0.002	3.80± 0.35	0.002± 0.001
300	6.85± 0.17	0.006± 0.005	7.37± 0.17	0.008± 0.003	3.59± 0.30	0.000± 0.001	3.82± 0.35	0.002± 0.001
350	6.96± 0.17	0.007± 0.004	7.48± 0.18	0.007± 0.002	3.61± 0.30	0.001± 0.005	3.83± 0.34	0.002± 0.001
400	7.07± 0.18	0.007± 0.005	7.58± 0.19	0.007± 0.001	3.63± 0.30	0.002± 0.002	3.85± 0.35	0.002± 0.001
450	7.19± 0.19	0.005± 0.003	7.69± 0.19	0.008± 0.000	3.65± 0.31	0.002± 0.002	3.87± 0.35	0.002± 0.001
500	7.31± 0.21	0.010± 0.003	7.79± 0.20	0.009± 0.001	3.68± 0.31	0.001± 0.001	3.89± 0.35	0.003± 0.001
550	7.44± 0.23	0.015± 0.003	7.90± 0.20	0.011± 0.002	3.71± 0.31	0.002± 0.002	3.91± 0.35	0.003± 0.001
600	7.60± 0.24	0.030± 0.006	8.01± 0.21	0.017± 0.005	3.73± 0.30	0.004± 0.002	3.93± 0.35	0.003± 0.001
650	7.74± 0.24	0.040± 0.014	8.12± 0.22	0.022± 0.003	3.75± 0.28	0.005± 0.002	3.94± 0.34	0.004± 0.001
700	7.87± 0.25	0.048± 0.012	8.22± 0.22	0.026± 0.005	3.76± 0.27	0.006± 0.000	3.96± 0.34	0.004± 0.000
750	7.99± 0.26	0.044± 0.011	8.30± 0.23	0.027± 0.007	3.79± 0.27	0.008± 0.001	3.97± 0.34	0.005± 0.000
800	8.09± 0.28	0.040± 0.012	8.33± 0.25	0.027± 0.005	3.81± 0.26	0.012± 0.003	3.99± 0.34	0.006± 0.001
850	8.09± 0.31	0.049± 0.005	8.27± 0.29	0.028± 0.002	3.83± 0.25	0.017± 0.001	4.01± 0.33	0.007± 0.001
900	7.76 0.52	0.057± 0.014	7.84± 0.52	0.033± 0.006	3.86± 0.25	0.019± 0.001	4.02± 0.34	0.009± 0.000
950	6.28± 1.23	0.065± 0.011	6.19± 1.21	0.034± 0.008	3.89± 0.25	0.029± 0.000	4.04± 0.34	0.012± 0.001

Table B.9- Dielectric constants and loss factors between 20-950 ºC at 912 MHz and 2470 MHz for mineral slabs at void fractions ranging 0.17±0.07 for orthoclase and 0.35±0.06 for albite. These results are the average of three repeats. The standard uncertainties are indicated in the table.

	Orthoclase				Albite			
Frequency (MHz)	**912**		**2470**		**912**		**2470**	
T (°C)	**ε'**	**ε''**	**ε'**	**ε''**	**ε'**	**ε''**	**ε'**	**ε''**
20	3.72± 0.24	0.001± 0.006	3.88± 0.25	0.007± 0.001	3.07± 0.20	0.009± 0.017	3.19± 0.21	0.008± 0.008
50	3.77± 0.25	0.010± 0.005	3.91± 0.26	0.007± 0.000	3.10± 0.20	0.014± 0.019	3.22± 0.21	0.012± 0.010
100	3.84± 0.26	0.015± 0.002	3.96± 0.26	0.011± 0.001	3.13± 0.21	0.017± 0.020	3.25± 0.21	0.018± 0.011
150	3.90± 0.28	0.024± 0.004	4.01± 0.27	0.014± 0.001	3.16± 0.22	0.027± 0.021	3.28± 0.22	0.022± 0.012
200	3.96± 0.30	0.026± 0.016	4.05± 0.27	0.018± 0.002	3.19± 0.23	0.043± 0.024	3.31± 0.22	0.029± 0.014
250	4.04± 0.32	0.038± 0.004	4.10± 0.28	0.022± 0.001	3.22± 0.23	0.055± 0.028	3.34± 0.22	0.035± 0.014
300	4.10± 0.33	0.034± 0.007	4.13± 0.28	0.022± 0.001	3.25± 0.23	0.065± 0.024	3.36± 0.22	0.039± 0.015
350	4.17± 0.33	0.026± 0.001	4.17± 0.27	0.018± 0.002	3.29± 0.22	0.072± 0.027	3.39± 0.22	0.041± 0.015
400	4.27± 0.35	0.026± 0.002	4.23± 0.29	0.016± 0.003	3.32± 0.22	0.066± 0.027	3.42± 0.22	0.039± 0.014
450	4.37± 0.36	0.026± 0.006	4.29± 0.30	0.015± 0.003	3.36± 0.22	0.057± 0.024	3.45± 0.22	0.034± 0.012
500	4.49± 0.38	0.024± 0.009	4.35± 0.30	0.016± 0.003	3.40± 0.21	0.047± 0.020	3.48± 0.21	0.030± 0.012
550	4.61± 0.41	0.028± 0.006	4.41± 0.32	0.016± 0.004	3.44± 0.21	0.041± 0.023	3.51± 0.21	0.028± 0.010
600	4.74± 0.41	0.027± 0.006	4.48± 0.32	0.017± 0.004	3.50± 0.21	0.049± 0.014	3.54± 0.21	0.027± 0.008
650	4.84± 0.43	0.028± 0.002	4.54± 0.32	0.018± 0.004	3.55± 0.19	0.055± 0.009	3.57± 0.20	0.029± 0.007
700	4.93± 0.45	0.034± 0.005	4.59± 0.34	0.019± 0.005	3.61± 0.19	0.056± 0.007	3.61± 0.20	0.031± 0.008
750	5.03± 0.47	0.046± 0.016	4.65± 0.34	0.021± 0.007	3.67± 0.17	0.054± 0.016	3.65± 0.19	0.029± 0.009
800	5.13± 0.49	0.049± 0.012	4.70± 0.35	0.024± 0.007	3.74± 0.16	0.062± 0.021	3.68± 0.18	0.032± 0.008
850	5.23± 0.52	0.064± 0.018	4.76± 0.36	0.028± 0.007	3.80± 0.15	0.082± 0.010	3.72± 0.18	0.034± 0.010
900	5.34± 0.57	0.090± 0.025	4.82± 0.37	0.039± 0.011	3.87± 0.14	0.103± 0.016	3.76± 0.18	0.041± 0.011
950	5.48± 0.61	0.135± 0.038	4.89± 0.39	0.050± 0.010	3.95± 0.14	0.142± 0.023	3.80± 0.18	0.052± 0.012

Table B.10- Dielectric constants and loss factors between 20-950 ºC at 912 MHz and 2470 MHz for mineral powders at void fractions ranging 0.56±0.04 for montmorillonite, muscovite and kaolinite. These results are the average of three repeats. The standard uncertainties are indicated in the table.

	Kaolinite				Montmorillonite				Muscovite			
Frequency (MHz)	912		2470		912		2470		912		2470	
T (°C)	ε'	ε''	ε'	ε''	ε'	ε''	ε'	ε''	ε'	ε''	ε'	ε''
20	2.76± 0.04	0.108± 0.006	2.81± 0.03	0.104± 0.003	3.03± 0.09	0.559± 0.009	2.90± 0.09	0.390± 0.006	2.66± 0.02	0.198± 0.010	2.66± 0.02	0.152± 0.005
50	2.81± 0.05	0.165± 0.013	2.85± 0.04	0.119± 0.005	3.45± 0.12	0.862± 0.024	3.12± 0.11	0.611± 0.016	2.80± 0.02	0.325± 0.014	2.73± 0.02	0.220± 0.008
100	2.62± 0.03	0.077± 0.012	2.67± 0.02	0.060± 0.007	3.51± 0.13	0.841± 0.033	3.13± 0.11	0.669± 0.022	2.38± 0.17	0.153± 0.019	2.35± 0.16	0.112± 0.015
150	2.52± 0.06	0.026± 0.002	2.59± 0.04	0.023± 0.001	2.35± 0.09	0.102± 0.007	2.35± 0.09	0.080± 0.007	2.26± 0.03	0.024± 0.001	2.28± 0.02	0.020± 0.001
200	2.50± 0.07	0.017± 0.001	2.57± 0.05	0.017± 0.000	2.30± 0.09	0.064± 0.003	2.31± 0.08	0.053± 0.003	2.28± 0.04	0.021± 0.006	2.29± 0.02	0.018± 0.003
250	2.49± 0.07	0.008± 0.001	2.56± 0.05	0.011± 0.000	2.30± 0.09	0.062± 0.004	2.31± 0.08	0.052± 0.003	2.30± 0.05	0.020± 0.007	2.30± 0.03	0.017± 0.004
300	2.50± 0.07	0.004± 0.001	2.55± 0.05	0.008± 0.000	2.30± 0.10	0.066± 0.003	2.31± 0.08	0.050± 0.002	2.33± 0.06	0.024± 0.007	2.32± 0.03	0.018± 0.005
350	2.50± 0.07	0.003± 0.002	2.55± 0.05	0.007± 0.000	2.31± 0.12	0.076± 0.003	2.30± 0.09	0.049± 0.003	2.36± 0.06	0.027± 0.007	2.34± 0.03	0.019± 0.006
400	2.50± 0.08	0.003± 0.001	2.54± 0.05	0.006± 0.000	2.33± 0.13	0.100± 0.004	2.32± 0.09	0.056± 0.003	2.39± 0.06	0.034± 0.009	2.35± 0.03	0.021± 0.006
450	2.49± 0.08	0.004± 0.002	2.52± 0.06	0.005± 0.000	2.37± 0.15	0.130± 0.007	2.34± 0.10	0.067± 0.003	2.41± 0.07	0.040± 0.009	2.36± 0.04	0.024± 0.006
500	2.44± 0.08	0.004± 0.001	2.45± 0.05	0.005± 0.001	2.40± 0.17	0.150± 0.008	2.35± 0.10	0.072± 0.003	2.42± 0.07	0.047± 0.010	2.35± 0.04	0.025± 0.007
550	2.18± 0.27	0.006± 0.002	2.17± 0.22	0.006± 0.002	2.42± 0.19	0.154± 0.013	2.35± 0.11	0.072± 0.004	2.47± 0.08	0.061± 0.009	2.36± 0.04	0.030± 0.007
600	2.24± 0.18	0.009± 0.003	2.18± 0.16	0.008± 0.002	2.46± 0.19	0.176± 0.007	2.37± 0.11	0.081± 0.003	2.52± 0.07	0.079± 0.009	2.39± 0.04	0.037± 0.007
650	2.29± 0.15	0.013± 0.003	2.22± 0.12	0.010± 0.002	2.52± 0.21	0.204± 0.006	2.39± 0.12	0.093± 0.004	2.58± 0.07	0.097± 0.011	2.42± 0.04	0.045± 0.007
700	2.37± 0.07	0.016± 0.002	2.29± 0.03	0.012± 0.001	2.59± 0.21	0.237± 0.010	2.43± 0.11	0.107± 0.005	2.63± 0.07	0.116± 0.010	2.44± 0.04	0.053± 0.007
750	2.40± 0.07	0.019± 0.003	2.32± 0.03	0.014± 0.001	2.66± 0.20	0.257± 0.011	2.47± 0.11	0.116± 0.004	2.67± 0.07	0.131± 0.010	2.46± 0.04	0.058± 0.008
800	2.43± 0.06	0.021± 0.001	2.34± 0.03	0.015± 0.001	2.74± 0.21	0.260± 0.013	2.53± 0.11	0.123± 0.005	2.71± 0.06	0.144± 0.013	2.48± 0.04	0.061± 0.009
850	2.46± 0.06	0.025± 0.001	2.36± 0.02	0.016± 0.001	3.10± 0.21	0.386± 0.015	2.75± 0.12	0.202± 0.007	2.78± 0.06	0.137± 0.012	2.54± 0.04	0.058± 0.008
900	2.50± 0.06	0.035± 0.003	2.38± 0.02	0.018± 0.001	3.42± 0.23	0.585± 0.033	2.94± 0.12	0.309± 0.015	3.00± 0.05	0.186± 0.010	2.71± 0.03	0.084± 0.007
950	2.52± 0.06	0.046± 0.002	2.38± 0.02	0.023± 0.002	3.73± 0.24	0.79±1 0.041	3.16± 0.13	0.415± 0.015	3.27± 0.05	0.318± 0.020	2.88± 0.04	0.149± 0.012

Table B.11- Dielectric constants and loss factors between 20-950 ºC at 912 MHz and 2470 MHz for mineral powders at void fractions ranging 0.56±0.04 for calcite and quartz. These results are the average of three repeats. The standard uncertainties are indicated in the table.

	Calcite				Quartz			
Frequency (MHz)	**912**		**2470**		**912**		**2470**	
T (°C)	**ε'**	**ε''**	**ε'**	**ε''**	**ε'**	**ε''**	**ε'**	**ε''**
20	2.61± 0.05	0.003± 0.001	2.71± 0.06	0.005± 0.001	1.87± 0.05	0.009± 0.005	1.91± 0.05	0.009± 0.001
50	2.62± 0.05	0.003± 0.001	2.72± 0.06	0.004± 0.000	1.87± 0.05	0.004± 0.002	1.91± 0.05	0.006± 0.001
100	2.64± 0.06	0.002± 0.002	2.75± 0.06	0.003± 0.000	1.86± 0.05	0.004± 0.003	1.91± 0.05	0.003± 0.000
150	2.67± 0.08	0.003± 0.001	2.78± 0.06	0.004± 0.000	1.86± 0.06	0.002± 0.005	1.92± 0.05	0.002± 0.000
200	2.70± 0.11	0.003± 0.002	2.81± 0.07	0.004± 0.000	1.88± 0.06	0.001± 0.003	1.93± 0.05	0.002± 0.000
250	2.73± 0.14	0.003± 0.001	2.84± 0.08	0.004± 0.001	1.90± 0.06	0.002± 0.005	1.94± 0.04	0.002± 0.001
300	2.76± 0.15	0.002± 0.002	2.87± 0.08	0.004± 0.001	1.92± 0.06	0.003± 0.003	1.96± 0.04	0.002± 0.000
350	2.80± 0.16	0.001± 0.001	2.89± 0.08	0.004± 0.001	1.95± 0.06	0.004± 0.003	1.97± 0.04	0.003± 0.000
400	2.84± 0.16	0.001± 0.002	2.92± 0.08	0.004± 0.001	1.98± 0.05	0.005± 0.004	1.99± 0.04	0.004± 0.000
450	2.88± 0.17	0.006± 0.002	2.96± 0.08	0.003± 0.001	2.01± 0.05	0.005± 0.002	2.01± 0.03	0.004± 0.000
500	2.94± 0.17	0.004± 0.002	3.00± 0.07	0.004± 0.001	2.05± 0.05	0.006± 0.006	2.03± 0.03	0.004± 0.001
550	3.00± 0.17	0.004± 0.003	3.05± 0.07	0.004± 0.001	2.10± 0.05	0.007± 0.004	2.06± 0.03	0.005± 0.001
600	3.07± 0.17	0.005± 0.003	3.10± 0.07	0.005± 0.000	2.15± 0.06	0.010± 0.004	2.08± 0.03	0.006± 0.001
650	3.15± 0.18	0.007± 0.003	3.15± 0.07	0.005± 0.001	2.20± 0.05	0.015± 0.005	2.10± 0.03	0.007± 0.001
700	3.22± 0.19	0.012± 0.001	3.21± 0.07	0.006± 0.001	2.24± 0.05	0.016± 0.005	2.12± 0.03	0.008± 0.001
750	3.31± 0.20	0.012± 0.002	3.27± 0.08	0.007± 0.000	2.27± 0.05	0.017± 0.006	2.14± 0.02	0.010± 0.001
800	3.38± 0.21	0.015± 0.002	3.31± 0.08	0.008± 0.002	2.31± 0.05	0.020± 0.008	2.16± 0.02	0.013± 0.002
850	3.38± 0.20	0.022± 0.003	3.28± 0.09	0.010± 0.001	2.34± 0.05	0.024± 0.007	2.18± 0.02	0.014± 0.001
900	3.04± 0.15	0.025± 0.003	2.89± 0.16	0.011± 0.000	2.38± 0.05	0.030± 0.008	2.19± 0.01	0.016± 0.002
950	2.56± 0.23	0.028± 0.003	2.38± 0.07	0.012± 0.002	2.41± 0.05	0.043± 0.011	2.21± 0.01	0.019± 0.002

Table B.12- Dielectric constants and loss factors between 20-950 ºC at 912 MHz and 2470 MHz for mineral powders at void fractions ranging 0.56±0.04 for orthoclase and albite. These results are the average of three repeats. The standard uncertainties are indicated in the table.

	Orthoclase				Albite			
Frequency (MHz)	**912**		**2470**		**912**		**2470**	
T (°C)	**ε'**	**ε''**	**ε'**	**ε''**	**ε'**	**ε''**	**ε'**	**ε''**
20	2.12± 0.09	0.006± 0.003	2.18± 0.09	0.007± 0.002	2.19± 0.07	0.014± 0.002	2.25± 0.07	0.013± 0.002
50	2.13± 0.09	0.003± 0.003	2.19± 0.09	0.006± 0.001	2.20± 0.07	0.015± 0.003	2.26± 0.07	0.011± 0.001
100	2.12± 0.10	0.003± 0.001	2.19± 0.09	0.003± 0.000	2.20± 0.07	0.005± 0.004	2.26± 0.07	0.005± 0.000
150	2.11± 0.10	0.003± 0.001	2.20± 0.09	0.003± 0.000	2.21± 0.08	0.005± 0.001	2.28± 0.07	0.006± 0.001
200	2.12± 0.10	0.003± 0.002	2.21± 0.09	0.003± 0.001	2.22± 0.08	0.006± 0.002	2.29± 0.07	0.007± 0.000
250	2.14± 0.08	0.003± 0.003	2.22± 0.09	0.004± 0.000	2.25± 0.08	0.011± 0.003	2.31± 0.07	0.008± 0.000
300	2.16± 0.08	0.005± 0.002	2.24± 0.09	0.005± 0.001	2.27± 0.08	0.011± 0.002	2.33± 0.07	0.010± 0.000
350	2.19± 0.07	0.007± 0.002	2.26± 0.09	0.006± 0.001	2.31± 0.07	0.019± 0.002	2.36± 0.07	0.013± 0.001
400	2.22± 0.06	0.009± 0.000	2.28± 0.08	0.007± 0.001	2.35± 0.07	0.027± 0.002	2.38± 0.07	0.017± 0.000
450	2.24± 0.05	0.010± 0.002	2.30± 0.08	0.007± 0.001	2.39± 0.07	0.036± 0.002	2.41± 0.07	0.022± 0.001
500	2.27± 0.04	0.012± 0.001	2.32± 0.07	0.009± 0.000	2.43± 0.08	0.047± 0.001	2.44± 0.07	0.027± 0.001
550	2.31± 0.04	0.020± 0.001	2.34± 0.07	0.012± 0.001	2.47± 0.09	0.059± 0.003	2.46± 0.07	0.033± 0.001
600	2.35± 0.04	0.024± 0.001	2.36± 0.07	0.014± 0.001	2.53± 0.10	0.080± 0.000	2.49± 0.07	0.042± 0.001
650	2.40± 0.05	0.029± 0.003	2.39± 0.07	0.016± 0.000	2.57± 0.11	0.105± 0.001	2.52± 0.08	0.053± 0.002
700	2.45± 0.07	0.038± 0.004	2.41± 0.07	0.020± 0.001	2.63± 0.11	0.130± 0.000	2.55± 0.08	0.064± 0.001
750	2.49± 0.07	0.049± 0.004	2.44± 0.06	0.024± 0.001	2.66± 0.11	0.138± 0.003	2.57± 0.08	0.065± 0.002
800	2.52± 0.08	0.057± 0.003	2.46± 0.07	0.029± 0.002	2.65± 0.11	0.104± 0.008	2.56± 0.08	0.044± 0.002
850	2.56± 0.08	0.071± 0.002	2.48± 0.07	0.034± 0.002	2.64± 0.10	0.075± 0.009	2.55± 0.07	0.031± 0.004
900	2.61± 0.08	0.087± 0.007	2.51± 0.07	0.041± 0.002	2.67± 0.09	0.083± 0.008	2.57± 0.07	0.033± 0.004
950	2.66± 0.08	0.104± 0.006	2.54± 0.07	0.045± 0.003	2.72± 0.09	0.102± 0.011	2.60± 0.07	0.040± 0.003

Appendix B3: Dielectric properties of Fibercon wool and Vitcas firebrick

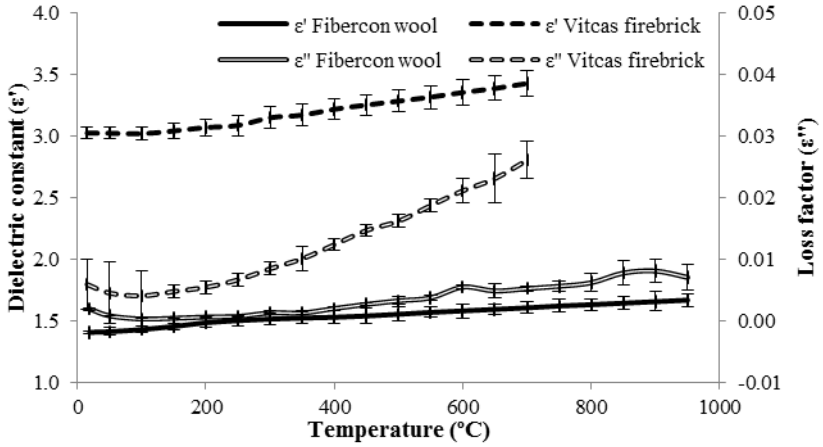


Figure B.1- Average trends of dielectric constants and loss factors of Fibercon 1600 wool and Vitcas grade 30 firebrick at 2470 MHz and across the firing range of 20-950 ºC and 20-700 ºC, respectively. These results are the average of three repeats using the resonant cavity method. Standard deviations average for the dielectric constants and loss factors around ±0.05 and ±0.001 for the wool, and ±0.08 and ±0.002 for the firebrick.

Table B.13- Average dielectric constants and loss factors of Fibercon 1600 wool and Vitcas grade 30 firebrick at 2470 MHz and across the firing range of 20-950 ºC and 20-700 ºC, respectively. These results are the average of three repeats using the resonant cavity method. The standard uncertainties are indicated in the table.

Temperature (ºC)	Fibercon 1600 wool		Vitcas grade 30 firebrick	
	ε'	ε''	ε'	ε''
20	1.41±0.01	0.002±0.000	3.02±0.05	0.006±0.004
50	1.41±0.02	0.001±0.000	3.02±0.05	0.005±0.005
100	1.43±0.03	0.000±0.000	3.02±0.05	0.004±0.004
150	1.46±0.04	0.000±0.000	3.04±0.06	0.005±0.001
200	1.49±0.04	0.001±0.000	3.07±0.07	0.005±0.001
250	1.50±0.04	0.001±0.000	3.09±0.08	0.007±0.001
300	1.52±0.04	0.001±0.000	3.15±0.09	0.008±0.001
350	1.52±0.04	0.001±0.000	3.17±0.09	0.010±0.002
400	1.53±0.04	0.002±0.000	3.22±0.08	0.012±0.001
450	1.54±0.04	0.003±0.000	3.25±0.08	0.015±0.001
500	1.55±0.05	0.003±0.001	3.28±0.09	0.016±0.001
550	1.57±0.05	0.004±0.000	3.32±0.09	0.019±0.001
600	1.58±0.06	0.006±0.000	3.35±0.10	0.021±0.002
650	1.59±0.07	0.005±0.001	3.39±0.10	0.023±0.004
700	1.61±0.04	0.005±0.001	3.43±0.10	0.026±0.003
750	1.62±0.06	0.006±0.001		
800	1.63±0.08	0.006±0.001		
850	1.64±0.08	0.008±0.002		
900	1.66±0.08	0.008±0.002		
950	1.67±0.08	0.007±0.002		

Appendix C: Dielectric property estimations

Appendix C1: Estimations of binary clay-air mixtures

Appendix C1.1: Powder to slab estimations

Table C.1- Binary clay-air mixing rules dielectric property estimations of slabs of Vedstaarup yellow clay at 0.37±0.02 void fraction at 912 MHz across the 20-950 C firing range from clay powders at void fractions ranging 0.56±0.03. The standard uncertainties are indicated in the table.

	Complex Refractive Index		Landau-Lifshitz-Looyenga		Bruggeman-Hanai		Böttcher		Lichtenecker		Rayleigh		Sen-Scala-Cohen		Complex Refractive Index α=0.65	
T (°C)	ε'	ε''	ε'	ε''	ε'	ε''	ε'	ε''	ε'	ε''	ε'	ε''	ε'	ε''	ε'	ε''
20	3.06± 0.04	0.050± 0.002	3.15± 0.04	0.053± 0.002	3.08± 0.04	0.050± 0.002	3.25± 0.04	0.059± 0.002	3.38± 0.04	0.064± 0.002	3.00± 0.04	0.046± 0.002	3.33± 0.04	0.065± 0.002	3.00± 0.04	0.047± 0.002
50	3.12± 0.05	0.060± 0.003	3.21± 0.05	0.065± 0.003	3.14± 0.05	0.060± 0.003	3.32± 0.05	0.072± 0.003	3.44± 0.05	0.078± 0.003	3.05± 0.05	0.056± 0.003	3.40± 0.05	0.080± 0.003	3.05± 0.05	0.057± 0.003
100	3.04± 0.09	0.046± 0.005	3.12± 0.09	0.049± 0.005	3.06± 0.09	0.046± 0.005	3.22± 0.09	0.054± 0.005	3.35± 0.09	0.059± 0.005	2.98± 0.09	0.043± 0.005	3.30± 0.09	0.060± 0.005	2.98± 0.09	0.043± 0.005
150	3.01± 0.10	0.055± 0.003	3.09± 0.10	0.059± 0.003	3.03± 0.10	0.056± 0.003	3.19± 0.10	0.065± 0.003	3.31± 0.10	0.071± 0.003	2.95± 0.10	0.052± 0.003	3.26± 0.10	0.072± 0.003	2.95± 0.10	0.053± 0.003
200	3.03± 0.13	0.054± 0.004	3.11± 0.13	0.057± 0.004	3.05± 0.13	0.054± 0.004	3.21± 0.13	0.063± 0.004	3.33± 0.13	0.069± 0.004	2.97± 0.13	0.050± 0.004	3.29± 0.13	0.070± 0.004	2.96± 0.13	0.051± 0.004
250	3.06± 0.15	0.054± 0.003	3.15± 0.15	0.058± 0.003	3.08± 0.15	0.054± 0.003	3.25± 0.15	0.064± 0.003	3.38± 0.15	0.070± 0.003	3.00± 0.15	0.050± 0.003	3.33± 0.15	0.071± 0.003	3.00± 0.15	0.051± 0.003
300	3.09± 0.17	0.055± 0.004	3.18± 0.17	0.059± 0.004	3.11± 0.17	0.055± 0.004	3.29± 0.17	0.065± 0.004	3.42± 0.17	0.071± 0.004	3.03± 0.17	0.051± 0.004	3.37± 0.17	0.072± 0.004	3.03± 0.17	0.052± 0.004
350	3.13± 0.18	0.058± 0.004	3.22± 0.18	0.062± 0.004	3.15± 0.18	0.058± 0.004	3.33± 0.18	0.069± 0.004	3.46± 0.18	0.075± 0.004	3.06± 0.18	0.053± 0.004	3.42± 0.18	0.077± 0.004	3.06± 0.18	0.055± 0.004
400	3.17± 0.19	0.060± 0.004	3.27± 0.19	0.064± 0.004	3.19± 0.19	0.060± 0.004	3.38± 0.19	0.071± 0.004	3.52± 0.19	0.078± 0.004	3.10± 0.19	0.055± 0.004	3.47± 0.19	0.080± 0.004	3.10± 0.19	0.057± 0.004
450	3.22± 0.20	0.066± 0.004	3.32± 0.20	0.071± 0.004	3.24± 0.20	0.066± 0.004	3.44± 0.20	0.080± 0.004	3.58± 0.20	0.087± 0.004	3.14± 0.20	0.061± 0.004	3.54± 0.20	0.090± 0.004	3.15± 0.20	0.063± 0.004
500	3.26± 0.20	0.074± 0.004	3.36± 0.20	0.080± 0.004	3.28± 0.20	0.074± 0.004	3.49± 0.20	0.089± 0.004	3.63± 0.20	0.097± 0.004	3.18± 0.20	0.069± 0.004	3.59± 0.20	0.101± 0.004	3.18± 0.20	0.070± 0.004
550	3.31± 0.20	0.081± 0.003	3.41± 0.20	0.087± 0.003	3.33± 0.20	0.081± 0.003	3.54± 0.20	0.098± 0.003	3.69± 0.20	0.107± 0.003	3.23± 0.20	0.075± 0.003	3.66± 0.20	0.111± 0.003	3.23± 0.20	0.077± 0.003
600	3.37± 0.18	0.092± 0.004	3.48± 0.18	0.100± 0.004	3.39± 0.18	0.092± 0.004	3.62± 0.18	0.112± 0.004	3.78± 0.18	0.122± 0.004	3.29± 0.18	0.085± 0.004	3.75± 0.18	0.128± 0.004	3.29± 0.18	0.087± 0.004
650	3.44± 0.16	0.105± 0.005	3.55± 0.16	0.114± 0.005	3.45± 0.16	0.105± 0.005	3.70± 0.16	0.128± 0.005	3.86± 0.16	0.140± 0.005	3.34± 0.16	0.097± 0.005	3.83± 0.16	0.147± 0.005	3.35± 0.16	0.099± 0.005
700	3.48± 0.16	0.115± 0.005	3.60± 0.16	0.124± 0.005	3.50± 0.16	0.114± 0.005	3.75± 0.16	0.140± 0.005	3.92± 0.16	0.153± 0.005	3.38± 0.16	0.105± 0.005	3.90± 0.16	0.162± 0.005	3.39± 0.16	0.108± 0.005
750	3.52± 0.17	0.121± 0.006	3.64± 0.17	0.131± 0.006	3.54± 0.17	0.121± 0.006	3.80± 0.17	0.148± 0.006	3.98± 0.17	0.162± 0.006	3.42± 0.17	0.111± 0.006	3.96± 0.17	0.173± 0.006	3.43± 0.17	0.114± 0.006
800	3.60± 0.18	0.127± 0.006	3.73± 0.18	0.137± 0.006	3.62± 0.18	0.126± 0.006	3.90± 0.18	0.155± 0.006	4.08± 0.18	0.170± 0.006	3.49± 0.18	0.116± 0.006	4.07± 0.18	0.183± 0.006	3.50± 0.18	0.119± 0.006
850	3.72± 0.19	0.149± 0.006	3.86± 0.19	0.162± 0.006	3.74± 0.19	0.148± 0.006	4.05± 0.19	0.184± 0.006	4.24± 0.19	0.202± 0.006	3.60± 0.19	0.136± 0.006	4.24± 0.19	0.220± 0.006	3.62± 0.19	0.140± 0.006
900	3.73± 0.21	0.181± 0.006	3.87± 0.21	0.196± 0.006	3.75± 0.21	0.179± 0.006	4.06± 0.21	0.223± 0.006	4.25± 0.21	0.246± 0.006	3.61± 0.21	0.165± 0.006	4.25± 0.21	0.268± 0.006	3.63± 0.21	0.170± 0.006
950	3.81± 0.22	0.233± 0.008	3.96± 0.22	0.253± 0.008	3.83± 0.22	0.231± 0.008	4.16± 0.22	0.289± 0.008	4.37± 0.22	0.319± 0.008	3.69± 0.22	0.212± 0.008	4.38± 0.22	0.351± 0.008	3.70± 0.22	0.219± 0.008

Table C.2- Binary clay-air mixing rules dielectric property estimations of slabs of Vedstaarup yellow clay at 0.37±0.02 void fraction at 2470 MHz across the 20-950 C firing range from clay powders at void fractions ranging 0.56±0.03. The standard uncertainties are indicated in the table.

	Complex Refractive Index		Landau-Lifshitz-Looyenga		Bruggeman-Hanai		Böttcher		Lichtenecker		Rayleigh		Sen-Scala-Cohen		Complex Refractive Index α=0.65	
T (°C)	ε'	ε''	ε'	ε''	ε'	ε''	ε'	ε''	ε'	ε''	ε'	ε''	ε'	ε''	ε'	ε''
20	3.15± 0.02	0.025± 0.004	3.24± 0.02	0.027± 0.007	3.17± 0.02	0.025± 0.004	3.36± 0.02	0.030± 0.004	3.49± 0.02	0.033± 0.004	3.08± 0.02	0.023± 0.004	3.45± 0.02	0.034± 0.004	3.08± 0.02	0.024± 0.004
50	3.19± 0.02	0.031± 0.004	3.29± 0.02	0.034± 0.004	3.21± 0.02	0.031± 0.004	3.40± 0.02	0.037± 0.004	3.54± 0.02	0.041± 0.004	3.12± 0.02	0.029± 0.004	3.50± 0.02	0.042± 0.004	3.12± 0.02	0.030± 0.004
100	3.13± 0.04	0.021± 0.005	3.22± 0.04	0.023± 0.005	3.15± 0.04	0.021± 0.005	3.33± 0.04	0.025± 0.005	3.46± 0.04	0.027± 0.005	3.06± 0.04	0.020± 0.005	3.42± 0.04	0.028± 0.005	3.06± 0.04	0.020± 0.005
150	3.11± 0.04	0.019± 0.002	3.19± 0.04	0.020± 0.002	3.13± 0.04	0.019± 0.002	3.30± 0.04	0.022± 0.002	3.43± 0.04	0.024± 0.002	3.04± 0.04	0.017± 0.002	3.39± 0.04	0.025± 0.002	3.04± 0.04	0.018± 0.002
200	3.12± 0.04	0.017± 0.002	3.21± 0.04	0.018± 0.002	3.14± 0.04	0.017± 0.002	3.32± 0.04	0.020± 0.002	3.45± 0.04	0.022± 0.002	3.05± 0.04	0.015± 0.002	3.41± 0.04	0.022± 0.002	3.05± 0.04	0.016± 0.002
250	3.14± 0.04	0.017± 0.002	3.24± 0.04	0.018± 0.002	3.16± 0.04	0.017± 0.002	3.35± 0.04	0.020± 0.002	3.48± 0.04	0.022± 0.002	3.07± 0.04	0.015± 0.002	3.44± 0.04	0.022± 0.002	3.07± 0.04	0.016± 0.002
300	3.17± 0.05	0.016± 0.002	3.26± 0.05	0.017± 0.002	3.19± 0.05	0.016± 0.002	3.38± 0.05	0.019± 0.002	3.51± 0.05	0.021± 0.002	3.09± 0.05	0.015± 0.002	3.47± 0.05	0.021± 0.002	3.10± 0.05	0.015± 0.002
350	3.19± 0.05	0.017± 0.002	3.29± 0.05	0.018± 0.002	3.21± 0.05	0.016± 0.002	3.41± 0.05	0.019± 0.002	3.54± 0.05	0.021± 0.002	3.12± 0.05	0.015± 0.002	3.50± 0.05	0.022± 0.002	3.12± 0.05	0.016± 0.002
400	3.22± 0.05	0.018± 0.002	3.32± 0.05	0.020± 0.002	3.24± 0.05	0.018± 0.002	3.44± 0.05	0.022± 0.002	3.58± 0.05	0.024± 0.002	3.14± 0.05	0.017± 0.002	3.54± 0.05	0.025± 0.002	3.15± 0.05	0.017± 0.002
450	3.25± 0.05	0.021± 0.001	3.35± 0.05	0.022± 0.001	3.27± 0.05	0.021± 0.001	3.48± 0.05	0.025± 0.001	3.62± 0.05	0.027± 0.001	3.17± 0.05	0.019± 0.001	3.58± 0.05	0.028± 0.001	3.18± 0.05	0.020± 0.001
500	3.27± 0.06	0.023± 0.002	3.38± 0.06	0.025± 0.002	3.29± 0.06	0.023± 0.002	3.50± 0.06	0.028± 0.002	3.65± 0.06	0.030± 0.002	3.19± 0.06	0.021± 0.002	3.61± 0.06	0.031± 0.002	3.20± 0.06	0.022± 0.002
550	3.30± 0.05	0.027± 0.002	3.41± 0.05	0.029± 0.002	3.32± 0.05	0.027± 0.002	3.54± 0.05	0.032± 0.002	3.69± 0.05	0.035± 0.002	3.22± 0.05	0.025± 0.002	3.65± 0.05	0.037± 0.002	3.22± 0.05	0.025± 0.002
600	3.34± 0.05	0.033± 0.002	3.45± 0.05	0.036± 0.002	3.36± 0.05	0.033± 0.002	3.59± 0.05	0.040± 0.002	3.74± 0.05	0.044± 0.002	3.26± 0.05	0.031± 0.002	3.71± 0.05	0.046± 0.002	3.26± 0.05	0.031± 0.002
650	3.38± 0.05	0.038± 0.002	3.49± 0.05	0.041± 0.002	3.40± 0.05	0.037± 0.002	3.63± 0.05	0.045± 0.002	3.79± 0.05	0.050± 0.002	3.29± 0.05	0.035± 0.002	3.76± 0.05	0.052± 0.002	3.30± 0.05	0.035± 0.002
700	3.40± 0.04	0.040± 0.002	3.52± 0.04	0.044± 0.002	3.42± 0.04	0.040± 0.002	3.66± 0.04	0.049± 0.002	3.82± 0.04	0.053± 0.002	3.31± 0.04	0.037± 0.002	3.79± 0.04	0.056± 0.002	3.32± 0.04	0.038± 0.002
750	3.42± 0.04	0.042± 0.003	3.54± 0.04	0.045± 0.003	3.44± 0.04	0.042± 0.003	3.68± 0.04	0.051± 0.003	3.84± 0.04	0.055± 0.003	3.33± 0.04	0.038± 0.003	3.82± 0.04	0.058± 0.003	3.34± 0.04	0.039± 0.003
800	3.47± 0.05	0.043± 0.002	3.59± 0.05	0.046± 0.002	3.49± 0.05	0.043± 0.002	3.74± 0.05	0.052± 0.002	3.91± 0.05	0.057± 0.002	3.37± 0.05	0.039± 0.002	3.88± 0.05	0.060± 0.002	3.38± 0.05	0.040± 0.002
850	3.55± 0.06	0.053± 0.002	3.67± 0.06	0.057± 0.002	3.57± 0.06	0.052± 0.002	3.84± 0.06	0.064± 0.002	4.02± 0.06	0.071± 0.002	3.45± 0.06	0.048± 0.002	4.00± 0.06	0.075± 0.002	3.46± 0.06	0.050± 0.002
900	3.53± 0.06	0.063± 0.004	3.65± 0.06	0.068± 0.004	3.54± 0.06	0.063± 0.004	3.81± 0.06	0.077± 0.004	3.98± 0.06	0.084± 0.004	3.42± 0.06	0.058± 0.004	3.96± 0.06	0.090± 0.004	3.43± 0.06	0.059± 0.004
950	3.56± 0.06	0.079± 0.004	3.69± 0.06	0.085± 0.004	3.58± 0.06	0.078± 0.004	3.85± 0.06	0.095± 0.004	4.03± 0.06	0.106± 0.004	3.46± 0.06	0.072± 0.004	4.01± 0.06	0.113± 0.004	3.47± 0.06	0.074± 0.004

Table C.3- Binary clay-air mixing rules dielectric property estimations of slabs of Hammershoj yellow clay at 0.39±0.01 void fraction at 912 MHz across the 20-950 C firing range from clay powders at void fractions ranging 0.56±0.03. The standard uncertainties are indicated in the table.

	Complex Refractive Index		Landau-Lifshitz-Looyenga		Bruggeman-Hanai		Böttcher		Lichtenecker		Rayleigh		Sen-Scala-Cohen		Complex Refractive Index α=0.65	
T (°C)	**ε'**	**ε''**	**ε'**	**ε''**	**ε'**	**ε''**	**ε'**	**ε''**	**ε'**	**ε''**	**ε'**	**ε''**	**ε'**	**ε''**	**ε'**	**ε''**
20	3.20± 0.08	0.052± 0.018	3.29± 0.08	0.055± 0.018	3.22± 0.08	0.052± 0.018	3.41± 0.08	0.062± 0.018	3.53± 0.08	0.066± 0.018	3.13± 0.08	0.048± 0.018	3.50± 0.08	0.069± 0.018	3.13± 0.08	0.049± 0.018
50	3.28± 0.10	0.071± 0.028	3.38± 0.10	0.077± 0.028	3.30± 0.10	0.071± 0.028	3.50± 0.10	0.085± 0.028	3.63± 0.10	0.092± 0.028	3.20± 0.10	0.066± 0.028	3.61± 0.10	0.096± 0.028	3.21± 0.10	0.068± 0.028
100	3.13± 0.08	0.032± 0.011	3.21± 0.08	0.034± 0.011	3.15± 0.08	0.032± 0.011	3.32± 0.08	0.037± 0.011	3.44± 0.08	0.040± 0.011	3.06± 0.08	0.029± 0.011	3.41± 0.08	0.041± 0.011	3.07± 0.08	0.030± 0.011
150	3.05± 0.11	0.029± 0.005	3.13± 0.11	0.030± 0.005	3.07± 0.11	0.029± 0.005	3.24± 0.11	0.034± 0.005	3.34± 0.11	0.036± 0.005	2.99± 0.11	0.027± 0.005	3.31± 0.11	0.037± 0.005	2.99± 0.11	0.027± 0.005
200	3.07± 0.13	0.027± 0.004	3.16± 0.13	0.029± 0.004	3.09± 0.13	0.027± 0.004	3.26± 0.13	0.032± 0.004	3.37± 0.13	0.034± 0.004	3.01± 0.13	0.025± 0.004	3.33± 0.13	0.035± 0.004	3.01± 0.13	0.026± 0.004
250	3.11± 0.15	0.026± 0.004	3.19± 0.15	0.028± 0.004	3.13± 0.15	0.026± 0.004	3.30± 0.15	0.031± 0.004	3.41± 0.15	0.033± 0.004	3.04± 0.15	0.024± 0.004	3.38± 0.15	0.034± 0.004	3.05± 0.15	0.025± 0.004
300	3.14± 0.17	0.025± 0.003	3.22± 0.17	0.026± 0.003	3.15± 0.17	0.025± 0.003	3.33± 0.17	0.029± 0.003	3.45± 0.17	0.031± 0.003	3.07± 0.17	0.023± 0.003	3.41± 0.17	0.032± 0.003	3.07± 0.17	0.023± 0.003
350	3.18± 0.18	0.026± 0.003	3.27± 0.18	0.027± 0.003	3.20± 0.18	0.026± 0.003	3.38± 0.18	0.030± 0.003	3.50± 0.18	0.033± 0.003	3.11± 0.18	0.024± 0.003	3.47± 0.18	0.034± 0.003	3.11± 0.18	0.024± 0.003
400	3.25± 0.18	0.029± 0.004	3.34± 0.18	0.031± 0.004	3.26± 0.18	0.029± 0.004	3.46± 0.18	0.035± 0.004	3.59± 0.18	0.037± 0.004	3.17± 0.18	0.027± 0.004	3.56± 0.18	0.039± 0.004	3.18± 0.18	0.028± 0.004
450	3.31± 0.20	0.038± 0.004	3.41± 0.20	0.041± 0.004	3.33± 0.20	0.038± 0.004	3.55± 0.20	0.046± 0.004	3.67± 0.20	0.049± 0.004	3.23± 0.20	0.035± 0.004	3.65± 0.20	0.052± 0.004	3.24± 0.20	0.036± 0.004
500	3.36± 0.22	0.047± 0.003	3.46± 0.22	0.050± 0.003	3.38± 0.22	0.047± 0.003	3.60± 0.22	0.056± 0.003	3.74± 0.22	0.061± 0.003	3.28± 0.22	0.043± 0.003	3.72± 0.22	0.064± 0.003	3.29± 0.22	0.045± 0.003
550	3.42± 0.23	0.058± 0.004	3.52± 0.23	0.063± 0.004	3.43± 0.23	0.058± 0.004	3.67± 0.23	0.070± 0.004	3.81± 0.23	0.076± 0.004	3.33± 0.23	0.054± 0.004	3.79± 0.23	0.081± 0.004	3.34± 0.23	0.055± 0.004
600	3.48± 0.24	0.071± 0.005	3.59± 0.24	0.076± 0.005	3.50± 0.24	0.071± 0.005	3.74± 0.24	0.086± 0.005	3.89± 0.24	0.093± 0.005	3.39± 0.24	0.065± 0.005	3.88± 0.24	0.099± 0.005	3.40± 0.24	0.067± 0.005
650	3.55± 0.25	0.089± 0.004	3.66± 0.25	0.096± 0.004	3.56± 0.25	0.089± 0.004	3.82± 0.25	0.108± 0.004	3.97± 0.25	0.117± 0.004	3.45± 0.25	0.082± 0.004	3.97± 0.25	0.126± 0.004	3.46± 0.25	0.084± 0.004
700	3.59± 0.25	0.102± 0.005	3.71± 0.25	0.110± 0.005	3.61± 0.25	0.102± 0.005	3.88± 0.25	0.125± 0.005	4.03± 0.25	0.135± 0.005	3.49± 0.25	0.094± 0.005	4.04± 0.25	0.146± 0.005	3.50± 0.25	0.097± 0.005
750	3.53± 0.28	0.105± 0.010	3.64± 0.28	0.113± 0.010	3.55± 0.28	0.105± 0.010	3.80± 0.28	0.128± 0.010	3.95± 0.28	0.138± 0.010	3.43± 0.28	0.097± 0.010	3.95± 0.28	0.148± 0.010	3.44± 0.28	0.099± 0.010
800	3.72± 0.25	0.112± 0.005	3.85± 0.25	0.121± 0.005	3.74± 0.25	0.111± 0.005	4.04± 0.25	0.138± 0.005	4.21± 0.25	0.149± 0.005	3.61± 0.25	0.103± 0.005	4.23± 0.25	0.164± 0.005	3.63± 0.25	0.106± 0.005
850	3.86± 0.25	0.141± 0.007	4.00± 0.25	0.153± 0.007	3.87± 0.25	0.140± 0.007	4.21± 0.25	0.175± 0.007	4.39± 0.25	0.190± 0.007	3.73± 0.25	0.129± 0.007	4.42± 0.25	0.212± 0.007	3.76± 0.25	0.133± 0.007
900	3.80± 0.25	0.161± 0.007	3.94± 0.25	0.174± 0.007	3.82± 0.25	0.159± 0.007	4.14± 0.25	0.198± 0.007	4.31± 0.25	0.215± 0.007	3.68± 0.25	0.147± 0.007	4.34± 0.25	0.238± 0.007	3.70± 0.25	0.152± 0.007
950	3.80± 0.27	0.220± 0.010	3.94± 0.27	0.238± 0.010	3.82± 0.27	0.218± 0.010	4.14± 0.27	0.271± 0.010	4.31± 0.27	0.294± 0.010	3.68± 0.27	0.201± 0.010	4.34± 0.27	0.325± 0.010	3.70± 0.27	0.207± 0.010

Table C.4-Binary clay-air mixing rules dielectric property estimations of slabs of Hammershoj yellow clay at 0.39±0.01 void fraction at 2470 MHz across the 20-950 ºC firing range from clay powders at void fractions ranging 0.56±0.03. The standard uncertainties are indicated in the table.

	Complex Refractive Index		Landau-Lifshitz-Looyenga		Bruggeman-Hanai		Böttcher		Lichtenecker		Rayleigh		Sen-Scala-Cohen		Complex Refractive Index α=0.65	
T (°C)	ε'	ε''	ε'	ε''	ε'	ε''	ε'	ε''	ε'	ε''	ε'	ε''	ε'	ε''	ε'	ε''
20	3.28± 0.07	0.044± 0.012	3.38± 0.07	0.047± 0.012	3.30± 0.07	0.044± 0.012	3.51± 0.07	0.053± 0.012	3.63± 0.07	0.057± 0.012	3.21± 0.07	0.041± 0.012	3.61± 0.07	0.060± 0.012	3.21± 0.07	0.042± 0.012
50	3.34± 0.08	0.056± 0.017	3.44± 0.08	0.060± 0.017	3.36± 0.08	0.055± 0.017	3.57± 0.08	0.067± 0.017	3.70± 0.08	0.072± 0.017	3.26± 0.08	0.051± 0.017	3.68± 0.08	0.076± 0.017	3.26± 0.08	0.053± 0.017
100	3.23± 0.04	0.027± 0.007	3.32± 0.04	0.029± 0.007	3.25± 0.04	0.027± 0.007	3.44± 0.04	0.033± 0.007	3.57± 0.04	0.035± 0.007	3.16± 0.04	0.025± 0.007	3.54± 0.04	0.037± 0.007	3.16± 0.04	0.026± 0.007
150	3.17± 0.03	0.025± 0.003	3.25± 0.03	0.027± 0.003	3.19± 0.03	0.025± 0.003	3.37± 0.03	0.030± 0.003	3.49± 0.03	0.032± 0.003	3.10± 0.03	0.023± 0.003	3.46± 0.03	0.033± 0.003	3.10± 0.03	0.024± 0.003
200	3.18± 0.04	0.024± 0.003	3.27± 0.04	0.026± 0.003	3.20± 0.04	0.024± 0.003	3.39± 0.04	0.028± 0.003	3.50± 0.04	0.030± 0.003	3.11± 0.04	0.022± 0.003	3.48± 0.04	0.032± 0.003	3.12± 0.04	0.023± 0.003
250	3.21± 0.05	0.023± 0.003	3.30± 0.05	0.025± 0.003	3.22± 0.05	0.023± 0.003	3.42± 0.05	0.027± 0.003	3.53± 0.05	0.029± 0.003	3.13± 0.05	0.021± 0.003	3.51± 0.05	0.031± 0.003	3.14± 0.05	0.022± 0.003
300	3.22± 0.05	0.020± 0.003	3.31± 0.05	0.022± 0.003	3.24± 0.05	0.020± 0.003	3.44± 0.05	0.024± 0.003	3.56± 0.05	0.026± 0.003	3.15± 0.05	0.019± 0.003	3.53± 0.05	0.027± 0.003	3.16± 0.05	0.019± 0.003
350	3.25± 0.05	0.020± 0.003	3.34± 0.05	0.021± 0.003	3.27± 0.05	0.020± 0.003	3.47± 0.05	0.024± 0.003	3.59± 0.05	0.026± 0.003	3.18± 0.05	0.019± 0.003	3.57± 0.05	0.027± 0.003	3.18± 0.05	0.019± 0.003
400	3.29± 0.06	0.022± 0.003	3.38± 0.06	0.024± 0.003	3.31± 0.06	0.022± 0.003	3.51± 0.06	0.027± 0.003	3.64± 0.06	0.029± 0.003	3.21± 0.06	0.021± 0.003	3.62± 0.06	0.030± 0.003	3.22± 0.06	0.021± 0.003
450	3.33± 0.07	0.026± 0.003	3.42± 0.07	0.027± 0.003	3.34± 0.07	0.025± 0.003	3.56± 0.07	0.031± 0.003	3.69± 0.07	0.033± 0.003	3.25± 0.07	0.024± 0.003	3.67± 0.07	0.035± 0.003	3.25± 0.07	0.024± 0.003
500	3.35± 0.07	0.029± 0.003	3.45± 0.07	0.031± 0.003	3.37± 0.07	0.029± 0.003	3.59± 0.07	0.035± 0.003	3.72± 0.07	0.037± 0.003	3.26± 0.07	0.027± 0.003	3.70± 0.07	0.039± 0.003	3.27± 0.07	0.027± 0.003
550	3.37± 0.08	0.034± 0.003	3.48± 0.08	0.037± 0.003	3.39± 0.08	0.034± 0.003	3.62± 0.08	0.041± 0.003	3.75± 0.08	0.044± 0.003	3.29± 0.08	0.032± 0.003	3.73± 0.08	0.047± 0.003	3.30± 0.08	0.033± 0.003
600	3.42± 0.09	0.042± 0.004	3.52± 0.09	0.045± 0.004	3.43± 0.09	0.042± 0.004	3.67± 0.09	0.050± 0.004	3.80± 0.09	0.054± 0.004	3.33± 0.09	0.038± 0.004	3.79± 0.09	0.058± 0.004	3.34± 0.09	0.039± 0.004
650	3.46± 0.09	0.048± 0.004	3.56± 0.09	0.052± 0.004	3.47± 0.09	0.048± 0.004	3.72± 0.09	0.058± 0.004	3.86± 0.09	0.063± 0.004	3.36± 0.09	0.044± 0.004	3.85± 0.09	0.067± 0.004	3.38± 0.09	0.046± 0.004
700	3.47± 0.09	0.053± 0.004	3.58± 0.09	0.057± 0.004	3.49± 0.09	0.053± 0.004	3.74± 0.09	0.064± 0.004	3.88± 0.09	0.069± 0.004	3.38± 0.09	0.049± 0.004	3.87± 0.09	0.074± 0.004	3.39± 0.09	0.050± 0.004
750	3.42± 0.13	0.055± 0.004	3.53± 0.13	0.059± 0.004	3.44± 0.13	0.055± 0.004	3.67± 0.13	0.066± 0.004	3.81± 0.13	0.071± 0.004	3.33± 0.13	0.051± 0.004	3.80± 0.13	0.076± 0.004	3.34± 0.13	0.052± 0.004
800	3.55± 0.09	0.055± 0.004	3.67± 0.09	0.059± 0.004	3.57± 0.09	0.055± 0.004	3.83± 0.09	0.067± 0.004	3.98± 0.09	0.073± 0.004	3.45± 0.09	0.051± 0.004	3.98± 0.09	0.078± 0.004	3.47± 0.09	0.052± 0.004
850	3.65± 0.09	0.068± 0.004	3.78± 0.09	0.074± 0.004	3.67± 0.09	0.068± 0.004	3.96± 0.09	0.084± 0.004	4.12± 0.09	0.090± 0.004	3.55± 0.09	0.063± 0.004	4.13± 0.09	0.099± 0.004	3.56± 0.09	0.065± 0.004
900	3.59± 0.09	0.071± 0.004	3.71± 0.09	0.077± 0.004	3.61± 0.09	0.071± 0.004	3.88± 0.09	0.087± 0.004	4.03± 0.09	0.094± 0.004	3.49± 0.09	0.065± 0.004	4.04± 0.09	0.101± 0.004	3.50± 0.09	0.067± 0.004
950	3.59± 0.10	0.085± 0.005	3.71± 0.10	0.091± 0.005	3.61± 0.10	0.084± 0.005	3.88± 0.10	0.104± 0.005	4.03± 0.10	0.112± 0.005	3.49± 0.10	0.078± 0.005	4.03± 0.10	0.121± 0.005	3.50± 0.10	0.080± 0.005

Table C.5- Binary clay-air mixing rules dielectric property estimations of slabs of Helligsø red clay at 0.40±0.01 void fraction at 912 MHz across the 20-950 ºC firing range from clay powders at void fractions ranging 0.56±0.03. The standard uncertainties are indicated in the table.

	Complex Refractive Index		Landau-Lifshitz-Looyenga		Bruggeman-Hanai		Böttcher		Lichtenecker		Rayleigh		Sen-Scala-Cohen		Complex Refractive Index α=0.65	
T (°C)	ε'	ε''	ε'	ε''	ε'	ε''	ε'	ε''	ε'	ε''	ε'	ε''	ε'	ε''	ε'	ε''
20	3.14± 0.07	0.023± 0.004	3.22± 0.07	0.024± 0.004	3.16± 0.07	0.023± 0.004	3.33± 0.07	0.027± 0.004	3.43± 0.07	0.028± 0.004	3.07± 0.07	0.021± 0.004	3.41± 0.07	0.030± 0.004	3.08± 0.07	0.022± 0.004
50	3.26± 0.10	0.030± 0.008	3.35± 0.10	0.033± 0.008	3.28± 0.10	0.030± 0.008	3.48± 0.10	0.036± 0.008	3.59± 0.10	0.039± 0.008	3.19± 0.10	0.028± 0.008	3.57± 0.10	0.041± 0.008	3.20± 0.10	0.029± 0.008
100	3.15± 0.05	0.022± 0.012	3.23± 0.05	0.024± 0.012	3.17± 0.05	0.022± 0.012	3.34± 0.05	0.026± 0.012	3.45± 0.05	0.028± 0.012	3.08± 0.05	0.021± 0.012	3.42± 0.05	0.029± 0.012	3.09± 0.05	0.021± 0.012
150	2.93± 0.06	0.029± 0.004	3.00± 0.06	0.030± 0.004	2.95± 0.06	0.029± 0.004	3.09± 0.06	0.033± 0.004	3.18± 0.06	0.036± 0.004	2.88± 0.06	0.027± 0.004	3.15± 0.06	0.036± 0.004	2.88± 0.06	0.027± 0.004
200	2.92± 0.06	0.025± 0.006	2.99± 0.06	0.027± 0.006	2.94± 0.06	0.025± 0.006	3.08± 0.06	0.029± 0.006	3.17± 0.06	0.031± 0.006	2.87± 0.06	0.023± 0.006	3.13± 0.06	0.032± 0.006	2.87± 0.06	0.024± 0.006
250	2.97± 0.08	0.027± 0.006	3.04± 0.08	0.028± 0.006	2.98± 0.08	0.027± 0.006	3.13± 0.08	0.031± 0.006	3.22± 0.08	0.033± 0.006	2.91± 0.08	0.025± 0.006	3.19± 0.08	0.034± 0.006	2.91± 0.08	0.025± 0.006
300	3.01± 0.09	0.022± 0.004	3.09± 0.09	0.023± 0.004	3.03± 0.09	0.022± 0.004	3.18± 0.09	0.026± 0.004	3.28± 0.09	0.027± 0.004	2.95± 0.09	0.021± 0.004	3.25± 0.09	0.028± 0.004	2.96± 0.09	0.021± 0.004
350	3.08± 0.10	0.027± 0.004	3.16± 0.10	0.028± 0.004	3.10± 0.10	0.027± 0.004	3.27± 0.10	0.031± 0.004	3.36± 0.10	0.033± 0.004	3.02± 0.10	0.025± 0.004	3.34± 0.10	0.035± 0.004	3.02± 0.10	0.025± 0.004
400	3.15± 0.11	0.034± 0.005	3.23± 0.11	0.036± 0.005	3.17± 0.11	0.034± 0.005	3.35± 0.11	0.040± 0.005	3.45± 0.11	0.043± 0.005	3.08± 0.11	0.032± 0.005	3.43± 0.11	0.045± 0.005	3.09± 0.11	0.032± 0.005
450	3.22± 0.12	0.046± 0.004	3.31± 0.12	0.050± 0.004	3.24± 0.12	0.046± 0.004	3.43± 0.12	0.055± 0.004	3.54± 0.12	0.059± 0.004	3.15± 0.12	0.043± 0.004	3.52± 0.12	0.062± 0.004	3.16± 0.12	0.044± 0.004
500	3.30± 0.15	0.059± 0.005	3.39± 0.15	0.064± 0.005	3.31± 0.15	0.059± 0.005	3.52± 0.15	0.071± 0.005	3.63± 0.15	0.076± 0.005	3.22± 0.15	0.055± 0.005	3.62± 0.15	0.080± 0.005	3.23± 0.15	0.057± 0.005
550	3.30± 0.19	0.067± 0.007	3.39± 0.19	0.072± 0.007	3.32± 0.19	0.067± 0.007	3.52± 0.19	0.080± 0.007	3.64± 0.19	0.085± 0.007	3.22± 0.19	0.062± 0.007	3.62± 0.19	0.090± 0.007	3.23± 0.19	0.064± 0.007
600	3.42± 0.19	0.089± 0.005	3.52± 0.19	0.095± 0.005	3.43± 0.19	0.089± 0.005	3.66± 0.19	0.107± 0.005	3.79± 0.19	0.114± 0.005	3.33± 0.19	0.082± 0.005	3.78± 0.19	0.122± 0.005	3.34± 0.19	0.084± 0.005
650	3.50± 0.19	0.115± 0.006	3.61± 0.19	0.124± 0.006	3.52± 0.19	0.115± 0.006	3.77± 0.19	0.139± 0.006	3.90± 0.19	0.149± 0.006	3.41± 0.19	0.106± 0.006	3.90± 0.19	0.160± 0.006	3.42± 0.19	0.109± 0.006
700	3.59± 0.19	0.147± 0.008	3.71± 0.19	0.158± 0.008	3.61± 0.19	0.147± 0.008	3.88± 0.19	0.179± 0.008	4.02± 0.19	0.192± 0.008	3.49± 0.19	0.136± 0.008	4.03± 0.19	0.208± 0.008	3.51± 0.19	0.140± 0.008
750	3.68± 0.20	0.178± 0.008	3.80± 0.20	0.192± 0.008	3.70± 0.20	0.177± 0.008	3.98± 0.20	0.218± 0.008	4.13± 0.20	0.234± 0.008	3.57± 0.20	0.164± 0.008	4.15± 0.20	0.256± 0.008	3.59± 0.20	0.169± 0.008
800	3.77± 0.20	0.207± 0.008	3.90± 0.20	0.222± 0.008	3.78± 0.20	0.205± 0.008	4.09± 0.20	0.254± 0.008	4.25± 0.20	0.272± 0.008	3.66± 0.20	0.189± 0.008	4.28± 0.20	0.301± 0.008	3.68± 0.20	0.195± 0.008
850	3.89± 0.21	0.221± 0.005	4.03± 0.21	0.238± 0.005	3.91± 0.21	0.219± 0.005	4.24± 0.21	0.273± 0.005	4.41± 0.21	0.293± 0.005	3.77± 0.21	0.202± 0.005	4.45± 0.21	0.330± 0.005	3.79± 0.21	0.208± 0.005
900	4.09± 0.22	0.281± 0.009	4.25± 0.22	0.304± 0.009	4.11± 0.22	0.278± 0.009	4.49± 0.22	0.351± 0.009	4.68± 0.22	0.379± 0.009	3.95± 0.22	0.256± 0.009	4.76± 0.22	0.436± 0.009	3.98± 0.22	0.265± 0.009
950	4.35± 0.22	0.394± 0.008	4.52± 0.22	0.428± 0.008	4.36± 0.22	0.389± 0.008	4.81± 0.22	0.499± 0.008	5.02± 0.22	0.540± 0.008	4.18± 0.22	0.357± 0.008	5.15± 0.22	0.645± 0.008	4.22± 0.22	0.371± 0.008

Table C.6- Binary clay-air mixing rules dielectric property estimations of slabs of Helligsø red clay at 0.40±0.01 void fraction at 2470 MHz across the 20-950 ºC firing range from clay powders at void fractions ranging 0.56±0.03. The standard uncertainties are indicated in the table.

	Complex Refractive Index		Landau-Lifshitz-Looyenga		Bruggeman-Hanai		Böttcher		Lichtenecker		Rayleigh		Sen-Scala-Cohen		Complex Refractive Index α=0.65	
T (°C)	**ε'**	**ε''**	**ε'**	**ε''**	**ε'**	**ε''**	**ε'**	**ε''**	**ε'**	**ε''**	**ε'**	**ε''**	**ε'**	**ε''**	**ε'**	**ε''**
20	3.20± 0.06	0.024± 0.006	3.28± 0.06	0.025± 0.006	3.21± 0.06	0.024± 0.006	3.40± 0.06	0.028± 0.006	3.51± 0.06	0.030± 0.006	3.13± 0.06	0.022± 0.006	3.48± 0.06	0.031± 0.006	3.13± 0.06	0.023± 0.006
50	3.29± 0.07	0.027± 0.007	3.38± 0.07	0.029± 0.007	3.30± 0.07	0.027± 0.007	3.51± 0.07	0.033± 0.007	3.62± 0.07	0.035± 0.007	3.21± 0.07	0.025± 0.007	3.61± 0.07	0.037± 0.007	3.22± 0.07	0.026± 0.007
100	3.19± 0.03	0.021± 0.009	3.27± 0.03	0.022± 0.009	3.20± 0.03	0.021± 0.009	3.39± 0.03	0.024± 0.009	3.49± 0.03	0.026± 0.009	3.12± 0.03	0.019± 0.009	3.47± 0.03	0.027± 0.009	3.12± 0.03	0.020± 0.009
150	2.99± 0.05	0.027± 0.004	3.07± 0.05	0.029± 0.004	3.01± 0.05	0.027± 0.004	3.16± 0.05	0.032± 0.004	3.25± 0.05	0.034± 0.004	2.94± 0.05	0.026± 0.004	3.22± 0.05	0.035± 0.004	2.94± 0.05	0.026± 0.004
200	2.96± 0.05	0.022± 0.004	3.03± 0.05	0.023± 0.004	2.98± 0.05	0.022± 0.004	3.13± 0.05	0.026± 0.004	3.22± 0.05	0.027± 0.004	2.91± 0.05	0.020± 0.004	3.19± 0.05	0.028± 0.004	2.91± 0.05	0.021± 0.004
250	2.98± 0.05	0.021± 0.005	3.05± 0.05	0.022± 0.005	3.00± 0.05	0.021± 0.005	3.14± 0.05	0.025± 0.005	3.23± 0.05	0.026± 0.005	2.92± 0.05	0.020± 0.005	3.20± 0.05	0.027± 0.005	2.92± 0.05	0.020± 0.005
300	3.00± 0.06	0.019± 0.004	3.07± 0.06	0.021± 0.004	3.01± 0.06	0.019± 0.004	3.17± 0.06	0.023± 0.004	3.26± 0.06	0.024± 0.004	2.94± 0.06	0.018± 0.004	3.23± 0.06	0.025± 0.004	2.94± 0.06	0.019± 0.004
350	3.03± 0.06	0.021± 0.005	3.10± 0.06	0.023± 0.005	3.05± 0.06	0.021± 0.005	3.20± 0.06	0.025± 0.005	3.30± 0.06	0.027± 0.005	2.97± 0.06	0.020± 0.005	3.27± 0.06	0.028± 0.005	2.97± 0.06	0.020± 0.005
400	3.06± 0.06	0.026± 0.005	3.14± 0.06	0.028± 0.005	3.08± 0.06	0.026± 0.005	3.24± 0.06	0.031± 0.005	3.34± 0.06	0.033± 0.005	3.00± 0.06	0.024± 0.005	3.31± 0.06	0.034± 0.005	3.00± 0.06	0.025± 0.005
450	3.10± 0.06	0.032± 0.005	3.18± 0.06	0.034± 0.005	3.12± 0.06	0.032± 0.005	3.29± 0.06	0.038± 0.005	3.39± 0.06	0.040± 0.005	3.04± 0.06	0.030± 0.005	3.36± 0.06	0.042± 0.005	3.04± 0.06	0.031± 0.005
500	3.13± 0.07	0.036± 0.005	3.21± 0.07	0.039± 0.005	3.14± 0.07	0.036± 0.005	3.32± 0.07	0.043± 0.005	3.42± 0.07	0.046± 0.005	3.06± 0.07	0.034± 0.005	3.40± 0.07	0.048± 0.005	3.07± 0.07	0.035± 0.005
550	3.12± 0.09	0.042± 0.005	3.20± 0.09	0.044± 0.005	3.13± 0.09	0.042± 0.005	3.30± 0.09	0.049± 0.005	3.41± 0.09	0.052± 0.005	3.05± 0.09	0.039± 0.005	3.38± 0.09	0.054± 0.005	3.06± 0.09	0.040± 0.005
600	3.17± 0.09	0.051± 0.005	3.26± 0.09	0.055± 0.005	3.19± 0.09	0.051± 0.005	3.37± 0.09	0.061± 0.005	3.48± 0.09	0.065± 0.005	3.10± 0.09	0.048± 0.005	3.46± 0.09	0.067± 0.005	3.11± 0.09	0.049± 0.005
650	3.22± 0.09	0.060± 0.005	3.31± 0.09	0.064± 0.005	3.24± 0.09	0.060± 0.005	3.43± 0.09	0.071± 0.005	3.54± 0.09	0.076± 0.005	3.15± 0.09	0.056± 0.005	3.52± 0.09	0.079± 0.005	3.16± 0.09	0.057± 0.005
700	3.27± 0.09	0.070± 0.005	3.36± 0.09	0.074± 0.005	3.28± 0.09	0.069± 0.005	3.48± 0.09	0.083± 0.005	3.60± 0.09	0.088± 0.005	3.19± 0.09	0.065± 0.005	3.58± 0.09	0.093± 0.005	3.20± 0.09	0.066± 0.005
750	3.31± 0.09	0.079± 0.005	3.40± 0.09	0.085± 0.005	3.33± 0.09	0.079± 0.005	3.53± 0.09	0.095± 0.005	3.65± 0.09	0.101± 0.005	3.23± 0.09	0.074± 0.005	3.63± 0.09	0.107± 0.005	3.24± 0.09	0.075± 0.005
800	3.35± 0.10	0.091± 0.006	3.45± 0.10	0.097± 0.006	3.37± 0.10	0.090± 0.006	3.58± 0.10	0.109± 0.006	3.70± 0.10	0.116± 0.006	3.27± 0.10	0.084± 0.006	3.69± 0.10	0.123± 0.006	3.28± 0.10	0.086± 0.006
850	3.43± 0.10	0.107± 0.006	3.53± 0.10	0.115± 0.006	3.45± 0.10	0.107± 0.006	3.68± 0.10	0.129± 0.006	3.81± 0.10	0.138± 0.006	3.34± 0.10	0.099± 0.006	3.80± 0.10	0.147± 0.006	3.36± 0.10	0.102± 0.006
900	3.57± 0.10	0.146± 0.007	3.68± 0.10	0.157± 0.007	3.59± 0.10	0.145± 0.007	3.85± 0.10	0.178± 0.007	3.99± 0.10	0.190± 0.007	3.47± 0.10	0.135± 0.007	3.99± 0.10	0.206± 0.007	3.49± 0.10	0.139± 0.007
950	3.75± 0.10	0.207± 0.008	3.87± 0.10	0.223± 0.008	3.76± 0.10	0.205± 0.008	4.06± 0.10	0.254± 0.008	4.22± 0.10	0.272± 0.008	3.63± 0.10	0.190± 0.008	4.24± 0.10	0.301± 0.008	3.65± 0.10	0.196± 0.008

Table C.7- Binary clay-air mixing rules dielectric property estimations of slabs of Hammershoj red clay at 0.42±0.03 void fraction at 912 MHz across the 20-950 ºC firing range from clay powders at void fractions ranging 0.56±0.03. The standard uncertainties are indicated in the table.

	Complex Refractive Index		Landau-Lifshitz-Looyenga		Bruggeman-Hanai		Böttcher		Lichtenecker		Rayleigh		Sen-Scala-Cohen		Complex Refractive Index α=0.65	
T (°C)	**ε'**	**ε''**	**ε'**	**ε''**	**ε'**	**ε''**	**ε'**	**ε''**	**ε'**	**ε''**	**ε'**	**ε''**	**ε'**	**ε''**	**ε'**	**ε''**
20	2.93± 0.12	0.037± 0.033	3.00± 0.12	0.039± 0.033	2.94± 0.12	0.037± 0.033	3.08± 0.12	0.043± 0.033	3.18± 0.12	0.046± 0.033	2.87± 0.12	0.034± 0.033	3.14± 0.12	0.047± 0.033	2.87± 0.12	0.035± 0.033
50	3.09± 0.10	0.057± 0.040	3.17± 0.10	0.060± 0.040	3.11± 0.10	0.057± 0.040	3.28± 0.10	0.067± 0.040	3.39± 0.10	0.072± 0.040	3.03± 0.10	0.053± 0.040	3.36± 0.10	0.074± 0.040	3.03± 0.10	0.054± 0.040
100	2.94± 0.17	0.029± 0.012	3.01± 0.17	0.031± 0.012	2.95± 0.17	0.029± 0.012	3.10± 0.17	0.034± 0.012	3.19± 0.17	0.037± 0.012	2.88± 0.17	0.028± 0.012	3.16± 0.17	0.037± 0.012	2.88± 0.17	0.028± 0.012
150	2.79± 0.16	0.029± 0.007	2.85± 0.16	0.030± 0.007	2.81± 0.16	0.029± 0.007	2.93± 0.16	0.033± 0.007	3.01± 0.16	0.035± 0.007	2.75± 0.16	0.027± 0.007	2.97± 0.16	0.036± 0.007	2.74± 0.16	0.027± 0.007
200	2.76± 0.16	0.015± 0.002	2.82± 0.16	0.016± 0.002	2.78± 0.16	0.015± 0.002	2.89± 0.16	0.017± 0.002	2.97± 0.16	0.019± 0.002	2.71± 0.16	0.014± 0.002	2.93± 0.16	0.019± 0.002	2.71± 0.16	0.014± 0.002
250	2.77± 0.18	0.014± 0.002	2.83± 0.18	0.015± 0.002	2.79± 0.18	0.014± 0.002	2.90± 0.18	0.017± 0.002	2.98± 0.18	0.018± 0.002	2.72± 0.18	0.014± 0.002	2.95± 0.18	0.018± 0.002	2.72± 0.18	0.014± 0.002
300	2.79± 0.20	0.015± 0.003	2.85± 0.20	0.015± 0.003	2.80± 0.20	0.015± 0.003	2.92± 0.20	0.017± 0.003	3.01± 0.20	0.018± 0.003	2.74± 0.20	0.014± 0.003	2.97± 0.20	0.018± 0.003	2.74± 0.20	0.014± 0.003
350	2.81± 0.21	0.017± 0.003	2.88± 0.21	0.018± 0.003	2.83± 0.21	0.017± 0.003	2.95± 0.21	0.019± 0.003	3.04± 0.21	0.021± 0.003	2.77± 0.21	0.016± 0.003	3.00± 0.21	0.021± 0.003	2.76± 0.21	0.016± 0.003
400	2.85± 0.23	0.022± 0.003	2.91± 0.23	0.024± 0.003	2.87± 0.23	0.022± 0.003	3.00± 0.23	0.026± 0.003	3.08± 0.23	0.027± 0.003	2.80± 0.23	0.021± 0.003	3.05± 0.23	0.028± 0.003	2.80± 0.23	0.021± 0.003
450	2.88± 0.24	0.033± 0.003	2.95± 0.24	0.036± 0.003	2.90± 0.24	0.034± 0.003	3.04± 0.24	0.039± 0.003	3.13± 0.24	0.042± 0.003	2.83± 0.24	0.031± 0.003	3.09± 0.24	0.042± 0.003	2.83± 0.24	0.032± 0.003
500	2.87± 0.19	0.042± 0.004	2.94± 0.19	0.045± 0.004	2.89± 0.19	0.043± 0.004	3.02± 0.19	0.049± 0.004	3.11± 0.19	0.053± 0.004	2.82± 0.19	0.040± 0.004	3.08± 0.19	0.053± 0.004	2.82± 0.19	0.041± 0.004
550	2.76± 0.28	0.053± 0.011	2.82± 0.28	0.056± 0.011	2.78± 0.28	0.053± 0.011	2.89± 0.28	0.061± 0.011	2.97± 0.28	0.065± 0.011	2.72± 0.28	0.050± 0.011	2.93± 0.28	0.065± 0.011	2.71± 0.28	0.051± 0.011
600	2.85± 0.26	0.065± 0.014	2.91± 0.26	0.069± 0.014	2.87± 0.26	0.065± 0.014	3.00± 0.26	0.075± 0.014	3.08± 0.26	0.080± 0.014	2.80± 0.26	0.061± 0.014	3.05± 0.26	0.081± 0.014	2.80± 0.26	0.062± 0.014
650	2.95± 0.24	0.086± 0.018	3.02± 0.24	0.092± 0.018	2.97± 0.24	0.086± 0.018	3.12± 0.24	0.101± 0.018	3.21± 0.24	0.108± 0.018	2.90± 0.24	0.081± 0.018	3.18± 0.24	0.110± 0.018	2.90± 0.24	0.082± 0.018
700	3.05± 0.23	0.106± 0.020	3.13± 0.23	0.113± 0.020	3.07± 0.23	0.106± 0.020	3.23± 0.23	0.125± 0.020	3.34± 0.23	0.134± 0.020	2.99± 0.23	0.099± 0.020	3.30± 0.23	0.137± 0.020	2.99± 0.23	0.101± 0.020
750	3.15± 0.22	0.131± 0.023	3.23± 0.22	0.140± 0.023	3.16± 0.22	0.131± 0.023	3.34± 0.22	0.156± 0.023	3.46± 0.22	0.167± 0.023	3.08± 0.22	0.122± 0.023	3.43± 0.22	0.173± 0.023	3.08± 0.22	0.125± 0.023
800	3.29± 0.21	0.156± 0.018	3.39± 0.21	0.167± 0.018	3.31± 0.21	0.155± 0.018	3.52± 0.21	0.186± 0.018	3.65± 0.21	0.200± 0.018	3.22± 0.21	0.144± 0.018	3.62± 0.21	0.210± 0.018	3.22± 0.21	0.148± 0.018
850	3.47± 0.21	0.178± 0.020	3.58± 0.21	0.192± 0.020	3.49± 0.21	0.177± 0.020	3.73± 0.21	0.216± 0.020	3.88± 0.21	0.232± 0.020	3.38± 0.21	0.164± 0.020	3.87± 0.21	0.248± 0.020	3.39± 0.21	0.169± 0.020
900	3.65± 0.22	0.234± 0.025	3.77± 0.22	0.252± 0.025	3.67± 0.22	0.232± 0.025	3.95± 0.22	0.286± 0.025	4.11± 0.22	0.309± 0.025	3.54± 0.22	0.214± 0.025	4.12± 0.22	0.337± 0.025	3.56± 0.22	0.221± 0.025
950	3.90± 0.22	0.348± 0.035	4.04± 0.22	0.377± 0.035	3.92± 0.22	0.345± 0.035	4.26± 0.22	0.432± 0.035	4.44± 0.22	0.469± 0.035	3.77± 0.22	0.317± 0.035	4.48± 0.22	0.525± 0.035	3.80± 0.22	0.328± 0.035

Table C.8- Binary clay-air mixing rules dielectric property estimations of slabs of Hammershoj red clay at 0.42±0.03 void fraction at 2470 MHz across the 20-950 ºC firing range from clay powders at void fractions ranging 0.56±0.03. The standard uncertainties are indicated in the table.

	Complex Refractive Index		Landau-Lifshitz-Looyenga		Bruggeman-Hanai		Böttcher		Lichtenecker		Rayleigh		Sen-Scala-Cohen		Complex Refractive Index α=0.65	
T (°C)	**ε'**	**ε''**	**ε'**	**ε''**	**ε'**	**ε''**	**ε'**	**ε''**	**ε'**	**ε''**	**ε'**	**ε''**	**ε'**	**ε''**	**ε'**	**ε''**
20	2.98± 0.10	0.034± 0.007	3.06± 0.10	0.036± 0.007	3.00± 0.10	0.034± 0.007	3.15± 0.10	0.040± 0.007	3.25± 0.10	0.042± 0.007	2.93± 0.10	0.032± 0.007	3.21± 0.10	0.043± 0.007	2.93± 0.10	0.032± 0.007
50	3.09± 0.08	0.044± 0.009	3.17± 0.08	0.047± 0.009	3.11± 0.08	0.044± 0.009	3.28± 0.08	0.052± 0.009	3.38± 0.08	0.056± 0.009	3.02± 0.08	0.041± 0.009	3.35± 0.08	0.058± 0.009	3.03± 0.08	0.042± 0.009
100	2.96± 0.06	0.025± 0.004	3.03± 0.06	0.027± 0.004	2.98± 0.06	0.025± 0.004	3.13± 0.06	0.029± 0.004	3.22± 0.06	0.031± 0.004	2.91± 0.06	0.023± 0.004	3.19± 0.06	0.032± 0.004	2.91± 0.06	0.024± 0.004
150	2.84± 0.04	0.026± 0.003	2.90± 0.04	0.028± 0.003	2.85± 0.04	0.026± 0.003	2.98± 0.04	0.030± 0.003	3.07± 0.04	0.032± 0.003	2.79± 0.04	0.024± 0.003	3.03± 0.04	0.033± 0.003	2.79± 0.04	0.025± 0.003
200	2.80± 0.03	0.013± 0.003	2.86± 0.03	0.014± 0.003	2.82± 0.03	0.013± 0.003	2.94± 0.03	0.015± 0.003	3.02± 0.03	0.016± 0.003	2.75± 0.03	0.012± 0.003	2.98± 0.03	0.016± 0.003	2.75± 0.03	0.013± 0.003
250	2.80± 0.03	0.012± 0.002	2.87± 0.03	0.013± 0.002	2.82± 0.03	0.012± 0.002	2.94± 0.03	0.014± 0.002	3.03± 0.03	0.015± 0.002	2.76± 0.03	0.012± 0.002	2.99± 0.03	0.015± 0.002	2.75± 0.03	0.012± 0.002
300	2.81± 0.04	0.011± 0.002	2.88± 0.04	0.012± 0.002	2.83± 0.04	0.011± 0.002	2.95± 0.04	0.013± 0.002	3.04± 0.04	0.014± 0.002	2.77± 0.04	0.011± 0.002	3.00± 0.04	0.014± 0.002	2.76± 0.04	0.011± 0.002
350	2.83± 0.04	0.013± 0.002	2.89± 0.04	0.014± 0.002	2.85± 0.04	0.013± 0.002	2.97± 0.04	0.015± 0.002	3.06± 0.04	0.016± 0.002	2.78± 0.04	0.012± 0.002	3.02± 0.04	0.016± 0.002	2.78± 0.04	0.012± 0.002
400	2.85± 0.04	0.016± 0.002	2.92± 0.04	0.017± 0.002	2.87± 0.04	0.016± 0.002	3.00± 0.04	0.019± 0.002	3.09± 0.04	0.020± 0.002	2.80± 0.04	0.015± 0.002	3.05± 0.04	0.020± 0.002	2.80± 0.04	0.015± 0.002
450	2.87± 0.05	0.021± 0.003	2.93± 0.05	0.022± 0.003	2.89± 0.05	0.021± 0.003	3.02± 0.05	0.024± 0.003	3.11± 0.05	0.026± 0.003	2.82± 0.05	0.020± 0.003	3.07± 0.05	0.026± 0.003	2.82± 0.05	0.020± 0.003
500	2.83± 0.08	0.026± 0.003	2.90± 0.08	0.028± 0.003	2.85± 0.08	0.026± 0.003	2.98± 0.08	0.030± 0.003	3.07± 0.08	0.032± 0.003	2.79± 0.08	0.024± 0.003	3.03± 0.08	0.033± 0.003	2.78± 0.08	0.025± 0.003
550	2.71± 0.20	0.030± 0.004	2.77± 0.20	0.032± 0.004	2.73± 0.20	0.030± 0.004	2.84± 0.20	0.034± 0.004	2.91± 0.20	0.037± 0.004	2.67± 0.20	0.028± 0.004	2.87± 0.20	0.037± 0.004	2.67± 0.20	0.029± 0.004
600	2.76± 0.20	0.037± 0.004	2.82± 0.20	0.040± 0.004	2.77± 0.20	0.038± 0.004	2.89± 0.20	0.043± 0.004	2.97± 0.20	0.046± 0.004	2.71± 0.20	0.035± 0.004	2.93± 0.20	0.046± 0.004	2.71± 0.20	0.036± 0.004
650	2.84± 0.21	0.045± 0.004	2.90± 0.21	0.047± 0.004	2.85± 0.21	0.045± 0.004	2.98± 0.21	0.052± 0.004	3.07± 0.21	0.055± 0.004	2.79± 0.21	0.042± 0.004	3.03± 0.21	0.056± 0.004	2.79± 0.21	0.043± 0.004
700	2.91± 0.19	0.052± 0.004	2.98± 0.19	0.056± 0.004	2.93± 0.19	0.052± 0.004	3.07± 0.19	0.061± 0.004	3.16± 0.19	0.065± 0.004	2.86± 0.19	0.049± 0.004	3.12± 0.19	0.066± 0.004	2.86± 0.19	0.050± 0.004
750	2.97± 0.16	0.062± 0.005	3.04± 0.16	0.066± 0.005	2.99± 0.16	0.062± 0.005	3.14± 0.16	0.072± 0.005	3.24± 0.16	0.077± 0.005	2.91± 0.16	0.057± 0.005	3.20± 0.16	0.079± 0.005	2.91± 0.16	0.059± 0.005
800	3.08± 0.11	0.072± 0.004	3.16± 0.11	0.076± 0.004	3.09± 0.11	0.072± 0.004	3.26± 0.11	0.084± 0.004	3.37± 0.11	0.090± 0.004	3.01± 0.11	0.067± 0.004	3.33± 0.11	0.093± 0.004	3.01± 0.11	0.068± 0.004
850	3.18± 0.12	0.084± 0.004	3.26± 0.12	0.090± 0.004	3.19± 0.12	0.084± 0.004	3.38± 0.12	0.100± 0.004	3.49± 0.12	0.107± 0.004	3.10± 0.12	0.078± 0.004	3.47± 0.12	0.111± 0.004	3.11± 0.12	0.080± 0.004
900	3.30± 0.13	0.117± 0.004	3.40± 0.13	0.126± 0.004	3.32± 0.13	0.117± 0.004	3.53± 0.13	0.140± 0.004	3.65± 0.13	0.151± 0.004	3.22± 0.13	0.108± 0.004	3.63± 0.13	0.158± 0.004	3.23± 0.13	0.111± 0.004
950	3.47± 0.14	0.176± 0.006	3.58± 0.14	0.190± 0.006	3.49± 0.14	0.176± 0.006	3.73± 0.14	0.214± 0.006	3.87± 0.14	0.230± 0.006	3.38± 0.14	0.162± 0.006	3.86± 0.14	0.246± 0.006	3.39± 0.14	0.167± 0.006

Appendix C1.2: Slab to powder estimations

Table C.9- Binary clay-air mixing rules dielectric property estimations of powders of Vedstaarup yellow clay at 0.56±0.03void fraction at 912 MHz across the 20-950 ºC firing range from clay slabs at 0.37±0.02void fractions. The standard uncertainties are indicated in the table.

	Complex Refractive Index		Landau-Lifshitz-Looyenga		Bruggeman-Hanai		Böttcher		Lichtenecker		Rayleigh		Sen-Scala-Cohen		Complex Refractive Index α=0.65	
T (°C)	ε'	ε''	ε'	ε''	ε'	ε''	ε'	ε''	ε'	ε''	ε'	ε''	ε'	ε''	ε'	ε''
20	2.45± 0.06	0.063± 0.006	2.39± 0.06	0.059± 0.006	2.44± 0.06	0.063± 0.006	2.33± 0.06	0.053± 0.006	2.26± 0.06	0.049± 0.006	2.51± 0.06	0.069± 0.006	2.28± 0.06	0.048± 0.006	2.50± 0.06	0.067± 0.006
50	2.48± 0.07	0.082± 0.008	2.42± 0.07	0.076± 0.008	2.47± 0.07	0.082± 0.008	2.35± 0.07	0.069± 0.008	2.29± 0.07	0.064± 0.008	2.54± 0.07	0.089± 0.008	2.31± 0.07	0.062± 0.008	2.54± 0.07	0.087± 0.008
100	2.46± 0.08	0.071± 0.009	2.40± 0.08	0.066± 0.009	2.45± 0.08	0.071± 0.009	2.34± 0.08	0.060± 0.009	2.27± 0.08	0.055± 0.009	2.52± 0.08	0.078± 0.009	2.29± 0.08	0.054± 0.009	2.52± 0.08	0.075± 0.009
150	2.44± 0.05	0.027± 0.004	2.38± 0.05	0.025± 0.004	2.43± 0.05	0.027± 0.004	2.32± 0.05	0.022± 0.004	2.26± 0.05	0.021± 0.004	2.50± 0.05	0.029± 0.004	2.28± 0.05	0.020± 0.004	2.49± 0.05	0.028± 0.004
200	2.45± 0.06	0.026± 0.003	2.39± 0.06	0.024± 0.003	2.44± 0.06	0.026± 0.003	2.33± 0.06	0.021± 0.003	2.27± 0.06	0.020± 0.003	2.51± 0.06	0.028± 0.003	2.29± 0.06	0.019± 0.003	2.50± 0.06	0.027± 0.003
250	2.46± 0.07	0.026± 0.004	2.40± 0.07	0.024± 0.004	2.45± 0.07	0.026± 0.004	2.34± 0.07	0.021± 0.004	2.28± 0.07	0.020± 0.004	2.52± 0.07	0.028± 0.004	2.30± 0.07	0.019± 0.004	2.52± 0.07	0.027± 0.004
300	2.47± 0.07	0.026± 0.005	2.41± 0.07	0.024± 0.005	2.46± 0.07	0.026± 0.005	2.35± 0.07	0.022± 0.005	2.28± 0.07	0.020± 0.005	2.53± 0.07	0.028± 0.005	2.30± 0.07	0.019± 0.005	2.53± 0.07	0.027± 0.005
350	2.49± 0.07	0.028± 0.006	2.42± 0.07	0.026± 0.006	2.47± 0.07	0.028± 0.006	2.36± 0.07	0.023± 0.006	2.29± 0.07	0.021± 0.006	2.55± 0.07	0.030± 0.006	2.31± 0.07	0.021± 0.006	2.54± 0.07	0.029± 0.006
400	2.50± 0.07	0.033± 0.006	2.44± 0.07	0.030± 0.006	2.49± 0.07	0.033± 0.006	2.37± 0.07	0.027± 0.006	2.30± 0.07	0.025± 0.006	2.56± 0.07	0.036± 0.006	2.32± 0.07	0.024± 0.006	2.55± 0.07	0.035± 0.006
450	2.51± 0.07	0.041± 0.005	2.45± 0.07	0.038± 0.005	2.50± 0.07	0.041± 0.005	2.38± 0.07	0.034± 0.005	2.31± 0.07	0.031± 0.005	2.58± 0.07	0.044± 0.005	2.33± 0.07	0.030± 0.005	2.57± 0.07	0.043± 0.005
500	2.52± 0.07	0.046± 0.007	2.46± 0.07	0.043± 0.007	2.51± 0.07	0.046± 0.007	2.39± 0.07	0.039± 0.007	2.32± 0.07	0.036± 0.007	2.59± 0.07	0.050± 0.007	2.34± 0.07	0.034± 0.007	2.58± 0.07	0.049± 0.007
550	2.53± 0.08	0.054± 0.008	2.47± 0.08	0.050± 0.008	2.52± 0.08	0.054± 0.008	2.40± 0.08	0.045± 0.008	2.33± 0.08	0.042± 0.008	2.60± 0.08	0.059± 0.008	2.35± 0.08	0.040± 0.008	2.59± 0.08	0.057± 0.008
600	2.56± 0.10	0.068± 0.008	2.49± 0.10	0.063± 0.008	2.55± 0.10	0.068± 0.008	2.42± 0.10	0.056± 0.008	2.35± 0.10	0.052± 0.008	2.62± 0.10	0.074± 0.008	2.36± 0.10	0.050± 0.008	2.62± 0.10	0.072± 0.008
650	2.58± 0.12	0.084± 0.011	2.51± 0.12	0.078± 0.011	2.57± 0.12	0.085± 0.011	2.43± 0.12	0.070± 0.011	2.36± 0.12	0.065± 0.011	2.64± 0.12	0.092± 0.011	2.38± 0.12	0.062± 0.011	2.64± 0.12	0.089± 0.011
700	2.59± 0.13	0.099± 0.011	2.52± 0.13	0.092± 0.011	2.58± 0.13	0.100± 0.011	2.45± 0.13	0.082± 0.011	2.37± 0.13	0.076± 0.011	2.66± 0.13	0.108± 0.011	2.39± 0.13	0.073± 0.011	2.65± 0.13	0.105± 0.011
750	2.61± 0.15	0.110± 0.012	2.54± 0.15	0.101± 0.012	2.60± 0.15	0.111± 0.012	2.46± 0.15	0.091± 0.012	2.39± 0.15	0.084± 0.012	2.68± 0.15	0.120± 0.012	2.40± 0.15	0.080± 0.012	2.67± 0.15	0.117± 0.012
800	2.64± 0.18	0.106± 0.012	2.56± 0.18	0.098± 0.012	2.63± 0.18	0.107± 0.012	2.48± 0.18	0.088± 0.012	2.41± 0.18	0.081± 0.012	2.71± 0.18	0.117± 0.012	2.42± 0.18	0.077± 0.012	2.70± 0.18	0.113± 0.012
850	2.65± 0.19	0.112± 0.011	2.58± 0.19	0.104± 0.011	2.64± 0.19	0.113± 0.011	2.50± 0.19	0.093± 0.011	2.42± 0.19	0.086± 0.011	2.73± 0.19	0.124± 0.011	2.44± 0.19	0.081± 0.011	2.72± 0.19	0.120± 0.011
900	2.65± 0.16	0.150± 0.017	2.58± 0.16	0.139± 0.017	2.64± 0.16	0.151± 0.017	2.49± 0.16	0.124± 0.017	2.42± 0.16	0.114± 0.017	2.72± 0.16	0.165± 0.017	2.43± 0.16	0.109± 0.017	2.71± 0.16	0.160± 0.017
950	2.66± 0.16	0.189± 0.019	2.58± 0.16	0.174± 0.019	2.65± 0.16	0.190± 0.019	2.50± 0.16	0.156± 0.019	2.43± 0.16	0.144± 0.019	2.74± 0.16	0.208± 0.019	2.44± 0.16	0.136± 0.019	2.72± 0.16	0.201± 0.019

Table C.10- Binary clay-air mixing rules dielectric property estimations of powders of Vedstaarup yellow clay at 0.56±0.03void fraction at 2470 MHz across the 20-950 ºC firing range from clay slabs at 0.37±0.02void fractions. The standard uncertainties are indicated in the table.

	Complex Refractive Index		Landau-Lifshitz-Looyenga		Bruggeman-Hanai		Böttcher		Lichtenecker		Rayleigh		Sen-Scala-Cohen		Complex Refractive Index α=0.65	
T (°C)	**ε'**	**ε''**	**ε'**	**ε''**	**ε'**	**ε''**	**ε'**	**ε''**	**ε'**	**ε''**	**ε'**	**ε''**	**ε'**	**ε''**	**ε'**	**ε''**
20	2.52± 0.07	0.058± 0.006	2.45± 0.07	0.053± 0.006	2.50± 0.07	0.058± 0.006	2.38± 0.07	0.048± 0.006	2.32± 0.07	0.045± 0.006	2.58± 0.07	0.063± 0.006	2.33± 0.07	0.043± 0.006	2.57± 0.07	0.061± 0.006
50	2.55± 0.07	0.073± 0.009	2.48± 0.07	0.068± 0.009	2.54± 0.07	0.073± 0.009	2.41± 0.07	0.061± 0.009	2.34± 0.07	0.056± 0.009	2.61± 0.07	0.080± 0.009	2.36± 0.07	0.054± 0.009	2.61± 0.07	0.078± 0.009
100	2.54± 0.07	0.064± 0.008	2.47± 0.07	0.059± 0.008	2.53± 0.07	0.064± 0.008	2.40± 0.07	0.053± 0.008	2.34± 0.07	0.049± 0.008	2.61± 0.07	0.070± 0.008	2.35± 0.07	0.047± 0.008	2.60± 0.07	0.068± 0.008
150	2.50± 0.07	0.023± 0.003	2.43± 0.07	0.022± 0.003	2.49± 0.07	0.023± 0.003	2.37± 0.07	0.020± 0.003	2.30± 0.07	0.018± 0.003	2.56± 0.07	0.025± 0.003	2.32± 0.07	0.017± 0.003	2.55± 0.07	0.025± 0.003
200	2.50± 0.08	0.022± 0.002	2.43± 0.08	0.021± 0.002	2.49± 0.08	0.022± 0.002	2.37± 0.08	0.019± 0.002	2.30± 0.08	0.017± 0.002	2.56± 0.08	0.024± 0.002	2.32± 0.08	0.017± 0.002	2.55± 0.08	0.024± 0.002
250	2.50± 0.10	0.024± 0.002	2.44± 0.10	0.022± 0.002	2.49± 0.10	0.024± 0.002	2.37± 0.10	0.020± 0.002	2.30± 0.10	0.018± 0.002	2.56± 0.10	0.026± 0.002	2.32± 0.10	0.018± 0.002	2.55± 0.10	0.025± 0.002
300	2.49± 0.11	0.022± 0.003	2.43± 0.11	0.020± 0.003	2.48± 0.11	0.022± 0.003	2.36± 0.11	0.018± 0.003	2.30± 0.11	0.017± 0.003	2.56± 0.11	0.024± 0.003	2.32± 0.11	0.016± 0.003	2.55± 0.11	0.023± 0.003
350	2.49± 0.12	0.022± 0.003	2.43± 0.12	0.021± 0.003	2.48± 0.12	0.023± 0.003	2.36± 0.12	0.019± 0.003	2.30± 0.12	0.017± 0.003	2.56± 0.12	0.024± 0.003	2.32± 0.12	0.017± 0.003	2.55± 0.12	0.024± 0.003
400	2.50± 0.13	0.025± 0.004	2.44± 0.13	0.023± 0.004	2.49± 0.13	0.025± 0.004	2.37± 0.13	0.021± 0.004	2.30± 0.13	0.019± 0.004	2.56± 0.13	0.027± 0.004	2.32± 0.13	0.019± 0.004	2.55± 0.13	0.026± 0.004
450	2.51± 0.13	0.028± 0.005	2.44± 0.13	0.026± 0.005	2.50± 0.13	0.028± 0.005	2.37± 0.13	0.023± 0.005	2.31± 0.13	0.022± 0.005	2.57± 0.13	0.031± 0.005	2.33± 0.13	0.021± 0.005	2.56± 0.13	0.030± 0.005
500	2.51± 0.13	0.030± 0.004	2.44± 0.13	0.028± 0.004	2.50± 0.13	0.030± 0.004	2.38± 0.13	0.025± 0.004	2.31± 0.13	0.023± 0.004	2.57± 0.13	0.033± 0.004	2.33± 0.13	0.023± 0.004	2.56± 0.13	0.032± 0.004
550	2.51± 0.14	0.034± 0.004	2.45± 0.14	0.032± 0.004	2.50± 0.14	0.035± 0.004	2.38± 0.14	0.029± 0.004	2.31± 0.14	0.027± 0.004	2.57± 0.14	0.038± 0.004	2.33± 0.14	0.026± 0.004	2.56± 0.14	0.036± 0.004
600	2.52± 0.15	0.040± 0.005	2.46± 0.15	0.037± 0.005	2.51± 0.15	0.040± 0.005	2.39± 0.15	0.033± 0.005	2.32± 0.15	0.031± 0.005	2.59± 0.15	0.044± 0.005	2.34± 0.15	0.030± 0.005	2.58± 0.15	0.042± 0.005
650	2.54± 0.15	0.046± 0.006	2.47± 0.15	0.043± 0.006	2.52± 0.15	0.046± 0.006	2.40± 0.15	0.038± 0.006	2.33± 0.15	0.035± 0.006	2.60± 0.15	0.050± 0.006	2.35± 0.15	0.034± 0.006	2.59± 0.15	0.049± 0.006
700	2.54± 0.15	0.050± 0.007	2.48± 0.15	0.047± 0.007	2.53± 0.15	0.051± 0.007	2.40± 0.15	0.042± 0.007	2.34± 0.15	0.039± 0.007	2.61± 0.15	0.055± 0.007	2.35± 0.15	0.037± 0.007	2.60± 0.15	0.053± 0.007
750	2.56± 0.15	0.053± 0.006	2.49± 0.15	0.049± 0.006	2.55± 0.15	0.053± 0.006	2.42± 0.15	0.044± 0.006	2.35± 0.15	0.041± 0.006	2.62± 0.15	0.058± 0.006	2.36± 0.15	0.039± 0.006	2.61± 0.15	0.056± 0.006
800	2.59± 0.15	0.051± 0.007	2.52± 0.15	0.047± 0.007	2.58± 0.15	0.051± 0.007	2.44± 0.15	0.042± 0.007	2.37± 0.15	0.039± 0.007	2.66± 0.15	0.056± 0.007	2.39± 0.15	0.037± 0.007	2.65± 0.15	0.054± 0.007
850	2.60± 0.16	0.059± 0.007	2.53± 0.16	0.055± 0.007	2.59± 0.16	0.060± 0.007	2.45± 0.16	0.049± 0.007	2.38± 0.16	0.045± 0.007	2.67± 0.16	0.065± 0.007	2.40± 0.16	0.043± 0.007	2.66± 0.16	0.063± 0.007
900	2.58± 0.15	0.068± 0.007	2.51± 0.15	0.063± 0.007	2.57± 0.15	0.069± 0.007	2.43± 0.15	0.057± 0.007	2.36± 0.15	0.052± 0.007	2.65± 0.15	0.075± 0.007	2.38± 0.15	0.050± 0.007	2.64± 0.15	0.072± 0.007
950	2.59± 0.13	0.080± 0.008	2.52± 0.13	0.074± 0.008	2.58± 0.13	0.081± 0.008	2.45± 0.13	0.067± 0.008	2.38± 0.13	0.062± 0.008	2.66± 0.13	0.088± 0.008	2.39± 0.13	0.059± 0.008	2.65± 0.13	0.085± 0.008

Table C.11- Binary clay-air mixing rules dielectric property estimations of powders of Hammershoj yellow clay at 0.56±0.03void fraction at 912 MHz across the 20-950 ºC firing range from clay slabs at 0.39±0.01 void fractions. The standard uncertainties are indicated in the table.

	Complex Refractive Index		Landau-Lifshitz-Looyenga		Bruggeman-Hanai		Böttcher		Lichtenecker		Rayleigh		Sen-Scala-Cohen		Complex Refractive Index α=0.65	
T (°C)	**ε'**	**ε''**	**ε'**	**ε''**	**ε'**	**ε''**	**ε'**	**ε''**	**ε'**	**ε''**	**ε'**	**ε''**	**ε'**	**ε''**	**ε'**	**ε''**
20	2.55± 0.06	0.090± 0.003	2.49± 0.06	0.084± 0.003	2.54± 0.06	0.090± 0.003	2.42± 0.06	0.075± 0.003	2.37± 0.06	0.071± 0.003	2.61± 0.06	0.097± 0.003	2.38± 0.06	0.068± 0.003	2.60± 0.06	0.095± 0.003
50	2.60± 0.08	0.132± 0.002	2.53± 0.08	0.124± 0.002	2.59± 0.08	0.133± 0.002	2.46± 0.08	0.111± 0.002	2.40± 0.08	0.104± 0.002	2.66± 0.08	0.144± 0.002	2.41± 0.08	0.100± 0.002	2.65± 0.08	0.140± 0.002
100	2.56± 0.07	0.090± 0.001	2.50± 0.07	0.084± 0.001	2.55± 0.07	0.091± 0.001	2.43± 0.07	0.076± 0.001	2.37± 0.07	0.072± 0.001	2.62± 0.07	0.098± 0.001	2.38± 0.07	0.069± 0.001	2.61± 0.07	0.095± 0.001
150	2.52± 0.08	0.027± 0.005	2.46± 0.08	0.026± 0.005	2.51± 0.08	0.028± 0.005	2.39± 0.08	0.023± 0.005	2.34± 0.08	0.022± 0.005	2.57± 0.08	0.030± 0.005	2.35± 0.08	0.021± 0.005	2.57± 0.08	0.029± 0.005
200	2.53± 0.08	0.029± 0.006	2.47± 0.08	0.027± 0.006	2.52± 0.08	0.029± 0.006	±2.40± 0.08	0.025± 0.006	2.35± 0.08	0.023± 0.006	2.59± 0.08	0.032± 0.006	2.36± 0.08	0.022± 0.006	2.58± 0.08	0.031± 0.006
250	2.55± 0.08	0.030± 0.008	2.49± 0.08	0.028± 0.008	2.54± 0.08	0.030± 0.008	2.42± 0.08	0.025± 0.008	2.36± 0.08	0.024± 0.008	2.61± 0.08	0.033± 0.008	2.37± 0.08	0.023± 0.008	2.60± 0.08	0.032± 0.008
300	2.56± 0.06	0.031± 0.001	2.50± 0.06	0.029± 0.001	2.55± 0.06	0.031± 0.001	2.43± 0.06	0.026± 0.001	2.37± 0.06	0.024± 0.001	2.62± 0.06	0.033± 0.001	2.38± 0.06	0.023± 0.001	2.61± 0.06	0.032± 0.001
350	2.58± 0.05	0.023± 0.007	2.51± 0.05	0.021± 0.007	2.57± 0.05	0.023± 0.007	2.44± 0.05	0.018± 0.007	2.38± 0.05	0.018± 0.007	2.64± 0.05	0.025± 0.007	2.39± 0.05	0.017± 0.007	2.63± 0.05	0.024± 0.007
400	2.59± 0.04	0.026± 0.006	2.53± 0.04	0.025± 0.006	2.58± 0.04	0.026± 0.006	2.46± 0.04	0.021± 0.006	2.40± 0.04	0.021± 0.006	2.66± 0.04	0.029± 0.006	2.41± 0.04	0.020± 0.006	2.65± 0.04	0.028± 0.006
450	2.62± 0.02	0.039± 0.006	2.55± 0.02	0.036± 0.006	2.61± 0.02	0.039± 0.006	2.48± 0.02	0.033± 0.006	2.42± 0.02	0.031± 0.006	2.68± 0.02	0.042± 0.006	2.43± 0.02	0.029± 0.006	2.67± 0.02	0.041± 0.006
500	2.64± 0.02	0.038± 0.008	2.57± 0.02	0.036± 0.008	2.63± 0.02	0.038± 0.008	2.49± 0.02	0.032± 0.008	2.43± 0.02	0.030± 0.008	2.70± 0.02	0.042± 0.008	2.44± 0.02	0.029± 0.008	2.69± 0.02	0.040± 0.008
550	2.66± 0.04	0.045± 0.006	2.59± 0.04	0.042± 0.006	2.65± 0.04	0.046± 0.006	2.51± 0.04	0.038± 0.006	2.45± 0.04	0.035± 0.006	2.73± 0.04	0.049± 0.006	2.46± 0.04	0.034± 0.006	2.72± 0.04	0.048± 0.006
600	2.69± 0.06	0.052± 0.006	2.62± 0.06	0.048± 0.006	2.68± 0.06	0.052± 0.006	2.54± 0.06	0.043± 0.006	2.47± 0.06	0.040± 0.006	2.76± 0.06	0.057± 0.006	2.48± 0.06	0.038± 0.006	2.75± 0.06	0.055± 0.006
650	2.73± 0.07	0.066± 0.007	2.66± 0.07	0.061± 0.007	2.72± 0.07	0.066± 0.007	2.57± 0.07	0.054± 0.007	2.50± 0.07	0.051± 0.007	2.81± 0.07	0.072± 0.007	2.51± 0.07	0.048± 0.007	2.79± 0.07	0.070± 0.007
700	2.76± 0.09	0.082± 0.005	2.69± 0.09	0.076± 0.005	2.75± 0.09	0.083± 0.005	2.60± 0.09	0.068± 0.005	2.53± 0.09	0.064± 0.005	2.84± 0.09	0.090± 0.005	2.53± 0.09	0.060± 0.005	2.82± 0.09	0.087± 0.005
750	2.80± 0.10	0.087± 0.005	2.72± 0.10	0.081± 0.005	2.79± 0.10	0.088± 0.005	2.63± 0.10	0.072± 0.005	2.56± 0.10	0.067± 0.005	2.88± 0.10	0.095± 0.005	2.56± 0.10	0.063± 0.005	2.86± 0.10	0.092± 0.005
800	2.84± 0.08	0.089± 0.006	2.76± 0.08	0.083± 0.006	2.84± 0.08	0.090± 0.006	2.66± 0.08	0.074± 0.006	2.59± 0.08	0.069± 0.006	2.93± 0.08	0.098± 0.006	2.59± 0.08	0.064± 0.006	2.91± 0.08	0.095± 0.006
850	2.86± 0.05	0.099± 0.007	2.78± 0.05	0.091± 0.007	2.85± 0.05	0.100± 0.007	2.68± 0.05	0.081± 0.007	2.60± 0.05	0.076± 0.007	2.95± 0.05	0.109± 0.007	2.60± 0.05	0.070± 0.007	2.93± 0.05	0.105± 0.007
900	2.86± 0.08	0.112± 0.008	2.78± 0.08	0.103± 0.008	2.85± 0.08	0.113± 0.008	2.68± 0.08	0.092± 0.008	2.60± 0.08	0.086± 0.008	2.95± 0.08	0.123± 0.008	2.60± 0.08	0.079± 0.008	2.93± 0.08	0.118± 0.008
950	2.91± 0.10	0.137± 0.006	2.82± 0.10	0.127± 0.006	2.90± 0.10	0.138± 0.006	2.72± 0.10	0.112± 0.006	2.64± 0.10	0.105± 0.006	3.00± 0.10	0.151± 0.006	2.64± 0.10	0.096± 0.006	2.98± 0.10	0.145± 0.006

Table C.12- Binary clay-air mixing rules dielectric property estimations of powders of Hammershoj yellow clay at 0.56±0.03void fraction at 2470 MHz across the 20-950 ºC firing range from clay slabs at 0.39±0.01 void fractions. The standard uncertainties are indicated in the table.

	Complex Refractive Index		Landau-Lifshitz-Looyenga		Bruggeman-Hanai		Böttcher		Lichtenecker		Rayleigh		Sen-Scala-Cohen		Complex Refractive Index α=0.65	
T (°C)	ε'	ε''	ε'	ε''	ε'	ε''	ε'	ε''	ε'	ε''	ε'	ε''	ε'	ε''	ε'	ε''
20	2.60± 0.05	0.085± 0.003	2.53± 0.05	0.079± 0.003	2.59± 0.05	0.086± 0.003	2.46± 0.05	0.071± 0.003	2.40± 0.05	0.067± 0.003	2.66± 0.05	0.093± 0.003	2.41± 0.05	0.064± 0.003	2.65± 0.05	0.090± 0.003
50	2.64± 0.07	0.112± 0.001	2.57± 0.07	0.104± 0.001	2.63± 0.07	0.113± 0.001	2.49± 0.07	0.093± 0.001	2.43± 0.07	0.088± 0.001	2.70± 0.07	0.122± 0.001	2.44± 0.07	0.083± 0.001	2.69± 0.07	0.118± 0.001
100	2.61± 0.06	0.084± 0.001	2.54± 0.06	0.079± 0.001	2.60± 0.06	0.085± 0.001	2.47± 0.06	0.071± 0.001	2.41± 0.06	0.066± 0.001	2.67± 0.06	0.092± 0.001	2.42± 0.06	0.063± 0.001	2.66± 0.06	0.089± 0.001
150	2.57± 0.06	0.025± 0.006	2.51± 0.06	0.023± 0.006	2.56± 0.06	0.025± 0.006	2.43± 0.06	0.020± 0.006	2.38± 0.06	0.019± 0.006	2.63± 0.06	0.027± 0.006	2.39± 0.06	0.019± 0.006	2.62± 0.06	0.026± 0.006
200	2.58± 0.05	0.026± 0.002	2.52± 0.05	0.024± 0.002	2.57± 0.05	0.026± 0.002	2.44± 0.05	0.022± 0.002	2.38± 0.05	0.020± 0.002	2.64± 0.05	0.028± 0.002	2.40± 0.05	0.020± 0.002	2.63± 0.05	0.027± 0.002
250	2.59± 0.05	0.026± 0.008	2.53± 0.05	0.024± 0.008	2.58± 0.05	0.026± 0.008	2.45± 0.05	0.021± 0.008	2.39± 0.05	0.020± 0.008	2.65± 0.05	0.028± 0.008	2.41± 0.05	0.019± 0.008	2.64± 0.05	0.027± 0.008
300	2.60± 0.03	0.025± 0.000	2.54± 0.03	0.023± 0.000	2.59± 0.03	0.025± 0.000	2.46± 0.03	0.021± 0.000	2.40± 0.03	0.019± 0.000	2.66± 0.03	0.027± 0.000	2.41± 0.03	0.019± 0.000	2.65± 0.03	0.026± 0.000
350	2.61± 0.03	0.017± 0.003	2.54± 0.03	0.016± 0.003	2.60± 0.03	0.017± 0.003	2.47± 0.03	0.015± 0.003	2.41± 0.03	0.013± 0.003	2.67± 0.03	0.018± 0.003	2.42± 0.03	0.013± 0.003	2.66± 0.03	0.018± 0.003
400	2.62± 0.02	0.020± 0.003	2.55± 0.02	0.018± 0.003	2.61± 0.02	0.020± 0.003	2.48± 0.02	0.017± 0.003	2.42± 0.02	0.015± 0.003	2.69± 0.02	0.021± 0.003	2.43± 0.02	0.015± 0.003	2.67± 0.02	0.021± 0.003
450	2.63± 0.01	0.026± 0.005	2.57± 0.01	0.024± 0.005	2.62± 0.01	0.026± 0.005	2.49± 0.01	0.022± 0.005	2.43± 0.01	0.020± 0.005	2.70± 0.01	0.028± 0.005	2.44± 0.01	0.019± 0.005	2.69± 0.01	0.027± 0.005
500	2.64± 0.01	0.023± 0.002	2.58± 0.01	0.021± 0.002	2.63± 0.01	0.023± 0.002	2.50± 0.01	0.019± 0.002	2.43± 0.01	0.018± 0.002	2.71± 0.01	0.025± 0.002	2.44± 0.01	0.017± 0.002	2.70± 0.01	0.024± 0.002
550	2.66± 0.02	0.027± 0.004	2.59± 0.02	0.025± 0.004	2.65± 0.02	0.027± 0.004	2.51± 0.02	0.022± 0.004	2.45± 0.02	0.021± 0.004	2.73± 0.02	0.029± 0.004	2.46± 0.02	0.020± 0.004	2.72± 0.02	0.028± 0.004
600	2.68± 0.03	0.030± 0.004	2.61± 0.03	0.028± 0.004	2.67± 0.03	0.030± 0.004	2.53± 0.03	0.025± 0.004	2.46± 0.03	0.024± 0.004	2.75± 0.03	0.033± 0.004	2.47± 0.03	0.022± 0.004	2.73± 0.03	0.032± 0.004
650	2.70± 0.04	0.036± 0.002	2.63± 0.04	0.033± 0.002	2.69± 0.04	0.036± 0.002	2.55± 0.04	0.030± 0.002	2.48± 0.04	0.028± 0.002	2.78± 0.04	0.039± 0.002	2.49± 0.04	0.026± 0.002	2.76± 0.04	0.038± 0.002
700	2.72± 0.05	0.042± 0.005	2.65± 0.05	0.039± 0.005	2.71± 0.05	0.042± 0.005	2.56± 0.05	0.035± 0.005	2.50± 0.05	0.033± 0.005	2.80± 0.05	0.046± 0.005	2.50± 0.05	0.031± 0.005	2.78± 0.05	0.045± 0.005
750	2.75± 0.05	0.043± 0.008	2.67± 0.05	0.040± 0.008	2.74± 0.05	0.043± 0.008	2.58± 0.05	0.035± 0.008	2.52± 0.05	0.033± 0.008	2.83± 0.05	0.047± 0.008	2.52± 0.05	0.031± 0.008	2.81± 0.05	0.045± 0.008
800	2.78± 0.04	0.042± 0.009	2.70± 0.04	0.039± 0.009	2.77± 0.04	0.043± 0.009	2.61± 0.04	0.035± 0.009	2.54± 0.04	0.033± 0.009	2.86± 0.04	0.046± 0.009	2.54± 0.04	0.031± 0.009	2.84± 0.04	0.045± 0.009
850	2.77± 0.03	0.046± 0.005	2.70± 0.03	0.043± 0.005	2.77± 0.03	0.047± 0.005	2.61± 0.03	0.038± 0.005	2.54± 0.03	0.036± 0.005	2.85± 0.03	0.051± 0.005	2.54± 0.03	0.034± 0.005	2.84± 0.03	0.049± 0.005
900	2.76± 0.04	0.049± 0.004	2.68± 0.04	0.046± 0.004	2.75± 0.04	0.049± 0.004	2.59± 0.04	0.041± 0.004	2.53± 0.04	0.038± 0.004	2.84± 0.04	0.054± 0.004	2.53± 0.04	0.036± 0.004	2.82± 0.04	0.052± 0.004
950	2.78± 0.05	0.055± 0.002	2.71± 0.05	0.051± 0.002	2.77± 0.05	0.056± 0.002	2.61± 0.05	0.046± 0.002	2.54± 0.05	0.043± 0.002	2.86± 0.05	0.061± 0.002	2.55± 0.05	0.040± 0.002	2.85± 0.05	0.059± 0.002

Table C.13- Binary clay-air mixing rules dielectric property estimations of powders of Helligsø red clay at 0.56±0.03void fraction at 912 MHz across the 20-950 ºC firing range from clay slabs at 0.40±0.01void fractions. The standard uncertainties are indicated in the table.

	Complex Refractive Index		Landau-Lifshitz-Looyenga		Bruggeman-Hanai		Böttcher		Lichtenecker		Rayleigh		Sen-Scala-Cohen		Complex Refractive Index α=0.65	
T (°C)	**ε'**	**ε''**	**ε'**	**ε''**	**ε'**	**ε''**	**ε'**	**ε''**	**ε'**	**ε''**	**ε'**	**ε''**	**ε'**	**ε''**	**ε'**	**ε''**
20	2.31± 0.05	0.092± 0.005	2.26± 0.05	0.086± 0.005	2.30± 0.05	0.091± 0.005	2.22± 0.05	0.079± 0.005	2.17± 0.05	0.075± 0.005	2.35± 0.05	0.098± 0.005	2.19± 0.05	0.074± 0.005	2.34± 0.05	0.096± 0.005
50	2.33± 0.04	0.121± 0.007	2.29± 0.04	0.114± 0.007	2.32± 0.04	0.121± 0.007	2.24± 0.04	0.104± 0.007	2.20± 0.04	0.099± 0.007	2.38± 0.04	0.129± 0.007	2.21± 0.04	0.097± 0.007	2.37± 0.04	0.126± 0.007
100	2.30± 0.04	0.109± 0.009	2.26± 0.04	0.103± 0.009	2.29± 0.04	0.109± 0.009	2.21± 0.04	0.095± 0.009	2.17± 0.04	0.090± 0.009	2.34± 0.04	0.117± 0.009	2.18± 0.04	0.088± 0.009	2.34± 0.04	0.114± 0.009
150	2.25± 0.07	0.017± 0.005	2.21± 0.07	0.016± 0.005	2.24± 0.07	0.017± 0.005	2.17± 0.07	0.015± 0.005	2.13± 0.07	0.014± 0.005	2.29± 0.07	0.018± 0.005	2.15± 0.07	0.014± 0.005	2.29± 0.07	0.018± 0.005
200	2.26± 0.10	0.018± 0.004	2.22± 0.10	0.017± 0.004	2.25± 0.10	0.018± 0.004	2.17± 0.10	0.016± 0.004	2.13± 0.10	0.015± 0.004	2.29± 0.10	0.019± 0.004	2.15± 0.10	0.014± 0.004	2.29± 0.10	0.019± 0.004
250	2.27± 0.15	0.020± 0.003	2.23± 0.15	0.019± 0.003	2.26± 0.15	0.020± 0.003	2.18± 0.15	0.017± 0.003	2.14± 0.15	0.016± 0.003	2.30± 0.15	0.021± 0.003	2.16± 0.15	0.016± 0.003	2.30± 0.15	0.021± 0.003
300	2.27± 0.15	0.020± 0.004	2.23± 0.15	0.019± 0.004	2.26± 0.15	0.020± 0.004	2.19± 0.15	0.017± 0.004	2.15± 0.15	0.017± 0.004	2.31± 0.15	0.022± 0.004	2.16± 0.15	0.017± 0.004	2.31± 0.15	0.021± 0.004
350	2.28± 0.15	0.025± 0.006	2.24± 0.15	0.024± 0.006	2.27± 0.15	0.025± 0.006	2.20± 0.15	0.021± 0.006	2.15± 0.15	0.021± 0.006	2.32± 0.15	0.027± 0.006	2.17± 0.15	0.020± 0.006	2.32± 0.15	0.026± 0.006
400	2.29± 0.14	0.030± 0.007	2.25± 0.14	0.028± 0.007	2.28± 0.14	0.030± 0.007	2.20± 0.14	0.026± 0.007	2.16± 0.14	0.024± 0.007	2.33± 0.14	0.032± 0.007	2.18± 0.14	0.024± 0.007	2.33± 0.14	0.031± 0.007
450	2.30± 0.13	0.039± 0.010	2.26± 0.13	0.037± 0.010	2.29± 0.13	0.039± 0.010	2.21± 0.13	0.034± 0.010	2.17± 0.13	0.032± 0.010	2.34± 0.13	0.042± 0.010	2.19± 0.13	0.032± 0.010	2.34± 0.13	0.041± 0.010
500	2.32± 0.14	0.044± 0.011	2.27± 0.14	0.042± 0.011	2.31± 0.14	0.044± 0.011	2.23± 0.14	0.038± 0.011	2.18± 0.14	0.036± 0.011	2.36± 0.14	0.048± 0.011	2.20± 0.14	0.036± 0.011	2.35± 0.14	0.047± 0.011
550	2.34± 0.16	0.057± 0.014	2.30± 0.16	0.054± 0.014	2.33± 0.16	0.057± 0.014	2.25± 0.16	0.050± 0.014	2.20± 0.16	0.047± 0.014	2.38± 0.16	0.062± 0.014	2.22± 0.16	0.046± 0.014	2.38± 0.16	0.060± 0.014
600	2.38± 0.19	0.068± 0.018	2.33± 0.19	0.064± 0.018	2.36± 0.19	0.068± 0.018	2.27± 0.19	0.058± 0.018	2.23± 0.19	0.055± 0.018	2.42± 0.19	0.073± 0.018	2.25± 0.19	0.054± 0.018	2.42± 0.19	0.071± 0.018
650	2.41± 0.19	0.083± 0.021	2.37± 0.19	0.078± 0.021	2.40± 0.19	0.083± 0.021	2.31± 0.19	0.070± 0.021	2.26± 0.19	0.067± 0.021	2.46± 0.19	0.089± 0.021	2.28± 0.19	0.065± 0.021	2.46± 0.19	0.087± 0.021
700	2.45± 0.19	0.100± 0.025	2.40± 0.19	0.094± 0.025	2.44± 0.19	0.100± 0.025	2.34± 0.19	0.085± 0.025	2.29± 0.19	0.081± 0.025	2.50± 0.19	0.107± 0.025	2.30± 0.19	0.078± 0.025	2.49± 0.19	0.105± 0.025
750	2.48± 0.21	0.116± 0.029	2.42± 0.21	0.109± 0.029	2.47± 0.21	0.117± 0.029	2.36± 0.21	0.099± 0.029	2.31± 0.21	0.094± 0.029	2.53± 0.21	0.125± 0.029	2.33± 0.21	0.091± 0.029	2.52± 0.21	0.122± 0.029
800	2.52± 0.21	0.129± 0.022	2.46± 0.21	0.121± 0.022	2.51± 0.21	0.130± 0.022	2.40± 0.21	0.110± 0.022	2.35± 0.21	0.104± 0.022	2.57± 0.21	0.140± 0.022	2.36± 0.21	0.100± 0.022	2.57± 0.21	0.136± 0.022
850	2.59± 0.21	0.147± 0.025	2.53± 0.21	0.137± 0.025	2.58± 0.21	0.147± 0.025	2.46± 0.21	0.124± 0.025	2.40± 0.21	0.117± 0.025	2.65± 0.21	0.159± 0.025	2.41± 0.21	0.112± 0.025	2.64± 0.21	0.154± 0.025
900	2.71± 0.23	0.200± 0.035	2.64± 0.23	0.187± 0.035	2.70± 0.23	0.202± 0.035	2.56± 0.23	0.167± 0.035	2.50± 0.23	0.158± 0.035	2.78± 0.23	0.218± 0.035	2.50± 0.23	0.149± 0.035	2.77± 0.23	0.211± 0.035
950	2.85± 0.23	0.288± 0.049	2.77± 0.23	0.268± 0.049	2.84± 0.23	0.291± 0.049	2.67± 0.23	0.238± 0.049	2.61± 0.23	0.225± 0.049	2.93± 0.23	0.316± 0.049	2.61± 0.23	0.208± 0.049	2.91± 0.23	0.305± 0.049

Table C.14- Binary clay-air mixing rules dielectric property estimations of powders of Helligsø red clay at 0.56±0.03void fraction at 2470 MHz across the 20-950 ºC firing range from clay slabs at 0.40±0.01 void fractions. The standard uncertainties are indicated in the table.

	Complex Refractive Index		Landau-Lifshitz-Looyenga		Bruggeman-Hanai		Böttcher		Lichtenecker		Rayleigh		Sen-Scala-Cohen		Complex Refractive Index α=0.65	
T (°C)	**ε'**	**ε''**	**ε'**	**ε''**	**ε'**	**ε''**	**ε'**	**ε''**	**ε'**	**ε''**	**ε'**	**ε''**	**ε'**	**ε''**	**ε'**	**ε''**
20	2.37± 0.05	0.095± 0.004	2.32± 0.05	0.089± 0.004	2.36± 0.05	0.095± 0.004	2.27± 0.05	0.081± 0.004	2.22± 0.05	0.077± 0.004	2.41± 0.05	0.102± 0.004	2.24± 0.05	0.075± 0.004	2.41± 0.05	0.099± 0.004
50	2.40± 0.05	0.116± 0.005	2.35± 0.05	0.109± 0.005	2.39± 0.05	0.116± 0.005	2.29± 0.05	0.100± 0.005	2.25± 0.05	0.095± 0.005	2.44± 0.05	0.125± 0.005	2.26± 0.05	0.092± 0.005	2.44± 0.05	0.122± 0.005
100	2.37± 0.05	0.100± 0.004	2.33± 0.05	0.094± 0.004	2.36± 0.05	0.100± 0.004	2.27± 0.05	0.086± 0.004	2.23± 0.05	0.082± 0.004	2.42± 0.05	0.108± 0.004	2.24± 0.05	0.080± 0.004	2.41± 0.05	0.105± 0.004
150	2.34± 0.06	0.016± 0.001	2.30± 0.06	0.016± 0.001	2.33± 0.06	0.016± 0.001	2.25± 0.06	0.014± 0.001	2.20± 0.06	0.013± 0.001	2.38± 0.06	0.018± 0.001	2.22± 0.06	0.013± 0.001	2.38± 0.06	0.017± 0.001
200	2.35± 0.07	0.016± 0.001	2.30± 0.07	0.015± 0.001	2.34± 0.07	0.016± 0.001	2.25± 0.07	0.013± 0.001	2.21± 0.07	0.013± 0.001	2.39± 0.07	0.017± 0.001	2.22± 0.07	0.013± 0.001	2.39± 0.07	0.017± 0.001
250	2.36± 0.08	0.017± 0.001	2.31± 0.08	0.016± 0.001	2.35± 0.08	0.017± 0.001	2.26± 0.08	0.014± 0.001	2.21± 0.08	0.014± 0.001	2.40± 0.08	0.018± 0.001	2.23± 0.08	0.014± 0.001	2.40± 0.08	0.018± 0.001
300	2.36± 0.09	0.017± 0.001	2.31± 0.09	0.016± 0.001	2.35± 0.09	0.017± 0.001	2.26± 0.09	0.014± 0.001	2.22± 0.09	0.014± 0.001	2.40± 0.09	0.018± 0.001	2.23± 0.09	0.014± 0.001	2.40± 0.09	0.018± 0.001
350	2.37± 0.09	0.019± 0.005	2.32± 0.09	0.018± 0.005	2.36± 0.09	0.019± 0.005	2.27± 0.09	0.017± 0.005	2.22± 0.09	0.015± 0.005	2.41± 0.09	0.020± 0.005	2.24± 0.09	0.015± 0.005	2.41± 0.09	0.020± 0.005
400	2.38± 0.08	0.022± 0.005	2.33± 0.08	0.021± 0.005	2.37± 0.08	0.022± 0.005	2.28± 0.08	0.018± 0.005	2.23± 0.08	0.018± 0.005	2.42± 0.08	0.023± 0.005	2.25± 0.08	0.017± 0.005	2.42± 0.08	0.023± 0.005
450	2.38± 0.08	0.026± 0.007	2.34± 0.08	0.025± 0.007	2.37± 0.08	0.026± 0.007	2.28± 0.08	0.023± 0.007	2.24± 0.08	0.021± 0.007	2.43± 0.08	0.028± 0.007	2.25± 0.08	0.021± 0.007	2.42± 0.08	0.028± 0.007
500	2.39± 0.09	0.030± 0.008	2.34± 0.09	0.028± 0.008	2.38± 0.09	0.030± 0.008	2.29± 0.09	0.024± 0.008	2.24± 0.09	0.024± 0.008	2.43± 0.09	0.032± 0.008	2.26± 0.09	0.023± 0.008	2.43± 0.09	0.031± 0.008
550	2.40± 0.09	0.034± 0.008	2.35± 0.09	0.032± 0.008	2.39± 0.09	0.034± 0.008	2.30± 0.09	0.029± 0.008	2.25± 0.09	0.028± 0.008	2.45± 0.09	0.037± 0.008	2.26± 0.09	0.027± 0.008	2.44± 0.09	0.036± 0.008
600	2.42± 0.10	0.040± 0.010	2.37± 0.10	0.037± 0.010	2.41± 0.10	0.040± 0.010	2.31± 0.10	0.034± 0.010	2.27± 0.10	0.032± 0.010	2.47± 0.10	0.043± 0.010	2.28± 0.10	0.031± 0.010	2.46± 0.10	0.042± 0.010
650	2.44± 0.10	0.044± 0.011	2.39± 0.10	0.042± 0.011	2.43± 0.10	0.044± 0.011	2.33± 0.10	0.038± 0.011	2.28± 0.10	0.036± 0.011	2.49± 0.10	0.048± 0.011	2.30± 0.10	0.035± 0.011	2.49± 0.10	0.047± 0.011
700	2.46± 0.10	0.049± 0.013	2.41± 0.10	0.046± 0.013	2.45± 0.10	0.049± 0.013	2.35± 0.10	0.042± 0.013	2.30± 0.10	0.039± 0.013	2.51± 0.10	0.053± 0.013	2.31± 0.10	0.038± 0.013	2.51± 0.10	0.051± 0.013
750	2.48± 0.10	0.054± 0.013	2.42± 0.10	0.050± 0.013	2.47± 0.10	0.054± 0.013	2.36± 0.10	0.045± 0.013	2.31± 0.10	0.043± 0.013	2.53± 0.10	0.058± 0.013	2.32± 0.10	0.042± 0.013	2.52± 0.10	0.056± 0.013
800	2.50± 0.11	0.060± 0.016	2.45± 0.11	0.057± 0.016	2.49± 0.11	0.061± 0.016	2.38± 0.11	0.051± 0.016	2.33± 0.11	0.049± 0.016	2.55± 0.11	0.065± 0.016	2.34± 0.11	0.047± 0.016	2.55± 0.11	0.063± 0.016
850	2.55± 0.10	0.073± 0.019	2.49± 0.10	0.068± 0.019	2.54± 0.10	0.073± 0.019	2.42± 0.10	0.062± 0.019	2.37± 0.10	0.058± 0.019	2.61± 0.10	0.079± 0.019	2.38± 0.10	0.056± 0.019	2.60± 0.10	0.077± 0.019
900	2.63± 0.11	0.105± 0.026	2.57± 0.11	0.099± 0.026	2.62± 0.11	0.106± 0.026	2.49± 0.11	0.089± 0.026	2.43± 0.11	0.084± 0.026	2.69± 0.11	0.115± 0.026	2.44± 0.11	0.080± 0.026	2.68± 0.11	0.111± 0.026
950	2.72± 0.11	0.149± 0.039	2.65± 0.11	0.139± 0.039	2.71± 0.11	0.150± 0.039	2.56± 0.11	0.124± 0.039	2.50± 0.11	0.117± 0.039	2.79± 0.11	0.162± 0.039	2.51± 0.11	0.110± 0.039	2.77± 0.11	0.157± 0.039

Table C.15- Binary clay-air mixing rules dielectric property estimations of powders of Hammershoj red clay at 0.56±0.03void fraction at 912 MHz across the 20-950 ºC firing range from clay slabs at 0.42±0.03 void fractions. The standard uncertainties are indicated in the table.

	Complex Refractive Index		Landau-Lifshitz-Looyenga		Bruggeman-Hanai		Böttcher		Lichtenecker		Rayleigh		Sen-Scala-Cohen		Complex Refractive Index α=0.65	
T (°C)	**ε'**	**ε''**	**ε'**	**ε''**	**ε'**	**ε''**	**ε'**	**ε''**	**ε'**	**ε''**	**ε'**	**ε''**	**ε'**	**ε''**	**ε'**	**ε''**
20	2.52± 0.06	0.168± 0.009	2.47± 0.06	0.159± 0.009	2.51± 0.06	0.168± 0.009	2.40± 0.06	0.144± 0.009	2.36± 0.06	0.138± 0.009	2.57± 0.06	0.180± 0.009	2.37± 0.06	0.133± 0.009	2.56± 0.06	0.176± 0.009
50	2.59± 0.05	0.245± 0.046	2.53± 0.05	0.231± 0.046	2.58± 0.05	0.246± 0.046	2.46± 0.05	0.209± 0.046	2.42± 0.05	0.200± 0.046	2.64± 0.05	0.264± 0.046	2.43± 0.05	0.192± 0.046	2.63± 0.05	0.257± 0.046
100	2.56± 0.10	0.205± 0.033	2.51± 0.10	0.194± 0.033	2.55± 0.10	0.206± 0.033	2.44± 0.10	0.176± 0.033	2.39± 0.10	0.168± 0.033	2.61± 0.10	0.221± 0.033	2.40± 0.10	0.162± 0.033	2.60± 0.10	0.215± 0.033
150	2.46± 0.11	0.031± 0.007	2.42± 0.11	0.030± 0.007	2.45± 0.11	0.031± 0.007	2.36± 0.11	0.027± 0.007	2.32± 0.11	0.026± 0.007	2.51± 0.11	0.034± 0.007	2.33± 0.11	0.025± 0.007	2.50± 0.11	0.033± 0.007
200	2.45± 0.09	0.017± 0.015	2.41± 0.09	0.016± 0.015	2.44± 0.09	0.017± 0.015	2.35± 0.09	0.015± 0.015	2.31± 0.09	0.014± 0.015	2.50± 0.09	0.019± 0.015	2.32± 0.09	0.014± 0.015	2.49± 0.09	0.018± 0.015
250	2.48± 0.06	0.025± 0.010	2.43± 0.06	0.024± 0.010	2.47± 0.06	0.025± 0.010	2.37± 0.06	0.022± 0.010	2.33± 0.06	0.021± 0.010	2.53± 0.06	0.027± 0.010	2.34± 0.06	0.020± 0.010	2.52± 0.06	0.026± 0.010
300	2.51± 0.05	0.019± 0.003	2.46± 0.05	0.018± 0.003	2.50± 0.05	0.019± 0.003	2.40± 0.05	0.016± 0.003	2.35± 0.05	0.016± 0.003	2.56± 0.05	0.020± 0.003	2.36± 0.05	0.015± 0.003	2.55± 0.05	0.020± 0.003
350	2.54± 0.04	0.023± 0.018	2.49± 0.04	0.022± 0.018	2.53± 0.04	0.023± 0.018	2.42± 0.04	0.020± 0.018	2.38± 0.04	0.019± 0.018	2.59± 0.04	0.025± 0.018	2.39± 0.04	0.018± 0.018	2.58± 0.04	0.024± 0.018
400	2.57± 0.02	0.037± 0.005	2.52± 0.02	0.035± 0.005	2.56± 0.02	0.037± 0.005	2.45± 0.02	0.031± 0.005	2.41± 0.02	0.030± 0.005	2.63± 0.02	0.039± 0.005	2.41± 0.02	0.029± 0.005	2.62± 0.02	0.038± 0.005
450	2.61± 0.00	0.038± 0.009	2.55± 0.00	0.036± 0.009	2.60± 0.00	0.038± 0.009	2.48± 0.00	0.032± 0.009	2.44± 0.00	0.031± 0.009	2.67± 0.00	0.041± 0.009	2.44± 0.00	0.030± 0.009	2.66± 0.00	0.040± 0.009
500	2.65± 0.00	0.049± 0.002	2.59± 0.00	0.046± 0.002	2.64± 0.00	0.050± 0.002	2.52± 0.00	0.042± 0.002	2.47± 0.00	0.040± 0.002	2.71± 0.00	0.053± 0.002	2.47± 0.00	0.038± 0.002	2.70± 0.00	0.052± 0.002
550	2.68± 0.06	0.051± 0.016	2.62± 0.06	0.048± 0.016	2.67± 0.06	0.051± 0.016	2.54± 0.06	0.043± 0.016	2.49± 0.06	0.041± 0.016	2.74± 0.06	0.055± 0.016	2.50± 0.06	0.039± 0.016	2.73± 0.06	0.053± 0.016
600	2.73± 0.05	0.068± 0.002	2.67± 0.05	0.064± 0.002	2.72± 0.05	0.069± 0.002	2.59± 0.05	0.057± 0.002	2.54± 0.05	0.055± 0.002	2.80± 0.05	0.074± 0.002	2.54± 0.05	0.052± 0.002	2.78± 0.05	0.072± 0.002
650	2.78± 0.05	0.084± 0.005	2.72± 0.05	0.079± 0.005	2.77± 0.05	0.084± 0.005	2.63± 0.05	0.070± 0.005	2.58± 0.05	0.067± 0.005	2.85± 0.05	0.091± 0.005	2.58± 0.05	0.063± 0.005	2.84± 0.05	0.088± 0.005
700	2.83± 0.07	0.095± 0.023	2.76± 0.07	0.089± 0.023	2.82± 0.07	0.096± 0.023	2.67± 0.07	0.079± 0.023	2.62± 0.07	0.076± 0.023	2.91± 0.07	0.103± 0.023	2.61± 0.07	0.071± 0.023	2.89± 0.07	0.100± 0.023
750	2.88± 0.08	0.120± 0.028	2.81± 0.08	0.112± 0.028	2.88± 0.08	0.121± 0.028	2.71± 0.08	0.100± 0.028	2.66± 0.08	0.095± 0.028	2.96± 0.08	0.130± 0.028	2.65± 0.08	0.088± 0.028	2.94± 0.08	0.126± 0.028
800	2.93± 0.10	0.132± 0.012	2.86± 0.10	0.123± 0.012	2.93± 0.10	0.133± 0.012	2.76± 0.10	0.109± 0.012	2.70± 0.10	0.105± 0.012	3.02± 0.10	0.143± 0.012	2.69± 0.10	0.096± 0.012	3.00± 0.10	0.139± 0.012
850	3.01± 0.10	0.128± 0.016	2.93± 0.10	0.120± 0.016	3.00± 0.10	0.130± 0.016	2.82± 0.10	0.106± 0.016	2.76± 0.10	0.101± 0.016	3.10± 0.10	0.140± 0.016	2.74± 0.10	0.092± 0.016	3.08± 0.10	0.135± 0.016
900	3.13± 0.10	0.175± 0.018	3.04± 0.10	0.163± 0.018	3.13± 0.10	0.177± 0.018	2.92± 0.10	0.144± 0.018	2.85± 0.10	0.137± 0.018	3.23± 0.10	0.192± 0.018	2.83± 0.10	0.123± 0.018	3.20± 0.10	0.185± 0.018
950	3.28± 0.11	0.255± 0.011	3.19± 0.11	0.237± 0.011	3.28± 0.11	0.259± 0.011	3.05± 0.11	0.207± 0.011	2.97± 0.11	0.197± 0.011	3.40± 0.11	0.280± 0.011	2.94± 0.11	0.174± 0.011	3.37± 0.11	0.270± 0.011

Table C.16- Binary clay-air mixing rules dielectric property estimations of powders of Hammershoj red clay at 0.56±0.03void fraction at 2470 MHz across the 20-950 ºC firing range from clay slabs at 0.42±0.03void fractions. The standard uncertainties are indicated in the table.

	Complex Refractive Index		Landau-Lifshitz-Looyenga		Bruggeman-Hanai		Böttcher		Lichtenecker		Rayleigh		Sen-Scala-Cohen		Complex Refractive Index α=0.65	
T (°C)	ε'	ε''	ε'	ε''	ε'	ε''	ε'	ε''	ε'	ε''	ε'	ε''	ε'	ε''	ε'	ε''
20	2.55± 0.05	0.175± 0.022	2.50± 0.05	0.165± 0.022	2.54± 0.05	0.176± 0.022	2.43± 0.05	0.150± 0.022	2.39± 0.05	0.144± 0.022	2.60± 0.05	0.188± 0.022	2.39± 0.05	0.138± 0.022	2.59± 0.05	0.183± 0.022
50	2.60± 0.04	0.220± 0.027	2.55± 0.04	0.207± 0.027	2.59± 0.04	0.221± 0.027	2.47± 0.04	0.187± 0.027	2.43± 0.04	0.179± 0.027	2.65± 0.04	0.236± 0.027	2.44± 0.04	0.171± 0.027	2.64± 0.04	0.230± 0.027
100	2.58± 0.12	0.192± 0.020	2.52± 0.12	0.181± 0.020	2.57± 0.12	0.193± 0.020	2.46± 0.12	0.164± 0.020	2.41± 0.12	0.157± 0.020	2.63± 0.12	0.206± 0.020	2.42± 0.12	0.150± 0.020	2.62± 0.12	0.201± 0.020
150	2.50± 0.10	0.030± 0.003	2.45± 0.10	0.028± 0.003	2.49± 0.10	0.030± 0.003	2.39± 0.10	0.026± 0.003	2.34± 0.10	0.025± 0.003	2.54± 0.10	0.032± 0.003	2.35± 0.10	0.024± 0.003	2.54± 0.10	0.031± 0.003
200	2.47± 0.07	0.015± 0.003	2.43± 0.07	0.014± 0.003	2.46± 0.07	0.015± 0.003	2.37± 0.07	0.013± 0.003	2.33± 0.07	0.013± 0.003	2.52± 0.07	0.016± 0.003	2.34± 0.07	0.012± 0.003	2.51± 0.07	0.016± 0.003
250	2.49± 0.04	0.020± 0.002	2.44± 0.04	0.019± 0.002	2.48± 0.04	0.020± 0.002	2.38± 0.04	0.017± 0.002	2.34± 0.04	0.016± 0.002	2.54± 0.04	0.021± 0.002	2.35± 0.04	0.016± 0.002	2.53± 0.04	0.021± 0.002
300	2.50± 0.03	0.017± 0.002	2.45± 0.03	0.016± 0.002	2.49± 0.03	0.017± 0.002	2.39± 0.03	0.015± 0.002	2.35± 0.03	0.014± 0.002	2.55± 0.03	0.018± 0.002	2.36± 0.03	0.013± 0.002	2.54± 0.03	0.018± 0.002
350	2.51± 0.02	0.018± 0.010	2.46± 0.02	0.017± 0.010	2.50± 0.02	0.019± 0.010	2.40± 0.02	0.016± 0.010	2.35± 0.02	0.015± 0.010	2.56± 0.02	0.020± 0.010	2.36± 0.02	0.015± 0.010	2.55± 0.02	0.019± 0.010
400	2.52± 0.01	0.028± 0.003	2.47± 0.01	0.027± 0.003	2.51± 0.01	0.028± 0.003	2.41± 0.01	0.024± 0.003	2.37± 0.01	0.023± 0.003	2.57± 0.01	0.030± 0.003	2.38± 0.01	0.022± 0.003	2.57± 0.01	0.029± 0.003
450	2.54± 0.00	0.026± 0.005	2.49± 0.00	0.025± 0.005	2.53± 0.00	0.026± 0.005	2.43± 0.00	0.023± 0.005	2.38± 0.00	0.022± 0.005	2.59± 0.00	0.028± 0.005	2.39± 0.00	0.021± 0.005	2.58± 0.00	0.028± 0.005
500	2.56± 0.00	0.030± 0.001	2.51± 0.00	0.029± 0.001	2.55± 0.00	0.031± 0.001	2.44± 0.00	0.026± 0.001	2.40± 0.00	0.025± 0.001	2.61± 0.00	0.033± 0.001	2.40± 0.00	0.024± 0.001	2.60± 0.00	0.032± 0.001
550	2.58± 0.03	0.032± 0.006	2.53± 0.03	0.030± 0.006	2.57± 0.03	0.032± 0.006	2.46± 0.03	0.027± 0.006	2.41± 0.03	0.026± 0.006	2.63± 0.03	0.034± 0.006	2.42± 0.03	0.025± 0.006	2.62± 0.03	0.034± 0.006
600	2.60± 0.04	0.040± 0.002	2.55± 0.04	0.037± 0.002	2.59± 0.04	0.040± 0.002	2.47± 0.04	0.034± 0.002	2.43± 0.04	0.032± 0.002	2.65± 0.04	0.043± 0.002	2.44± 0.04	0.031± 0.002	2.64± 0.04	0.041± 0.002
650	2.63± 0.07	0.044± 0.002	2.57± 0.07	0.042± 0.002	2.62± 0.07	0.044± 0.002	2.50± 0.07	0.037± 0.002	2.45± 0.07	0.036± 0.002	2.69± 0.07	0.048± 0.002	2.46± 0.07	0.034± 0.002	2.68± 0.07	0.046± 0.002
700	2.65± 0.09	0.045± 0.013	2.60± 0.09	0.043± 0.013	2.65± 0.09	0.046± 0.013	2.52± 0.09	0.039± 0.013	2.47± 0.09	0.037± 0.013	2.71± 0.09	0.049± 0.013	2.48± 0.09	0.035± 0.013	2.70± 0.09	0.048± 0.013
750	2.68± 0.12	0.054± 0.008	2.62± 0.12	0.051± 0.008	2.67± 0.12	0.055± 0.008	2.54± 0.12	0.046± 0.008	2.49± 0.12	0.044± 0.008	2.74± 0.12	0.058± 0.008	2.50± 0.12	0.042± 0.008	2.73± 0.12	0.057± 0.008
800	2.71± 0.14	0.059± 0.005	2.65± 0.14	0.055± 0.005	2.70± 0.14	0.059± 0.005	2.57± 0.14	0.050± 0.005	2.52± 0.14	0.048± 0.005	2.77± 0.14	0.064± 0.005	2.52± 0.14	0.045± 0.005	2.76± 0.14	0.062± 0.005
850	2.76± 0.14	0.064± 0.013	2.70± 0.14	0.060± 0.013	2.75± 0.14	0.064± 0.013	2.61± 0.14	0.054± 0.013	2.56± 0.14	0.051± 0.013	2.83± 0.14	0.069± 0.013	2.56± 0.14	0.048± 0.013	2.82± 0.14	0.067± 0.013
900	2.85± 0.14	0.093± 0.008	2.78± 0.14	0.087± 0.008	2.84± 0.14	0.094± 0.008	2.69± 0.14	0.078± 0.008	2.63± 0.14	0.074± 0.008	2.92± 0.14	0.101± 0.008	2.63± 0.14	0.069± 0.008	2.91± 0.14	0.098± 0.008
950	2.96± 0.16	0.137± 0.008	2.88± 0.16	0.128± 0.008	2.95± 0.16	0.138± 0.008	2.78± 0.16	0.113± 0.008	2.72± 0.16	0.108± 0.008	3.04± 0.16	0.149± 0.008	2.71± 0.16	0.100± 0.008	3.02± 0.16	0.144± 0.008

Appendix C2: Estimations of multicomponent clay-minerals mixtures

Table C.17- Multicomponent clay-minerals mixing rules dielectric property estimations of slabs of Vedstaarup yellow clay at 0.37±0.02void fraction at 912 MHz across the 20-950 ºC firing range from mineral powders at 0.56±0.04 void fractions. The standard uncertainties are indicated in the table.

	Complex Refractive Index		Landau-Lifshitz-Looyenga		Bruggeman-Hanai		Böttcher		Lichtenecker		Rayleigh		Sen-Scala-Cohen		Complex Refractive Index α=0.65	
T (°C)	ε'	ε''	ε'	ε''	ε'	ε''	ε'	ε''	ε'	ε''	ε'	ε''	ε'	ε''	ε'	ε''
20	3.07± 0.06	0.046± 0.005	3.02± 0.06	0.051± 0.005	3.34± 0.06	0.052± 0.005	3.46± 0.06	0.061± 0.005	3.52± 0.06	0.060± 0.005	3.23± 0.06	0.047± 0.005	3.70± 0.06	0.072± 0.005	3.07± 0.06	0.051± 0.005
50	3.21± 0.06	0.049± 0.009	3.15± 0.06	0.073± 0.009	3.48± 0.06	0.074± 0.009	3.64± 0.06	0.064± 0.009	3.67± 0.06	0.085± 0.009	3.35± 0.06	0.044± 0.009	3.88± 0.06	0.081± 0.009	3.21± 0.06	0.075± 0.009
100	3.18± 0.08	0.040± 0.013	3.12± 0.08	0.065± 0.013	3.45± 0.08	0.066± 0.013	3.59± 0.08	0.052± 0.013	3.63± 0.08	0.075± 0.013	3.31± 0.08	0.036± 0.013	3.84± 0.08	0.069± 0.013	3.18± 0.08	0.067± 0.013
150	2.83± 0.07	0.012± 0.004	2.78± 0.07	0.011± 0.004	3.10± 0.07	0.011± 0.004	3.31± 0.07	0.021± 0.004	3.24± 0.07	0.013± 0.004	3.01± 0.07	0.012± 0.004	3.38± 0.07	0.017± 0.004	2.84± 0.07	0.010± 0.004
200	2.84± 0.08	0.027± 0.003	2.79± 0.08	0.027± 0.003	3.11± 0.08	0.028± 0.003	3.32± 0.08	0.035± 0.003	3.25± 0.08	0.034± 0.003	3.02± 0.08	0.026± 0.003	3.40± 0.08	0.037± 0.003	2.84± 0.08	0.026± 0.003
250	2.87± 0.09	0.027± 0.004	2.82± 0.09	0.027± 0.004	3.15± 0.09	0.028± 0.004	3.36± 0.09	0.034± 0.004	3.29± 0.09	0.034± 0.004	3.05± 0.09	0.026± 0.004	3.44± 0.09	0.037± 0.004	2.87± 0.09	0.026± 0.004
300	2.91± 0.09	0.028± 0.003	2.86± 0.09	0.029± 0.003	3.18± 0.09	0.030± 0.003	3.41± 0.09	0.037± 0.003	3.33± 0.09	0.036± 0.003	3.08± 0.09	0.028± 0.003	3.50± 0.09	0.039± 0.003	2.91± 0.09	0.027± 0.003
350	2.95± 0.10	0.034± 0.003	2.90± 0.10	0.035± 0.003	3.23± 0.10	0.036± 0.003	3.46± 0.10	0.045± 0.003	3.39± 0.10	0.044± 0.003	3.12± 0.10	0.034± 0.003	3.56± 0.10	0.048± 0.003	2.95± 0.10	0.033± 0.003
400	3.00± 0.10	0.045± 0.004	2.95± 0.10	0.046± 0.004	3.28± 0.10	0.047± 0.004	3.53± 0.10	0.059± 0.004	3.45± 0.10	0.058± 0.004	3.17± 0.10	0.044± 0.004	3.63± 0.10	0.063± 0.004	2.99± 0.10	0.043± 0.004
450	3.06± 0.10	0.058± 0.004	3.01± 0.10	0.060± 0.004	3.35± 0.10	0.062± 0.004	3.56± 0.10	0.077± 0.004	3.53± 0.10	0.076± 0.004	3.23± 0.10	0.057± 0.004	3.72± 0.10	0.083± 0.004	3.05± 0.10	0.056± 0.004
500	3.11± 0.11	0.068± 0.005	3.07± 0.11	0.071± 0.005	3.41± 0.11	0.072± 0.005	3.59± 0.11	0.090± 0.005	3.60± 0.11	0.090± 0.005	3.29± 0.11	0.067± 0.005	3.82± 0.11	0.098± 0.005	3.11± 0.11	0.065± 0.005
550	3.16± 0.12	0.075± 0.006	3.12± 0.12	0.077± 0.006	3.47± 0.12	0.079± 0.006	3.65± 0.12	0.098± 0.006	3.67± 0.12	0.099± 0.006	3.34± 0.12	0.073± 0.006	3.90± 0.12	0.108± 0.006	3.15± 0.12	0.072± 0.006
600	3.25± 0.12	0.090± 0.004	3.21± 0.12	0.094± 0.004	3.57± 0.12	0.096± 0.004	3.73± 0.12	0.120± 0.004	3.79± 0.12	0.121± 0.004	3.43± 0.12	0.089± 0.004	4.05± 0.12	0.134± 0.004	3.24± 0.12	0.087± 0.004
650	3.35± 0.12	0.110± 0.005	3.31± 0.12	0.114± 0.005	3.67± 0.12	0.116± 0.005	3.80± 0.12	0.146± 0.005	3.91± 0.12	0.148± 0.005	3.53± 0.12	0.107± 0.005	4.20± 0.12	0.166± 0.005	3.33± 0.12	0.105± 0.005
700	3.44± 0.13	0.131± 0.005	3.41± 0.13	0.136± 0.005	3.77± 0.13	0.138± 0.005	3.93± 0.13	0.176± 0.005	4.04± 0.13	0.177± 0.005	3.62± 0.13	0.127± 0.005	4.36± 0.13	0.202± 0.005	3.42± 0.13	0.125± 0.005
750	3.54± 0.13	0.143± 0.006	3.50± 0.13	0.149± 0.006	3.87± 0.13	0.150± 0.006	4.06± 0.13	0.193± 0.006	4.16± 0.13	0.194± 0.006	3.71± 0.13	0.139± 0.006	4.52± 0.13	0.225± 0.006	3.51± 0.13	0.136± 0.006
800	3.62± 0.13	0.143± 0.008	3.59± 0.13	0.149± 0.008	3.96± 0.13	0.151± 0.008	4.17± 0.13	0.194± 0.008	4.27± 0.13	0.195± 0.008	3.79± 0.13	0.139± 0.008	4.66± 0.13	0.231± 0.008	3.59± 0.13	0.137± 0.008
850	3.76± 0.13	0.181± 0.008	3.74± 0.13	0.188± 0.008	4.11± 0.13	0.188± 0.008	4.37± 0.13	0.246± 0.008	4.47± 0.13	0.243± 0.008	3.93± 0.13	0.171± 0.008	4.90± 0.13	0.310± 0.008	3.73± 0.13	0.174± 0.008
900	3.78± 0.12	0.248± 0.013	3.76± 0.12	0.254± 0.013	4.13± 0.12	0.254± 0.013	4.39± 0.12	0.332± 0.013	4.50± 0.12	0.321± 0.013	3.96± 0.12	0.228± 0.013	4.89± 0.12	0.445± 0.013	3.74± 0.12	0.242± 0.013
950	3.73± 0.14	0.324± 0.017	3.71± 0.14	0.327± 0.017	4.08± 0.14	0.327± 0.017	4.32± 0.14	0.426± 0.017	4.42± 0.14	0.401± 0.017	3.91± 0.14	0.289± 0.017	4.79± 0.14	0.614± 0.017	3.70± 0.14	0.319± 0.017

Table C.18- Multicomponent clay-minerals mixing rules dielectric property estimations of slabs of Vedstaarup yellow clay at 0.37±0.02 void fraction at 2470 MHz across the 20-950 ºC firing range from mineral powders at 0.56±0.04void fractions. The standard uncertainties are indicated in the table.

	Complex Refractive Index		Landau-Lifshitz-Looyenga		Bruggeman-Hanai		Böttcher		Lichtenecker		Rayleigh		Sen-Scala-Cohen		Complex Refractive Index α=0.65	
T (°C)	ε'	ε''	ε'	ε''	ε'	ε''	ε'	ε''	ε'	ε''	ε'	ε''	ε'	ε''	ε'	ε''
20	3.12± 0.06	0.041± 0.003	3.07± 0.06	0.038± 0.003	3.40± 0.06	0.039± 0.003	3.68± 0.06	0.064± 0.003	3.59± 0.06	0.046± 0.003	3.28± 0.06	0.042± 0.003	3.78± 0.06	0.064± 0.003	3.11± 0.06	0.038± 0.003
50	3.20± 0.06	0.044± 0.006	3.15± 0.06	0.056± 0.006	3.48± 0.06	0.056± 0.006	3.78± 0.06	0.074± 0.006	3.69± 0.06	0.066± 0.006	3.35± 0.06	0.043± 0.006	3.89± 0.06	0.070± 0.006	3.19± 0.06	0.055± 0.006
100	3.16± 0.07	0.034± 0.009	3.11± 0.07	0.055± 0.009	3.44± 0.07	0.056± 0.009	3.73± 0.07	0.060± 0.009	3.64± 0.07	0.066± 0.009	3.32± 0.07	0.032± 0.009	3.83± 0.07	0.055± 0.009	3.16± 0.07	0.055± 0.009
150	2.93± 0.06	0.012± 0.002	2.88± 0.06	0.009± 0.002	3.21± 0.06	0.009± 0.002	3.44± 0.06	0.029± 0.002	3.36± 0.06	0.011± 0.002	3.11± 0.06	0.012± 0.002	3.53± 0.06	0.018± 0.002	2.93± 0.06	0.008± 0.002
200	2.94± 0.06	0.024± 0.001	2.89± 0.06	0.024± 0.001	3.22± 0.06	0.025± 0.001	3.45± 0.06	0.031± 0.001	3.37± 0.06	0.031± 0.001	3.11± 0.06	0.023± 0.001	3.55± 0.06	0.033± 0.001	2.94± 0.06	0.023± 0.001
250	2.96± 0.06	0.024± 0.001	2.91± 0.06	0.024± 0.001	3.24± 0.06	0.025± 0.001	3.48± 0.06	0.031± 0.001	3.41± 0.06	0.031± 0.001	3.14± 0.06	0.023± 0.001	3.58± 0.06	0.034± 0.001	2.96± 0.06	0.023± 0.001
300	2.99± 0.06	0.024± 0.001	2.94± 0.06	0.024± 0.001	3.27± 0.06	0.025± 0.001	3.52± 0.06	0.031± 0.001	3.44± 0.06	0.031± 0.001	3.16± 0.06	0.023± 0.001	3.62± 0.06	0.034± 0.001	2.98± 0.06	0.023± 0.001
350	3.01± 0.06	0.024± 0.002	2.96± 0.06	0.025± 0.002	3.30± 0.06	0.026± 0.002	3.55± 0.06	0.032± 0.002	3.47± 0.06	0.032± 0.002	3.19± 0.06	0.024± 0.002	3.66± 0.06	0.035± 0.002	3.01± 0.06	0.023± 0.002
400	3.05± 0.06	0.028± 0.002	3.00± 0.06	0.029± 0.002	3.33± 0.06	0.030± 0.002	3.59± 0.06	0.037± 0.002	3.51± 0.06	0.037± 0.002	3.22± 0.06	0.028± 0.002	3.71± 0.06	0.040± 0.002	3.04± 0.06	0.027± 0.002
450	3.08± 0.06	0.033± 0.002	3.03± 0.06	0.034± 0.002	3.37± 0.06	0.035± 0.002	3.64± 0.06	0.044± 0.002	3.56± 0.06	0.043± 0.002	3.25± 0.06	0.032± 0.002	3.77± 0.06	0.047± 0.002	3.07± 0.06	0.031± 0.002
500	3.11± 0.06	0.036± 0.002	3.06± 0.06	0.037± 0.002	3.40± 0.06	0.038± 0.002	3.68± 0.06	0.048± 0.002	3.60± 0.06	0.048± 0.002	3.29± 0.06	0.036± 0.002	3.82± 0.06	0.052± 0.002	3.10± 0.06	0.035± 0.002
550	3.13± 0.07	0.039± 0.002	3.08± 0.07	0.040± 0.002	3.42± 0.07	0.041± 0.002	3.70± 0.07	0.051± 0.002	3.62± 0.07	0.052± 0.002	3.30± 0.07	0.038± 0.002	3.85± 0.07	0.056± 0.002	3.12± 0.07	0.037± 0.002
600	3.18± 0.07	0.045± 0.002	3.13± 0.07	0.046± 0.002	3.47± 0.07	0.048± 0.002	3.77± 0.07	0.059± 0.002	3.68± 0.07	0.060± 0.002	3.35± 0.07	0.044± 0.002	3.93± 0.07	0.066± 0.002	3.17± 0.07	0.043± 0.002
650	3.23± 0.07	0.053± 0.002	3.18± 0.07	0.055± 0.002	3.53± 0.07	0.056± 0.002	3.84± 0.07	0.070± 0.002	3.75± 0.07	0.071± 0.002	3.40± 0.07	0.052± 0.002	4.02± 0.07	0.078± 0.002	3.22± 0.07	0.050± 0.002
700	3.29± 0.06	0.062± 0.003	3.24± 0.06	0.064± 0.003	3.59± 0.06	0.065± 0.003	3.92± 0.06	0.082± 0.003	3.82± 0.06	0.083± 0.003	3.46± 0.06	0.061± 0.003	4.11± 0.06	0.092± 0.003	3.28± 0.06	0.059± 0.003
750	3.34± 0.06	0.068± 0.003	3.30± 0.06	0.070± 0.003	3.65± 0.06	0.072± 0.003	3.99± 0.06	0.090± 0.003	3.89± 0.06	0.091± 0.003	3.51± 0.06	0.066± 0.003	4.20± 0.06	0.102± 0.003	3.33± 0.06	0.065± 0.003
800	3.39± 0.07	0.069± 0.003	3.35± 0.07	0.072± 0.003	3.70± 0.07	0.073± 0.003	4.06± 0.07	0.092± 0.003	3.96± 0.07	0.093± 0.003	3.56± 0.07	0.068± 0.003	4.28± 0.07	0.106± 0.003	3.37± 0.07	0.066± 0.003
850	3.47± 0.07	0.092± 0.004	3.43± 0.07	0.096± 0.004	3.79± 0.07	0.097± 0.004	4.17± 0.07	0.124± 0.004	4.07± 0.07	0.123± 0.004	3.64± 0.07	0.089± 0.004	4.40± 0.07	0.145± 0.004	3.45± 0.07	0.089± 0.004
900	3.42± 0.09	0.128± 0.006	3.38± 0.09	0.131± 0.006	3.74± 0.09	0.133± 0.006	4.09± 0.09	0.160± 0.006	4.01± 0.09	0.165± 0.006	3.60± 0.09	0.121± 0.006	4.28± 0.09	0.205± 0.006	3.39± 0.09	0.125± 0.006
950	3.31± 0.06	0.164± 0.006	3.27± 0.06	0.165± 0.006	3.63± 0.06	0.167± 0.006	3.94± 0.06	0.203± 0.006	3.86± 0.06	0.201± 0.006	3.49± 0.06	0.150± 0.006	4.10± 0.06	0.267± 0.006	3.29± 0.06	0.161± 0.006

Table C.19- Multicomponent clay-minerals mixing rules dielectric property estimations of slabs of Hammershoj yellow clay at 0.39±0.01 void fraction at 912 MHz across the 20-950 ºC firing range from mineral powders at 0.56±0.04void fractions. The standard uncertainties are indicated in the table.

	Complex Refractive Index		Landau-Lifshitz-Looyenga		Bruggeman-Hanai		Böttcher		Lichtenecker		Rayleigh		Sen-Scala-Cohen		Complex Refractive Index α=0.65	
T (°C)	ε'	ε''	ε'	ε''	ε'	ε''	ε'	ε''	ε'	ε''	ε'	ε''	ε'	ε''	ε'	ε''
20	2.98± 0.06	0.054± 0.005	2.92± 0.06	0.059± 0.005	3.25± 0.06	0.060± 0.005	3.49± 0.06	0.083± 0.005	3.38± 0.06	0.069± 0.005	3.14± 0.06	0.055± 0.005	3.55± 0.06	0.081± 0.005	2.99± 0.06	0.059± 0.005
50	3.11± 0.07	0.057± 0.011	3.05± 0.07	0.085± 0.011	3.38± 0.07	0.087± 0.011	3.65± 0.07	0.088± 0.011	3.53± 0.07	0.097± 0.011	3.26± 0.07	0.052± 0.011	3.72± 0.07	0.091± 0.011	3.12± 0.07	0.088± 0.011
100	3.08± 0.09	0.047± 0.016	3.02± 0.09	0.075± 0.016	3.35± 0.09	0.077± 0.016	3.61± 0.09	0.067± 0.016	3.49± 0.09	0.085± 0.016	3.22± 0.09	0.043± 0.016	3.69± 0.09	0.077± 0.016	3.09± 0.09	0.079± 0.016
150	2.76± 0.08	0.014± 0.004	2.70± 0.08	0.012± 0.004	3.02± 0.08	0.013± 0.004	3.21± 0.08	0.026± 0.004	3.12± 0.08	0.015± 0.004	2.93± 0.08	0.014± 0.004	3.26± 0.08	0.019± 0.004	2.77± 0.08	0.012± 0.004
200	2.76± 0.08	0.025± 0.003	2.70± 0.08	0.026± 0.003	3.02± 0.08	0.027± 0.003	3.22± 0.08	0.042± 0.003	3.13± 0.08	0.032± 0.003	2.94± 0.08	0.025± 0.003	3.27± 0.08	0.034± 0.003	2.77± 0.08	0.025± 0.003
250	2.79± 0.09	0.025± 0.004	2.73± 0.09	0.026± 0.004	3.06± 0.09	0.027± 0.004	3.26± 0.09	0.042± 0.004	3.17± 0.09	0.032± 0.004	2.97± 0.09	0.025± 0.004	3.32± 0.09	0.034± 0.004	2.80± 0.09	0.025± 0.004
300	2.83± 0.10	0.027± 0.003	2.77± 0.10	0.028± 0.003	3.09± 0.10	0.029± 0.003	3.30± 0.10	0.044± 0.003	3.21± 0.10	0.034± 0.003	3.00± 0.10	0.027± 0.003	3.36± 0.10	0.037± 0.003	2.83± 0.10	0.026± 0.003
350	2.87± 0.10	0.033± 0.003	2.81± 0.10	0.033± 0.003	3.14± 0.10	0.035± 0.003	3.35± 0.10	0.042± 0.003	3.26± 0.10	0.041± 0.003	3.04± 0.10	0.032± 0.003	3.42± 0.10	0.044± 0.003	2.87± 0.10	0.032± 0.003
400	2.91± 0.11	0.043± 0.004	2.85± 0.11	0.044± 0.004	3.19± 0.11	0.045± 0.004	3.41± 0.11	0.055± 0.004	3.32± 0.11	0.054± 0.004	3.09± 0.11	0.042± 0.004	3.49± 0.11	0.058± 0.004	2.92± 0.11	0.041± 0.004
450	2.97± 0.11	0.056± 0.004	2.91± 0.11	0.057± 0.004	3.25± 0.11	0.059± 0.004	3.48± 0.11	0.071± 0.004	3.39± 0.11	0.071± 0.004	3.15± 0.11	0.055± 0.004	3.57± 0.11	0.077± 0.004	2.97± 0.11	0.054± 0.004
500	3.02± 0.12	0.065± 0.005	2.97± 0.12	0.067± 0.005	3.31± 0.12	0.069± 0.005	3.56± 0.12	0.074± 0.005	3.46± 0.12	0.084± 0.005	3.21± 0.12	0.064± 0.005	3.66± 0.12	0.091± 0.005	3.02± 0.12	0.063± 0.005
550	3.07± 0.14	0.071± 0.007	3.02± 0.14	0.073± 0.007	3.36± 0.14	0.075± 0.007	3.62± 0.14	0.081± 0.007	3.52± 0.14	0.092± 0.007	3.26± 0.14	0.070± 0.007	3.74± 0.14	0.101± 0.007	3.07± 0.14	0.069± 0.007
600	3.16± 0.13	0.086± 0.005	3.11± 0.13	0.089± 0.005	3.46± 0.13	0.091± 0.005	3.74± 0.13	0.100± 0.005	3.63± 0.13	0.112± 0.005	3.34± 0.13	0.085± 0.005	3.88± 0.13	0.124± 0.005	3.15± 0.13	0.083± 0.005
650	3.25± 0.14	0.105± 0.005	3.20± 0.14	0.108± 0.005	3.56± 0.14	0.111± 0.005	3.86± 0.14	0.125± 0.005	3.75± 0.14	0.137± 0.005	3.43± 0.14	0.103± 0.005	4.02± 0.14	0.153± 0.005	3.24± 0.14	0.101± 0.005
700	3.34± 0.14	0.125± 0.006	3.29± 0.14	0.129± 0.006	3.66± 0.14	0.132± 0.006	3.98± 0.14	0.152± 0.006	3.87± 0.14	0.164± 0.006	3.52± 0.14	0.122± 0.006	4.16± 0.14	0.186± 0.006	3.33± 0.14	0.120± 0.006
750	3.43± 0.14	0.136± 0.007	3.38± 0.14	0.141± 0.007	3.75± 0.14	0.144± 0.007	4.10± 0.14	0.163± 0.007	3.98± 0.14	0.180± 0.007	3.61± 0.14	0.133± 0.007	4.31± 0.14	0.207± 0.007	3.41± 0.14	0.131± 0.007
800	3.50± 0.15	0.136± 0.008	3.46± 0.15	0.141± 0.008	3.83± 0.15	0.144± 0.008	4.21± 0.15	0.164± 0.008	4.08± 0.15	0.181± 0.008	3.68± 0.15	0.133± 0.008	4.44± 0.15	0.212± 0.008	3.49± 0.15	0.131± 0.008
850	3.64± 0.15	0.173± 0.009	3.60± 0.15	0.177± 0.009	3.98± 0.15	0.179± 0.009	4.39± 0.15	0.210± 0.009	4.26± 0.15	0.224± 0.009	3.82± 0.15	0.164± 0.009	4.65± 0.15	0.282± 0.009	3.62± 0.15	0.167± 0.009
900	3.66± 0.13	0.237± 0.016	3.62± 0.13	0.240± 0.016	4.00± 0.13	0.242± 0.016	4.42± 0.13	0.292± 0.016	4.29± 0.13	0.296± 0.016	3.84± 0.13	0.219± 0.016	4.65± 0.13	0.403± 0.016	3.63± 0.13	0.232± 0.016
950	3.61± 0.16	0.309± 0.020	3.57± 0.16	0.309± 0.020	3.95± 0.16	0.312± 0.020	4.35± 0.16	0.379± 0.020	4.22± 0.16	0.370± 0.020	3.80± 0.16	0.278± 0.020	4.57± 0.16	0.553± 0.020	3.59± 0.16	0.306± 0.020

Table C.20- Multicomponent clay-minerals mixing rules dielectric property estimations of slabs of Hammershoj yellow clay at 0.39±0.01 void fraction at 2470 MHz across the 20-950 ºC firing range from mineral powders at 0.56±0.04void fractions. The standard uncertainties are indicated in the table.

	Complex Refractive Index		Landau-Lifshitz-Looyenga		Bruggeman-Hanai		Böttcher		Lichtenecker		Rayleigh		Sen-Scala-Cohen		Complex Refractive Index α=0.65	
T (°C)	**ε'**	**ε''**	**ε'**	**ε''**	**ε'**	**ε''**	**ε'**	**ε''**	**ε'**	**ε''**	**ε'**	**ε''**	**ε'**	**ε''**	**ε'**	**ε''**
20	3.03± 0.07	0.048± 0.003	2.97± 0.07	0.045± 0.003	3.30± 0.07	0.046± 0.003	3.55± 0.07	0.078± 0.003	3.45± 0.07	0.053± 0.003	3.19± 0.07	0.050± 0.003	3.63± 0.07	0.072± 0.003	3.03± 0.07	0.044± 0.003
50	3.11± 0.07	0.051± 0.008	3.05± 0.07	0.064± 0.008	3.38± 0.07	0.066± 0.008	3.65± 0.07	0.093± 0.008	3.54± 0.07	0.075± 0.008	3.26± 0.07	0.051± 0.008	3.73± 0.07	0.079± 0.008	3.11± 0.07	0.065± 0.008
100	3.07± 0.08	0.040± 0.010	3.01± 0.08	0.064± 0.010	3.34± 0.08	0.065± 0.010	3.61± 0.08	0.069± 0.010	3.49± 0.08	0.075± 0.010	3.23± 0.08	0.037± 0.010	3.68± 0.08	0.061± 0.010	3.07± 0.08	0.065± 0.010
150	2.85± 0.07	0.014± 0.003	2.79± 0.07	0.010± 0.003	3.12± 0.07	0.011± 0.003	3.33± 0.07	0.032± 0.003	3.24± 0.07	0.013± 0.003	3.03± 0.07	0.014± 0.003	3.40± 0.07	0.020± 0.003	2.86± 0.07	0.010± 0.003
200	2.86± 0.07	0.023± 0.001	2.80± 0.07	0.023± 0.001	3.13± 0.07	0.024± 0.001	3.34± 0.07	0.044± 0.001	3.25± 0.07	0.029± 0.001	3.03± 0.07	0.022± 0.001	3.41± 0.07	0.031± 0.001	2.86± 0.07	0.022± 0.001
250	2.88± 0.07	0.023± 0.002	2.82± 0.07	0.023± 0.002	3.15± 0.07	0.024± 0.002	3.37± 0.07	0.044± 0.002	3.28± 0.07	0.029± 0.002	3.06± 0.07	0.022± 0.002	3.44± 0.07	0.031± 0.002	2.89± 0.07	0.022± 0.002
300	2.90± 0.07	0.023± 0.002	2.84± 0.07	0.023± 0.002	3.18± 0.07	0.024± 0.002	3.40± 0.07	0.044± 0.002	3.30± 0.07	0.029± 0.002	3.08± 0.07	0.022± 0.002	3.48± 0.07	0.031± 0.002	2.91± 0.07	0.022± 0.002
350	2.93± 0.07	0.023± 0.002	2.87± 0.07	0.024± 0.002	3.20± 0.07	0.025± 0.002	3.43± 0.07	0.045± 0.002	3.33± 0.07	0.030± 0.002	3.11± 0.07	0.023± 0.002	3.52± 0.07	0.032± 0.002	2.93± 0.07	0.023± 0.002
400	2.96± 0.07	0.027± 0.002	2.90± 0.07	0.027± 0.002	3.24± 0.07	0.028± 0.002	3.47± 0.07	0.034± 0.002	3.37± 0.07	0.034± 0.002	3.14± 0.07	0.027± 0.002	3.56± 0.07	0.037± 0.002	2.96± 0.07	0.026± 0.002
450	2.99± 0.07	0.031± 0.002	2.93± 0.07	0.032± 0.002	3.27± 0.07	0.033± 0.002	3.51± 0.07	0.040± 0.002	3.42± 0.07	0.040± 0.002	3.17± 0.07	0.031± 0.002	3.61± 0.07	0.044± 0.002	2.99± 0.07	0.030± 0.002
500	3.02± 0.07	0.034± 0.002	2.96± 0.07	0.035± 0.002	3.31± 0.07	0.037± 0.002	3.55± 0.07	0.044± 0.002	3.45± 0.07	0.045± 0.002	3.20± 0.07	0.034± 0.002	3.66± 0.07	0.048± 0.002	3.02± 0.07	0.033± 0.002
550	3.04± 0.08	0.037± 0.003	2.98± 0.08	0.038± 0.003	3.32± 0.08	0.039± 0.003	3.58± 0.08	0.047± 0.003	3.47± 0.08	0.048± 0.003	3.22± 0.08	0.037± 0.003	3.69± 0.08	0.052± 0.003	3.04± 0.08	0.036± 0.003
600	3.08± 0.08	0.043± 0.002	3.03± 0.08	0.044± 0.002	3.37± 0.08	0.045± 0.002	3.64± 0.08	0.054± 0.002	3.53± 0.08	0.056± 0.002	3.26± 0.08	0.042± 0.002	3.76± 0.08	0.061± 0.002	3.08± 0.08	0.041± 0.002
650	3.13± 0.08	0.050± 0.002	3.08± 0.08	0.052± 0.002	3.43± 0.08	0.054± 0.002	3.70± 0.08	0.064± 0.002	3.59± 0.08	0.066± 0.002	3.31± 0.08	0.050± 0.002	3.84± 0.08	0.072± 0.002	3.13± 0.08	0.048± 0.002
700	3.19± 0.07	0.059± 0.003	3.14± 0.07	0.061± 0.003	3.49± 0.07	0.062± 0.003	3.78± 0.07	0.072± 0.003	3.66± 0.07	0.077± 0.003	3.37± 0.07	0.058± 0.003	3.93± 0.07	0.085± 0.003	3.19± 0.07	0.056± 0.003
750	3.24± 0.07	0.064± 0.003	3.19± 0.07	0.067± 0.003	3.54± 0.07	0.069± 0.003	3.85± 0.07	0.077± 0.003	3.73± 0.07	0.085± 0.003	3.41± 0.07	0.064± 0.003	4.01± 0.07	0.095± 0.003	3.24± 0.07	0.062± 0.003
800	3.29± 0.07	0.066± 0.003	3.24± 0.07	0.068± 0.003	3.59± 0.07	0.070± 0.003	3.91± 0.07	0.078± 0.003	3.79± 0.07	0.087± 0.003	3.46± 0.07	0.065± 0.003	4.09± 0.07	0.098± 0.003	3.28± 0.07	0.063± 0.003
850	3.36± 0.08	0.088± 0.004	3.32± 0.08	0.090± 0.004	3.67± 0.08	0.092± 0.004	4.01± 0.08	0.106± 0.004	3.89± 0.08	0.114± 0.004	3.54± 0.08	0.085± 0.004	4.20± 0.08	0.134± 0.004	3.35± 0.08	0.085± 0.004
900	3.31± 0.10	0.122± 0.007	3.27± 0.10	0.124± 0.007	3.63± 0.10	0.127± 0.007	3.94± 0.10	0.151± 0.007	3.84± 0.10	0.153± 0.007	3.50± 0.10	0.116± 0.007	4.09± 0.10	0.188± 0.007	3.30± 0.10	0.119± 0.007
950	3.21± 0.07	0.156± 0.008	3.16± 0.07	0.156± 0.008	3.52± 0.07	0.160± 0.008	3.80± 0.07	0.192± 0.008	3.70± 0.07	0.186± 0.008	3.40± 0.07	0.144± 0.008	3.93± 0.07	0.245± 0.008	3.20± 0.07	0.155± 0.008

Table C.21- Multicomponent clay-minerals mixing rules dielectric property estimations of slabs of Helligsø red clay at 0.40±0.01 void fraction at 912 MHz across the 20-950 ºC firing range from mineral powders at 0.56±0.04void fractions. The standard uncertainties are indicated in the table.

	Complex Refractive Index		Landau-Lifshitz-Looyenga		Bruggeman-Hanai		Böttcher		Lichtenecker		Rayleigh		Sen-Scala-Cohen		Complex Refractive Index α=0.65	
T (°C)	**ε'**	**ε''**	**ε'**	**ε''**	**ε'**	**ε''**	**ε'**	**ε''**	**ε'**	**ε''**	**ε'**	**ε''**	**ε'**	**ε''**	**ε'**	**ε''**
20	2.80± 0.07	0.065± 0.006	2.77± 0.07	0.064± 0.006	2.95± 0.07	0.065± 0.006	3.10± 0.07	0.079± 0.006	3.05± 0.07	0.070± 0.006	2.87± 0.07	0.064± 0.006	3.14± 0.07	0.088± 0.006	2.79± 0.07	0.065± 0.006
50	2.92± 0.08	0.066± 0.013	2.90± 0.08	0.093± 0.013	3.07± 0.08	0.093± 0.013	3.24± 0.08	0.079± 0.013	3.19± 0.08	0.099± 0.013	2.98± 0.08	0.060± 0.013	3.30± 0.08	0.094± 0.013	2.92± 0.08	0.097± 0.013
100	2.86± 0.10	0.052± 0.018	2.83± 0.10	0.079± 0.018	3.01± 0.10	0.080± 0.018	3.17± 0.10	0.061± 0.018	3.11± 0.10	0.083± 0.018	2.92± 0.10	0.046± 0.018	3.22± 0.10	0.075± 0.018	2.86± 0.10	0.083± 0.018
150	2.56± 0.07	0.015± 0.005	2.53± 0.07	0.013± 0.005	2.71± 0.07	0.013± 0.005	2.82± 0.07	0.018± 0.005	2.79± 0.07	0.015± 0.005	2.65± 0.07	0.015± 0.005	2.84± 0.07	0.019± 0.005	2.55± 0.07	0.012± 0.005
200	2.56± 0.07	0.024± 0.003	2.54± 0.07	0.024± 0.003	2.71± 0.07	0.025± 0.003	2.82± 0.07	0.029± 0.003	2.80± 0.07	0.028± 0.003	2.66± 0.07	0.023± 0.003	2.85± 0.07	0.030± 0.003	2.56± 0.07	0.024± 0.003
250	2.59± 0.07	0.025± 0.004	2.57± 0.07	0.025± 0.004	2.74± 0.07	0.025± 0.004	2.86± 0.07	0.030± 0.004	2.83± 0.07	0.029± 0.004	2.68± 0.07	0.024± 0.004	2.89± 0.07	0.031± 0.004	2.58± 0.07	0.024± 0.004
300	2.62± 0.08	0.027± 0.003	2.60± 0.08	0.028± 0.003	2.77± 0.08	0.028± 0.003	2.89± 0.08	0.033± 0.003	2.87± 0.08	0.032± 0.003	2.71± 0.08	0.026± 0.003	2.93± 0.08	0.034± 0.003	2.61± 0.08	0.027± 0.003
350	2.66± 0.08	0.034± 0.003	2.63± 0.08	0.035± 0.003	2.81± 0.08	0.035± 0.003	2.94± 0.08	0.041± 0.003	2.91± 0.08	0.040± 0.003	2.75± 0.08	0.033± 0.003	2.97± 0.08	0.043± 0.003	2.65± 0.08	0.033± 0.003
400	2.70± 0.08	0.044± 0.004	2.68± 0.08	0.045± 0.004	2.86± 0.08	0.046± 0.004	2.99± 0.08	0.053± 0.004	2.96± 0.08	0.053± 0.004	2.79± 0.08	0.043± 0.004	3.03± 0.08	0.056± 0.004	2.69± 0.08	0.043± 0.004
450	2.75± 0.09	0.056± 0.005	2.73± 0.09	0.058± 0.005	2.91± 0.09	0.058± 0.005	3.05± 0.09	0.068± 0.005	3.03± 0.09	0.067± 0.005	2.84± 0.09	0.054± 0.005	3.10± 0.09	0.072± 0.005	2.74± 0.09	0.055± 0.005
500	2.80± 0.10	0.067± 0.006	2.78± 0.10	0.069± 0.006	2.96± 0.10	0.069± 0.006	3.11± 0.10	0.082± 0.006	3.09± 0.10	0.080± 0.006	2.89± 0.10	0.065± 0.006	3.16± 0.10	0.086± 0.006	2.79± 0.10	0.065± 0.006
550	2.85± 0.12	0.075± 0.008	2.83± 0.12	0.077± 0.008	3.02± 0.12	0.078± 0.008	3.18± 0.12	0.092± 0.008	3.15± 0.12	0.091± 0.008	2.94± 0.12	0.073± 0.008	3.23± 0.12	0.098± 0.008	2.83± 0.12	0.074± 0.008
600	2.92± 0.12	0.093± 0.005	2.91± 0.12	0.096± 0.005	3.10± 0.12	0.096± 0.005	3.27± 0.12	0.114± 0.005	3.24± 0.12	0.113± 0.005	3.02± 0.12	0.090± 0.005	3.34± 0.12	0.122± 0.005	2.91± 0.12	0.091± 0.005
650	3.00± 0.12	0.114± 0.006	2.99± 0.12	0.117± 0.006	3.18± 0.12	0.117± 0.006	3.37± 0.12	0.140± 0.006	3.34± 0.12	0.139± 0.006	3.10± 0.12	0.110± 0.006	3.44± 0.12	0.152± 0.006	2.98± 0.12	0.111± 0.006
700	3.08± 0.12	0.135± 0.007	3.07± 0.12	0.139± 0.007	3.26± 0.12	0.139± 0.007	3.47± 0.12	0.168± 0.007	3.44± 0.12	0.165± 0.007	3.17± 0.12	0.130± 0.007	3.55± 0.12	0.183± 0.007	3.06± 0.12	0.132± 0.007
750	3.15± 0.12	0.148± 0.008	3.15± 0.12	0.153± 0.008	3.34± 0.12	0.152± 0.008	3.56± 0.12	0.184± 0.008	3.52± 0.12	0.182± 0.008	3.24± 0.12	0.142± 0.008	3.65± 0.12	0.203± 0.008	3.13± 0.12	0.144± 0.008
800	3.21± 0.12	0.146± 0.010	3.20± 0.12	0.150± 0.010	3.40± 0.12	0.149± 0.010	3.63± 0.12	0.182± 0.010	3.59± 0.12	0.179± 0.010	3.30± 0.12	0.140± 0.010	3.73± 0.12	0.202± 0.010	3.18± 0.12	0.142± 0.010
850	3.34± 0.12	0.174± 0.010	3.34± 0.12	0.179± 0.010	3.54± 0.12	0.177± 0.010	3.80± 0.12	0.218± 0.010	3.76± 0.12	0.211± 0.010	3.43± 0.12	0.164± 0.010	3.92± 0.12	0.252± 0.010	3.31± 0.12	0.170± 0.010
900	3.48± 0.13	0.240± 0.018	3.49± 0.13	0.245± 0.018	3.68± 0.13	0.241± 0.018	3.97± 0.13	0.299± 0.018	3.93± 0.13	0.285± 0.018	3.56± 0.13	0.221± 0.018	4.11± 0.13	0.364± 0.018	3.45± 0.13	0.236± 0.018
950	3.62± 0.14	0.325± 0.023	3.63± 0.14	0.330± 0.023	3.82± 0.14	0.324± 0.023	4.15± 0.14	0.405± 0.023	4.09± 0.14	0.382± 0.023	3.69± 0.14	0.293± 0.023	4.31± 0.14	0.523± 0.023	3.58± 0.14	0.321± 0.023

Table C.22- Multicomponent clay-minerals mixing rules dielectric property estimations of slabs of Helligsø red clay at 0.40±0.01 void fraction at 2470 MHz across the 20-950 ºC firing range from mineral powders at 0.56±0.04void fractions. The standard uncertainties are indicated in the table

	Complex Refractive Index		Landau-Lifshitz-Looyenga		Bruggeman-Hanai		Böttcher		Lichtenecker		Rayleigh		Sen-Scala-Cohen		Complex Refractive Index α=0.65	
T (°C)	ε'	ε''	ε'	ε''	ε'	ε''	ε'	ε''	ε'	ε''	ε'	ε''	ε'	ε''	ε'	ε''
20	2.82± 0.07	0.057± 0.004	2.80± 0.07	0.048± 0.004	2.98± 0.07	0.049± 0.004	3.14± 0.07	0.069± 0.004	3.10± 0.07	0.054± 0.004	2.90± 0.07	0.056± 0.004	3.18± 0.07	0.077± 0.004	2.82± 0.07	0.048± 0.004
50	2.90± 0.07	0.060± 0.009	2.88± 0.07	0.070± 0.009	3.05± 0.07	0.070± 0.009	3.22± 0.07	0.073± 0.009	3.18± 0.07	0.076± 0.009	2.97± 0.07	0.057± 0.009	3.27± 0.07	0.082± 0.009	2.89± 0.07	0.071± 0.009
100	2.84± 0.08	0.043± 0.012	2.81± 0.08	0.066± 0.012	2.99± 0.08	0.067± 0.012	3.15± 0.08	0.051± 0.012	3.10± 0.08	0.072± 0.012	2.91± 0.08	0.039± 0.012	3.19± 0.08	0.059± 0.012	2.83± 0.08	0.068± 0.012
150	2.63± 0.07	0.015± 0.004	2.61± 0.07	0.011± 0.004	2.79± 0.07	0.011± 0.004	2.91± 0.07	0.017± 0.004	2.88± 0.07	0.012± 0.004	2.73± 0.07	0.015± 0.004	2.94± 0.07	0.019± 0.004	2.63± 0.07	0.010± 0.004
200	2.64± 0.06	0.021± 0.002	2.61± 0.06	0.022± 0.002	2.79± 0.06	0.022± 0.002	2.91± 0.06	0.026± 0.002	2.89± 0.06	0.025± 0.002	2.73± 0.06	0.021± 0.002	2.95± 0.06	0.027± 0.002	2.63± 0.06	0.021± 0.002
250	2.66± 0.06	0.022± 0.002	2.63± 0.06	0.022± 0.002	2.81± 0.06	0.022± 0.002	2.94± 0.06	0.026± 0.002	2.91± 0.06	0.026± 0.002	2.75± 0.06	0.021± 0.002	2.97± 0.06	0.027± 0.002	2.65± 0.06	0.021± 0.002
300	2.67± 0.06	0.022± 0.002	2.65± 0.06	0.022± 0.002	2.83± 0.06	0.023± 0.002	2.96± 0.06	0.026± 0.002	2.94± 0.06	0.026± 0.002	2.77± 0.06	0.021± 0.002	3.00± 0.06	0.028± 0.002	2.67± 0.06	0.021± 0.002
350	2.70± 0.06	0.023± 0.002	2.68± 0.06	0.024± 0.002	2.86± 0.06	0.024± 0.002	2.99± 0.06	0.028± 0.002	2.96± 0.06	0.028± 0.002	2.79± 0.06	0.022± 0.002	3.03± 0.06	0.029± 0.002	2.69± 0.06	0.023± 0.002
400	2.72± 0.06	0.027± 0.002	2.70± 0.06	0.028± 0.002	2.88± 0.06	0.028± 0.002	3.02± 0.06	0.033± 0.002	3.00± 0.06	0.032± 0.002	2.82± 0.06	0.026± 0.002	3.06± 0.06	0.034± 0.002	2.71± 0.06	0.026± 0.002
450	2.75± 0.06	0.032± 0.002	2.73± 0.06	0.033± 0.002	2.92± 0.06	0.033± 0.002	3.06± 0.06	0.039± 0.002	3.03± 0.06	0.038± 0.002	2.85± 0.06	0.031± 0.002	3.10± 0.06	0.041± 0.002	2.74± 0.06	0.031± 0.002
500	2.78± 0.07	0.036± 0.003	2.76± 0.07	0.036± 0.003	2.94± 0.07	0.037± 0.003	3.09± 0.07	0.043± 0.003	3.06± 0.07	0.043± 0.003	2.87± 0.07	0.034± 0.003	3.14± 0.07	0.046± 0.003	2.77± 0.07	0.035± 0.003
550	2.79± 0.08	0.039± 0.003	2.78± 0.08	0.040± 0.003	2.96± 0.08	0.040± 0.003	3.11± 0.08	0.047± 0.003	3.08± 0.08	0.047± 0.003	2.89± 0.08	0.038± 0.003	3.16± 0.08	0.050± 0.003	2.78± 0.08	0.038± 0.003
600	2.83± 0.08	0.046± 0.003	2.81± 0.08	0.047± 0.003	3.00± 0.08	0.047± 0.003	3.15± 0.08	0.056± 0.003	3.13± 0.08	0.055± 0.003	2.92± 0.08	0.044± 0.003	3.21± 0.08	0.059± 0.003	2.82± 0.08	0.044± 0.003
650	2.87± 0.07	0.054± 0.003	2.86± 0.07	0.056± 0.003	3.04± 0.07	0.056± 0.003	3.20± 0.07	0.066± 0.003	3.17± 0.07	0.066± 0.003	2.96± 0.07	0.053± 0.003	3.26± 0.07	0.071± 0.003	2.86± 0.07	0.053± 0.003
700	2.91± 0.07	0.064± 0.003	2.90± 0.07	0.065± 0.003	3.08± 0.07	0.066± 0.003	3.26± 0.07	0.078± 0.003	3.23± 0.07	0.077± 0.003	3.01± 0.07	0.061± 0.003	3.32± 0.07	0.084± 0.003	2.90± 0.07	0.062± 0.003
750	2.95± 0.07	0.069± 0.003	2.94± 0.07	0.071± 0.003	3.12± 0.07	0.072± 0.003	3.30± 0.07	0.085± 0.003	3.27± 0.07	0.084± 0.003	3.04± 0.07	0.067± 0.003	3.37± 0.07	0.092± 0.003	2.93± 0.07	0.067± 0.003
800	2.98± 0.07	0.069± 0.004	2.97± 0.07	0.071± 0.004	3.16± 0.07	0.071± 0.004	3.34± 0.07	0.085± 0.004	3.31± 0.07	0.084± 0.004	3.08± 0.07	0.067± 0.004	3.42± 0.07	0.092± 0.004	2.97± 0.07	0.067± 0.004
850	3.07± 0.07	0.087± 0.005	3.06± 0.07	0.089± 0.005	3.25± 0.07	0.089± 0.005	3.45± 0.07	0.107± 0.005	3.42± 0.07	0.105± 0.005	3.16± 0.07	0.083± 0.005	3.53± 0.07	0.119± 0.005	3.05± 0.07	0.085± 0.005
900	3.15± 0.07	0.122± 0.008	3.14± 0.07	0.125± 0.008	3.33± 0.07	0.124± 0.008	3.55± 0.07	0.151± 0.008	3.51± 0.07	0.145± 0.008	3.24± 0.07	0.115± 0.008	3.64± 0.07	0.171± 0.008	3.13± 0.07	0.120± 0.008
950	3.23± 0.07	0.163± 0.009	3.22± 0.07	0.165± 0.009	3.41± 0.07	0.163± 0.009	3.65± 0.07	0.199± 0.009	3.61± 0.07	0.190± 0.009	3.31± 0.07	0.150± 0.009	3.74± 0.07	0.234± 0.009	3.20± 0.07	0.160± 0.009

Table C.23- Multicomponent clay-minerals mixing rules dielectric property estimations of slabs of Hammershoj red clay at 0.42±0.03 void fraction at 912 MHz across the 20-950 ºC firing range from mineral powders at 0.56±0.04void fractions. The standard uncertainties are indicated in the table.

	Complex Refractive Index		Landau-Lifshitz-Looyenga		Bruggeman-Hanai		Böttcher		Lichtenecker		Rayleigh		Sen-Scala-Cohen		Complex Refractive Index α=0.65	
T (°C)	ε'	ε''	ε'	ε''	ε'	ε''	ε'	ε''	ε'	ε''	ε'	ε''	ε'	ε''	ε'	ε''
20	2.80± 0.07	0.065± 0.006	2.77± 0.07	0.064± 0.006	2.95± 0.07	0.065± 0.006	3.25± 0.07	0.079± 0.006	3.05± 0.07	0.070± 0.006	2.87± 0.07	0.064± 0.006	3.14± 0.07	0.088± 0.006	2.79± 0.07	0.065± 0.006
50	2.92± 0.07	0.066± 0.012	2.90± 0.07	0.093± 0.012	3.07± 0.07	0.093± 0.012	3.39± 0.07	0.079± 0.012	3.19± 0.07	0.099± 0.012	2.98± 0.07	0.060± 0.012	3.30± 0.07	0.094± 0.012	2.92± 0.07	0.097± 0.012
100	2.86± 0.10	0.052± 0.016	2.83± 0.10	0.079± 0.016	3.01± 0.10	0.080± 0.016	3.32± 0.10	0.061± 0.016	3.11± 0.10	0.083± 0.016	2.92± 0.10	0.046± 0.016	3.22± 0.10	0.075± 0.016	2.86± 0.10	0.083± 0.016
150	2.56± 0.08	0.015± 0.004	2.53± 0.08	0.013± 0.004	2.71± 0.08	0.013± 0.004	2.97± 0.08	0.018± 0.004	2.79± 0.08	0.015± 0.004	2.65± 0.08	0.015± 0.004	2.84± 0.08	0.019± 0.004	2.55± 0.08	0.012± 0.004
200	2.56± 0.08	0.024± 0.003	2.54± 0.08	0.024± 0.003	2.71± 0.08	0.025± 0.003	2.97± 0.08	0.029± 0.003	2.80± 0.08	0.028± 0.003	2.66± 0.08	0.023± 0.003	2.85± 0.08	0.030± 0.003	2.56± 0.08	0.024± 0.003
250	2.59± 0.08	0.025± 0.004	2.57± 0.08	0.025± 0.004	2.74± 0.08	0.025± 0.004	3.01± 0.08	0.030± 0.004	2.83± 0.08	0.029± 0.004	2.68± 0.08	0.024± 0.004	2.89± 0.08	0.031± 0.004	2.58± 0.08	0.024± 0.004
300	2.62± 0.08	0.027± 0.003	2.60± 0.08	0.028± 0.003	2.77± 0.08	0.028± 0.003	3.04± 0.08	0.033± 0.003	2.87± 0.08	0.032± 0.003	2.71± 0.08	0.026± 0.003	2.93± 0.08	0.034± 0.003	2.61± 0.08	0.027± 0.003
350	2.66± 0.08	0.034± 0.003	2.63± 0.08	0.035± 0.003	2.81± 0.08	0.035± 0.003	3.09± 0.08	0.041± 0.003	2.91± 0.08	0.040± 0.003	2.75± 0.08	0.033± 0.003	2.97± 0.08	0.043± 0.003	2.65± 0.08	0.033± 0.003
400	2.70± 0.08	0.044± 0.004	2.68± 0.08	0.045± 0.004	2.86± 0.08	0.046± 0.004	3.14± 0.08	0.053± 0.004	2.96± 0.08	0.053± 0.004	2.79± 0.08	0.043± 0.004	3.03± 0.08	0.056± 0.004	2.69± 0.08	0.043± 0.004
450	2.75± 0.09	0.056± 0.004	2.73± 0.09	0.058± 0.004	2.91± 0.09	0.058± 0.004	3.20± 0.09	0.068± 0.004	3.03± 0.09	0.067± 0.004	2.84± 0.09	0.054± 0.004	3.10± 0.09	0.072± 0.004	2.74± 0.09	0.055± 0.004
500	2.80± 0.10	0.067± 0.006	2.78± 0.10	0.069± 0.006	2.96± 0.10	0.069± 0.006	3.26± 0.10	0.082± 0.006	3.09± 0.10	0.080± 0.006	2.89± 0.10	0.065± 0.006	3.16± 0.10	0.086± 0.006	2.79± 0.10	0.065± 0.006
550	2.85± 0.11	0.075± 0.007	2.83± 0.11	0.077± 0.007	3.02± 0.11	0.078± 0.007	3.33± 0.11	0.092± 0.007	3.15± 0.11	0.091± 0.007	2.94± 0.11	0.073± 0.007	3.23± 0.11	0.098± 0.007	2.83± 0.11	0.074± 0.007
600	2.92± 0.11	0.093± 0.005	2.91± 0.11	0.096± 0.005	3.10± 0.11	0.096± 0.005	3.42± 0.11	0.114± 0.005	3.24± 0.11	0.113± 0.005	3.02± 0.11	0.090± 0.005	3.34± 0.11	0.122± 0.005	2.91± 0.11	0.091± 0.005
650	3.00± 0.12	0.114± 0.005	2.99± 0.12	0.117± 0.005	3.18± 0.12	0.117± 0.005	3.52± 0.12	0.140± 0.005	3.34± 0.12	0.139± 0.005	3.10± 0.12	0.110± 0.005	3.44± 0.12	0.152± 0.005	2.98± 0.12	0.111± 0.005
700	3.08± 0.12	0.135± 0.006	3.07± 0.12	0.139± 0.006	3.26± 0.12	0.139± 0.006	3.62± 0.12	0.168± 0.006	3.44± 0.12	0.165± 0.006	3.17± 0.12	0.130± 0.006	3.55± 0.12	0.183± 0.006	3.06± 0.12	0.132± 0.006
750	3.15± 0.12	0.148± 0.007	3.15± 0.12	0.153± 0.007	3.34± 0.12	0.152± 0.007	3.71± 0.12	0.184± 0.007	3.52± 0.12	0.182± 0.007	3.24± 0.12	0.142± 0.007	3.65± 0.12	0.203± 0.007	3.13± 0.12	0.144± 0.007
800	3.21± 0.12	0.146± 0.009	3.20± 0.12	0.150± 0.009	3.40± 0.12	0.149± 0.009	3.78± 0.12	0.182± 0.009	3.59± 0.12	0.179± 0.009	3.30± 0.12	0.140± 0.009	3.73± 0.12	0.202± 0.009	3.18± 0.12	0.142± 0.009
850	3.34± 0.12	0.174± 0.009	3.34± 0.12	0.179± 0.009	3.54± 0.12	0.177± 0.009	3.95± 0.12	0.218± 0.009	3.76± 0.12	0.211± 0.009	3.43± 0.12	0.164± 0.009	3.92± 0.12	0.252± 0.009	3.31± 0.12	0.170± 0.009
900	3.48± 0.12	0.240± 0.016	3.49± 0.12	0.245± 0.016	3.68± 0.12	0.241± 0.016	4.12± 0.12	0.299± 0.016	3.93± 0.12	0.285± 0.016	3.56± 0.12	0.221± 0.016	4.11± 0.12	0.364± 0.016	3.45± 0.12	0.236± 0.016
950	3.62± 0.13	0.325± 0.021	3.63± 0.13	0.330± 0.021	3.82± 0.13	0.324± 0.021	4.30± 0.13	0.405± 0.021	4.09± 0.13	0.382± 0.021	3.69± 0.13	0.293± 0.021	4.31± 0.13	0.523± 0.021	3.58± 0.13	0.321± 0.021

Table C.24- Multicomponent clay-minerals mixing rules dielectric property estimations of slabs of Hammershoj red clay at 0.42±0.03 void fraction at 2470 MHz across the 20-950 ºC firing range from mineral powders at 0.56±0.04void fractions. The standard uncertainties are indicated in the table.

	Complex Refractive Index		Landau-Lifshitz-Looyenga		Bruggeman-Hanai		Böttcher		Lichtenecker		Rayleigh		Sen-Scala-Cohen		Complex Refractive Index α=0.65	
T (°C)	ε'	ε''	ε'	ε''	ε'	ε''	ε'	ε''	ε'	ε''	ε'	ε''	ε'	ε''	ε'	ε''
20	2.82± 0.07	0.057± 0.003	2.80± 0.07	0.048± 0.003	2.98± 0.07	0.049± 0.003	3.23± 0.07	0.069± 0.003	3.10± 0.07	0.054± 0.003	2.90± 0.07	0.056± 0.003	3.18± 0.07	0.077± 0.003	2.82± 0.07	0.048± 0.003
50	2.90± 0.07	0.060± 0.008	2.88± 0.07	0.070± 0.008	3.05± 0.07	0.070± 0.008	3.31± 0.07	0.073± 0.008	3.18± 0.07	0.076± 0.008	2.97± 0.07	0.057± 0.008	3.27± 0.07	0.082± 0.008	2.89± 0.07	0.071± 0.008
100	2.84± 0.09	0.043± 0.011	2.81± 0.09	0.066± 0.011	2.99± 0.09	0.067± 0.011	3.24± 0.09	0.051± 0.011	3.10± 0.09	0.072± 0.011	2.91± 0.09	0.039± 0.011	3.19± 0.09	0.059± 0.011	2.83± 0.09	0.068± 0.011
150	2.63± 0.07	0.015± 0.003	2.61± 0.07	0.011± 0.003	2.79± 0.07	0.011± 0.003	3.00± 0.07	0.017± 0.003	2.88± 0.07	0.012± 0.003	2.73± 0.07	0.015± 0.003	2.94± 0.07	0.019± 0.003	2.63± 0.07	0.010± 0.003
200	2.64± 0.07	0.021± 0.002	2.61± 0.07	0.022± 0.002	2.79± 0.07	0.022± 0.002	3.00± 0.07	0.026± 0.002	2.89± 0.07	0.025± 0.002	2.73± 0.07	0.021± 0.002	2.95± 0.07	0.027± 0.002	2.63± 0.07	0.021± 0.002
250	2.66± 0.07	0.022± 0.002	2.63± 0.07	0.022± 0.002	2.81± 0.07	0.022± 0.002	3.03± 0.07	0.026± 0.002	2.91± 0.07	0.026± 0.002	2.75± 0.07	0.021± 0.002	2.97± 0.07	0.027± 0.002	2.65± 0.07	0.021± 0.002
300	2.67± 0.07	0.022± 0.002	2.65± 0.07	0.022± 0.002	2.83± 0.07	0.023± 0.002	3.05± 0.07	0.026± 0.002	2.94± 0.07	0.026± 0.002	2.77± 0.07	0.021± 0.002	3.00± 0.07	0.028± 0.002	2.67± 0.07	0.021± 0.002
350	2.70± 0.06	0.023± 0.002	2.68± 0.06	0.024± 0.002	2.86± 0.06	0.024± 0.002	3.08± 0.06	0.028± 0.002	2.96± 0.06	0.028± 0.002	2.79± 0.06	0.022± 0.002	3.03± 0.06	0.029± 0.002	2.69± 0.06	0.023± 0.002
400	2.72± 0.06	0.027± 0.002	2.70± 0.06	0.028± 0.002	2.88± 0.06	0.028± 0.002	3.11± 0.06	0.033± 0.002	3.00± 0.06	0.032± 0.002	2.82± 0.06	0.026± 0.002	3.06± 0.06	0.034± 0.002	2.71± 0.06	0.026± 0.002
450	2.75± 0.06	0.032± 0.003	2.73± 0.06	0.033± 0.003	2.92± 0.06	0.033± 0.003	3.15± 0.06	0.039± 0.003	3.03± 0.06	0.038± 0.003	2.85± 0.06	0.031± 0.003	3.10± 0.06	0.041± 0.003	2.74± 0.06	0.031± 0.003
500	2.78± 0.07	0.036± 0.003	2.76± 0.07	0.036± 0.003	2.94± 0.07	0.037± 0.003	3.18± 0.07	0.043± 0.003	3.06± 0.07	0.043± 0.003	2.87± 0.07	0.034± 0.003	3.14± 0.07	0.046± 0.003	2.77± 0.07	0.035± 0.003
550	2.79± 0.08	0.039± 0.003	2.78± 0.08	0.040± 0.003	2.96± 0.08	0.040± 0.003	3.20± 0.08	0.047± 0.003	3.08± 0.08	0.047± 0.003	2.89± 0.08	0.038± 0.003	3.16± 0.08	0.050± 0.003	2.78± 0.08	0.038± 0.003
600	2.83± 0.07	0.046± 0.003	2.81± 0.07	0.047± 0.003	3.00± 0.07	0.047± 0.003	3.24± 0.07	0.056± 0.003	3.13± 0.07	0.055± 0.003	2.92± 0.07	0.044± 0.003	3.21± 0.07	0.059± 0.003	2.82± 0.07	0.044± 0.003
650	2.87± 0.07	0.054± 0.003	2.86± 0.07	0.056± 0.003	3.04± 0.07	0.056± 0.003	3.29± 0.07	0.066± 0.003	3.17± 0.07	0.066± 0.003	2.96± 0.07	0.053± 0.003	3.26± 0.07	0.071± 0.003	2.86± 0.07	0.053± 0.003
700	2.91± 0.07	0.064± 0.003	2.90± 0.07	0.065± 0.003	3.08± 0.07	0.066± 0.003	3.35± 0.07	0.078± 0.003	3.23± 0.07	0.077± 0.003	3.01± 0.07	0.061± 0.003	3.32± 0.07	0.084± 0.003	2.90± 0.07	0.062± 0.003
750	2.95± 0.07	0.069± 0.003	2.94± 0.07	0.071± 0.003	3.12± 0.07	0.072± 0.003	3.39± 0.07	0.085± 0.003	3.27± 0.07	0.084± 0.003	3.04± 0.07	0.067± 0.003	3.37± 0.07	0.092± 0.003	2.93± 0.07	0.067± 0.003
800	2.98± 0.07	0.069± 0.004	2.97± 0.07	0.071± 0.004	3.16± 0.07	0.071± 0.004	3.43± 0.07	0.085± 0.004	3.31± 0.07	0.084± 0.004	3.08± 0.07	0.067± 0.004	3.42± 0.07	0.092± 0.004	2.97± 0.07	0.067± 0.004
850	3.07± 0.07	0.087± 0.005	3.06± 0.07	0.089± 0.005	3.25± 0.07	0.089± 0.005	3.54± 0.07	0.107± 0.005	3.42± 0.07	0.105± 0.005	3.16± 0.07	0.083± 0.005	3.53± 0.07	0.119± 0.005	3.05± 0.07	0.085± 0.005
900	3.15± 0.07	0.122± 0.007	3.14± 0.07	0.125± 0.007	3.33± 0.07	0.124± 0.007	3.64± 0.07	0.151± 0.007	3.51± 0.07	0.145± 0.007	3.24± 0.07	0.115± 0.007	3.64± 0.07	0.171± 0.007	3.13± 0.07	0.120± 0.007
950	3.23± 0.07	0.163± 0.008	3.22± 0.07	0.165± 0.008	3.41± 0.07	0.163± 0.008	3.74± 0.07	0.199± 0.008	3.61± 0.07	0.190± 0.008	3.31± 0.07	0.150± 0.008	3.74± 0.07	0.234± 0.008	3.20± 0.07	0.160± 0.008

Table C.25- Multicomponent clay-minerals mixing rules dielectric property estimations of slabs of Spanish yellow clay at 0.10±0.01void fraction at 912 MHz across the 20-950 ºC firing range from mineral powders at 0.56±0.04void fractions. The standard uncertainties are indicated in the table.

	Complex Refractive Index		Landau-Lifshitz-Looyenga		Bruggeman-Hanai		Böttcher		Lichtenecker		Rayleigh		Sen-Scala-Cohen		Complex Refractive Index α=0.65	
T (°C)	ε'	ε''	ε'	ε''	ε'	ε''	ε'	ε''	ε'	ε''	ε'	ε''	ε'	ε''	ε'	ε''
20	4.25± 0.05	0.080± 0.005	4.46± 0.05	0.036± 0.005	4.50± 0.05	0.031± 0.005	5.05± 0.05	0.112± 0.005	5.76± 0.05	0.056± 0.005	4.24± 0.05	0.079± 0.005	5.78± 0.05	0.156± 0.005	4.07± 0.05	0.029± 0.005
50	4.32± 0.05	0.060± 0.006	4.53± 0.05	0.050± 0.006	4.57± 0.05	0.044± 0.006	5.14± 0.05	0.083± 0.006	5.88± 0.05	0.078± 0.006	4.29± 0.05	0.055± 0.006	5.92± 0.05	0.128± 0.006	4.13± 0.05	0.041± 0.006
100	4.16± 0.08	0.041± 0.008	4.35± 0.08	0.026± 0.008	4.40± 0.08	0.023± 0.008	4.92± 0.08	0.056± 0.008	5.59± 0.08	0.042± 0.008	4.15± 0.08	0.039± 0.008	5.60± 0.08	0.077± 0.008	3.98± 0.08	0.021± 0.008
150	4.14± 0.07	0.021± 0.003	4.33± 0.07	0.006± 0.003	4.38± 0.07	0.006± 0.003	4.90± 0.07	0.029± 0.003	5.56± 0.07	0.010± 0.003	4.13± 0.07	0.020± 0.003	5.58± 0.07	0.041± 0.003	3.97± 0.07	0.005± 0.003
200	4.19± 0.08	0.015± 0.003	4.39± 0.08	0.017± 0.003	4.44± 0.08	0.015± 0.003	4.97± 0.08	0.020± 0.003	5.66± 0.08	0.027± 0.003	4.18± 0.08	0.013± 0.003	5.70± 0.08	0.028± 0.003	4.02± 0.08	0.013± 0.003
250	4.27± 0.09	0.015± 0.004	4.48± 0.09	0.017± 0.004	4.52± 0.09	0.015± 0.004	5.07± 0.09	0.020± 0.004	5.80± 0.09	0.028± 0.004	4.25± 0.09	0.013± 0.004	5.85± 0.09	0.029± 0.004	4.09± 0.09	0.013± 0.004
300	4.35± 0.10	0.017± 0.003	4.57± 0.10	0.019± 0.003	4.60± 0.10	0.017± 0.003	5.19± 0.10	0.023± 0.003	5.96± 0.10	0.031± 0.003	4.33± 0.10	0.015± 0.003	6.02± 0.10	0.032± 0.003	4.16± 0.10	0.015± 0.003
350	4.44± 0.11	0.019± 0.003	4.67± 0.11	0.022± 0.003	4.70± 0.11	0.020± 0.003	5.31± 0.11	0.027± 0.003	6.13± 0.11	0.038± 0.003	4.41± 0.11	0.018± 0.003	6.22± 0.11	0.038± 0.003	4.24± 0.11	0.017± 0.003
400	4.54± 0.11	0.024± 0.005	4.78± 0.11	0.028± 0.005	4.80± 0.11	0.025± 0.005	5.44± 0.11	0.034± 0.005	6.31± 0.11	0.048± 0.005	4.50± 0.11	0.022± 0.005	6.43± 0.11	0.049± 0.005	4.32± 0.11	0.022± 0.005
450	4.64± 0.11	0.032± 0.004	4.91± 0.11	0.037± 0.004	4.91± 0.11	0.033± 0.004	5.59± 0.11	0.045± 0.004	6.52± 0.11	0.063± 0.004	4.60± 0.11	0.029± 0.004	6.67± 0.11	0.069± 0.004	4.42± 0.11	0.029± 0.004
500	4.76± 0.11	0.037± 0.005	5.05± 0.11	0.043± 0.005	5.03± 0.11	0.038± 0.005	5.76± 0.11	0.052± 0.005	6.76± 0.11	0.075± 0.005	4.70± 0.11	0.034± 0.005	6.95± 0.11	0.080± 0.005	4.53± 0.11	0.033± 0.005
550	4.90± 0.12	0.045± 0.005	5.21± 0.12	0.053± 0.005	5.17± 0.12	0.046± 0.005	5.95± 0.12	0.063± 0.005	7.03± 0.12	0.092± 0.005	4.83± 0.12	0.040± 0.005	7.29± 0.12	0.100± 0.005	4.65± 0.12	0.040± 0.005
600	5.08± 0.12	0.061± 0.004	5.42± 0.12	0.072± 0.004	5.36± 0.12	0.063± 0.004	6.21± 0.12	0.086± 0.004	7.41± 0.12	0.128± 0.004	4.99± 0.12	0.055± 0.004	7.76± 0.12	0.142± 0.004	4.81± 0.12	0.054± 0.004
650	5.26± 0.12	0.080± 0.006	5.63± 0.12	0.095± 0.006	5.54± 0.12	0.082± 0.006	6.47± 0.12	0.114± 0.006	7.78± 0.12	0.171± 0.006	5.15± 0.12	0.072± 0.006	8.23± 0.12	0.194± 0.006	4.97± 0.12	0.070± 0.006
700	5.43± 0.12	0.097± 0.005	5.83± 0.12	0.115± 0.005	5.71± 0.12	0.098± 0.005	6.71± 0.12	0.138± 0.005	8.13± 0.12	0.210± 0.005	5.29± 0.12	0.086± 0.005	8.71± 0.12	0.248± 0.005	5.12± 0.12	0.085± 0.005
750	5.59± 0.13	0.108± 0.006	6.02± 0.13	0.129± 0.006	5.88± 0.13	0.109± 0.006	6.94± 0.13	0.155± 0.006	8.48± 0.13	0.239± 0.006	5.43± 0.13	0.095± 0.006	9.22± 0.13	0.288± 0.006	5.26± 0.13	0.094± 0.006
800	5.74± 0.13	0.119± 0.007	6.20± 0.13	0.143± 0.007	6.02± 0.13	0.121± 0.007	7.15± 0.13	0.172± 0.007	8.80± 0.13	0.269± 0.007	5.56± 0.13	0.105± 0.007	9.70± 0.13	0.334± 0.007	5.39± 0.13	0.104± 0.007
850	5.83± 0.13	0.128± 0.007	6.30± 0.13	0.153± 0.007	6.11± 0.13	0.129± 0.007	7.28± 0.13	0.185± 0.007	9.00± 0.13	0.290± 0.007	5.64± 0.13	0.112± 0.007	9.93± 0.13	0.378± 0.007	5.47± 0.13	0.112± 0.007
900	5.61± 0.10	0.158± 0.007	6.05± 0.10	0.187± 0.007	5.92± 0.10	0.158± 0.007	6.99± 0.10	0.225± 0.007	8.58± 0.10	0.343± 0.007	5.48± 0.10	0.136± 0.007	9.03± 0.10	0.452± 0.007	5.27± 0.10	0.139± 0.007
950	5.25± 0.14	0.227± 0.011	5.63± 0.14	0.263± 0.011	5.57± 0.14	0.224± 0.011	6.48± 0.14	0.314± 0.011	7.82± 0.14	0.458± 0.011	5.18± 0.14	0.191± 0.011	8.07± 0.14	0.665± 0.011	4.95± 0.14	0.203± 0.011

Table C.26- Multicomponent clay-minerals mixing rules dielectric property estimations of slabs of Spanish yellow clay at 0.10±0.01void fraction at 2470 MHz across the 20-950 ºC firing range from mineral powders at 0.56±0.04void fractions. The standard uncertainties are indicated in the table.

	Complex Refractive Index		Landau-Lifshitz-Looyenga		Bruggeman-Hanai		Böttcher		Lichtenecker		Rayleigh		Sen-Scala-Cohen		Complex Refractive Index α=0.65	
T (°C)	ε'	ε''	ε'	ε''	ε'	ε''	ε'	ε''	ε'	ε''	ε'	ε''	ε'	ε''	ε'	ε''
20	4.42± 0.05	0.079± 0.002	4.65± 0.05	0.030± 0.002	4.68± 0.05	0.027± 0.002	5.29± 0.05	0.111± 0.002	6.09± 0.05	0.049± 0.002	4.39± 0.05	0.077± 0.002	6.16± 0.05	0.160± 0.002	4.23± 0.05	0.024± 0.002
50	4.48± 0.05	0.068± 0.003	4.71± 0.05	0.038± 0.003	4.73± 0.05	0.033± 0.003	5.36± 0.05	0.095± 0.003	6.18± 0.05	0.061± 0.003	4.44± 0.05	0.064± 0.003	6.27± 0.05	0.141± 0.003	4.27± 0.05	0.031± 0.003
100	4.34± 0.08	0.034± 0.006	4.56± 0.08	0.021± 0.006	4.59± 0.08	0.018± 0.006	5.17± 0.08	0.047± 0.006	5.93± 0.08	0.034± 0.006	4.32± 0.08	0.032± 0.006	6.00± 0.08	0.069± 0.006	4.15± 0.08	0.016± 0.006
150	4.34± 0.05	0.024± 0.000	4.56± 0.05	0.006± 0.000	4.60± 0.05	0.006± 0.000	5.18± 0.05	0.032± 0.000	5.94± 0.05	0.010± 0.000	4.32± 0.05	0.022± 0.000	6.02± 0.05	0.049± 0.000	4.15± 0.05	0.005± 0.000
200	4.39± 0.05	0.015± 0.001	4.62± 0.05	0.017± 0.001	4.65± 0.05	0.015± 0.001	5.25± 0.05	0.021± 0.001	6.04± 0.05	0.029± 0.001	4.37± 0.05	0.014± 0.001	6.13± 0.05	0.031± 0.001	4.20± 0.05	0.014± 0.001
250	4.45± 0.06	0.016± 0.002	4.69± 0.06	0.018± 0.002	4.71± 0.06	0.016± 0.002	5.32± 0.06	0.022± 0.002	6.14± 0.06	0.030± 0.002	4.41± 0.06	0.014± 0.002	6.26± 0.06	0.033± 0.002	4.25± 0.06	0.014± 0.002
300	4.51± 0.06	0.017± 0.002	4.75± 0.06	0.019± 0.002	4.77± 0.06	0.017± 0.002	5.40± 0.06	0.023± 0.002	6.25± 0.06	0.032± 0.002	4.47± 0.06	0.015± 0.002	6.39± 0.06	0.035± 0.002	4.30± 0.06	0.015± 0.002
350	4.57± 0.06	0.018± 0.002	4.82± 0.06	0.021± 0.002	4.83± 0.06	0.019± 0.002	5.49± 0.06	0.025± 0.002	6.37± 0.06	0.035± 0.002	4.52± 0.06	0.016± 0.002	6.53± 0.06	0.039± 0.002	4.36± 0.06	0.016± 0.002
400	4.63± 0.06	0.020± 0.002	4.90± 0.06	0.023± 0.002	4.89± 0.06	0.020± 0.002	5.58± 0.06	0.027± 0.002	6.49± 0.06	0.038± 0.002	4.58± 0.06	0.018± 0.002	6.68± 0.06	0.042± 0.002	4.41± 0.06	0.017± 0.002
450	4.70± 0.05	0.021± 0.002	4.97± 0.05	0.025± 0.002	4.96± 0.05	0.022± 0.002	5.67± 0.05	0.030± 0.002	6.62± 0.05	0.042± 0.002	4.64± 0.05	0.019± 0.002	6.84± 0.05	0.046± 0.002	4.47± 0.05	0.019± 0.002
500	4.77± 0.05	0.023± 0.003	5.05± 0.05	0.027± 0.003	5.03± 0.05	0.024± 0.003	5.76± 0.05	0.032± 0.003	6.75± 0.05	0.046± 0.003	4.70± 0.05	0.021± 0.003	7.01± 0.05	0.051± 0.003	4.53± 0.05	0.020± 0.003
550	4.84± 0.06	0.028± 0.003	5.13± 0.06	0.033± 0.003	5.10± 0.06	0.029± 0.003	5.86± 0.06	0.039± 0.003	6.88± 0.06	0.057± 0.003	4.76± 0.06	0.026± 0.003	7.20± 0.06	0.063± 0.003	4.59± 0.06	0.025± 0.003
600	4.94± 0.05	0.034± 0.003	5.25± 0.05	0.040± 0.003	5.20± 0.05	0.035± 0.003	6.00± 0.05	0.047± 0.003	7.09± 0.05	0.069± 0.003	4.85± 0.05	0.031± 0.003	7.46± 0.05	0.076± 0.003	4.69± 0.05	0.030± 0.003
650	5.04± 0.05	0.040± 0.003	5.37± 0.05	0.047± 0.003	5.31± 0.05	0.041± 0.003	6.15± 0.05	0.056± 0.003	7.29± 0.05	0.084± 0.003	4.94± 0.05	0.036± 0.003	7.75± 0.05	0.092± 0.003	4.78± 0.05	0.035± 0.003
700	5.15± 0.05	0.047± 0.003	5.49± 0.05	0.056± 0.003	5.41± 0.05	0.049± 0.003	6.29± 0.05	0.067± 0.003	7.51± 0.05	0.101± 0.003	5.03± 0.05	0.043± 0.003	8.04± 0.05	0.113± 0.003	4.87± 0.05	0.042± 0.003
750	5.25± 0.05	0.054± 0.003	5.61± 0.05	0.065± 0.003	5.51± 0.05	0.056± 0.003	6.43± 0.05	0.077± 0.003	7.70± 0.05	0.117± 0.003	5.11± 0.05	0.049± 0.003	8.34± 0.05	0.133± 0.003	4.96± 0.05	0.048± 0.003
800	5.33± 0.06	0.059± 0.004	5.70± 0.06	0.070± 0.004	5.59± 0.06	0.061± 0.004	6.54± 0.06	0.084± 0.004	7.87± 0.06	0.129± 0.004	5.18± 0.06	0.054± 0.004	8.59± 0.06	0.148± 0.004	5.03± 0.06	0.052± 0.004
850	5.34± 0.06	0.059± 0.003	5.72± 0.06	0.071± 0.003	5.61± 0.06	0.061± 0.003	6.57± 0.06	0.085± 0.003	7.92± 0.06	0.129± 0.003	5.20± 0.06	0.054± 0.003	8.57± 0.06	0.152± 0.003	5.04± 0.06	0.052± 0.003
900	5.05± 0.10	0.074± 0.003	5.39± 0.10	0.087± 0.003	5.34± 0.10	0.075± 0.003	6.17± 0.10	0.104± 0.003	7.37± 0.10	0.152± 0.003	4.98± 0.10	0.066± 0.003	7.55± 0.10	0.178± 0.003	4.77± 0.10	0.065± 0.003
950	4.60± 0.04	0.101± 0.005	4.88± 0.04	0.115± 0.005	4.90± 0.04	0.101± 0.005	5.56± 0.04	0.137± 0.005	6.51± 0.04	0.190± 0.005	4.60± 0.04	0.087± 0.005	6.52± 0.04	0.237± 0.005	4.38± 0.04	0.091± 0.005

Table C.27- Multicomponent clay-minerals mixing rules dielectric property estimations of slabs of English red clay at 0.30±0.02 void fraction at 912 MHz across the 20-950 ºC firing range from mineral powders at 0.56±0.04void fractions. The standard uncertainties are indicated in the table.

	Complex Refractive Index		Landau-Lifshitz-Looyenga		Bruggeman-Hanai		Böttcher		Lichtenecker		Rayleigh		Sen-Scala-Cohen		Complex Refractive Index α=0.65	
T (°C)	**ε'**	**ε''**	**ε'**	**ε''**	**ε'**	**ε''**	**ε'**	**ε''**	**ε'**	**ε''**	**ε'**	**ε''**	**ε'**	**ε''**	**ε'**	**ε''**
20	2.68± 0.04	0.079± 0.006	2.73± 0.04	0.019± 0.006	2.73± 0.04	0.018± 0.006	2.87± 0.04	0.097± 0.006	2.93± 0.04	0.021± 0.006	2.66± 0.04	0.075± 0.006	2.92± 0.04	0.103± 0.006	2.64± 0.04	0.018± 0.006
50	2.71± 0.04	0.046± 0.009	2.75± 0.04	0.023± 0.009	2.76± 0.04	0.022± 0.009	2.90± 0.04	0.055± 0.009	2.96± 0.04	0.025± 0.009	2.68± 0.04	0.042± 0.009	2.95± 0.04	0.062± 0.009	2.66± 0.04	0.023± 0.009
100	2.62± 0.08	0.034± 0.010	2.66± 0.08	0.013± 0.010	2.67± 0.08	0.012± 0.010	2.79± 0.08	0.042± 0.010	2.86± 0.08	0.015± 0.010	2.60± 0.08	0.032± 0.010	2.84± 0.08	0.044± 0.010	2.58± 0.08	0.012± 0.010
150	2.60± 0.06	0.017± 0.004	2.65± 0.06	0.003± 0.004	2.66± 0.06	0.003± 0.004	2.78± 0.06	0.021± 0.004	2.84± 0.06	0.004± 0.004	2.59± 0.06	0.016± 0.004	2.82± 0.06	0.022± 0.004	2.56± 0.06	0.003± 0.004
200	2.63± 0.06	0.006± 0.003	2.67± 0.06	0.007± 0.003	2.68± 0.06	0.006± 0.003	2.81± 0.06	0.007± 0.003	2.88± 0.06	0.008± 0.003	2.62± 0.06	0.006± 0.003	2.85± 0.06	0.008± 0.003	2.59± 0.06	0.006± 0.003
250	2.67± 0.06	0.007± 0.005	2.71± 0.06	0.007± 0.005	2.72± 0.06	0.007± 0.005	2.86± 0.06	0.008± 0.005	2.92± 0.06	0.008± 0.005	2.65± 0.06	0.006± 0.005	2.90± 0.06	0.009± 0.005	2.62± 0.06	0.007± 0.005
300	2.71± 0.06	0.009± 0.003	2.76± 0.06	0.009± 0.003	2.77± 0.06	0.009± 0.003	2.91± 0.06	0.010± 0.003	2.98± 0.06	0.011± 0.003	2.69± 0.06	0.008± 0.003	2.96± 0.06	0.011± 0.003	2.66± 0.06	0.008± 0.003
350	2.76± 0.06	0.011± 0.004	2.81± 0.06	0.012± 0.004	2.82± 0.06	0.011± 0.004	2.97± 0.06	0.014± 0.004	3.05± 0.06	0.014± 0.004	2.74± 0.06	0.010± 0.004	3.02± 0.06	0.015± 0.004	2.71± 0.06	0.011± 0.004
400	2.81± 0.06	0.014± 0.005	2.87± 0.06	0.014± 0.005	2.87± 0.06	0.014± 0.005	3.04± 0.06	0.017± 0.005	3.12± 0.06	0.017± 0.005	2.79± 0.06	0.013± 0.005	3.10± 0.06	0.018± 0.005	2.76± 0.06	0.013± 0.005
450	2.87± 0.06	0.015± 0.004	2.94± 0.06	0.016± 0.004	2.94± 0.06	0.015± 0.004	3.11± 0.06	0.018± 0.004	3.20± 0.06	0.019± 0.004	2.85± 0.06	0.014± 0.004	3.18± 0.06	0.020± 0.004	2.82± 0.06	0.014± 0.004
500	2.94± 0.06	0.019± 0.006	3.01± 0.06	0.020± 0.006	3.00± 0.06	0.019± 0.006	3.20± 0.06	0.024± 0.006	3.29± 0.06	0.024± 0.006	2.91± 0.06	0.017± 0.006	3.27± 0.06	0.026± 0.006	2.88± 0.06	0.018± 0.006
550	3.01± 0.14	0.022± 0.005	3.09± 0.14	0.023± 0.005	3.08± 0.14	0.022± 0.005	3.29± 0.14	0.027± 0.005	3.38± 0.14	0.028± 0.005	2.98± 0.14	0.020± 0.005	3.37± 0.14	0.030± 0.005	2.95± 0.14	0.021± 0.005
600	3.12± 0.10	0.032± 0.005	3.20± 0.10	0.034± 0.005	3.18± 0.10	0.032± 0.005	3.42± 0.10	0.039± 0.005	3.52± 0.10	0.041± 0.005	3.07± 0.10	0.029± 0.005	3.52± 0.10	0.045± 0.005	3.05± 0.10	0.030± 0.005
650	3.21± 0.09	0.042± 0.006	3.30± 0.09	0.045± 0.006	3.28± 0.09	0.042± 0.006	3.53± 0.09	0.053± 0.006	3.65± 0.09	0.056± 0.006	3.16± 0.09	0.039± 0.006	3.65± 0.09	0.061± 0.006	3.13± 0.09	0.040± 0.006
700	3.29± 0.06	0.047± 0.006	3.39± 0.06	0.051± 0.006	3.36± 0.06	0.048± 0.006	3.64± 0.06	0.060± 0.006	3.75± 0.06	0.063± 0.006	3.23± 0.06	0.043± 0.006	3.77± 0.06	0.070± 0.006	3.21± 0.06	0.045± 0.006
750	3.36± 0.06	0.053± 0.006	3.46± 0.06	0.057± 0.006	3.43± 0.06	0.053± 0.006	3.73± 0.06	0.067± 0.006	3.85± 0.06	0.071± 0.006	3.30± 0.06	0.048± 0.006	3.87± 0.06	0.079± 0.006	3.28± 0.06	0.050± 0.006
800	3.43± 0.05	0.061± 0.008	3.53± 0.05	0.065± 0.008	3.49± 0.05	0.061± 0.008	3.81± 0.05	0.077± 0.008	3.94± 0.05	0.082± 0.008	3.36± 0.05	0.055± 0.008	3.97± 0.05	0.092± 0.008	3.34± 0.05	0.057± 0.008
850	3.50± 0.05	0.067± 0.007	3.61± 0.05	0.072± 0.007	3.57± 0.05	0.067± 0.007	3.91± 0.05	0.086± 0.007	4.04± 0.05	0.091± 0.007	3.42± 0.05	0.061± 0.007	4.09± 0.05	0.103± 0.007	3.41± 0.05	0.063± 0.007
900	3.59± 0.05	0.085± 0.007	3.71± 0.05	0.092± 0.007	3.66± 0.05	0.085± 0.007	4.02± 0.05	0.109± 0.007	4.16± 0.05	0.116± 0.007	3.50± 0.05	0.076± 0.007	4.22± 0.05	0.136± 0.007	3.49± 0.05	0.080± 0.007
950	3.68± 0.05	0.130± 0.011	3.81± 0.05	0.140± 0.011	3.75± 0.05	0.128± 0.011	4.14± 0.05	0.167± 0.011	4.29± 0.05	0.176± 0.011	3.59± 0.05	0.115± 0.011	4.37± 0.05	0.217± 0.011	3.58± 0.05	0.123± 0.011

Table C.28- Multicomponent clay-minerals mixing rules dielectric property estimations of slabs of English red clay at 0.30±0.02 void fraction at 2470 MHz across the 20-950 ºC firing range from mineral powders at 0.56±0.04void fractions. The standard uncertainties are indicated in the table.

	Complex Refractive Index		Landau-Lifshitz-Looyenga		Bruggeman-Hanai		Böttcher		Lichtenecker		Rayleigh		Sen-Scala-Cohen		Complex Refractive Index α=0.65	
T (°C)	**ε'**	**ε''**	**ε'**	**ε''**	**ε'**	**ε''**	**ε'**	**ε''**	**ε'**	**ε''**	**ε'**	**ε''**	**ε'**	**ε''**	**ε'**	**ε''**
20	2.76± 0.04	0.074± 0.003	2.81± 0.04	0.016± 0.003	2.81± 0.04	0.015± 0.003	2.96± 0.04	0.091± 0.003	3.03± 0.04	0.018± 0.003	2.73± 0.04	0.070± 0.003	3.02± 0.04	0.097± 0.003	2.71± 0.04	0.015± 0.003
50	2.78± 0.04	0.058± 0.004	2.83± 0.04	0.019± 0.004	2.83± 0.04	0.018± 0.004	2.99± 0.04	0.071± 0.004	3.06± 0.04	0.021± 0.004	2.75± 0.04	0.055± 0.004	3.05± 0.04	0.078± 0.004	2.73± 0.04	0.018± 0.004
100	2.70± 0.07	0.025± 0.007	2.75± 0.07	0.010± 0.007	2.76± 0.07	0.009± 0.007	2.90± 0.07	0.030± 0.007	2.97± 0.07	0.011± 0.007	2.69± 0.07	0.023± 0.007	2.95± 0.07	0.033± 0.007	2.66± 0.07	0.009± 0.007
150	2.70± 0.04	0.017± 0.001	2.75± 0.04	0.003± 0.001	2.76± 0.04	0.003± 0.001	2.90± 0.04	0.020± 0.001	2.97± 0.04	0.004± 0.001	2.68± 0.04	0.016± 0.001	2.94± 0.04	0.022± 0.001	2.65± 0.04	0.003± 0.001
200	2.72± 0.04	0.007± 0.001	2.77± 0.04	0.007± 0.001	2.78± 0.04	0.007± 0.001	2.92± 0.04	0.008± 0.001	3.00± 0.04	0.008± 0.001	2.70± 0.04	0.006± 0.001	2.97± 0.04	0.009± 0.001	2.67± 0.04	0.006± 0.001
250	2.74± 0.04	0.007± 0.002	2.80± 0.04	0.008± 0.002	2.80± 0.04	0.007± 0.002	2.95± 0.04	0.009± 0.002	3.03± 0.04	0.009± 0.002	2.73± 0.04	0.007± 0.002	3.00± 0.04	0.010± 0.002	2.70± 0.04	0.007± 0.002
300	2.77± 0.04	0.008± 0.002	2.83± 0.04	0.008± 0.002	2.83± 0.04	0.008± 0.002	2.99± 0.04	0.009± 0.002	3.06± 0.04	0.010± 0.002	2.75± 0.04	0.007± 0.002	3.04± 0.04	0.010± 0.002	2.72± 0.04	0.007± 0.002
350	2.80± 0.04	0.009± 0.002	2.86± 0.04	0.009± 0.002	2.86± 0.04	0.009± 0.002	3.02± 0.04	0.010± 0.002	3.10± 0.04	0.011± 0.002	2.78± 0.04	0.008± 0.002	3.08± 0.04	0.011± 0.002	2.75± 0.04	0.008± 0.002
400	2.84± 0.04	0.010± 0.002	2.90± 0.04	0.010± 0.002	2.89± 0.04	0.010± 0.002	3.06± 0.04	0.012± 0.002	3.15± 0.04	0.012± 0.002	2.81± 0.04	0.009± 0.002	3.13± 0.04	0.013± 0.002	2.78± 0.04	0.009± 0.002
450	2.87± 0.04	0.011± 0.003	2.93± 0.04	0.012± 0.003	2.93± 0.04	0.011± 0.003	3.10± 0.04	0.013± 0.003	3.19± 0.04	0.014± 0.003	2.84± 0.04	0.010± 0.003	3.17± 0.04	0.015± 0.003	2.81± 0.04	0.010± 0.003
500	2.90± 0.04	0.012± 0.003	2.96± 0.04	0.012± 0.003	2.96± 0.04	0.012± 0.003	3.14± 0.04	0.014± 0.003	3.23± 0.04	0.015± 0.003	2.87± 0.04	0.011± 0.003	3.21± 0.04	0.016± 0.003	2.84± 0.04	0.011± 0.003
550	2.92± 0.12	0.014± 0.003	2.99± 0.12	0.015± 0.003	2.99± 0.12	0.015± 0.003	3.18± 0.12	0.017± 0.003	3.26± 0.12	0.019± 0.003	2.89± 0.12	0.013± 0.003	3.25± 0.12	0.020± 0.003	2.87± 0.12	0.014± 0.003
600	2.97± 0.09	0.017± 0.003	3.04± 0.09	0.018± 0.003	3.03± 0.09	0.017± 0.003	3.23± 0.09	0.021± 0.003	3.32± 0.09	0.022± 0.003	2.94± 0.09	0.016± 0.003	3.31± 0.09	0.023± 0.003	2.91± 0.09	0.016± 0.003
650	3.01± 0.07	0.020± 0.003	3.09± 0.07	0.021± 0.003	3.08± 0.07	0.020± 0.003	3.29± 0.07	0.025± 0.003	3.38± 0.07	0.026± 0.003	2.98± 0.07	0.019± 0.003	3.37± 0.07	0.028± 0.003	2.95v 0.07	0.019± 0.003
700	3.06± 0.03	0.024± 0.003	3.13± 0.03	0.026± 0.003	3.12± 0.03	0.024± 0.003	3.34± 0.03	0.030± 0.003	3.44± 0.03	0.032± 0.003	3.02± 0.03	0.022± 0.003	3.43± 0.03	0.034± 0.003	2.99± 0.03	0.023± 0.003
750	3.09± 0.03	0.028± 0.003	3.17± 0.03	0.030± 0.003	3.15± 0.03	0.028± 0.003	3.38± 0.03	0.035± 0.003	3.49± 0.03	0.037± 0.003	3.05± 0.03	0.026± 0.003	3.48± 0.03	0.040± 0.003	3.02± 0.03	0.027± 0.003
800	3.13± 0.02	0.033± 0.004	3.21± 0.02	0.035± 0.004	3.19± 0.02	0.033± 0.004	3.43± 0.02	0.041± 0.004	3.53± 0.02	0.044± 0.004	3.08± 0.02	0.030± 0.004	3.53± 0.02	0.047± 0.004	3.06± 0.02	0.031± 0.004
850	3.17± 0.02	0.034± 0.003	3.25± 0.02	0.036± 0.003	3.23± 0.02	0.034± 0.003	3.48± 0.02	0.042± 0.003	3.59± 0.02	0.045± 0.003	3.12± 0.02	0.031± 0.003	3.59± 0.02	0.049± 0.003	3.10± 0.02	0.032± 0.003
900	3.22± 0.02	0.043± 0.003	3.31± 0.02	0.046± 0.003	3.29± 0.02	0.043± 0.003	3.55± 0.02	0.054± 0.003	3.66± 0.02	0.057± 0.003	3.17± 0.02	0.039± 0.003	3.67± 0.02	0.062± 0.003	3.15± 0.02	0.040± 0.003
950	3.28± 0.02	0.058± 0.005	3.37± 0.02	0.062± 0.005	3.34± 0.02	0.058± 0.005	3.62± 0.02	0.073± 0.005	3.73± 0.02	0.076± 0.005	3.22± 0.02	0.053± 0.005	3.75± 0.02	0.087± 0.005	3.20± 0.02	0.055± 0.005

Table C.29- Multicomponent clay-minerals mixing rules dielectric property estimations of slabs of Dutch red clay at 0.38±0.01void fraction at 912 MHz across the 20-950 ºC firing range from mineral powders at 0.56±0.04void fractions. The standard uncertainties are indicated in the table.

	Complex Refractive Index		Landau-Lifshitz-Looyenga		Bruggeman-Hanai		Böttcher		Lichtenecker		Rayleigh		Sen-Scala-Cohen		Complex Refractive Index α=0.65	
T (°C)	**ε'**	**ε''**	**ε'**	**ε''**	**ε'**	**ε''**	**ε'**	**ε''**	**ε'**	**ε''**	**ε'**	**ε''**	**ε'**	**ε''**	**ε'**	**ε''**
20	2.68± 0.05	0.079± 0.006	2.73± 0.05	0.019± 0.006	2.73± 0.05	0.018± 0.006	2.87± 0.05	0.034± 0.006	2.93± 0.05	0.021± 0.006	2.66± 0.05	0.075± 0.006	2.92± 0.05	0.103± 0.006	2.64± 0.05	0.018± 0.006
50	2.71± 0.05	0.046± 0.005	2.75± 0.05	0.023± 0.005	2.76± 0.05	0.022± 0.005	2.90± 0.05	0.045± 0.005	2.96± 0.05	0.025± 0.005	2.68± 0.05	0.042± 0.005	2.95± 0.05	0.062± 0.005	2.66± 0.05	0.023± 0.005
100	2.62± 0.07	0.034± 0.007	2.66± 0.07	0.013± 0.007	2.67± 0.07	0.012± 0.007	2.79± 0.07	0.032± 0.007	2.86± 0.07	0.015± 0.007	2.60± 0.07	0.032± 0.007	2.84± 0.07	0.044± 0.007	2.58± 0.07	0.012± 0.007
150	2.60± 0.06	0.017± 0.004	2.65± 0.06	0.003± 0.004	2.66± 0.06	0.003± 0.004	2.78± 0.06	0.016± 0.004	2.84± 0.06	0.004± 0.004	2.59± 0.06	0.016± 0.004	2.82± 0.06	0.022± 0.004	2.56± 0.06	0.003± 0.004
200	2.63± 0.06	0.006± 0.003	2.67± 0.06	0.007± 0.003	2.68± 0.06	0.006± 0.003	2.81± 0.06	0.007± 0.003	2.88± 0.06	0.008± 0.003	2.62± 0.06	0.006± 0.003	2.85± 0.06	0.008± 0.003	2.59± 0.06	0.006± 0.003
250	2.67± 0.06	0.007± 0.005	2.71± 0.06	0.007± 0.005	2.72± 0.06	0.007± 0.005	2.86± 0.06	0.008± 0.005	2.92± 0.06	0.008± 0.005	2.65± 0.06	0.006± 0.005	2.90± 0.06	0.009± 0.005	2.62± 0.06	0.007± 0.005
300	2.71± 0.06	0.009± 0.003	2.76± 0.06	0.009± 0.003	2.77± 0.06	0.009± 0.003	2.91± 0.06	0.010± 0.003	2.98± 0.06	0.011± 0.003	2.69± 0.06	0.008± 0.003	2.96± 0.06	0.011± 0.003	2.66± 0.06	0.008± 0.003
350	2.76± 0.06	0.011± 0.003	2.81± 0.06	0.012± 0.003	2.82± 0.06	0.011± 0.003	2.97± 0.06	0.014± 0.003	3.05± 0.06	0.014± 0.003	2.74± 0.06	0.010± 0.003	3.02± 0.06	0.015± 0.003	2.71± 0.06	0.011± 0.003
400	2.81± 0.05	0.014± 0.005	2.87± 0.05	0.014± 0.005	2.87± 0.05	0.014± 0.005	3.04± 0.05	0.017± 0.005	3.12± 0.05	0.017± 0.005	2.79± 0.05	0.013± 0.005	3.10± 0.05	0.018± 0.005	2.76± 0.05	0.013± 0.005
450	2.87± 0.05	0.015± 0.004	2.94± 0.05	0.016± 0.004	2.94± 0.05	0.015± 0.004	3.11± 0.05	0.018± 0.004	3.20± 0.05	0.019± 0.004	2.85± 0.05	0.014± 0.004	3.18± 0.05	0.020± 0.004	2.82± 0.05	0.014± 0.004
500	2.94± 0.05	0.019± 0.006	3.01± 0.05	0.020± 0.006	3.00± 0.05	0.019± 0.006	3.20± 0.05	0.024± 0.006	3.29± 0.05	0.024± 0.006	2.91± 0.05	0.017± 0.006	3.27± 0.05	0.026± 0.006	2.88± 0.05	0.018± 0.006
550	3.01± 0.07	0.022± 0.005	3.09± 0.07	0.023± 0.005	3.08± 0.07	0.022± 0.005	3.29± 0.07	0.027± 0.005	3.38± 0.07	0.028± 0.005	2.98± 0.07	0.020± 0.005	3.37± 0.07	0.030± 0.005	2.95± 0.07	0.021± 0.005
600	3.12± 0.07	0.032± 0.005	3.20± 0.07	0.034± 0.005	3.18± 0.07	0.032± 0.005	3.42± 0.07	0.039± 0.005	3.52± 0.07	0.041± 0.005	3.07± 0.07	0.029± 0.005	3.52± 0.07	0.045± 0.005	3.05± 0.07	0.030± 0.005
650	3.21± 0.06	0.042± 0.006	3.30± 0.06	0.045± 0.006	3.28± 0.06	0.042± 0.006	3.53± 0.06	0.053± 0.006	3.65± 0.06	0.056± 0.006	3.16± 0.06	0.039± 0.006	3.65± 0.06	0.061± 0.006	3.13± 0.06	0.040± 0.006
700	3.29± 0.06	0.047± 0.006	3.39± 0.06	0.051± 0.006	3.36± 0.06	0.048± 0.006	3.64± 0.06	0.060± 0.006	3.75± 0.06	0.063± 0.006	3.23± 0.06	0.043± 0.006	3.77± 0.06	0.070± 0.006	3.21± 0.06	0.045± 0.006
750	3.36± 0.05	0.053± 0.007	3.46± 0.05	0.057± 0.007	3.43± 0.05	0.053± 0.007	3.73± 0.05	0.067± 0.007	3.85± 0.05	0.071± 0.007	3.30± 0.05	0.048± 0.007	3.87± 0.05	0.079± 0.007	3.28± 0.05	0.050± 0.007
800	3.43± 0.05	0.061± 0.008	3.53± 0.05	0.065± 0.008	3.49± 0.05	0.061± 0.008	3.81± 0.05	0.077± 0.008	3.94± 0.05	0.082± 0.008	3.36± 0.05	0.055± 0.008	3.97± 0.05	0.092± 0.008	3.34± 0.05	0.057± 0.008
850	3.50± 0.05	0.067± 0.007	3.61± 0.05	0.072± 0.007	3.57± 0.05	0.067± 0.007	3.91± 0.05	0.086± 0.007	4.04± 0.05	0.091± 0.007	3.42± 0.05	0.061± 0.007	4.09± 0.05	0.103± 0.007	3.41± 0.05	0.063± 0.007
900	3.59± 0.05	0.085± 0.008	3.71± 0.05	0.092± 0.008	3.66± 0.05	0.085± 0.008	4.02± 0.05	0.109± 0.008	4.16± 0.05	0.116± 0.008	3.50± 0.05	0.076± 0.008	4.22± 0.05	0.136± 0.008	3.49± 0.05	0.080± 0.008
950	3.68± 0.05	0.130± 0.012	3.81± 0.05	0.140± 0.012	3.75± 0.05	0.128± 0.012	4.14± 0.05	0.167± 0.012	4.29± 0.05	0.176± 0.012	3.59± 0.05	0.115± 0.012	4.37± 0.05	0.217± 0.012	3.58± 0.05	0.123± 0.012

Table C.30- Multicomponent clay-minerals mixing rules dielectric property estimations of slabs of Dutch red clay at 0.38±0.01void fraction at 2470 MHz across the 20-950 ºC firing range from mineral powders at 0.56±0.04void fractions. The standard uncertainties are indicated in the table.

	Complex Refractive Index		Landau-Lifshitz-Looyenga		Bruggeman-Hanai		Böttcher		Lichtenecker		Rayleigh		Sen-Scala-Cohen		Complex Refractive Index α=0.65	
T (°C)	ε'	ε''	ε'	ε''	ε'	ε''	ε'	ε''	ε'	ε''	ε'	ε''	ε'	ε''	ε'	ε''
20	2.76± 0.05	0.074± 0.002	2.81± 0.05	0.016± 0.002	2.81± 0.05	0.015± 0.002	2.96± 0.05	0.042± 0.002	3.03± 0.05	0.018± 0.002	2.73± 0.05	0.070± 0.002	3.02± 0.05	0.097± 0.002	2.71± 0.05	0.015± 0.002
50	2.78± 0.05	0.058± 0.003	2.83± 0.05	0.019± 0.003	2.83± 0.05	0.018± 0.003	2.99± 0.05	0.051± 0.003	3.06± 0.05	0.021± 0.003	2.75± 0.05	0.055± 0.003	3.05± 0.05	0.078± 0.003	2.73± 0.05	0.018± 0.003
100	2.70± 0.07	0.025± 0.005	2.75± 0.07	0.010± 0.005	2.76± 0.07	0.009± 0.005	2.90± 0.07	0.030± 0.005	2.97± 0.07	0.011± 0.005	2.69± 0.07	0.023± 0.005	2.95± 0.07	0.033± 0.005	2.66± 0.07	0.009± 0.005
150	2.70± 0.05	0.017± 0.000	2.75± 0.05	0.003± 0.000	2.76± 0.05	0.003± 0.000	2.90± 0.05	0.020± 0.000	2.97± 0.05	0.004± 0.000	2.68± 0.05	0.016± 0.000	2.94± 0.05	0.022± 0.000	2.65± 0.05	0.003± 0.000
200	2.72± 0.05	0.007± 0.001	2.77± 0.05	0.007± 0.001	2.78± 0.05	0.007± 0.001	2.92± 0.05	0.008± 0.001	3.00± 0.05	0.008± 0.001	2.70± 0.05	0.006± 0.001	2.97± 0.05	0.009± 0.001	2.67± 0.05	0.006± 0.001
250	2.74± 0.04	0.007± 0.001	2.80± 0.04	0.008± 0.001	2.80± 0.04	0.007± 0.001	2.95± 0.04	0.009± 0.001	3.03± 0.04	0.009± 0.001	2.73± 0.04	0.007± 0.001	3.00± 0.04	0.010± 0.001	2.70± 0.04	0.007± 0.001
300	2.77± 0.04	0.008± 0.002	2.83± 0.04	0.008± 0.002	2.83± 0.04	0.008± 0.002	2.99± 0.04	0.009± 0.002	3.06± 0.04	0.010± 0.002	2.75± 0.04	0.007± 0.002	3.04± 0.04	0.010± 0.002	2.72± 0.04	0.007± 0.002
350	2.80± 0.04	0.009± 0.002	2.86± 0.04	0.009± 0.002	2.86± 0.04	0.009± 0.002	3.02± 0.04	0.010± 0.002	3.10± 0.04	0.011± 0.002	2.78± 0.04	0.008± 0.002	3.08± 0.04	0.011± 0.002	2.75± 0.04	0.008± 0.002
400	2.84± 0.04	0.010± 0.002	2.90± 0.04	0.010± 0.002	2.89± 0.04	0.010± 0.002	3.06± 0.04	0.012± 0.002	3.15± 0.04	0.012± 0.002	2.81± 0.04	0.009± 0.002	3.13± 0.04	0.013± 0.002	2.78± 0.04	0.009± 0.002
450	2.87± 0.03	0.011± 0.002	2.93± 0.03	0.012± 0.002	2.93± 0.03	0.011± 0.002	3.10± 0.03	0.013± 0.002	3.19± 0.03	0.014± 0.002	2.84± 0.03	0.010± 0.002	3.17± 0.03	0.015± 0.002	2.81± 0.03	0.010± 0.002
500	2.90± 0.03	0.012± 0.002	2.96± 0.03	0.012± 0.002	2.96± 0.03	0.012± 0.002	3.14± 0.03	0.014± 0.002	3.23± 0.03	0.015± 0.002	2.87± 0.03	0.011± 0.002	3.21± 0.03	0.016± 0.002	2.84± 0.03	0.011± 0.002
550	2.92± 0.05	0.014± 0.002	2.99± 0.05	0.015± 0.002	2.99± 0.05	0.015± 0.002	3.18± 0.05	0.017± 0.002	3.26± 0.05	0.019± 0.002	2.89± 0.05	0.013± 0.002	3.25± 0.05	0.020± 0.002	2.87± 0.05	0.014± 0.002
600	2.97± 0.04	0.017± 0.002	3.04± 0.04	0.018± 0.002	3.03± 0.04	0.017± 0.002	3.23± 0.04	0.021± 0.002	3.32± 0.04	0.022± 0.002	2.94± 0.04	0.016± 0.002	3.31± 0.04	0.023± 0.002	2.91± 0.04	0.016± 0.002
650	3.01± 0.04	0.020± 0.002	3.09± 0.04	0.021± 0.002	3.08± 0.04	0.020± 0.002	3.29± 0.04	0.025± 0.002	3.38± 0.04	0.026± 0.002	2.98± 0.04	0.019± 0.002	3.37± 0.04	0.028± 0.002	2.95± 0.04	0.019± 0.002
700	3.06± 0.03	0.024± 0.002	3.13± 0.03	0.026± 0.002	3.12± 0.03	0.024± 0.002	3.34± 0.03	0.030± 0.002	3.44± 0.03	0.032± 0.002	3.02± 0.03	0.022± 0.002	3.43± 0.03	0.034± 0.002	2.99± 0.03	0.023± 0.002
750	3.09± 0.03	0.028± 0.003	3.17± 0.03	0.030± 0.003	3.15± 0.03	0.028± 0.003	3.38± 0.03	0.035± 0.003	3.49± 0.03	0.037± 0.003	3.05± 0.03	0.026± 0.003	3.48± 0.03	0.040± 0.003	3.02± 0.03	0.027± 0.003
800	3.13± 0.02	0.033± 0.003	3.21± 0.02	0.035± 0.003	3.19± 0.02	0.033± 0.003	3.43± 0.02	0.041± 0.003	3.53± 0.02	0.044± 0.003	3.08± 0.02	0.030± 0.003	3.53± 0.02	0.047± 0.003	3.06± 0.02	0.031± 0.003
850	3.17± 0.02	0.034± 0.003	3.25± 0.02	0.036± 0.003	3.23± 0.02	0.034± 0.003	3.48± 0.02	0.042± 0.003	3.59± 0.02	0.045± 0.003	3.12± 0.02	0.031± 0.003	3.59± 0.02	0.049± 0.003	3.10± 0.02	0.032± 0.003
900	3.22± 0.02	0.043± 0.003	3.31± 0.02	0.046± 0.003	3.29± 0.02	0.043± 0.003	3.55± 0.02	0.054± 0.003	3.66± 0.02	0.057± 0.003	3.17± 0.02	0.039± 0.003	3.67± 0.02	0.062± 0.003	3.15± 0.02	0.040± 0.003
950	3.28± 0.02	0.058± 0.005	3.37± 0.02	0.062± 0.005	3.34± 0.02	0.058± 0.005	3.62± 0.02	0.073± 0.005	3.73± 0.02	0.076± 0.005	3.22± 0.02	0.053± 0.005	3.75± 0.02	0.087± 0.005	3.20± 0.02	0.055± 0.005

Appendix D: Thermal modelling of microwave trials

Appendix D1: Parameters used in the thermal models calculations

Table D.1- Rig parameters and clay characteristics used for the developed thermal models.

Specimen	25x20 mm		25x35 mm	
	Sides	Top-Bottom	Sides	Top-Bottom
Temperature ambient (T_A)	20 °C			
Mass of clay specimen (m)	14.3±0.4 g		38.8±0.5 g	
Clay thermal conductivity (K_C)	$10^{-7}\,T_{CAvg}{}^2$+9 $10^{-5}\,T_{CAvg}$+0.1453 (Campbell et al., 1994)			
Firebrick thermal conductivity(K_F)	$10^{-4}\,T_{FAvg}$+0.3027 (BNZ, 2016)			
Fibercon wool thermal conductivity (K_W)	3 $10^{-7}\,T_{WAvg}{}^2$-3 $10^{-4}T_{WAvg}$+0.2064 (INSULCON, 2014)			
Clay thickness (e_c)	0.010 m	0.013 m	0.018 m	0.013 m
Vitcas firebrick thickness (e_F)	0.021 m	0.030 m	0.014 m	0.030 m
Fibercon wool thickness (e_W)	0.010 m	0.110 m	0.075 m	0.110 m
Vitcas firebrick diameter or height(L_F)	0.037 m	0.084 m	0.037 m	0.211 m
Heat exchange area of Fibercon wool(A_W)	0.007 m^2	0.001 m^2	0.007 m^2	0.002 m^2
Heat exchange area of clay(A_C)	0.001 m	0.001 m	0.002 m	0.002 m

Appendix D2: Specific heat capacity of Danish clays

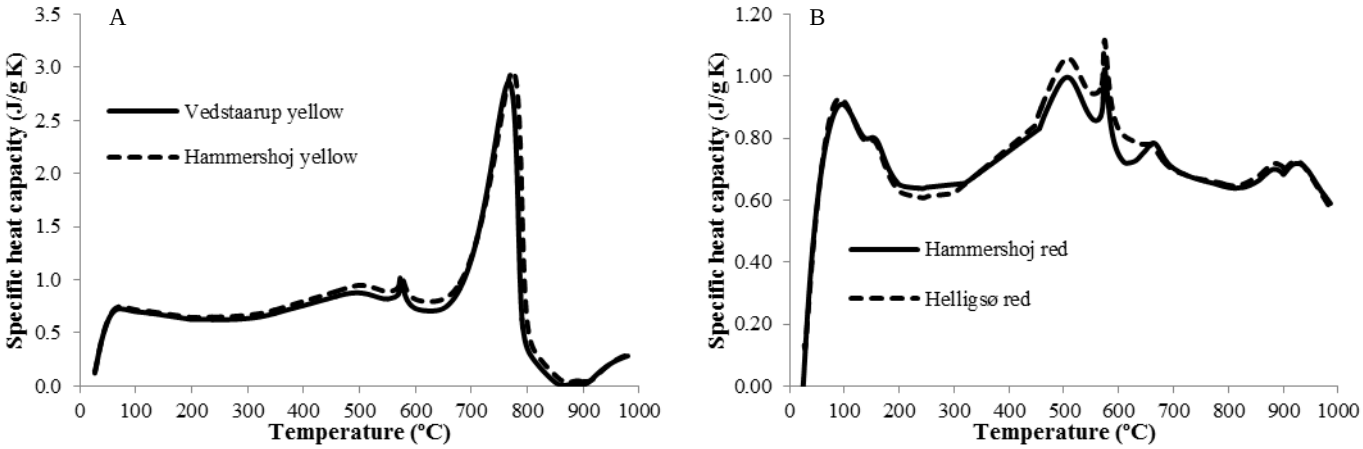


Figure D.1- Average specific heat capacity across the temperature range of 25-1000 °C at 20 °C/min in a N_2 atmosphere for yellow (A) and red (B) Danish clays. These results are the average of three repeats. Standard deviations average around ±0.007 for Vedstaarup yellow, ±0.011 for Hammershoj yellow, ±0.014 for Helligsø red and ±0.010 for Hammershoj red.

Appendix D3: Temperature relations and heating losses across clay firing

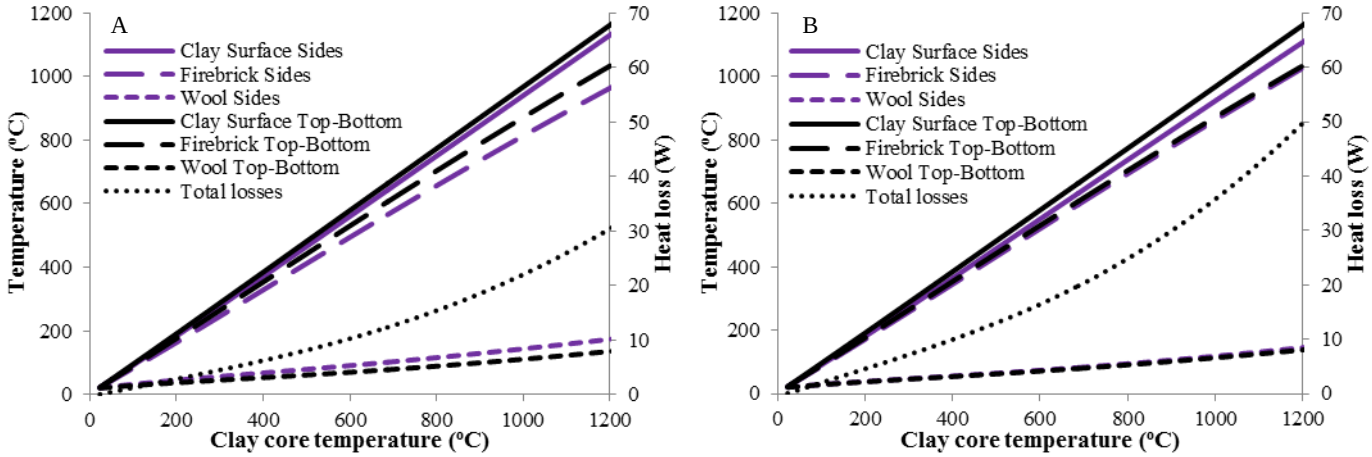


Figure D.2- Temperature equilibrium relations between different parts of the heating system with the clay core and total heating losses of the system across firing for 25x20 mm (A) and 25x35 mm (B) clay specimens.

Appendix E: LabVIEW software interface for automatic power input control during microwave heating trials

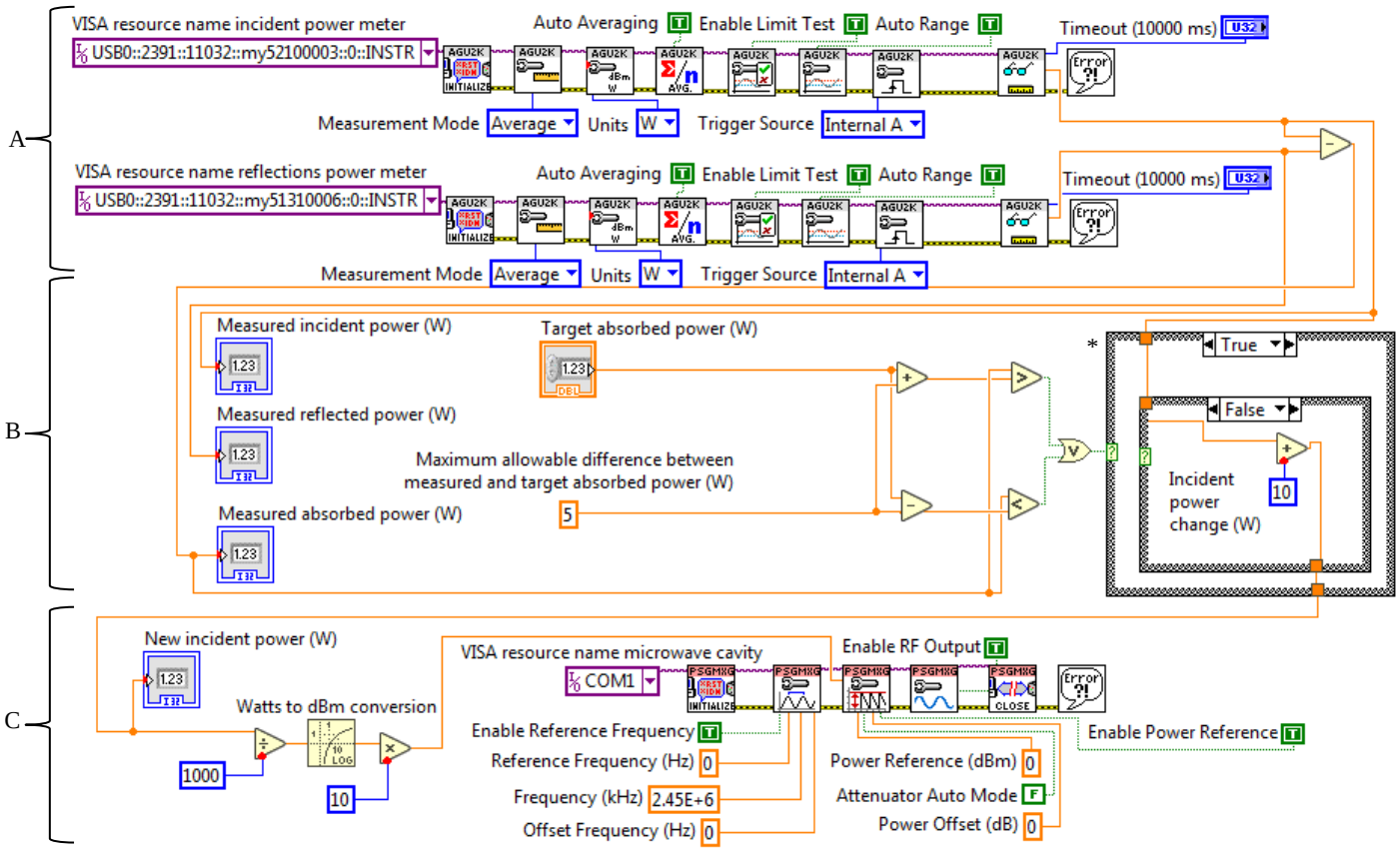


Figure E.1- Diagram of LabVIEW software interface used to automatically control the power absorbed by the clay samples during microwave heating trials. The system can be divided in input of measured incident and reflected powers (A), assessment of power readings and computation of new incident power through an "If block" represented by nested case structures (B) and output of new incident power to microwave generator (C).*In the diagram, the case structure displays the event where the incident power needs to be increased.